3-D Computer Graphics
A Mathematical Introduction with OpenGL

Revision draft Draft C.4.a. November 21, 2022

Samuel R. Buss

November 21, 2022

This is a draft of a second edition of the book, intended for use by students in Math 155AB at UCSD during Winter-Spring 2019 and onwards. This draft is available for general use for your personal study or projects. Reports of errata or other corrections will be *greatly* appreciated.

Contents

Table of Contents iii

Preface ix

I Introduction 1

I.1 Points, lines and triangles 2

I.1.1 Rectangular arrays of pixels 2

I.1.2 Vector graphics 4

I.1.3 Triangles 5

I.2 Coordinate systems 5

I.3 Points, lines and triangles in OpenGL 7

I.3.1 Loading vertices into a VAO and VBO 7

I.3.2 Drawing points and lines 11

I.3.3 Drawing triangles 13

I.3.4 Rendering with element arrays 17

I.3.5 Different colors per vertex 19

I.3.6 Face orientation and culling 21

I.3.7 Wireframe triangles 22

I.4 Vertex shaders and fragment shaders 22

I.4.1 Very simple vertex and fragment shader example . 25

I.4.2 A fragment shader modifying the color 26

I.4.3 Flat shading 27

I.4.4 Hidden surfaces 28

I.5 Animation with double buffering 29

I.6 Antialiasing with supersampling 31

I.7 Additional exercises 31

II Transformations and Viewing 35

II.1 Transformations and the graphics pipeine 35

II.2 Transformations in 2-space 38

II.2.1 Basic definitions 39

II.2.2 Matrix representation of linear transformations . . 42

II.2.3 Rigid transformations and rotations 46

II.2.4 Homogeneous coordinates 52

II.2.5 Matrix representation of an affine transformation . 53
II.2.6 Using two dimensional transformations 55
II.2.7 Another outlook on composing transformations . . 59
II.2.8 Two dimensional projective geometry 61
II.3 Transformations in 3-space 63
II.3.1 Moving from 2-space to 3-space 63
II.3.2 A solar system example 67
II.3.3 Transformations and OpenGL 70
II.3.4 Uniform variables and generic vertex attributes. . . 73
II.3.5 Solar system in OpenGL 75
II.3.6 Derivation of the rotation matrix 77
II.3.7 Euler's theorem 81
II.3.8 Three dimensional projective geometry 83
II.4 Projection transformations and perspective 84
II.4.1 Orthographic viewing transformations 86
II.4.2 Perspective viewing transformations 88
II.4.3 The power of 4×4 matrices 93
II.4.4 Mapping lines to lines 94
II.4.5 Another use for projection: shadows 95
II.4.6 z-fighting 96
II.4.7 The OpenGL perspective transformations 97
II.5 Additional exercises 100

III The Rendering Pipeline 109
III.1 The core rendering pipeline 109
III.2 Rendering pipeline with a geometry shader 114
III.3 Rasterization: mapping to pixels 119
III.3.1 Bresenham algorithm 125
III.3.2 The perils of floating point roundoff 126
III.4 Additional exercises 128

IV Lighting and Shading 131
IV.1 The Phong lighting model 133
IV.1.1 Diffuse reflection 137
IV.1.2 Specular reflection 139
IV.1.3 Ambient reflection and emissivity 142
IV.1.4 Putting it together: multiple lights and colors . . . 143
IV.1.5 Schlick's Fresnel term for specular reflection 144
IV.1.6 Attenuation and spotlight effects 146
IV.2 Gouraud and Phong shading 147
IV.3 Computing surface normals 150
IV.4 Affine transformations and normal vectors 155
IV.5 Shader programs for Phong lighting 157
IV.6 The Cook-Torrance lighting model 164
IV.6.1 Bidirectional reflectivity 164
IV.6.2 Overview of Cook-Torrance lighting 166

IV.6.3 The microfacet distribution term, D 168
IV.6.4 The geometric surface occlusion term, G 169
IV.6.5 The Fresnel term, F 175
IV.7 Additional exercises 177

V Averaging and Interpolation 183
V.1 Linear interpolation 184
V.1.1 Interpolation between two points 184
V.1.2 Weighted averages and affine combinations 185
V.1.3 Interpolation on three points: barycentric coordinates187
V.2 Bilinear and trilinear interpolation 195
V.2.1 Bilinear interpolation 195
V.2.2 Properties of bilinear interpolation 198
V.2.3 Inverting bilinear interpolation 202
V.2.4 Trilinear interpolation 207
V.3 Convex sets and weighted averages 208
V.4 Interpolation and homogeneous coordinates 210
V.5 Hyperbolic interpolation 213
V.6 Spherical linear interpolation 215
V.7 Interpolation with GLSL shaders 218
V.8 Additional exercises 220

VI Texture Mapping 225
VI.1 Texture mapping an image 225
VI.1.1 Interpolating a texture to a surface 227
VI.1.2 Assigning texture coordinates 229
VI.1.3 Mipmapping and anti-aliasing 233
VI.1.4 Stochastic supersampling 236
VI.2 Bump mapping 237
VI.3 Environment mapping 240
VI.4 Texture mapping in OpenGL 243
VI.4.1 Loading a texture map 243
VI.4.2 Managing multiple texture maps 245
VI.4.3 Environment mapping in OpenGL 246

VII Color 249
VII.1 Color perception 249
VII.2 Representation of color values 252
VII.2.1 Additive and subtractive colors 253
VII.2.2 Representation of RGB colors 254
VII.2.3 Hue, saturation, and luminance 256
VII.3 Gamma correction and sRGB color 259
VII.3.1 Using sRGB versus RGB 261
VII.4 Additional exercises 264

VIII Bézier Curves **265**
VIII.1 Bézier curves of degree three 266
VIII.2 De Casteljau's method 270
VIII.3 Recursive subdivision 271
VIII.4 Piecewise Bézier curves 274
VIII.5 Hermite polynomials 277
VIII.6 Bézier curves of general degree 278
VIII.7 De Casteljau's method, revisited 282
VIII.8 Recursive subdivision, revisited 284
VIII.9 Degree elevation 285
VIII.10Bézier surface patches 287
VIII.10.1Basic properties of Bézier patches 288
VIII.10.2Joining Bézier patches 291
VIII.11Bézier curves and surfaces in OpenGL 294
VIII.11.1Bézier curves 294
VIII.11.2Bézier patches 296
VIII.12Rational Bézier curves 297
VIII.13Conic sections with rational Bézier curves 299
VIII.14Surface of revolution example 306
VIII.15Interpolating with Bézier curves 309
VIII.15.1Catmull-Rom splines 309
VIII.15.2Bessel-Overhauser splines 311
VIII.15.3Tension-continuity-bias splines 314
VIII.16Interpolating with Bézier surfaces 317
VIII.17Additional exercises 322

IX B-Splines **325**
IX.1 Uniform B-splines of degree three 326
IX.2 Nonuniform B-splines 330
IX.3 Examples of nonuniform B-splines 334
IX.4 Properties of nonuniform B-splines 341
IX.5 The de Boor algorithm 345
IX.6 Blossoms 350
IX.7 Derivatives and smoothness of B-spline curves 355
IX.8 Knot insertion 358
IX.9 Bézier and B-spline curves 362
IX.10 Degree elevation 364
IX.11 Rational B-splines and NURBS 364
IX.12 Interpolating with B-splines 365
IX.13 Additional exercises 370

X Ray Tracing **371**
X.1 Basic ray tracing 372
X.1.1 Local lighting and reflection rays 377
X.1.2 Transmission rays 379
X.1.3 Putting it all together 383

X.2 Advanced ray tracing techniques 385
X.2.1 Distributed ray tracing 385
X.2.2 Backwards ray tracing 394
X.3 Special effects without ray tracing 396

XI Intersection Testing 403
XI.1 Fast intersections with rays 404
XI.1.1 Ray versus sphere intersections 404
XI.1.2 Ray versus plane intersections 407
XI.1.3 Ray versus triangle intersections 409
XI.1.4 Ray versus convex polytope intersections 411
XI.1.5 Ray versus cylinder intersections 415
XI.1.6 Ray versus quadric intersections 416
XI.1.7 Ray versus Bézier patch intersections 417
XI.2 Pruning intersection tests 417

XII Radiosity 423
XII.1 The radiosity equations 425
XII.1.1 Patches, light levels, and form factors 425
XII.1.2 High-level description of the radiosity algorithm . . 429
XII.2 Calculation of form factors 430
XII.2.1 The ray tracing method 433
XII.2.2 The hemicube method 433
XII.3 Solving the radiosity equations 436
XII.3.1 Iterative methods 436
XII.3.2 Jacobi iteration 440
XII.3.3 Gauss-Seidel iteration 441
XII.3.4 The shooting method 442

XIII Animation and Kinematics 445
XIII.1 Overview 445
XIII.1.1 Techniques evolved from traditional animation . . . 446
XIII.1.2 Computerized animation 448
XIII.2 Animation of position 450
XIII.2.1 Ease in: fixed target 450
XIII.2.2 Ease in: moving target 451
XIII.3 Representations of orientations 452
XIII.3.1 Rotation matrices 453
XIII.3.2 Yaw, pitch, and roll 454
XIII.3.3 Quaternions 456
XIII.3.4 Theoretical development of quaternions 458
XIII.3.5 Representing rotations with quaternions 461
XIII.3.6 Quaternion and rotation matrix conversions 463
XIII.3.7 Interpolation of quaternions 465
XIII.4 Kinematics 467
XIII.4.1 Rigid links and joints 468

XIII.4.2 Forward kinematics 469
XIII.4.3 Inverse kinematics, setting it up 472
XIII.4.4 Inverse kinematics, finding a local solution 475

A Mathematics Background 483
A.1 Preliminaries 483
A.2 Vectors and vector products 484
A.2.1 Vectors in $\mathbb{R}^2$ 484
A.2.2 Vectors in $\mathbb{R}^3$ 489
A.3 Matrices 491
A.3.1 Matrices and vector products in $\mathbb{R}^3$ 492
A.3.2 Determinants, inverses, and adjoints 493
A.3.3 Linear subspaces 494
A.4 Multivariable calculus 495
A.4.1 Multivariable functions 495
A.4.2 Vector-valued functions 497
A.4.3 Multivariable vector-valued functions 498

B Answers to Selected Exercises 499

Bibliography 509

Index 519

Preface

Preface to the Second Edition

The second edition has updated the first edition in several ways. The most notable change is use of the "modern" OpenGL approach instead of the older "direct" OpenGL commands. This much better reflects present-day programming practice in computer graphics, not only in OpenGL, but also in other computer graphics API's (application programming interfaces) such as Direct3D, Vulkan and Metal. A new Chapter III includes a more detailed discussion of the graphics rendering pipeline, including vertex shaders, fragment shaders and geometry.

Switching to modern OpenGL induced a range of concommittant changes throughout the text. In addition, Chapter II has been revised to improve the exposition. Chapter IV now includes the Schlick Fresnel approximation. And, Chapter VII now discusses sRGB encodings and gamma correction. Quite a few other small updates have been included as well.

Many new exercises have been added, and answers for some of the exercises can be found in the new Appendix B. The old Appendix B on the ray tracing software has been removed, but the software continues to be available freely online and is occasionally updated.

This second edition has been used for teaching Math 155A at UC San Diego during 2019-2022 while being written. There are web pages that give supplementary examples of OpenGL software along with detailed introduction to the use of the OpenGL API in C++. These web pages, along with substantial other materials including videos covering many of the topics from the first eight chapters, are available online at `http://math.ucsd.edu/~sbuss/MathCG2/`.

Preface to the First Edition

Computer graphics has grown phenomenally in recent decades, progressing from simple 2-D graphics to complex, high-quality, three dimensional environments. In entertainment, computer graphics is used extensively in movies and computer games. Animated movies are increasingly being made entirely with computers. Even nonanimated movies depend heavily on computer graphics to develop special effects: witness, for instance, the success of the *Star Wars* movies beginning already in the mid-1970's. The capabilities of computer graphics in personal computers and home game consoles have now improved to the extent that low-cost systems are able to display millions of polygons per second.

There are also significant uses of computer graphics in nonentertainment applications. For example, virtual reality systems are often used in training. Computer graphics is an indispensable tool for scientific visualization and for computer aided design (CAD). We need good methods for displaying large data sets in a comprehensible manner and for showing the results of large-scale scientific simulations.

The art and science of computer graphics has been evolving since the advent of computers and started in earnest in the early 1960's. Since then, computer graphics has developed into a rich, deep, and coherent field. The aim of this book is to present the mathematical foundations of computer graphics, along with a practical introduction to programming computer graphics using OpenGL. I believe that understanding the mathematical basis is important for any advanced use of computer graphics. For this reason, this book attempts to cover the underlying mathematics thoroughly. The principle guiding the selection of topics for this book has been to choose topics that are of practical significance for computer graphics practitioners — in particular for software developers. My hope is that this book will serve as a comprehensive introduction to the standard tools used in computer graphics and especially to the mathematical theory behind these tools.

About this book The plan for this book has been shaped by my personal experiences as an academic mathematician and by my participation in various applied computer projects, including projects in computer games and virtual reality. This book was started while I was teaching a mathematics class at the University of California, San Diego (UCSD) on computer graphics and geometry. That course was structured as an introduction to programming 3-D graphics in OpenGL, and to the mathematical foundations of computer graphics. While teaching that course, I became convinced of the need for a book that brings together the mathematical theory underlying computer graphics in an introductory and unified setting.

The other motivation for writing this book has been my involvement in several virtual reality and computer game projects. Many of the topics included in this book are present mainly because I have found them useful in computer game applications. Modern-day computer games and virtual reality applications are demanding software projects: these applications require software capable of displaying convincing three dimensional environments. Generally, the software must keep track of the motion of multiple objects; maintain information about the lighting, colors, and textures of many objects; and display them on the screen at 30 or 60 frames per second. In addition, considerable artistic and creative skills are needed to make a worthwhile three dimensional environment. Not surprisingly, this requires sophisticated software development by large teams of programmers, artists, and designers.

Perhaps it is a little more surprising that 3-D computer graphics requires extensive mathematics. This is however the case. Furthermore, the mathematics tends to be elegant and interdisciplinary. The mathematics needed in computer graphics brings together constructions and methods from several areas of mathematics, including geometry, calculus, linear algebra, numerical analysis, abstract algebra, data structures, and algorithms. In fact, computer graphics is arguably the best example of a practical area where so much mathematics combines so elegantly.

This book includes a blend of applied and theoretical topics. On the more applied side, I recommend the use of OpenGL, a readily available, free, cross-platform programming environment for 3-D graphics. The `C` and `C++` code for OpenGL programs which can be freely downloaded from the Internet has been included, and I discuss how OpenGL implements many of the mathematical concepts discussed in this book. A ray tracer software package is also described; this software can also be downloaded from the Internet. On the theoretical side, this book stresses the mathematical foundations of computer graphics, more so than any other text of which I am aware. I strongly believe that knowing the mathematical foundations of computer graphics is important for being able to use tools such as OpenGL or Direct3D, or, to a lesser extent, CAD programs properly.

The mathematical topics in this book are chosen because of their importance and relevance to graphics. However, I have not hesitated to introduce more abstract concepts when they are crucial to computer graphics, for instance the projective geometry interpretation of homogeneous coordinates, In our opinion, a good knowledge of mathematics is invaluable if you want to properly use the techniques of computer graphics software, and even more important if you want to develop new or innovative uses of computer graphics.

Using this book and OpenGL

This book is intended for use as a textbook, as a source for self-study, or as a reference. It is strongly recommended that you try running the programs supplied with the book, and that you write OpenGL programs of your own.

OpenGL is a platform independent API (application programming interface) for rendering 3-D graphics. A big advantage of using OpenGL is that it is a widely supported industry standard. There are a number of 3-D programming environments with capabilities similar to OpenGL; these include Microsoft's Direct3D and Apple's Metal, which are specific to the Windows and Macintosh operating systems, as well as Vulkan, which is a successor to OpenGL. The new programming interfaces allow more fine-grained control of GPU resources than OpenGL; however, all these systems are based on the same mathematical and conceptual approaches.

This book is intended to be supplemented with other resources to help you learn OpenGL. The book contains code snippets, of C++ programs using OpenGL features. It also discusses the architecture of OpenGL programs, including how vertex and fragment shaders work within an OpenGL program. We also provide some substantial shader programs, including a shader that implements Phong lighting.

The textbook's web page at

`http://math.ucsd.edu/~sbuss/MathCG2/`

contains a number of sample OpenGL programs. That web page starts with *SimpleDrawModern*, which is essentially the simplest possible nontrivial modern-style OpenGL program. It works up to programs that use sophisticated shaders for Phong light and that manage multiple shaders. It also has a complete Ray Tracing package available. These programs all use the "modern" OpenGL programming style, not the older "immediate mode" OpenGL. All the OpenGL programs include full source code and are accompanied by web pages explaining the code features line-by-line. OpenGL programming can be complex, but it is hoped that these will give you a straightforward and accessible introduction to OpenGL programming.

The textbook's software may be used without any restriction except that its use in commercial products or any kind of substantial project must be acknowledged.

There are many other sources available to learn OpenGL. One very nice source is the `https://learnopengl.com` web pages created by Joey De Vries. This web site also has the option to download a complete copy of the `learnopengl.com` tutorials as a PDF e-book. (As of 2022, this is free online, but a hardcopy can be purchased; donations are also accepted.) The *OpenGL SuperBible* is a book-length tutorial introduction to OpenGL. For more official sources, there are the *OpenGL Programming Guide* and the *OpenGL Shading Language Book* written by some of the OpenGL developers. These last two books can be difficult to read for the beginner however. Whatever source you use, it should cover OpenGL version 3.3, or later.

Finally, it is scarcely necessary to mention it, but the internet is a wonderful resource: there is plenty of great information online about OpenGL! In fact, it is recommended that as you read the book, you do an internet search for every OpenGL command encountered.

Outline of the book

The chapters are arranged more or less in the order the material might be covered in a course. However, it is not necessary to read the material in order. In particular, the later chapters can be read largely independently, with the exception that Chapter IX depends on Chapter VIII.

Chapter I. Introduction. Introduces the basic concepts of computer graphics. Drawing points, lines, and triangles. Modeling with triangles. A little bit of color. Simple vertex and fragment shaders. Flat and smooth shading. Hidden surfaces. Animation. Getting started with OpenGL programming.

Chapter II. Transformations and viewing. The rendering pipeline. Linear and affine transformations matrices in two and three dimensions. Translations and rotations. Homogeneous coordinates. Orthographic and perspective viewing transformations. Projective geometry. Matrix representations of linear, affine and perspective transformations. Working with transformations and matrices in C++ and OpenGL.

Chapter III. The rendering pipeline. The rendering pipeline in more detail. Vertex and fragment shaders. Geometry shaders. Pixelization, Gouraud and scan line interpolation, and the Bresenham algorithm.

Chapter IV. Lighting, illumination, and shading. The Phong lighting model. Ambient, diffuse, and specular lighting. A shader program for Phong lighting. The Cook-Torrance lighting model.

Chapter V. Averaging and interpolation. Linear interpolation. Barycentric coordinates. Bilinear interpolation. Convexity. Hyperbolic interpolation. Spherical linear interpolation. This is a more mathematical chapter with a lot of tools that are used elsewhere in the book: you may wish to skip much of this on the first reading, and come back to it as needed.

Chapter VI. Texture mapping. Textures and texture coordinates. Mipmapping. Supersampling and jittering. Bump mapping. Environment mapping. Texture maps in OpenGL.

Chapter VII. Color. Color perception. Additive and subtractive colors. RGB and HSL. Gamma correction. RGB and sRGB.

Chapter VIII. Bézier curves. Bézier curves of degree three and of general degree. De Casteljau methods. Subdivision. Piecewise Bézier curves. Hermite polynomials. Bézier surface patches. Bézier curves in OpenGL. Rational curves and conic sections. Surfaces of revolution. Degree elevation. Interpolation with Catmull-Rom, Bessel-Overhauser, and tension-continuity-bias splines. Interpolation with Bézier surfaces.

Chapter IX. B-splines. Uniform and nonuniform B-splines and their properties. The de Boor algorithm. Blossoms. Smoothness properties. NURBS and conic sections. Knot insertion. Relationship with Bézier curves. Interpolation with spline curves. This chapter has a mix of introductory topics and more specialized topics. We include all proofs, but recommend that many of the proofs be skipped on the first reading.

Chapter X. Ray tracing. Recursive ray tracing. Reflection and transmission. Distributed ray tracing. Backwards ray tracing.

Chapter XI. Intersection testing. Testing rays for intersections with spheres, planes, triangles, polytopes, and other surfaces. Bounding volumes and hierarchical pruning.

Chapter XII. Radiosity. Patches, form factors, and the radiosity equation. The hemicube method. The Jacobi, Gauss-Seidel, and Southwell iterative methods.

Chapter XIII. Animation and kinematics. Key framing. Ease in and ease out. Representations of orientation. Quaternions. Interpolating quaternions. Forward and inverse kinematics for articulated rigid multibodies.

Appendix A. Mathematics background. A review of topics from vectors, matrices, linear algebra, and calculus.

Appendix B. Answer to selected exercises. Answers to many of the inline exercises.

There are exercises at the end of most chapters, and more "inline" exercises scattered throughout the book, especially in the introductory chapters. Answers to the inline exercises are available in the final appendix. The exercises are often supplied with hints and they should not be terribly difficult. It is highly recommended that you do the exercises to master the material!

A few sections in the book, as well as some of the theorems, proofs, and exercises, are labeled with a star symbol (★). This indicates that the material is optional or less important, and can be safely skipped without affecting your understanding of the rest of the book.

Theorems, lemmas, definitions, etc. are numbered uniformly for each chapter; for example, in Chapter V, Definition V.1 is followed by Theorem V.2. Figures and exercises are numbered separately. For instance, Figure V.1 is the first figure of Chapter V.

For the instructor

This book is intended for use with advanced junior or senior level undergraduate courses. It is based in large part on my teaching computer graphics courses mostly at the upper division level. In a two quarter, undergraduate course, I cover most of the material in the book, more-or-less in the order presented in the book. Some of the more advanced topics would be skipped however; most notably Cook-Torrance lighting and some of the material on Bézier and B-spline curves and patches are best omitted from an undergraduate course. I also omit the more difficult proofs from an undergraduate course, especially some the proofs for B-splines.

It is certainly recommended that students using this book do programming assignments using OpenGL. Although this book covers a lot of OpenGL material in outline form, students will need to have an additional source for learning the details of programming in OpenGL. Programming prerequisites include some experience in a C-like language such as C, C++ or Java. The first quarters of my own courses have included programming assignments first on two dimensional graphing, second on 3-D transformations based on the solar system exercise on page 75, third on polygonal modeling (often asking students to do something creative based on their initials, plus asking them to dynamically render surfaces of revolution or another circularly symmetric object such as the torus in Figure I.15 on page 23), fourth on adding materials and lighting to a scene, fifth on textures, and then ending with an open ended assignment where students choose a project on their own. The second quarter of the course has included assignments on modeling objects with Bézier patches (Blinn's article [15] on how to construct the Utah teapot is sometimes used to help with this); on writing a program that draws Catmull-Rom and Overhauser spline curves which interpolate points picked with the mouse; on writing vertex, geometry, and fragment shaders; on using the ray tracing software supplied with this book; on implementing some aspect of distributed ray tracing; and then ending with another final project of their choosing. Extensive past course materials can be found online at `http://math.ucsd.edu/~sbuss/CourseWeb`.

Acknowledgements

Very little of the material in this book is original. The aspects that are original mostly concern matters of organization and presentation: in a number of places, I have tried to present new, simpler proofs than what was known before. In many cases, material is presented without attribution or credit, but in most cases this material is due to others. I have included references for items that I learned by consulting the original literature, and for topics for which it was easy to ascertain what the original source was. However, the book does not try to be comprehensive in assigning credit.

I learned computer graphics from several sources. First, I worked on a computer graphics project with several people at SAIC including Tom Yonkman and my wife, Teresa Buss. Subsequently, I have worked over a period of years

on computer games applications at Angel Studios and later at Rockstar Games. At Angel Studios, I benefited greatly, and learned an immense amount, from working with Steve Rotenberg, Brad Hunt, Dave Etherton, Santi Bacerra, Nathan Brown, Ted Carson, Jeff Roorda, Daniel Blumenthal, and others. I am particularly indebted to Steve Rotenberg who has been my "guru" for advanced topics and current research in computer graphics.

When first teaching computer graphics courses at UCSD, I benefitted especially from the textbooks by Watt and Watt [119], Watt [118], and Hill [66]. This book is written partly from notes developed while teaching these classes.

I am greatly indebted to Frank Chang and Malachi Pust for a thorough proofreading of an early draft of the first edition. In addition, I'd like to thank Michael Bailey, Stephanie Buss (my daughter), Chris Calabro, Joseph Chow, Daniel Curtis, Tamsen Dunn, Rosalie Iemhoff, Cyrus Jam, Jin-Su Kim, Vivek Manpuria, Jason McAuliffe, Jong-Won Oh, Horng Bin Ou, Chris Pollett, John Rapp, Don Quach, Daryl Sterling, Aubin Whitley, and anonymous referees for corrections to preliminary drafts of this book and Tak Chu, Craig Donner, Jason Eng, Igor Kaplounenko, Alex Kulungowski, Allan Lam, Peter Olcott, Nevin Shenoy, Mara Silva, Abbie Whynot, and George Yue for corrections incorporated into the second printing of the first edition.

Students and teaching assistants from my Math 155AB courses in the 2019-2022 contributed corrections and suggestions for preliminary drafts of the second edition of the book. They included Fariza Ahmed, Michael Bradley, Yeonil Cho, Yuelin Dai, Jiangmeng Ding, Dylan Greicius, Tina Jin, Nathaniel Karter, Qihao Leng, Bright Lian, Stephen Rabin, Dominic Ricci, Christopher Rocha, Mihai Ruber, Arshia Sehgal, Ronan Sullivan, Joshua Sun, Luan Tran, Phap Tran, Yujie Wang, Yuming Ma, Wenjie Zhu, and more names to come I hope.

Finally, I am indebted to the teaching assistants for my courses, including Chaitanya Animesh, Jonathan Conder, Patrick Girardet, Abhinav Gupta, Tina Jin, Arseniy Kryazhev, Srivastava Shanmukha Kuchibhotla, Janine LoBue, Soham Pachpande, Jefferson Ng, Jon Pham, Inderjot Singh Saggu, Nicholas Sieger, Xiudi Tang, and Jingwen Wang.

The figures in this book were prepared with several software systems. The majority of the figures were created using T. van Zandt's `pstricks` macro package for LaTeX. Some of the figures were created with a modified version of C. Geuzaine's program `GL2PS` for converting OpenGL images into postscript files. A few figures were created from screen dump bitmaps and converted to postscript images with Adobe Photoshop.

Chapter I

Introduction

This is a ***preliminary*** *draft of a second edition of the book* 3-D Computer Graphics: A Mathematical Introduction with OpenGL. *So please read it cautiously and critically! Corrections are appreciated. Draft C.4.a*

Author: Sam Buss, `sbuss@ucsd.edu`

This introductory chapter will explain some of the basic concepts of 3-D graphics, with an emphasis on explaining how to get started with simple drawing in OpenGL. We will use the so-called “Modern OpenGL” programming interface. Modern OpenGL is designed to take advantage of the power of graphics processing units (GPU’s). A GPU is a kind of micro-supercomputer, typically containing hundreds or even thousands of cores. Each core in a GPU is a small computer, able to run small programs and handle small computations. This allows a GPU to act like a powerful parallel computer, able to perform multiple computations at once. GPUs were originally developed for handling graphics computations, for example to run a separate program for each pixel on a computer display. But they have evolved to become much more powerful and capable of handling many applications in diverse fields such as scientific computation, bioinformatics, data science, and machine learning.

A graphics program using OpenGL is designed to run on the central processing unit (CPU) of a computer; the CPU is used to generate high-level graphics data and small GPU programs called “shaders”. The graphics data and the shaders are uploaded from the CPU into the GPU. The GPU runs these programs to generate the image which appears on the computer screen.

In a typical application rendering a 3-D scene, the CPU will specify a set of triangles in terms of their vertices. The information about the vertices and triangles is uploaded into the GPU’s memory. The GPU first runs programs called “vertex shaders” that operate independently on each vertex, then the vertices are used to form triangles, and finally the GPU runs small programs called “fragment shaders” that operate independently on each pixel covered by each triangle. All this happens every time the screen is rendered, say 30 or 60 times per second!

This chapter will first discuss the conceptual display modes of points, lines and triangles and how they are described in 3-space using x, y, z coordinates. The crucial idea is that an arbitrary three dimensional surface can be approximated by a set of triangles. The second part of this chapter describes some simple C++ programs using OpenGL vertex shaders and fragment shaders. It also describes setting colors, orienting triangles, using hidden surface removal, and making animation work with double buffering. The website `https://math.ucsd.edu/~sbuss/MathCG2/OpenGLsoft` has C++ programs that illustrate how to use OpenGL. The first two, *SimpleDrawModern* and *SimpleAnimModern*, give some of the simplest possible examples of complete C++ programs using shaders and OpenGL. The program *Chapter1Figs* was used to generate some of the figures in this chapter.

Later chapters will discuss how to use transformations, how to set the viewpoint, how to add lighting and shading, how to add textures, and other topics.

I.1 Points, lines and triangles

We start by describing three models for graphics display modes: (1) drawing points, (2) drawing lines, and (3) drawing triangles. These three models correspond to different hardware architectures for graphics displays. Drawing points corresponds roughly to the model of a graphics image as a rectangular array of pixels. Drawing lines corresponds to vector graphics displays. Drawing triangles corresponds to the methods used by modern graphics systems to display three dimensional images.

I.1.1 Rectangular arrays of pixels

The most common low-level model is to treat a graphics image as a rectangular array of pixels, where each pixel can be independently set to a different color and brightness. This is the display model used for LCD's, CRT's, projectors, etc.; namely for computer screens, televisions, cell phones, and many movies. If the pixels are small enough, they cannot be individually seen by the human eye, and the image, although composed of points, appears as a single smooth image. This principle is used in art as well, notably in mosaics and even more so in pointillism, where pictures are composed of small patches of solid color, yet appear to form a continuous image when viewed from a sufficient distance.

The model of graphics images as a rectangular array of pixels is only a convenient abstraction, and is not entirely accurate. For instance, on most graphics displays, each pixel actually consists of *three* separate points: each point generates one of three primary colors, red, blue, and green, and can be independently set to a brightness value. Thus, each pixel is formed from three colored dots. With a sufficiently good magnifying glass, you can see the pixel as separate colors. (It is easiest to try this with a low resolution device such as an old-style CRT television: depending on the physical design of the screen,

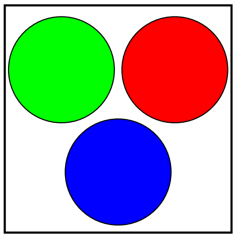

Figure I.1: A pixel is formed from subregions or subpixels, each of which displays one of three colors. See color plate C.1.

the separate colors may appear in individual dots or in stripes.) The three primary colors of red, green and blue can be blended to generate a wide palette of colors; however, they cannot reproduce all possible visible colors.

A second way in which the rectangular array model is not accurate is that sometimes sub-pixel addressing of images is used. For instance, laser printers and inkjet printers reduce aliasing problems, such as jagged edges on lines and symbols, by micro-positioning toner or ink dots. Some computers use subpixel rendering to display text at a higher resolution than would otherwise be possible by treating each pixel as three independently addressable subpixels. In this way, the device is able to position text at the subpixel level and achieve a higher level of detail and better-formed characters.

In this book however, we rarely examine issues of subpixels; instead, we will model a pixel as being a single rectangular point that can be set to a desired color and brightness. But there are many occasions when the fact that a computer graphics image is composed of pixels will be important. Section III.3 discusses the Bresenham algorithm for approximating a straight sloping line with pixels. Also, when using texture maps and ray tracing, it is important to avoid the aliasing problems that can arise with sampling a continuous or high-resolution image into a set of pixels.

In principle, any picture can be rendered by directly setting the brightness levels for each pixel in the image. But in practice, this would be difficult and time-consuming. It is far easier to not consider the pixels at all, and to work instead at the higher level of triangle-based modeling. In high-level graphics programming applications, we generally ignore the fact that the graphics image is rendered using a rectangular array of pixels. Most OpenGL programs work by drawing triangles, and let the graphics hardware handle most of the work of translating the results into pixel brightness levels. This builds on top of a variety of sophisticated techniques for drawing triangles as arrays of pixels, including methods for shading and smoothing and for applying texture maps.

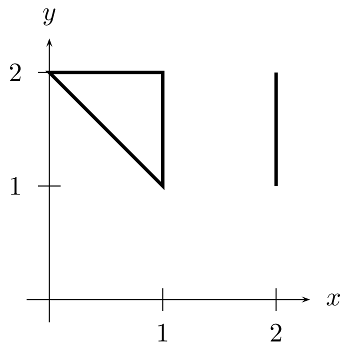

```
penup();
moveto(2,2);
pendown();
moveto(2,1);
penup();
moveto(1,2);
pendown();
moveto(0,2);
moveto(1,1);
moveto(1,2);
```

Figure I.2: Examples of vector graphics commands.

I.1.2 Vector graphics

Traditional vector graphics renders images as a set of lines. This does not allow drawing surfaces or solid objects; instead it draws two dimensional shapes, graphs of functions, or wireframe images of three dimensional objects. The prototypical example of vector graphics systems are pen plotters: this includes also the "turtle geometry" systems. Pen plotters have a drawing pen that moves over a flat sheet of paper. The commands available might include (a) *pen up*, which lifts the pen up from the surface of the paper, (b) *pen down*, which lowers the tip of the pen onto the paper, and (c) *move-to*(x,y), which moves the pen in a straight line from its current position to the point with coordinates $\langle x,y\rangle$. When the pen is up, it moves without drawing; when the pen is down, it draws as it moves. In addition, there may be commands for switching to a different color pen and commands for moving along curved paths such as circular or elliptical arcs and Bézier curves.

Another example of vector graphics devices is vector graphics display terminals, which traditionally are monochrome monitors that can draw arbitrary lines. On these vector graphics display terminals, the screen is a large expanse of phosphor, and does not have pixels. A old-style traditional oscilloscope is another example of a vector graphics display device. A laser light show is also a kind of vector graphics image.

Vector graphics display terminals have not been commonly used for decades, so vector graphics images are usually rendered on pixel-based displays. In pixel-based systems, the screen image is stored as a bitmap, namely, as a table containing all the pixel colors. In contrast, a vector graphics system stores the image as a list of commands, for instance as a list of pen up/down and move commands. Such a list of commands is called a display list.

Since pixel-based graphics hardware is so very prevalent, modern vector graphics images are typically displayed on hardware that is pixel-based. This has the disadvantage that the pixel-based hardware cannot directly draw arbitrary lines or curves and must instead approximate lines and curves with pixels.

On the other hand, it has the advantage that more sophisticated images can be drawn, including rendering regions that are filled in or "shaded" with a color, a pattern or an image. Adobe's postscript language is a prominent example of a modern vector graphics system. Another accessible example is the `<canvas>` element of JavaScript which makes it very easy to display vector graphics on a web page. The `<canvas>` element uses commands `moveto(`x`,`y`)` and `lineto(`x`,`y`)` that provide the same functionality as `penup`, `pendown` and `moveto`. For an example, see this book's web page for a very simple JavaScript program drawing the lines shown in Figure I.2.

I.1.3 Triangles

One step up, in both abstraction and sophistication, is the polygonal model of graphics images. It is very common for three dimensional graphics images to be modeled first as a set of polygons: these are converted to triangles to be displayed on a (two dimensional) display. Triangle-based modeling is used in nearly every three dimensional computer graphics system. It is a central tool for the generation of interactive three dimensional graphics, and is used for photo-realistic rendering, including in movies and computer games.

Most computers have special-purpose graphics hardware for processing triangles, often in the form of a separate GPU. One of the essential operations for a GPU is drawing a single triangle on the display and filling in its interior. The interior can be filled with a solid color or, more usually, it can be shaded with the color varying across the triangle. In addition, texture mapping may be used to paint an image or a texture onto the triangle. GPU's are incredibly effective at this: with proper programming and initialization, it is possible to render many millions of triangles per second (or even billions in simplified applications). This is a lot of triangles!

The purpose of techniques such as shading or texturing triangles is to make polygonally modeled objects look more realistic. For example, Figure IV.1 on page 132 shows six models of a teapot. Part (a) of the figure shows a wireframe teapot, as could be modeled on a vector graphics device. Part (b) shows the same shape, but with all triangles filled in with the same solid, unvarying, color; the result shows a silhouette with no three dimensionality. Parts (c) through (f) show the teapot rendered with lighting effects: Parts (c) and (e) show flat shaded (i.e., unshaded) triangles where the polygonal nature of the teapot is clearly evident; parts (d) and (f) incorporate shading in which the triangles are shaded with color that varies across the triangles. The shading does a fairly good job of masking the polygonal nature of the teapot, and greatly increases the realism of the image.

I.2 Coordinate systems

When rendering a geometric object, its position and shape are specified in terms of the positions of its vertices. For instance, a triangle is specified in terms of

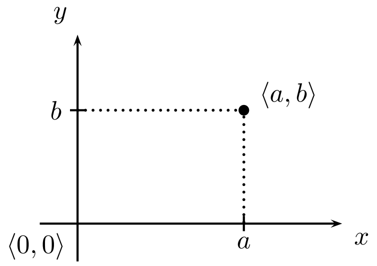

Figure I.3: The xy-plane, $\mathbb{R}^2$, and the point $\langle a, b\rangle$.

the positions of its three vertices. Graphics programming languages, including OpenGL, allow you to set up your own coordinate systems for specifying positions of points; this is done by using a matrix to define a mapping from your coordinate system into the screen coordinates. Chapter II describes how these matrices define linear or affine transformations; they allow you to position points in either 2-space ($\mathbb{R}^2$) or 3-space ($\mathbb{R}^3$) and have OpenGL automatically map the points into the proper location in the graphics image.

In the two dimensional xy-plane, also called $\mathbb{R}^2$, a vertex's position is set by specifying its x- and y-coordinates. The usual convention, see Figure I.3, is that the x-axis is horizontal and pointing to the right, and the y-axis is vertical and pointing upwards.

In three dimensional xyz-space, $\mathbb{R}^3$, positions are specified by triples $\langle a, b, c\rangle$ giving the x-, y- and z-coordinates of the vertex. However, the convention for how the three coordinate axes are positioned is different for computer graphics than is usual in mathematics. In computer graphics, the x-axis is pointing to the right, the y-axis is pointing upwards, and the z-axis is pointing towards the viewer. This is different from what you may be used to: for example, in calculus, the x-, y- and z-axes usually point forwards, rightwards, and upwards (respectively). The computer graphics convention was adopted presumably because it keeps the x- and y-axes in the same position as for the xy-plane. But of course it has the disadvantage of taking some getting used to. Figure I.4 shows the orientation of the coordinate axes as used in computer graphics.

It is useful to note that the coordinates axes used in computer graphics form a righthanded coordinate system. This means that if you position your right hand with your thumb and index finger extended to make an “L” shape, and place your hand so that your thumb points along the positive x-axis and your index finger points along the positive y-axis, then your palm will be facing towards the positive z-axis. This means that the usual righthand rule applies to cross products of vectors in $\mathbb{R}^3$.

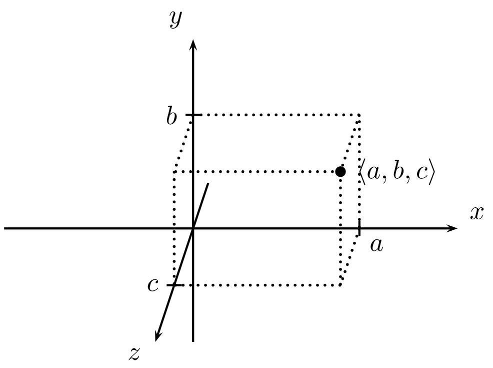

Figure I.4: The coordinate axes in $\mathbb{R}^3$, and the point $\langle a,b,c\rangle$. The z-axis is pointing towards the viewer.

I.3 Points, lines and triangles in OpenGL

This section gives an overview of how OpenGL specifies the geometries of points, lines and triangles, focusing on the simplest and most common methods. Sample code and explanations of these, and other OpenGL features, can be found in the programs *SimpleDrawModern*, *SimpleAnimModern*, *BasicDrawModes* and *Chapter1Figs* available from the book's website. These programs also illustrate how the C++ code, OpenGL function calls and shader programs fit together in a fully functioning program.

For now, we discuss only drawing vertices at fixed positions in the xy-plane or in xyz-space. These are specified by giving an array of vertex positions, plus the information about how they are joined to form lines or triangles.

Later on in this chapter, we will show some simple shader programs and discuss shading triangles with color, culling front- or back-faces, using the depth buffer for hidden surfaces, and double buffering for animation. Chapter II will explain how to move vertices and geometric shapes around with rotations, translations, and other transformations.

I.3.1 Loading vertices into a VAO and VBO

Points, lines and triangles are always specified in terms of vertex positions. Vertex positions are generally given in terms of their x, y-coordinates in $\mathbb{R}^2$ or their x, y, z-coordinates[1] in $\mathbb{R}^3$. Let's start with a simple example of six vertices in $\mathbb{R}^2$. In a C or C++ program, they can be given explicitly in an array as:

[1] However, later on, when working with homogeneous coordinates, we will see that positions might be given in terms x, y, z, w-coordinates instead of x, y, z-coordinates.

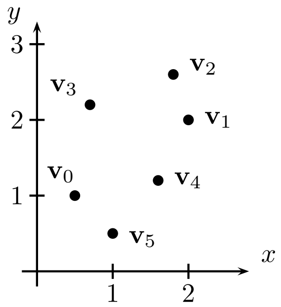

Figure I.5: The six points in the `verts` array.

```
// Array of x,y coordinates for six vertices
float verts[] = {
     0.5, 1.0,           // Vertex v0
     2.0, 2.0,           // Vertex v1
     1.8, 2.6,           // Vertex v2
     0.7, 2.2,           // Vertex v3
     1.6, 1.2,           // Vertex v4
     1.0, 0.5,           // Vertex v5
};
```

This declaration of the array `verts` allocates space for 12 `float`'s (floating point numbers) giving the x, y coordinates of vertices $\mathbf{v}_0$ through $\mathbf{v}_5$. For example, `verts[4]` and `verts[5]` are equal to 1.8 and 2.6, and give the x- and y-coordinates of the point $\mathbf{v}_2 = \langle 1.8, 2.6 \rangle$. Figure I.5 shows the positions of these vertices.

The array `verts` is allocated in the memory space of the C++ program, perhaps even in temporary storage in the C++ execution stack. To render objects using these vertices, it is necessary to load the data into OpenGL's memory space. This is unfortunately a bit complex, but it can be accomplished with the following (minimalistic) code:

```
unsigned int theVAO;           // Name of a Vertex Array Object (VAO)
glGenVertexArrays(1, &theVAO);

unsigned int theVBO;           // Name of a Vertex Buffer Object (VBO)
glGenBuffers(1, &theVBO);

glBindBuffer(GL_ARRAY_BUFFER, theVBO);   // Select the active VBO
glBufferData(GL_ARRAY_BUFFER, sizeof(verts), verts, GL_STATIC_DRAW);

unsigned int vPos_loc = 0;     // Shader's 'location' for positions
glBindVertexArray(theVAO);   // Select the active VAO
glVertexAttribPointer(vPos_loc, 2, GL_FLOAT, GL_FALSE, 0, (void*)0 );
glEnableVertexAttribArray(vPos_loc);
```

There is a lot going on in this code. It starts off by asking OpenGL to set up a Vertex Array Object (VAO) and a Vertex Buffer Object (VBO). A VBO holds vertex data; in our example, it holds the x, y coordinates of vertices. In other applications, the VBO might also hold texture coordinates, surface normals, color or material properties, etc. A VAO holds information about the way the vertex data is stored in the VBO: the primary purpose of a VAO is to let shader programs know how to access the data stored in the VBO. The code copies the vertex data into the VBO by calling `glBufferData`. The call to `glVertexAttribPointer` tells the VAO that the vertex data consists of pairs of floating point numbers and that the data starts at the beginning of the VBO.

Vertex Buffer Object. The VBO holds *per-vertex* data; namely, in our example, each vertex has its own x, y coordinates. These vertex data are also called *vertex attributes.* The two lines

```
    unsigned int theVBO;
    glGenBuffers(1, &theVBO);
```

ask OpenGL to set up a new VBO. The first parameter to `glGenBuffers` is the number of VBO's to be set up. Each VBO is referenced (or, named) by an unsigned integer; the second parameter to `glGenBuffers` is the address where the names of the new VBO's are returned.

The two lines

```
glBindBuffer(GL_ARRAY_BUFFER, theVBO);
glBufferData(GL_ARRAY_BUFFER, sizeof(verts), verts, GL_STATIC_DRAW);
```

copy the per-vertex data into the VBO. OpenGL uses several kinds of buffers; one kind is the `GL_ARRAY_BUFFER` and the call to `glBindBuffer` makes `theVBO` the current `GL_ARRAY_BUFFER`. `glBufferData` is used to copy the per-vertex data to this buffer. Its function prototype is:[2]

```
  glBufferData(GLenum target, int size, void* data, GLenum usage);
```

The *target* specifies which OpenGL buffer to copy data to. The fourth parameter provides a hint as how the data will be used. `GL_STATIC_DRAW` specifies that the data is used frequently but not changed often; this encourages OpenGL to store the data in the GPU memory for better rendering speed.[3] The second parameter, for us `sizeof(verts)`, is the number of bytes of data to be uploaded. The VBO will be resized as needed to accommodate the data. The

[2] This function prototype is not quite correct. We will simplify function prototypes for the sake of simplicity of understanding. For the same reason, we often gloss over many of the command features. You are encouraged to learn more about these OpenGL functions by searching online; when you do so, be careful to find the OpenGL documentation (not the OpenGL ES documentation).

[3] The option `GL_DYNAMIC_DRAW` can be used instead of to `GL_STATIC_DRAW` to indicate the data will change frequently; for instance, if the data is updated every time the scene is rendered.

third parameter is a pointer to the beginning of data to be copied into the VBO.

Vertex Array Object. The VAO holds the information about the vertex attributes. In our case, this information is that the per-vertex data consists of pairs of floating point numbers and that they are stored in adjacent locations starting at the beginning of the VBO. This is accomplished with following lines of code:

```
glBindBuffer(GL_ARRAY_BUFFER, theVBO);
...
unsigned int vPos_loc = 0;        // Shader's 'location' for positions
glBindVertexArray(theVAO);
glVertexAttribPointer(vPos_loc, 2, GL_FLOAT, GL_FALSE, 0, (void*)0 );
```

We first call `glBindBuffer` and `glBindVertexArray` to select the current VAO and VBO. The function prototype for `glVertexAttribPointer` is:

```
glVertexAttribPointer( int index, int size, GLenum type,
                       bool normalize, int stride, void* bufferOffset );
```

The first parameter, *index*, is the shader program's "location" for the data: later on, our vertex shader will use "`location=0`" to access this data. The second and third parameters specify the number of data values per vertex and their type: in our example, each vertex has two (2) floating point numbers, so we used "`2, GL_FLOAT`". The final parameter gives the offset in bytes into the VBO where the data starts. For us, this was "`(void*)0`", as the vertex data starts at the beginning of the VBO. The fifth parameter, called the *stride*, specifies the spacing between the data for successive vertices. The "stride" is the number of bytes from the start of the data for one vertex to the start of the data to the next vertex. We used "`0`" for the stride, which tells OpenGL to calculate the stride based on the assumption the data is tightly packed. We could have instead used the command

```
glVertexAttribPointer( vPos_loc, 2, GL_FLOAT, GL_FALSE,
                       2*sizeof(float), (void*)0 );
```

with "`0`" replaced by "`2*sizeof(float)`" to give the stride explicitly.

The fourth parameter, *normalize*, controls how integer values are converted to floating point when uploaded to the VBO. We are uploading floating point values, so this parameter is ignored in our example.

The final step is to tell the VAO to "enable" the per-vertex data in the VBO. Our code did this with the command

```
 glEnableVertexAttribArray(vPos_loc);
```

This tells the VAO that the vertex attribute with index `vertPos_loc` is specified on a per-vertex basis from the VBO. (As is discussed later in Chapter II.3.4, an alternative is to use a vertex attribute which uses the same value for multiple vertices.)

I.3.2 Drawing points and lines

Once we have defined an array of vertex positions, and loaded the needed data into the VBO and VAO, we are ready to give the code that actually renders the points. To render the vertices as six isolated points, we use the C++ code[4]

```
  glBindVertexArray(theVAO);
  int vColor_loc = 1;
  glVertexAttrib3f(vColor_loc, 0.0, 0.0, 0.0); // Black color ⟨0,0,0⟩
  glDrawArrays(GL_POINTS, 0, 6);
```

The result of these commands is to draw the six points as shown in Figure I.6a (compare to Figure I.5). The call to `glBindVertexArray` selects the VAO. Since the VAO knows which VBO holds the per-vertex data, there is no need to explicitly bind the VBO.[5]

The `glVertexAttrib3f` function call sets a color value, in this case, the color is black. The color is given by three floating point numbers, in the range 0 to 1.0, giving the red, green and blue (RGB) components of the color. In our code, the color is a *generic* attribute; this means that all the vertices have the same color. Consequently, the color value must be set just before rendering the points, instead of being stored in the VBO on a per-vertex basis.[6] The `vColor_loc` value is 1, as our vertex shader program will use `location=1` to access the color.

The call to `glDrawArrays` is the command that causes the vertices to be actually rendered. The first parameter, `GL_POINTS`, tells OpenGL to draw the vertices as isolated points. The second parameter, `0`, says to start with vertex number 0, i.e., the first vertex. The third parameter, `6`, is the number of vertices to be rendered.

You can also render the points joined by lines. The first mode, `GL_LINES`, uses the code

```
glBindVertexArray(theVAO);
int vColor_loc = 1;
glVertexAttrib3f(vColor_loc, 0.0, 0.0, 0.0); // Black color (0,0,0)
glDrawArrays(GL_LINES, 0, 6);
```

This is identical to the code used to render the vertices as points, but uses GL_LINES in place of `GL_POINTS`. It results in drawing the lines shown in

[4] Before giving this code, one also has to state which shader program to use. Shaders will be discussed soon.

[5] In fact, it is possible that multiple VBO's are used to hold different vertex attributes.

[6] The advantage of this is that if the vertices all have the same color, there is no need to waste memory in the VBO specifying the same color repeatedly. This disadvantage is, at least in the most widely used versions of OpenGL, that one has to call `glVertexAttrib3f` each time the color changes during rendering.

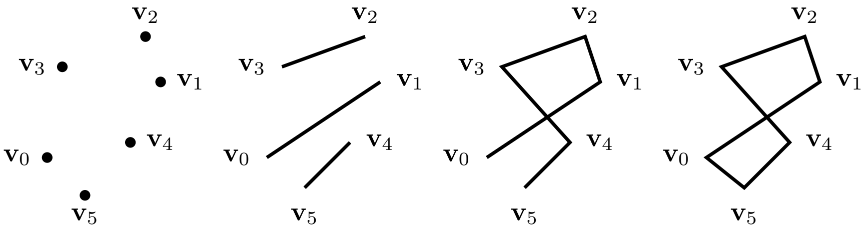

(a) `GL_POINTS` (b) `GL_LINES` (c) `GL_LINE_STRIP` (d) `GL_LINE_LOOP`

Figure I.6: The three line drawing modes, as controlled by the first parameter to `glDrawArrays`.

Figure I.6b. The effect is to use each successive pair of vertices as endpoints of a line segment. Namely, if there are n vertices $\mathbf{v}_0, \ldots, \mathbf{v}_{n-1}$, it draws the line segments with endpoints $\mathbf{v}_{2i}$ and $\mathbf{v}_{2i+1}$ for $0 \le i < n/2$. This is shown in Figure I.6b.

Another option for lines is `GL_LINE_STRIP` which draws a connected sequence of line segments, starting with the first vertex, joining a line segment to each successive vertex, ending at the last vertex. In other words, when there are n vertices, it draws the line segments joining $\mathbf{v}_i$ and $\mathbf{v}_{i+1}$ for $0 \le i < n-1$. This is pictured in Figure I.6c.

The option `GL_LINE_LOOP` draws these line segments, plus a line from the final vertex back to the first vertex, thus rendering a closed loop of line segments. This draws, in addition, the line segment joining $\mathbf{v}_{n-1}$ and $\mathbf{v}_0$. For this, see Figure I.6d.

There is a sample OpenGL program, *SimpleDrawModern*, available at the book's website, which contains a complete C++ program with the above code for drawing the six vertices as line segments, as a line strip, and as a line loop. (It also draws a couple other images.) If OpenGL is new to you, it is recommended that you examine the source code and try compiling and running the program.

If you run OpenGL with default settings, you will probably discover that the points are drawn as very small, single pixel points — perhaps so small as to be almost invisible. Similarly, the lines may look much too thin, and may be visibly jagged because of the lines being drawn only one pixel wide. By default, OpenGL draws thin lines, one pixel wide, and does not do any "anti-aliasing" to smooth out the lines. On most OpenGL systems, you can call the following functions to make points display as large, round dots to make lines be drawn wider and smoother.

```
glPointSize(n);          // Points are n pixels in diameter
glEnable(GL_POINT_SMOOTH);
glHint(GL_POINT_SMOOTH_HINT, GL_NICEST);
glLineWidth( m );        // Lines are m pixels wide
glEnable(GL_LINE_SMOOTH);
glHint(GL_LINE_SMOOTH_HINT, GL_NICEST); // Antialias lines
glEnable(GL_BLEND);
glBlendFunc(GL_SRC_ALPHA, GL_ONE_MINUS_SRC_ALPHA);
```

In the first line, a number such as 6 for n may give good results so that points are six pixels in diameter. In the fourth, using $m = 3$ so that lines are three pixels wide may work well. The *SimpleDrawModern* program already includes the above function calls. If you are lucky, executing these lines in the program before the drawing code will cause the program to draw nice round dots for points. However, the effect of these commands varies with different implementations of OpenGL, so you may see square dots instead of round dots, or even no change at all. How well, and whether, the point sizing and blending works and the line width specification and the anti-aliasing work will depend on your implementation of OpenGL.

Exercise I.1. The OpenGL program *SimpleDrawModern* includes code to draw the images shown in Figure I.6, and a colorized version of Figure I.16. Run this program, examine its source code, and read the online explanation of how the code works. (At this point, you should be able to understand most of the code apart from the parts that draw triangles and use the vertex and fragment shaders.) Learn how to compile the program. Then try disabling the code for making bigger points, and wider, smoother lines. What changes does this cause?

Exercise I.2. Write an OpenGL program to generate the two star-shaped images of Figure I.7 as line drawings. You will probably want modify the source code of *SimpleDrawModern* for this. (Exercises I.5 and I.6 use the same figure.)

I.3.3 Drawing triangles

The fundamental rendering operation for 3-D graphics is to draw a triangle. Ordinarily, triangles are drawn as solid, filled-in shapes. The most basic way to draw triangles is to use the `glDrawArrays` command with one of the options `GL_TRIANGLES`, `GL_TRIANGLE_STRIP` or `GL_TRIANGLE_FAN`.

Figure I.8a illustrates how triangles are rendered with `GL_TRIANGLES` and `glDrawArrays`. Here it is assumed that the six vertices $\mathbf{u}_0, \ldots, \mathbf{u}_5$ are stored in the VBO: these vertices are grouped into triples, and each triple defines the three vertices of a triangle. More generally, if there are n vertices $\mathbf{u}_0, \ldots, \mathbf{u}_{n-1}$ then, for each $i < n/3$, the vertices $\mathbf{u}_{3i}, \mathbf{u}_{3i+1}, \mathbf{u}_{3i+2}$ are used to form a triangle.

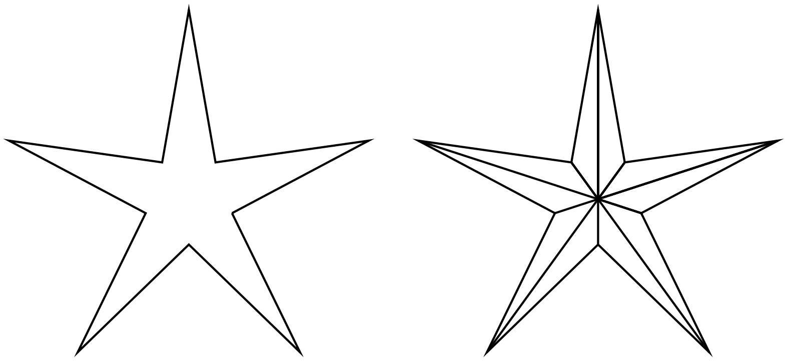

Figure I.7: Figures for Exercises I.2, I.5, and I.6.

Each triangle can be viewed from two sides. The two sides are called the *front face* and the *back face*. A common convention is that, when rendering a solid object, the surface of the object is rendered as triangles all with their front faces visible from outside the object.

When rendering with GL_TRIANGLES, the determintion of which side of the triangle is the front face is based on whether the viewer sees the three vertices of the triangle in counter-clockwise or clockwise order. The usual convention is that on the front side of the i-th triangle, the viewer sees the vertices $\mathbf{u}_{3i}, \mathbf{u}_{3i+1}, \mathbf{u}_{3i+2}$ ordered in counter-clockwise (CCW) order around the triangle. Then, from the back side, a viewer sees these vertices going around the triangle in clockwise (CW) order. For example, Figure I.8a shows the front faces of the two triangles.

Figure I.8b illustrates how triangles are rendered with GL_TRIANGLE_FAN in a fan-like pattern, sharing a common vertex $\mathbf{u}_0$. Again, there are six vertices $\mathbf{u}_0, \ldots, \mathbf{u}_5$ (but different ones than in Figure I.8a). If there are n vertices $\mathbf{u}_0, \ldots, \mathbf{u}_{n-1}$ with GL_TRIANGLE_FAN, then for each $1 \le i < n-1$, the vertices $\mathbf{u}_0, \mathbf{u}_i, \mathbf{u}_{i+1}$ are used to form a triangle. These triangles again have a front face and back face. The front faces are viewed with the vertices $\mathbf{u}_0, \mathbf{u}_i, \mathbf{u}_{i+1}$ in counter-clockwise order. The triangles in Figure I.8b are all front facing.

Figure I.8c illustrates how triangles are rendered with GL_TRIANGLE_STRIP. Once again, there are six vertices, $\mathbf{u}_0, \ldots, \mathbf{u}_5$, but ordered differently. This renders the triangle with vertices $\mathbf{u}_0, \mathbf{u}_1, \mathbf{u}_2$, then the triangle with vertices $\mathbf{u}_1, \mathbf{u}_2, \mathbf{u}_3$, then the triangle with vertices $\mathbf{u}_2, \mathbf{u}_3, \mathbf{u}_4$, and then the triangle with vertices $\mathbf{u}_3, \mathbf{u}_4, \mathbf{u}_5$. The orders of the vertices are chosen so that the front face of the *first* triangle is on the side where the vertices are seen in counter-clockwise order. The same holds in general for the third, fifth, seventh, etc. triangles. The second, fourth, sixth, etc. triangles have front faces on the side where the vertices are seen in clockwise order. These conventions allow the triangle strip to make a well-formed surface; for instance, in the shape of ribbon. For

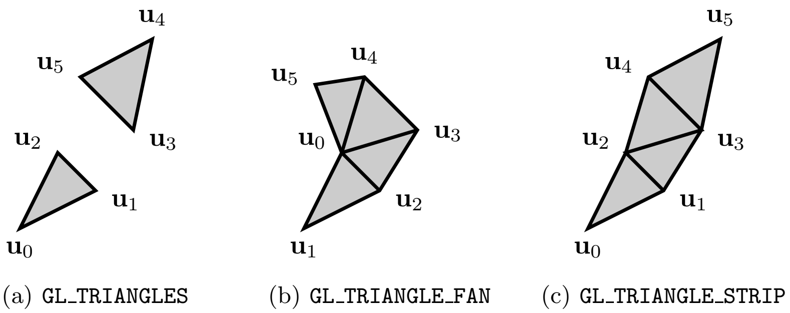

(a) `GL_TRIANGLES` (b) `GL_TRIANGLE_FAN` (c) `GL_TRIANGLE_STRIP`

Figure I.8: The three triangle drawing modes. These are shown with the default front face visible to the viewer. The vertices $\mathbf{u}_i$ are numbered in the order needed for the drawing modes. For this, it is important to note the difference in the placement and numberings of vertices in each figure, especially of vertices $\mathbf{u}_4$ and $\mathbf{u}_5$ in the first and last figures.

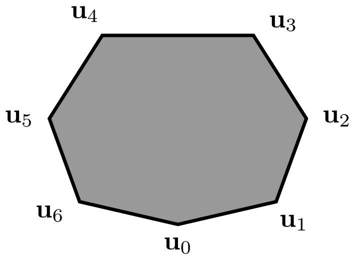

Figure I.9: The region for Exercise I.3.

example, the second triangle of Figure I.8c has its front face visible since the vertices are seen in counter-clockwise order as $\mathbf{u}_1, \mathbf{u}_3, \mathbf{u}_2$, not $\mathbf{u}_1, \mathbf{u}_2, \mathbf{u}_3$. In fact, all the triangles shown in Figure I.8c are front facing.

Exercise I.3. A convex planar region bounded by seven edges, with vertices v_0 through v_6, is shown in Figure I.9. Your answers for for (a) and (b) should cover this region with triangles so that the triangles do not overlap (beyond sharing edges) and so that all triangles are front facing using the default `GL_CCW` convention.

(a) Give a ordering of the vertices (with repetitions if necessary) that will render in the region as a triangle fan. Draw a copy of the figure, showing the triangles in the triangle fan.

(b) Give a ordering of the vertices (with repetitions if necessary) that will render in the region as a triangle strip. Draw a copy of the region, showing the triangles in the triangle strip.

The triangles shown in Figure I.8a can be rendered using the code shown below. First, an array `verts2` is loaded with seven vertices, given by their x, y, z coordinates (the z-coordinates are all zero):

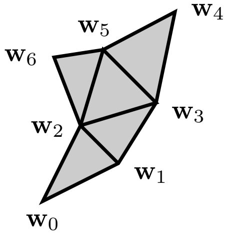

Figure I.10: The points used for rendering the triangles with glDrawElements.

```
// Array of x,y,z coordinates for seven vertices
float verts2[] = {
    0.25, 0.5, 0.0,         // Vertex $\mathbf{w}_0$
    1.25, 1.0, 0.0,         // Vertex $\mathbf{w}_1$
    0.75, 1.5, 0.0,         // Vertex $\mathbf{w}_2$
    1.75, 1.8, 0.0,         // Vertex $\mathbf{w}_3$
    2.0,  3.0, 0.0,         // Vertex $\mathbf{w}_4$
    1.05, 2.5, 0.0,         // Vertex $\mathbf{w}_5$
    0.4,  2.4, 0.0,         // Vertex $\mathbf{w}_6$
};
```

Figure I.10 shows all the points of verts2. The verts2 array is loaded into a VAO and VBO with the following code (we assume the VAO and VBO have already been set up and that vPos_loc has been defined):

```
glBindBuffer(GL_ARRAY_BUFFER, theVBO);
glBufferData(GL_ARRAY_BUFFER, sizeof(verts2), verts2, GL_STATIC_DRAW);
glBindVertexArray(theVAO);
glVertexAttribPointer( vPos_loc, 3, GL_FLOAT, GL_FALSE,
                       3*sizeof(float), (void*)0 );
glEnableVertexAttribArray(vPos_loc);
```

The triangles shown in Figure I.8a can be rendered with the following code (assuming vColor_loc is defined as before):

```
glBindVertexArray(theVAO);
glVertexAttrib3f(vColor_loc, 0.7, 0.7, 0.7); // Light gray
glDrawArrays(GL_TRIANGLES, 0, 6);
```

The code as written above will render the triangles as light gray triangles without any borders.

The call to glDrawArrays specifies to draw triangles using a total of six vertices, starting with vertex number 0; hence it draws two triangles. There is a seventh vertex in verts2 which has also been loaded into the VBO, but it is ignored since the third parameter to glDrawArrays is 6. (The seventh vertex will be used by the code in Section I.3.4 when we discuss how to reuse vertices with the `glDrawElements` command.) Similar calls to `glDrawArrays` can be used to render the triangle fan and triangle strip of Figure I.8 using `GL_TRIANGLE_FAN` and `GL_TRIANGLE_STRIP`, but they require using different arrays with the vertices reordered as shown in Figure I.8.

I.3.4 Rendering with element arrays

An element array allows using *indices* of vertices for drawing. This can be useful when vertices are reused for several drawing commands. For example, a single vertex might appear in multiple triangles drawn in `GL_TRIANGLES` mode, or in multiple triangle strips or triangle fans. (For an example of this, see the spheres of Figure I.11.) An element array holds *indices* of vertices, so that the VBO does not need to hold multiple copies of same vertex. This means that the VBO can hold a single copy of a vertex and its attributes; but the vertex can be referenced multiple times and used in multiple triangles. For this, it is necessary that the vertex attributes are *exactly* the same each time the vertex is referenced.

An element array is sometimes called an "element array buffer", "element buffer object" (EBO), or "index buffer object" (IBO). For an example of how to use element arrays, the following code can draw the triangles shown in Figure I.8. First, we allocate and define the element array by:

```
unsigned int elements[] = {
    0, 1, 2, 3, 4, 5,      // For GL_TRIANGLES
    2, 0, 1, 3, 5, 6,      // For GL_TRIANGLE_FAN
    0, 1, 2, 3, 5, 4       // For GL_TRIANGLE_STRIP
};
```

The indices in the `elements` array indicate which vertices from the `verts` array are to be used with `glDrawArrays`. For example, the triangle fan will be drawn with vertices $\mathbf{w}_2, \mathbf{w}_0, \mathbf{w}_1, \mathbf{w}_3, \mathbf{w}_5, \mathbf{w}_6$.

The following code allocates an element buffer object (EBO) and loads the data from the `elements` array into the EBO:

```
unsigned int theEBO;
glGenBuffers( 1, &theEBO );
glBindVertexArray(theVAO);
glBindBuffer(GL_ELEMENT_ARRAY_BUFFER, theEBO);
glBufferData(GL_ELEMENT_ARRAY_BUFFER, sizeof(elements), elements, GL_STATIC_DRAW);
```

These commands work just like the earlier code that loaded data into the VBO. The triangles of Figure I.8a can then be drawn with

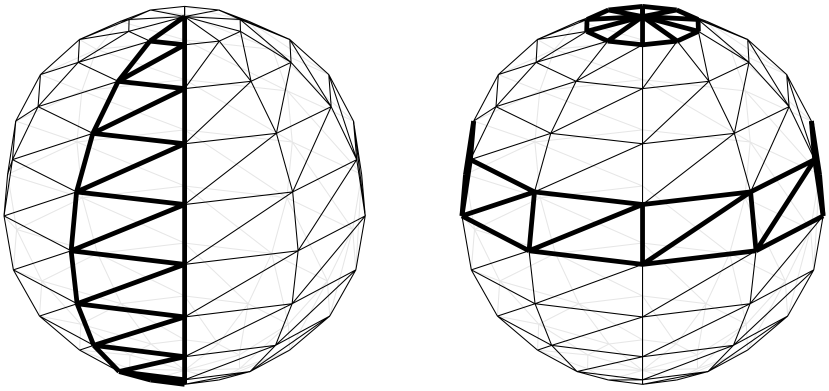

(a) A triangle strip

(b) A triangle strip and a triangle fan

Figure I.11: Part (a) shows how a sphere can be drawn with triangle strips running vertically between the "south pole" and "north pole" of the sphere. Part (b) shows how to render a sphere with horizontal strips formed from triangle fans, plus triangle fans at the "north pole" and "south pole".

```
glBindVertexArray(theVAO);
glVertexAttrib3f(vColor_loc, 0.7, 0.7, 0.7); // Light gray
glDrawElements(GL_TRIANGLES, 6, GL_UNSIGNED_INT, 0 );
```

Note that we are now using `glDrawElements` instead of `glDrawArrays`. The second and fourth parameters to `glDrawElements` are 6 and 0: they specify that the drawing should use the vertices referenced by the six (6) indices starting at position 0 in the EBO (the position is measured bytes and hence has C++ type `void*`). The third parameter tells OpenGL that the indices are stored as unsigned integers. To draw the triangle fan of Figure I.8b, the `glDrawElements` call is replaced with

```
glDrawElements( GL_TRIANGLE_FAN, 6, GL_UNSIGNED_INT,
                (void*)(6*sizeof(unsigned int)) );
```

This again uses six vertices, but now the indices start at byte position `6*sizeof(unsigned int)` in the EBO, i.e., at the seventh index in the array.

Similarly, to draw the triangle strip of Figure I.8c, use

```
glDrawElements( GL_TRIANGLE_STRIP, 6, GL_UNSIGNED_INT,
                (void*)(12*sizeof(unsigned int)) );
```

The program *BasicDrawModes* at the book's website shows a complete program using `glDrawElements` along with a description of how it works.

It is common to use triangles, triangle strips and triangle fans to form complex shapes. For example, Figure I.11 shows two ways of rendering a sphere

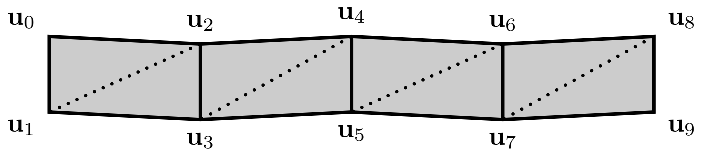

Figure I.12: A quad strip with four quadrilaterals. The edges of the quadrilaterals are shown as solid lines. When rendered as triangles using $\mathbf{u}_0$ through $\mathbf{u}_9$, the dotted lines show the additional edges for triangles. (Compare this to Figure I.8c.)

with triangles. The first method is to use multiple triangle strips, each running "north-to-south" on the sphere. The second method uses triangle fans around the north and south poles, and uses triangle strips going horizontally completely around the sphere. Both methods render the sphere as a collection of triangles. (We shall see later how lighting and shading can be used to hide the triangles and make the sphere appear to be perfectly smooth.)

Each triangle strip going horizontally around the sphere is a "quad strip", of quadrilaterals connected end-to-end, and joined at the ends to form a closed loop. Figure I.12 shows an example of quad strip, consisting of four quadrilaterals. This can be rendered as a triangle strip using the vectices in the order $\mathbf{u}_0$ through $\mathbf{u}_9$. If the first two vertices, $\mathbf{u}_0$ and $\mathbf{u}_1$, are identical to the final two vertices, $\mathbf{u}_8$ and $\mathbf{u}_9$, then the quad strip forms a closed loop.

Exercise I.4. Suppose the vertices of Figure I.12 were used to form a triangle strip with the vertices ordered as $\mathbf{u}_1, \mathbf{u}_0, \mathbf{u}_3, \mathbf{u}_2, \mathbf{u}_5, \mathbf{u}_4, \mathbf{u}_7, \mathbf{u}_6, \mathbf{u}_9, \mathbf{u}_8$. What would this do to the geometry of the quad strip? How would this change the constituent triangles? What would be the direction of the front faces?

Now answer the same questions supposing the vertices were instead ordered as $\mathbf{u}_9, \mathbf{u}_8, \mathbf{u}_7, \mathbf{u}_6, \mathbf{u}_5, \mathbf{u}_4, \mathbf{u}_3, \mathbf{u}_2, \mathbf{u}_1, \mathbf{u}_0$.

I.3.5 Different colors per vertex

The earlier code example assigned the same color to all the vertices, using `glVertexAttrib3f` to set the color as a generic attribute. It is also possible to set the vertex colors on a per-vertex basis, storing them in the VBO similarly to the way the vertex positions are set. We illustrate next how to do this by interleaving vertex positions and colors into a single array. Similar methods can be used for other vertex attributes, such as texture coordinates, normals, material properties, etc.[7]

[7] It is also possible to store different vertex attributes in different arrays or even in different VBO's, instead of interleaving them in a single array.

Color		R	G	B	Color		R	G	B
Black:	⬛	0	0	0	White:	⬜	1	1	1
Red:	🟥	1	0	0	Cyan:	🟦	0	1	1
Green:	🟩	0	1	0	Magenta:	🟪	1	0	1
Blue:	🟦	0	0	1	Yellow:	🟨	1	1	0

Figure I.13: Eight colors and their RGB values.

```
// Array of x,y coordinates and r,g,b colors for three vertices
float verts3[] = {
    // x, y position;  R, G, B color
    0.0, 0.0,          1.0, 0.0, 0.0,   // 1st vertex, Red ⟨1,0,0⟩
    2.0, 0.0,          0.0, 1.0, 0.0,   // 2nd vertex, Green ⟨0,1,0⟩
    1.0, 1.5,          0.0, 0.0, 1.0,   // 3rd vertex, Blue ⟨0,0,1⟩
};
```

The verts3 array gives the three vertices different colors by giving the red, green and blue component of the color using a number in the interval $[0,1]$. Other colors can be specified by blending different amounts of red, green, and blue. For example, white is specified by the color $\langle 1,1,1\rangle$, yellow is specified by $\langle 1,1,0\rangle$, magenta by $\langle 1,0,1\rangle$, and cyan by $\langle 0,1,1\rangle$. You can find many other color codes by searching online for “RGB colors”; often they are specified with color components given by integers between 0 and 255: they can be converted to the range $[0,1]$ by dividing by 255.[8]

The verts3 data can be loaded into the VAO and VBO by:

```
glBindBuffer(GL_ARRAY_BUFFER, theVBO);
glBufferData(GL_ARRAY_BUFFER, sizeof(verts3), verts3, GL_STATIC_DRAW);
glBindVertexArray(theVAO);
glVertexAttribPointer( vPos_loc, 2, GL_FLOAT, GL_FALSE,
                       5*sizeof(float), (void*)0 );
glVertexAttribPointer( vColor_loc, 3, GL_FLOAT, GL_FALSE,
                       5*sizeof(float), (void*)(2*sizeof(float)) );
glEnableVertexAttribArray(vPos_loc);
glEnableVertexAttribArray(vColor_loc);
```

The first call to glVertexAttribPointer specifies that the vertex position data consists of two float’s per vertex, that the stride from one vertex to the next is 5*sizeof(float) bytes, and that the first vertex’s position data starts at the beginning of the VBO. The second call to glVertexAttribPointer specifies that the vertex color data consists of three float’s per vertex, that the stride

[8] It is also possible to use integers in the range 0 to 255 with OpenGL: for example, you can use GL_UNSIGNED_BYTE instead of GL_FLOAT when calling glVertexAttribPointer.

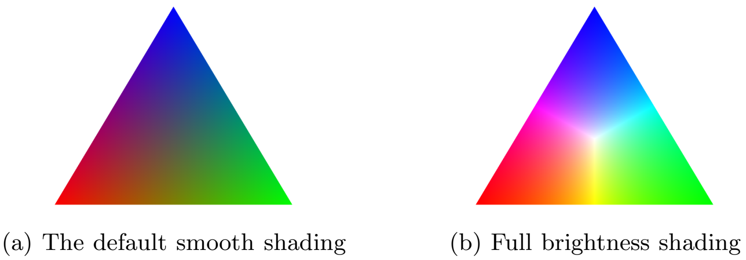

(a) The default smooth shading

(b) Full brightness shading

Figure I.14: Two triangles: with the default smooth shading and the "full brightness" shading. The latter is created with the fragment shader on page 26.

is again `5*sizeof(float)` bytes, and that the first vertex's color data starts at position `2*sizeof(float)` in the VBO (measured in bytes). The two calls to `glEnableVertexAttribArray` specify that the position and color data are stored on a per-vertex basis in the VBO; in other words, that they are not generic attributes.

Rendering the three colored vertices as a triangle is done with the usual command, now using only three vertices to render a single triangle,

```
glDrawArrays( GL_TRIANGLES, 0, 3 );
```

The result is shown in Figure C.3a. The color of the triangle at each vertex is the red, green or blue color as specified in the `verts3` array. Interior points are colored as an average of the colors of the vertices: this is called *shading* or *smooth shading*. For instance, midway between the red and green vertex, the color is a dark yellow. Dark yellow is the average of red and green and it is represented by the triple $\langle\frac{1}{2},\frac{1}{2},0\rangle$. The center of the triangle is a dark gray, represented by the triple $\langle\frac{1}{3},\frac{1}{3},\frac{1}{3}\rangle$. We will learn more about how shading is calculated when we discuss barycentric coordinates (and hyperbolic interpolation) in Chapter V.

I.3.6 Face orientation and culling

OpenGL keeps track of whether triangles are facing towards the viewer or away from the viewer, that is to say, OpenGL assigns each triangle a front face and a back face. Sometimes, it is desirable for only the front faces of triangles to be viewable, and at other times you may want both the front and back faces of a triangle to be visible. If we set the back faces to be invisible by "culling" them, then any triangle whose back face would ordinarily be seen is not drawn at all. In effect, a culled face becomes transparent. By default, no faces are culled so both front- and back-faces are visible.

As we already discussed, OpenGL determines which face of a triangle is the front face by the default convention that vertices on a triangle are specified in counter-clockwise order (with some exceptions for triangle strips). The triangles shown in Figures I.8 and I.14 are all shown with their front faces visible.

You can change the convention for which face is the front face by using the `glFrontFace` command. This command has the format

$$\texttt{glFrontFace(}\left\{\begin{array}{c}\texttt{GL\_CW}\\ \texttt{GL\_CCW}\end{array}\right\}\texttt{);}\qquad\qquad \texttt{// Use either GL\_CW or GL\_CCW}$$

where "CW" and "CCW" stand for clockwise and counter-clockwise. `GL_CCW` is the default. Using `GL_CW` causes the opposite convention for front and back faces to be used on subsequent triangles.

To cull front and/or back faces, use the commands

$$\texttt{glCullFace(}\left\{\begin{array}{c}\texttt{GL\_FRONT}\\ \texttt{GL\_BACK}\\ \texttt{GL\_FRONT\_AND\_BACK}\end{array}\right\}\texttt{);}$$

```
glEnable( GL_CULL_FACE );
```

You must explicitly turn on the face culling with the call to `glEnable`. Face culling can be turned back off with the corresponding `glDisable` command. When culling is enabled, the default setting for `glCullFace` is `GL_BACK`.

The wireframe torus of Figure I.15a is shown without any face culling. Figure I.15b shows the same torus with back face culling.

The spheres in Figure I.11 are rendered with back faces culled. Since the sphere is convex, culling back faces is good enough to correctly remove hidden surfaces. On the other hand, a torus is not convex; as Figure I.15 shows, culling back faces does not do a very good job of removing hidden surfaces on a torus.

I.3.7 Wireframe triangles

By default, OpenGL draws triangles as filled in. It is possible to change this by using the `glPolygonMode` function to specify whether to draw solid triangles, wireframe triangles, or just the vertices of triangles. This makes it easy for a program to switch between wireframe and non-wireframe mode. The syntax for the `glPolygonMode` command is

$$\texttt{glPolygonMode(}\left\{\begin{array}{c}\texttt{GL\_FRONT}\\ \texttt{GL\_BACK}\\ \texttt{GL\_FRONT\_AND\_BACK}\end{array}\right\}\texttt{,}\left\{\begin{array}{c}\texttt{GL\_FILL}\\ \texttt{GL\_LINE}\\ \texttt{GL\_POINT}\end{array}\right\}\texttt{);}$$

The first parameter to `glPolygonMode` specifies whether the mode applies to front and/or back faces. The second parameter sets whether triangles are drawn filled in, as lines, or as just vertices.

I.4 Vertex shaders and fragment shaders

Modern graphics systems provide a huge amount of flexibility in how rendering occurs. The simplest functionality is obtained by writing a vertex shader and fragment shader. A vertex shader is a small program that is run once for each

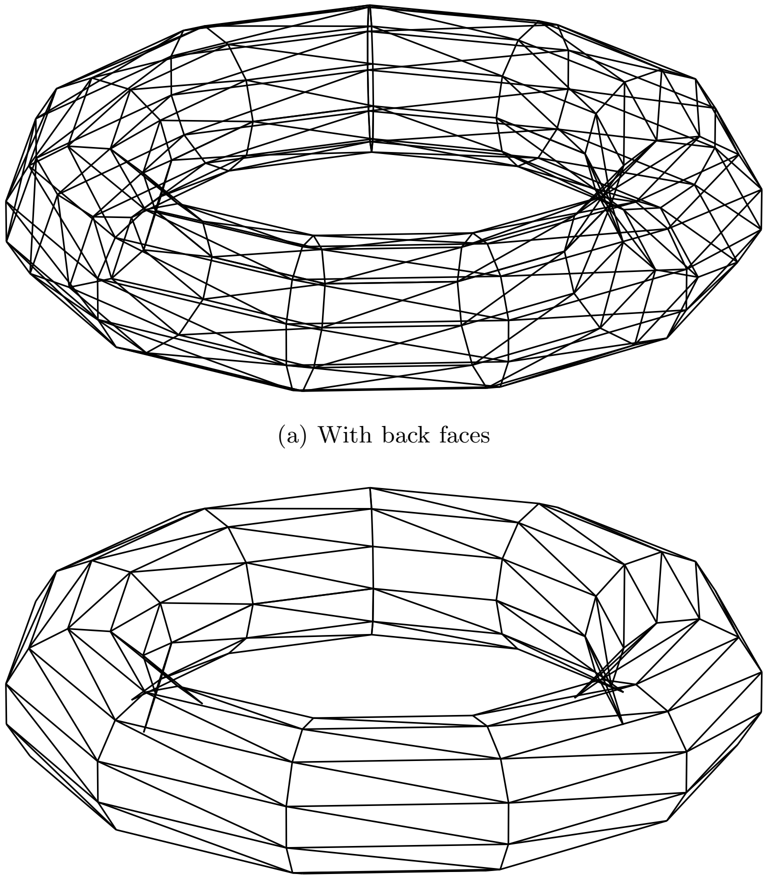

(a) With back faces

(b) With back faces culled

Figure I.15: Two wireframe tori, without hidden surfaces

vertex. A fragment shader is a small program that is run once for each pixel rendered. (Fragment shaders are sometimes called “pixel shaders”, and in most cases, you can think of “fragment” as being a synonym for “pixel”.) In this section, we’ll discuss some simple uses of vertex and fragment shaders. Later on, we’ll describe more sophisticated shaders.

The terminology “shader” comes from the idea of shading a triangle. The term “shading” means the process of letting the color or brightness vary smoothly across a surface. Later on, we shall see that shading is an important tool for creating realistic images, particularly when combined with lighting models that compute colors from material properties and light properties, rather than using colors that are explicitly set by the programmer. Shader programs are so-named because they were originally intended mostly for controlling shading of triangles; however, they can be used for many other purposes as well.

The main inputs to a vertex shader are the attributes of a single vertex; usually some of these attributes come from a VBO, while others are specified globally, either as generic attributes or "uniform variables". In a typical application, the vertex shader may receive the x, y, z-coordinates of a vertex, and perhaps a color or texture coordinates. The vertex shader can then do rather sophisticated computations, including changing the per-vertex data, possibly changing the color or texture coordinates or even the position of the vertex. The main output of the vertex shader is a value `gl_Position` which gives the x, y-coordinates of the vertex *in screen coordinates.* The `gl_Position` also gives a "depth" value which will be used for hidden surface computation as discussed later in Section I.4.4 and Chapter II. This depth value is often called the "z-value". (In actuality, `gl_Position` has a w-component so that values are represented in homogeneous coordinates; this will be discussed in Chapter II.) For now, we just think of the `gl_Position` as giving the x- and y-coordinate of a pixel on the screen, with x and y both ranging from -1 to 1, plus a depth value giving information about how far the vertex is from the viewer. As x varies from -1 to 1, the pixel position varies from left to right. As y varies from -1 to 1, the pixel position varies from the bottom of the image to the top. The depth value also varies from -1 to 1 and provides information about how far the contents of the pixel is from the viewer. (See Sections I.4.4 and II.4 for more on depth values.)

A vertex shader will output other, shader-specific values in addition to the `gl_Position`. For example, the shader-specific output values might be the red, green and blue components of the color of the pixel.

The fragment shader is invoked when a pixel is rendered in a *framebuffer.* The framebuffer is two dimensional array of values, usually holding a color value and a depth value for each pixel in the image. Consider a triangle with three vertices. The vertex shader is run on each vertex, and the three output values `gl_Position` give three pixels on the screen. These three pixels specify a triangle of pixels. Usually, the triangle will be filled in ("shaded"), with each pixel of the triangle being rendered as some color. Figures III.4 and III.5 on pages 120 and 122 give an idea of how this works. Note that the edges of the filled in triangle will in general be a bit "jaggy" because of the fact that pixels are rectangularly arranged.

When a triangle is rendered, OpenGL determines which framebuffer pixels it covers. OpenGL then calls the fragment shader once per pixel. The job of the fragment shader is to calculate the color that should be placed into the corresponding pixel.

The inputs to the fragment shader correspond to the shader-specific values output by the vertex shader. By default, each such input to the fragment shader is calculated as an average of the corresponding shader-specific values output by the vertex shader. That is, when rendering a triangle, an input to the fragment shader is an average of the outputs from the vertex shaders for the three triangle vertices. This averaging works in the same way that colors were averaged in the triangle in Figure C.3a in the last code example above. The fragment shader's main output is a vector giving the red, green, and blue components of the pixel (plus an alpha or transparency value). This output from the fragment shader is the color displayed in that pixel — unless some other triangle overwrites it.

I.4.1 Very simple vertex and fragment shader example

Vertex and fragment shaders can be quite complex, but for now, we illustrate the idea with some very simple shaders. The following program is a vertex shader that can work with the earlier code examples:

```
#version 330 core
layout (location = 0) in vec3 vertPos;      // Position, at ‘location’ 0
layout (location = 1) in vec3 vertColor;    // Color, at ‘location’ 1
out vec3 theColor;                          // Output a color
void main() {
  gl_Position = vec4(vertPos.x-1.0, 0.666*vertPos.y-1.0, vertPos.z, 1.0);
  theColor = vertColor;
}
```

The shader is written in the OpenGL Shader Language (GLSL). The first line indicates the version of the language being used. The next two lines give the "locations" of the two vertex attributes (position and color) and specify that they are 3-vectors (vec3's). Note how x, y, z-components of the vecs3's are referenced by using the suffixes .x, .y, and .z. The earlier code samples with the vert array specified only the x- and y-coordinates of vertices in the VBO; however, the vertPos variable is still allowed to be a vec3 as the z-component defaults to 0. The fourth line specifies that there is a shader-specific output value called theColor. The vertex shader's main program sets the pixel position in gl_Position and sets the shader-specific output theColor equal to the vertex attribute vertColor.

Note that the x- and y-coordinates of the position are transformed by the equations

$$\texttt{vertPos.x-1.0} \qquad \text{and} \qquad \texttt{0.666*vertPos.y-1.0}. \tag{I.1}$$

The input x-coordinates vertPos.x from all our examples range between 0 and 2, and thus vertPos.x-1.0 ranges between -1 and 1. Similarly, the input y-coordinates vertPos.y range between 0 and 3, and 0.666*vertPos.x-1.0 ranges between -1 and 1. Therefore the transformations (I.1) ensure that the output x- and y-coordinates in gl_Position lie in the range $[-1, 1]$. If output coordinates were outside $[-1, 1]$, the pixel would lie outside the visible part of the screen: the vertex would not be rendered (and triangles containing that vertex would be either clipped or culled).

The transformations of (I.1) are ad-hoc and very specific to our earlier examples. Chapter II will discuss more general matrix methods for transforming points to lie in the visible part of the screen.

The simplest possible fragment shader is:

```
#version 330 core
in vec3 theColor;        // Input color (averaged)
out vec4 FragColor;      // Output color
void main() {
  FragColor = vec4(theColor, 1.0f);    // Alpha value is 1.0
}
```

The only thing this fragment shader does is copy the input color to the output color. Note that the "`in`" declaration of `theColor` in the fragment shader exactly matches the "`out`" declaration in the vertex shader. The output `FragColor` has four components: red, green, blue and alpha (RGBA).

I.4.2 A fragment shader modifying the color

For a small, very simple, example of the power of shaders, we give a second fragment shader. This fragment shader can be used with the same vertex shader as above; it takes the same color (`theColor`) as input, but increases to maximum brightness while maintaining its hue. It does this by multiplying the color by a scalar to increase its maximum component to 1. Here is the code:

```
#version 330 core
in vec3 theColor;       // Input color (averaged)
out vec4 FragColor;     // Output color
void main() {
    float mx = max(theColor.r,max(theColor.g,theColor.b));
    if ( mx!=0 ) {
        FragColor = vec4(theColor/mx, 1.0f);    // Scale maximum component to 1.0
    }
    else {
        FragColor = vec4(1.0, 1.0, 1.0, 1.0);    // Replace black with white
    }
}
```

This code uses the suffixes `.r`, `.g` and `.b` to access the three components of the 3-vector `theColor`. (These have exactly the same meaning as `.x`, `.y` and `.z`, and are used here just as a reminder that `theColor` represents an RGB color.) Thus `mx` is equal to the maximum of the RGB components of the input color. Figure C.3b shows the triangle as rendered by this fragment shader. For the pixel midway between the red and green vertices, `theColor` is equal to $\langle \frac{1}{2}, \frac{1}{2}, 0 \rangle$, so the fragment shader computes `mx` to equal $\frac{1}{2}$, and outputs the color as $\langle 1, 1, 0 \rangle$, namely a bright yellow instead a dark yellow. For the pixel at the middle of the triangle, `theColor` is equal to $\langle \frac{1}{3}, \frac{1}{3}, \frac{1}{3} \rangle$, `mx` equals $\frac{1}{3}$, and the `FragColor` color is $\langle 1, 1, 1 \rangle$, namely white instead of a dark gray.

I.4.3 Flat shading

In *flat shading*, the shader-specific values output by the vertex shader are not averaged across the triangle. Instead, one of the vertices has its values used for the entire triangle. To use flat shading, the vertex and fragment shaders have to be modified to declare the out/in variable as being `flat`. For example, a simple vertex shader with flat shading could be

```
#version 330 core
layout (location = 0) in vec3 vertPos;       // Position, at ‘location’ 0
layout (location = 1) in vec3 vertColor;     // Color, at ‘location’ 1
flat out vec3 theColor;                      // Output a color
void main() {
  gl_Position = vec4(vertPos.x-1.0, 0.666*vertPos.y-1.0, vertPos.z, 1.0);
  theColor = vertColor;
}
```

This can be paired with a fragment shader such as

```
#version 330 core
flat in vec3 theColor;   // Input color (averaged)
out vec4 FragColor;      // Output color
void main() {
  FragColor = vec4(theColor, 1.0f);   // Alpha value is 1.0
}
```

The only difference in these two new shaders is the addition of the keyword `flat` to modify the declaration of `theColor`.[9] When a variable is declared to be `flat` then one of the vertices has its value used for the *entire* triangle. Usually, the last specified vertex of the triangle is the one whose value is used. Thus if the `verts3` triangle (see Figure C.3a) was rendered with shaders using `flat` it would be rendered as a solid blue triangle — even though it has a red vertex and green vertex.[10]

Exercise I.5. Draw the five-pointed star of Figure I.7 as filled-in triangles formed from smoothly varying colors. Use a single triangle fan, with the initial point of the triangle fan at the center of the star. (Save your program to modify for the next exercise.)

Exercise I.6. Modify the program you wrote for Exercise I.5 to use flat shading. For this, modify the vertex shader and fragment shader used in the previous exercise to include the `flat` keyword. Compare the flat colors to the smooth colors of Exercise I.5. Are the colors being picked according to the last specified vertex of each triangle?

[9] Some implementations of GLSL allow you to omit the qualifier “`flat`” in the vertex shader.

[10] The `glProvokingIndex` command allows you to make `flat` mode use the first vertex of the triangle instead of the last vertex.

I.4.4 Hidden surfaces

When we render three dimensional scenes, objects that are closer to the viewpoint may occlude, or hide, objects which are farther from the viewer. OpenGL uses a depth buffer that holds a distance or depth value for each pixel.[11] The depth buffer lets OpenGL do hidden surface computations by the simple expedient of drawing into a pixel only if the new distance will be less than the old distance. The typical use of the depth buffer is as follows: When an object, such as a triangle, is rendered, OpenGL determines which pixels need to be drawn and computes a measure of the distance from the viewer to each pixel. That distance is compared to the distance associated with the current contents of the pixel. The lesser of these two distances determines which pixel value is saved, since the closer object is presumed to occlude the farther object.

To better appreciate the elegance and simplicity of the depth buffer approach to hidden surfaces, we consider some alternative hidden surface methods. One alternative method, called the *painter's algorithm*, sorts the triangles from most distant to closest and renders them in back-to-front order, letting subsequent triangles overwrite earlier ones. The painter's algorithm is conceptually easy, but not completely reliable. In fact, it is not always possible to consistently sort triangles according to their distance from the viewer (cf. Figure I.16). In addition, the painter's algorithm cannot handle interpenetrating triangles.

Another hidden surface method is to work out geometrically all the information about how the triangles occlude each other, and render only the visible portions of each triangle. This, however, can require sophisticated algorithms to implement efficiently and robustly.

The depth buffer method, in contrast, is very simple and requires only an extra depth, or distance, value to be stored per pixel. Another big advantage of the depth buffer method is that it allows triangles to be rendered independently and in any order. The painter's algorithm needs to collect a complete list of the triangles before starting the rendering, so that they can be sorted before rendering. Similarly, calculating occlusions requires processing all the triangles before any rendering occurs. The depth buffer method can render each triangle by storing colors and depths into the pixels covered by the triangle, and immediately discard all information about the triangle; it does not need to collect all the triangles before rendering into pixels.

The depth buffer is not activated by default in OpenGL. To enable it, you must enable `GL_DEPTH_TEST`:

```
glEnable(GL_DEPTH_TEST); // Enable depth buffering
glDepthFunc(GL_LEQUAL);
```

The call to `glDepthFunc` says that a pixel should be overwritten if its new value has depth less than or equal to the current contents of the pixel. The default

[11] The depth value of a vertex is the z-coordinate of the `gl_Position` value output by the vertex shader (after perspective division); see Chapter II.

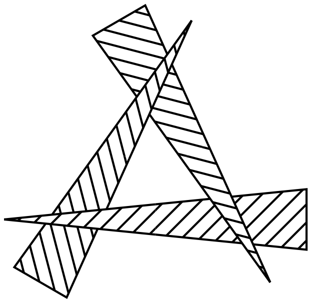

Figure I.16: Three triangles. The triangles are slanting upwards to the viewer so that the top portion of each triangle is in front of the base portion of another. This means that the painter's algorithm is unable to sort the triangles in an order that correctly handles hidden surfaces.

depth test function is `GL_LESS` only keeps a new value if its depth is less than the old depth; in most applications this will work equally well.[12]

It is also important to clear the depth buffer each time you begin to render an image. This is typically done with a command such as

```
    glClear( GL_COLOR_BUFFER_BIT | GL_DEPTH_BUFFER_BIT );
```

which both clears the color (i.e., initializes the entire image to the default color) and clears the depth values (by setting them to the maximum possible depth). The default color and depth for `glClear` can be changed by calling `glClearColor()` or `glClearDepth`.[13]

The *SimpleDrawModern* program illustrates the use of the depth buffering for hidden surfaces. It shows three triangles, each of which partially hides another, as in Figure I.16. This example shows why ordering polygons from back-to-front is not a reliable means of performing hidden surface computation.

I.5 Animation with double buffering

The term "animation" refers to drawing moving objects or scenes. The movement is only a visual illusion however; in practice, animation is achieved by drawing a succession of still scenes, called frames, each showing a static snapshot at an instance in time. The illusion of motion is obtained by rapidly displaying successive frames. Movies and videos typically have a frame rate

[12] Handling depth testing for exactly coincident object can be tricky, especially in the presence of floating point roundoff errors. The `glPolygonOffset` function, discussed in Section II.4.6, can help handle this.

[13] It is also possible to use `glClearBuffer` commands instead of `glClearColor` and `glClear`. See the *SimpleAnimModern* program for an example.

of 24 or 48 frames per second; higher frame rates give much better results for higher speed motion. The frame rates in computer graphics can vary with the power of the computer and the complexity of the graphics rendering, but typically it is desirable to have 30 frames per second, and more ideally to get at lesat 60 frames per second. In most cases, hese frame rates are quite adequate to give the appearance smooth motion. For head mounted displays, where the view changes with the position of the viewer's head, even higher frame rates are needed to get good effects.

Double buffering can be used to generate successive frames cleanly. While one image is displayed on the screen, the next frame is being created in another part of memory. When the next frame is ready to be displayed, the new frame replaces the old frame on the screen instantaneously (or rather: the next time the screen is redrawn, the new image is used). A region of memory where an image is being created or stored is called a buffer. The image being displayed is stored in the *front buffer*, and the *back buffer* holds the next frame as it is being created. When the buffers are swapped, the new image replaces the old on the screen. Note that swapping buffers does not generally require copying from one buffer to the other; instead, one can just update pointers to switch the identities of the front and back buffers.

A simple example of animation using double buffering in OpenGL is shown in the program *SimpleAnimModern* that accompanies this book. The main loop in that program uses the GLFW interface for OpenGL as follows:

```
while (!glfwWindowShouldClose(window)) {
  myRenderScene();                 // Render new scene
  glfwSwapBuffers(window);         // Display new scene
  glfwWaitEventsTimeout(1.0/60.0); // Approximately 60 frames/sec
}
```

This call to `myRenderScene` renders into the current frame buffer, the so-called *back buffer*. While rendering, the display is showing the contents of the front buffer so that the rendering does not show up instantaneously on the display. Instead, the rendering becomes visible after the call to `glfwSwapBuffers` interchanges the front and back buffers. This causes the just-rendered scene to be shown on the display. The previous screen image is now ready to be overwritten in the next rendering pass.

The call to `glfwWaitEventsTimeout` tells OpenGL to wait until some "event" has occurred or until 1/60 of second has elapsed. An "event" can be a mouse click or a mouse movement or a keystroke, or a window resizing, etc. When there are no events, the scene is redrawn approximately 60 times per second. This timing is not particularly accurate: for more reliable results, your program can either check the actual elapsed time. If it is supported, vertical synchronization can also be used.

If the scene is fixed and not animating, you can use

```
glfwWaitEvents();     // Use this if no animation.
```

instead of glfwWaitEventsTimeout. This will cause the image to be redrawn only when an event has occurred. For instance, if the window is resized, the scene will need to be rerendered.

In some cases, you may wish animate as fast as possible, but still check for events. For this, you can use

```
glfwPollEvents();     // Just check for events
```

The OpenGL programs *SimpleDrawModern* and *SimpleAnimModern* on the book's website provide examples of capturing keystrokes and resizing the graphics window. In addition, *ConnectDotsModern* shows how to capture mouse clicks.

I.6 Antialiasing with supersampling

Aliasing problems arise when converting between analog and digital representations, or when converting between different resolution digital representations. A simple example is the jagged lines that result when drawing a straight line on a rectangular array of pixels. These aliasing problems can be particularly distracting for animated scenes.

A simple way to dramatically reduce aliasing problems in an OpenGL program is to include the following two lines to turn on multisampling antialiasing (MSAA):

```
glfwWindowHint(GLFW_SAMPLES, 4);   // Invoke MSAA
glEnable(GL_MULTISAMPLE);
```

The parameter "4" instructs OpenGL to use "multisample aliasing" with each screen pixel holding four color and depth values — in a 2x2 arrangement of subpixels. Each screen pixel has its color calculated once per triangle that overlaps the screen pixel: the color and depth values are saved into only those subpixels which are actually covered by the triangle. This can greatly improve many common aliasing problems with edges of triangles.

Multisample antialiasing (MSAA) is fairly expensive in terms of memory, since it requires four color and depth values per pixel: this can sometimes cause a noticeable slowdown in graphics performance. However, the fact that it is handled directly by the GPU hardware makes it relatively efficient. Other antialiasing methods will be discussed in Sections VI.1.3, VI.1.4 and X.2.1.

I.7 Additional exercises

Exercise I.7. Write an OpenGL program that renders a cube with six faces of different colors. Form the cube from eight vertices and twelve triangles, making sure that the front faces are facing outwards. The eight vertices may be placed at $\langle \pm 1, \pm 1, \pm 1 \rangle$. You can do this with either with twelve separate triangles using GL_TRIANGLES, or with two or more triangle strips.

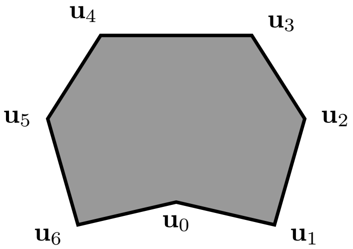

Figure I.17: The region for Exercise I.10.

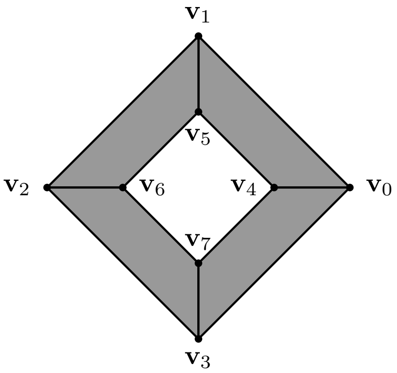

Figure I.18: The region for Exercise I.11.

Experiment with changing between smooth shading and flat shading. If you already know how to perform rotations, let your program include the ability to spin the cube around.

Exercise I.8. Repeat the previous exercise, but render the cube using two triangle fans. See Exercise I.14 for the related question about how to order the vertices in the two triangle fans.

Exercise I.9. Modify the *SimpleDrawModern* program at the book's web page to draw the three triangles with white borders. This will require toggling the polygon mode. The program will first render the triangles first shaded with colors, and then redraw them with the polygon mode set to `GL_LINE`. Does it matter if the polygon modes are used in the opposite order?

(Depending on your OpenGL implementation, it is possible, but not likely, that there will be z-fighting between the lines and the polygons. If so, this can be fixed with `glPolygonOffset`.)

Exercise I.10. A non-convex planar region bounded by seven edges, with vertices $\mathbf{u}_0$ through $\mathbf{u}_6$, is shown in Figure I.17. Your answers for (a) and (b) should cover this region with triangles so that the triangles do not overlap (beyond sharing edges) and so that all triangles are front facing using the default `GL_CCW` convention. (Compare with Exercise I.3.)

(a) Give a ordering of the vertices (with repetitions if necessary) that will render in the region as a triangle fan. Draw a copy of the figure, showing the triangles in the triangle fan.

(b) Give a ordering of the vertices (with repetitions if necessary) that will render in the region as a triangle strip. Draw a copy of the region, showing the triangles in the triangle strip.

Exercise I.11. Eight vertices, $\mathbf{v}_0$ through $\mathbf{v}_7$, are used to specify four gray quadrangles to form the region with a hole in the middle shown in Figure I.18.

(a) List the vertices in the correct order to render the shaded region as a single triangle strip with the faces are facing towards the viewer as shown in the figure. (With the default convention, `GL_CCW`, for front faces.)

(b) Now express the region as two triangle fans, again with all triangles facing towards the viewer.

Exercise I.12. An octahedron centered at the origin is formed from the six vertices $\langle \pm 1, 0, 0\rangle$, $\langle 0, \pm 1, 0\rangle$ and $\langle 0, 0, \pm 1\rangle$. Describe a way to order the vertices to render the octahedron as two triangle fans, with all faces facing outward.

Exercise I.13. A tetrahedron-like shape is formed from the four vertices $\langle -1, 0, -1\rangle$, $\langle 1, 0, -1\rangle$, $\langle 0, 1, 0\rangle$ and $\langle 0, 1, 0\rangle$. Describe a vertex order for rendering the four faces of this shape with a single triangle strip, with all faces facing outward.

Exercise I.14. A $2\times 2\times 2$ cube has the eight vertices $\langle \pm 1, \pm 1, \pm 1\rangle$. Show how to render the six faces of the cube with two triangle fans, by explicitly listing the vertices used for the triangle fans. Make sure that the usual CCW front faces are facing outwards. There are many possible vertex orderings, choose one that uses $\langle 1, 1, 1\rangle$ as the first (central) vertex for one of the triangle fans.

Exercise I.15. Consider rendering one triangle strip of a sphere as shown in Figure I.11a. Suppose the sphere is formed from k slices and ℓ stacks. The k slices cut the sphere like an orange with k slices, each slice takes up $2\pi/k$ radians around the central axis. The ℓ stacks are formed from $\ell - 1$ horizonal cuts (perpendicular to the central axis): the north pole is in the top stack and the south pole is in the bottom stack. How many triangles are in the triangle strip shown in Figure I.11a running from the south pole to the north pole? How many triangles are in the triangle strip shown in Figure I.11b running around the equator? How many vertices are present in the VBO or VEO arrays for these strips? How many of these vertices are distinct?

Exercise I.16. Gamma correction (which will be discussed Chapter VII) alters an RGB color $\langle r, g, b\rangle$ to the color $\langle r^\gamma, g^\gamma, b^\gamma\rangle$. The value γ is a fixed constant, usually between $\frac{1}{3}$ and 3. The values r, g, b should be in the range $[0, 1]$. Write a fragment shader that implements gamma correction. This will be similar to the fragment shader on page 26, but with a different algorithm for modifying the color. The suggestion is to modify the program *Chapter1Figs* available on the book's webpage and change the way the triangle of Figure C.3b is rendered by that program's fragment shader. The GLSL function `pow` will be useful for this. Try this with several values of γ between 0.5 and 3.

Chapter II

Transformations and Viewing

*This is a **preliminary** draft of a second edition of the book* 3-D Computer Graphics: A Mathematical Introduction with OpenGL. *So please read it cautiously and critically! Corrections are appreciated. Draft C.4.a*
Author: Sam Buss, `sbuss@ucsd.edu`
Copyright 2001, 2002, 2003. 2018, 2019, 2020, 2021, 2022.

This chapter discusses the mathematics of linear, affine, and perspective transformations, as well as their uses in OpenGL. The basic purpose of these transformations is to provide methods of changing the shape and position of objects, but their use is pervasive throughout computer graphics. In fact, affine and perspective transformations are arguably the most fundamental mathematical tool for computer graphics. They are mathematically very elegant, and even more importantly, are fairly easy for an artist or programmer to use. In addition they have efficient software and hardware implementations.

II.1 Transformations and the graphics pipeine

An obvious use of transformations is to organize and simplify the task of geometric modeling. As an example, suppose an artist is designing a computerized geometric model of a Ferris wheel. A Ferris wheel has a lot of symmetry and includes many repeated elements, such as multiple cars and struts. The artist could design a single model of the car, and then place multiple instances of the car around the Ferris wheel, attached at the proper points. Similarly, the artist could build the main structure of the Ferris wheel by designing one radial "slice" of the wheel and using multiple, rotated copies of this slice to form the entire structure. Affine transformations are used to describe how the parts are placed and oriented.

A second important use of transformations is to describe animation. If the Ferris wheel is animated, then the positions and orientations of its individual geometric components are constantly changing. Thus, for animation, it is necessary to compute time-varying affine transformations to simulate the motion of the Ferris wheel.

A third, more hidden, use of transformations in computer graphics is for rendering. After a 3-D geometric model has been created, it is necessary to render it on a two dimensional surface called the *viewport*. Some common examples of viewports are a window on a computer monitor or a smartphone screen, a frame of a movie, and a hardcopy image. There are special transformations, called perspective transformations, that are used to map points from a 3-D model to points on a 2-D viewport.

To appreciate the uses of transformations, it is useful to understand how they are usually used in the *rendering pipeline* to render and model a 3-D scene. Figure II.1 shows the transformations that are most commonly used in 3-D graphics rendering. As we discuss later, these transformations are generally represented by 4×4 matrices acting on homogeneous coordinates. The following elements go into modelling and transforming a vertex:

Vertex position: We start with a vertex position $\mathbf{x}$, usually as a point in 3-space, denoting a position for the vertex in *local coordinates.* For example, in the Ferris wheel example, to model a single chair of the Ferris wheel it might be the most convenient to model it as being centered at the origin. Vertices are specified relative to a local coordinate system for the chair. In this way, the chair can be modeled once without having to consider where the chairs will be placed in the final scene.

As we see later, it is common to use homogeneous coordinates, so that a 4-vector $\mathbf{x}$ represents a position in 3-space. For OpenGL, these vertex positions $\mathbf{x}$ would be stored in the VBO as vertex attributes.

The model matrix: The model matrix M transforms vertex positions $\mathbf{x}$ from local coordinates into *world coordinates* (also called *global coordinates*). The world coordinates can be viewed as the "real" coordinates. In the Ferris wheel example, multiple chairs are rendered at different positions and orientations on the Ferris wheel, since the chairs go around with the wheel plus they may rock back-and-forth. Each chair will have its own model matrix M. The model matrix transforms vertex positions $\mathbf{x}$ from local coordinates into global coordinates. Usually, the model matrix is a 4×4 matrix M, and the matrix-vector product $M\mathbf{x}$ gives the world coordinates for the point with local coordinates $\mathbf{x}$.

Model matrix transformations usually represent "affine transformations"; these provide a flexible set of tools for positioning vertices, including methods for rotating, scaling, and re-shaping objects. The next sections will discuss affine transformations in some detail.

The view matrix: The view matrix V transforms vertex positions from world coordinates into *view coordinates* (also called *camera coordinates*). The 3-D scene is rendered from the viewpoint of some viewer or camera. The viewer has a viewpoint position, a view direction, and a field of view. All this

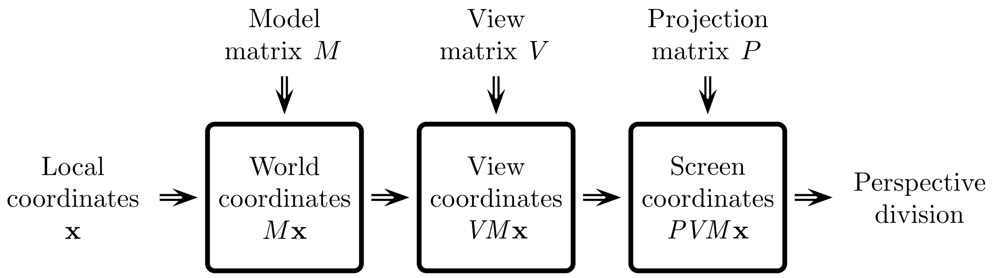

Figure II.1: The rendering pipeline: The transformation matrices and coordinate systems most often used in 3-D rendering. These matrices transform local coordinates for vertices into device independent screen coordinates. The final stage of the rendering pipeline's transformation of coordinates is perspective division. The final result consists of x, y screen coordinates and a z-value representing the depth.

information defines the view coordinates. A typical convention is that the viewer is positioned at the origin of the view coordinate system, and looking down the negative z-axis, with the viewer's y-axis pointing in the viewer's "up" direction and the viewer's x-axis pointing in the viewer's "rightward" direction.

Like the model matrix M, the view matrix V is a 4×4 matrix and typically represents an affine transformation. If $\mathbf{y} = M\mathbf{x}$ describes a position in world coordinates, then $V\mathbf{y}$ is the position in view coordinates. This can be equivalently expressed as $(VM)\mathbf{x}$.

The matrix product VM is also a 4×4 matrix, called the modelview matrix. It is fairly common to work with just the modelview matrix, and instead of using separate model and view matrices.

The projection matrix: The projection matrix P transforms vertex positions from view coordinates into *device independent screen coordinates.* The x, y-coordinates of the screen coordinates determine the position in the final image. OpenGL requires the x, y coordinates of the device independent screen coordinates to be in the range $[-1, 1]$; but they ultimately determine the coordinates of a single pixel in the final image. The z-component of the screen coordinates are based on the distance of the point from the viewer. We call the z-component the "pseudo-distance", as it is a nonlinear function of the actual distance from the viewer. The pseudo-distance is defined in Section II.4.2; it is used for hidden surface computations using the depth buffer method.

The projection matrix is also a 4×4 matrix, and applies either an "orthographic projection" or, more commonly, a "perspective transformation."

Perspective division: The model, view and projection matrices are all 4×4 matrices operating on homogeneous representations of points in 3-space. The homogeneous coordinates are a 4-vector $\langle x, y, z, w\rangle$ with an extra fourth component w. Division by w gives the ordinary screen components as the 3-vector $\langle x/w, y/w, z/w\rangle$. The values x/w and y/w are the x- and y-coordinates of the screen position and z/w gives the pseudo-distance. All three of these values x/w, y/w and z/w need to be in the range $[-1, 1]$: otherwise the point is not visible, either by virtue of being outside of the field of view or being with too close or too far from the viewer.

The mathematics behind all this is described later in this chapter. The use of homogeneous coordinates is particularly useful because it handles both translations and perspective at the same time.

The model matrix, view matrix, and perspective matrix are used by the vertex shader to transform vertex positions from local coordinates to screen coordinates. Perspective division occurs after the vertex shader has processed the vertices. The fragment shader is not able to alter the screen position, and in most applications does not alter the z-value (depth) value. In some applications, the fragment shader needs to use the world coordinates or the view coordinates of a point, for instance when calculating global lighting. (For this, see Chapter IV.) If so, they come from the vertex shader as shader-specific output values.

II.2 Transformations in 2-space

We start by discussing linear and affine transformations on a fairly abstract level. After that, we will give some examples of using transformations in OpenGL. We begin by considering affine transformations in 2-space since they are much simpler than transformations in 3-space. As we shall see, most of the important properties of affine transformations already apply in 2-space.

The xy-plane, denoted $\mathbb{R}^2 = \mathbb{R} \times \mathbb{R}$, is the usual cartesian plane consisting of points $\langle x, y\rangle$. To avoid writing too many coordinates, we often use the vector notation $\mathbf{x}$ for a point in $\mathbb{R}^2$, with the usual convention being that $\mathbf{x} = \langle x_1, x_2\rangle$, where $x_1, x_2 \in \mathbb{R}$. This notation is convenient, but potentially confusing, since we will use the same notation for vectors as for points.[1]

We write $\mathbf{0}$ for the origin, or zero vector. So, $\mathbf{0} = \langle 0, 0\rangle$. We write $\mathbf{x} + \mathbf{y}$ and $\mathbf{x} - \mathbf{y}$ for the component-wise sum and difference of $\mathbf{x}$ and $\mathbf{y}$. A real number $\alpha \in \mathbb{R}$ is called a *scalar*, and the product of a scalar and a vector is defined by $\alpha\mathbf{x} = \langle \alpha x_1, \alpha x_2\rangle$.[2] The *magnitude* or *norm* of a vector $\mathbf{x} = \langle x_1, x_2\rangle$

[1] Points and vectors in 2-space both consist of a pair of real numbers. The difference is that a point specifies a particular location, whereas a vector specifies a particular displacement, or change in location. That is to say, a vector is the difference of two points. Rather than adopting a confusing and nonstandard notation that clearly distinguishes between points and vectors, we will instead follow the more common, but ambiguous, convention of using the same notation for points as for vectors.

[2] In view of the distinction between points and vectors, it can be useful to form the sums and differences of two vectors, or of a point and a vector, or the difference of two points, but it is not generally useful to form the sum of two points. The sum or difference of two vectors is a vector. The sum or difference of a point and a vector is a point. The difference

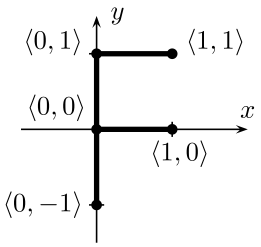

Figure II.2: The "F" shape.

is equal to $||\mathbf{x}|| = \sqrt{x_1^2 + x_2^2}$. A *unit* vector is a vector with magnitude equal to 1. See Appendix 1 for more basic facts about vectors.

II.2.1 Basic definitions

A *transformation* on $\mathbb{R}^2$ is any mapping $A : \mathbb{R}^2 \mapsto \mathbb{R}^2$. That is to say, each point $\mathbf{x} \in \mathbb{R}^2$ is mapped to a unique point, $A(\mathbf{x})$, also in $\mathbb{R}^2$.

Definition II.1. Let $A : \mathbb{R}^2 \to \mathbb{R}^2$ be a transformation. A is a *linear transformation* provided the following two conditions hold:

1. For all $\alpha \in \mathbb{R}$ and all $\mathbf{x} \in \mathbb{R}^2$, $A(\alpha\mathbf{x}) = \alpha A(\mathbf{x})$.
2. For all $\mathbf{x}, \mathbf{y} \in \mathbb{R}^2$, $A(\mathbf{x}+\mathbf{y}) = A(\mathbf{x}) + A(\mathbf{y})$.

Note that $A(\mathbf{0}) = \mathbf{0}$ for any linear transformation A. This follows from condition 1. with $\alpha = 0$.

We defined transformations as acting on a single point at a time, but of course a transformation also acts on arbitrary geometric objects by mapping the points in the object. Figure II.3 shows six examples of linear transformations and how they act on the "F" shape of Figure II.2. These include

(a) $\langle x, y\rangle \mapsto \langle x, y\rangle$. The identity transformation I.

(b) $\langle x, y\rangle \mapsto \langle \frac{1}{2}x, \frac{1}{2}y\rangle$. The uniform scaling $S_{\frac{1}{2}}$

(c) $\langle x, y\rangle \mapsto \langle \frac{3}{2}x, \frac{1}{2}y\rangle$. The nonuniform scaling $S_{\langle \frac{3}{2}, \frac{1}{2}\rangle}$.

(d) $\langle x, y\rangle \mapsto \langle -y, x\rangle$. Rotation 90° counter-clockwise, R_{90°.

(e) $\langle x, y\rangle \mapsto \langle x+y, y\rangle$. A shearing transformation.

(f) $\langle x, y\rangle \mapsto \langle -y, -x\rangle$. Reflection across the line $y = -x$.

Exercise II.1. Verify that the five transformations A_1-A_5 below are linear. Draw pictures showing how they transform the "F" shape.

- $A_1 : \langle x, y\rangle \mapsto \langle -y, x\rangle$.

of two points is a vector. However, we gloss over these issues, and define the sums and products on all combinations of points and vectors. In any event, we frequently blur the distinction between points and vectors.

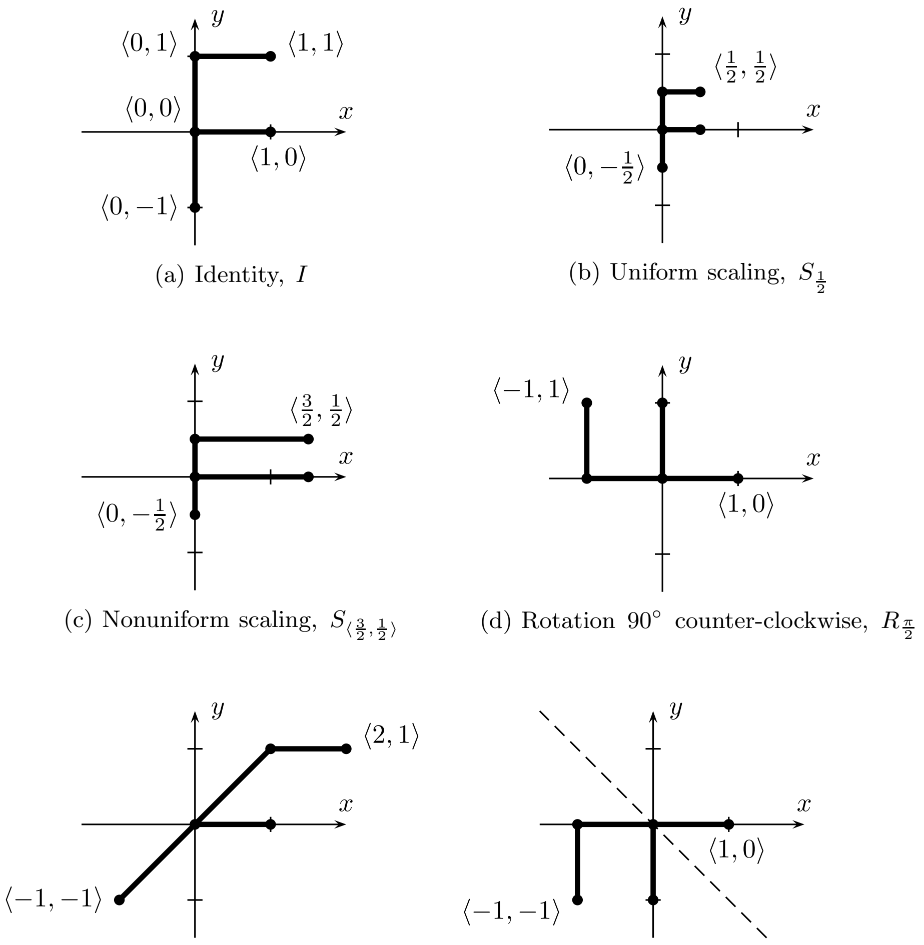

(a) Identity, I

(b) Uniform scaling, $S_{\frac{1}{2}}$

(c) Nonuniform scaling, $S_{\langle\frac{3}{2},\frac{1}{2}\rangle}$

(d) Rotation 90° counter-clockwise, $R_{\frac{\pi}{2}}$

(e) A shearing transformation

(f) Reflection across $y=-x$

Figure II.3: Transformations of the “F” shape.

- $A_2 : \langle x,y\rangle \mapsto \langle x,2y\rangle$.
- $A_3 : \langle x,y\rangle \mapsto \langle x-y,y\rangle$.
- $A_4 : \langle x,y\rangle \mapsto \langle x,-y\rangle$.
- $A_5 : \langle x,y\rangle \mapsto \langle -x,-y\rangle$.

Figure II.3b shows the *uniform scaling* $S_{\frac{1}{2}}$. For α any scalar, the uniform scaling $S_\alpha : \langle x,y\rangle \mapsto \langle \alpha x,\alpha y\rangle$ is the linear transformation which changes the sizes of object (centered at the origin) by a factor α. Figure II.3c shows an example, of nonuniform scaling. In general, the nonuniform scaling $S_{\langle\alpha,\beta\rangle}$:

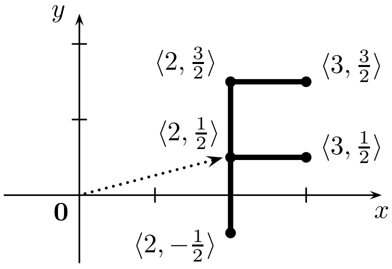
y
$\langle 2, \frac{3}{2}\rangle$
$\langle 3, \frac{3}{2}\rangle$
$\langle 2, \frac{1}{2}\rangle$
$\langle 3, \frac{1}{2}\rangle$
$\mathbf{0}$
x
$\langle 2, -\frac{1}{2}\rangle$

Figure II.4: The translation $T_{\mathbf{u}}$, where $\mathbf{u} = \langle 2, \frac{1}{2}\rangle$, applied to the "F" shape of Figure II.2.

$\langle x, y\rangle \mapsto \langle \alpha x, \beta y\rangle$ scales x-coordinates by the factor α and y-coordinates by β. Figure II.3d shows a rotation by 90° in the counter-clockwise direction. More generally, for θ a scalar, R_θ performs a rotation around the origin by θ radians in the counter-clockwise direction. A matrix formula for R_θ is given later in Equation (II.3).

One simple, but important, kind of nonlinear transformation is a "translation," which changes the position of objects by a fixed amount but does not change the orientations or shapes of geometric objects.

Definition II.2. A transformation $A : \mathbb{R}^2 \to \mathbb{R}^2$ is a *translation* provided that there is a fixed $\mathbf{u} \in \mathbb{R}^2$ such that $A(\mathbf{x}) = \mathbf{x} + \mathbf{u}$ for all $\mathbf{x} \in \mathbb{R}^2$.

The notation $T_{\mathbf{u}}$ is used to denote this translation; thus $T_{\mathbf{u}}(\mathbf{x}) = \mathbf{x} + \mathbf{u}$.

The *composition* of two transformations A and B is the transformation which is computed by first applying B and then applying A. This transformation is denoted $A \circ B$, or just AB, and satisfies

$$(A \circ B)(\mathbf{x}) = A(B(\mathbf{x})).$$

The *identity* transformation maps every point to itself. The *inverse* of a transformation A is the transformation A^{-1} such that $A \circ A^{-1}$ and $A^{-1} \circ A$ are both the identity transformation. Not every transformation has an inverse, but when A is one-to-one and onto, the inverse transformation A^{-1} always exists.

Note that the inverse of $T_{\mathbf{u}}$ is $T_{-\mathbf{u}}$.

Definition II.3. A transformation A is *affine* provided it can be written as the composition of a translation and a linear transformation. That is to say, provided it can be written in the form $A = T_{\mathbf{u}} \circ B$ for some $\mathbf{u} \in \mathbb{R}^2$ and some linear transformation B.

In other words, a transformation A is affine if it equals

$$A(\mathbf{x}) \;=\; B(\mathbf{x}) + \mathbf{u}, \tag{II.1}$$

with B a linear transformation and $\mathbf{u}$ a point.

Since it is permitted that $\mathbf{u} = \mathbf{0}$, every linear transformation is affine. However, not every affine transformation is linear. In particular, if $\mathbf{u} \neq \mathbf{0}$, then the transformation (II.1) is not linear, since it does not map $\mathbf{0}$ to $\mathbf{0}$.

Proposition II.4. *Let A be an affine transformation. The translation vector $\mathbf{u}$ and the linear transformation B are uniquely determined by A.*

Proof. First, let's see how to determine $\mathbf{u}$ from A. We claim that in fact $\mathbf{u} = A(\mathbf{0})$. This is proved by the following equalities:

$$A(\mathbf{0}) \;=\; T_{\mathbf{u}}(B(\mathbf{0})) \;=\; T_{\mathbf{u}}(\mathbf{0}) \;=\; \mathbf{0}+\mathbf{u} \;=\; \mathbf{u}.$$

Then $B = T_{\mathbf{u}}^{-1} \circ A = T_{-\mathbf{u}} \circ A$, so B is also uniquely determined. □

Corollary II.5. *An affine transformation A is linear iff $A(\mathbf{0}) = \mathbf{0}$.*

Another useful fact is that linear transformations and affine transformations are perserved under composition:

Theorem II.6. *Let A and B be transformations of $\mathbb{R}^2$.*

a. *If A and B are linear, then $A \circ B$ is a linear transformation.*

b. *If A and B are affine transformations, then $A \circ B$ is an affine transformation.*

Proof. First suppose A and B are linear. Then

$$(A\circ B)(\alpha\mathbf{x}) \;=\; A(B(\alpha\mathbf{x})) \;=\; A(\alpha B(\mathbf{x})) \;=\; \alpha A(B(\mathbf{x})) \;=\; \alpha(A\circ B)(\mathbf{x}),$$

and

$$(A\circ B)(\mathbf{x}+\mathbf{y}) \;=\; A(B(\mathbf{x}+\mathbf{y})) \;=\; A(B(\mathbf{x}))+A(B(\mathbf{y})) \;=\; (A\circ B)(\mathbf{x})+(A\circ B)(\mathbf{y}).$$

That shows $A \circ B$ is linear.

Now suppose A and B are affine, with $A = T_{\mathbf{u}} \circ C$ and $B = T_{\mathbf{v}} \circ D$, where C and D are linear transformations. Then

$$(A\circ B)(\mathbf{x}) \;=\; A(D(\mathbf{x})+\mathbf{v}) \;=\; A(D(\mathbf{x}))+A(\mathbf{v}) \;=\; C(D(\mathbf{x}))+\mathbf{u}+A(\mathbf{v}).$$

Therefore $(A\circ B)(\mathbf{x}) = E(\mathbf{x})+\mathbf{w}$ where $E = C\circ D$ is linear and $\mathbf{w} = \mathbf{u}+A(\mathbf{v})$. Thus $A \circ B$ is affine. □

II.2.2 Matrix representation of linear transformations

The above mathematical definition of linear transformations is stated rather abstractly. However, there is a very concrete way to represent a linear transformation $A : \mathbb{R}^2 \to \mathbb{R}^2$, namely as a 2×2 matrix.

Define $\mathbf{i} = \langle 1, 0\rangle$ and $\mathbf{j} = \langle 0, 1\rangle$. The two vectors $\mathbf{i}$ and $\mathbf{j}$ are the unit vectors which are aligned with the x-axis and y-axis, respectively. Any vector $\mathbf{x} = \langle x_1, x_2\rangle$ can be uniquely expressed as a linear combination of $\mathbf{i}$ and $\mathbf{j}$, namely as $\mathbf{x} = x_1\mathbf{i} + x_2\mathbf{j}$.

Let A be a linear transformation. Let $\mathbf{u} = \langle u_1, u_2\rangle = A(\mathbf{i})$ and $\mathbf{v} = \langle v_1, v_2\rangle = A(\mathbf{j})$. Then, by linearity, for any $\mathbf{x} \in \mathbb{R}^2$,

$$\begin{aligned} A(\mathbf{x}) &= A(x_1\mathbf{i} + x_2\mathbf{j}) \;=\; x_1A(\mathbf{i}) + x_2A(\mathbf{j}) \;=\; x_1\mathbf{u} + x_2\mathbf{v} \\ &= \langle u_1x_1 + v_1x_2, u_2x_1 + v_2x_2\rangle. \end{aligned}$$

Now let M be the matrix $\begin{pmatrix} u_1 & v_1 \\ u_2 & v_2 \end{pmatrix}$. Then,

$$M\begin{pmatrix} x_1 \\ x_2 \end{pmatrix} = \begin{pmatrix} u_1 & v_1 \\ u_2 & v_2 \end{pmatrix}\begin{pmatrix} x_1 \\ x_2 \end{pmatrix} = \begin{pmatrix} u_1x_1 + v_1x_2 \\ u_2x_1 + v_2x_2 \end{pmatrix}, \tag{II.2}$$

so the matrix M computes the same thing as the transformation A. We call M the *matrix representation of* A.

We have just shown that every linear transformation A is represented by some matrix. Conversely, it is easy to check that every matrix represents a linear transformation. Thus, it is reasonable to henceforth think of linear transformations on $\mathbb{R}^2$ as being the same as 2×2 matrices.

One notational complication is that a linear transformation A operates on points $\mathbf{x} = \langle x_1, x_2\rangle$, whereas a matrix M acts on column vectors. It would be convenient, however, to use both of the notations $A(\mathbf{x})$ and $M\mathbf{x}$. To make both notations be correct, we adopt the following rather special conventions about the meaning of angle brackets and the representation of points as column vectors:

Notation The point or vector $\langle x_1, x_2\rangle$ is identical to the column vector $\begin{pmatrix} x_1 \\ x_2 \end{pmatrix}$. So 'point,' 'vector,' and 'column vector' all mean the same thing. A column vector is the same as a matrix with a single column. A *row vector* is a vector of the form (x_1, x_2); i.e., a matrix with a single row.

A superscript 'T' denotes the matrix transpose operator. In particular, the transpose of a row vector is a column vector, and vice-versa. Thus, if $\mathbf{x} = \langle x_1, x_2\rangle$, then $\mathbf{x}^{\mathrm{T}}$ equals the row vector (x_1, x_2).

It is a simple, but important, fact that the columns of a matrix M are the images of $\mathbf{i}$ and $\mathbf{j}$ under M. That is to say, the first column of M is equal to $M\mathbf{i}$ and the second column of M is equal to $M\mathbf{j}$. So, using the notation of (II.2),

$$M\mathbf{i} = M\begin{pmatrix} 1 \\ 0 \end{pmatrix} = \begin{pmatrix} u_1 \\ u_2 \end{pmatrix} \qquad \text{and} \qquad M\mathbf{j} = M\begin{pmatrix} 0 \\ 1 \end{pmatrix} = \begin{pmatrix} v_1 \\ v_2 \end{pmatrix}.$$

This fact gives an intuitive method of constructing the matrix for a linear transformation. For example, consider the reflection across the line $y = -x$ shown in Figure II.3f. Just by the shape of the transformed "F", we see that it maps $\mathbf{i}$ to $\langle 0, -1\rangle$ and $\mathbf{j}$ to $\langle -1, 0\rangle$. Taking these vectors as the first and second columns of the matrix, we get immediately that this reflection is represented by the matrix $\begin{pmatrix} 0 & -1 \\ -1 & 0 \end{pmatrix}$.

We occasionally use a compact "block notation" for matrices. For example, with M as in Equation (II.2) and $\mathbf{u} = \langle u_1, u_2 \rangle$ and $\mathbf{v} = \langle v_1, v_2 \rangle$, we can write $M = (\mathbf{u}\ \mathbf{v})$ to indicate that $\mathbf{u}$ and $\mathbf{v}$ are the two columns of M.

Exercise II.2. Determine the 2×2 matrices representing the other five transformations shown in Figure II.3.

A more complicated use of this method for determining matrices is shown in the next example.

Example II.7. Let $M = \begin{pmatrix} 1 & 0 \\ 1 & 2 \end{pmatrix}$. The action of M on the "F" is shown in Figure II.5. We'll use a purely geometric method to find the matrix representation of its inverse M^{-1}. For this, it is enough to determine $M^{-1}\mathbf{i}$ and $M^{-1}\mathbf{j}$ since they will be the columns of M^{-1}. Looking at the graph on the right in Figure II.5, there are two vectors drawn with dotted lines: one of these is the vector $\mathbf{i} = \langle 1, 0 \rangle$ and the other is $2\mathbf{j} = \langle 0, 2 \rangle$. The preimages of these two vectors are drawn as dotted vectors on the lefthand graph are equal to $\langle 1, -1/2 \rangle$ and $\langle 0, 1 \rangle$. From this, we get immediately that

$$M^{-1}\mathbf{i} = M^{-1}\begin{pmatrix} 1 \\ 0 \end{pmatrix} = \begin{pmatrix} 1 \\ -1/2 \end{pmatrix} \qquad \text{and} \qquad M^{-1}\mathbf{j} = \tfrac{1}{2}M^{-1}\begin{pmatrix} 0 \\ 2 \end{pmatrix} = \begin{pmatrix} 0 \\ 1/2 \end{pmatrix}.$$

Therefore, M^{-1} is equal to $\begin{pmatrix} 1 & 0 \\ -1/2 & 1/2 \end{pmatrix}$.

The example illustrates a rather intuitive way to find the inverse of a matrix, but it depends on being able to visually find preimages of $\mathbf{i}$ and $\mathbf{j}$. It is worth explaining in a little more detail how to visualize the preimages above. Let's consider the preimage of $\mathbf{j}$. For this, we note that the two vertices in the image $\langle 1, 3 \rangle$ and $\langle 1, 1 \rangle$ have difference equal to $\langle 0, 2 \rangle = 2\mathbf{j}$, which is a scalar multiple of $\mathbf{j}$. This is shown as the vertical dotted vector in the righthand side of Figure II.5. And, it is clear from the picture that $A(\langle 1, 1 \rangle) = \langle 1, 3 \rangle$ and $A(\langle 1, 0 \rangle) = \langle 1, 1 \rangle$. The vector between these two points is shown as a dotted vector in the lefthand side of Figure II.5, By linearity, we have

$$\begin{aligned} A(\langle 0, 1 \rangle) &= A(\langle 1, 1 \rangle - \langle 1, 0 \rangle) \ = \ A(\langle 1, 1 \rangle) - A(\langle 1, 0 \rangle) \\ &= \langle 1, 3 \rangle - \langle 1, 1 \rangle \ = \ \langle 0, 2 \rangle \ = \ 2\mathbf{j}. \end{aligned}$$

From this, $A(\langle 0, \frac{1}{2} \rangle) = \mathbf{j}$, so $A^{-1}(\mathbf{j}) = \langle 0, \frac{1}{2} \rangle$. A similar method, using the other two dotted arrows in Figure II.5, can be used to visual $A^{-1}(\mathbf{i}) = \langle 1, -\frac{1}{2} \rangle$:

$$A(\langle 1, -\tfrac{1}{2} \rangle) \ = \ A(\langle 1, 0 \rangle) - A(\langle 0, \tfrac{1}{2} \rangle) \ = \ \langle 1, 1 \rangle - \langle 0, 1 \rangle \ = \ \mathbf{i}.$$

Of course, one can alternately compute the inverse of a 2×2 matrix by the well-known formula

$$\begin{pmatrix} a & b \\ c & d \end{pmatrix}^{-1} \ = \ \frac{1}{det(M)}\begin{pmatrix} d & -b \\ -c & a \end{pmatrix},$$

where $det(M) = ad - bc$ is the determinant of M.

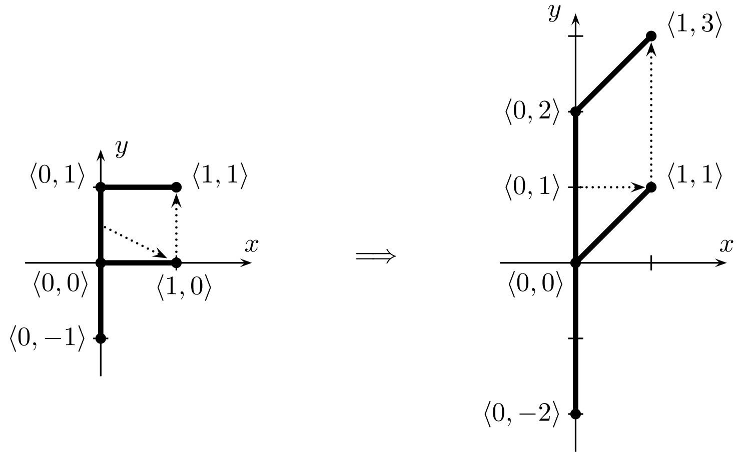

Figure II.5: An "F" shape transformed by a linear transformation from Example II.7. The dotted vectors in the graph on the right are the vectors $\mathbf{i}$ and $2\mathbf{j}$. The horizontal dotted vector going from $\langle 0,1\rangle$ to $\langle 1,1\rangle$ is equal to $\mathbf{i}$ since $\langle 1,1\rangle - \langle 0,1\rangle = \langle 1,0\rangle$. Similarly, the vertical dotted vector going from $\langle 1,1\rangle$ to $\langle 1,3\rangle$ is equal to $2\mathbf{j}$. The preimages of these two vectors are shown as dotted vectors in the lefthand graph.

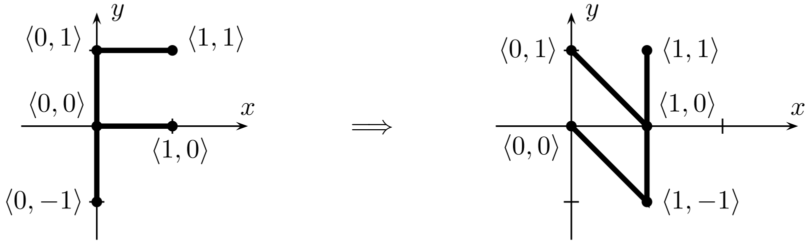

Figure II.6: The affine transformation for Exercises II.3, and II.44.

Exercise II.3. Figure II.6 shows an affine transformation f acting on an "F". (a) Is this a linear transformation? Why or why not? (b) Express this affine transformation in the form $\mathbf{x} \mapsto M\mathbf{x} + \mathbf{u}$, by explicitly giving M and $\mathbf{u}$.

Exercise II.4. Let f again be the affine transformation in Figure II.6. Express $f^{-1}(\mathbf{x})$ in the form $N\mathbf{x} + \mathbf{v}$ where N is a 2×2 matrix.

A *rotation* is a transformation which rotates the points in $\mathbb{R}^2$ by a fixed angle around the origin. Figure II.7 shows the effect of a rotation of θ degrees in the counter-clockwise (CCW) direction. As shown in Figure II.7, the images of $\mathbf{i}$ and $\mathbf{j}$ under a rotation of θ degrees are $\langle \cos\theta, \sin\theta\rangle$ and $\langle -\sin\theta, \cos\theta\rangle$. Therefore, a counter-clockwise rotation through an angle θ is represented by the matrix

$$R_\theta \;=\; \begin{pmatrix} \cos\theta & -\sin\theta \\ \sin\theta & \cos\theta \end{pmatrix}. \qquad \text{(II.3)}$$

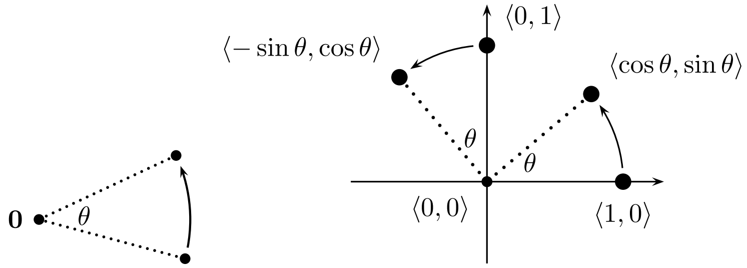

Figure II.7: Effect of a rotation through angle θ. The origin $\mathbf{0}$ is held fixed by the rotation.

Conventions on row and column vectors, and transposes. The conventions adopted in this book are that points in space are represented by *column* vectors, and linear transformations with matrix representation M are computed as $M\mathbf{x}$. In other words, our matrices are applied to column vectors by multiplying on the left. Unfortunately, this convention is not universally followed and it is also common in computer graphics applications to use *row* vectors for points and vectors, and to use matrix representations which act on the right. That is to say, many workers in computer graphics use a *row* vector to represent a point: instead of using $\mathbf{x}$, they use the row vector $\mathbf{x}^{\mathrm{T}}$.[3] Then, instead of multiplying $\mathbf{x}$ on the left with M, they multiply on the right with its transpose M^{T}. Since $\mathbf{x}^{\mathrm{T}}M^{\mathrm{T}}$ equals $(M\mathbf{x})^{\mathrm{T}}$ this has the same meaning. Similarly, when multiplying matrices to compose transformations, the fact that $(MN)^{\mathrm{T}} = N^{\mathrm{T}}M^{\mathrm{T}}$ means that the order of the multiplications is reversed when working with transposed matrices.

II.2.3 Rigid transformations and rotations

A rigid transformation is a transformation which only repositions objects, leaving their shape and size unchanged. If the rigid transformation also preserves the notions of "clockwise" versus "counter-clockwise," then it is called orientation preserving.

Definition II.8. A transformation is called *rigid* if and only if it preserves both:

1. Distances between points.
2. Angles between lines.[4]

[3] The notation $\mathbf{x}^{\mathrm{T}}$ means "$\mathbf{x}$ transpose". This treats the column vector x as a 2×1 matrix, and the row vector $\mathbf{x}^{\mathrm{T}}$ as a 1×2 matrix.

[4] Strictly speaking, the second condition could be omitted from the definition of "rigid". This is because the SSS Theorem (Side-Side-Side Theorem) of geometry implies that if distances are preserved, then also angles are preserved.

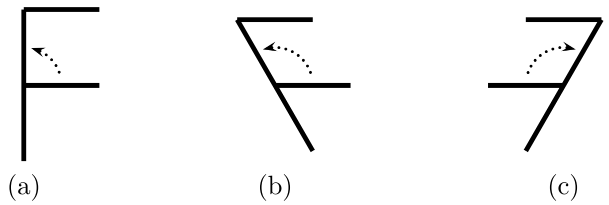

Figure II.8: The original "F" shape in (a) is transformed by an orientation preserving transformation in (b), and by an orientation reversing transformation in (c).

A transformation is said to be *orientation preserving* if it preserves the direction of angles; i.e., if a counter-clockwise direction between two intersecting lines stays counter-clockwise after being transformed by A.

Rigid, orientation preserving transformations are widely used. One application of these transformations is in animation: the position and orientation of a moving rigid body can be described by a time-varying transformation $A(t)$. This transformation $A(t)$ will be rigid and orientation preserving, provided the body does not deform or change size or shape.

The two most common examples of rigid, orientation preserving transformations are rotations and translations. Another example of a rigid, orientation preserving transformation is a "generalized rotation" which performs a rotation around an arbitrary center point. We prove below that every rigid, orientation preserving transformation over $\mathbb{R}^2$ is either a translation or a generalized rotation.

Exercise II.5. Which of the five linear transformations in Exercise II.1 on page 39 are rigid? Which ones are both rigid and orientation preserving?

For *linear* transformations, an equivalent definition of rigid transformation is that a linear transformation A is rigid if and only if it preserves dot products. That is to say, if and only if, for all $\mathbf{x}, \mathbf{y} \in \mathbb{R}^2$, $\mathbf{x} \cdot \mathbf{y} = A(\mathbf{x}) \cdot A(\mathbf{y})$. To see that this preserves distances, recall that $||\mathbf{x}||^2 = \mathbf{x} \cdot \mathbf{x}$ is the square of the magnitude of $\mathbf{x}$, or the square of $\mathbf{x}$'s distance from the origin. Thus, if A preserves dot products, $||\mathbf{x}||^2 = \mathbf{x} \cdot \mathbf{x} = A(\mathbf{x}) \cdot A(\mathbf{x}) = ||A(\mathbf{x})||^2$. From the definition of the dot product as $\mathbf{x} \cdot \mathbf{y} = ||\mathbf{x}|| \cdot ||\mathbf{y}|| \cos\theta$, where θ is the angle between $\mathbf{x}$ and $\mathbf{y}$, if the transformation A preserves dot products, it must also preserve angles between lines.

Exercise II.6. Let A be a linear transformation. Prove more fully the assertions in the previous paragraph by showing that if $A(\mathbf{0}) = \mathbf{0}$ and A preserves distances between points, then A preserves dot products. Conversely, prove that if A preserves dot products, then $A(\mathbf{0}) = \mathbf{0}$ and A preserves distances between points.

Exercise II.7. Let $M = (\mathbf{u}, \mathbf{v})$, i.e., $M = \begin{pmatrix} u_1 & v_1 \\ u_2 & v_2 \end{pmatrix}$. Show that the linear transformation represented by the matrix M is rigid if and only if $||\mathbf{u}|| = ||\mathbf{v}|| = 1$, and $\mathbf{u} \cdot \mathbf{v} = 0$.

A matrix M of the type in the previous exercise is called an *orthonormal* matrix.

Exercise II.8. Prove that the linear transformation represented by the matrix M is rigid if and only if $M^{\mathrm{T}} = M^{-1}$.

Exercise II.9. Prove that if $M = \langle \mathbf{u}, \mathbf{v} \rangle$ represents a rigid transformation, then $det(M) = \pm 1$.

Exercise II.10. Show that the linear transformation represented by the matrix M is orientation preserving if and only if $det(M) > 0$. [Hint: Let $M = (\mathbf{u}, \mathbf{v})$. Let $\mathbf{u}'$ be $\mathbf{u}$ rotated counter-clockwise 90°. Then M is orientation preserving if and only if $\mathbf{u}' \cdot \mathbf{v} > 0$.]

Theorem II.9. *Every rigid, orientation preserving, linear transformation is a rotation.*

The converse to Theorem II.9 holds too: every rotation is obviously a rigid, orientation preserving, linear transformation.

Proof. Let A be a rigid, orientation preserving, linear transformation. Let $\langle a, b \rangle = A(\mathbf{i})$. By rigidity, $A(\mathbf{i}) \cdot A(\mathbf{i}) = a^2 + b^2 = 1$. Also, $A(\mathbf{j})$ must be the vector which is obtained by rotating $A(\mathbf{i})$ counter-clockwise 90°; thus, $A(\mathbf{j}) = \langle -b, a \rangle$, as shown in Figure II.9.

Therefore, the matrix M which represents A is equal to $\begin{pmatrix} a & -b \\ b & a \end{pmatrix}$. Since $a^2 + b^2 = 1$, there must be an angle θ such that $\cos\theta = a$ and $\sin\theta = b$, namely, either $\theta = \cos^{-1} a$ or $\theta = -\cos^{-1} a$. From Equation (II.3), we see that A is a rotation through the angle θ. □

Many programming languages, including `C` and `C++`, have a two parameter version of the arctangent function which lets you compute the rotation angle as

$$\theta \;=\; \mathtt{atan2}(b, a).$$

This is often more robust, and more useful, than using C++'s arctangent `atan`, arcsine (`asin`) or arccosine (`acos`). In the shader programming language GLSL, the arctangent function is named just `atan` instead of `atan2`, and can take either one or two inputs.

We can improve on Theorem II.9 by weakening the assumption that A is linear to assume only that $A(\mathbf{0}) = \mathbf{0}$.

Theorem II.10. *Suppose A is a rigid, orientation preserving transformation with $A(\mathbf{0}) = \mathbf{0}$. Then A is a rotation.*

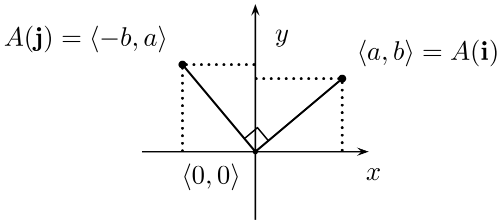
$A(\mathbf{j}) = \langle -b, a\rangle$
y
$\langle a, b\rangle = A(\mathbf{i})$
$\langle 0, 0\rangle$
x

Figure II.9: A rigid, orientation preserving, linear transformation acting on the unit vectors $\mathbf{i}$ and $\mathbf{j}$.

Proof. As in the proof of Theorem II.9, there are scalars a and b such that $a^2 + b^2 = 1$ and such that $A(\mathbf{i}) = \langle a, b\rangle$ and $A(\mathbf{j}) = \langle -b, a\rangle$. (That part of the proof used only the rigid and orientation preserving properties.) Let θ satisfy $\cos(\theta) = a$ and $\sin(\theta) = b$. Define $B = R_{-\theta} \circ A$. Then $B(\mathbf{0}) = \mathbf{0}$, and $B(\mathbf{i}) = \mathbf{i}$ and $B(\mathbf{j}) = \mathbf{j}$. Furthermore, as a composition of two rigid and orientation preserving transformations, B is also rigid and orientation preserving.

It is not hard to verify that every point $\mathbf{x} \in \mathbb{R}^2$ is uniquely characterized by its distances from the three points $\mathbf{0}$, $\mathbf{i}$ and $\mathbf{j}$. Therefore, since B is rigid and maps those three points to themselves, B must map every point $\mathbf{x}$ in $\mathbb{R}^2$ to itself. In other words, B is the identity. Therefore, $A = (R_{-\theta})^{-1} = R_\theta$, and so is a rotation. □

Theorem II.10, and the definition of affine transformations, gives the following characterization.

Corollary II.11. *Every rigid, orientation preserving transformation A can be (uniquely) expressed as the composition of a translation and a rotation. Hence A is an affine transformation.*

Corollary II.11 is proved by applying Theorem II.10 to the rigid, orientation preserving transformation $T_{-\mathbf{u}} \circ A$ where $\mathbf{u} = A(\mathbf{0})$.

Definition II.12. A *generalized rotation* is a transformation which holds a *center point* $\mathbf{u}$ fixed and rotates all other points around $\mathbf{u}$ through a fixed angle θ. This transformation is denoted $R_\theta^{\mathbf{u}}$.

An example of a generalized rotation is given in Figure II.10. Clearly, a generalized rotation is a rigid, orientation preserving, affine transformation.

One way to perform a generalized rotation is to first apply a translation to move the point $\mathbf{u}$ to the origin, then rotate around the origin, and then translate the origin back to $\mathbf{u}$. Thus, the generalized rotation $R_\theta^{\mathbf{u}}$ can be expressed as

$$R_\theta^{\mathbf{u}} \;=\; T_{\mathbf{u}} \circ R_\theta \circ T_{-\mathbf{u}}. \tag{II.4}$$

You should convince yourself that formula (II.4) is correct. Note especially the order in which the compositions are applied.

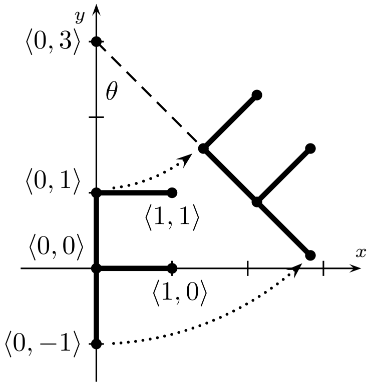

Figure II.10: A generalized rotation $R_\theta^{\mathbf{u}}$. The center of rotation is $\mathbf{u} = \langle 0,3\rangle$. The angle is $\theta = 45^\circ$.

Exercise II.11. Prove that $R_\theta^{\mathbf{u}}$ is equal to

$$R_\theta^{\mathbf{u}}(\mathbf{x}) \;=\; R_\theta(\mathbf{x}) + (\mathbf{u} - R_\theta(\mathbf{u})).$$

[Hint: Use the reasoning of the proof of part b. of Theorem II.6.]

Theorem II.13. *Every rigid, orientation preserving transformation is either a translation or a generalized rotation.*

Obviously, the converse of this theorem holds too.

Proof. Let A be a rigid, orientation preserving transformation. By Corollary II.11, A is affine. Let $\mathbf{u} = A(\mathbf{0})$. If $\mathbf{u} = \mathbf{0}$, A is actually a linear transformation, and Theorem II.9 implies that A is a rotation. So suppose $\mathbf{u} \neq \mathbf{0}$. It will suffice to prove that either A is a translation or there is some point $\mathbf{v} \in \mathbb{R}^2$ which is a fixed point of A, i.e., such that $A(\mathbf{v}) = \mathbf{v}$. This is sufficient since then the reasoning of the proofs of Theorems II.9 and II.10 shows that A is a generalized rotation around $\mathbf{v}$.

Let L be the line that contains the two points $\mathbf{0}$ and $\mathbf{u}$. We consider two cases. First, suppose that A maps L to itself. By rigidity, and by choice of $\mathbf{u}$, $A(\mathbf{u})$ is distance $||\mathbf{u}||$ from $\mathbf{u}$, so we must have either $A(\mathbf{u}) = \mathbf{u}+\mathbf{u}$ or $A(\mathbf{u}) = \mathbf{0}$. If $A(\mathbf{u}) = \mathbf{u}+\mathbf{u}$, then A must be the translation $T_{\mathbf{u}}$. This follows since, again by the rigidity of A, every point $\mathbf{x} \in L$ must map to $\mathbf{x}+\mathbf{u}$ and, by the rigidity and orientation preserving properties, the same holds for every point not on L. On the other hand, if $A(\mathbf{u}) = \mathbf{0}$, then rigidity implies that $\mathbf{v} = \frac{1}{2}\mathbf{u}$ is a fixed point of A, and thus A is a generalized rotation around $\mathbf{v}$.

Second, suppose that the line L is mapped to a different line L'. Let L' make an angle of θ with L, as shown in Figure II.11. Since $L' \neq L$, θ is nonzero and is not a multiple of 180°; thus $-180^\circ < \theta < 180^\circ$. Let w be the point on L midway between $\mathbf{0}$ and $\mathbf{u}$, and let w' be the point on L' midway between $\mathbf{u}$ and $A(\mathbf{u})$ Let $\mathbf{w}$ and $\mathbf{w}'$ be the midpoints of L and L'. Let L_2

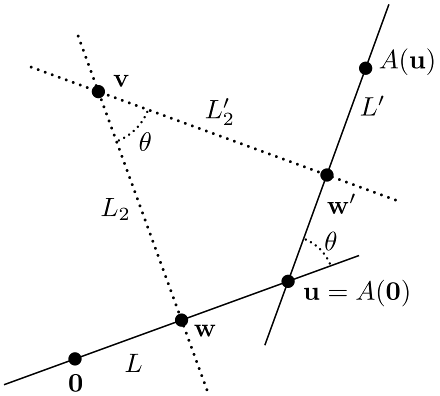

Figure II.11: Finding the center of rotation. The point $\mathbf{v}$ is fixed by the rotation.

and L_2' be the lines perpendicular to L and L' at $\mathbf{w}$ and $\mathbf{w}'$, respectively. These two lines are not parallel, and thus they intersect at a point $\mathbf{v}$. By rigidity, A sends L_2 to L_2'. Rigidity plus the orientation preserving property imply that $A(\mathbf{v}) = \mathbf{v}$. Therefore A is the generalized rotation $R_\theta^{\mathbf{v}}$ which performs a rotation by angle θ around the point $\mathbf{v}$. □

The proof method for Theorem II.13 can be slightly generalized to give a geometric method for determining the fixed point $\mathbf{v}$ of A when A is a generalized rotation. Suppose $\mathbf{y} = A(\mathbf{x})$ with $\mathbf{y} \neq \mathbf{x}$. Let $\overline{\mathbf{xy}}$ denote the line segment joining $\mathbf{x}$ and $\mathbf{y}$. Then the fixed point must lie on the perpendicular bisector of $\overline{\mathbf{xy}}$. If also $\mathbf{w} = A(\mathbf{u})$ with $\mathbf{u} \neq \mathbf{w}$, and if line segments $\overline{\mathbf{xy}}$ and $\overline{\mathbf{uw}}$ are not parallel, then their perpendicular bisectors will intersect at the center of rotation $\mathbf{v}$. (The proof of Theorem II.13 applied this principle with the line segment joining $\mathbf{0}$ and $\mathbf{u}$ and the line segment joining $\mathbf{u}$ and $A(\mathbf{u})$.)

Example II.14. Let A be the affine transformation that acts on the "F" shape as shown in Figure II.12. This is clearly a rigid, orientation preserving transformation, and must be a generalized rotation $R_\theta^{\mathbf{v}}$. From the picture, θ is equal to 90°. The fixed point $\mathbf{v}$ is harder to visualize, but we can find it as follows.

Let $\mathbf{x} = \langle 1, 1\rangle$ and $\mathbf{y} = \langle 2, 1\rangle$, so $A(\mathbf{x}) = \mathbf{y}$.[5] Also let $\mathbf{u} = \langle 1, 0\rangle$ and $\mathbf{w} = \langle 3, 1\rangle$, so $A(\mathbf{u}) = \mathbf{w}$. The line segments $\overline{\mathbf{xy}}$ and $\overline{\mathbf{uw}}$ are shown as dashed lines in Figure II.12. Their midpoints are $\langle \frac{3}{2}, 1\rangle$ and $\langle 2, \frac{1}{2}\rangle$; and their perpendicular bisectors are the lines $x = \frac{3}{2}$ and $2x + y = \frac{9}{2}$, shown as dotted lines in the figure. The perpendicular bisectors are not parallel, and intersect

[5] An alternate choice would be to let $\mathbf{x} = \mathbf{0}$ and $\mathbf{y} = \langle 3, 0\rangle$, but we choose instead values for $\mathbf{x}$ and $\mathbf{y}$ that make the Figure II.12 easier to understand.

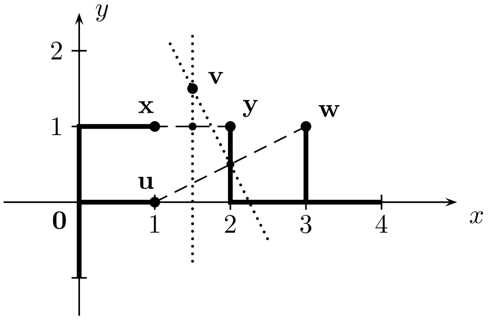

Figure II.12: The transformation for Example II.14. The line segments $\overline{\mathbf{xy}}$ and $\overline{\mathbf{uw}}$ are drawn as dashed lines. Their perpendicular bisectors are drawn as dotted lines. The "F" shape at the origin is mapped to the "F" shape on the right.

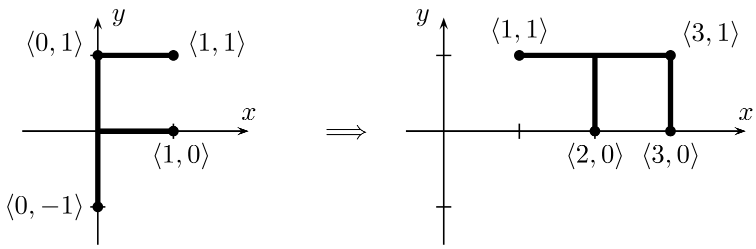

Figure II.13: The transformation for Exercise II.12.

at the point $\mathbf{v} = \langle \frac{3}{2}, \frac{3}{2} \rangle$. This point is fixed by A, so A is the generalized rotation $R^{\mathbf{v}}_{90^\circ}$.

An alternative, algebraic way to work the example is to express A in matrix form as $A(\mathbf{x}) = \begin{pmatrix} 0 & -1 \\ 1 & 0 \end{pmatrix} \mathbf{x} + \begin{pmatrix} 3 \\ 0 \end{pmatrix}$, and then solve $A(\mathbf{v}) = \mathbf{v}$ for $\mathbf{v}$.

Exercise II.12. Let $f : \mathbb{R}^2 \to \mathbb{R}^2$ be the rigid, orientation preserving transformation shown in Figure II.13. Express f as a generalized rotation $R^{\mathbf{v}}_{\theta}$.

II.2.4 Homogeneous coordinates

Homogeneous coordinates provide a method of using a triple of numbers $\langle x, y, w \rangle$ to represent a point in $\mathbb{R}^2$.

Definition II.15. If $x, y, w \in \mathbb{R}$ and $w \neq 0$, then $\langle x, y, w \rangle$ is a *homogeneous coordinate representation* of the point $\langle x/w, y/w \rangle \in \mathbb{R}^2$.

Note that any given point in $\mathbb{R}^2$ has many representations in homogeneous coordinates. For example, the point $\langle 2,1\rangle$ can be represented by any of the following sets of homogeneous coordinates:

$$\langle 2,1,1\rangle,\ \langle 4,2,2\rangle,\ \langle 6,3,3\rangle,\ \langle -2,-1,-1\rangle,\ \text{etc.}$$

More generally, the triples $\langle x,y,w\rangle$ and $\langle x',y',w'\rangle$ represent the same point in homogeneous coordinates if and only if there is a nonzero scalar α such that $x'=\alpha x$, $y'=\alpha y$ and $w'=\alpha w$.

So far, we have only specified the meaning of the homogeneous coordinates $\langle x,y,w\rangle$ when $w\neq 0$, since the definition of the meaning of $\langle x,y,w\rangle$ required dividing by w. However, we shall see in Section II.2.8 below that when $w=0$, $\langle x,y,w\rangle$ is the homogeneous coordinate representation of a "point at infinity." (Alternatively, graphics software such as OpenGL will sometimes use homogeneous coordinates with $w=0$ as a representation of a direction.) However, as we shall see, it is always required that at least one of the components x, y, w is nonzero.

The use of homogeneous coordinates may at first seem somewhat strange or poorly motivated; however, it is an important mathematical tool for the representation of points in computer graphics. There are several reasons for this. First, as we shall see next, using homogeneous coordinates allows an affine transformation to be represented by a single matrix. The second reason will become apparent in Section II.4, where perspective transformations and interpolation is discussed. A third important reason will arise in Chapters VIII and IX, where homogeneous coordinates will allow Bézier curves and B-spline curves to represent circles and other conic sections.

Exercise II.13. Give five different homogeneous representations for the point $\langle -1,\frac{1}{2}\rangle\in\mathbb{R}^2$. Include at least two representations with $w<0$.

II.2.5 Matrix representation of an affine transformation

Recall that any affine transformation A can be expressed as a linear transformation B followed by a translation $T_{\mathbf{u}}$, that is, $A=T_{\mathbf{u}}\circ B$. Let M be a 2×2 matrix representing B and suppose

$$M \;=\; \begin{pmatrix} a & b\\ c & d\end{pmatrix} \qquad \text{and} \qquad \mathbf{u} \;=\; \begin{pmatrix} e\\ f\end{pmatrix}.$$

Then the mapping A can be defined by

$$\begin{pmatrix} x_1\\ x_2\end{pmatrix} \mapsto M\begin{pmatrix} x_1\\ x_2\end{pmatrix}+\begin{pmatrix} e\\ f\end{pmatrix} \;=\; \begin{pmatrix} a & b\\ c & d\end{pmatrix}\begin{pmatrix} x_1\\ x_2\end{pmatrix}+\begin{pmatrix} e\\ f\end{pmatrix} \;=\; \begin{pmatrix} ax_1+bx_2+e\\ cx_1+dx_2+f\end{pmatrix}.$$

Now define N to be the 3×3 matrix

$$N \;=\; \begin{pmatrix} a & b & e\\ c & d & f\\ 0 & 0 & 1\end{pmatrix}.$$

Using the homogeneous representation $\langle x_1, x_2, 1\rangle$ of $\langle x_1, x_2\rangle$, we see that

$$N\begin{pmatrix} x_1 \\ x_2 \\ 1 \end{pmatrix} \quad = \quad \begin{pmatrix} a & b & e \\ c & d & f \\ 0 & 0 & 1 \end{pmatrix}\begin{pmatrix} x_1 \\ x_2 \\ 1 \end{pmatrix} \quad = \quad \begin{pmatrix} ax_1 + bx_2 + e \\ cx_1 + dx_2 + f \\ 1 \end{pmatrix}.$$

The effect of N acting on $\langle x, y, 1\rangle$ is identical to the effect of the affine transformation A acting on $\langle x, y\rangle$. The only difference is that the third coordinate of "1" is being carried around. More generally, for any other homogeneous representation of the same point, $\langle \alpha x_1, \alpha x_2, \alpha\rangle$ with $\alpha \neq 0$, the effect of multiplying by N is

$$N\begin{pmatrix} \alpha x_1 \\ \alpha x_2 \\ \alpha \end{pmatrix} \quad = \quad \begin{pmatrix} \alpha(ax_1 + bx_2 + e) \\ \alpha(cx_1 + dx_2 + f) \\ \alpha \end{pmatrix},$$

which is another representation of the point $A(\mathbf{x})$ in homogeneous coordinates.

Thus, the 3×3 matrix N provides a faithful representation of the affine map A in that, when working with homogeneous coordinates, multiplying by the matrix N provides exactly the same results as applying the transformation A. Further, N acts consistently on different homogeneous representations of the same point.

Note that the matrix N can also be written in block form as $N = \begin{pmatrix} M & \mathbf{x} \\ \mathbf{0}^{\mathrm{T}} & 1 \end{pmatrix}$. Here $\mathbf{0}^{\mathrm{T}}$ means the row vector $(0\ 0)$.

The method used to obtain N from A was completely general, and therefore any affine transformation can be represented as a 3×3 matrix which acts on homogeneous coordinates. So far, we have used only matrices that have the bottom row $(0\ 0\ 1)$; these matrices are sufficient for representing any affine transformation. In fact, an affine transformation may henceforth be viewed as being identical to a 3×3 matrix that has bottom row $(0\ 0\ 1)$.

When we discuss perspective transformations, which are more general than affine transformations, it will be necessary to have other values in the bottom row of the matrix.

Exercise II.14. Figure II.14 shows an affine transformation acting on an "F". (a) Is this a linear transformation? Why or why not? (b) Give a 3×3 matrix which represents the affine transformation. [Hint: In this case, the easiest way to find the matrix is to split the transformation into a linear part and a translation. Then consider what the linear part does to the vectors $\mathbf{i}$ and $\mathbf{j}$.]

For the next exercise, it is not necessary to invert a 3×3 matrix. Instead, note that if a transformation is defined by $\mathbf{y} = A\mathbf{x} + \mathbf{u}$, then its inverse is $\mathbf{x} = A^{-1}\mathbf{y} - A^{-1}\mathbf{u}$. Alternatively, the matrix inverse can be determined by "inspection", using the methods of Example II.7.

Exercise II.15. Give the 3×3 matrix which represents the inverse of the transformation in the previous exercise.

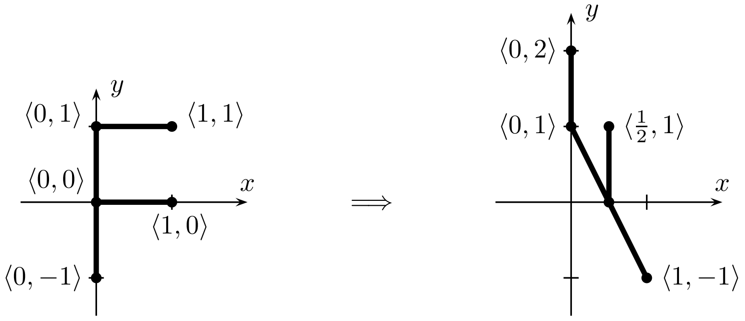

Figure II.14: The affine transformation for Exercise II.14.

Exercise II.16. Give an example of how two different 3×3 homogeneous matrices can represent the same affine transformation. [Hint: The bottom row can contain $0\ 0\ \alpha$.]

II.2.6 Using two dimensional transformations

The next two sections take a break from the mathematical theory of affine transformations and discuss how they are used in computer graphics when forming the model matrix M. Recall that the model matrix is used for positioning objects in space. The model matrix will operate on homogeneous coordinates, and thus can be used to apply translations, rotations, uniform and nonuniform scalings, reflections, shearings, and in fact any affine transformation.[6] This section will only discuss the intuitions, not the details, of how this is done. In particular, we illustrate the ideas with a simple example in 2-space, whereas OpenGL programs generally work in 3-space. This section does not give any actual OpenGL code; instead it gives only high-level pseudo-code. Sections II.3.3 through II.3.5 will describe how this kind of pseudo-code can be translated into OpenGL code.

The purpose of the model matrix M is to hold a homogeneous matrix representing an affine transformation. We shall therefore think of M as being a 3×3 matrix acting on homogeneous representations of points in 2-space. (In actual practice, M is a 4×4 matrix operating on points in 3-space.) We illustrate using model matrices to render the "F" shapes shown in Figures II.15 and II.16.

Figure II.15 shows an example of how rotation and translation transformation are not commutative; in other words, that different orders of operations can yield different results. Define two transformations A_1 and A_2 by

$$A_1 \;=\; T_{\langle \ell,0\rangle} \circ R_\theta \qquad \text{and} \qquad A_2 \;=\; R_\theta \circ T_{\langle \ell,0\rangle}. \tag{II.5}$$

The two transformed "F" shapes $A_1(\mathsf{F})$ and $A_2(\mathsf{F})$ are shown in Figure II.15. Namely, the "F" shape is modeled in standard position as shown in Figure II.2,

[6] It is can also apply perspective transformations, but this is usually not so useful for the model matrix.

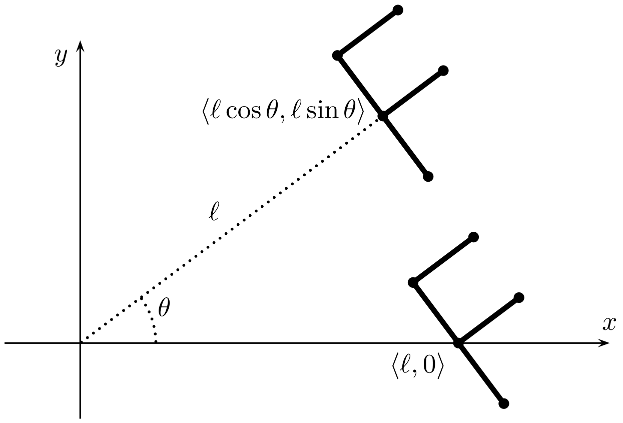

Figure II.15: The results of drawing the "F" shape with the two transformations A_1 and A_2 of Equation (II.5).

by drawing lines joining the five points $\langle 0,-1\rangle$, $\langle 0,0\rangle$, $\langle 0,1\rangle$, $\langle 1,0\rangle$ and $\langle 1,1\rangle$. Transforming the points in this F in standard position by A_1 or by A_2 gives the "F" shapes $A_1(\mathsf{F})$ and $A_2(\mathsf{F})$. The lower "F" shape (the one on the x-axis) is $A_1(\mathsf{F})$; the upper one is $A_2(\mathsf{F})$.

To understand this, first observe that $R_\theta(\mathsf{F})$ is an "F" shape still positioned at the origin, but rotated counter-clockwise by the angle θ. Then $A_1(\mathsf{F}) = T_{\langle \ell,0\rangle}(R_\theta(\mathsf{F}))$ is this rotated "F" shape translated distance ℓ along the positive x-axis; so $A_1(\mathsf{F})$ is the rotated "F" shape positioned at $\langle \ell,0\rangle$. On the other hand, $T_{\langle \ell,0\rangle}(\mathsf{F})$ is an upright "F" shape positioned at $\langle \ell,0\rangle$; and $A_2(\mathsf{F})$ is this "F" shape rotated around the origin, so as to be positioned at $\langle \ell\cos\theta, \ell\sin\theta\rangle$.

The intuition behind forming $A_1(\mathsf{F})$ and $A_2(\mathsf{F})$ is that transformations are applied in right-to-left order. For $A_1(\mathsf{F}) = (T_{\langle \ell,0\rangle} \circ R_\theta)(\mathsf{F})$, this means we first apply the rotation R_θ to the F, and then apply the translation $T_{\langle \ell,0\rangle}$. However for $A_2(\mathsf{F})$, the translation is applied first and the rotation is applied to the result. The pseudo-code for this is as follows. We use the notation "M_1" and "M_2" instead of "A_1" and "A_2" to indicate matrices representing the transformations. Likewise, R_θ and $T_{\langle \ell,0\rangle}$ denote the matrices for these transformations acting on homogeneous coordinates.

```
Set $M_1$ = $Identity$;                 // Identity matrix
Set $M_1$ = $M_1 \cdot T_{\langle \ell,0\rangle}$ ;        // Multiply on the right
Set $M_1$ = $M_1 \cdot R_\theta$ ;           // Multiply on the right
Render $M_1(\mathsf{F})$ ;                 // Render the lower F

Set $M_2$ = $Identity$;                 // Identity matrix
Set $M_2$ = $M_2 \cdot R_\theta$ ;           // Multiply on the right
Set $M_2$ = $M_2 \cdot T_{\langle \ell,0\rangle}$ ;        // Multiply on the right
Render $M_2(\mathsf{F})$ ;                 // Render the upper F
```

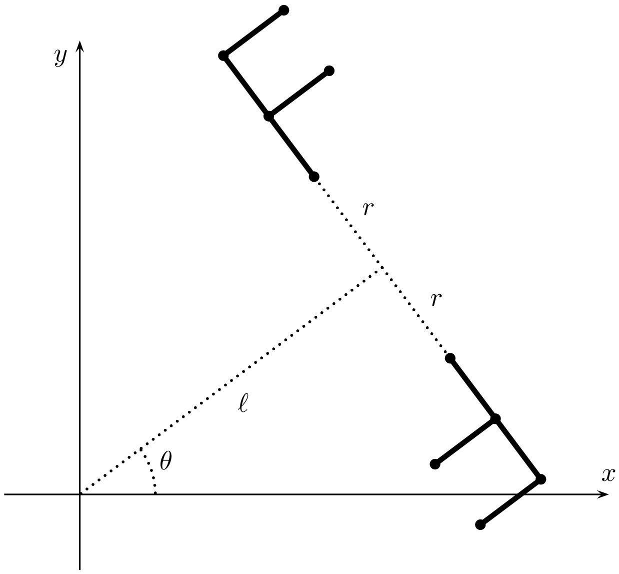

Figure II.16: The results of drawing the "F" shape with two different model matrices. The dotted lines are not rendered by the code and are present only to indicate the placement of the shapes. This figure is used for the pseudo-code on page 58.

This pseudo-code generates the "F" shapes of Figure II.15. The matrix multiplication commands update the model matrix by multiplying with a rotation or translation on the right. This means that if you read the program line-by-line in forward order, the "F" shape is transformed by these operations in *reverse order*. For example, the matrix M_1 is formed by multiplying first with $T_{\langle \ell,0\rangle}$ and then with R_θ; however, forming $M_1(\mathsf{F})$ has the same effect as transforming the "F" first with R_θ and then with $T_{\langle \ell,0\rangle}$. This reversal of the order of transformations may seem counterintuitive, but it can help with hierarchically modeling a scene.

Now let's look at the two "F" shapes shown in Figure II.16. We'll define two transformations represented by matrices M_3 and M_4, so that $M_3(\mathsf{F})$ generates the upper "F" shape in Figure II.16 and $M_4(\mathsf{F})$ generates the lower one. We claim that for the upper "F", the matrix M_3 should represent the transformation

$$R_\theta \circ T_{\langle \ell,0\rangle} \circ T_{\langle 0,r+1\rangle}. \tag{II.6}$$

This is illustrated in Figure II.17, where three F's are shown. The first one, placed above the origin is the shape $T_{\langle 0,r+1\rangle}(\mathsf{F})$; namely, is the 'F" shape translated up the positive y-axis a distance $r+1$. The second one is $T_{\langle \ell,0\rangle} \circ T_{\langle 0,r+1\rangle}(\mathsf{F})$; namely it is further translated distance ℓ in the direction of the positive x-axis. The third one is $R_\theta \circ T_{\langle \ell,0\rangle} \circ T_{\langle 0,r+1\rangle}(\mathsf{F})$; namely the second "F" is rotated around the origin.

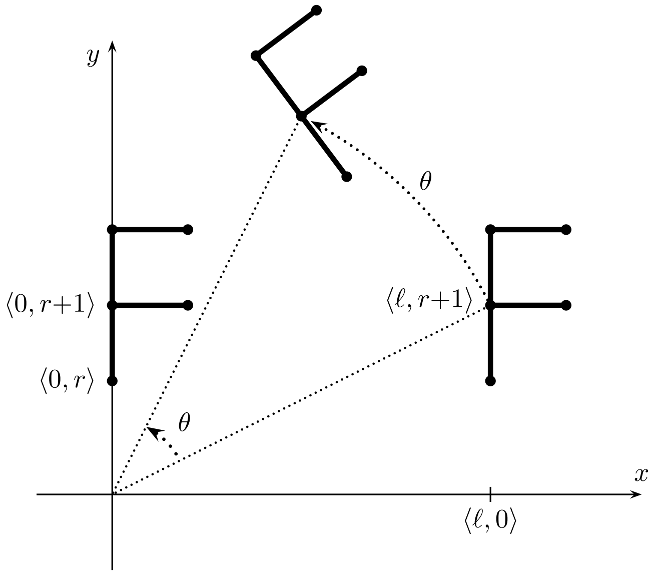

Figure II.17: The intermediate stages of placing the upper "F" shape of Figure II.16. The two upright "F" shapes are $T_{\langle 0,r+1\rangle}(\mathsf{F})$ and $T_{\langle \ell,0\rangle}\circ T_{\langle 0,r+1\rangle}(\mathsf{F})$. The "F" is never actually placed in these two intermediate positions; rather this just helps us figure out what the model matrix should be.

The same kind of reasoning shows that the lower "F" shape is equal to $M_4(\mathsf{F})$ where matrix M_4 represents the transformation

$$R_\theta \circ T_{\langle \ell,0\rangle} \circ R_\pi \circ T_{\langle 0,r+1\rangle}. \tag{II.7}$$

You should try working this out to verify that this transformation is correct. Note that R_π performs a 180° rotation around the origin, so that $R_\pi \circ T_{\langle 0,r+1\rangle}(\mathsf{F})$ is an upside down F with its center vertex positioned at $\langle 0, -(r{+}1)\rangle$.

Here is some possible pseudo-code for rendering the two "F" shapes of Figure II.16:

```
Set $M_0$ = $Identity$;
Set $M_0$ = $M_0 \cdot R_\theta$ ;
Set $M_0$ = $M_0 \cdot T_{\langle \ell,0\rangle}$ ;
Set $M_3$ = $M_0 \cdot T_{\langle 0,r+1\rangle}$ ;      // Calculate $M_3$ from $M_0$
Render $M_3(\mathsf{F})$ ;                    // Render the lower F
Set $M_4$ = $M_0 \cdot R_\pi$ ;               // Calculate $M_4$ from $M_0$
Set $M_4$ = $M_4 \cdot T_{\langle 0,r+1\rangle}$ ;
Render $M_4(\mathsf{F})$ ;                    // Render the upper F
```

As before, the matrix multiplication commands update the model matrix by multiplying with a rotation or translation on the right, the "F" shapes are

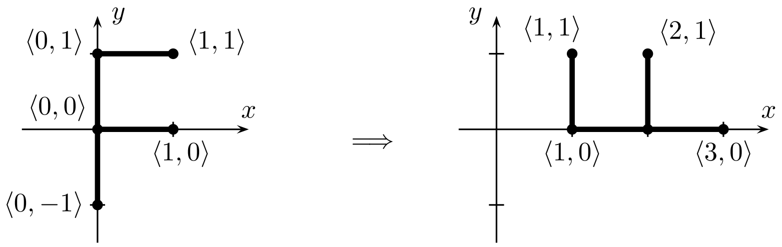

Figure II.18: The affine transformation for Exercise II.17.

transformed by these operations in the reverse of the order given the code. This example shows how it can help with hierarchically rendering scenes. For example, changing just the second line (the multiplication by R_θ) causes both "F" shapes to be rotated together as a group around the origin. Similarly the translation by $T_{\langle \ell,0\rangle}$ moves both "F" shapes together.

Exercise II.17. Consider the transformation shown in Figure II.18.

(a) Give pseudo-code that will draw the "F" as shown on the righthand side of Figure II.18.

(b) Give the 3×3 homogeneous matrix which represents the affine transformation shown in the figure.

II.2.7 Another outlook on composing transformations

So far we have discussed the actions of transformations (rotations and translations) as acting on the objects being drawn, and viewed them as being applied in reverse order from the order given in the (pseudo-)code. However, it is also possible to view transformations as acting not on objects, but instead on coordinate systems. In this alternative viewpoint, one thinks of the transformations acting on local coordinate systems (and *within* the local coordinate system), and now the transformations are applied in the same order as given in the code.

To illustrate the alternate view of transformations, consider the "F" shape that is shown uppermost in Figures II.16 and II.17. Recall this is transformed by

$$R_\theta \circ T_{\langle \ell,0\rangle} \circ T_{\langle 0,r+1\rangle}.$$

Figure II.19 shows four local coordinate systems placed a different positions and orientations on the xy-plane. These four coordinate systems are based on the four pairs of unit vectors $\mathbf{x}^0, \mathbf{y}^0$ and $\mathbf{x}^1, \mathbf{y}^1$ and $\mathbf{x}^2, \mathbf{y}^2$ and $\mathbf{x}^3, \mathbf{y}^3$. The first set of local coordinates $\mathbf{x}^0$ and $\mathbf{y}^0$ is identical to the original xy-coordinate axes.

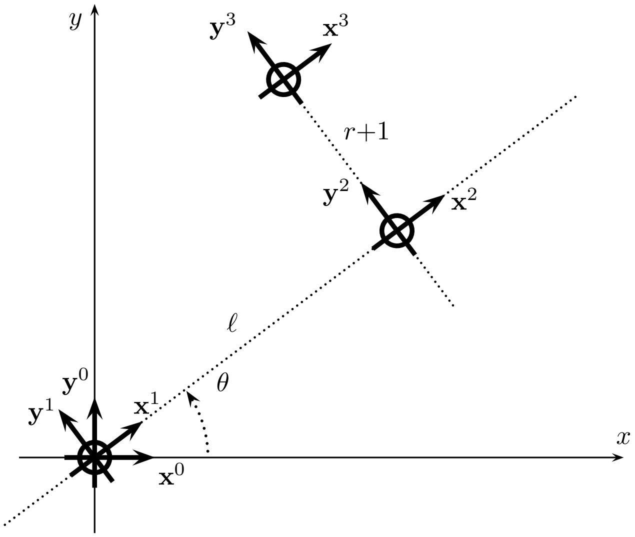

Figure II.19: The four local coordinate systems implicit in the transformation (II.6) used to position the upper "F" shape of Figures II.16 and II.17. The successive transformations are carried out relative to the previous local coordinate system.

The second set of local coordinates uses the axes $\mathbf{x}^1$ and $\mathbf{y}^1$. These are obtained by applying the rotation R_θ to the $\mathbf{x}^0, \mathbf{y}^0$ coordinate system, namely the coordinate axes are rotated counter-clockwise by the angle θ.

The third set of local coordinates uses $\mathbf{x}^2$ and $\mathbf{y}^2$. This is obtained by translating the $\mathbf{x}^1, \mathbf{y}^1$ coordinate system by $\langle 0, \ell \rangle$, doing the translation *relative to the* $\mathbf{x}^1, \mathbf{y}^1$ *coordinate system.* The fourth set of local coordinates is obtained by an additional translation by $\langle 0, r{+}1 \rangle$, relative to the local coordinate system of $\mathbf{x}^2$ and $\mathbf{y}^2$. The upper "F" shape shown in Figures II.16 and II.17 is obtained by placing an "F" shape in standard position relative to the $\mathbf{x}^3, \mathbf{y}^3$ coordinate system.

It should be stressed again that in this framework where transformations are viewed as acting on local coordinate systems, the meanings of the transformations are to be interpreted within the local coordinate system. In some applications, it can be useful to use this framework. For instance, when setting up a view matrix for defining a camera position and direction, it might be intuitive to think of the camera moving through a scene with the movements being specified relative to a local coordinate system attached to the camera. In this case, the intuition is that the scene is being transformed by the inverse of the camera movements (basing everything on the local coordinate systm attached to the camera).

Exercise II.18. Review the transformations used to draw the lower "F" shape shown in Figure II.16. Understand how this works from the viewpoint that transformations act on local coordinate systems. Draw a figure similar to Figure II.19 showing all the intermediate local coordinate systems that are implicitly defined by transformation (II.7).

II.2.8 Two dimensional projective geometry*

Projective geometry provides an elegant mathematical interpretation of the homogeneous coordinates for points in the xy-plane. In this interpretation, the triples $\langle x, y, w\rangle$ do not represent points just in the usual flat Euclidean plane, but in a larger geometric space known as the *projective plane*. The projective plane is an example of a projective geometry. A projective geometry is a system of points and lines which satisfy the following two axioms:[7]

P1. Any two distinct points lie on exactly one line.

P2. Any two distinct lines contain exactly one common point (i.e., intersect in exactly one point).

Of course, the usual Euclidean plane, $\mathbb{R}^2$, does not satisfy the second axiom since parallel lines do not intersect in $\mathbb{R}^2$. However, by adding appropriate "points at infinity" and a "line at infinity," the Euclidean plane $\mathbb{R}^2$ can be enlarged so as to become a projective geometry. In addition, homogeneous coordinates are a suitable way of representing the points in the projective plane.

The intuitive idea of the construction of the projective plane is as follows: for each family of parallel lines in $\mathbb{R}^2$, we create a new point, called a *point at infinity*. This new point is added to each of these parallel lines. In addition, we add one new line: the *line at infinity*, which contains exactly all the new points at infinity. It is not hard to verify that the axioms P1 and P2 hold.

Consider a line L in Euclidean space $\mathbb{R}^2$: it can be specified by a point $\mathbf{u}$ on L and by a nonzero vector $\mathbf{v}$ in the direction of L. In this case, L consists of the set of points

$$\{\mathbf{u} + \alpha\mathbf{v} : \alpha \in \mathbb{R}\} \;=\; \{\langle u_1 + \alpha v_1, u_2 + \alpha v_2\rangle : \alpha \in \mathbb{R}\}.$$

For each value of α, the corresponding point on the line L has homogeneous coordinates $\langle u_1/\alpha + v_1, u_2/\alpha + v_2, 1/\alpha\rangle$. As $\alpha \to \infty$, this triple approaches the limit $\langle v_1, v_2, 0\rangle$. This limit is a point at infinity and is added to the line L when we extend the Euclidean plane to the projective plane. If one takes the limit as $\alpha \to -\infty$, then the triple $\langle -v_1, -v_2, 0\rangle$ is approached in the limit. This is viewed as being the same point as $\langle v_1, v_2, 0\rangle$, since multiplication by the nonzero scalar -1 does not change the meaning of homogeneous coordinates. Thus, the intuition is that the *same* point at infinity on the line is found at both ends of the line.

[7] This is not a complete list of the axioms for projective geometry. For instance, it is required that every line has at least three points, etc.

Note that the point at infinity, $\langle v_1, v_2, 0\rangle$, on the line L did not depend on $\mathbf{u}$. If the point $\mathbf{u}$ is replaced by some point not on L, then a different line is obtained; this line will be parallel to L in the Euclidean plane, and any line parallel to L can be obtained by appropriately choosing $\mathbf{u}$. Thus, any line parallel to L has the same point infinity as the line L.

More formally, the *projective plane* is defined as follows. Two triples, $\langle x, y, w\rangle$ and $\langle x', y', w'\rangle$, are *equivalent* if there is a nonzero $\alpha \in \mathbb{R}$ such that $x = \alpha x'$, $y = \alpha y'$ and $w = \alpha w'$. We write $\langle x, y, w\rangle^P$ to denote the equivalence class which contains the triples which are equivalent to $\langle x, y, w\rangle$. The *projective points* are the equivalence classes $\langle x, y, w\rangle^P$ such that at least one of x, y, w is nonzero. A projective point is called a *point at infinity* if $w = 0$.

A *projective line* is either a usual line in $\mathbb{R}^2$ plus a point at infinity, or the line at infinity. Formally, for any triple a, b, c of real numbers, with at least one of a, b, c nonzero, there is a projective line L defined by

$$L \;=\; \{\langle x, y, w\rangle^P : ax + by + cw = 0, x, y, w \text{ not all zero}\}. \tag{II.8}$$

Suppose at least one of a, b is nonzero. Considering the $w = 1$ case, the projective line L contains a point $\langle x, y, 1\rangle$ provided $ax + by + c = 0$: this is the equation of a general line in the Euclidean space $\mathbb{R}^2$. Thus L contains all triples which are representations of points on the Euclidean line $ax + by + c = 0$. In addition, the line L contains the point at infinity $\langle -b, a, 0\rangle^P$. Note that $\langle -b, a\rangle$ is a Euclidean vector parallel to the line defined by $ax + by + c = 0$.

The projective line defined by (II.8) with $a = b = 0$ and $c \neq 0$ is the *line at infinity*; it contains those points $\langle x, y, 0\rangle^P$ such that x and y are not both zero.

Exercise II.19★ Another geometric model for the two dimensional projective plane is provided by the 2-sphere, with antipodal points identified. The 2-sphere is the sphere in $\mathbb{R}^3$ which is centered at the origin and has radius 1. Points on the 2-sphere are represented by normalized triples $\langle x, y, w\rangle$, which have $x^2 + y^2 + w^2 = 1$. In addition, the antipodal points $\langle x, y, w\rangle$ and $\langle -x, -y, -w\rangle$ are treated as equivalent. Prove that lines in projective space correspond to great circles on the sphere, where a *great circle* is defined as the intersection of the sphere with a plane containing the origin. For example, the line at infinity corresponds to the intersection of the 2-sphere with the xy-plane. [Hint: Equation (II.8) can be viewed as defining L in terms of a dot product with $\langle a, b, c\rangle$.]

Yet another way of mathematically understanding the two dimensional projective space is to view it as the space of linear subspaces of three dimensional Euclidean space. To understand this, let $\mathbf{x} = \langle x_1, x_2, x_3\rangle$ be a representation of a point in the projective plane. This point is equivalent to the points $\alpha\mathbf{x}$ for all nonzero $\alpha \in \mathbb{R}$; these points plus the origin form a line through the origin in $\mathbb{R}^3$. A line through the origin is of course a one dimensional subspace, and we identify this one dimensional subspace of $\mathbb{R}^3$ with the point $\mathbf{x}$.

Now consider a line L in the projective plane. If L is not the line at infinity, then it corresponds to a line in $\mathbb{R}^2$. One way to specify the line L is choose

$\mathbf{u} = \langle u_1, u_2 \rangle$ on L and a vector $\mathbf{v} = \langle v_1, v_2 \rangle$ in the direction of L. The line L then is the set of points $\{\mathbf{u} + \alpha\mathbf{v} : \alpha \in \mathbb{R}\}$. It is easy to verify that, after adding the point at infinity, the line L contains exactly the following set of homogeneous points:

$$\{\beta\langle u_1, u_2, 1\rangle + \gamma\langle v_1, v_2, 0\rangle : \beta, \gamma \in \mathbb{R} \text{ s.t. } \beta \neq 0 \text{ or } \gamma \neq 0\}.$$

This set of triples is, of course, a plane in $\mathbb{R}^3$ with a hole at the origin. Thus, we can identify this two dimensional subspace of $\mathbb{R}^3$ (that is, the plane) with the line in the projective plane. If, on the other hand, L is the line at infinity, then it corresponds in the same way to the two dimensional subspace $\{\langle x_1, x_2, 0\rangle : x_1, x_2 \in \mathbb{R}\}$.

These considerations give rise to another way of understanding the two dimensional projective plane. The "points" of the projective plane are one dimensional subspaces of $\mathbb{R}^3$. The "lines" of the projective plane are two dimensional subspaces of $\mathbb{R}^3$. A "point" lies on a "line" if and only if the corresponding one dimensional subspace is a subset of the two dimensional subspace.

The historical development of projective geometry arose from the development of the theory of perspective by Brunelleschi in the early 15th century. The basic tenet of the theory of perspective for drawings and paintings is that families of parallel lines point towards a common "vanishing point," which is essentially a point at infinity. The modern mathematical development of projective geometry based on homogeneous coordinates came much later of course, being developed by Feuerbach and Möbius in 1827 and Klein in 1871. Homogeneous coordinates have long been recognized as being useful for many computer graphics applications; see, for example, the early textbook by Newman and Sproull [82]. An accessible mathematical introduction to abstract projective geometry is the textbook by Coxeter [31].

II.3 Transformations in 3-space

We turn next to transformations in 3-space $\mathbb{R}^3$. This turns out to be very similar in many regards to transformations in 2-space. There are however some new features, most notably, rotations are more complicated in 3-space than in 2-space. First, we discuss how to extend, to 3-space, the concepts of linear and affine transformations, matrix representations for transformations, and homogeneous coordinates. We then explain the basic modeling commands in OpenGL for manipulating matrices. After that, we give a mathematical derivation of the rotation matrices needed in 3-space and give a proof of Euler's theorem.

II.3.1 Moving from 2-space to 3-space

In 3-space, points, or vectors, are triples $\langle x_1, x_2, x_3\rangle$ of real numbers. We denote 3-space by $\mathbb{R}^3$ and use the notation $\mathbf{x}$ for a point, with it being understood that $\mathbf{x} = \langle x_1, x_2, x_3 \rangle$. The origin, or zero vector, now is $\mathbf{0} = \langle 0, 0, 0 \rangle$. As before, we will identify $\langle x_1, x_2, x_3 \rangle$ with the column vector with the same entries. By convention, we always use a "righthanded" coordinate system, as shown in Figure I.4 on page 7.[8] This means that if you position your right hand so that your thumb points along the x-axis and your index finger is extended straight and points along the y-axis, then your palm will be facing in the positive z-axis direction. It also means that vector cross products are defined with the righthand rule. As discussed in Section I.2, it is common in computer graphics applications to visualize the x-axis as pointing to the right, the y-axis as pointing upwards, and the z-axis as pointing towards you.

Homogeneous coordinates for points in $\mathbb{R}^3$ are vectors of four numbers. The homogeneous coordinates $\langle x, y, z, w \rangle$ represents the point $\langle x/w, y/w, z/w \rangle$ in $\mathbb{R}^3$. The 2-dimensional projective geometry described in Section II.2.8 can be straightforwardly extended to a 3-dimensional geometry, by adding a "plane at infinity": each line has a single point at infinity, and each plane has a line of points at infinity. (See Section II.3.8 for more on projective geometry.)

A *transformation* on $\mathbb{R}^3$ is any mapping from $\mathbb{R}^3$ to $\mathbb{R}^3$. The definition of a *linear transformation* on $\mathbb{R}^3$ is identical to the definition used for $\mathbb{R}^2$, except that now the vectors $\mathbf{x}$ and $\mathbf{y}$ range over $\mathbb{R}^3$. Similarly, the definitions of *translation* and of *affine transformation* are word-for-word identical to the definitions given for $\mathbb{R}^2$, except that now the translation vector $\mathbf{u}$ is in $\mathbb{R}^3$. In particular, an affine transformation is still defined as the composition of a translation and a linear transformation.

Every linear transformation A in $\mathbb{R}^3$ can be represented by a 3×3 matrix M as follows. Let $\mathbf{i} = \langle 1, 0, 0 \rangle$, $\mathbf{j} = \langle 0, 1, 0 \rangle$, and $\mathbf{k} = \langle 0, 0, 1 \rangle$, and let $\mathbf{u} = A(\mathbf{i})$, $\mathbf{v} = A(\mathbf{j})$, and $\mathbf{w} = A(\mathbf{k})$. Set M equal to the matrix $(\mathbf{u}, \mathbf{v}, \mathbf{w})$, i.e., the matrix whose columns are $\mathbf{u}$, $\mathbf{v}$, and $\mathbf{w}$, so

$$M = \begin{pmatrix} u_1 & v_1 & w_1 \\ u_2 & v_2 & w_2 \\ u_3 & v_3 & w_3 \end{pmatrix}. \tag{II.9}$$

Then $M\mathbf{x} = A(\mathbf{x})$ for all $\mathbf{x} \in \mathbb{R}^3$, that is to say, M represents A. In this way, any linear transformation of $\mathbb{R}^3$ can be viewed as being a 3×3 matrix. (Compare this to the analogous construction for $\mathbb{R}^2$ explained at the beginning of Section II.2.2.)

A *rigid* transformation is one that preserves the size and shape of an object, and changes only its position and orientation. Formally, a transformation A is defined to be rigid provided it preserves distances between points and preserves angles between lines. Recall that the length of a vector $\mathbf{x}$ is equal to $||\mathbf{x}|| = \sqrt{\mathbf{x} \cdot \mathbf{x}} = \sqrt{x_1^2 + x_2^2 + x_3^2}$. An equivalent definition of rigidity is that a transformation A is rigid if it preserves dot products, that is to say, if $A(\mathbf{x}) \cdot A(\mathbf{y}) = \mathbf{x} \cdot \mathbf{y}$ for all $\mathbf{x}, \mathbf{y} \in \mathbb{R}^3$. It is not hard to prove that $M = (\mathbf{u}, \mathbf{v}, \mathbf{w})$ represents a rigid transformation if and only if $||\mathbf{u}|| = ||\mathbf{v}|| = ||\mathbf{w}|| = 1$ and

[8] The only exception is that in "screen space coordinates" where z represents a depth value, it is usual to use a left-handed coordinate system.

$\mathbf{u} \cdot \mathbf{v} = \mathbf{v} \cdot \mathbf{w} = \mathbf{u} \cdot \mathbf{w} = \mathbf{0}$. From this, it is straightforward to show that M represents a rigid transformation if and only if $M^{-1} = M^{\mathrm{T}}$ (c.f. Exercises II.7 and II.8 on page 48).

We define an *orientation preserving* transformation to be one which preserves "righthandedness." Formally, we say that A is orientation preserving provided that $(A(\mathbf{u}) \times A(\mathbf{v})) \cdot A(\mathbf{u} \times \mathbf{v}) > 0$ for all noncollinear $\mathbf{u}, \mathbf{v} \in \mathbb{R}^3$. By recalling the righthand rule used to determine the direction of a cross product, you should be able to convince yourself that this definition makes sense.

Exercise II.20. Let $M = (\mathbf{u}, \mathbf{v}, \mathbf{w})$ be a 3×3 matrix. Prove that $\mathit{det}(M)$ is equal to $(\mathbf{u} \times \mathbf{v}) \cdot \mathbf{w}$. Conclude that M represents an orientation preserving transformation if and only if $\mathit{det}(M) > 0$. Also, prove that if $\mathbf{u}$ and $\mathbf{v}$ are unit vectors which are orthogonal to each other, then setting $\mathbf{w} = \mathbf{u} \times \mathbf{v}$ makes $M = (\mathbf{u}, \mathbf{v}, \mathbf{w})$ a rigid, orientation preserving transformation.

Any affine transformation is the composition of a linear transformation and a translation. Since a linear transformation can be represented by a 3×3 matrix, any affine transformation can be represented by a 3×3 matrix and a vector in $\mathbb{R}^3$ representing a translation amount. That is, any affine transformation A can be written as:

$$A \; : \; \begin{pmatrix} x \\ y \\ z \end{pmatrix} \mapsto \begin{pmatrix} a & b & c \\ d & e & f \\ g & h & i \end{pmatrix} \begin{pmatrix} x \\ y \\ z \end{pmatrix} + \begin{pmatrix} u \\ v \\ w \end{pmatrix},$$

so that $A(\mathbf{x}) = B(\mathbf{x}) + \mathbf{u}$ where B is the linear transformation with matrix representation

$$\begin{pmatrix} a & b & c \\ d & e & f \\ g & h & i \end{pmatrix},$$

and $\mathbf{u}$ is the vector $\langle u, v, w \rangle$. We can rewrite this using a single 4×4 homogeneous matrix which acts on homogeneous coordinates, as follows:

$$\begin{pmatrix} x \\ y \\ z \\ 1 \end{pmatrix} \mapsto \begin{pmatrix} a & b & c & u \\ d & e & f & v \\ g & h & i & w \\ 0 & 0 & 0 & 1 \end{pmatrix} \begin{pmatrix} x \\ y \\ z \\ 1 \end{pmatrix}$$

This 4×4 matrix contains the matrix representing linear transformation B in its upper left 3×3 submatrix and the translation vector $\mathbf{u}$ in the upper three entries of the last column. Thus, affine transformations can be identified with 4×4 matrices with bottom row $(0\ 0\ 0\ 1)$. When we study transformations for perspective, we shall see some nontrivial uses of the bottom row of a 4×4 homogeneous matrix, but for now, we are only interested in matrices whose fourth row is $(0, 0, 0, 1)$.

Simple examples of transformations in 3-space include translations $T_{\mathbf{u}}$, uniform scalings S_α and nonuniform scalings $S_{\mathbf{u}}$ where α is a scalar, and

$\mathbf{u} = \langle u_1, u_2, u_3 \rangle$. These have 4×4 matrix representations

$$T_{\mathbf{u}} = \begin{pmatrix} 1 & 0 & 0 & u_1 \\ 0 & 1 & 0 & u_2 \\ 0 & 0 & 1 & u_3 \\ 0 & 0 & 0 & 1 \end{pmatrix} \qquad S_\alpha = \begin{pmatrix} \alpha & 0 & 0 & 0 \\ 0 & \alpha & 0 & 0 \\ 0 & 0 & \alpha & 0 \\ 0 & 0 & 0 & 1 \end{pmatrix} \qquad S_{\mathbf{u}} = \begin{pmatrix} u_1 & 0 & 0 & 0 \\ 0 & u_2 & 0 & 0 \\ 0 & 0 & u_3 & 0 \\ 0 & 0 & 0 & 1 \end{pmatrix}.$$

Rotations in 3-space are considerably more complicated than in 2-space. The reason for this is that a rotation can be performed about any axis whatsoever. This includes not just rotations around the x-, y- and z-axes, but also rotations around an axis pointing in an arbitrary direction. A rotation which fixes the origin can be specified by giving a rotation axis $\mathbf{u}$ and a rotation angle θ, where the axis $\mathbf{u}$ can be any nonzero vector. We think of the base of the vector being placed at the origin, and the axis of rotation is the line through the origin parallel to the vector $\mathbf{u}$. The angle θ gives the amount of rotation. The *direction* of the rotation is determined by the *righthand rule*; namely, if one mentally grasps the vector $\mathbf{u}$ with one's right hand so that the thumb, when extended, is pointing in the direction of the vector $\mathbf{u}$, then one's fingers will curl around $\mathbf{u}$ pointing in the direction of the rotation. In other words, if one views the vector $\mathbf{u}$ head-on, namely looking down the axis of rotation in the opposite direction that $\mathbf{u}$ is pointing, then the rotation direction is counter-clockwise (for positive values of θ). A rotation of this type is denoted $R_{\theta,\mathbf{u}}$. By convention, the axis of rotation always passes through the origin, and thus the rotation fixes the origin. Figure II.22 on page 78 illustrates the action of $R_{\theta,\mathbf{u}}$ on a point $\mathbf{v}$. Clearly, $R_{\theta,\mathbf{u}}$ is a linear transformation and is rigid and orientation preserving.

The general formula for the matrix representation of the rotation $R_{\theta,\mathbf{u}}$ is quite complicated:

$$\begin{pmatrix} (1-c)u_1^2 + c & (1-c)u_1u_2 - su_3 & (1-c)u_1u_3 + su_2 & 0 \\ (1-c)u_1u_2 + su_3 & (1-c)u_2^2 + c & (1-c)u_2u_3 - su_1 & 0 \\ (1-c)u_1u_3 - su_2 & (1-c)u_2u_3 + su_1 & (1-c)u_3^2 + c & 0 \\ 0 & 0 & 0 & 1 \end{pmatrix}. \tag{II.10}$$

The formula (II.10) for $R_{\theta,\mathbf{u}}$ will be derived later in Section II.3.6. This complicated formula is not needed in common simple cases. In particular, it is easy to compute by hand the matrix representation of a rotation around the three xyz coordinate axes. For instance, $R_{\theta,\mathbf{j}}$ is represented by

$$\begin{pmatrix} \cos\theta & 0 & \sin\theta & 0 \\ 0 & 1 & 0 & 0 \\ -\sin\theta & 0 & \cos\theta & 0 \\ 0 & 0 & 0 & 1 \end{pmatrix}.$$

To calculate this matrix, you just need to notice that the images of the $\mathbf{i}$, $\mathbf{j}$ and $\mathbf{k}$ vectors are $R_{\theta,\mathbf{j}}(\mathbf{i}) = \langle \cos\theta, 0, -\sin\theta \rangle$, $R_{\theta,\mathbf{j}}(\mathbf{j}) = \mathbf{j}$, and $R_{\theta,\mathbf{j}}(\mathbf{k}) = \langle \sin\theta, 0, \cos\theta \rangle$. These three vectors form the columns of the upper left 3×3 submatrix in the matrix representation of $R_{\theta,\mathbf{j}}$.

Exercise II.21. What are the 4×4 matrix representations for $R_{\frac{\pi}{3},\mathbf{i}}$, $R_{-\frac{2\pi}{3},\mathbf{k}}$, and $R_{\frac{\pi}{4},-\mathbf{j}}$?

Section II.3.7 below shows that every rigid, orientation preserving, linear transformation in 3-space is a rotation. As a corollary, every rigid, orientation preserving, affine transformation can be (uniquely) expressed as the composition of a translation and a rotation about a line through the origin.

It is of course possible to have rotations about axes that do not pass through the origin. These are called "glide rotations" or "screw transformations", and are discussed in Section II.3.7.

II.3.2 A solar system example

This section illustrates how to use transformations to position objects in a solar system containing a sun, an earth and a moon. It uses a view matrix V to set the viewer's position, and multiple model matrices to position the sun, earth and moon. We'll describe this in terms of matrices first; the next section will give C++ code based on the *SolarModern* program available at the book's website.

We model the sun as placed at the origin, and the earth and moon lying in the xz-plane, as shown in Figure II.20. The earth has a circular orbit around the sun of orbital radius r_E. The moon has a circular orbit around the earth of orbital radius r_M. At some instant in time, the earth has orbited by θ_E radians as measured by the angle from the z-axis. And, the moon has orbited θ_M radians around the earth as measured by the angle from the line containing the centers of the sun and the earth. Finally, the earth has rotated φ radians on its axis. This is all pictured in Figure II.20 showing a top view of the solar system: in this view, the y-axis is pointing up out of the image towards the viewer, the z-axis is pointing downwards, and the x-axis is pointing rightwards.

We first give pseudo-code for placing the sun, earth and moon as shown in Figure II.20. After that, we describe how to modify the code to use the view matrix to position the solar system in front of the viewer. We will render the sun as a sphere of radius 1, the earth as a sphere of radius 0.7, and the moon as a sphere of radius 0.4. We let $\mathcal{S}$ denote a sphere of radius 1 centered at the origin; then $M(\mathcal{S})$ denotes $\mathcal{S}$ as transformed by a model matrix M.

Here is the pseudo-code for rendering the sun and the earth; it uses three modelview matrices, M_S, M_{E_0} and M_{E_1}. M_S is for the sun; M_{E_0} is for the earth-moon system; and M_{E_1} is for the earth.

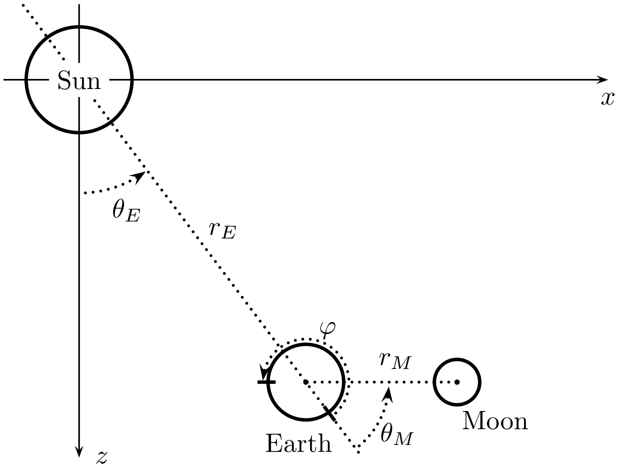

Figure II.20: A solar system with a sun, an earth, and a mooon. This is a top view, from a viewpoint looking down the y-axis, with the z-axis pointing downward, and the x-axis rightward. The sun is at the origin.

```
Set $M_S = Identity$.
Render $M_S(\mathcal{S})$.                // Render the sun
Set $M_{E_0} = M_S$.
Set $M_{E_0} = M_{E_0} \cdot R_{\theta_E,\mathbf{j}}$.          // Revolve around the sun.
Set $M_{E_0} = M_{E_0} \cdot T_{\langle 0,0,r_E \rangle}$.   // Translate to earth's orbit.
Set $M_{E_1} = M_{E_0}$.                  // Save $M_{E_0}$ for use with the moon.
Set $M_{E_1} = M_{E_1} \cdot R_{\varphi,\mathbf{j}}$.           // Rotate earth on its axis.
Set $M_{E_1} = M_{E_1} \cdot S_{0.7}$.          // Scale the earth smaller.
Render $M_{E_1}(\mathcal{S})$.              // Render the earth
```

The second line of pseudo-code renders the sun as transformed by only the identity matrix, hence as a unit sphere at the origin. The final line renders the earth as a unit sphere transformed by the matrix $R_{\theta_E,\mathbf{j}} \cdot T_{\langle 0,0,r_E \rangle} \cdot R_{\varphi,\mathbf{j}} \cdot S_{0.7}$. The effect of the final two matrices, $R_{\varphi,\mathbf{j}} \cdot S_{0.7}$ is to rotate the earth on its axis and scale it by the factor 0.7. These two operations commute, so they could be have equivalently been applied in the reverse order. The first matrices, $R_{\theta_E,\mathbf{j}} \cdot T_{\langle 0,0,r_E \rangle}$, have the effect of positioning the earth onto its orbit, and then revolving it around the sun. The order of the matrices is important of course, since rotations and translation in general do not commute. You should verify that these operations place the earth as illustrated in Figure II.20: the constructions are very similar to the methods used in Section II.2.6 to position the "F" shapes.

The next block of pseudo-code positions the moon. It uses M_m as a modelview matrix for the moon, and bases it off the model matrix M_{E_0} for the earth-system.

```
Set $M_m = M_{E_0}$ .                      // Copy earth-system matrix.
Set $M_m = M_m \cdot R_{\theta_M,\mathbf{j}}$ .          // Revolve around the earth.
Set $M_m = M_m \cdot T_{\langle 0,0,r_M \rangle}$ .      // Translate to the moon's orbit.
Set $M_m = M_m \cdot S_{0.4}$ .             // Scale the moon smaller.
Render $M_m(\mathcal{S})$ .                  // Render the moon
```

This has the effect of rendering the moon as a unit sphere at the origin, but transformed by the matrix

$$R_{\theta_E,\mathbf{j}} \cdot T_{\langle 0,0,r_E \rangle} \cdot R_{\theta_M,\mathbf{j}} \cdot T_{\langle 0,0,r_M \rangle} \cdot S_{0.4}.$$

The point of basing the model matrix M_m for the moon off of M_{E_0} instead of the model matrix M_{E_1} for the earth is that this means that the moon is not affected by the matrices that rotated and scaled the earth.

So far we have discussed only the model matrices; it is also necessary compute also a view matrix.[9] The purpose of the view matrix is to position the scene in front of the viewer to that we render the correct part of the scene. The usual convention in OpenGL is that the viewer is positioned at the origin looking in the direction of the negative z-axis. The view matrix is used to place the scene in front of the viewer; for this, the center of the viewed scene should be placed on the negative z-axis.

We give some sample code that makes the sun the center of the view. The viewer will be placed slightly above the xz-plane so that the viewer is looking slightly downward with the sun in the center of the view. The view matrix V is set with the following code:

```
Set $V = \textit{Identity}$ .
Set $V = V \cdot T_{\langle 0,0,-30 \rangle}$ .      // Translate 30 units down the $-z$ axis.
Set $V = V \cdot R_{\pi/20,\mathbf{i}}$ .          // Tilt the solar system down about $16^\circ$ .
```

The rotation $R_{\pi/20,\mathbf{i}}$ rotates the solar system down approximately 16°: the rotation holds the x-axis fixed, and moves the front of the solar system downward and the back of the solar system upward. The translation $T_{\langle 0,0,-25 \rangle}$ pushes the solar system away, so that its center (the sun) is 25 units in front of the viewer.

The view matrix V is sometimes incorporated in the modelview matrix M, and sometimes calculated as a separate matrix. In the former case, the vertex shader uses the modelview matrix in the calculation of the position `gl_Position` of the vertex. (It also uses the projection matrix.) In the latter case, the vertex shader receives separate V and M matrices, and applies them both to calculate `gl_Position`.

When incorporating the view matrix V into the modelview matrices, the first line of pseudo-code above changes from `Set` $M = \textit{Identity}$ to `Set` $M = V$.

[9] There is almost always also a projection matrix, which controls the field of view and depth of field of the viewer. This will be discussed later in this chapter.

This is the method used in the *SolarModern*, whose code is discussed in the next section.

II.3.3 Transformations and OpenGL

This section describes how the model and view matrices can be used with a C++/OpenGL program. The older "legacy" or "immediate mode" OpenGL system had built-in methods (called the "fixed function pipeline") for working with modelview and projection matrices, including using a stack for hierarchial use of modelview matrices, and automatic application of modelview and projection matrices. Much of this fixed function pipeline has been removed in the "modern" OpenGL system. In modern OpenGL, a programmer must maintain all matrices the C++ code, plus must program the GPU shader programs to correctly apply the matrices. This removes a lot of the built-in functionality that was supported in legacy OpenGL, but has the advantage of providing the programmer much more flexibility and customizability.

Nonetheless, a lot of the features of legacy of OpenGL are still used in modern OpenGL systems. For instance, although it is not required to use the modelview and projection matrices in the same way they were used in OpenGL, it is still common to use the same general approach, albeit now explicitly coded into the shader programs. We will illustrate this with some code fragments from the *SolarModern* program.

First though, we describe the *GlLinearMath* software, available from the book's website that we use for handling matrices and vectors. We then describe how matrices are given a shader program as a uniform variable. At the same time, for completeness, we show how colors are given to a vertex shader as a generic attribute. After that, we present some code fragments from *SolarModern*.

The *GlLinearMath* package. The *GlLinearMath* package contains full-featured support for C++ classes encapsulating vectors and matrices over $\mathbb{R}^2$, $\mathbb{R}^3$ and $\mathbb{R}^4$. We describe only a small set of its features here. The main C++ class we use is the `LinearMapR4` class, which defines 4×4 matrices. It includes special functions for reproducing the functionality of the functions `glTranslatef`, `glRotatef`, `glScalef`, `glLoadMatrixf`, `glFrustum`, `glOrtho`, `gluPerspective` and `gluLookAt`, which are in legacy OpenGL but are no longer available in modern OpenGL.

The basic classes are `VectorR3`, `VectorR4` and `LinearMapR4`. Members of these classes are declared by

```
VectorR3 vec3;                  // A 3-vector
VectorR3 vec4;                  // A 4-vector
LinearMapR4 mat;                // A 4 × 4 matrix
```

To initialize the matrix `mat` to the identity, use

```
    mat.SetIdentity();
```

To set `mat` equal to the 4×4 translation matrix $T_{\mathbf{u}}$, where $\mathbf{u} = \langle u_1, u_2, u_3 \rangle$, use the command

```
    mat.Set_glTranslate( $u_1$ , $u_2$ , $u_3$ );
```

To multiply `mat` *on the right* by $T_{\mathbf{u}}$, use instead the command

```
    mat.Mult_glTranslate( $u_1$ , $u_2$ , $u_3$ );
```

To either set the matrix `mat` equal to the uniform scaling matrix S_α, or to multiply it on the right with S_α, use

```
    mat.Set_glScale( $\alpha$ );
```

or

```
    mat.Mult_glScale( $\alpha$ );
```

The corresponding commands for the nonuniform scaling $S_{\langle \alpha,\beta,\gamma \rangle}$ are

```
    mat.Set_glScale( $\alpha$ , $\beta$ , $\gamma$ );
    mat.Mult_glScale( $\alpha$ , $\beta$ , $\gamma$ );
```

To set the matrix `mat` equal to the rotation matrix $R_{\theta,\mathbf{u}}$, or to multiply it on the right by $R_{\theta,\mathbf{u}}$, use

```
    mat.Set_glRotate( $\theta$ , $u_1$ , $u_2$ , $u_3$ );
```

or

```
    mat.Mult_glRotate( $\theta$ , $u_1$ , $u_2$ , $u_3$ );
```

The vector $\mathbf{u} = \langle u_1, u_2, u_3 \rangle$ should be non-zero, but does not need to be a unit vector. `Set_glRotate` and `Mult_glRotate` normalize their input $\mathbf{u}$ before using the rotation matrix formula (II.10).

All of the "`Mult`" methods multiply on the right by the transformation matrix. There are no built-in methods for multiplying on the left; however, this can be done with explicit multiplication. For example, you multiply on left by $R_{\theta,\mathbf{u}}$ by using

```
    LinearMapR4 rotMat;
    rotMat.Set_glRotate( $\theta$ , $u_1$ , $u_2$ , $u_3$ );
    mat = rotMat * mat;
```

The `glTranslate` and `glRotate` methods can also take a `VectorR3` argument. For example, if we first initialize a vector with

```
     VectorR3 uVec( $u_1$ , $u_2$ , $u_3$ );
```

then the `Mult_glTranslate` and `Mult_glRotate` commands above can be equivalently expressed as

```
    mat.Mult_glTranslate( uVec );
```

and

```
    mat.Mult_glRotate( θ, uVec );
```

Neither legacy OpenGL nor *GlLinearMath* have special functions for reflections or shearing transformations. A reflection transformation is a transformation which transforms points to their "mirror image" across some plane, as illustrated in Figures II.3f and II.39. A reflection across the coordinate planes can easily be done with a nonuniform scaling. For example, $S_{\langle -1,1,1\rangle}$ performs a reflection across the yz-plane by negating the x-coordinate of a point. Reflections across other planes can in principle be done by combining $S_{\langle -1,1,1,\rangle}$ with rotations, but this would generally be unnecessarily complicated.

A *shearing* transformation is an even more complicated kind of transformation; a two dimensional example is shown in Figure II.3e. In principle, one can use nonuniform scalings in combination with rotations to perform arbitrary shearing transformations. In practice, this is usually difficult and much more trouble than it is worth. It is often much more efficient and convenient to just explicitly give the components of a 4×4 matrix which perform any desired affine transformation. For example, the formulas from Exercises II.58 and II.59 below can be used to get the entries of a 4×4 matrix that carries out a reflection.

GlLinearMath has a number of methods to set the contents of a matrix explicitly. (These replace the legacy OpenGL `LoadMatrix` method.) The primary methods are the `Set` methods which set the 16 entries of the 4×4 matrix of a `LinearMapR4` in column order. These are used as

```
    mat.Set( m11, m21, m31, m41, m12, ..., m44 );
```

or

```
    mat.Set( uVec1, uVec2, uVec3, uVec4 );
```

where `uVec1`,`uVec2`,`uVec3`,`uVec4` are `VectorR4` objects. Again, these methods set the entries of `mat` by column order. There are similar `SetByRows` methods to set the entries in row order.

GlLinearMath also implements three legacy OpenGL methods for perspective transformations. These will be discussed later, in Section II.4.7. For the record, these functions are:

```
    Set_glOrtho( left, right, bottom, top, near, far );
    Set_glFrustum( left, right, bottom, top, near, far );
    Set_gluPerspective( fieldofview_y, aspectratio, near, far, );
```

GlLinearMath also implements a version of the `gluLookAt` function of legacy OpenGL, which makes it easy to position the viewpoint at an arbitrary location, looking in an arbitrary direction with an arbitrary orientation. The *GlLinearMath* function is invoked by

```
Set_gluLookAt( eyePos, lookAtPos, upDir);
```

The variables *eyePos*, *lookAtPos* and *upDir* are `VectorR3` objects. The vector *eyePos* specifies a location in 3-space for the viewpoint. The *lookAtPos* vector specifies the point in the center of the field of view. This of course should be different than the view position *eyePos*. The vector *upDir* specifies an upward direction for the y-axis of the viewer. It is not necessary for *upDir* vector to be orthogonal to the vector *eyePos* to *lookAtPos*, but it must not be parallel to it.

The `Set_gluLookAt` command should be used to set the set the view matrix or model matrix (not the projection matrix discussed later). This is to maintain the convention that the viewer should always be placed at the origin.

Exercise II.22. Modify the *SolarModern* program to use `Set_gluLookAt` to set the view matrix instead of calling `Set_glTranslate` and `Mult_glRotate`.

II.3.4 Uniform variables and generic vertex attributes.

After the C++ program has computed the matrices needed for rendering, they need to be sent to the shader program so that they can be used to transform vertices within the shader program. This is typically done by making the matrices a “uniform variable” in the shader program.

Chapter I described using vertex attributes that were specified on a per-vertex basis and stored in a VBO. Transformation matrices, however, are typically fixed for a large number of vertices. For example, when rendering a sphere, the VBO might hold the vertices for a unit sphere centered at the origin, and the transformation matrices would be used to position the sphere’s vertices for rendering. Since the same matrices are used for all the vertices of the sphere, it would make no sense to store the matrices on a per-vertex basis.

OpenGL provides two ways to provide data to a shader program that is the same for a range of vertices: *generic vertex attributes* and *uniform variables.* Generic vertex attributes are available as inputs only to the vertex shader, but not to the fragment shader or other shaders. On the other hand, uniform variables are available as inputs to all the shaders, including both the vertex shader and the fragment shader.

Generic vertex attributes are specified with the `glVertexAttrib` family of commands. An example of this will be shown in the C++ solar system code below to set the color of the spheres. Uniform variables are set with the `glUniform` family of commands. This will be illustrated by using the `glUniformMatrix4f` command to load a 4×4 modelview matrix into the shader.

Let’s start with the vertex shader code used by the *SolarModern* program.

```
#version 330 core
layout (location = 0) in vec3 vertPos;     // Input position
layout (location = 1) in vec3 vertColor;   // Input color
out vec3 theColor;                         // Output color
uniform mat4 projectionMatrix;    // The projection matrix
uniform mat4 modelviewMatrix;     // The model-view matrix
void main() {
    gl_Position = projectionMatrix * modelviewMatrix *
                    vec4(vertPos.x, vertPos.y, vertPos.z, 1.0);
    theColor = vertColor;
}
```

The vertex shader has two vertex attributes as input, `vertPos` and `vertColor`. The `vertPos` values are given on a per-vertex basis, obtained from the VBO. The `vertColor` is a generic vertex attribute and will be specified by a `glVertexAttrib3f` command; it is the same for many vertices. Note that the vertex shader does not distinguish between generic vertex attributes and per-vertex vertex attributes. Indeed, it is possible that the same variable is a generic vertex attribute for some VAO's and a per-vertex attribute for other VAO's.

There are also two uniform inputs, the `projectionMatrix` and the `modelviewMatrix`. These matrices are also the same for many vertices at a time. As uniform variables, they are available as inputs to both the vertex shader and the fragment shader; however, the *SolarModern* program uses them only in the vertex shader. Nonetheless it is traditional to specify matrices as uniform inputs instead of generic vertex attributes, since some applications such as Phong interpolation need to access the matrices in the fragment shader.[10]

An example of how to set a generic vertex attribute can be found in the *SolarModern* program:

```
unsigned int vertColor_loc = 1;
glVertexAttrib3f(vertColor_loc, 1.0f, 1.0f, 0.0f);
```

The effect of this command is that a vertex shader program accessing the variable at location `vertColor_loc` will use the value $\langle 1, 1, 0 \rangle$ (representing bright yellow).[11] This happens unless `glEnableVertexAttribArray` has been used to tell the VAO to take the vertex attribute from the VBO.

A uniform matrix variable is set by the commands below. The input to `glUniformMatrix4fv` is an array of single precision floating point numbers (`float`'s). The *GlLinearMath* package works with double precision numbers so

[10] It would possible to for the matrices to be generic inputs in the *SolarModern* program, but OpenGL makes this awkward as it would require the matrix to be loaded column-by-column with four calls to `glVertexAttrib4f`.

[11] This code example hard-codes the location of `vertColor` as 1. If this cannot be hard-coded for some reason, it is also possible to use `glGetAttribLocation` to get the location for the vertex attribute `vertColor`.

it is necessary to first dump out the matrix entries into an array of 16 `float`'s. The matrix `mat` is the modelview matrix.

```
unsigned int vertColor_loc = 1;
int modelviewMatLocation = glGetUniformLocation(shaderProgram1,
                                                "modelviewMatrix");
float matEntries[16];
...
glUseProgram(shaderProgram1);
...
mat.DumpByColumns(matEntries);
glUniformMatrix4fv(modelviewMatLocation, 1, false, matEntries);
```

The shader program is the compiled program containing both the vertex shader and the fragment shader. It is set as the current shader program by the command `glUseProgram`. The `glUniformMatrix4fv` command sets the uniform variable in only the current shader program.

Unfortunately, the more commonly used versions of OpenGL do not allow hard-coding the locations of uniform variables. Thus the function `glGetUniformLocation` must be used to get the location of the uniform variable based on its name.

There are a lot of different forms of the `glVertexAttrib` and `glUniform` commands; for these, see the OpenGL documentation.

II.3.5 Solar system in OpenGL

The *SolarModern* program creates a simple solar system with a central yellow sun, a blue planet revolving around the sun every 365 days, and a moon revolving around the planet 12 times per (simulated) year. In addition, the planet rotates on its axis once per day, i.e., once per 24 hours. The planets are drawn as wire spheres, using the *GlGeomSpheres* C++ class.

Figure II.21 shows the code fragments of the *SolarModern* C++ code that deal with the modelview matrix and set the uniform variables and generic vertex attributes. This uses the OpenGL features discussed in the last two section, and follows the pseudo-code of Section II.3.2. The complete *SolarModern* program and its documentation is available at the book's website.

Exercise II.23. Review the `Solar` program and understand how it works. Try making some of the following extensions to create a more complicated solar system.

a. Add one or more planets.

b. Add more moons. Make a geostationary moon, which always stays above the same point on the planet. Make a moon with a retrograde orbit. (A retrograde orbit means the moon revolves opposite to the usual direction, that is, in the clockwise direction instead of counter-clockwise.)

```
int modelviewMatLocation = glGetUniformLocation(shaderProgram1,
                                                "modelviewMatrix");
float matEntries[16];

viewMatrix.Set_glTranslate(0.0, 0.0, -CameraDistance);
viewMatrix.Mult_glRotate(viewAzimuth, 1.0, 0.0, 0.0);

glUseProgram(shaderProgram1);
LinearMapR4 SunPosMatrix = viewMatrix;
SunPosMatrix.DumpByColumns(matEntries);
glUniformMatrix4fv(modelviewMatLocation, 1, false, matEntries);
glVertexAttrib3f(vertColor_loc, 1.0f, 1.0f, 0.0f); // Yellow
Sun.Render();

LinearMapR4 EarthPosMatrix = SunPosMatrix;
double revolveAngle = (DayOfYear / 365.0)*PI2;
EarthPosMatrix.Mult_glRotate(revolveAngle, 0.0, 1.0, 0.0);
EarthPosMatrix.Mult_glTranslate(0.0, 0.0, 5.0);
LinearMapR4 EarthMatrix = EarthPosMatrix;
double earthRotationAngle = (HourOfDay / 24.0)*PI2;
EarthMatrix.Mult_glRotate(earthRotationAngle, 0.0, 1.0, 0.0);
EarthMatrix.Mult_glScale(0.5);
EarthMatrix.DumpByColumns(matEntries);
glUniformMatrix4fv(modelviewMatLocation, 1, false, matEntries);
glVertexAttrib3f(vertColor_loc, 0.2f, 0.4f, 1.0f); // Cyan-blue
Earth.Render();

LinearMapR4 MoonMatrix = EarthPosMatrix;
double moonRotationAngle = (DayOfYear*12.0 / 365.0)*PI2;
MoonMatrix.Mult_glRotate(moonRotationAngle, 0.0, 1.0, 0.0);
MoonMatrix.Mult_glTranslate(0.0, 0.0, 1.0);
MoonMatrix.Mult_glScale(0.2);
MoonMatrix.DumpByColumns(matEntries);
glUniformMatrix4fv(modelviewMatLocation, 1, false, matEntries);
glVertexAttrib3f(vertColor_loc, 0.9f, 0.9f, 0.9f); // Bright gray
Moon1.Render();
```

Figure II.21: Selected *SolarModern* code, showing the use of the use of the modelview matrix and setting generic vertex attributes and uniform variables. See Sections II.3.2, II.3.3 and II.3.4 for discussions of how the code works.

c. Give the moon a satellite of its own.

d. Give the planet and its moon(s) a tilt. The tilt should be in a fixed direction. This is similar to the tilt of the Earth which causes the seasons. The tilt of the earth is always in the direction of the North Star, Polaris. Thus, during part of a year, the northern hemisphere tilts towards the sun, and during the rest of the year, the northern hemisphere tilts away from the sun.

e. Change the length of the year so that the planet revolves around the sun once every 365.25 days. Be sure not to introduce any discontinuities in the orientation of the planet at the end of a year.

f. Make the moon rotate around the planet every 29 days. Make sure there is no discontinuity in the moon's position at the end of a year.

II.3.6 Derivation of the rotation matrix

This section contains the mathematical derivation of formula (II.10) for the matrix representing a rotation, $R_{\theta,\mathbf{u}}$, through an angle θ around axis $\mathbf{u} = \langle u_1, u_2, u_3\rangle$. Recall that that formula for $R_{\theta,\mathbf{u}}$ was

$$\begin{pmatrix} (1-c)u_1^2+c & (1-c)u_1u_2-su_3 & (1-c)u_1u_3+su_2 & 0 \\ (1-c)u_1u_2+su_3 & (1-c)u_2^2+c & (1-c)u_2u_3-su_1 & 0 \\ (1-c)u_1u_3-su_2 & (1-c)u_2u_3+su_1 & (1-c)u_3^2+c & 0 \\ 0 & 0 & 0 & 1 \end{pmatrix}, \qquad \text{(II.10)}$$

where $c = \cos\theta$ and $s = \sin\theta$, and where $\mathbf{u}$ must be a unit vector. There is no loss of generality in assuming that $\mathbf{u}$ is a unit vector, since if not, it may be normalized by dividing by $||\mathbf{u}||$.

To derive Equation (II.10), let $\mathbf{v}$ be an arbitrary point and consider what $\mathbf{w} = R_{\theta,\mathbf{u}}(\mathbf{v})$ is equal to. For this, we split $\mathbf{v}$ into two components, $\mathbf{v}_1$ and $\mathbf{v}_2$, so that $\mathbf{v} = \mathbf{v}_1 + \mathbf{v}_2$, with $\mathbf{v}_1$ parallel to $\mathbf{u}$ and $\mathbf{v}_2$ orthogonal to $\mathbf{u}$. (Refer to Figure II.22.) The vector $\mathbf{v}_1$ is the projection of $\mathbf{v}$ onto the line of $\mathbf{u}$, and is equal to $\mathbf{v}_1 = (\mathbf{u}\cdot\mathbf{v})\mathbf{u}$, since the dot product $\mathbf{u}\cdot\mathbf{v}$ is equal to $||\mathbf{u}||\cdot||\mathbf{v}||\cos\varphi$ where φ is the angle between $\mathbf{u}$ and $\mathbf{v}$, and since $||\mathbf{u}|| = 1$.[12] We rewrite this as

$$\mathbf{v}_1 \;=\; (\mathbf{u}\cdot\mathbf{v})\mathbf{u} \;=\; \mathbf{u}(\mathbf{u}\cdot\mathbf{v}) \;=\; \mathbf{u}(\mathbf{u}^{\mathrm{T}}\mathbf{v}) \;=\; (\mathbf{u}\mathbf{u}^{\mathrm{T}})\mathbf{v}.$$

The above equation uses the fact that a dot product $\mathbf{u}\cdot\mathbf{v}$ can be rewritten as a matrix product $\mathbf{u}^{\mathrm{T}}\mathbf{v}$ (recall that our vectors are all column vectors) and the fact that matrix multiplication is associative. The product $\mathbf{u}\mathbf{u}^{\mathrm{T}}$ is the symmetric 3×3 matrix

$$\mathit{Proj}_{\mathbf{u}} \;=\; \mathbf{u}\mathbf{u}^{\mathrm{T}} \;=\; \begin{pmatrix} u_1 \\ u_2 \\ u_3 \end{pmatrix} (u_1 \;\; u_2 \;\; u_3) \;=\; \begin{pmatrix} u_1^2 & u_1u_2 & u_1u_3 \\ u_1u_2 & u_2^2 & u_2u_3 \\ u_1u_3 & u_2u_3 & u_3^2 \end{pmatrix}. \qquad \text{(II.11)}$$

[12] See Appendix A and Figure A.3 for a discussion of why $(\mathbf{v}\cdot\mathbf{u})\mathbf{u}$ gives the projection of $\mathbf{v}$ onto the unit vector $\mathbf{u}$.

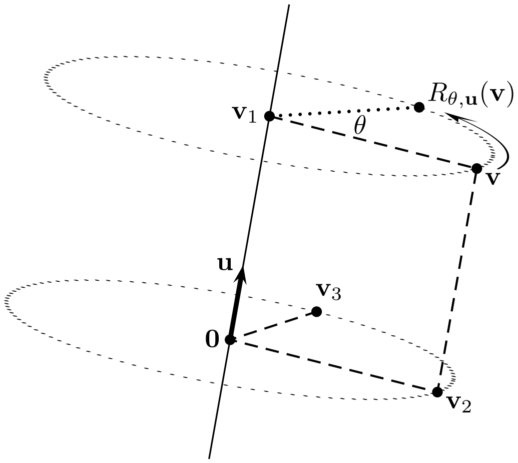

Figure II.22: The vector $\mathbf{v}$ being rotated around $\mathbf{u}$. The vector $\mathbf{v}_1$ is $\mathbf{v}$'s projection onto $\mathbf{u}$. The vector $\mathbf{v}_2$ is the component of $\mathbf{v}$ orthogonal to $\mathbf{u}$. The vector $\mathbf{v}_3$ is $\mathbf{v}_2$ rotated 90° around $\mathbf{u}$. The dashed line segments in the figure all meet at right angles.

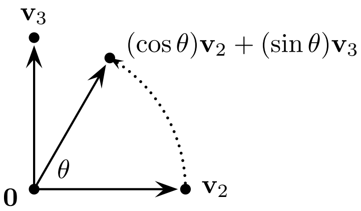

Figure II.23: The vector $\mathbf{v}_2$ being rotated around $\mathbf{u}$. This is the same situation as shown in Figure II.22, but viewed looking directly down the vector $\mathbf{u}$.

Since $\mathbf{v} = \mathbf{v}_1 + \mathbf{v}_2$, we therefore have

$$\mathbf{v}_1 \;=\; \mathit{Proj}_{\mathbf{u}}\mathbf{v} \qquad \text{and} \qquad \mathbf{v}_2 \;=\; (I - \mathit{Proj}_{\mathbf{u}})\mathbf{v},$$

where I is the 3×3 identity matrix.

We know that $R_{\theta,\mathbf{u}}(\mathbf{v}_1) = \mathbf{v}_1$, since $\mathbf{v}_1$ is a scalar multiple of $\mathbf{u}$ and is not affected by a rotation around $\mathbf{u}$. Thus $R_{\theta,\mathbf{u}}(\mathbf{v}) = \mathbf{v}_1 + R_{\theta,\mathbf{u}}(\mathbf{v}_2)$. In order to compute $R_{\theta,\mathbf{u}}(\mathbf{v}_2)$, we further define $\mathbf{v}_3$ to be the vector

$$\mathbf{v}_3 \;=\; \mathbf{u} \times \mathbf{v}_2 \;=\; \mathbf{u} \times \mathbf{v}.$$

The second equality holds since $\mathbf{v}$ and $\mathbf{v}_2$ differ by a multiple of $\mathbf{u}$. The vector $\mathbf{v}_3$ is orthogonal to both $\mathbf{u}$ and $\mathbf{v}_2$. Furthermore, since $\mathbf{u}$ is a unit vector orthogonal to $\mathbf{v}_2$, $\mathbf{v}_3$ has the same magnitude as $\mathbf{v}_2$. That is to say, $\mathbf{v}_3$ is equal to the rotation of $\mathbf{v}_2$ around the axis $\mathbf{u}$ through an angle of 90°.

Figure II.23 shows a view of $\mathbf{v}_2$ and $\mathbf{v}_3$ looking straight down the $\mathbf{u}$ axis of rotation. From the figure, it is obvious that rotating $\mathbf{v}_2$ through an angle of θ around $\mathbf{u}$ results in the vector

$$(\cos\theta)\mathbf{v}_2 + (\sin\theta)\mathbf{v}_3. \tag{II.12}$$

Therefore, $R_{\theta,\mathbf{u}}(\mathbf{v})$ is equal to

$$\begin{aligned} R_{\theta,\mathbf{u}}(\mathbf{v}) &= R_{\theta,\mathbf{u}}(\mathbf{v}_1) + R_{\theta,\mathbf{u}}(\mathbf{v}_2) \\ &= \mathbf{v}_1 + (\cos\theta)\mathbf{v}_2 + (\sin\theta)\mathbf{v}_3 \\ &= \mathit{Proj}_{\mathbf{u}}\mathbf{v} + (\cos\theta)(I - \mathit{Proj}_{\mathbf{u}})\mathbf{v} + (\sin\theta)(\mathbf{u}\times\mathbf{v}). \end{aligned}$$

To finish deriving the matrix for $R_{\theta,\mathbf{u}}$, we define the matrix

$$M_{\mathbf{u}\times} = \begin{pmatrix} 0 & -u_3 & u_2 \\ u_3 & 0 & -u_1 \\ -u_2 & u_1 & 0 \end{pmatrix} \tag{II.13}$$

and see, by a simple calculation, that $(M_{\mathbf{u}\times})\mathbf{v} = \mathbf{u}\times\mathbf{v}$ holds for all $\mathbf{v}$. From this, it is immediate that

$$\begin{aligned} R_{\theta,\mathbf{u}}(\mathbf{v}) &= [\mathit{Proj}_{\mathbf{u}} + (\cos\theta)(I - \mathit{Proj}_{\mathbf{u}}) + (\sin\theta)M_{\mathbf{u}\times}]\mathbf{v} \qquad \text{(II.14)} \\ &= [(1-\cos\theta)\mathit{Proj}_{\mathbf{u}} + (\cos\theta)I + (\sin\theta)M_{\mathbf{u}\times})]\mathbf{v}. \end{aligned}$$

The quantity inside the square brackets is a 3×3 matrix, so this completes the derivation of the matrix representation of $R_{\theta,\mathbf{u}}$. An easy calculation shows that this corresponds to the representation given earlier (in homogeneous form) by Equation (II.10).

Exercise II.24. Carry out the calculation to show that the formula (II.14) for $R_{\theta,\mathbf{u}}$ is equivalent to the formula in Equation (II.10).

Exercise II.25* Let $\mathbf{u}$, $\mathbf{v}$ and $\mathbf{w}$ be orthogonal unit vectors with $\mathbf{w} = \mathbf{u}\times\mathbf{v}$. Prove that $R_{\theta,\mathbf{u}}$ is represented by the following 3×3 matrix:

$$\mathbf{u}\mathbf{u}^{\mathrm{T}} + (\cos\theta)(\mathbf{v}\mathbf{v}^{\mathrm{T}} + \mathbf{w}\mathbf{w}^{\mathrm{T}}) + (\sin\theta)(\mathbf{w}\mathbf{v}^{\mathrm{T}} - \mathbf{v}\mathbf{w}^{\mathrm{T}}).$$

[Hint: For any vector $\mathbf{x}$, the values $\mathbf{u}^{\mathrm{T}}\cdot\mathbf{x}$, $\mathbf{v}^{\mathrm{T}}\cdot\mathbf{x}$ and $\mathbf{w}^{\mathrm{T}}\cdot\mathbf{x}$ are equal to the magnitudes of the projections of $\mathbf{x}$ onto the unit vectors $\mathbf{u}$, $\mathbf{u}$ and $\mathbf{w}$.]

It is also possible to convert a rotation matrix back into a unit rotation vector $\mathbf{u}$ and a rotation angle θ. For this, suppose we are given a rotation matrix M, and want to find values for θ and $\mathbf{u}$ so that M is equal to the matrix $R_{\theta,\mathbf{u}}$ in Equation (II.10). The matrix is given to us as a 4×4 rotation matrix $M = (m_{i,j})_{i,j}$ so that the entry in row i and column j is $m_{i,j}$. By (II.10). the sum of the first three entries on the diagonal of M (that is to say, the trace of the 3×3 submatrix representing the rotation) is equal to

$$m_{1,1} + m_{2,2} + m_{3,3} = (1-c) + 3c = 1 + 2c$$

since $u_1^2 + u_2^2 + u_3^2 = 1$. Thus, $\cos\theta = (m_{1,1} + m_{2,2} + m_{3,3} - 1)/2$, or

$$\theta = \arccos(\alpha/2), \tag{II.15}$$

where $\alpha = m_{1,1} + m_{2,2} + m_{3,3} - 1$. Letting $s = \sin\theta$, we can determine $\mathbf{u}$'s components from:

$$\begin{aligned} u_1 &= \frac{m_{3,2} - m_{2,3}}{2s} \\ u_2 &= \frac{m_{1,3} - m_{3,1}}{2s} \\ u_3 &= \frac{m_{2,1} - m_{1,2}}{2s}. \end{aligned} \tag{II.16}$$

Equations (II.15) and (II.16) give a method to computing θ and $\mathbf{u}$ from M. However, this calculation will have problems with numerical instability if θ is very close to 0 since, in that case, $\sin\theta \approx 0$, and then the determination of the values of u_i requires dividing by values near zero. The problem is that dividing by a near-zero value tends to introduce unstable or inaccurate results, since small roundoff errors can have a large effect on the results of the division. This problem is compounded by the fact that for $\theta \approx 0$, we have $\alpha/2 \approx 1$, so the computation of $\arccos(\alpha/2)$ also loses accuracy.

Of course, if θ, and thus $\sin\theta$, are exactly equal to zero, then the rotation angle is zero and any vector $\mathbf{u}$ will work. Absent roundoff errors, this situation occurs only if M is the identity matrix.

To mitigate the problems caused dividing by a near-zero value, one should instead compute

$$\beta = \sqrt{(m_{3,2} - m_{2,3})^2 + (m_{1,3} - m_{3,1})^2 + (m_{2,1} - m_{1,2})^2}.$$

Note that β will equal $2s = 2\sin\theta$, since dividing by $2s$ in equations (II.16) was what was needed to normalize the vector $\mathbf{u}$. If β is zero, then the rotation angle θ is zero and, in this case, $\mathbf{u}$ may be an arbitrary unit vector. If β is nonzero, then

$$\begin{aligned} u_1 &= (m_{3,2} - m_{2,3})/\beta \\ u_2 &= (m_{1,3} - m_{3,1})/\beta \\ u_3 &= (m_{2,1} - m_{1,2})/\beta. \end{aligned}$$

This way of computing $\mathbf{u}$ makes it more likely that a (nearly) unit vector will be obtained for $\mathbf{u}$ when the rotation angle θ is near zero. From α and β, the angle θ can be computed as

$$\theta \;=\; \mathtt{atan2}(\beta, \alpha).$$

This is a more robust way to compute θ than using the arccos function.

For an alternative, and often better, method of representing rotations in terms of 4-vectors, see the parts of Section XIII.3 on quaternions (pages 456-467).

II.3.7 Euler's theorem

A fundamental fact about rigid, orientation preserving, linear transformations is that they are always equivalent to a rotation around an axis passing through the origin.

Theorem II.16. *If A is a rigid, orientation preserving, linear transformation of $\mathbb{R}^3$, then A is the same as some rotation $R_{\theta,\mathbf{v}}$.*

This theorem was formulated by Euler in 1776. We give a concrete proof based on symmetries; it is also possible to give a proof based on matrix properties.

Proof. The idea of the proof is similar to the proof of Theorem II.13, which showed that every rigid, orientation preserving, affine transformation is either a generalized rotation or a translation. However, now we shall consider the action of A on points on the unit sphere instead of on points in the plane.

Since A is rigid, unit vectors are mapped to unit vectors. In particular, A maps the unit sphere onto itself. In fact, it will suffice to show that A maps some point $\mathbf{v}$ on the unit sphere to itself, since if $\mathbf{v}$ is a fixed point, then A fixes the line through the origin containing $\mathbf{v}$. The rigidity and orientation preserving properties then imply that A is a rotation around this line, because the action of A on $\mathbf{v}$ and on a vector perpendicular to $\mathbf{v}$ determines all the values of A.

Assume that A is not the identity map. First, note that A cannot map every point $\mathbf{u}$ on the unit sphere to its antipodal point $-\mathbf{u}$, since otherwise, A would not be orientation preserving. Therefore, there is some unit vector $\mathbf{u}_0$ on the sphere such that $A(\mathbf{u}_0) \neq -\mathbf{u}_0$. Fix such a point, and let $\mathbf{u} = A(\mathbf{u}_0)$. If $\mathbf{u} = \mathbf{u}_0$, this is a fixed point and we are done. So suppose $\mathbf{u} \neq \mathbf{u}_0$. Let C be the great circle containing both $\mathbf{u}_0$ and $\mathbf{u}$, and let L be the shorter portion of C connecting $\mathbf{u}_0$ to $\mathbf{u}$, i.e., L is spanning less than 180° around the unit sphere. Let L' be the image of L under A and let C' be the great circle containing L'. Suppose that $L = L'$, i.e., that A maps this arc to itself. In this case, rigidity implies that A maps $\mathbf{u}$ to $\mathbf{u}_0$. Then, rigidity further implies that the point $\mathbf{v}$ midway between $\mathbf{u}_0$ and $\mathbf{u}$ is a fixed point of A, so A is a rotation around $\mathbf{v}$.

Otherwise, suppose $L \neq L'$. Let $\mathbf{w}$ and $\mathbf{w}'$ be the midpoints of the arcs L and L'. Let C_2 be the great circle which is perpendicular to L at $\mathbf{w}$, and let C_2' be the great circle which is perpendicular to L' at $\mathbf{w}'$. Let $\mathbf{v}$ be the point where C_2 and C_2' intersect (they also intersect at $-\mathbf{v}$). The points on C_2 are equidistant from $\mathbf{u}_0$ and $\mathbf{u}$; similarly the points on C_2' are equidistant from $\mathbf{u}$ and $\mathbf{u}'$. Therefore $\mathbf{v}$ is equidistant from all three of $\mathbf{u}_0$, $\mathbf{u}$ and $\mathbf{u}'$. It is also equidistant from $\mathbf{w}$ and $\mathbf{w}'$.

By the rigidity and orientation-preserving properties, A maps C_2 to C_2' and $\mathbf{v}$ is a fixed point of A. Thus, A is a rotation around the vector $\mathbf{v}$. □

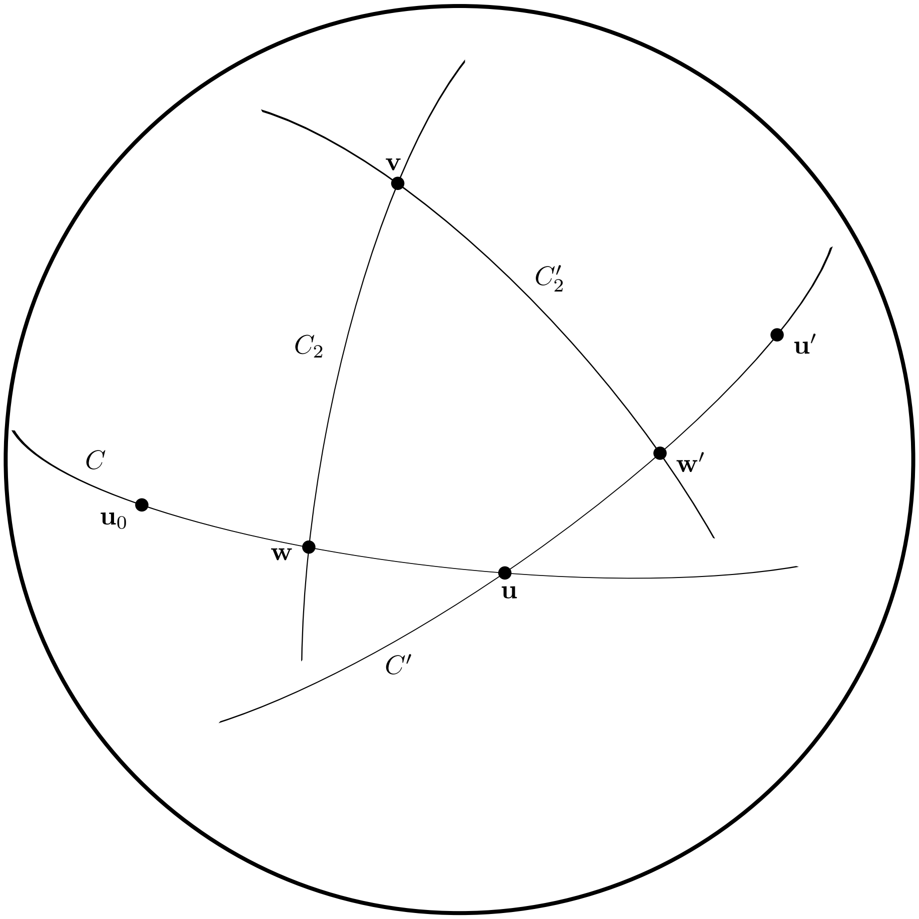

Figure II.24: Finding the axis of rotation around the fixed point $\mathbf{v}$. The image shows the unit sphere. We have $\mathbf{u}_0 = A(\mathbf{u})$ and $A(\mathbf{u}) = \mathbf{u}'$ and $\mathbf{v} = A(\mathbf{v})$. C, C', C_2 and C_2' are great circles. L is the shorter portion of C joining u_0 to u, and L' is the shorter portion of C' joining u to u'. $\mathbf{w}$ and $\mathbf{w}'$ are the midpoints of L and L'. At $\mathbf{w}$ and $\mathbf{w}'$, the great circles meet at right angles. Compare this with Figure II.11.

Exercise II.26. Give a different proof of Euler's Theorem (Theorem II.16) using matrices instead of a geometric argument. [Hint: The Wikipedia page on "Euler's rotation theorem" (as of October 2022) gives a short direct matrix-based proof in which the key step is to show that the matrix associated with a rigid, orientation preserving transformation has an eigenvalue equal to 1. It is not hard to translate that proof into our conventions.]

One can define a *generalized rotation* in 3-space to be a transformation $R^{\mathbf{v}}_{\theta,\mathbf{u}}$ which performs a rotation through angle θ around the line L, where L is the line which contains the point $\mathbf{v}$ and is parallel to $\mathbf{u}$. However, unlike the situation for 2-space (see Theorem II.13), it is not the case that every rigid, orientation preserving, affine transformation in 3-space is equivalent to either a translation or a generalized rotation of this type. Instead, we need a more general notion of "glide rotation", also called a "screw transformation" since it creates a motion similar to a wood screw or sheet metal screw which simultaneously rotates on its central axis and translates on the same axis. For example, consider a transformation which both rotates around the y-axis and translates along the y-axis.

More formally, a *glide rotation* is a mapping which can be expressed as a translation along an axis $\mathbf{u}$ composed with a rotation $R^{\mathbf{v}}_{\theta,\mathbf{u}}$ along the line which contains $\mathbf{v}$ and is parallel to $\mathbf{u}$.

Exercise II.27$^{\bigstar}$ Prove that every rigid, orientation preserving, affine transformation is a glide rotation. (This is the "Mozzi-Chasles theorem", formulated by Mozzi in 1763, and by Chasles in 1830.) [Hint: Suppose A is not a translation. First consider A's action on planes, and define a linear transformation B as follows: let $\mathbf{r}$ be a unit vector perpendicular to a plane P, and define $B(\mathbf{r})$ to be the unit vector perpendicular to the plane $A(P)$. B is a rigid, orientation preserving map on the unit sphere. Furthermore, $B(\mathbf{r}) = A(\mathbf{r}) - A(\mathbf{0})$, so B is a linear transformation. By Euler's theorem, B is a rotation. Let $\mathbf{w}$ be a unit vector fixed by B, and let Q be the plane through the origin perpendicular to $\mathbf{w}$, so $A(Q)$ is parallel to Q. Let C be a transformation on Q defined by letting $C(\mathbf{x})$ be the value of $A(\mathbf{x})$ projected onto Q. Then C is a two dimensional, generalized rotation around a point $\mathbf{v}$ in the plane Q. (Why?) From this, deduce that A has the desired form.]

II.3.8 Three dimensional projective geometry$^{\bigstar}$

Three dimensional projective geometry can be developed analogously to the two dimensional geometry discussed in Section II.2.8, and three dimensional projective space can be viewed either as the usual three dimensional Euclidean space augmented with points at infinity, or as the space of linear subspaces of the four dimensional $\mathbb{R}^4$.

We first consider how to represent three dimensional projective space as $\mathbb{R}^3$ plus points at infinity. The new points at infinity are obtained as follows: let L be a line in $\mathbb{R}^3$, and let $\mathcal{F}$ be family of lines parallel to L. We have a new point at infinity, $\mathbf{u}_{\mathcal{F}}$, and this point is added to every line in $\mathcal{F}$. The three dimensional projective space consists of $\mathbb{R}^3$ plus these new points at infinity. Each plane P in $\mathbb{R}^3$ gets a new line of points at infinity in the projective space, namely the points at infinity that belong to the lines in the plane P. The set of lines of the projective space are (a) the lines of $\mathbb{R}^3$ (including their new point at infinity), and (b) the points at infinity on the lines lying in a single common plane. Finally, the set of all points at infinity forms the plane at infinity.

You should check that, in three dimensional projective space, any two distinct planes intersect in a unique line.

Three dimensional projective space can also be represented by linear subspaces of the four dimensional space $\mathbb{R}^4$. This corresponds to the representation of points in $\mathbb{R}^3$ by homogeneous coordinates. A point in the projective space is equal to a one dimensional subspace of $\mathbb{R}^4$, namely, a set of points of the form $\{\alpha\mathbf{u} : \alpha \in \mathbb{R}\}$ for $\mathbf{u}$ a *fixed* nonzero point of $\mathbb{R}^4$. The 4-tuple $\mathbf{u}$ is just a homogeneous representation of a point; if its fourth component (w-component) is zero, then the point is a point at infinity. The lines in projective space are just the two dimensional subspaces of $\mathbb{R}^4$. A line is a line at infinity if and only if all its 4-tuples have zero as fourth component. The planes in projective space are precisely the three dimensional subspaces of $\mathbb{R}^4$.

Exercise II.28. Work out the correspondence between the two ways of representing three dimensional projective space.

OpenGL and other similar systems use 4-tuples as homogeneous coordinates for points in 3-space extensively, by letting a 4-tuple $\langle a, b, c, d\rangle$ specify the point $\langle a/d, b/d, c/d\rangle$. Of course, when modelling shapes, it is more common for a programmer to specify a point with only three (not homogeneous) coordinates. But, internally, the OpenGL pipeline and the shader programs automatically convert points $\langle x, y, z\rangle$ to their homogeneous representation $\langle x, y, z, 1\rangle$.

3-D modelling programs often implicitly use homogeneous representations of points. This happens when a point $\langle x, y, z\rangle$ is given a weight w. Internally, the program will treat the point as having the homogeneous representation $\langle wx, wy, wz, w\rangle$. The homogeneous representation is usually hidden from the user, as it is more intuitive to think of the point as being placed at $\langle x, y, z\rangle$ and then given a weight w. It is necessary to use homogeneous coordinates in this way when forming circular and elliptical arcs. This is discussed later in Sections V.4, V.5 and especially VIII.13.

II.4 Projection transformations and perspective

So far, we have used affine transformations as a method for placing geometric models of objects in 3-space. This is represented by the first two stages of the rendering pipeline shown in Figure II.1 on page 37. In these stages, points are placed in 3-space, controlled by the model and view matrices.

We now turn our attention to the final stages of the pipeline. These stages deals with how the geometric model in 3-space is viewed; namely, the field of view of the camera or eye. Of course, there is no actual camera, it is only virtual; instead, transformations are used to map the geometric model in 3-space into the xy-plane of the final image. Transformations used for this purpose are called *viewing transformations.* Viewing transformations include not only the affine transformations discussed earlier, but also a new class of "perspective transformations."

To understand properly the purposes and uses of viewing transformations, it is necessary to consider the end result of the rendering pipeline (Figure II.1). The final output of the rendering pipeline is usually a rectangular array of pixels. Each pixel has an xy-position in the graphics image. In addition, each pixel has a color or grayscale value. Finally, each pixel to stores a "depth value" or "distance value" which measures the distance to the object visible in that pixel.

Storing the depth is important since it is used by the hidden surface algorithm. When rendering a scene, there may be multiple objects that lie behind a given pixel. As the objects are drawn onto the screen, the depth value, or distance, to the relevant part of the object is stored into each pixel location. By comparing depths, it can be determined whether one object is in front of another object, and thereby that the further object, being hidden behind the closer object, is not visible.

The use of the depth values is discussed more in Section III.3, but for now it is enough to keep in mind that it is important to keep track of the distances of objects from the camera position.

The last two stages of the rendering pipeline shown in Figure II.1 consist of multiplication by the projection matrix P and perspective division. These two stages generate *device independent screen coordinates* to specify the position of a vertex in the final image. The third stages uses a 4×4 projection matrix P to map vertices represented by homogeneous coordinates to new homogeneous coordinates $\langle x, y, z, w \rangle$. The final stage, *perspective division*, further transforms these points by converting them back to points in $\mathbb{R}^3$ by the usual map

$$\langle x, y, z, w \rangle \;\mapsto\; \langle x/w, y/w, z/w \rangle.$$

The end result of these two stages is to map the viewable objects into device independent screen coordinates. These coordinates must lie in the $2 \times 2 \times 2$ cube centered at the origin, which contains the points with $-1 \le x \le 1$, $-1 \le y \le 1$, and $-1 \le z \le 1$. The points with $x = 1$ (respectively, $x = -1$) are to be at the right (respectively, left) side of the screen or final image, and points with $y = 1$ (respectively, $y = -1$) are at the top (respectively, bottom) of the screen. Points with $z = -1$ are closest to the viewer and points with $z = 1$ are farthest from the viewer.[13]

[13] This convention on z means that now we are using a lefthand coordinate system instead of a righthand coordinate system, with the x-axis pointing rightward, the y-axis pointing upward, and the z-axis pointing away from the viewer. This is the common convention for OpenGL, so that $z = -1$ for the closest objects and $z = 1$ for the farthest objects. Since it is rare to use cross products in these screen space coordinates, this fact that this system is lefthanded does not usually cause any problems.

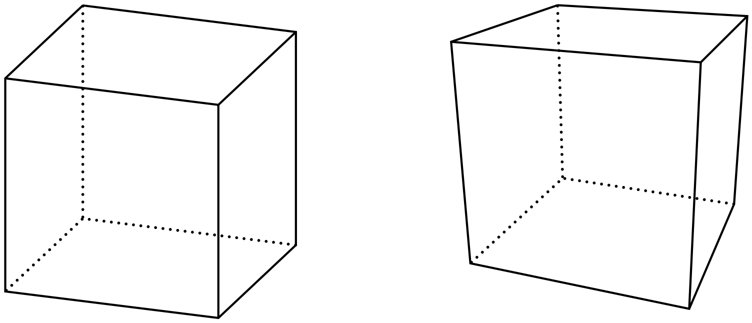

Figure II.25: The cube on the left is rendered with an orthographic projection. The one on the right with a perspective transformation. With the orthographic projection, the rendered size of a face of the cube is independent of its distance from the viewer; compare, for example, the front and back faces. Under a perspective transformation, the closer a face is, the larger it is rendered.

There are two kinds of viewing transformations: orthographic projections and perspective transformations. An orthographic projection acts similarly to placing the viewer at an infinite distance (with a suitable telescope). Thus orthographic projections map the geometric model by projecting at right angles onto a plane perpendicular to the view direction. Perspective transformations put the viewer at a finite position, and perspective makes closer objects appear larger than distant objects of the same size. The difference between orthographic and perspective transformations is illustrated in Figure II.25.

To simplify the definitions of orthographic and perspective transformations, it is convenient to define them only for a viewer who is placed at the origin and is looking in the direction of the negative z-axis. If the viewpoint is to be placed elsewhere or directed elsewhere, the view matrix should be used to perform ordinary affine transformations that adjust the view accordingly.

II.4.1 Orthographic viewing transformations

Orthographic viewing transformations carry out a parallel projection of a 3-D model onto a plane. Unlike the perspective transformations described later, orthographic viewing projections do not cause closer objects to appear larger and distant objects to appear smaller. For this reason, orthographic viewing projections are generally preferred for applications such as architecture or engineering applications, including computer aided design and manufacturing (CAD/CAM), since the parallel projection is better at preserving relative sizes and angles.

For convenience, orthographic projections are defined in terms of an observer who is at the origin and is looking down the z-axis in the negative z-direction. The view direction is perpendicular to the xy-plane, and if two points differ in only their z-coordinate, then the one with higher z-coordinate is closer to the viewer.

An orthographic projection is generally specified by giving six axis-aligned "clipping planes" which form a rectangular prism (a box shape). The orthographic projection transforms the rectangular prism by scaling it to have dimensions $2 \times 2 \times 2$ and translating it to be centered at the origin. The rectangular prism is specified by six values ℓ, r, b, t, n and f. These variable names are mnemonics for "left," "right," "bottom," "top," "near" and "far." The rectangular prism then consists of the points $\langle x, y, z\rangle$ such that

$$\begin{array}{rcccl} & \ell & \le & x & \le & r, \\ & b & \le & y & \le & t, \\ \text{and} & -f & \le & z & \le & -n. \end{array}$$

By convention that the viewer is looking down the z-axis, facing in the negative z direction. This means that the distance of a point $\langle x, y, z\rangle$ from the viewer is equal to $-z$. The plane $z = -n$ is called the *near clipping plane* and the plane $z = -f$ is called the *far clipping plane*. Objects which are closer than the near clipping plane or farther than the far clipping plane will be clipped or culled and not be rendered.

The orthographic projection must map points from the rectangular prism into the $2 \times 2 \times 2$ cube centered at the origin. This consists of, firstly, scaling along the coordinate axes and, secondly, translating so that the cube is centered at the origin. The x coordinate is scaled by a factor $2/(r - \ell)$ and then translated so that the x values ℓ and r are mapped to -1 and 1, respectively. Similarly, the y coordinate is scaled by a factor $2/(t-b)$ and then translated so that the y values b and t are mapped to -1 and 1, respectively. The z component is scaled by the factor $-2/(f-n)$ and translated so that the z values $-n$ and $-f$ are mapped to -1 and 1, respectively. The negative sign in the scaling factor for z is due to OpenGL's convention that depth values are increasing from -1 to 1 as objects are further away from the viewer. We leave it as exercise to figure out the translation amounts needed to center the $2 \times 2 \times 2$ cube. The resulting orthographic projection is given the following 4×4 matrix, which acts on homogeneous coordinates.

$$\begin{pmatrix} \dfrac{2}{r-\ell} & 0 & 0 & -\dfrac{r+\ell}{r-\ell} \\ 0 & \dfrac{2}{t-b} & 0 & -\dfrac{t+b}{t-b} \\ 0 & 0 & \dfrac{-2}{f-n} & \dfrac{f+n}{f-n} \\ 0 & 0 & 0 & 1 \end{pmatrix}. \tag{II.17}$$

Exercise II.29. Verify that the matrix (II.17) maps $\langle \ell, b, -n, 1\rangle$ and $\langle r, t, -f, 1\rangle$ to $\langle -1, -1, -1, 1\rangle$ and $\langle 1, 1, 1, 1\rangle$. This justifies the entries in the final column of (II.17).

II.4.2 Perspective viewing transformations

Perspective transformations are used when the camera or eye position is placed at a finite distance from the scene. The use of perspective means that the closer an object is to the viewer, the larger is will be displayed. Perspective is useful for giving the viewer the sense of being "in" a scene, since a perspective view shows the scene from a particular viewpoint. Perspective is heavily used in entertainment applications where it is desired to give an immersive experience; it is particularly useful in dynamic situations where the combination of motion and correct perspective gives a strong sense of the three dimensionality of the scene. It is also used in applications as diverse as computer games, animated movies and architectural modeling, to show the view from a particular viewpoint.

As was mentioned in Section II.2.8, perspective was originally discovered for applications in drawing and painting. An important principle in the classic theory of perspective is the notion of a "vanishing point" shared by a family of parallel lines. An artist who is incorporating perspective in a drawing will choose appropriate vanishing points to aid the composition of the drawing. In computer graphics applications, we are able to avoid all considerations of vanishing points, etc. Instead, we place objects in 3-space, choose a viewpoint (camera position), and mathematically calculate the correct perspective transformation to create the scene as viewed from the viewpoint.

To derive the mathematical formula for a perspective transformation, we consider a viewer who is placed at the origin looking down the negative z-axis. We mentally choose as a "viewscreen" the plane $z = -d$, which is parallel to the xy-plane at distance d from the viewpoint at the origin. Intuitively, the viewscreen serves as a display screen onto which viewable objects are projected. Let a vertex in the scene have position $\langle x, y, z\rangle$. We form the line from the vertex position to the origin, and calculate the point $\langle x', y', z'\rangle$ where the line intersects the viewscreen (see Figure II.26). Of course, we have $z' = -d$. Referring to Figure II.26 and arguing using similar triangles, we have

$$x' = \frac{d \cdot x}{-z} \qquad \text{and} \qquad y' = \frac{d \cdot y}{-z}. \tag{II.18}$$

The values x', y' give the position of the vertex as seen on the viewscreen from the viewpoint at the origin.

So far, projective transformations have been very straightforward, but now it is necessary to incorporate also the "depth" of the vertex, i.e., its distance from the viewer, since the depth information is needed for the hidden surface algorithm. An obvious first attempt would be to use the value $-z$ for the depth. Another, albeit less appealing, possibility would be to record the true distance $\sqrt{x^2 + y^2 + z^2}$ as the depth. Both of these ideas, however, fail to work well. The reason they fail to work well is that if perspective mappings are defined with a depth defined in either of these ways, then lines in the three dimensional scene can be mapped to curves in the viewscreen space. That is to say, a line of points with coordinates x, y, z, will map to a curve of points with coordinates x', y', z' that is not a line in the viewscreen space.

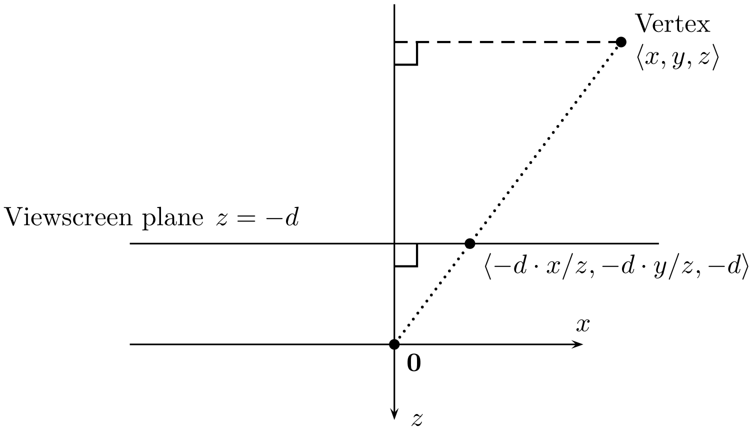
Vertex
$\langle x, y, z\rangle$
Viewscreen plane $z = -d$
$\langle -d\cdot x/z, -d\cdot y/z, -d\rangle$
x
$\mathbf{0}$
z

Figure II.26: Perspective projection onto a viewscreen at distance d. The viewer is at the origin, looking in the direction of the negative z axis. The point $\langle x, y, z\rangle$ is perspectively projected onto the plane $z = -d$, which is at distance d in front of the viewer at the origin.

An example of how a line can map to a curve is shown in Figure II.27. For this figure, we use the transformation

$$x \;\mapsto\; \frac{d\cdot x}{-z} \qquad y \;\mapsto\; \frac{d\cdot y}{-z} \qquad z \;\mapsto\; z \tag{II.19}$$

so that the z-coordinate directly serves a measure of depth. (Since the viewpoint is looking down the negative z-axis, greater values of z correspond to closer points.) In Figure II.27, we see points A, B, and C that are mapped by (II.19) to points A', B', and C'. Obviously, A and C are fixed points of the transformation, so $A = A'$ and $C = C'$. However, the point B is mapped to the point B' which is not on the line segment from A' to C'. Thus, the image of the line segment is not straight.

One might question at this point why it is undesirable for lines to map to curves. The answer to this question lies in the way the fourth stage of the graphics rendering pipeline works. In the fourth stage, the endpoints of a line segment are used to place a line in the screen space. This line in screen space typically has not only a position on the screen, but also depth (distance) values stored in a *depth buffer*.[14] When the fourth stage processes a line segment, say as shown in Figure II.27, it is given only the endpoints A' and C' as points $\langle x_{A'}, y_{A'}, z_{A'}\rangle$ and $\langle x_{C'}, y_{C'}, z_{C'}\rangle$. It then uses linear interpolation (averaging) to determine the rest of the points on the line segment.

In Figure II.27, the problem is that the point B is midway between A and C and has depth value ($-z$) midway between the depth values for A

[14] Other information, such as color values, is also stored along with depth, but this does not concern the present discussion.

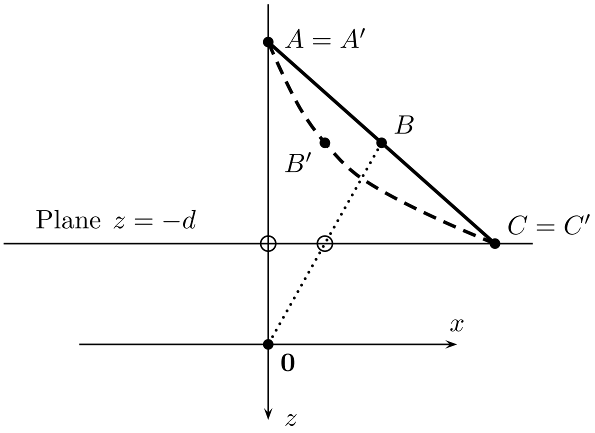

Figure II.27: The undesirable transformation of a line to a curve. The mapping used is $\langle x, y, z\rangle \mapsto \langle -d\cdot x/z, -d\cdot y/z, z\rangle$. The points A and C are fixed by the transformation and B is mapped to B'. The dashed curve is the image of the line segment AC. (The small unlabeled circles show the images of A and B under the mapping of Figure II.26.) The figure shows a top view, with the y-axis pointing upward out of the image.

and C, but the position of B on the viewscreen (the plane $z = -d$) is approximately one-fourth of the way from A to C, not halfway from A to C. The result is that the depth values for intermediate points such as B' cannot be straightforwardly linearly interpolated from the depth values of A' and C'. If the intermediate depth values are not computed correctly, the hidden surface algorithm can fail dramatically, since the depth values are used to determine which points are in front of other points. Another practical consideration is that we want perspective transformations to map lines to lines, so that perspective transformations can be represented by 4×4 matrices.

Thus, we need another way to handle depth information. In fact, it is enough to find a definition of a "fake" distance or a "pseudo-distance" function *pseudo-dist*(z) which has the following two properties:

1. The pseudo-distance respects relative order of z values. Namely, if $z > z'$, then *pseudo-dist*(z) < *pseudo-dist*(z').
2. It causes lines to map to lines.

Property 1. means that if $\langle x, y, z\rangle$ and $\langle x', y', z'\rangle$ lie in the same view direction, and if $z > z'$ so that $\langle x, y, z\rangle$ is closer to the viewer than $\langle x', y', z'\rangle$, then *pseudo-dist*$(z)$ < *pseudo-dist*(z'). In other words, the closer point has the smaller pseudo-distance value.

As it turns out, a good choice for a pseudo-distance satisfying properties 1. and 2. is any function of the form:

$$\textit{pseudo-dist}(z) \;=\; A + B/z,$$

with A and B constants such that $B > 0$. Since $B > 0$, property 1. certainly holds, as $\textit{pseudo-dist}(z) < \textit{pseudo-dist}(z')$ holds whenever $z > z'$.

It is common to choose the values for A and B so that points on the near and far clipping planes have pseudo-distances equal to -1 and 1, respectively. The near and far clipping planes have $z = -n$ and $z = -f$ with $0 < n < f$, so we need:

$$\begin{array}{rcccl} \textit{pseudo-dist}(-n) & = & A - B/n & = & -1 \\ \textit{pseudo-dist}(-f) & = & A - B/f & = & 1. \end{array}$$

Solving these two equations for A and B yields

$$A \;=\; \frac{f+n}{f-n} \qquad \text{and} \qquad B \;=\; \frac{2fn}{f-n}. \tag{II.20}$$

Before discussing property 2., it is helpful to see how this definition of the pseudo-distance function fits into the framework of homogeneous representation of points. With the use of the *pseudo-dist* function, the perspective transformation becomes the mapping

$$\langle x, y, z \rangle \;\mapsto\; \langle -d \cdot x/z,\, -d \cdot y/z,\, A + B/z \rangle. \tag{II.21}$$

We can rewrite this in homogeneous coordinates as

$$\langle x, y, z, 1 \rangle \;\mapsto\; \langle d \cdot x,\, d \cdot y,\, -A \cdot z - B,\, -z \rangle, \tag{II.22}$$

since multiplying through by $(-z)$ does not change the point represented by the homogeneous coordinates. More generally, because the homogeneous representation $\langle x, y, z, w \rangle$ is equivalent to $\langle x/w, y/w, z/w, 1 \rangle$, the mapping (II.22) acting on this point is

$$\langle x/w,\, y/w,\, z/w,\, 1 \rangle \;\mapsto\; \langle d \cdot x/w,\;\, d \cdot y/w,\;\, -A \cdot (z/w) - B,\;\, -z/w \rangle,$$

and, multiplying both sides by w, this becomes

$$\langle x, y, z, w \rangle \;\mapsto\; \langle d \cdot x,\;\, d \cdot y,\;\, -A \cdot z - B \cdot w,\;\, -z \rangle. \tag{II.23}$$

This equation (II.23) for the perspective transformation incorporating the *pseudo-dist* function is represented by the 4×4 homogeneous matrix:

$$\begin{pmatrix} d & 0 & 0 & 0 \\ 0 & d & 0 & 0 \\ 0 & 0 & -A & -B \\ 0 & 0 & -1 & 0 \end{pmatrix}. \tag{II.24}$$

The fact that the perspective transformation based on pseudo-distance can be expressed as a 4×4 matrix has two unexpected benefits. First, homogeneous matrices provide a uniform framework for representing both affine transformations and perspective transformations. Second, in Section II.4.4, we shall prove the following theorem:

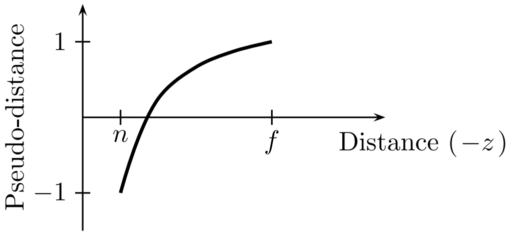

Figure II.28: Pseudo-distance varies nonlinearly with distance. Larger pseudo-distance values correspond to more distant points.

Theorem II.17. *The perspective transformation represented by the* 4×4 *matrix (II.24) maps lines to lines.*

In choosing a perspective transformation, it is important to select values for n and f, the near and far clipping plane distances, so that all the desired objects are included in the field of view. At the same time, it is also important not to choose the near clipping plane to be too near, or the far clipping plane to be too distant. The reason is that the depth buffer values need to have enough resolution so as to allow different (pseudo-)distance values to be distinguished. To understand how the use of pseudo-distance affects how much resolution is needed to distinguish between different distances, consider the graph of pseudo-distance versus distance in Figure II.28. Qualitatively, it is clear from the graph that pseudo-distance varies faster for small distance values than for large distance values (since the graph of the pseudo-distance function is sloping more steeply at smaller distances than at larger distances). Therefore, the pseudo-distance function is better at distinguishing differences in distance at small distances than at large distances. In most applications this is good, since, as a general rule, small objects tend to be close to the viewpoint, whereas more distant objects tend to either be larger or, if not larger, then errors in depth comparisons for distant objects make less noticeable errors in the graphics image.

It is common for final (device dependent) output of the rendering pipeline to convert the pseudo-distance into a value in the range 0 to 1, with 0 used for points at the near clipping plane and with 1 representing points at the far clipping plane. This number, in the range 0 to 1, is then represented in fixed point, binary notation, i.e. as an integer, with 0 representing the value at the near clipping plane and the maximum integer value representing the value at the far clipping plane. In modern graphics hardware systems, it is common to use a 32 bit integer to store the depth information, and this gives sufficient depth resolution to allow the hidden surface calculations to work well in most situations. That is, it will work well provided the near and far clipping distances are chosen wisely. Older systems used 16 bit depth buffers, and this tended to occasionally cause resolution problems. By comparison, the usual single-precision floating point numbers have 24 bits of resolution.

II.4.3 The power of 4×4 matrices

The previous section introduced an important new ability of 4×4 matrices to represent transformations in $\mathbb{R}^3$. Equations (II.21)-(II.23) defined a function for perspective that used ratios x/y, x/z and x/w, y/w. These are *not* linear functions, but nonetheless perspective transformation could be represented over homogeneous coordinates with 4×4 matrix.

More generally, we define a degree one polynomial over x_1, x_2, x_3 to be an expression of the form $p(x_1, x_2, x_3) = ax_1 + bx_2 + cx_3 + d$, where $a, b, c, d \in \mathbb{R}$ are constants. (A degree one polynomial is also called an "affine function".) Suppose a transformation A of $\mathbb{R}^3$ is defined by

$$A(\mathbf{x}) \;=\; \left\langle \frac{p(x_1,x_2,x_3)}{w(x_1,x_2,x_3)}, \frac{q(x_1,x_2,x_3)}{w(x_1,x_2,x_3)}, \frac{r(x_1,x_2,x_3)}{w(x_1,x_2,x_3)} \right\rangle.$$

where p, q, r and w are degree one polynomials and $\mathbf{x} = \langle x_1, x_2, x_3 \rangle$. We claim that A can be represented by a 4×4 matrix acting on homogeneous coordinates.

Instead of proving this abstractly, we give an example. Let $A : \mathbb{R}^3 \to \mathbb{R}^3$ be defined by

$$A(\langle x, y, z \rangle) \;=\; \left\langle \frac{x+1}{3z-2}, 0, \frac{x-2y+5}{3z-2} \right\rangle. \qquad \text{(II.25)}$$

Writing this over homogeneous coordinates,

$$A : \langle x, y, z, 1 \rangle \mapsto \left\langle \frac{x+1}{3z-2}, 0, \frac{x-2y+5}{3z-2}, 1 \right\rangle.$$

Multiplying the righthand side by $3z-2$, which does not change what point is represented, means

$$A : \langle x, y, z, 1 \rangle \mapsto \langle x+1,\, 0,\, x-2y+5,\, 3z-2 \rangle. \qquad \text{(II.26)}$$

This map can be represented by a 4×4 matrix as

$$\begin{pmatrix} x+1 \\ 0 \\ x-2y+5 \\ 3z-2 \end{pmatrix} \;=\; \begin{pmatrix} 1 & 0 & 0 & 1 \\ 0 & 0 & 0 & 0 \\ 1 & -2 & 0 & 5 \\ 0 & 0 & 3 & -2 \end{pmatrix} \begin{pmatrix} x \\ y \\ z \\ 1 \end{pmatrix}.$$

Equation (II.26) only showed the action of A on homogeneous coordinates with fourth component 1. Replacing x, y and z with x/w, y/w and z/w, (II.26) becomes

$$A : \langle x/w, y/w, z/w, 1 \rangle \mapsto \langle x/w+1,\, 0,\, x/w-2y/w+5,\, 3z/w-2 \rangle.$$

So, multiplying through by w,

$$A : \langle x, y, z, w \rangle \mapsto \langle x+w,\, 0,\, x-2y+5w,\, 3z-2w \rangle.$$

The same 4×4 matrix still represents the transformation A:

$$\begin{pmatrix} x+w \\ 0 \\ x-2y+5w \\ 3z-2w \end{pmatrix} = \begin{pmatrix} 1 & 0 & 0 & 1 \\ 0 & 0 & 0 & 0 \\ 1 & -2 & 0 & 5 \\ 0 & 0 & 3 & -2 \end{pmatrix} \begin{pmatrix} x \\ y \\ z \\ w \end{pmatrix}. \tag{II.27}$$

It is interesting to note that the original definition of A in (II.25) was undefined for inputs with $z = 2/3$ since that gives a division by zero. However the representation (II.27) for A is defined for inputs with $z/w = 2/3$. These are sent to points at infinity. For instance, $\langle 0,0,2,3\rangle$ is mapped by A to the point $\langle 3,0,15,0\rangle$ at infinity. In this way, although (II.25) was undefined for points in the plane $z = 2/3$ in $\mathbb{R}^3$, the representation (II.27) maps (the homogeneous representations of) the points in the plane $z = 2/3$ to the plane at infinity.

Exercise II.30.

a. Define $A : \mathbb{R}^2 \to \mathbb{R}^2$ by $A(\langle x,y\rangle = \langle x/(x-y-2), (y-1)/(x-y-2)\rangle$. Give a 3×3 matrix representing A over homogeneous coordinates.

b. Define $B : \mathbb{R}^3 \to \mathbb{R}^3$ by $B(\langle x,y,z\rangle = \langle z/(z+2), 1 + ((y-1)/(z+2)), 3\rangle$. Give a 4×4 matrix representing B over homogeneous coordinates.

II.4.4 Mapping lines to lines

As discussed earlier, the fact that perspective transformations map lines in 3-space to lines in screen space is important for interpolation of depth values in the screen space. In fact, more than this is true: any transformation which is represented by a 4×4 homogeneous matrix maps lines in 3-space to lines in 3-space. Since the perspective maps are represented by 4×4 matrices, as shown by Equation (II.24), the same is true *a fortiori* of perspective transformations.

Theorem II.18. *Let M be a 4×4 homogeneous matrix acting on homogeneous coordinates for points in $\mathbb{R}^3$. If L is a line in $\mathbb{R}^3$, then the image of L under the transformation represented by M, if defined, is either a line or a point in $\mathbb{R}^3$.*

This immediately gives the following corollary.

Corollary II.19. *Perspective transformations map lines to lines.*

For proving Theorem II.18, the most convenient way to represent the three dimensional projective space is as the set of linear subspaces of the Euclidean space $\mathbb{R}^4$, as was described in Section II.3.8. The “points” of the three dimensional projective space are the one dimensional subspaces of $\mathbb{R}^4$. The “lines” of the three dimensional projective space are the two dimensional subspaces of $\mathbb{R}^4$. The “planes” of the three dimensional projective geometry are the three dimensional subspaces of $\mathbb{R}^4$.

The proof of Theorem II.18 is now immediate. Since M is represented by a 4×4 matrix, it acts linearly on $\mathbb{R}^4$. Therefore, M must map a two dimensional subspace representing a line onto a subspace of dimension at most two: i.e., onto either a two dimensional subspace representing a line, or a one dimensional subspace representing a point, or a zero dimensional subspace. In the last case, the value of M on points on the line is undefined, since the point $\langle 0,0,0,0\rangle$ is not a valid set of homogeneous coordinates for a point in $\mathbb{R}^3$.

II.4.5 Another use for projection: shadows

In the next chapter, we shall study local lighting and illumination models. These lighting models, by virtue of their tracking only local features, cannot handle phenomena such as shadows or indirect illumination. There are global methods for calculating lighting that do handle shadows and indirect illumination (see Chapters X and XII), but these global methods are often computationally very difficult, and cannot be done with ordinary OpenGL commands in any event. There are however multi-pass rendering techniques for rendering shadows that can be used in OpenGL, see Section X.3.

An alternative way to cast shadows that works well for casting shadows onto flat, planar surfaces is to render the shadow of an object explicitly. This can be done in OpenGL by setting the current color to black (or whatever shadow color is desired), and then drawing the shadow as a flat object on the plane. Determining the shape of a shadow of a complex object can be complicated, since it depends on the orientation of the object and the position of the light source and object relative to the plane. Instead of attempting to explicitly calculate the shape of the shadow, you can instead first set the modelview matrix to hold a projection transformation, and then render the object in 3-space, letting the modelview matrix map the rendered object down onto the plane.

This has several advantages, chief among them being that it requires very little coding effort. One can merely render the object twice: once in its proper location in 3-space, and once with the modelview matrix set to project it down flat onto the plane. This handles arbitrarily complex shapes properly, including objects that contain holes.

To determine what the modelview matrix should be for shadow projections, suppose that the light is positioned at $\langle 0, y_0, 0\rangle$, that is, at height y_0 up the y-axis, and that the plane of projection is the xz-plane where $y=0$. It is not difficult to see using similar triangles that the projection transformation needed to cast shadows should be (see Figure II.29)

$$\langle x,y,z\rangle \;\mapsto\; \langle \frac{x}{1-y/y_0},\, 0,\, \frac{z}{1-y/y_0}\rangle. \tag{II.28}$$

This transformation is represented by the following homogeneous matrix:

$$\begin{pmatrix} 1 & 0 & 0 & 0\\ 0 & 0 & 0 & 0\\ 0 & 0 & 1 & 0\\ 0 & -\frac{1}{y_0} & 0 & 1 \end{pmatrix}.$$

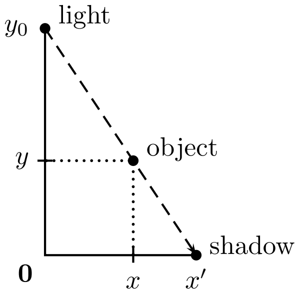

Figure II.29: A light is positioned at $\langle 0, y_0, 0\rangle$. An object is positioned at $\langle x, y, z\rangle$. The shadow of the point is projected to the point $\langle x', 0, z'\rangle$, where $x' = x/(1 - y/y_0)$ and $z' = z/(1 - y/y_0)$.

Exercise II.31. Prove the correctness of Equation (II.28) for the shadow transformation and the homogeneous matrix representation.

Exercise II.32. A light source is placed at $\langle 0, 10, 0\rangle$ and casts shadows onto the horizontal plane P defined by $y = 1$. When $\langle x, y, z\rangle$ is a point in $\mathbb{R}^3$ with $1 \le y < 10$, define $A(\langle x, y, z\rangle)$ to be the position of the shadow of the point on the plane P. For example, $A(\langle 1, 7, 2\rangle) = \langle 3, 1, 6\rangle$, and $A(\langle -2, 4, -4\rangle) = \langle -3, 1, -6\rangle$.

(a) Working in ordinary coordinates (not homogeneous) give the formula expressing the mapping $A(\langle x, y, z\rangle) = \langle x', y', z'\rangle$. That is, give formulas for x', y', z' in terms of x, y, z.

(b) Give a 4×4-matrix that represents the transformation A over homogeneous coordinates.

II.4.6 z-fighting

One potential pitfall with drawing shadows on a flat plane is that if the shadow is drawn exactly coincident with the plane, then *z-fighting* may cause the plane and shadow to show through each other. z-fighting occurs when two objects are drawn at the same depth from the viewer: due to roundoff errors, it can happen that some pixel positions have the first object closer than the other object and other pixels have the second object closer than the first object. The effect is a pattern of pixels where one object shows through the other. One way to combat z-fighting is to slightly lift the shadow up from the plane, but this can cause problems from some viewpoints where the gap between the plane and the shadow can become apparent. To solve this problem, you can use the OpenGL polygon offset feature. The polygon offset mode perturbs the depth values (pseudo-distance values) of points before performing depth testing against the pixel buffer. This allows the depth values to be perturbed for depth comparison purposes without affecting the position of the object on the screen.

To use polygon offset to draw a shadow on a plane, you would first enable polygon offset mode with a positive offset value, then draw the plane, and finally disable polygon offset mode for subsequent rendering. Finally, you would render the shadow without any polygon offset.

The OpenGL commands for enabling polygon offset mode are

```
glPolygonOffset( 1.0, 1.0 );
          ⎧  GL_POLYGON_OFFSET_FILL  ⎫
glEnable( ⎨  GL_POLYGON_OFFSET_LINE  ⎬ );
          ⎩ GL_POLYGON_OFFSET_POINT  ⎭
```

Similar options for `glDisable` will disable polygon offset. The amount of offset is controlled by the `glPolygonOffset()` command; setting both parameters to `1.0` is a good choice in most cases where you wish to increase the distance from the viewer. You can also use negative values such as `-1.0` instead of `-1.0` to decrease the distance from the viewer. For details on what these parameters mean, see the OpenGL documentation.

II.4.7 The OpenGL perspective transformations

The older legacy version of OpenGL provided special functions for setting up viewing transformations as either orthographic projections or perspective transformations. These included `glOrtho` for orthographic projections, and `glFrustum` and `gluPerspective` for perspective transformations. These functions are no longer available in modern OpenGL, but the *GlLinearMath* software includes direct replacements.

To set up a `LinearMapR4` matrix for an orthographic projection you can use the *GlLinearMath* methods:

```
LinearMapR4 mat;
mat.Set_glOrtho( float ℓ, float r, float b, float t, float n, float f );
```

As discussed in Section II.4.1, the purpose of this is to set up the camera or eye position so as to be looking down the negative z-axis, at the rectangular prism of points with $\ell \leq x \leq r$ and $b \leq y \leq t$ and $-f \leq z \leq -n$. Any part of the scene which lies outside this prism is clipped and not displayed. In particular, objects which are closer than the *near clipping plane*, defined by $z = -n$, are not visible, and do not even obstruct the view of more distant objects. In addition, objects further than the *far clipping plane*, defined by $z = -f$ are likewise not visible. Of course, objects, or parts of objects, outside the left, right, bottom, and top planes are not visible.

The `Set_glOrtho` command sets the matrix `mat` equal to

$$S = \begin{pmatrix} \frac{2}{r-\ell} & 0 & 0 & -\frac{r+\ell}{r-\ell} \\ 0 & \frac{2}{t-b} & 0 & -\frac{t+b}{t-b} \\ 0 & 0 & \frac{-2}{f-n} & -\frac{f+n}{f-n} \\ 0 & 0 & 0 & 1 \end{pmatrix}.$$

This is the same as the matrix shown in Equation (II.17).

Older versions of OpenGL had two commands that implement perspective transformations, `glFrustum` and `gluPerspective`; in *GlLinearMath*, they are replaced by `Set_glFrustum` and `Set_gluPerspective`. These functions make the usual assumption that the viewpoint is at the origin and the view direction is towards the negative z-axis. The most basic function is the `Set_glFrustum` function, which is used as follows:

```
LinearMapR4 mat;
mat.Set_glFrustum( float ℓ, float r , float b , float t , float n , float f );
```

A *frustum* is a six-sided geometric shape formed from a rectangular pyramid by removing a top portion. In this case, the frustum consists of the points $\langle x, y, z\rangle$ satisfying the conditions (II.29) and (II.30). (Refer to Figure II.30.)

a. The points lie between the near and far clipping planes:

$$-f \;\le\; z \;\le\; -n. \tag{II.29}$$

b. The perspective mapping that performs a perspective projection onto the near clipping plane, maps $\langle x, y, z\rangle$ to a point $\langle x', y', z'\rangle$ with $\ell \le x' \le r$ and $b \le y' \le t$. In view of Equation (II.18) on page 88, this is equivalent to

$$\ell \;\le\; \frac{n\cdot x}{-z} \;\le\; r \qquad \text{and} \qquad b \;\le\; \frac{n\cdot y}{-z} \;\le\; t. \tag{II.30}$$

The `Set_glFrustum` function above sets the matrix `mat` equal to

$$S = \begin{pmatrix} \frac{2n}{r-\ell} & 0 & \frac{r+\ell}{r-\ell} & 0 \\ 0 & \frac{2n}{t-b} & \frac{t+b}{t-b} & 0 \\ 0 & 0 & -\frac{(f+n)}{f-n} & -\frac{2fn}{f-n} \\ 0 & 0 & -1 & 0 \end{pmatrix}. \tag{II.31}$$

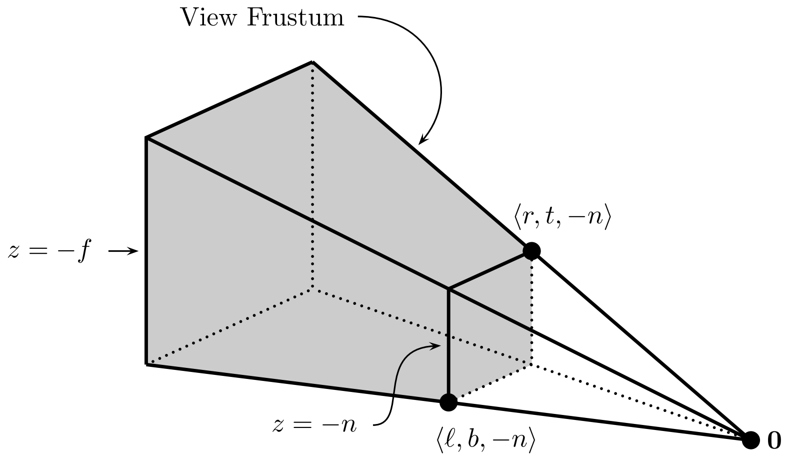

Figure II.30: The frustum viewed with `Set_glFrustum(`ℓ`, `r`, `b`, `t`, `n`, `f`)`. The near clipping plane is $z = -n$. The far clipping plane is $z = -f$. The frustum is the set of points satisfying (II.29) and (II.30).

This matrix S is chosen so that the frustum is mapped onto the $2 \times 2 \times 2$ cube centered at the origin. The formula for the matrix S is obtained in a manner similar to the derivation of the Equation (II.24) for the perspective transformation in Section II.4.2. There are two differences between Equations (II.31) and (II.24). First, the OpenGL matrix causes the final x and y values to lie in the range -1 to 1 by performing appropriate scaling and translation: the scaling is caused by the first two diagonal entries, and the translation is effected by the top two values in the third column. The second difference is that (II.24) was derived under the assumption that the view frustum was centered on the z-axis. For `Set_glFrustum`, this happens if $\ell = -r$ and $b = -t$. But, `Set_glFrustum` also allows more general view frustums that are not centered on the z-axis.

Exercise II.33. Prove that the matrix S of (II.31), when applied to homogeneous representations, maps the $\mathbb{R}^3$-points $\langle \ell, b, -n\rangle$ and $\langle r, t, -n\rangle$ in $\mathbb{R}^3$ to $\langle -1, -1, -1\rangle$ and $\langle 1, 1, -1\rangle$, respectively. Show that the back center point of the frustum is located at $\langle \frac{f(\ell+r)}{2n}, \frac{f(b+t)}{2n}, -f\rangle$. Prove that S maps this $\mathbb{R}^3$-point to $\langle 0, 0, 1\rangle$. Thus the matrix maps the back center point of the frustum is to the back center point of the $2 \times 2 \times 2$ cube of device independent screen coordinates (where $z = 1$ under OpenGL's conventions).

Exercise II.34* Derive Equation (II.31) for the `Set_glFrustum` matrix.

The function `Set_gluPerspective` can be used as an alternative to `Set_glFrustum`. `Set_gluPerspective` limits you to perspective transformations for which the z-axis is in the center of the field of view; but this is usually what is wanted anyway. `Set_gluPerspective` works by making a single call to `Set_glFrustum`. The usage of `Set_gluPerspective` is

```
LinearMapR4 mat;
Set_gluPerspective( float θ , float aspectRatio, float n , float f );
```

where θ is an angle (measured in radians) specifying the vertical field of view. That is to say, θ is the solid angle between the top bounding plane and the bottom bounding plane of the frustum in Figure II.30. The *aspect ratio* of an image is the ratio of its width to its height, so the parameter *aspectRatio* specifies the ratio of the width of the frustum to the height of the frustum. It follows that a call to `Set_gluPerspective` is equivalent to calling `Set_glFrustum` with

$$\begin{aligned} t &= n \cdot \tan(\theta/2) \\ b &= -n \cdot \tan(\theta/2) \\ r &= (\mathit{aspectRatio}) \cdot t \\ \ell &= (\mathit{aspectRatio}) \cdot b. \end{aligned}$$

For an example of `Set_glFrustum`, see the program *SolarModern* on the book's web page, and the accompanying explanation of the code.

II.5 Additional exercises

Exercise II.35. Define functions f_1-f_4 by:

- $f_1 : \langle x_1, x_2 \rangle \mapsto \langle x_2, -x_1 \rangle$, and
- $f_2 : \langle x_1, x_2 \rangle \mapsto \langle 2x_1, -\frac{1}{2}x_2 \rangle$, and
- $f_3 : \langle x_1, x_2 \rangle \mapsto \langle x_1 - \frac{1}{2}x_2, x_2 \rangle$, and
- $f_4 : \langle x_1, x_2 \rangle \mapsto \langle x_2, x_1 - \frac{1}{2}x_2 \rangle$.

Verify (but do not show your work) that each f_i is linear. Draw figures showing how these four functions transform the "F"-shape. Your four figures should be similar to the images in Figures II.3, II.5 and II.6. Label enough of the points to make it clear your answer is correct.

Exercise II.36. Consider the functions $f_1, \ldots, f_4$ from the previous Exercise II.35. Which of the four f_i's are affine? Which of the four f_i's are rigid? Which of the f_i's are orientation preserving?

Exercise II.37. Define functions

- $g_1 : \langle x_1, x_2 \rangle \mapsto \langle 2 - x_2, -x_1 \rangle$, and
- $g_2 : \langle x_1, x_2 \rangle \mapsto \langle 2x_1, x_2 - x_1 - 2 \rangle$.

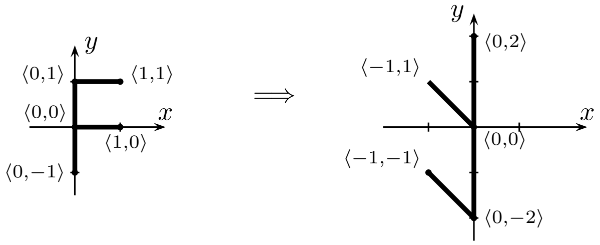

Figure II.31: The transformation for Exercise II.39 and II.40.

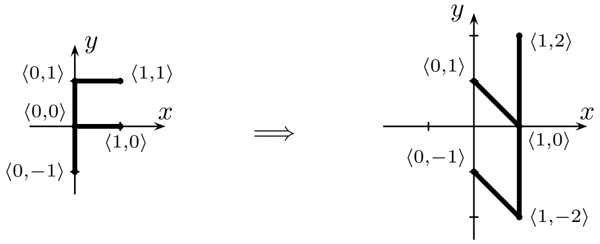

Figure II.32: The transformation for Exercises II.41 and II.42.

Verify (but do not show your work) that each g_i is affine.

(a) Draw figures showing how these two functions transform the “F”-shape.

(b) Express the two functions in form $M\mathbf{x}+\mathbf{c}$ where M is a 2×2 matrix and $\mathbf{c}\in\mathbb{R}$.

Exercise II.38. Prove the angle sum formulas for sin and cos:

$$\begin{aligned}\sin(\theta+\varphi) &= \sin\theta\cos\varphi+\cos\theta\sin\varphi\\ \cos(\theta+\varphi) &= \cos\theta\cos\varphi-\sin\theta\sin\varphi,\end{aligned}$$

by considering what the rotation R_θ does to the point $\mathbf{x}=\langle\cos\varphi,\sin\varphi\rangle$ and using the matrix representation of R_θ given by Equation (II.3).

Exercise II.39. Let A be the transformation of $\mathbb{R}^2$ shown in Figure II.31. Is A linear? Is A rigid? Is A orientation preserving? Give a matrix representing A: either a 2×2 matrix if A is linear, or a 3×3 matrix if A is only affine.

Exercise II.40. Again let A be the transformation of $\mathbb{R}^2$ shown in Figure II.31. Is A^{-1} linear? Is A^{-1} rigid? Is A^{-1} orientation preserving? Give a matrix representing A^{-1}: either a 2×2 matrix if A^{-1} is linear, or a 3×3 matrix if A^{-1} is only affine.

Exercise II.41. Let A be the transformation of $\mathbb{R}^2$ shown in Figure II.32. Is A linear? Is A rigid? Is A orientation preserving? Give a matrix representing A: either a 2×2 matrix if A is linear, or a 3×3 matrix if A is only affine.

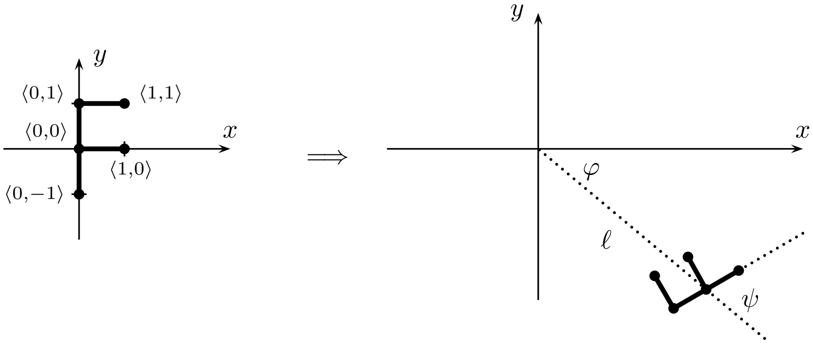

Figure II.33: The transformation for Exercise II.43.

Exercise II.42. Again let A be the transformation of $\mathbb{R}^2$ shown in Figure II.32. Is A^{-1} linear? Is A^{-1} rigid? Is A^{-1} orientation preserving? Give a matrix representing A^{-1}: either a 2×2 matrix if A^{-1} is linear, or a 3×3 matrix if A^{-1} is only affine.

Exercise II.43. Let an affine transformation C of $\mathbb{R}^2$ act on the "F" shape as shown in Figure II.33. The "F" shape has been scaled uniformly by a factor of $\frac{1}{2}$ and moved to a new position and orientation. Express C as a composition of transformations of the forms $T_{\mathbf{u}}$, R_θ, and $S_{\frac{1}{2}}$. The vector $\mathbf{u}$ and the angle θ should be expressed in terms of ℓ, φ and ψ.

Exercise II.44. Let $f : \mathbb{R}^2 \to \mathbb{R}^2$ be the affine transformation in Figure II.6 on page 45.

(a) Express f as a 3×3 matrix acting on homogeneous coordinates.

(b) Express f^{-1} as a 3×3 matrix acting on homogeneous coordinates.

[Hint: These will be easy if you have already worked Exercises II.3 and II.4.]

Exercise II.45. Let f be the affine transformation in Figure II.34.

(a) Is f a linear map?

(b) Is f a rigid map?

(c) Is f an orientation preserving map?

(d) Express f as a composition of translations $T_{\mathbf{u}}$ and rotations R_θ.

(e) Express f as a generalized rotation $R_\theta^{\mathbf{v}}$ (i.e., around a point $\mathbf{v}$).

(f) Give a 3×3 matrix that represents f over homogeneous coordinates.

(g) Give a 3×3 matrix that represents f^{-1} over homogeneous coordinates.

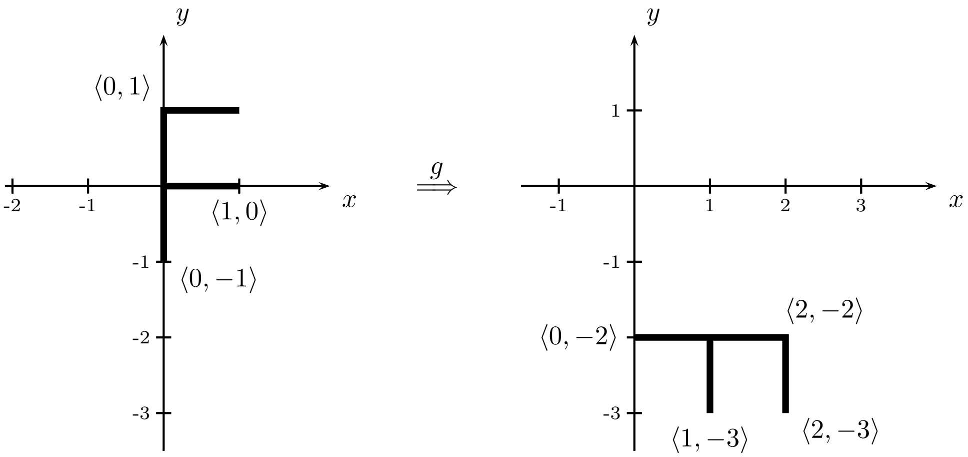

Figure II.34: The transformation for Exercise II.45.

Exercise II.46. Let $S_{\langle a,b,c\rangle|}$ be the nonuniform scaling transformation defined by $S_{\langle a,b,c\rangle}(\langle x_1,x_2,x_3\rangle) = \langle ax_1,bx_2,cx_3\rangle$ acting on points in $\mathbb{R}^3$. Express $S_{a,b,c}$ as a 4×4 matrix acting on homogeneous coordinates.

Exercise II.47. Let A be the transformation $S_{\langle\frac{1}{2},\frac{1}{2},\frac{1}{2}\rangle} \circ T_{\langle 4,2,0\rangle}$. What is $A(\langle 0,0,0\rangle)$? Give the 4×4 matrix representation for A.

Exercise II.48. Let B be the transformation $R_{\pi,\mathbf{j}} \circ T_{\langle 1,2,0\rangle}$. What is $B(\langle 0,0,0\rangle)$? Give the 4×4 matrix representation for B.

Exercise II.49. Give the 4×4 matrix representations of $T_{\mathbf{i}-\mathbf{j}} \circ R_{\pi/2,\mathbf{k}}$ and of $R_{\pi/2,\mathbf{k}} \circ T_{\mathbf{i}-\mathbf{j}}$. What are the images of $\mathbf{0}$, $\mathbf{i}$, $\mathbf{j}$ and $\mathbf{k}$ under these two compositions? (It is recommended to do this by visualizing the action of the composed transformations. The problem can also be worked by multiplying matrices, but in this case it is highly recommended to try visualizing afterwards.)

Exercise II.50. Give the 4×4 matrix representations of $T_{\mathbf{i}-\mathbf{j}} \circ S_2$ and of $S_2 \circ T_{\mathbf{i}-\mathbf{j}}$. Recall S_2 is a uniform scaling transformation. What are the images of $\mathbf{0}$, $\mathbf{i}$, $\mathbf{j}$ and $\mathbf{k}$ under these two compositions? As in the previous exercise, this problem can be solved by either visualization or matrix multiplication.

Exercise II.51. Suppose $\mathcal{C}$ is a radius 1, height 2 cylinder centered at the origin, with central axis the y-axis. The top face of $\mathcal{C}$ is the horizontal disk of radius one centered $\langle 0,1,0\rangle$. The bottom face of $\mathcal{C}$ is the horizontal disk of radius one centered $\langle 0,-1,0\rangle$. ("Horizontal" means parallel to the xz-plane.)

Let $\mathcal{D}$ a skewed cylinder (also called an "oblique cylinder") which has central axis the line where $y=x+2$ and $z=0$, and has perpendicular height 4, with the top face of $\mathcal{D}$ the horizontal radius $\frac{1}{2}$ disk centered at $\langle 2,4,0\rangle$ and the bottom face of $\mathcal{D}$ the horizontal radius $\frac{1}{2}$ disk centered at $\langle -2,0,0\rangle$.

(a) Draw a picture of D. What is the center point of D?

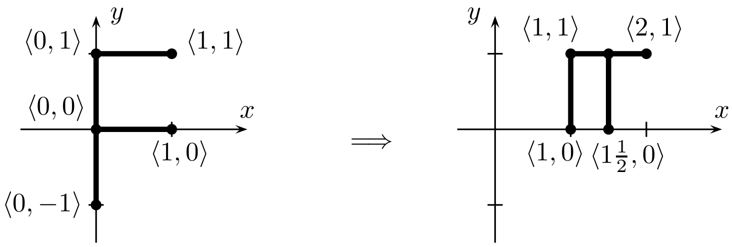

Figure II.35: The affine transformation for Exercise II.54.

(b) Give a 4×4 matrix M so that M represents the affine transformation sending $\mathcal{C}$ to $\mathcal{D}$.

Exercise II.52. Let A be the linear transformation such that $A(\langle x, y, z\rangle) = \langle z, x, y\rangle$. That is, A cyclically permutes the three coordinate axes. What 4×4 matrix represents A over homogeneous coordinates? Express A as a rotation $A = R_{\theta,\mathbf{u}}$ by giving values for θ and $\mathbf{u}$. [Hint: You can visualize this by considering the symmetries in the way A acts.]

Exercise II.53. A light source is placed at $\langle -10, 1, 0\rangle$ and casts shadows onto the plane P defined by $x = 2$. This plane is parallel to the yz-plane and acts like an infinite wall.

When $\langle x, y, z\rangle$ is a point in $\mathbb{R}^3$ with $-10 < x \le 2$, define $A(\langle x, y, z\rangle)$ to be the position of the shadow of the point on the plane P. For example, $A(\langle -4, 2, 2\rangle) = \langle 2, 3, 4\rangle$, and $A(\langle -7, 2, 2\rangle) = \langle 2, 5, 8\rangle$.

(a) Working in ordinary coordinates (not homogeneous) give the formula expressing the mapping $A(\langle x, y, z\rangle) = \langle x', y', z'\rangle$. That is, give formulas for x', y', z' in terms of x, y, z. (The fact that the light source does not lie on the x-axis means that the formulas for y' and z' are not the same.)

(b) Give a 4×4-matrix that represents the transformation A over homogeneous coordinates.

Exercise II.54. Consider the affine transformation of $\mathbb{R}^2$ shown in Figure II.35.

(a) Give pseudo-code in the style of Section II.2.6 that will draw the "F" as shown on the righthand side of Figure II.35. You may use $S_{\langle a,b\rangle}$ with one of a or b negative to perform a reflection.

(b) Give a 3×3 homogeneous matrix which represents this transformation.

Exercise II.55. This problem concerns transformations in $\mathbb{R}^2$. Suppose you are given a function `DrawCircle()` that draws a unit circle centered the origin.

(a) Give pseudo-code in the style of Section II.2.6 that uses `DrawCircle()` to draw the ellipse shown in Figure II.36. The major axis length is ℓ; the

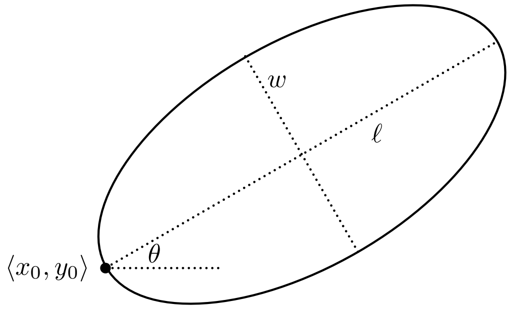

Figure II.36: The unit circle transformed into a tilted ellipse for Exercise II.55.

ellipse's width (minor axis length) is w. One end of the major axis is at $\langle x_0, y_0 \rangle$, and the major axis is tilted by an angle θ counter-clockwise. [Hint: There are several possible good answers.]

(b) Express the transformation used in part (a) as a composition of translations $T_{\mathbf{u}}$, rotations R_θ and scalings $S_{\langle a,b \rangle}$.

Exercise II.56. The problem concerns transformations in $\mathbb{R}^3$. Suppose you are given a function `DrawCone()` that draws a cone of height 1 and base radius 1. `DrawCone()` draws the cone centered around the y-axis with its base on the xz-plane and the tip of the code at $\langle 0, 1, 0 \rangle$.

(a) Give pseudo-code in the style of Section II.2.6 that draws the cone as shown in Figure II.37, upside down, with height 2 and base radius 1. The tip is now at the origin, and the cone is still centered on the y-axis. [Hint: There are several possible good answers.]

(b) Express the transformation applied to the `DrawCone()` cone to yield the cone positioned as in Figure II.37 as a composition of translations $T_{\mathbf{u}}$, rotations $R_{\theta,\mathbf{u}}$ and scalings $S_{\langle a,b,c \rangle}$.

Exercise II.57. Repeat Exercise II.56 for the cone show in Figure II.38.

Exercise II.58. A plane P containing the origin can be specified by giving a unit vector $\mathbf{u}$ which is orthogonal to the plane. That is, let $P = \{\mathbf{x} \in \mathbb{R}^3 : \mathbf{u} \cdot \mathbf{x} = 0\}$. A *reflection across* P is the linear transformation which maps each point $\mathbf{x}$ to its 'mirror image' directly across P, as illustrated in Figure II.39. Prove that, for a plane containing the origin, this reflection is represented by the 3×3 matrix $I - 2\mathbf{u}\mathbf{u}^{\mathrm{T}}$. Write out this matrix in component form too. [Hint: If $\mathbf{v} = \mathbf{v}_1 + \mathbf{v}_2$ as in the derivation of the rotation matrix, then the reflection maps $\mathbf{v}$ to $\mathbf{v}_2 - \mathbf{v}_1$.]

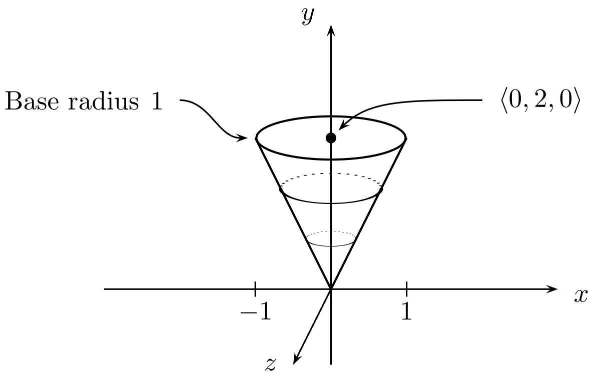

Figure II.37: The transformed cone for Exercise II.56.

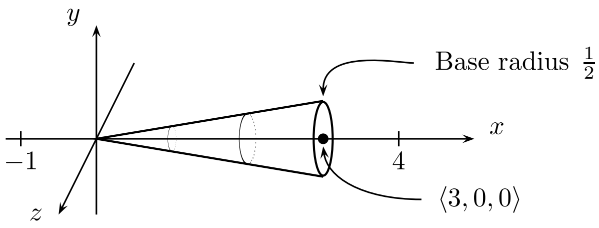

Figure II.38: The transformed cone for Exercise II.57.

Exercise II.59. Now let P be the plane $\{\mathbf{x}\in\mathbb{R}^3 : \mathbf{u}\cdot\mathbf{x}=a\}$ for some unit vector $\mathbf{u}$ and scalar a, where P does not necessarily contain the origin. Derive the 4×4 matrix which represents the transformation which reflects points across P. [Hint: This is an affine transformation. It is the composition of the linear map from Exercise II.58 and a translation.]

Exercise II.60. Let B be the transformation $\langle x,y,z\rangle \mapsto \langle \frac{1+x}{1-y}-1,\, 0,\, \frac{z}{1-y}\rangle$. Give a 4×4 matrix which represents this transformation over homogeneous coordinates. (When $0<y<1$, B gives the transformation for a shadow cast from a light at $\langle -1,1,0\rangle$ onto the plane $y=0$. You do **not** need to use this fact to work the problem!)

Exercise II.61. Consider a scaling $S_{\langle\alpha,\beta\rangle}$ with α and β both non-zero. Prove that if $|\alpha|=|\beta|$, then $S_{\langle\alpha,\beta\rangle}$ preserves angles between lines. Second, prove that if $|\alpha|\neq|\beta|$, then $S_{\langle\alpha,\beta\rangle}$ does not preserve angles between lines.

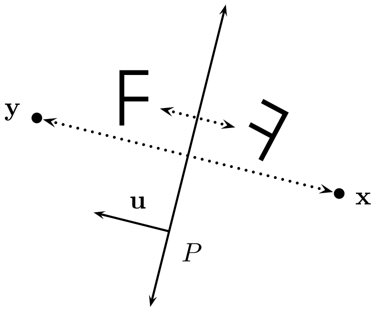

Figure II.39: Reflection across the plane P. The vector $\mathbf{u}$ is the unit vector perpendicular to the plane. A reflection maps a point to its mirror image across the plane. The point $\mathbf{x}$ is mapped to the point $\mathbf{y}$ directly across the plane, and vice-versa. Each “F” is mapped to the mirror image “F”.

Chapter III

The Rendering Pipeline

This chapter gives the highlights of the overall rendering pipeline as used by OpenGL. This pipeline is a combination of built-in OpenGL functionality and user-written shader programs. Section III.1 describes the simplest version of the OpenGL rendering pipeline, for shader programs that use only a vertex shader and fragment shader. It also describes the basic inputs and outputs for shader programs. Section III.2 describes more advanced features of the rendering pipeline, including geometry shaders. The final sections of the chapter discuss rasterization (mapping lines and triangles to pixels), the Bresenham algorithm and scan line interpolation.

III.1 The core rendering pipeline

The simplest and most common OpenGL rendering pipeline consists of a vertex shader and a fragment shader; see Figure III.1. The vertex shader is invoked on a per-vertex basis. The fragment shader is invoked on a per-fragment basis. A "fragment" is generally the same as a pixel, but could also be a pixel in a buffer other than the screen buffer. The primitive assembly, vertex post-processing, and rasterization stages transfer data from the vertex shaders to the fragment shaders.

Vertex shaders. In its simplest usage, the vertex shader:

- Is invoked with vertex attributes from the VBO and with generic attributes. The latter are given by `glVertexAttrib*` commands.
- Can also use uniform inputs, given by `glUniform*` commands.
- Can use `gl_VertexID` to obtain the vertex's position in the VBO's attribute array.
- Can use `gl_InstanceID` to get the instance number, when the C++ program uses "instanced" drawing commands (`glDraw*Instanced` commands) to render from the same VBO repeatedly.

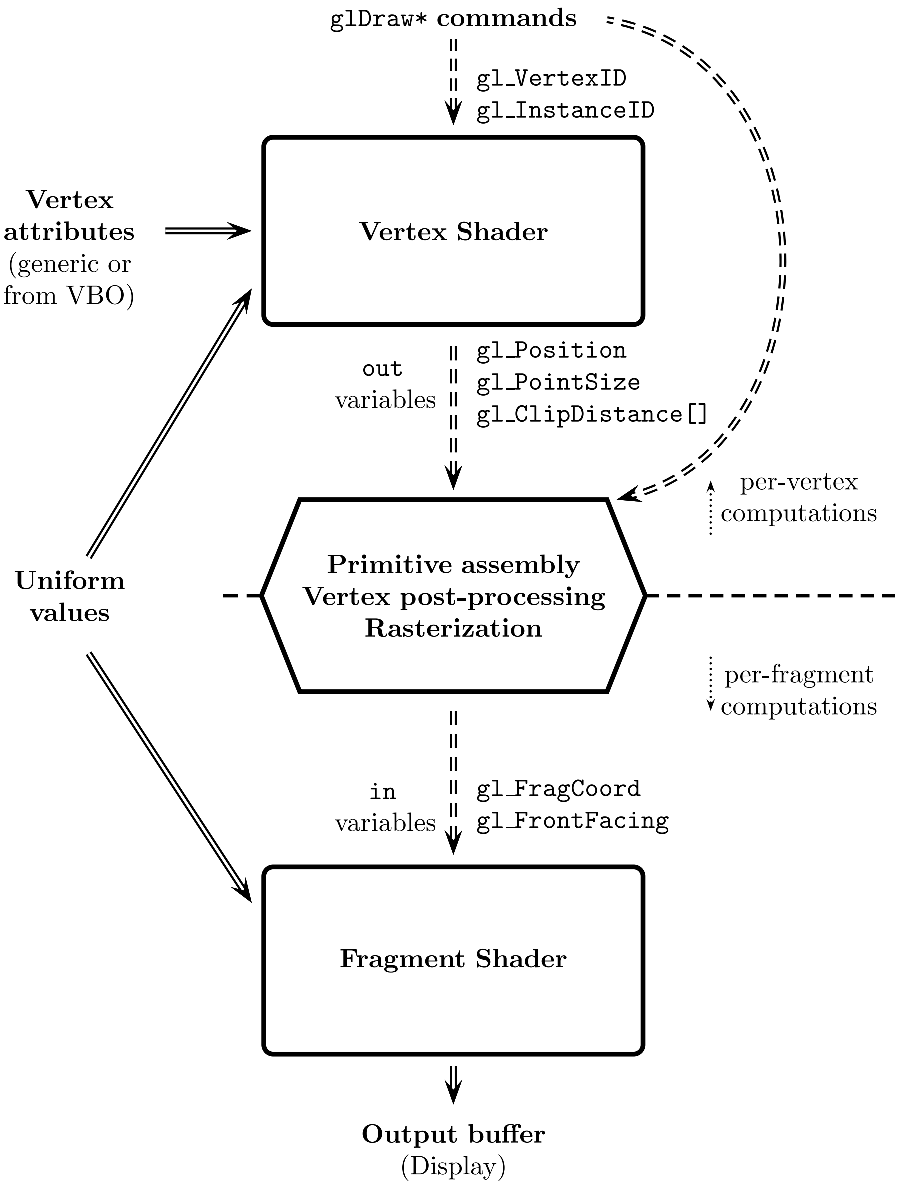

Figure III.1: The core shader rendering pipeline. The primary inputs to the shaders are the vertex attributes and the uniform variables. The rasterization is controlled by commands such as `glFrontFace`, `glCullFace`, `glPolygonMode`, `glPointSize`, `glLineWidth`, `glDepthFunc`, etc. `glBlendFunc` controls the way the fragment shader's outputs are written into the output buffer.

- Is ideally run once per vertex entry in the VBO. However, it may need to run multiple times on a vertex when VBO entries are used in the geometry multiple times.[1] If the vertex shader is run multiple times on the same vertex (with the same index in the VBO), it always produces exactly the same results.
- Has as its main output the `vec4` value `gl_Position` which is a homogeneous representation of a point $\langle x, y, z\rangle$ in $[-1,1]^3$. The x and y values give the position of the pixel (or, fragment) on the screen; the z value is the depth.
- Generates shader-specific outputs, declared with type keyword `out`. When rendering edges or triangles, these vertex specific outputs are interpolated before being sent to the fragment shader. By default, hyperbolic interpolation (called `smooth`) is used. However, `flat` shading can be used to use a single vertex's values across the entire edge or triangle. Much less commonly, `noperspective` shading can also be used; this uses ordinary linear interpolation (i.e., barycentric interpolation for triangles) in screen coordinates without taking depth or perspective into account. For more on this, see Sections V.7 and VI.1.1.
- May also specify a `gl_PointSize` for points; this lets a points be rendered as multiple pixel in the final image. For instance, in conjunction with the fragment shader, it allows a point to specify the position of a sprite.
- May also give an array of user-defined clipping distances using an array `gl_ClipDistance[]`. Clipping and culling are performed by the vertex post-processing stage described next. By default, OpenGL only clips and culls against the viewable volume, but the `gl_ClipDistance` values may be used to define additional clipping planes.

Primitive assembly, vertex post-processing and rasterization. The primitive assembly, vertex post-processing, and rasterization stages run after the vertex shader processes vertices. These stages determine which pixel (fragments) need to be rendered. First, *primitive assembly* combines the vertices into "primitives", namely into the points, edges and triangles as specified by `glDraw*` and `glPolygonMode` commands. *Vertex post-processing* and *rasterization* together determine which screen pixels are written to by each primitive. Most commonly:

- If the point size, as specified by `glPointSize` or `gl_PointSize`, is greater than one, then a point covers a square region of pixels.
- If the line width, as specified by `glLineWidth`, is greater than one, an edge covers a rectangle (usually long and skinny) of pixels.

[1] OpenGL maintains a small cache holding the output of the vertex shader on recent vertices to reduce the need to run the vertex shader multiple times on the same vertex.

- A triangle covers a triangle of pixels. For both triangles and lines, the methods discussed in Section III.3.1 determine the exact coverage of pixels.
- Clipping and culling are used to discard a primitive, or a portion of a primitive, that is not in the visible region. "Clipping" means to discard part of a triangle or line or point region. "Culling" means to completely discard a triangle or line or point. The most common use of clipping and culling is to dicard pixels outside the viewable volume. This includes near- and far-depth clipping and culling which discard primitives, or parts of primitives, which are behind the viewer or are too close to or too far from the viewer. It is also possible for the vertex shader to specify additional clipping/culling conditions.[2]
- Back face culling, if enabled, is used to discard triangles at that are not facing the viewer correctly. The functions `glFrontFace` and `glCullFace` control the culling of back faces (or front faces).
- Depth-culling (when enabled) is used to discard pixels whose depth, as specified in `gl_Position`, is larger than the depth of the current contents of the pixel. The function `glDepthFunc` can be used to control how depth-culling is performed.

The rasterization process is internal to OpenGL. There are a variety of ways to customize it; however, is not directly programmable.

Fragment shaders. The results from the rasterizer are sent to the fragment shader. In its simplest usage, the fragment shader

- Is invoked once for each fragment (i.e., pixel) output by the rasterization stage. Under normal usage with depth testing enabled, it is invoked only when the incoming fragment is not farther from the viewer than the current contents of the fragment.
- Uses the `out` variables from the vertex shader as inputs by declaring them as `in` variables. As discussed above, values these are shaded (interpolated) from the vertices' values before being received by the fragment shader.
- Can also use uniform inputs, given by `glUniform*` commands.
- Has as input a Boolean `bool` variable `gl_FrontFacing` that indicates whether the current triangle is being viewed from the front face side or the back face side. If back faces are being culled by the rasterizer, `gl_FrontFacing` will have value *true*.
- Has available as an input, the `vec4` variable `gl_FragCoord` giving the screen coordinates and depth buffer value for the current fragment. In most OpenGL implementations, the x and y coordinates,

[2] Clipping and culling are performed as part of the vertex processing before rasterization, not as part of the fragment processing. Clipping may require replacing a single triangle by multiple triangles.

`gl_FragCoord.x` and `gl_FragCoord.y` are half-integer values: the values $\langle 0.5, 0.5\rangle$ indicate the lower left pixel of the output buffer; the values $\langle w-\frac{1}{2}, h-\frac{1}{2}\rangle$ indicate the upper right pixel if the output buffer has dimensions $w \times h$. `gl_FragCoord.z` gives the depth value in the range $[-1, 1]$, with greater values indicating greater relative distance from the viewer. Note that `gl_FragCoord.x`, `gl_FragCoord.y` and `gl_FragCoord.z` are used directly, without first dividing by `gl_FragCoord.w`.

- Has as its main output, a `vec4` variable giving the red, green, blue and alpha values for the current fragment. This variable can be given any name, but must be declared with the type keyword `out`.
- The output from the fragment shader is typically written into the output buffer without further modification. However, `glBlendFunc` can be used to specify how the fragment shader's output is blended (averaged) with the prior value in the output buffer.

See Figure III.1 for a schematic of the core shader rendering pipeline.

Exercise III.1. For these three multiple choice questions, two vertices are considered to be the "same vertex" if they have exactly the same values for their vertex attributes — even if they are at different locations in the VBO and thus have different vertex ID's. Recall that `glDrawElements` uses an element array (an EBO), but `glDrawArrays` does not.

a. Suppose `glDrawArrays` is used to render vertices from data in a VBO using `GL_TRIANGLES`. If the same vertex v appears as a vertex in multiple triangles, then a vertex shader is invoked for v:

i. At most once, possibly not at all.

ii. Exactly once.

iii. One or more times, but possibly not for every triangle containing v.

iv. Exactly once per triangle containing v.

b. Now suppose `glDrawArrays` is used to render vertices from data in a VBO using `GL_TRIANGLE_STRIP`. If the same vertex v appears as a vertex in multiple triangles, then a vertex shader is invoked for v:

i. At most once, possibly not at all.

ii. Exactly once.

iii. One or more times, but possibly not for every triangle containing v.

iv. Exactly once per triangle containing v.

c. Suppose `glDrawElements` is used to render vertices from data in a VBO and EBO using `GL_TRIANGLE_STRIP`. If the same vertex v appears as a vertex in multiple triangles, then a vertex shader is invoked for v:

i. At most once, possibly not at all.

ii. Exactly once.

iii. One or more times, but possibly not for every triangle containing v.

iv. Exactly once per triangle containing v.

III.2 Rendering pipeline with a geometry shader

A geometry shader is an optional stage the rendering pipeline that can programmatically create new primitives. As shown in Figure III.2, the geometry shader lies between the vertex shader and the fragment shader. The inputs to the geometry shader are primitives of a fixed type, usually points, lines strips, or triangle strips. The outputs of the geometry shader are also primitives of a fixed type. The input types and output types can be different; for instance, a geometry shader might take triangles as inputs and output line strips.

Figure III.3 shows an example of a geometry shader.[3] This geometry shader takes a triangle as an input, and outputs line strips. It first generates a line strip consisting of the three edges the triangle, and then draws three lines showing the positions of the normal vectors at the three vertices. The vertex shader has already generated the `gl_Position` value and set two `out` values called `vertNormal` and `VertColor`. When the `glDraw*` commands create triangles, the vertices are first processed by the vertex shader as usual. Afterwards, the triangles are reassembled and sent to the geometry shader. The geometry shader outputs new primitives that are rasterized and sent to the fragment shader.

Another kind of shader, called a tessellation shader, can also be used to generate new primitives. The tessellation shader in the rendering pipeline sits immediately after the vertex shader and before the geometry shader. vertex shader in the rendering pipeline Tessellation shaders lack the flexibility of geometry shaders and are intended for generating highly structured primitives; for instance, a tessellation shader could be used to generate Catmull-Rom splines (see Section VIII.15.1 or interpolating Bézier surfaces (see Section VIII.16). For applications that suit tessellation shaders, they can be considerably faster than geometry shaders. Geometry shaders are much more versatile in what kinds of primitive can be rendered; they also have the advantage of supporting the so-called "transform feedback" which allows writing data to a buffer in addition to rendering primitives. Tessellation shaders support a complex set of options, and we do will not describe them further.

The important features of geometry shaders can be summarized as follows.

- A geometry shader accepts as inputs the vertices of a single kind of primitive. The most common types for input primitives are points, lines and triangles. For example, a vertex shader that takes triangles as inputs will include a declaration

[3] This is a simplified version of the geometry shader in the file *NormalViewer.glsl* in the C++ program *GlGeomShapesTester*, available at the book's web pages.

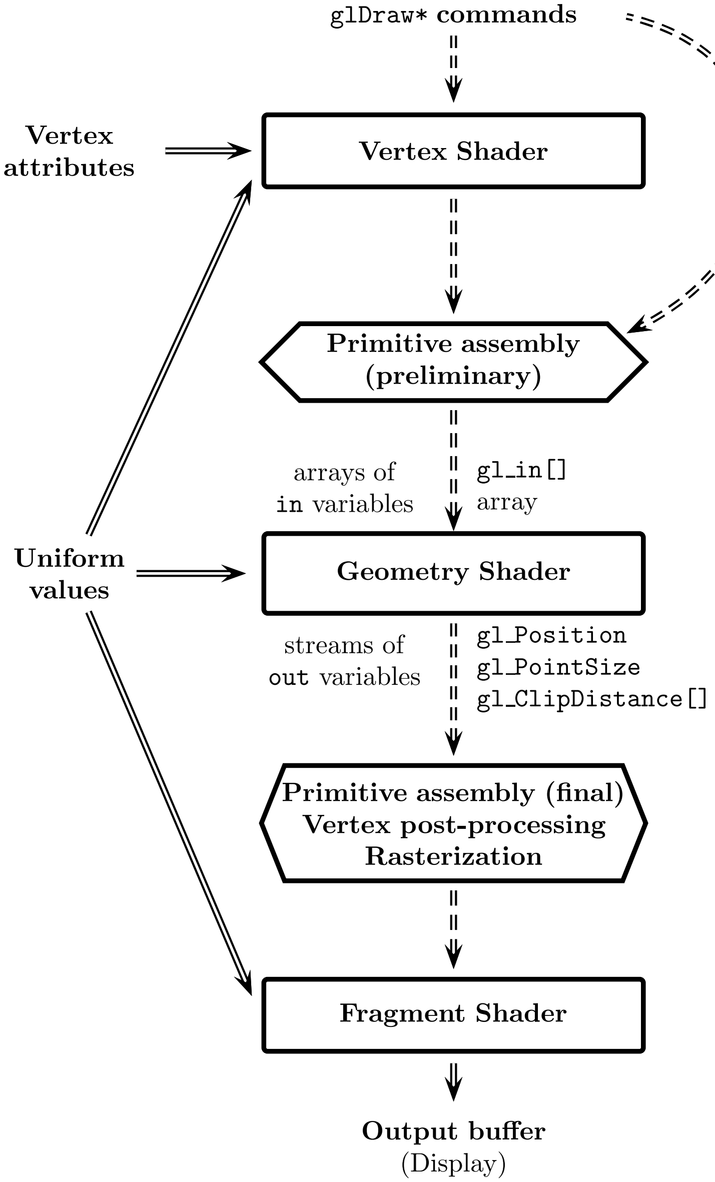

Figure III.2: A simplified view of the shader rendering pipeline with a geometry shader. The geometry shader receives a single primitive, with the vertex attributes passed in as an array. The geometry outputs multiple primitives; it outputs `out` variables for each vertex in each primitive. The first stage of primitive assembly collects vertex data into primitives to feed to the geometry shader. The second stage of primitive assembly collects the primitives output by the geometry shader.

```
#version 330 core
layout(triangles) in;
layout(line_strip, max_vertices = 12) out;
in vec3 vertColor[];        // Input: Array of vertex colors
in vec3 vertNormal[];       // Input: Array of vertex unit normals
out vec3 theColor;          // Output: Color for a vertex
uniform mat4 projectionMatrix;

void main() {
  // The next two variables control the color and length of normals.
  vec3 normalColor = vec3(1.0, 1.0, 1.0);
  float normalLength = 0.4;

  // Transform vertices by the projection matrix
  vec4 projVertPos[3];
  for (int i=0; i<3; i++ ) {
      projVertPos[i] = projectionMatrix * gl_in[i].gl_Position;
  }

  // Outline the triangle's edges as single line strip
  for (int i=0; i<=3; i++ ) {
      int j = i%3;
      gl_Position = projVertPos[j];
      theColor = vertColor[j];
      EmitVertex();
  }
  EndPrimitive();

  // Render each normal vector as a short line
  for (int i=0; i<gl_in.length(); i++ ) {
      vec3 vPos = vec3(gl_in[i].gl_Position)/gl_in[i].gl_Position.w;
      theColor = normalColor;
      gl_Position = projVertPos[i];
      EmitVertex();
      vPos += normalLength*vertNormal[i];
      theColor = normalColor;
      gl_Position = projectionMatrix*vec4(vPos,1.0);
      EmitVertex();
      EndPrimitive();
  }
}
```

Figure III.3: A (simplified) sample geometry shader. For the associated vertex and fragment shaders, see the file *NormalViewer.glsl*.

```
layout ( triangles ) in;
```

at the beginning.

- The geometry shader outputs multiple primitives (possibly none), each of which typically has multiple vertices. The output type is declared with a command such as

  ```
  layout(line_strip, max_vertices = 12) out;
  ```

  This particular command means that the output primitives are line strips, and that the total number of vertices in the line strips output by any particular invocation of the vertex shader will not exceed 12. The other permitted output types are `points` and `triangle_strip`. Note that the output types of "lines" and "triangles" are not permitted; however, they can be output by outputting individual lines as separate line strips, or individual triangles as separate triangle strips.
- The vertex shader receives arrays holding the vertex data for each vertex in the input primitive. These arrays are of length 1, 2, or 3 for points, lines or triangles (respectively). The `gl_in` array holds the position values output by the vertex shader; the i-th vertex's position is accessed using `gl_in[i].gl_Position`. The other `out` variables written by the vertex shader are passed to the vertex shader in separate arrays. For example, the code in Figure III.2 can use `vertColor[i]` to access the `vertColor` value generated by the vertex shader for the i-th vertex of the triangle. Since triangles have three vertices, i can be 0, 1 or 2.
- Although less-commonly used than `gl_Position`, the `gl_in` array also holds `gl_PointSize` values and potentially arrays of user-defined clip distances.
- The geometry shader outputs primitives by calling functions `EmitVertex()` and `EndPrimitive()`. First `EmitVertex` is called once per vertex in the primitive. For example, if outputting a line strip, `EmitVertex` two or more times. Once all the vertices of a primitive output via `EmitVertex`, then `EndPrimitive()` is called to indicate the end of the primitive. After that, a new primitive can be started.
- The geometry shader must set the value of `gl_Position` before calling `EmitVertex`. This is the position of the vertex in device independent screen coordinates, that is, as transformed by the projection matrix. This `gl_Position` value is an output value; it should not be confused with the input position values `gl_in[].gl_Position`.
- The geometry shader also must set the values of `out` variables before each call to `EmitVertex`.[4] The `out` variables from the geometry shader become

[4] The documentation for GLSL state that the `out` variables do not retain their values between calls to `EmitVertex`, and thus must be set explicitly for every vertex even their value has not changed. Nonetheless, inpractive, many GLSL implementations do save the previous `out` value.

in values for the fragment shader.

- Less commonly, the geometry shader can also set gl_PointSize and an array of clip distances for each output vertex.

The sample code in Figure III.3 shows the basic functionality of a geometry shader. This shader takes a triangle as input. Each vertex of the triangle has a gl_Position value, a color value vertColor and a normal vector vectNormal. The position values are given world coordinates: the vertex shader computed these by transforming positions a model view matrix, not the projection matrix. The vertices output by the geometry shader must output position values in device independent coordinates; for this, it transforms the positions with the projection matrix.

The geometry shader outputs first a line strip of length 3 that traces out the edges of the triangle. It then outputs three lines indicating the positions of the normal vectors. This is done with using three line strips of two vertices each. The fragment shader will use the out value from the geometry shader; it does not have access to any out values from the vertex shader (unless the geometry shader copies them into a new out variable.

Another important use of geometry shaders is *transform feedback.* Transform feedback allows the geometry shader to write data out to a buffer, that can later be used by the CPU or as a VBO, etc. Although we will not discuss transform feedback here, examples can be found in the programs *ParticlesTransformFeedback* and *Chap1TransformFeedback* at the book's web pages.

Exercise III.2. Why is the geometry shader of Figure III.2 designed so that the input positions are in world coordinates instead of device independent screen coordinates?

Exercise III.3. Answer the following true/false questions a.-g. about geometry shaders. Answer the cases under the assumption that the shader program has a vertex shader, a geometry shader and a fragment shader. Not all of these topics have been covered explicitly, but you should answer according to what would make the most sense in terms of how geometry shaders work.

a. A geometry shader can take as inputs any one of points, lines, line strips, triangles, triangle fans, or triangle strips.

b. A geometry shader that takes lines as inputs can output triangle strips.

c. The only way a geometry shader can output a triangle fan is to output it as multiple triangle strips.

d. A geometry shader can change the value of a uniform variable.

e. A geometry shader can access all vertex attributes, even vertex attributes that the vertex shader did not copy into "out" variables.

f. The vertices output by the geometry shader might be processed by a vertex shader before being sent to the fragment shader.

g. The fragment shader's "in" variables can be used to receive values directly from both the vertex shader and the geometry shader.

III.3 Rasterization: mapping to pixels

The rendering pipeline uses the model, view, and projection matrices followed by perspective division (see Figure II.1 on page 37), to map triangles with vertices in 3-space into triangles in a rectangular array of pixels. This array of pixels is called the *viewport*. By convention, the polygons are specified in terms of their vertices. The rendering pipeline positions these vertices in the $2 \times 2 \times 2$ cube centered at the origin. The resulting x and y coordinates of a vertex determine the position of the vertex in the viewport. The z-coordinate specifies a relative depth or distance value, possibly a pseudo-distance value. In addition, each vertex will usually have associated with it other values, most notably color values. The color values are commonly scalars r, g, b, α for the intensities of red, green, and blue light and the alpha channel value. Alternatively, the color may be a single scalar for gray-scale intensity in a black and white image. Other values may also be associated with pixels, for instance, u, v-values indexing into a texture map.

If the viewport has width w and height h, we index a pixel by a pair $\langle i, j \rangle$ with i, j integer values, $0 \le i < w$ and $0 \le j < h$. Suppose a vertex $\mathbf{v}$ has position $\langle x, y, z \rangle$ in the $2 \times 2 \times 2$ cube. We can remap the x, y values into the rectangle $[0, w) \times [0, h)$ to get values x', y' corresponding directly to pixel indices by letting

$$x' \;=\; \frac{x+1}{2} w \qquad \text{and} \qquad y' \;=\; \frac{y+1}{2} h.$$

Then the vertex $\mathbf{v}$ is mapped to the pixel $\langle i, j \rangle$, where[5]

$$i \;=\; \lfloor x' \rfloor \qquad \text{and} \qquad j \;=\; \lfloor y' \rfloor,$$

with the exceptions that $x' = w$ yields $i = w - 1$ and $y' = h$ yields $j = h - 1$. Thus, the pixel $\langle i, j \rangle$ corresponds to vertices with $\langle x', y' \rangle$ in the unit square centered at $\langle i + \frac{1}{2}, j + \frac{1}{2} \rangle$.

At the same time as the x' and y' values are quantized to pixel indices, the other values associated with the pixel are likewise quantized to integer values. The z-value is typically saved as a 16- or 32-bit integer, with 0 indicating the closest visible objects and larger values indicating more distant objects. Color values such as r, g, b are typically stored as 8-bit integers (for "millions of colors" mode with 16,777,216 colors). Texture coordinates are typically mapped to integer coordinates indexing a pixel in the texture.

Now suppose that a line segment has as endpoints the two vertices $\mathbf{v}_1$ and $\mathbf{v}_2$, and that these endpoints have been mapped to the pixels $\langle i_1, j_1 \rangle$ and $\langle i_2, j_2 \rangle$. Once the endpoints have been determined, it is still necessary to draw

[5] The notation $\lfloor a \rfloor$ denotes the least integer less than or equal to a.

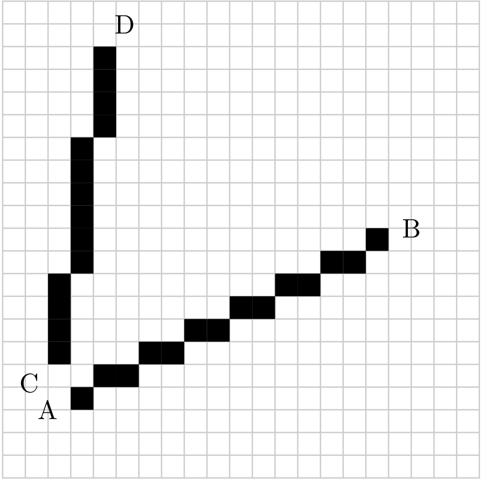

Figure III.4: The line segment AB has slope $\Delta j/\Delta i \leq 1$. The line segment CD has slope ≥ 1. The former segment is drawn with one pixel per column; the latter segment is drawn with one pixel per row.

the pixels that connect the two endpoints in a straight line. The problem is that the pixels are arranged rectangularly, so, for lines that are not exactly horizontal or vertical, there is some ambiguity about which pixels belong to the line segment. There are several possibilities here for how to decide which pixels are drawn as part of the line segment. The usual solution is the following.

First, when drawing the pixels that represent a line segment, we work only with the values $\langle i_1, j_1\rangle$ and $\langle i_2, j_2\rangle$: the floating point numbers from which they were derived have been forgotten.[6] Then let

$$\Delta i = i_2 - i_1 \qquad \text{and} \qquad \Delta j = j_2 - j_1.$$

Of course, we may assume that $i_1 \leq i_2$; otherwise, the vertices could be interchanged. We also can assume, without loss of any generality, that $j_1 \leq j_2$, since the case $j_1 > j_2$ is symmetric. We then distinguish the cases of whether the slope of the line segment is ≤ 1 or ≥ 1, i.e., whether $\Delta j/\Delta i \leq 1$, or $\Delta i/\Delta j \leq 1$. As illustrated in Figure III.4, in the first case, the line segment can be drawn so that there is exactly one pixel $\langle i, j\rangle$ drawn for each i between i_1 and i_2. In the second case, there is exactly one pixel $\langle i, j\rangle$ drawn for each j between j_1 and j_2.

[6] There is some loss of information in rounding to the nearest pixel and forgetting the floating point numbers. Some implementations of line drawing algorithms use subpixel levels of precision, that is rather than rounding to the nearest pixel, they use a fixed number of bits of extra precision to address subpixel locations. This extra precision does not change the essential nature of the Bresenham algorithm for line drawing which is described in the next section. In particular, the Bresenham algorithm can still work with integers.

Henceforth, it is assumed that the slope of the line is positive and ≤ 1, i.e., $0 \le \Delta j \le \Delta i$; and, in addition, $i_1 \ne i_2$. This does not cause any loss of generality since the case of slope > 1 can be handled by interchanging the roles of the variables i and j. Our goal is to find values $j(i)$ so that the line segment can be drawn using the pixels $\langle i, j(i)\rangle$, for $i = i_1, i_1{+}1, \ldots, i_2$. This is done by using linear interpolation to define an "ideal" value $y(i)$ for $j(i)$ and then rounding to the nearest integer. Namely, suppose $i_1 \le i \le i_2$. Let $\alpha = \frac{i-i_1}{i_2-i_1}$. Calculating the y-coordinate of the line to be drawn on the viewport, we have that

$$y(i) - y(i_1) \;=\; \alpha \cdot (y(i_2) - y(i_1)),$$

i.e.,

$$y(i) \;=\; j_1 + \frac{1}{2} + \alpha(j_2 - j_1) \;=\; j_1 + \frac{1}{2} + \alpha\Delta j,$$

since our best estimates for $y(i_1)$ and $y(i_2)$ are $y(i_1) = j_1{+}\frac{1}{2}$ and $y(i_2) = j_2{+}\frac{1}{2}$. We then obtain $j(i)$ by rounding down, namely,

$$j(i) \;=\; \left\lfloor j_1 + \frac{1}{2} + \alpha\Delta j \right\rfloor \;=\; \left\lfloor j_1 + \frac{1}{2} + \frac{i - i_1}{i_2 - i_1}\Delta j \right\rfloor. \tag{III.1}$$

Another, and more suggestive, way to write the formula for $j(i)$ is to use the notation $[x]$ to denote x rounded to the nearest integer. Then $[x] = \lfloor x + \frac{1}{2} \rfloor$, so Equation (III.1) is equivalent to

$$j(i) \;=\; [(1-\alpha)j_1 + \alpha j_2]. \tag{III.2}$$

As we shall see in Chapter V, this is the usual formula for linear interpolation. (The additive $\frac{1}{2}$ in the earlier formulas is thus seen to be just an artifact of the rounding process.)

The next section will present the Bresenham algorithm which gives an efficient, purely integer based, method for computing the interpolating values $y(i)$.

When working with ordinary Euclidean (nonhomogeneous) coordinates and orthographic projections, other scalar values, such as the depth value z, the color values r, g, b, the texture coordinates, etc., can be linearly interpolated in the same way. For the color values, this is what is called Gouraud interpolation.[7] For example, the interpolated values for the depth z would be computed so that

$$z(i) \;=\; [(1-\alpha)z_1 + \alpha z_2], \tag{III.3}$$

where z_1 and z_2 are the integer values at the first and last vertex which are obtained by appropriately scaling the z values and rounding to the nearest integer. The value $z(i)$is the calculated interpolating integer value at the pixel $\langle i, y(i)\rangle$.

However, it is very common to use perspective (non-orthographic) viewing transformation with homogeneous coordinates for vertex positions. In this case,

[7] Gouraud interpolation is named after H. Gouraud who proposed linear interpolation as a method of blending colors across polygons in 1971 in [57].

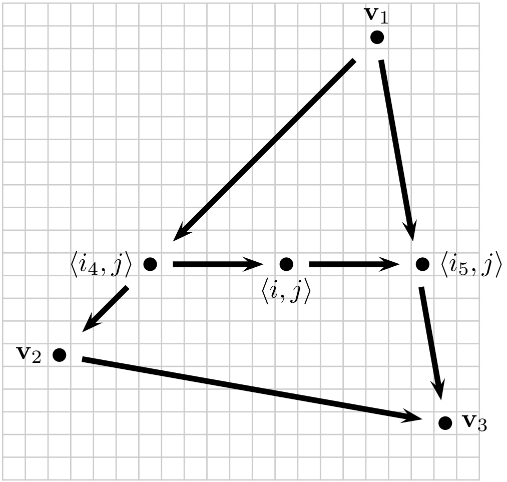

Figure III.5: The scan line interpolation method first interpolates along the edges of the triangle, then interpolates along the horizontal rows of pixels in the interior of the triangle. The interpolation directions are shown with arrows. If you look closely, you will note that the rightmost pixel, $\langle i_5, j\rangle$, on the horizontal scan line is not exactly on the line segment forming the right edge of the triangle — this is necessary since its position must be rounded to the nearest pixel.

Equation III.3 cannot be used to calculating the interpolated values for other scalar values $z(i)$. Section V.4 on "hyperbolic interpolation" describes what must be done in this case.

Before discussing the Bresenham algorithm, we consider how interpolation is used to interpolate values across a triangle of pixels in the viewport. Let a triangle have vertices $\mathbf{v}_1$, $\mathbf{v}_2$, and $\mathbf{v}_3$. After projecting and rounding to integer values, the vertices map to points $\langle i_m, j_m\rangle$, for $m = 1, 2, 3$. By the linear interpolation formulas above, the three sides of the triangle can be drawn as pixels, and the other values such as depth and color are also interpolated to the pixels along the sides of the triangle. The pixels in the interior of the triangle are filled in by interpolation along the horizontal rows of pixels. Thus, for instance, in Figure III.5, the scalar values at pixel $\langle i, j\rangle$ are interpolated from the values at the pixels $\langle i_4, j\rangle$ and $\langle i_5, j\rangle$. This method is called *scan line interpolation.*

The process of interpolating along a scan line is mathematically identical to the linear interpolation discussed above. Thus, it can also be carried out with the efficient Bresenham algorithm. In fact, the most natural implementation would involve nested loops that implement nested Bresenham algorithms.

Triangles are generally rendered as part of a larger surface. In some cases, it is important that rasterization assigns each pixels to a unique (closest) triangle on the surface. For example, if a surface is facing the viewer, the triangles

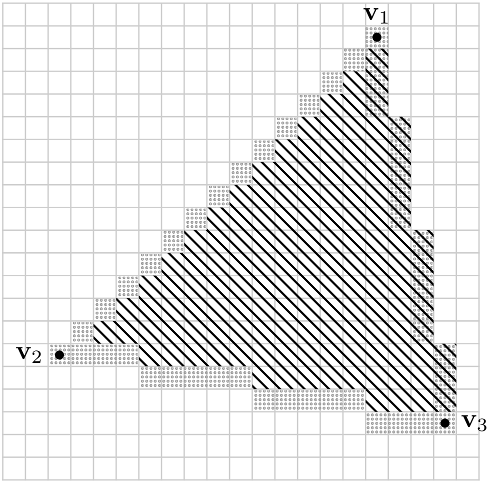

Figure III.6: Scan line interpolation can be used to assign pixels to the triangle with vertices $\mathbf{v}_1, \mathbf{v}_2, \mathbf{v}_3$. The dotted squares indicate pixels on the boundary of the triangle. The diagonally hatched squares are the pixels assigned to the triangle. When the triangles form a coherent surface facing the viewpoint, each pixel is assigned to exactly one triangle.

should be rasterized to disjoint sets of pixels. On the one hand, as discussed in the next section, we definitely do not want to have visible gaps between adjacent triangles, as these will leave pixel-sized holes in the surface. On the other hand, we also do not want two adjacent triangles to overlap and jointly contain triangles along their common edge, because this can create problems when transparency or other blending effects are used.

For this reason, it is important to have some method for deciding how pixels that lie along the common edge of two triangles are assigned to only one of the triangles. One possible solution to this is shown in Figure III.6. The idea here to arbitrarily decide that pixels that belong to the triangle to the left of the edge they lie on. (Some pixels may below to both a right edge and a left edge, e.g., the pixels for $\mathbf{v}_1$ and $\mathbf{v}_3$ in the figure; these also do not below to the triangle.) For horizontal edges, pixels can be assigned the triangle below the edge. This method is easy to implement as part of scan line interpolation, working with only a single triangle at a time.

Finally, there is a generalization of scan line interpolation that applies to general polygons, rather than just to triangles. The general scan line interpolation interpolates values along all the edges of the polygon. Then, every horizontal scan line of pixels in the interior of the polygon begins and ends on an edge or vertex, of course. The values on the horizontal scan line are filled in by interpolating from the values at the ends. With careful coding, general scan line interpolation can be implemented efficiently to carry out the

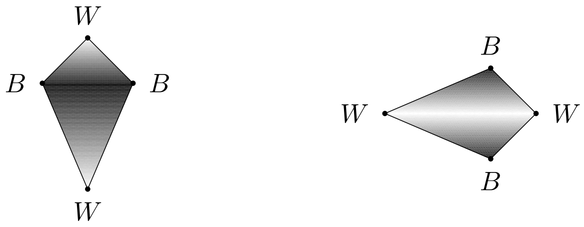

Figure III.7: Opposite vertices have the same black or white color. Scan line interpolation causes the appearance of the polygon to change radically when it is rotated. The two polygons are identical except for their orientation.

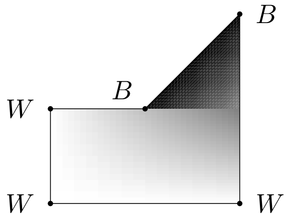

Figure III.8: Vertices are colored black or white as labeled. Scan line interpolation causes the non-convex polygon to be shaded discontinuously.

interpolation along edges and across scan lines simultaneously. However, scan line interpolation suffers from the serious drawback that the results of the interpolation can change greatly as the polygon is rotated, so it is generally not recommended for scenes that contain rotating polygons. Figure III.7 shows an example of how scan line interpolation can inconsistently render polygons as they rotate. There, a polygon is drawn twice, first upright and then rotated 90°. Two of the vertices of the polygon are labeled "W" and are assigned the color white. The other two vertices are labeled "B" and are colored black. The scan line interpolation imposes a top-to-bottom interpolation that drastically changes the appearance of the rotated polygon.

Another problem with scan line interpolation is shown in Figure III.8. Here a non-convex polygon has two black vertices and three white vertices. The non-convexity causes a discontinuous shading of the polygon.

Scan line interpolation on triangles does not suffer from the problems just discussed. Indeed, for triangles, scan line interpolation is equivalent to linear interpolation, at least up to round-off errors introduced by quantization. Since modern OpenGL renders only triangles and not general polygons, it is not susceptible to the kind of scan line interpolation problems discussed above.

Nonetheless, the examples in Figures III.7 and III.8 illustrate that you must be careful when splitting general polygons into triangles for rendering.

III.3.1 Bresenham algorithm

The Bresenham algorithm provides a fast iterative method for interpolating on integer values. It is traditionally presented as an algorithm for drawing pixels in a rectangular array to form a line. However, it applies equally well to perform linear interpolation of values in the depth buffer, linear interpolation for Gouraud shading, etc.

Before presenting the actual Bresenham algorithm, we present pseudo-code for an algorithm based on real numbers. Then we shall see how to rewrite the algorithm to use integers instead. The algorithm will calculate the integer values $j(i)$ for $i = i_1, i_1{+}1, \ldots, i_2$, so that $j(i_1) = j_1$ and $j(i_2) = j_2$. We are assuming without loss of generality that $i_1 < i_2$ and $j_1 \le j_2$ and that $\Delta j = j_2 - j_1$ and $\Delta i = i_2 - i_1$ with $\Delta j/\Delta i \le 1$. The first algorithm to compute the $j(i)$ values is (in pseudo-C++):

```
float dJ = j2-j1;
float dI = i2-i1;
float m = dJ/dI;     // Slope
writePixel(i1, j1);
float y = j1;
int i, j;
for ( i=i1+1; i<=i2; i++ ) {
    y = y+m;
    j = round(y);     // Round to nearest integer
    writePixel( i, j );
}
```

In the above code, the function `writePixel(i,j)` is called to indicate that $j(\mathtt{i}) = \mathtt{j}$. The function `round(y)` is not a real C++ function, but is intended to return y rounded to the nearest integer. The variables `i1` and `i2` are equal to i_1 and i_2.

The algorithm given above is very simple, but its implementation suffers from the fact that it uses floating point, and converts a floating point number to an integer number in each iteration of the loop. A more efficient algorithm, known as Bresenham's algorithm, can be designed to operate with only integers. The basic insight for Bresenham's algorithm is that the value of y in the algorithm is always a multiple of $1/(i_2 - i_1) = 1/\Delta i$. We shall rewrite the algorithm, using variables `j` and `ry` that have the property that $\mathtt{j} + (\mathtt{ry}/\Delta i)$ is equal to the value y of the previous pseudo-code. Furthermore, `j` is equal to $[y] = \mathtt{round}(y)$, so $-\Delta x/2 < \mathtt{ry} \le \Delta x/2$, where $\Delta x = \Delta i$. With these correspondences, it is straightforward to verify that the next algorithm is equivalent to the previous algorithm.

```
int deltaX = i2-i1;
int thresh = deltaX/2;          // Integer division rounds down
int ry = 0;
int deltaY = j2 - j1;
writePixel( i1, j1 );
int i;
int j = j1;
for ( i=i1+1; i<=i2; i++ ) {
    ry = ry + deltaY;
    if ( ry > thresh ) {
        j = j + 1;
        ry = ry - deltaX;
    }
    writePixel( i, j );
}
```

The above algorithm, the Bresenham algorithm, uses only integer operations and only straightforward operations such as addition, subtraction and comparison. In addition, the algorithm is simple enough that it can readily be implemented efficiently in special-purpose hardware.

III.3.2 The perils of floating point roundoff

The above algorithm for line drawing has the property that it attempts to draw lines which are "infinitely thin". Because of this there are several unavoidable pitfalls that can arise. The first and most common problem is the problem of aliasing. The term *aliasing* refers to a large variety of problems or effects that can occur when analog data is converted into digital data, or vice-versa. In the situation of drawing a line, we are converting floating point numbers which represent positions into integers which represent pixel positions. The floating point numbers usually have much more precision than the integer values and the conversion to integer values can cause problems.

For drawing lines on a screen, a major part of the problem is that the pixels on the screen are arranged rectangularly, whereas a line can be diagonal at an arbitrary angle. Therefore, a line at a diagonal is drawn as a "step function" consisting of straight segments which are horizontal (or vertical) with a one pixel jump between the segments. This can give the line drawn on the screen a jagged or saw-tooth look, that is to say, the line has "jaggies." In addition, if the line is animated, the positions of the "jaggies" on the line move with the line. This can cause undesirable effects where the jaggies become annoyingly visible, or where a moving line figure becomes "shimmery" from the changes in the digitization of the lines.

There are several anti-aliasing methods that can reduce the undesirable jaggies on lines, but we shall not discuss these here (see Sections X.2.1 and X.3). Instead, we shall discuss another problem that can arise in rendering lines if the programmer is not careful to avoid inconsistent roundoff errors. An example is shown in Figure III.9. In the figure, the program has attempted to draw two polygons, $ABCD$ and $BAEF$, which share the common edge $\overline{AB}$. However, due to roundoff errors, the second polygon was drawn as $B'A'EF$ where A' and B' are placed one pixel above and to the left of A and B, respectively. Because of this, the whole line segment $\overline{A'B'}$ is placed one pixel up and one pixel to the left of the segment $\overline{AB}$. The result is that the edges of the polygons do not exactly coincide, and there are pixels between the two polygons that are left undrawn. Each time the line segments "jog" up one pixel, an undrawn pixel is left behind. These undrawn pixels can create unsightly pixel-sized holes in the surface being formed from the two polygons.

In actuality, the problems of matching up edges between two abutting polygons is more even sensitive to roundoff error than is indicated in the previous paragraph. As discussed earlier, when two polygons share an edge,they should be rendered so that each pixel on the boundary edge belongs to exactly one of the two polygons. That is to say, the image needs to be drawn without leaving any gaps between the polygons *and* without having the polygons overlap in any pixel. There are several reasons why it is important to not have the polygons overlap and share a pixel. First, it is desirable for the image to be drawn the same regardless of the order in which the two polygons are processed. Second, for some applications, such as blending or shadow volumes, polygons will leave visible seams where they overlap. Scan line interpolation gives an easy method to accomplish this. But this does mean, unfortunately, that almost any roundoff error that moves a vertex to a different pixel position can cause rendering errors.

This kind of misplacement from roundoff errors can happen no matter how small the roundoff error is. The only way to avoid this kind of roundoff error is to compute the positions A' and B' in *exactly* the same way that A and B were computed. By "exactly the same way," we do not mean by a mathematically equivalent way, rather we mean by the same sequence of calculations.[8]

Figure III.10 shows another situation where discretization errors can cause pixel-sized holes, even if there are no roundoff errors. In the figure, three triangles are being drawn: $\triangle\mathbf{uyx}$, $\triangle\mathbf{uzy}$, and $\triangle\mathbf{vxz}$. The point $\mathbf{y}$ lies on the boundary of the third triangle. Of course, if the color assigned to the vertex $\mathbf{y}$ is not the appropriate weighted average of the colors assigned to $\mathbf{x}$ and $\mathbf{z}$, then there will be a discontinuity in color across the line $\overline{\mathbf{xz}}$. But there can be problems even if all vertices are assigned the same color. When the Bresenham algorithm draws the lines $\overline{\mathbf{xy}}$, $\overline{\mathbf{yz}}$, and $\overline{\mathbf{xz}}$, it starts by mapping the endpoints to the nearest pixel centers. This can sufficiently perturb the positions of the three points so that there are pixel-size gaps left undrawn between the line $\overline{\mathbf{xz}}$ and the two lines $\overline{\mathbf{xy}}$ and $\overline{\mathbf{yz}}$.

This kind of discretization error can easily arise when approximating

[8] In rare cases, even using exactly the same sequence of calculations may not be good enough if the CPU or floating point coprocessor has flexibility in when it performs rounding of intermediate results — as is the default setting on many PC's.

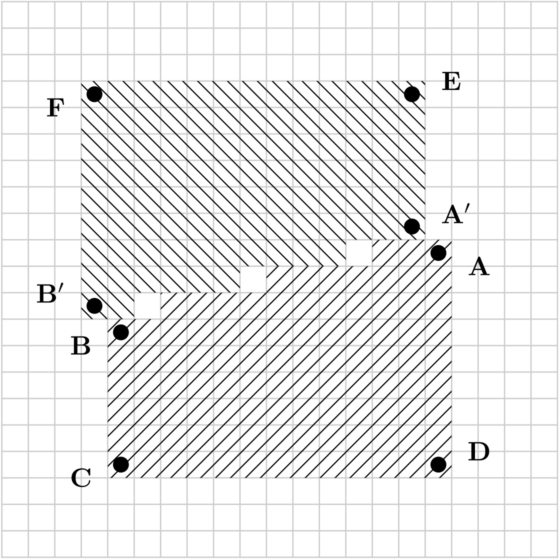

Figure III.9: The polygons $ABCD$ and $B'A'EF$ are supposed to share an edge, but arbitrarily small roundoff errors can cause a small displacement of the edge. This can lead to pixel-sized holes appearing between the two polygons. In the figure, the pixelized polygons are shown with different crosshatching: the three white pixels between the polygons are errors introduced by roundoff errors and will cause unwanted visual artifacts. This same effect can occur even in cases where only one of the vertices is affected by roundoff errors.

a curved surface with flat polygons; see the discussion on "cracking" in Section VIII.10.2. It can also occur when two flat polygons that abut each other are subdivided into subpolygons, for example in radiosity algorithms. If you look closely, you may be able to see examples of this problem in Figures XII.1-XII.3 on pages 426-427. (This depends on how precisely the figures were rendered in the printing process!)

To avoid this problem, you should subdivide the triangle $\triangle\mathbf{vxz}$ and draw the two triangles $\triangle\mathbf{vxy}$ and $\triangle\mathbf{vyz}$ instead of $\triangle\mathbf{vxz}$.

III.4 Additional exercises

Exercise III.4. Answer the following "True/False" questions a.-h. about a shader program with a vertex shader, a geometry shader and a fragment shader. It is assumed that the C++ program issues a `glDrawElements()` command with the option `GL_TRIANGLE_FAN`. The geometry shader is set up to take triangles as input (using `layout ( triangles ) in;`).

a. Each invocation of the geometry shader has access to the three vertices of a

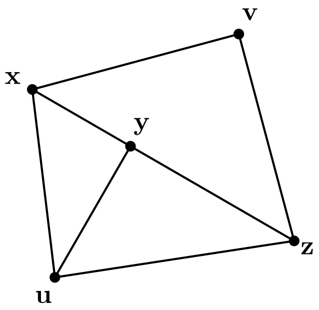

Figure III.10: Three triangles as placed by `glVertex*`. Even if no roundoff errors occur, the pixel-level discretization inherent in the Bresenham algorithm can leave pixel-sized gaps along the line $\overline{\mathbf{xz}}$.

triangle.

b. Each invocation of the geometry shader has access to all the vertices in the triangle fan.

c. The geometry shader can determine whether the draw command used `GL_TRIANGLE_FAN` instead of `GL_TRIANGLES` or `GL_TRIANGLE_STRIP`.

d. The geometry shader has access to all the vertex attributes of the vertices in the input triangle, even the ones that the vertex shader did not copy to “out” variables.

e. The geometry shader can access the `gl_VertexID`'s of the vertices of the input primitive, even if the vertex shader does not copy `gl_VertexID` to an `out` variable.

f. The geometry shader can read the values of uniform variables.

g. The geometry shader can change the values of uniform variables.

h. The geometry shader can (be programmed to) determine whether the input triangle lies entirely within the viewable region.

Chapter IV

Lighting and Shading

This is a ***preliminary*** *draft of a second edition of the book* 3-D Computer Graphics: A Mathematical Introduction with OpenGL. *So please read it cautiously and critically! Corrections are appreciated. Draft C.4.a*

Author: Sam Buss, `sbuss@ucsd.edu`

Lighting and shading are important tools for making graphics images appear more realistic, more attractive, and more understandable. Lighting and shading provide crucial visual cues about the curvature and orientation of surfaces, and are important in making three dimensionality apparent in a graphics image. Indeed, good lighting and shading is probably more important than correct perspective in making a scene understandable.

Lighting and illumination models in computer graphics are based on a modular approach where the artist or programmer specifies the positions and properties of light sources, and, independently, specifies the surface properties of materials. The properties of the lights and the materials interact to create the illumination, color, and shading that is seen from a given viewpoint.

For an example of the importance of lighting and shading for rendering three dimensional images, refer to Figure IV.1. Figure IV.1(b) shows a teapot rendered with a solid color with no shading. This flat, featureless teapot is just a silhouette with no three dimensionality. Figure IV.1(c) shows the same teapot, but now rendered with the Phong lighting model. This teapot now looks three dimensional, but the individual triangles are clearly visible. Figure IV.1(d) further improves the teapot by using Gouraud interpolation to create a smooth, rounded appearance. Finally, Figures IV.1(e) and (f) show the teapot with specular lighting added; the brightly reflecting spot shown in (e) and (f) is called a specular highlight.

"Shading" refers to the practice of letting colors and brightness vary smoothly across a surface. The two most popular kinds of shading are Gouraud interpolation [57] and Phong interpolation [88]. (These are also called "Gourand shading" and "Phong shading".) Either of these shading methods can be used to give a smooth appearance to surfaces. If fact, even surfaces which are

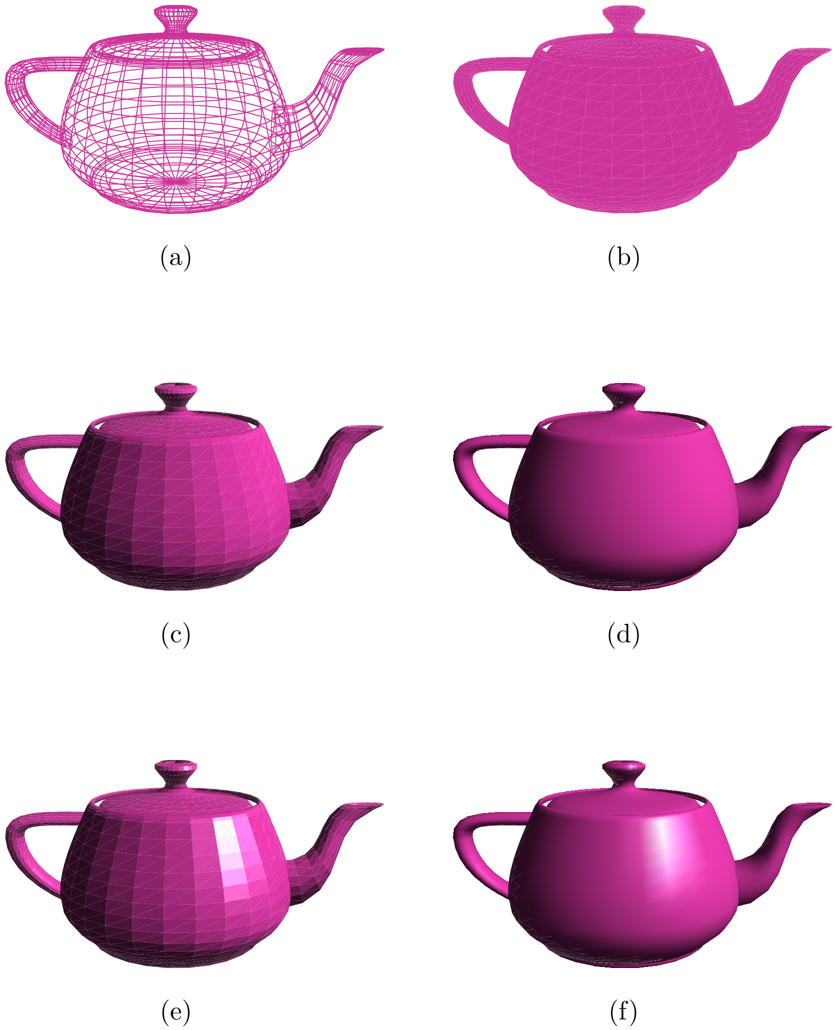

(a)

(b)

(c)

(d)

(e)

(f)

Figure IV.1: Six teapots with various shading and lighting options. (a) Wireframe teapot. (b) Teapot drawn with solid color, but no lighting or shading. (c) Teapot with flat shading, with only ambient and diffuse lighting. (d) Teapot drawn with Gouraud interpolation, with only ambient and diffuse reflection. (e) Teapot drawn with flat shading, with ambient, diffuse, and specular lighting. (f) Teapot with Gouraud shading, with ambient, diffuse, and specular lighting. See color plate C.6.

modeled as flat facets can appear smooth, as illustrated in Figure IV.1(d) and (f).

This chapter discusses two *local* models of illumination and shading. The first model is the popular Phong lighting model. The Phong lighting model gives good shading and illumination; in addition, it lends itself to efficient implementation in either software or hardware. Phong lighting models light as having diffuse and specular components: these concepts are very widely used in nearly all real-time graphics systems. The Phong lighting model was introduced by B.T. Phong in 1975 in the same paper [88] that introduced Phong shading.

The second local lighting model is the Cook-Torrance lighting model. This is computationally more difficult to implement, but gives better flexibility and the ability to model a wider variety of surfaces.

These lighting and shading models are at least partly based on the physics of how light reflects off surfaces. However, the actual physics of reflection is quite complicated, and it is more accurate to say that the Phong and Cook-Torrance models are physically *inspired*, rather than physically *correct*.

As "local" lighting models, the Phong and Cook-Torrance models consider only the effects of a light source shining directly onto a surface and then being reflected directly to the viewpoint. Local lighting models do not consider secondary reflections, where light may reflect from several surfaces before reaching the viewpoint. Nor do the local lighting models, at least in their simplest forms, properly handle shadows cast by lights. We will discuss nonlocal, or "global," lighting models later: Chapter X discusses ray tracing and Chapter XII discusses radiosity.

Section IV.1 describes the Phong lighting model, including the modelling of ambient, diffuse and specular reflection. We also discuss the Schlick Fresnel approximation for specular light at grazing angles. Section IV.2 then discusses how either Gouraud or Phong shading can be used to apply Phong lighting to pixels in the interior of triangles. Phong lighting uses surfaces normal in a very important way, and Section IV.3 describes methods for calculating surface normals. Section IV.4 describes how normal vectors are affected by affine (modelview) transformations. Section IV.5 gives shader code for Phong lighting, and Phong lighting with Schlick's Fresnel approximation.

Finally, Section IV.6 describes the Cook-Torrance model. The Cook-Torrance model and its extensions are usually not fully implemented because of their complexity, but it common to use an approximation (due to Schlick [97]) to the Fresnel term in the Cook-Torrance model. This is described in Sections IV.1.5 and IV.6.

IV.1 The Phong lighting model

The Phong lighting model is one of the simplest, but still very powerful, lighting and shading model for three dimensional computer graphics. Its popularity is due, firstly, to the fact that it is flexible enough to achieve a wide range of visual effects, and, secondly, to the fact that it is easy to implement efficiently

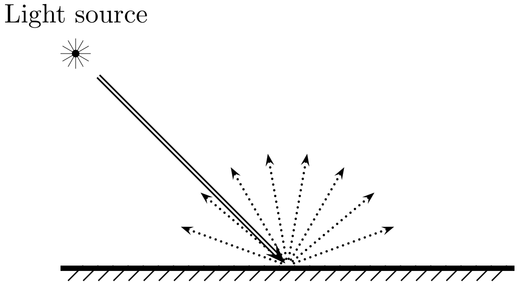

Figure IV.2: Diffusely reflected light is reflected equally brightly in all directions. The double line is a beam of incoming light. The dotted arrows indicate outgoing light.

in software and especially hardware. Modern graphics systems use modified and extended versions of Phong lighting, but the essential notions of diffuse and specular lighting are widely used.

The Phong lighting model is, at its heart, a model of how light reflects off of surfaces. For Phong lighting, all light sources are modeled as point light sources. Also, light is modeled as consisting of the three discrete color components, red, green, and blue. That is to say, it is assumed that all light consists of a pure red component, a pure green component, and a pure blue component. By the *superposition principle*, we can calculate light reflection intensities independently for each light source and for each of the three color components.

The Phong model allows for two kinds of reflection:

Diffuse reflection. Diffusely reflected light is light which is reflected evenly in all directions away from the surface. This is the predominant mode of reflection for non-shiny surfaces. Figure IV.2 shows the graphical idea of diffuse reflection.

Specular reflection. Specularly reflected light is light which is reflected in a mirror-like fashion, as from a shiny surface. As shown in Figure IV.3, specularly reflected light leaves a surface with its angle of reflection approximately equal to its angle of incidence. This is a large part of the reflected light from a polished or glossy surface. Specular reflections are the cause of “specular highlights,” i.e., bright spots on curved surfaces where intense specular reflection occurs.

In addition to dividing reflections into two categories, the Phong lighting model treats light or illumination as being of three distinct kinds:

Specular light. Specular light is light from a point light source which will be reflected specularly.

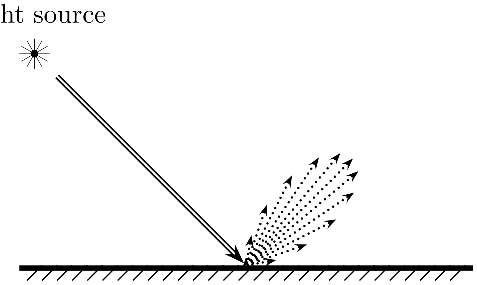

Figure IV.3: Specularly reflected light is reflected primarily in the direction with the angle of incidence equal to the angle of reflection. The double line is a beam of incoming light. The dotted arrows indicate outgoing light; the longer the arrow, the more intense the reflection in that direction.

Diffuse light. Diffuse light is light from a point light source which will be reflected diffusely.

Ambient light. Ambient light is light that arrives equally from all directions, rather than from a point light source. Ambient light is intended to model light which has spread around the environment through multiple reflections.

As mentioned earlier, light is modeled as coming in a small number of distinct wavelengths, i.e., in a small number of colors. In keeping with the fact that monitors have red, green, and blue pixels, light is usually modeled as consisting of a blend of red, green, and blue. Each of the color components is treated independently with its own specular, diffuse, and ambient properties.

Finally, the Phong lighting model gives material properties to each surface; the material properties control how lights illuminate the surface. Except for the specular exponent, these properties are set independently for each of the three colors.

Specular reflection properties. A *specular reflectivity coefficient*, $\rho_{\rm s}$, controls the amount of specular reflection. A *specular exponent*, f, controls the shininess of the surface by controlling the narrowness of the spread of specularly reflected light.

Diffuse reflection properties. A *diffuse reflectivity coefficient*, $\rho_{\rm d}$, controls the relative intensity of diffusely reflected light.

Ambient reflection properties. An *ambient reflectivity coefficient*, $\rho_{\rm a}$, controls the amount of ambient light reflected from the surface.

Emissive properties. The *emissivity* of a surface controls how much light the surface emits in the absence of any incident light. Light emitted from

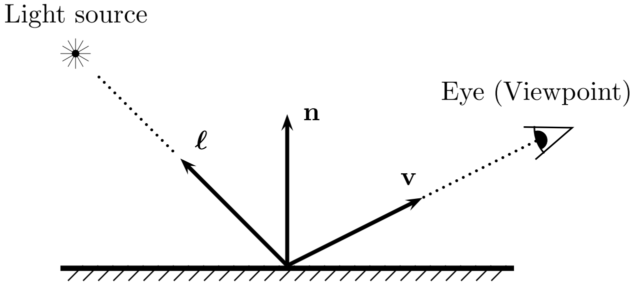

Figure IV.4: The fundamental vectors of the Phong lighting model. The surface normal is the unit vector $\mathbf{n}$. The point light source is in the direction of the unit vector $\boldsymbol{\ell}$. The viewpoint (eye) is in the direction of the unit vector $\mathbf{v}$. The vectors $\boldsymbol{\ell}$, $\mathbf{n}$ and $\mathbf{v}$ are not necessarily coplanar.

a surface does not act as a light source that illuminates other surfaces; instead, it only affects the color seen by the observer.

The basic setup for reflection in the Phong reflection model is shown in Figure IV.4. As shown in the figure, there is a particular point on a surface being illuminated by a point light source, and being viewed from some viewpoint. The surface's orientation is specified by a unit vector $\mathbf{n}$ pointing perpendicularly up from the surface. The light's direction is specified by a unit vector $\boldsymbol{\ell}$ which points from the point on the surface towards the light. The viewpoint direction is similarly specified by a unit vector, $\mathbf{v}$, pointing from the surface towards the viewpoint. These three vectors, plus the properties of the light source and of the surface material, are used by the Phong model to determine the amount of light reaching the eye.

We assume that light from the point light source is shining with intensity I^{in}. Phong lighting assumes that light has separate ambient, diffuse and specular component expressed as

$$I^{\mathrm{in}} \;=\; I^{\mathrm{in}}_{\mathrm{a}} + I^{\mathrm{in}}_{\mathrm{d}} + I^{\mathrm{in}}_{\mathrm{s}}.$$

Phong lighting provides methods to calculate the intensity of the light reflected from the surface that arrives at the eye. For our purposes, it is not particularly important to worry about how light intensity is measured, except it is useful to think of it as measuring the energy flux per unit area, where the area is measured perpendicularly to the direction of the light.

The next two sections discuss how the Phong model calculates the amount of diffuse reflection and the amount of specular reflection. For the time being, we will restrict attention to light at a single wavelength (i.e., of a single, pure color) and coming from a single light source. Section IV.1.4 explains how the effects of multiple lights and of different colors are additively combined.

Light Properties	
$I_{\mathrm{a}}^{\mathrm{in}}$	Incoming ambient light
$I_{\mathrm{d}}^{\mathrm{in}}$	Incoming diffuse light
$I_{\mathrm{s}}^{\mathrm{in}}$	Incoming specular light

Material Properties	
ρ_{a}	Ambient reflectivity
ρ_{d}	Diffuse reflectivity
ρ_{s}	Specular reflectivity
f	Specular exponent
I_{e}	Emissivity

Figure IV.5: Phong lighting allows properties of lights and surface properties of materials to be set independently. This allows extra flexibility for designing lighting. The properties shown above are given separate values for each color (usually red, green and blue), except the specular exponent (shininess) is the same for all colors.

Phong lighting uses quite a few light properties and material properties; these are summarized in Figure IV.5.

IV.1.1 Diffuse reflection

Diffuse reflection refers to the process of light reflecting equally in all directions, as illustrated in Figure IV.2. The fundamental Phong vectors are shown again in Figure IV.6, now with the angle between $\boldsymbol{\ell}$ and $\mathbf{n}$ shown equal to θ: this is the angle of incidence of the light arriving from the point source. The amount of light which is diffusely reflected is calculated as

$$I_{\mathrm{d}} \;=\; \rho_{\mathrm{d}} I_{\mathrm{d}}^{\mathrm{in}} \cos\theta \;=\; \rho_{\mathrm{d}} I_{\mathrm{d}}^{\mathrm{in}} (\boldsymbol{\ell} \cdot \mathbf{n}), \tag{IV.1}$$

where the second equality holds because the vectors are unit vectors. Here $I_{\mathrm{d}}^{\mathrm{in}}$ is the intensity of the incoming diffuse light. I_{d} is the intensity of the diffusely reflected light in the direction of the viewpoint. The value ρ_{d} is a constant, which is called the *diffuse reflectivity coefficient* of the surface. This value represents a physical property of the surface material.

A surface which diffusely reflects light according to Equation (IV.1) is called *Lambertian*, and most non-shiny surfaces are fairly close to Lambertian. The defining characteristic of a Lambertian surface is that if a large flat region of the surface is uniformly lit, then the surface should have the same apparent (or, perceived) brightness and color from all viewing directions.

The presence of the $\cos\theta$ term in Equation (IV.1) requires some explanation. Recall that the incoming light intensity, $I_{\mathrm{d}}^{\mathrm{in}}$, is intended to measure energy flux per unit area, with unit area measured *perpendicularly* to the direction of the light. Since the light is incident onto the surface at an angle of θ away from the normal vector $\mathbf{n}$, a "perpendicularly measured unit area" worth of energy flux is spread over a larger area of the surface, namely, an area of the surface which is larger by a factor of $1/(\cos\theta)$. See Figure IV.7 for an illustration of how the area increases by a factor of $1/\cos\theta$. Because of this, the energy flux arriving per unit area of the surface is only $(\cos\theta)I_{\mathrm{d}}^{\mathrm{in}}$.

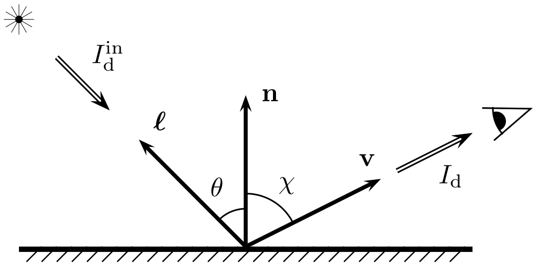

Figure IV.6: The setup for diffuse reflection in the Phong model. The angle of incidence is θ. $I_{\mathrm{d}}^{\mathrm{in}}$ and I_{d} are the incoming and outgoing light intensities in the indicated directions.

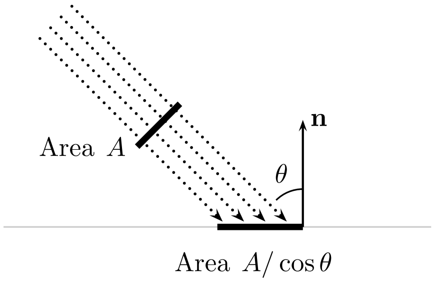

Figure IV.7: The perpendicular cross sectional area of a beam of light is A. The area of the surface tilted at an angle θ is larger by a factor of $1/\cos\theta$.

At this point, it would be reasonable to ask why there is not another cosine factor involving the angle of reflection. Of course, this is not what we generally perceive: that is, when one looks at a surface from a sharp angle we do not see the brightness of the surface drop off dramatically with the cosine of the angle of reflection. Otherwise, surfaces viewed from a sharply sidewise angle would appear almost black. Conversely, diffusely reflecting surfaces do not appear much brighter when viewed from straight on. [1]

However, more careful consideration of why there is no factor involving the angle of reflection reveals that Figure IV.2 was a little misleading. It is not the case that the probability of a single photon being reflected in a given direction is independent of the reflection direction. Instead, letting χ be the angle between the surface normal $\mathbf{n}$ and the outgoing light direction $\mathbf{v}$, the probability that a photon reflects out in the direction $\mathbf{v}$ is proportional to $\cos\chi$. The viewer

[1] We are describing Lambertian surfaces. However, not all surfaces are Lambertian, for example the moon as illuminated by the sun and viewed from the earth.

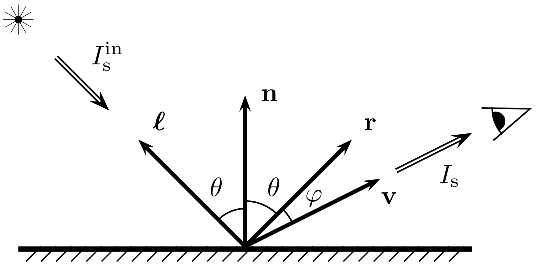

Figure IV.8: The setup for specular reflection in the Phong model. The angle of incidence is θ. The vector $\mathbf{r}$ points in the direction of perfect mirror-like reflection. $I_{\mathrm{s}}^{\mathrm{in}}$ and I_{s} are the incoming and outgoing specular light intensities in the indicated directions.

looking at the surface from this view angle of χ from the normal vector sees light coming from a surface area of $(1/\cos\chi)$ times the apparent field of view area. (This is similar to the justification of the $\cos\theta$ factor.) The two factors of $\cos\chi$ and $1/\cos\chi$ cancel out, and we are left with the Phong diffuse reflection formula (IV.1).

IV.1.2 Specular reflection

Specular reflection refers to the process of light reflecting primarily mirror-like, in the direction where the angle of incidence equals the angle of reflection. The purpose of specular reflection is to model shiny surfaces. A perfect mirror would reflect all of its light in exactly that direction, but most shiny surfaces do not reflect nearly as well as a mirror, so the specularly reflected light spreads out a little, as is shown in Figure IV.3. (In any event, the Phong lighting model is not capable of modeling true mirror-like reflections.)

Given the unit vector $\boldsymbol{\ell}$ in the direction of the light source, and the unit surface normal $\mathbf{n}$, the direction of a perfect mirror-like reflection is given by the vector $\mathbf{r}$ shown in Figure IV.8. The vector $\mathbf{r}$ is a unit vector, coplanar with $\boldsymbol{\ell}$ and $\mathbf{n}$. The angle of perfect reflection is the angle between $\mathbf{r}$ and $\mathbf{n}$, and this is equal to the angle of incidence, θ, which is the angle between $\boldsymbol{\ell}$ and $\mathbf{n}$.

It is best to compute $\mathbf{r}$ using the following formula:

$$\mathbf{r} \ = \ 2(\boldsymbol{\ell}\cdot\mathbf{n})\mathbf{n} - \boldsymbol{\ell}.$$

To derive this formula, note that $(\boldsymbol{\ell}\cdot\mathbf{n})\mathbf{n}$ is the projection of $\boldsymbol{\ell}$ onto $\mathbf{n}$, and that $\boldsymbol{\ell} - (\boldsymbol{\ell}\cdot\mathbf{n})\mathbf{n}$ is equal to $(\boldsymbol{\ell}\cdot\mathbf{n})\mathbf{n} - \mathbf{r}$. For this, see Figure IV.9.

In Figure IV.8, the angle between the view vector and the perfect reflection direction vector is φ. Let's assume for simplicity that $\varphi < \pi/2$ (that is, φ less than 90 degrees). The guiding principle for determining specular reflection is

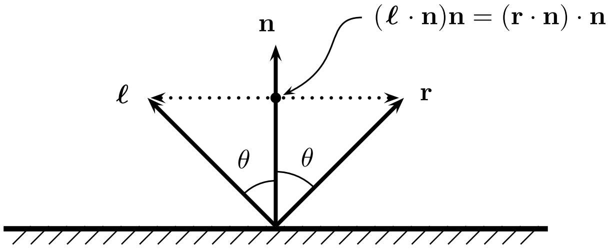
n
$(\boldsymbol{\ell}\cdot\mathbf{n})\mathbf{n} = (\mathbf{r}\cdot\mathbf{n})\cdot\mathbf{n}$
$\boldsymbol{\ell}$
r
θ
θ

Figure IV.9: The calculation of the reflection vector $\mathbf{r}$ for specular lighting. The two dotted vectors are $\boldsymbol{\ell} - (\boldsymbol{\ell}\cdot\mathbf{n})\mathbf{n}$ and $\mathbf{r} - (\boldsymbol{\ell}\cdot\mathbf{n})\mathbf{n}$; they are the negatives of each other.

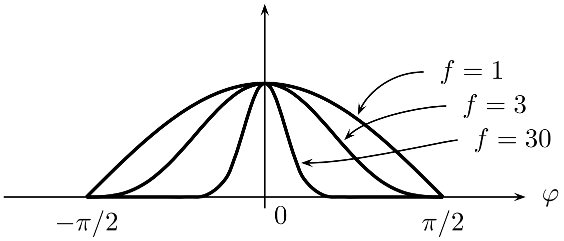

Figure IV.10: The function $(\cos\varphi)^f$ for $f = 1, 3, 30$ with φ in the range $[-\pi/2, \pi/2]$. As f increases, the graph of $(\cos\varphi)^f$ decreases and gets skinnier.

that the closer the angle φ is to zero, the more intense the specular reflection in the direction of the viewpoint. The Phong lighting model uses the factor

$$(\cos\varphi)^f \tag{IV.2}$$

to model the dropoff in light intensity in a reflection direction which differs by an angle of φ from the direction $\mathbf{r}$ of perfect reflection. Figure IV.10 shows some examples of the graph of $(\cos\theta)^f$ for some small values of f.

There is no particular physical justification for the use of the factor $(\cos\varphi)^f$; rather, it is used since the cosine can easily be computed by a dot product, and since the exponent f can be adjusted experimentally on an ad hoc basis to achieve the desired spread of specular light. The exponent f is ≥ 1, with values in the range 50 to 100 being typical for shiny surfaces; the larger the exponent, the narrower the beam of specularly reflected light. Higher exponent values make the specular highlights smaller and the surface appear shinier; however, exponents which are too high can lead to specular highlights being missed.

With the factor (IV.2), the Phong formula for the intensity $I_{\rm s}$ of specularly reflected light is:

$$I_{\rm s} \;=\; \rho_{\rm s} I_{\rm s}^{\rm in}(\cos\varphi)^f \;=\; \rho_{\rm s} I_{\rm s}^{\rm in}(\mathbf{v}\cdot\mathbf{r})^f, \tag{IV.3}$$

where $\rho_{\rm s}$ is a constant called the *specular reflectivity coefficient*, and $I_{\rm s}^{\rm in}$ is the intensity of the specular light from the light source. The value of $\rho_{\rm s}$ depends

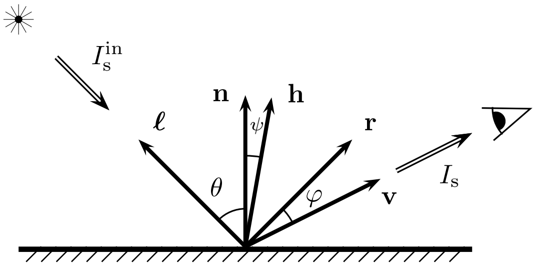

Figure IV.11: The setup for calculating the specular reflection using the halfway vector $\mathbf{h}$, the unit vector halfway between $\boldsymbol{\ell}$ and $\mathbf{v}$.

on the surface and on the wavelength of the light. For the time being, we are working under the assumption that all the light is a single pure color.

Equations (IV.2) and (IV.3) are correct under the assumption $\varphi \leq \pi/2$, so $\mathbf{v} \cdot \mathbf{r} \geq 0$. When $\varphi > \pi/2$ and $\mathbf{v} \cdot \mathbf{r} < 0$, there is no specular reflection as the direction of perfect reflection is not pointing in the direction towards the viewer. Thus, in the general formula for I_s is

$$I_s \;=\; \rho_s I_s^{in} (\max\{\cos\varphi, 0\})^f \;=\; \rho_s I_s^{in} (\max\{\mathbf{v} \cdot \mathbf{r}, 0\})^f. \tag{IV.4}$$

Equation IV.4 holds for all φ, not just $\varphi \leq \pi/2$.

Often a computational shortcut, based on the "halfway" vector, is used to simplify the calculation of I_s. The *halfway vector* $\mathbf{h}$ is defined to be the unit vector halfway between the light source direction and the view direction, namely

$$\mathbf{h} \;=\; \frac{\boldsymbol{\ell} + \mathbf{v}}{||\boldsymbol{\ell} + \mathbf{v}||}.$$

Let ψ be the angle between $\mathbf{h}$ and the surface normal $\mathbf{n}$. Referring to Figure IV.11, it is easy to see that if $\boldsymbol{\ell}$, $\mathbf{n}$, and $\mathbf{v}$ are (approximately) coplanar, then ψ is (approximately) equal to $\varphi/2$. Therefore, it is generally acceptable to use $(\cos\psi)^f$ instead of $(\cos\varphi)^f$ in the calculation of I_s, since the exponent f can be changed slightly to compensate for the factor of two change in the value of the angle. With the halfway vector, the Phong equation for the intensity of specular reflection becomes:

$$I_s \;=\; \rho_s I_s^{in} (\cos\psi)^f \;=\; \rho_s I_s^{in} (\mathbf{h} \cdot \mathbf{n})^f. \tag{IV.5}$$

Although (IV.5) is not exactly equal to (IV.3), it gives qualitatively similar results. One advantage to using the halfway vector is that $\mathbf{h} \cdot \mathbf{n}$ cannot be negative, so we do not need to use $\max\{\mathbf{h} \cdot \mathbf{n}, 0\}$.

For polygonally modeled objects, the calculation of the diffuse and specular components of Phong lighting is usually done at least once for each vertex in the geometric model. For points in the interior of polygons, either Phong shading calculates the entire Phong lighting equation for each pixel, or Gouraud shading is used to determine the lighting and colors by averaging values from the vertices (see Section IV.2 below). Thus the formula (IV.1) and the formulas (IV.3) or (IV.5) will need to be calculated at each pixel (in Phong shading) or at each vertex (in Gouraud shading). Each of these calculations needs the unit vectors $\boldsymbol{\ell}$ and $\mathbf{v}$. To calculate $\boldsymbol{\ell}$ and $\mathbf{v}$, one subtracts the surface position from the positions of the light and the viewpoint, and then normalizes the resulting differences. This is computationally expensive, since, for each of $\boldsymbol{\ell}$ and $\mathbf{v}$, it requires calculation of a square root and a division.

One way to avoid repeated calculation of $\boldsymbol{\ell}$ and $\mathbf{v}$ is to make the simplifying approximation that they are constants, and are the same for all vertices. In essence, this has the effect of placing the lights and the viewpoint at points at infinity, so that the view direction $\mathbf{v}$ and the light direction $\boldsymbol{\ell}$ are independent of the position of the surface being illuminated. When the light direction vector $\boldsymbol{\ell}$ is held constant, we call the light a *directional light.* Non-directional lights are called *positional* lights, since the light's position determines the direction of illumination of any given point. If the view direction is computed using the position of the viewpoint, then we say there is a *local viewer.* Otherwise, the view direction $\mathbf{v}$ is held fixed, and we call it a *nonlocal viewer.* Note that a nonlocal viewer can be used in conjunction with a perspective viewing transformation!

If we have a directional light and a nonlocal viewer, so that both $\boldsymbol{\ell}$ and $\mathbf{v}$ are held constant, then the vector $\mathbf{h}$ also remains constant. This makes the use of the halfway vector and formula (IV.5) even more advantageous: the only vector that needs to be recalculated for Phong lighting is the surface normal $\mathbf{n}$.

So far, we have mentioned two advantages to using the halfway vector. First, we do not need to handle the (impossible) case $\mathbf{h} \cdot \mathbf{n} < 0$. And second, with the directional viewers and positional lights, we do not need to repeatedly recalculate $\mathbf{h}$. An additional advantage of the halfway vector is that it can work better with very low specular exponent values f. A value $f \leq 1$ makes a very broad, spread-out specular highlight. However, when $f \leq 1$, although $\lim_{\theta \to (\pi/2)^-} (\cos\theta)^f)$ is equal to 0, the curve $(\cos\theta)^f$ does not have a continuous left derivative at $\theta = \pi/2$, and in fact, does not have a derivative there if $f < 1$. This discontinuous change in the rate of the light intensity can cause a visible border on the specular highlight, showing up exactly where $\mathbf{r} \cdot \mathbf{v} = 0$. This effect does not occur when using the halfway vector, since the $\mathbf{n} \cdot \mathbf{h} \geq 0$ always holds and there is no visible border.

IV.1.3 Ambient reflection and emissivity

Ambient light is light which comes from all directions, rather than from the direction of a light source. It is modeled as being reflected equally in all directions, so the ambient component of the surface lighting and shading is independent of the direction of view. We let $I_{\mathrm{a}}^{\mathrm{in}}$ represent the total intensity of the incoming ambient light. In the Phong model, the surface has an associated *ambient reflectivity coefficient*, $\rho_{\rm a}$, which specifies the fraction of the ambient light that is reflected. The formula for the intensity of the outgoing ambient light is:

$$I_{\rm a} \;=\; \rho_{\rm a} I_{\rm a}^{\rm in}. \tag{IV.6}$$

Finally, a surface can also be given an *emissive intensity constant*, $I_{\rm e}$. This is equal to the intensity of the light emitted by the surface in addition to the reflected light.

IV.1.4 Putting it together: multiple lights and colors

So far, the discussion of the Phong model has been restricted to a single wavelength (or pure color) of light, with illumination from a single light source. According to the superposition principle, the various types of reflection and emission can be combined by simple addition. Furthermore, the effect of multiple lights is likewise determined by adding the illumination from the lights considered individually. Finally, different wavelengths may be considered independently, with no interaction between the intensity of one wavelength and another.

First, for a single wavelength and a single light source, the total outgoing light intensity, I, is equal to

$$\begin{aligned} I &= I_{\rm a} + I_{\rm d} + I_{\rm s} + I_{\rm e} \\ &= \rho_{\rm a} I_{\rm a}^{\rm in} + \rho_{\rm d} I_{\rm d}^{\rm in} (\boldsymbol{\ell} \cdot \mathbf{n}) + \rho_{\rm s} I_{\rm s}^{\rm in} (\max\{\mathbf{r} \cdot \mathbf{v}, 0\})^f + I_{\rm e}. \end{aligned} \tag{IV.7}$$

The halfway vector formula for specular reflection may be used instead, with $\mathbf{h} \cdot \mathbf{n}$ replacing $\max\{\mathbf{r} \cdot \mathbf{v}, 0\}$ in the equation.

Second, to adapt this formula to multiple wavelengths, we write I^λ, $I_{\rm a}^{\lambda,{\rm in}}$, $I_{\rm d}^{\lambda,{\rm in}}$, $I_{\rm s}^{\lambda,{\rm in}}$, $I_{\rm e}^\lambda$ for the intensities of the light at wavelength λ. In addition, the material properties are also dependent on the wavelength λ, and can now be written as $\rho_{\rm a}^\lambda$, etc. It is usual, however, to make the specular exponent independent of the wavelength. Equation (IV.7) can be specialized to a single wavelength, yielding

$$I^\lambda \;=\; \rho_{\rm a}^\lambda I_{\rm a}^{\lambda,{\rm in}} + \rho_{\rm d}^\lambda I_{\rm d}^{\lambda,{\rm in}} (\boldsymbol{\ell} \cdot \mathbf{n}) + \rho_{\rm s}^\lambda I_{\rm s}^{\lambda,{\rm in}} (\max\{\mathbf{r} \cdot \mathbf{v}, 0\})^f + I_{\rm e}^\lambda. \tag{IV.8}$$

It is traditional to use the three wavelengths of red, green, and blue light, since these are the three colors displayed by computer monitors; however, more wavelengths can be used for greater realism.

To write a single equation incorporating all three wavelengths at once, we use boldface variables to denote a 3-tuple: we let $\boldsymbol{\rho}_{\rm a}$ denote the triple $\langle \rho_{\rm a}^{\rm red}, \rho_{\rm a}^{\rm green}, \rho_{\rm a}^{\rm blue} \rangle$, let $\mathbf{I}$ equal $\langle I^{\rm red}, I^{\rm green}, I^{\rm blue} \rangle$, etc. We also momentarily use $*$ for component-wise multiplication on 3-tuples. Then Equation (IV.8) can be written as:

$$\mathbf{I} \;=\; \boldsymbol{\rho}_{\rm a} * \mathbf{I}_{\rm a}^{\rm in} + \boldsymbol{\rho}_{\rm d} * \mathbf{I}_{\rm d}^{\rm in} (\boldsymbol{\ell} \cdot \mathbf{n}) + \boldsymbol{\rho}_{\rm s} * \mathbf{I}_{\rm s}^{\rm in} (\max\{\mathbf{r} \cdot \mathbf{v}, 0\})^f + \mathbf{I}_{\rm e}. \tag{IV.9}$$

Third, we consider the effect of multiple point light sources. We assume there are k light sources. When illuminating a given point on a surface, light number i has light direction vector $\boldsymbol{\ell}_i$. The i-th light also has an intensity value $\mathbf{I}^{\text{in},i}$ which represents the intensity of the light reaching that point on the surface. This intensity may be moderated by the distance of the surface from the light, and by various other effects, such as spotlight effects. In addition, if $\mathbf{n} \cdot \boldsymbol{\ell}_i \le 0$, then the light is not shining from above the surface, and in this case we take incoming diffuse and specular light intensities, $\mathbf{I}_{\text{d}}^{\text{in},i}$ and $\mathbf{I}_{\text{s}}^{\text{in},i}$, to be zero. However, the incoming ambient light, $\mathbf{I}_{\text{a}}^{\text{in},i}$, will typically not be zeroed out when the light is below the surface. We then add the terms of Equation (IV.9) over all light sources to get the overall illumination ($\mathbf{r}_i$ is the unit vector in the direction of perfect reflection for light i):

$$\mathbf{I} \;=\; \boldsymbol{\rho}_{\text{a}} * \mathbf{I}_{\text{a}}^{\text{in}} + \boldsymbol{\rho}_{\text{d}} * \sum_{i=1}^{k} \mathbf{I}_{\text{d}}^{\text{in},i}(\boldsymbol{\ell}_i \cdot \mathbf{n}) + \boldsymbol{\rho}_{\text{s}} * \sum_{i=1}^{k} \mathbf{I}_{\text{s}}^{\text{in},i}(\max\{\mathbf{r}_i \cdot \mathbf{v}, 0\})^f + \mathbf{I}_{\text{e}}. \quad \text{(IV.10)}$$

The first term in this equation is a 3-tuple $\mathbf{I}_{\text{a}}^{\text{in}}$ representing the incoming ambient light. It is common to specify a global value, $\mathbf{I}_{\text{a}}^{\text{in,global}}$, for global ambient light, and to have each light source contribute some additional ambient light, $\mathbf{I}_{\text{a}}^{\text{in},i}$ to the scene. Then,

$$\mathbf{I}_{\text{a}}^{\text{in}} = \mathbf{I}_{\text{a}}^{\text{in,global}} + \sum_{i=1}^{k} \mathbf{I}_{\text{a}}^{\text{in},i}. \quad \text{(IV.11)}$$

Exercise IV.1. Why is it customary to use the same specular exponent for all wavelengths? What would a specular highlight look like if different wavelengths had different specular exponents?

IV.1.5 Schlick's Fresnel term for specular reflection

The Phong lighting calculation treated the specular reflectivity coefficient, ρ_{s}, as being constant independent of the angle of incidence of light. However, many real-world materials show specular reflections at grazing angles, namely when the incoming light is close to parallel to the surface and thus close perpendicular to the normal vector $\mathbf{n}$. This true even for materials, like paper or cloth, that do not show specular highlights in other situations. Although Phong lighting does not take this into account, the more sophisticated Cook Torrance lighting model handles specular reflectivity with a physically-based calculation based on the Fresnel reflection equations and a microfacet model of surfaces. This is described in Section IV.6.

Schlick [97] gave a simplified approximation of the specular reflectivity that matches the Cook-Torrance method to a high degree of accuracy, but is much easier to compute. The Schlick approximation does not require any new material properties, so is easy to incorporate into the Phong lighting model. As before, let θ be the angle between the light vector $\boldsymbol{\ell}$ and the normal vector $\mathbf{n}$. The basic idea of the Schlick approximation is that for angles θ up to approximately

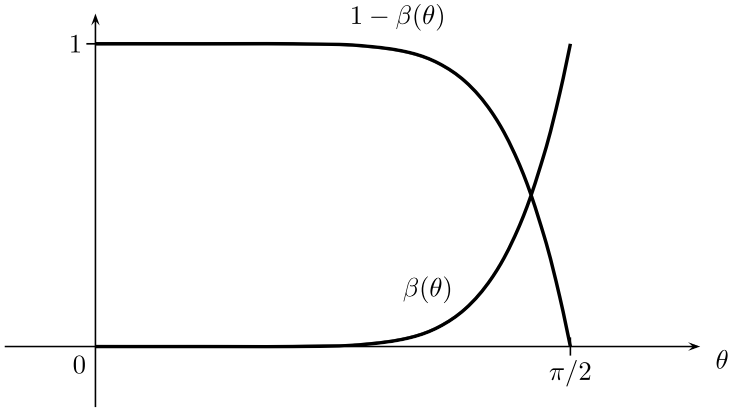

Figure IV.12: The curves $\beta(\theta)$ and $1-\beta(\theta)$ for $\beta(\theta) = (1-\cos\theta)^5$ where $0 \le \theta \le \pi/2$. The angle θ is the angle between the light direction $\boldsymbol{\ell}$ and the normal vector $\mathbf{n}$. At $\theta = \pi/3$ (60 degrees), $\beta(\pi/3) = 0.03125$ so $1-\beta(\pi/3) = 0.96875$ is still close to 1. The two curves cross where β is equal to $1/2$, with $\theta \approx 1.441$ radians, i.e. 82°.

$\pi/3$ radians (60°), the specular reflectively is very close to the Phong specular reflectivity coefficient $\rho_{\rm s}$, but for larger angles θ up to π radians (90°), the effective specularity coefficient approaches 1. The Schlick calculation defines

$$\beta(\theta) \;=\; (1-\cos\theta)^5 \;=\; (1-\boldsymbol{\ell}\cdot\mathbf{n})^5.$$

The value $\beta(\theta)$ is then used to linearly interpolate between $\rho_{\rm s}$ and 1 using the formula

$$\rho_{\rm Schlick} \;=\; (1-\beta(\theta))\cdot\rho_{\rm s} + \beta(\theta). \tag{IV.12}$$

Later, in Chapter V, we will see that this is just a linear interpolation from $\rho_{\rm s}$ to 1: the equation for $\rho_{\rm Schlick}$ will be written as $\mathit{lerp}(\rho_{\rm s}, 1, \beta(\theta))$. In GLSL, it would be expressed as `mix(` $\rho_{\rm s}$ `, 1,` $\beta(\theta)$`)`.

To understand Equation (IV.12), see Figure IV.12. The figure shows that $\beta(\theta)$ is very close to 0 until approximately $\theta = \pi/3$; for large values of θ, it transitions rather quickly to 1. Conversely, $1-\beta(\theta)$ is close to 1 for moderate values of θ, and transitions to 0 only as θ gets close to $\pi/2$. Consequently, the Schlick Fresnel term has a noticeable effect only when the light vector $\boldsymbol{\ell}$ starts getting close to parallel to the surface.

The Schlick Fresnel specular reflectivity coefficient $\rho_{\rm Schlick}$ is computed using Equation (IV.12). To incorporate this into Phong lighting, just replace $\rho_{\rm s}$ with $\rho_{\rm Schlick}$ in Equations (IV.3)-(IV.5). It is evident that Equation (IV.12) will have the most effect when $\rho_{\rm s}$ is not close to 1. Thus, the Fresnel adjustment is mostly useful for diffuse surfaces that have low specular reflectivity.

IV.1.6 Attenuation and spotlight effects

It is common to use distance attenuation and spotlights to achieve some special effects with lighting. Distance attenuation means making the light less intense, i.e. less bright, as the distance increases from the light. The usual formula[2] for the distance attenuation factor is:

$$\delta \;=\; \frac{1}{k_{\mathrm{c}} + k_{\mathrm{l}}d + k_{\mathrm{q}}d^2} \qquad \text{(IV.13)}$$

where d is the distance from the light, and the constant scalars k_{c}, k_{l} and k_{q} are the *constant attenuation factor*, the *linear attenuation factor*, and the *quadratic attenuation factor*, respectively. All three of the light intensity values, $\mathbf{I}^{\mathrm{in}}_{\mathrm{a}}$, $\mathbf{I}^{\mathrm{in}}_{\mathrm{d}}$, and $\mathbf{I}^{\mathrm{in}}_{\mathrm{s}}$, are multiplied by the distance attenuation factor δ before being used in the Phong lighting calculations.

Having three different parameters, k_{c}, k_{l} and k_{q}, provides some flexibility in using distance attenuation. The physically correct attenuation of light from a point source would use an inverse square law falloff in intensity. An inverse square law falloff, however, is more extreme than is desirable in most applications. The inverse square law also does not take into account that, in actuality, most lights are not point sources; nor does it take in account multiple interreflections of light. For these reasons, it is useful also have k_{c} and k_{l}, to give better artistic or visual effects from distance attenuation.

Spotlights are another kind of visual effect, based on attenuation and clipping of light. A spotlight is a positional light which shines a narrow beam of light. The spotlight models light shining in the direction of a circular cone around a central axis. A spotlight can be specified with three values:

- The direction $\mathbf{s}$ of the spotlight. This unit vector is the vector giving the direction of the center of the spotlight.

- The cutoff angle θ. This is the angle between the center vector $\mathbf{s}$ and the sides of the cone of light from the light source. (See Figure IV.13.) A cutoff angle of θ specifies that the light intensity drops abruptly to zero for any direction which is more than θ degrees away from the spotlight direction. Often, it is more efficient to give the cosine value $\cos\theta$ instead of the angle θ itself.

- The spotlight exponent $c \ge 0$. This constant controls how fast the light intensity decreases away from the center of the spotlight. The intensity of the light along a direction at an angle φ from the center of the spotlight (where φ is less than the spotlight cutoff angle) is reduced by a factor of $(\cos\varphi)^c = (-\mathbf{s}\cdot\boldsymbol{\ell})^c$.

Figure IV.13 shows the setup for spotlights. The vector $\boldsymbol{\ell}$ still gives the vector from the illuminated point to the spotlight position. Thus $\cos\varphi = -\mathbf{s}\cdot\boldsymbol{\ell}$.

[2] This is the approach used in legacy OpenGL.

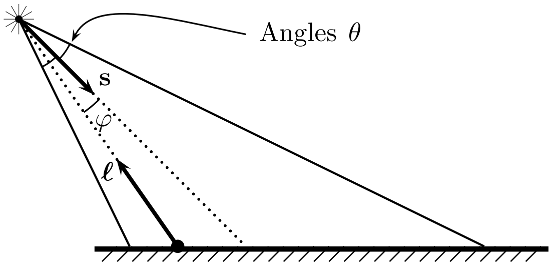

Figure IV.13: A spotlight. The spot direction is $\mathbf{s}$. The cone of the spotlight is the area within angle θ of the spot direction. The angle φ is the angle between the spot direction and the direction to the point on the surface. We have $\cos\varphi = -\boldsymbol{\ell}\cdot\mathbf{s}$.

The spotlight attenuation factor δ' can be computed as

$$\delta' \;=\; \begin{cases} (-\boldsymbol{\ell}\cdot\mathbf{s})^c & \text{if } (-\boldsymbol{\ell}\cdot\mathbf{s}) \ge \cos\theta \\ 0 & \text{otherwise.} \end{cases} \tag{IV.14}$$

Equations (IV.10) and (IV.11) are rewritten include the distance attenuation and spotlight effects as

$$\begin{aligned} \mathbf{I} \;=\;& \boldsymbol{\rho}_{\mathrm{a}} * \mathbf{I}_{\mathrm{a}}^{\mathrm{in,global}} + \mathbf{I}_{\mathrm{e}} \\ &+ \sum_{i=1}^{k} \delta_i \cdot \delta_i' \cdot \Big(\boldsymbol{\rho}_{\mathrm{a}} * \mathbf{I}_{\mathrm{a}}^{\mathrm{in},i} + \boldsymbol{\rho}_{\mathrm{d}} * \mathbf{I}_{\mathrm{d}}^{\mathrm{in},i}(\boldsymbol{\ell}_i\cdot\mathbf{n}) + \boldsymbol{\rho}_{\mathrm{s}} * \mathbf{I}_{\mathrm{s}}^{\mathrm{in},i}(\max\{\mathbf{r}_i\cdot\mathbf{v},0\})^f \Big). \end{aligned}$$

where δ_i and δ_i' are the factors for the i-th light. Note that the distance attenuation and spotlight effects apply to all aspects of the light including ambient light. This is one of the reasons for including global ambient light in the Phong lighting model.

This completes the theoretical description of Phong lighting. The next section takes up the two most common methods of interpolating, or shading, colors and brightness from the vertices of a triangle into the interior points of the triangle. The two sections after that discuss how to calculate and transform normals. Section IV.5 describes the shader code from the *EduPhong* package that implements Phong lighting calculations.

IV.2 Gouraud and Phong shading

The term “shading” refers to the use of interpolation to create a smoothly varying pattern of color and brightness on the surfaces of objects. Without shading, each triangle in a geometric model would be rendered as a solid, constant color; the resulting image would be noticeably polygonal. One way to avoid this problem is to use extremely small triangles, say with each triangle so small that it spans only one pixel, but often this is prohibitively expensive in terms of computational time. Instead, good shading effects can be obtained even for moderately large triangles by computing the lighting and colors at only the vertices of the polygons and using interpolation, or averaging, to set the lighting and colors of pixels in the interior of the triangles.

There are several ways that interpolation is used to create shading effects. As usual, suppose a surface is modeled as a set of triangles, and we render one triangle at a time. Consider the problem of determining the color at a single vertex of one of the patches. Once the light source, viewpoint, and material properties are fixed, it remains only to specify the normal vector $\mathbf{n}$ at the vertex. If the surface is intended to be a smooth surface, then the normal vector at the vertex should, of course, be set to be the normal to the underlying surface. On the other hand, some surfaces are faceted and consist of flat polygon patches, for example, the cube shown in part (a) of Figure IV.14. For these surfaces, the normal vector for the vertex should be the same as the normal vector for the polygon being rendered. Since vertices typically belong to more than one triangle, this means that a vertex might be rendered with different normal vectors for different triangles.

Parts (d) and (f) of Figure IV.1 show examples of Gouraud shading. Figure IV.14 shows a more extreme example of how Gouraud shading can hide, or partially hide, the edges of polygons. Both parts of Figure IV.14 show a reddish solid cube lit by only ambient and diffuse light, and both figures use Gouraud shading. The first cube was rendered by drawing each polygon independently, with the normals at all four vertices of each polygon normal to the plane of the polygon. The second cube was drawn with the normal to each vertex pointing outward from the center point of the cube; i.e., the normals at a vertex are an average of the normals of the three adjacent faces and thus are equal to $\langle \pm 1/\sqrt{3}, \pm 1/\sqrt{3}, \pm 1/\sqrt{3} \rangle$. The faces of the cube are clearly visible as flat surfaces in the first figure, but are somewhat disguised in the second picture.

The question of how to determine the surface normal at a vertex of a polygonal model will be discussed further in Section IV.3. However, first we consider the methods for interpolating the results of the Phong lighting model to shade interior points of a polygon. We assume the polygon is a triangle. This is a reasonable assumption, since rendering systems generally triangulate polygons. This assumption has the convenient effect that triangles are always planar, so we do not need to worry about the pathological situation of non-planar polygons.

There are two kinds of shading used with the Phong model, and both usually use the scan line interpolation described in Section III.3. Scan line interpolation is also equivalent to linear interpolation, which will be discussed in Section V.1.

The first kind of shading is *Gouraud shading*. In Gouraud shading, a color value is determined for each vertex, the color value being a triple $\langle r, g, b \rangle$ with red, green, and blue light intensities. After the three vertices of a triangle are rendered at pixel positions in the viewport, the interior pixels of the triangle in

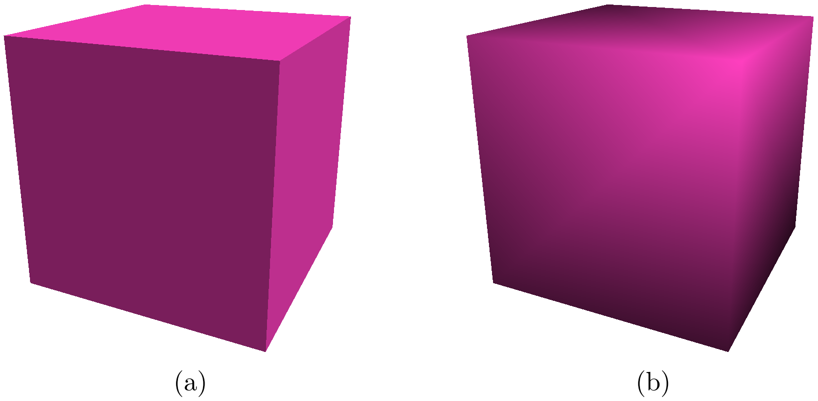

Figure IV.14: Two cubes with (a) normals at vertices perpendicular to each face, and (b) normals outward from the center of the cube. Note that (a) is rendered with Gouraud shading, not flat shading. See color plate C.7.

the viewport are shaded by simple linear interpolation. Recall that this means that if two vertices, $\mathbf{x}_0$, $\mathbf{x}_1$, have color values $\langle r_i, g_i, b_i\rangle$, for $i = 0, 1$, and if another pixel is positioned on the line segment between the points, at a fraction α of the way from $\mathbf{x}_0$ to $\mathbf{x}_1$, then the interpolated color is

$$(1-\alpha)\langle r_0, g_0, b_0\rangle \; + \; \alpha\langle r_1, g_1, b_1\rangle.$$

Gouraud interpolation works moderately well; however, for large polygons, it can miss specular highlights, or at least miss the brightest part of the specular highlight if this falls in the middle of a polygon. Another example of how Gouraud shading can fail is that a spotlight shining on a wall can be completely overlooked by Gouraud interpolation, since if the wall is modeled as a large polygon, then the four vertices of the polygon may not be illuminated by the spotlight at all. More subtly, Gouraud interpolation suffers from the fact that the brightness of a specular highlight depends strongly on how the highlight is centered on a vertex; this is particularly apparent when objects or lights are being animated. Nonetheless, Gouraud shading works acceptably in many cases and can be implemented efficiently in hardware.

The second kind of shading is *Phong shading.* In Phong shading, the surface normals are interpolated throughout the interior of the triangle, and the full Phong lighting is recalculated at each pixel in the triangle on the viewport. This is considerably more computational work than Gouraud shading. Gouraud shading does the Phong lighting calculations only at vertices, whereas Phong shading must do the Phong lighting calculation at each pixel. In other words, the vertex shader does the Phong light calculations for Gouraud shading, whereas the fragment shader has to do the Phong lighting calculations for Phong shading.

The interpolation of surface normals for Phong shading is not as simple as the usual linear interpolation described in Section III.3 since the interpolated surface normals must be unit vectors in order to be used in the Phong lighting calculations. The most common way to calculate interpolated surface normals is as follows: Suppose $\mathbf{x}_0, \mathbf{x}_1$ are pixels where the surface normals are $\mathbf{n}_0$ and $\mathbf{n}_1$, respectively. At a pixel at a fraction α of the distance along the line from $\mathbf{x}_0$ to $\mathbf{x}_1$, the interpolated normal is

$$\mathbf{n}_\alpha \;=\; \frac{(1-\alpha)\mathbf{n}_0 + \alpha\mathbf{n}_1}{||(1-\alpha)\mathbf{n}_0 + \alpha\mathbf{n}_1||}. \tag{IV.15}$$

This is computationally more work than Gouraud shading, especially because of the renormalization. Perhaps, the biggest disadvantage of Phong shading is that all the information about the colors and directions of lights needs to be made available to the fragment shader so that lighting can be calculated at every pixel in the final image. On the other hand, the big advantage of Phong shading is that small specular highlights and spotlights are not missed when they occur in the interior of a triangle or polygon. In addition, the brightness of a specular highlight is not nearly so sensitive to whether the specular highlight is centered over a vertex or in the interior of a polygon.

One problem with Phong shading is that normals should not be interpolated linearly across the polygonal approximation to a surface, since normals tend to change less rapidly in areas where the normals are pointing towards the viewer, and more rapidly in areas where the normals are pointing more sideways. One way to partly incorporate this observation in the Phong shading calculation is to use the following method to calculate normals. Let the normals be unit vectors $\mathbf{n}_i = \langle n_{x,i}, n_{y,i}, n_{z,i}\rangle$, $i = 0, 1$. Then replace the calculation of Equation (IV.15) by

$$\begin{aligned} n_{x,\alpha} &= (1-\alpha)n_{x,0} + \alpha n_{x,1} \\ n_{y,\alpha} &= (1-\alpha)n_{y,0} + \alpha n_{y,1} \\ n_{z,\alpha} &= \sqrt{1 - n_{x,\alpha}^2 - n_{y,\alpha}^2}\,. \end{aligned}$$

The equations above calculate the x and y components of $\mathbf{n}_\alpha$ by linear interpolation, and choose the z-component so as to make $\mathbf{n}_\alpha$ a unit vector.

Exercise IV.2* Prove that these alternate equations for normal vector interpolation provide the correct unit normal vectors in the case of a spherical surface viewed orthographically. Further prove that $1 - n_{x,\alpha}^2 - n_{y,\alpha}^2 \geq 0$.

IV.3 Computing surface normals

As we have seen, it is important to correctly set the values of surface normals in order to obtain good lighting and shading effects. In many cases, one can determine surface normals by understanding the surface clearly, and using symmetry properties. For example, the surface normals for symmetric objects like spheres, cylinders, tori, etc., are easy to determine. For more complicated surfaces, however, it is necessary to use more general methods. We discuss next three different methods for calculating surface normals on general surfaces.

First, suppose a surface has been modeled as a mesh of flat polygons with vertices that lie on the surface. Consider a particular vertex $\mathbf{v}$, and let $P_1, \ldots, P_k$ be the polygons which have that vertex as a corner. The unit surface normal $\mathbf{n}_i$ for each individual polygon P_i is easy to compute by taking two adjacent (and noncollinear) edges from the polygon, forming their cross product and normalizing. Then we can estimate the unit normal, $\mathbf{n}$, at the vertex as the average of the unit normals of the adjacent polygons, namely as

$$\mathbf{n} \;=\; \frac{\sum_i \mathbf{n}_i}{||\sum_i \mathbf{n}_i||}. \tag{IV.16}$$

Note that it is necessary to renormalize, since Phong lighting works with unit vectors.

Computing the normal vector by averaging the normals of adjacent polygons has the advantage that it can be done directly from the polygonal model of a surface, without using any direct knowledge of the surface. It also works even when there is no mathematical surface underlying the polygonal data, say in situations where the polygonal data has been generated by hand, or by measurement of some object. Of course, this method does not generally give the exactly correct surface normal, but if the polygons are small enough compared to the rate of change of the curvature of the surface, it will give normals that are close to the correct surface normals.

In some cases, Equation (IV.16 can be improved by taking the areas of the adjacent polygons $P_1, \ldots, P_k$ into account. The intuition is that smaller polygons should be better indicators of the surface normal than large polygons (at least if the polygons do not have bad aspect ratios). Letting A_i be the area of polygon P_i, then one can instead estimate the surface normal as

$$\mathbf{n} \;=\; \frac{\sum_i \mathbf{n}_i/A_i}{||\sum_i \mathbf{n}_i/A_i||}.$$

This is a kind of weighted average, as defined later in Section V.1.2.

The second method of computing surface normals can be used with surfaces that are defined parametrically. We say that a surface is defined *parametrically* if there is a function $\mathbf{f}(x,y)$ of two variables with a domain $A \subseteq \mathbb{R}^2$ such that the surface is the set of points $\{\mathbf{f}(x,y) : \langle x,y\rangle \in A\}$. We write "$\mathbf{f}$" in boldface, since it is a function which gives values in $\mathbb{R}^3$, i.e., it is a vector-valued function,

$$\mathbf{f}(x,y) \;=\; \langle f_1(x,y), f_2(x,y), f_3(x,y)\rangle.$$

The partial derivatives

$$\mathbf{f}_x := \frac{\partial \mathbf{f}}{\partial x} \qquad \text{and} \qquad \mathbf{f}_y := \frac{\partial \mathbf{f}}{\partial y}$$

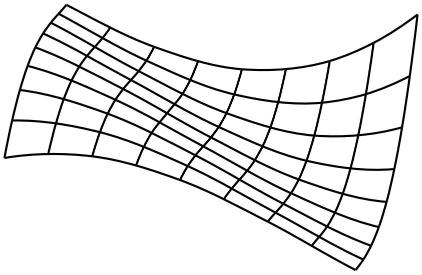

Figure IV.15: A polygonal mesh defined by a parametric function. The horizontal and vertical curves are lines of constant y values and constant x values, respectively.

are defined component-wise as usual, and are likewise vectors in $\mathbb{R}^3$. The partial derivatives are the rates of change of $\mathbf{f}$ with respect to changes in one of the variables while the other is held fixed. In Figures IV.15 and IV.16, this is illustrated with the partial derivative tangent to the surface cross sections where the other variable is constant. Except in degenerate cases, the cross product of the two partial derivatives gives a vector which is perpendicular to the surface.

Theorem IV.1. *Suppose* $\mathbf{f}$ *has partial derivatives at* $\langle x, y\rangle$. *If the cross product vector* $\mathbf{f}_x(x,y) \times \mathbf{f}_y(x,y)$ *is nonzero, then it is perpendicular to the surface at* $\mathbf{f}(x,y)$.

To prove the theorem, note that $\mathbf{f}_x$ and $\mathbf{f}_y$ are noncollinear and are both tangent to the surface parametrically defined by $\mathbf{f}$. □

Usually, the vector $\mathbf{f}_x \times \mathbf{f}_y$ must be normalized, and care must be taken to choose the correct outward direction. Therefore, the unit vector normal to a parametrically defined surface is given by the formula

$$\pm\frac{\mathbf{f}_x(x,y) \times \mathbf{f}_y(x,y)}{||\mathbf{f}_x(x,y) \times \mathbf{f}_y(x,y)||} \tag{IV.17}$$

whenever the vector $\mathbf{f}_x(x,y) \times \mathbf{f}_y(x,y)$ is nonzero. The sign is chosen to make the vector pointing outward.

Exercise IV.3. Let T be a torus (doughnut shape) with major radius R and minor radius r. This torus is a tube going around the y-axis. The center of the tube stays distance R from the y-axis and lies in the xz-plane. The radius of the tube is r.

(a) Show that the torus T is parametrically defined by $\mathbf{f}(\theta, \varphi)$, for $0 \le \theta \le 360^\circ$ and $0 \le \varphi \le 360^\circ$, where

$$\mathbf{f}(\theta,\varphi) \;=\; \langle (R + r\cos\varphi)\sin\theta, r\sin\varphi, (R + r\cos\varphi)\cos\theta\rangle. \tag{IV.18}$$

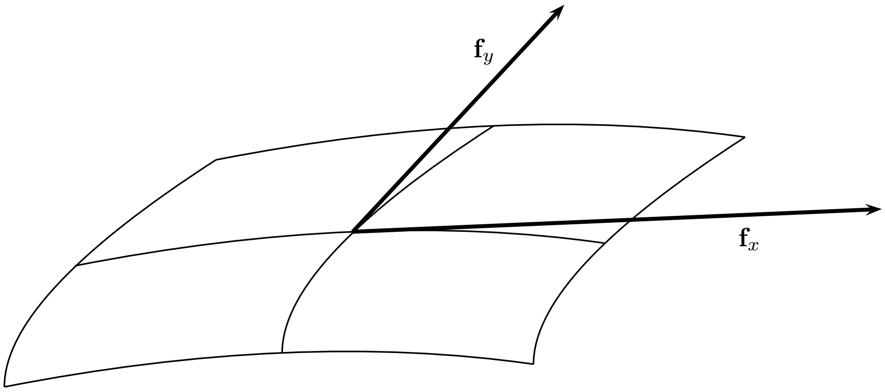

Figure IV.16: A close-up view of a polygonal mesh. The partial derivatives are tangent to the horizontal and vertical cross section curves.

Draw a picture of the torus and of a point on it for a representative value of θ and φ. [Hint: θ controls the angle measured around the y-axis, starting with $\theta = 0$ at the positive z-axis. The angle φ specifies the amount of turn around the centerline of the torus.]

(b) Use your picture and the symmetry of the torus to show that the unit normal vector to the torus at the point $\mathbf{f}(\theta, \varphi)$ is equal to

$$\langle \sin\theta\cos\varphi, \sin\varphi, \cos\theta\cos\varphi \rangle. \tag{IV.19}$$

Exercise IV.4. Let T be the torus from the previous exercise. Use Theorem IV.1 to compute a vector normal to the torus at the point $\mathbf{f}(\theta, \varphi)$. Compare your answer to Equation (IV.19). Is it the same? If not, why not?

The third method for computing surface normals applies to surfaces which are defined as level sets of functions. Such a surface can be defined as the set of points satisfying some equation, and is sometimes called an *implicitly defined surface*. (See Appendix A.4.) An implicitly defined surface is defined from a real-valued function $f(x, y, z)$, and the surface is the set of points $\{\langle x, y, z\rangle : f(x, y, z) = 0\}$. Recall that the gradient of f, ∇f, is defined by

$$\nabla f(x, y, z) \;=\; \left\langle \frac{\partial f}{\partial x}, \frac{\partial f}{\partial y}, \frac{\partial f}{\partial z} \right\rangle.$$

From multivariable calculus, it follows that the gradient of f is perpendicular to the level surface.

Theorem IV.2. *Let S be the level set defined as above as the set of zeroes of f. Let $\langle x, y, z\rangle$ be a point on the surface S. If the vector $\nabla f(x, y, z)$ is nonzero, then it is perpendicular to the surface at $\langle x, y, z\rangle$.*

Exercise IV.5. Show that the torus T considered in the previous two exercises can be defined as the set of zeros of the function

$$f(x,y,z) \;=\; (\sqrt{x^2+z^2}-R)^2+y^2-r^2.$$

Use Theorem IV.2 to derive a formula for a vector perpendicular to the surface at a point $\langle x,y,z\rangle$. The vector should be pointing outward from the torus, but it does not need to be a unit vector. Your answer should be independent of r. Why does this make sense?

A special kind of parametric surface is a *surface of revolution*; for these, there are computational short cuts that make it easier to compute surface normals. Assume we have a parametric function $\mathbf{g} : \mathbb{R} \to \mathbb{R}^2$ which defines a curve of points $\mathbf{g}(t) = \langle g_1(t), g_2(t)\rangle$ with $g_1(t)$ always greater than zero. Identifying the points $\langle g_1(t), g_2(t)\rangle$ with the points $\langle g_1(t), g_2(t), 0\rangle$ in $\mathbb{R}^3$, a surface of revolution is formed by revolving the curve $\mathbf{g}$ around the y-axis. This yields the parametric surface of points

$$\mathbf{f}(\theta,t) \;=\; \langle g_1(t)\sin\theta,\; g_2(t),\; g_1(t)\cos\theta\rangle, \tag{IV.20}$$

where θ ranges over $[0,2\pi]$ and t ranges over the domain of $\mathbf{g}$.

For example, the torus of Exercise IV.3 can be defined using

$$\mathbf{g}(t) \;=\; \langle\,(R+r\cos t),\; r\sin t\,\rangle,$$

for $t \in [0,2\pi]$. Here the parameter t is playing the role of φ of Exercise IV.3, and the surface of rotation is the same torus.

Let's assume that the vector derivative $\mathbf{g}'(t)$ is never equal to zero; that is, $g_1'(t)$ and $g_2'(t)$ are never both equal to zero simultaneously. Then at a fixed point $\mathbf{g}(t_0)$ on the curve $\mathbf{g}$, the vector

$$\mathbf{g}'(t_0) \;=\; \langle g_1'(t_0), g_2'(t_0)\rangle$$

it is a non-zero vector, tangent to the curve $\mathbf{g}(t)$ at $t=t_0$. Rotating this counter-clockwise by 90°, we have that

$$\mathbf{n}_g(t_0) \;=\; \langle -g_2'(t_0), g_1'(t_0)\rangle$$

is perpendicular to the curve $\mathbf{g}(t)$ at $t=t_0$. By rotating this vector around the y-axis, this implies that

$$\mathbf{n}_f(\theta,t_0) \;=\; \langle -g_2'(t_0)\sin\theta,\; g_1'(t_0),\; -g_2'(t_0)\cos\theta\rangle$$

is perpendicular to the surface $\mathbf{f}$ at the point (IV.20). It may be necessary to negate $\mathbf{n}_f(\theta,t_0)$ to make the normal be pointing outward from the surface instead of inward.

Exercise IV.6. Let the function $y=h(x)$ be defined for $x \geq 0$, and generate a surface of revolution by revolving the graph of h around the y-axis. This fits into the above framework by letting $\mathbf{g}(t) = \langle t, h(t)\rangle$. Give a formula for the points on the surface of revolution defined by $\mathbf{f}(\theta,t)$. Also give a formula for the *unit normal* vectors pointing *upward* from the surface of of revolution.

What condition is needed for the surface $\mathbf{f}(\theta,t)$ to have a well-defined normal when $t=0$?

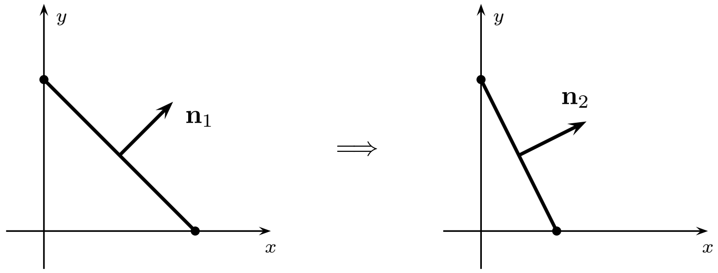

Figure IV.17: An example of how a nonuniform scaling transformation affects a normal. The transformation maps $\langle x,y\rangle$ to $\langle \frac{1}{2}x, y\rangle$. The line with unit normal $\mathbf{n}_1 = \langle \frac{1}{\sqrt{2}}, \frac{1}{\sqrt{2}}\rangle$ is transformed to a line with unit normal $\mathbf{n}_2 = \langle \frac{2}{\sqrt{5}}, \frac{1}{\sqrt{5}}\rangle$.

IV.4 Affine transformations and normal vectors

When using affine transformations to transform the positions of geometrically modeled objects, it is also important to transform the normal vectors appropriately. After all, things could get very mixed up if the vertices and polygons are rotated, but the normals are not!

For now, assume we have an affine transformation $A\mathbf{x} = B\mathbf{x} + \mathbf{u}_0$ where B is a linear transformation. Since translating a surface does not affect its normal vectors, we can ignore the translation $\mathbf{u}_0$ and just work with the linear mapping B.

If B is a rigid transformation (possibly not orientation preserving), then it is clear that after a surface is mapped by B, its normals are also mapped by B. That is to say, if a vertex $\mathbf{v}$ on the surface S has the normal $\mathbf{n}$, then on the transformed surface, $B(S)$, the transformed vertex $B(\mathbf{v})$ has surface normal $B(\mathbf{n})$.

However, the situation is more complicated for nonrigid transformations. To understand this on an intuitive level, consider an example in the xy-plane. In Figure IV.17(a), a line segment is shown with slope -1: the vector $\mathbf{n}_1 = \langle 1,1\rangle$ is perpendicular to this line. If B performs a scaling by a factor of $1/2$ in the x-axis dimension, then the line is transformed to a line with slope -2. But, the normal vector is mapped by B to $\langle \frac{1}{2}, 1\rangle$ which is *not* perpendicular to the transformed line. Instead, the correct perpendicular direction is $\mathbf{n}_2 = \langle 2,1\rangle$, so it looks almost like the inverse of B needs to be applied to the normal vector. This is not quite correct though; as we shall see next, it is the transpose of the inverse which needs to be applied to the normals.

We state the next theorem in terms of a vector normal to a plane, but the same results hold for a normal to a surface, since we can just use the plane tangent to the surface at a given point. We may assume without much loss of applicability that the transformation B is invertible, since otherwise the image of B is contained in a plane P, and any normal to the plane P is perpendicular to the surface.

Theorem IV.3. *Let B be a linear transformation represented by the invertible matrix M. Let N be the matrix*

$$N = (M^{\mathrm{T}})^{-1}, \qquad \textit{or equivalently,} \qquad N = (M^{-1})^{\mathrm{T}}. \tag{IV.21}$$

Let P be a plane and $\mathbf{n}$ be orthogonal to P. Then $N\mathbf{n}$ is orthogonal to the image, $B(P)$, of the plane P under the map B.

To prove the theorem, it is helpful to recall that for any vectors $\mathbf{x}$ and $\mathbf{y}$, the dot product $\mathbf{x}\cdot\mathbf{y}$ is equal to $\mathbf{x}^{\mathrm{T}}\mathbf{y}$ (see Appendix A).

Proof. Suppose that $\mathbf{x}$ is a vector lying in the plane P, so $\mathbf{n}\cdot\mathbf{x} = 0$. In order to prove the theorem, it will suffice to show that $(N\mathbf{n})\cdot(M\mathbf{x}) = 0$. But this follows immediately from

$$\begin{aligned}(N\mathbf{n})\cdot(M\mathbf{x}) &= ((M^{-1})^{\mathrm{T}}\mathbf{n})\cdot(M\mathbf{x}) = ((M^{-1})^{\mathrm{T}}\mathbf{n})^{\mathrm{T}}(M\mathbf{x}) = (\mathbf{n}^{\mathrm{T}}M^{-1})(M\mathbf{x}) \\ &= \mathbf{n}^{\mathrm{T}}(M^{-1}M\mathbf{x}) = \mathbf{n}^{\mathrm{T}}\mathbf{x} = \mathbf{n}\cdot\mathbf{x} = 0,\end{aligned}$$

and the theorem is proved. □

Recall that the adjoint of a matrix M is the transpose of the matrix formed from the cofactors of M (see Appendix A). In addition, the inverse of a matrix M is equal to the adjoint of M divided by the determinant of M. Therefore, it is immediate that Theorem IV.3 also holds for the transpose of the adjoint of M in place of the transpose of the inverse of M.

To summarize, a normal vector transforms under an affine transformation $\mathbf{x} \mapsto M\mathbf{x} + \mathbf{u}_0$, according to the formula

$$\mathbf{n} \;\mapsto\; N\mathbf{n},$$

where N is the transpose of either the inverse or the adjoint of M. Note that $N\mathbf{n}$ may not be a unit vector.

Exercise IV.7. The linear transformation of $\mathbb{R}^2$ depicted in Figure IV.17 is given by the matrix

$$M = \begin{pmatrix} 1/2 & 0 \\ 0 & 1 \end{pmatrix}.$$

Compute the transposes of the adjoint of M and the inverse of M. Prove that, for any line L in $\mathbb{R}^2$, these matrices correctly map a vector normal to the line L to a vector normal to the image, $M(L)$, of the line.

So far, we have only discussed how normal vectors are converted by *affine* transformations. However, the 4×4 homogeneous matrices allowed in OpenGL are more general than just affine transformations, and for these, a different construction is needed. Given a 4×4 matrix M, let N be the transpose of either the inverse or the adjoint of M. Let $\mathbf{n}$ be orthogonal to a plane P. As discussed in Section II.3.8, the plane P in 3-space corresponds to a three dimensional linear subspace P^{H} of $\mathbb{R}^4$ in homogeneous coordinates. Let $\mathbf{u}$ be a point on the plane P, and $\mathbf{x} = \langle x_1, x_2, x_3 \rangle$ and $\mathbf{y} = \langle y_1, y_2, y_3 \rangle$ be two noncollinear vectors parallel to P in 3-space. Form the vectors $\mathbf{x}^{\mathrm{H}} = \langle x_1, x_2, x_3, 0 \rangle$ and $\mathbf{y}^{\mathrm{H}} = \langle y_1, y_2, y_3, 0 \rangle$. These two vectors, plus $\mathbf{u}^{\mathrm{H}} = \langle u_1, u_2, u_3, 1 \rangle$, span P^{H}.

Let $\mathbf{n} = \langle n_1, n_2, n_3 \rangle$ be orthogonal to P, and let $\mathbf{n}^{\mathrm{H}} = \langle n_1, n_2, n_3, -\mathbf{u} \cdot \mathbf{n} \rangle$. Since $\mathbf{n}^{\mathrm{H}}$ is orthogonal to $\mathbf{x}^{\mathrm{H}}$, $\mathbf{y}^{\mathrm{H}}$ and $\mathbf{u}^{\mathrm{H}}$, it is perpendicular to the space P^{H} spanned by these three vectors. Therefore, by exactly the same proof as Theorem IV.3, we have that $N\mathbf{n}^{\mathrm{H}}$ is orthogonal to $M(P^{\mathrm{H}})$. Let $N\mathbf{n}^{\mathrm{H}} = \langle n_1', n_2', n_3', n_4' \rangle$, where we are now treating Nn^{H} as a vector in $\mathbb{R}^4$ and $M(P^{\mathrm{H}})$ as a subspace of $\mathbb{R}^4$. Then clearly, $\langle n_1', n_2', n_3' \rangle$ is a vector in 3-space orthogonal to the 3-space vectors which are parallel to $M(P)$. Therefore, $\langle n_1', n_2', n_3' \rangle$ is perpendicular to the plane $M(P)$ in 3-space.

When using perspective, spotlight directions must be transformed by the same inverse-transpose method in Equation (IV.21) as was used for surface normals.

IV.5 Shader programs for Phong lighting

The modern OpenGL system has no built-in lighting methods.[3] This lack of built-in lighting methods has both advantages and disadvantages: The disadvantage is that you must write your own Phong lighting routines. The advantage is that you can customize Phong lighting to fit your specific application. Fortunately, it is not too difficult to write shaders that implement Phong lighting, with either Gouraud shading or Phong shading. But implementing a robust version of Phong lighting requires handling a number of subtle cases.

The book's website includes GLSL shader programs (called *EduPhong*) that implement a full featured version of Phong lighting with Phong shading. They include the ability to use either Gouraud shading or Phong shading. There are also sample programs, including *SimpleLightModern*, that show how it is used in an OpenGL C++ program.

The *EduPhong* package implements Phong lighting with either Phong interpolation or Gouraud interpolation. It supports all the Phong lighting material properties, including the ambient, diffuse, and specular reflectivity coefficients, and emissivity. It also supports the Schlick Fresnel approximation. Light sources may be given independent ambient, diffuse, and specular intensities, and special effects for lights include spotlighting and distance attenuation.

We describe below the most important components of how *EduPhong*'s GLSL shader programs implement Phong lighting. We do not describe the C++ routines in *EduPhong* that interface with the shader programs: see the book's website for descriptions of these. Instead, we will concentrate on the data structures, and the core algorithms used for Phong lighting. This will show the details of what is needed for Phong lighting calculations. It also illustrates the design principles for a moderately complicated GLSL program. We do not

[3] This is in contrast to the legacy OpenGL interface which implemented Phong lighting with Gouraud shading.

cover all aspects of the code, but the complete source code can be found in the file *EduPhong.glsl*.

Vertex attributes

The *EduPhong* shaders uses vertex attributes for the material properties. These vertex attributes are defined in *EduPhong.glsl* as:

```
layout (location = 0) in vec3 vertPos;            // Position
layout (location = 1) in vec3 vertNormal;         // Surface normal
layout (location = 2) in vec2 vertTexCoords;      // Texture coordinates
layout (location = 3) in vec3 EmissiveColor;      // $\mathbf{I}_{\rm e}$
layout (location = 4) in vec3 AmbientColor;       // $\boldsymbol{\rho}_{\rm a}$
layout (location = 5) in vec3 DiffuseColor;       // $\boldsymbol{\rho}_{\rm d}$
layout (location = 6) in vec3 SpecularColor;      // $\boldsymbol{\rho}_{\rm s}$
layout (location = 7) in float SpecularExponent;// $f$
layout (location = 8) in float UseFresnel;        // 1.0 (Fresnel) or 0.0 (no Fresnel)
```

The first two vertex attributes give the vertex's position and surface normal in "local coordinates". There is a uniform variable `modelviewMatrix` which holds a 4×4 modelview matrix defined by

```
uniform mat4 modelviewMatrix;
```

This matrix is used by the vertex shader to transform the vertex's position and normal into "world coordinates" (also called "modelview coordinates") using the commands[4]

```
vec4 mvPos4 = modelviewMatrix * vec4(vertPos.x,vertPos.y,vertPos.z,1.0);
vec3 mvPos = vec3(mvPos4.x,mvPos4.y,mvPos4.z) / mvPos4.w;
vec3 mvNormalFront = normalize(inverse(transpose(mat3(modelviewMatrix)))*vertNormal);
```

The 4-vector `mvPos4` gives the vertex position in homogeneous coordinates. The position `mvPos` of the vertex as a 3-vector is computed by perspective division, namely by dividing by the w component. The unit vector normal to the surface, `mvNormalFront`, is computed using the method of Equation (IV.21) of Theorem IV.3.

The *EduPhong* code for Phong lighting assumes that the world coordinate system is an orthonormal coordinate system with the viewer (if it is local) placed at the origin and with the direction of view in the direction of the negative z axis, so that $\mathbf{v} = \langle 0, 0, 1 \rangle$. This is a standard assumption; in particular, it is the convention used by the legacy OpenGL routines `gluPerspective`, `glFrustum` and `glOrtho`, and by the corresponding routines `Set_gluPerspective`, `Set_glFrustum` and `Set_glOrtho` in the *GlLinearMath* package.

[4] We have slightly modified the code here; see the code in *EduPhong.glsl* to see how the variables are actually declared.

The four color values give the emissivity, $\mathbf{I}_{\rm e}$, and the ambient, diffuse and specular reflectivities, $\boldsymbol{\rho}_{\rm a}$, $\boldsymbol{\rho}_{\rm d}$ and $\boldsymbol{\rho}_{\rm s}$. These are 3-vectors; their xyz-components give the values for red, green and blue, in that order. The specular exponent, f, is a scalar (a `float`) since it is the same for all three colors.

The variable `UseFresnel`, which controls whether the Fresnel term is included, is a `float` variable instead of a Boolean value of type `bool`. This is because GLSL does not allow vertex attributes to be Boolean variables. The reason for this restriction is that vertex attributes are intended to be values that can be linearly interpolated. For us, it actually an advantage to use a `float`, since it gives the flexibility to transition smoothly between the use Fresnel lighting and non-Fresnel lighting, as will be shown in the code below.

The vector `vertTexCoords` gives the texture coordinates of the texture coordinates of the vertex. As is discussed below, a texture map can be used to modify the nonspecular component of the lighting.

There are two shader programs in *EduPhong*; one that does Phong lighting with Phong shading, and a second one that computes Phong lighting with Gouraud shading. The first vertex shader, `vertexShader_PhongPhong`, which computes Phong shading, sends the values of `mvPos` and `mvNormalFront` plus the rest of the vertex attributes to the corresponding fragment shader (named `fragmentShader_PhongPhong`) to do the Phong lighting calculation at every pixel. The Phong interpolation is carried out automatically by the averaging of vertex attributes. The other vertex shader, `vertexShader_PhongGouraud`, which uses Gouraud shading, computes the Phong lighting at the vertex and sends the resulting color to the corresponding fragment shader (named `fragmentShader_PhongGouraud`). For this shader program, the averaging of vertex attributes acts on the color value, and thus implements Gouraud shading.

Light properties

The *EduPhong* shaders use the following data structure to describe the properties of a light source. These are uniform variables, not vertex attributes.

```
struct phLight {
  bool IsEnabled;                // True if light is turned on
  bool IsAttenuated;             // True if attenuation is active
  bool IsSpotLight;              // True if spotlight
  bool IsDirectional;            // True if directional
  vec3 Position;
  vec3 AmbientColor;             // $\mathbf{I}_{\rm a}^{\rm in}$
  vec3 DiffuseColor;             // $\mathbf{I}_{\rm d}^{\rm in}$
  vec3 SpecularColor;            // $\mathbf{I}_{\rm s}^{\rm in}$
  vec3 SpotDirection;            // s.  A unit vector
  float SpotCosCutoff;           // $\cos\theta$.  Cosine of cutoff angle
  float SpotExponent;            // $c$.  Spotlight exponent
  float ConstantAttenuation;     // $k_{\rm c}$
  float LinearAttenuation;       // $k_{\rm l}$
  float QuadraticAttenuation;    // $k_{\rm q}$ };
```

The Boolean IsDirectional specifies whether the light is directional or positional. If it is positional, the 3-vector Position gives the location of the light. If directional, then Position is a unit vector and the negative of Position gives the incoming light direction $\boldsymbol{\ell}$. The 3-vectors AmbientColor, DiffuseColor and SpecularColor specify the red, green and blue components of the colors $\mathbf{I}_{\rm a}^{\rm in}$, $\mathbf{I}_{\rm d}^{\rm in}$ and $\mathbf{I}_{\rm s}^{\rm in}$.

The Boolean IsAttenuated specifies whether distance attenuation is used. If so, the variables ConstantAttenuation, LinearAttenuation and QuadraticAttenuation give the attenuation factors. The attenuation is calculated according to Equation (IV.13).

The Boolean IsSpotLight specifies whether spotlight effects are used. If so, the variables SpotDirection, SpotCosCutoff and SpotExponent give the spotlight parameters. The spotlight attenuation is calculated according to Equation (IV.14).

Global properties

There are also a number of global parameters used by *EduPhong*, that do not correspond to any particular light or vertex. These are collected in the following data structure as uniform variables.

```
layout (std140) uniform phGlobal {
  vec3 GlobalAmbientColor;    // $\mathbf{I}_{\rm a}^{\rm in,global}$.  Global ambient light
  int NumLights;              // Number of lights
  bool LocalViewer;           // True for local viewer; false for directional
  bool EnableEmissive;        // Control whether emissive colors are rendered
  bool EnableDiffuse;         // Control whether diffuse colors are rendered
  bool EnableAmbient;         // Control whether ambient colors are rendered
  bool EnableSpecular;        // Control whether specular colors are rendered
  bool UseHalfwayVector;      // Control whether halfway vector method is used
};
```

The four "`Enable`···" Boolean values specify whether to include the emissive, ambient, diffuse and specular components of the color. It is convenient to be able to enable these components independently, partly for illustrative or educational purposes, and partly to help design lighting and colors. The `UseHalfwayVector` Boolean controls whether or not to use the shortcut of Equation (IV.5). The 3-vector `GlobalAmbientColor` gives the red, green and blue components of the global ambient light, $\mathbf{I}_{\rm a}^{\rm in,global}$.

The Boolean value `LocalViewer` specifies whether the view is local or nonlocal. If the viewer is local, then it is camera is assumed to at the origin. In either case, the view direction is in the $-z$ direction. The integer `NumLights` specifies how many lights are present; only the lights that are enabled contribute to the Phong lighting.

Shader code for *EduPhong*

Here is the complete code for the Phong lighting calculation as used by *EduPhong* (with minor edits):

```
// Shared code for calculating Phong light.
// Inputs:
// (a) Material properties (mvPos through useFresnel).
// (b) Global light properties (phGlobal uniform structure)
// (c) Individual light properties (phLightArray, with phLight structures)
// Outputs:
// (a) nonspecColor (combined nonspecular components of the color)
// (b) specularColor (specular component of the color)
// Assumes normal vector mvNormal is for the side of the triangle facing the viewer.
vec3 nonspecColor;      // Returned value for $\mathbf{I}_{\rm e} + \mathbf{I}_{\rm a} + \mathbf{I}_{\rm d}$
vec3 specularColor;     // Returned value for $\mathbf{I}_{\rm s}$
void CalculatePhongLighting() {
  nonspecColor = vec3(0.0, 0.0, 0.0);
  specularColor = vec3(0.0, 0.0, 0.0);
  if ( EnableEmissive ) {
    nonspecColor = matEmissive;
  }
  if ( EnableAmbient ) {
    nonspecColor += matAmbient*GlobalAmbientColor;
  }
  // vVector = unit vector towards view direction ($\mathbf{v}$)
  vec3 vVector = LocalViewer ?  -mvPos :  vec3(0.0, 0.0, 1.0);
  vVector = normalize(vVector);
  for ( int i=0; i<NumLights; i++ ) {
    if ( Lights[i].IsEnabled ) {
      // nonspecColorLt and specularColorLt - color from this light
      vec3 nonspecColorLt = vec3(0.0, 0.0, 0.0);
```

```
vec3 specularColorLt = vec3(0.0, 0.0, 0.0);
// ellVector = unit vector towards light source $\boldsymbol{\ell}_i$
vec3 ellVector = -Lights[i].Position;
if ( !Lights[i].IsDirectional ) {
  ellVector = -(ellVector + mvPos);
}
ellVector = normalize(ellVector);
float dotEllNormal = dot(ellVector, mvNormal);
if (dotEllNormal > 0 ) {
  float spotCosine;
  if ( Lights[i].IsSpotLight ) {
    spotCosine = -dot(ellVector,Lights[i].SpotDirection);
  }
  if ( !Lights[i].IsSpotLight || spotCosine > Lights[i].SpotCosCutoff ) {
    if ( EnableDiffuse ) {
      nonspecColorLt += matDiffuse*Lights[i].DiffuseColor*dotEllNormal;
    }
    if ( EnableSpecular ) {
      float specFactor = 0.0; // Includes $(\cos)^f$ factor and Fresnel factor
      if ( UseHalfwayVector ) {
        vec3 hVector = normalize(ellVector+vVector); // Halfway vector $\mathbf{h}$
        specFactor = pow( dot(hVector,mvNormal), matSpecExponent );
      }
      else {
        vec3 rVector = 2.0*dotEllNormal*mvNormal - ellVector; // Reflection vector
        float rDotV = dot(vVector, rVector);
        if ( rDotV>0.0 ) {
          specFactor = pow( rDotV, matSpecExponent);
        }
      }
      vec3 matspec = matSpecular;
      if ( useFresnel!=0.0 ) {
        float d = 1.0 - dotEllNormal;
        float dd = d*d;
        float fresnelBlend = dd*dd*d*useFresnel; // Blending factor for Fresnel
        matspec = mix(matSpecular, vec3(1.0,1.0,1.0), fresnelBlend);
      }
      specularColorLt += specFactor*matspec*Lights[i].SpecularColor;
    }
    if ( Lights[i].IsSpotLight ) {
      float spotAtten = pow(spotCosine,Lights[i].SpotExponent);
      nonspecColorLt *= spotAtten;
      specularColorLt *= spotAtten;
    }
  }
```

```
      }
      if ( EnableAmbient ) {
        nonspecColorLt += matAmbient*Lights[i].AmbientColor;
      }
      if ( Lights[i].IsAttenuated ) {
        float dist = distance(mvPos,Lights[i].Position);
        float atten = 1.0/(Lights[i].ConstantAttenuation
                          + (Lights[i].LinearAttenuation
                             + Lights[i].QuadraticAttenuation*dist)*dist);
        nonspecColorLt *= atten;
        specularColorLt *= atten;
      }
      nonspecColor += nonspecColorLt;
      specularColor += specularColorLt;
    }
  }
}
```

The code above is fairly straightforward. It starts by setting the specular color to zero, and the nonspecular color equal to the emissive color. It then computes the view vector $\mathbf{v}$ from the surface to the viewer (`vVector`). It then loops over all enabled light sources accumulating the illumination from each light. For each enabled light, it computes the $\boldsymbol{\ell}$ vector towards the light, and checks if the dot product $\boldsymbol{\ell} \cdot \mathbf{n}$ of the light vector and the normal to the surface is positive. If so, then after checking that the light is not completely cut off by spotlight effects, it computes first the diffuse lighting and then the specular lighting. The specular lighting is computed by either halfway vector method or using the reflection direction $\mathbf{r}$ (`rVector`), and then applies the Fresnel adjustment if it is enabled. The last step is computing the lighting from a light source is to apply the attenuation factors from both distance attenuation and spotlight effects.

The end result is of the computation is the two 3-vectors `specularColor` and `nonSpecularColor`. *EduPhong* incorporates a texture mapping operation which may update the nonspecular component of the color first. Thus effectively allows a simple post-Phong computation to control the color of the surface. The specular color is not affected by the texture map, so that specular highlights are unchanged by the texture color. The final step of Phong lighting is to add the two values `specularColor` and `nonSpecularColor` to get the final color.

The GLSL code for Phong shading renders both front and back faces. This is accomplished by the following code fragment in the fragment shader `fragmentShader_PhongPhong` that uses Phong shading.

```
if ( gl_FrontFacing ) {
  mvNormal = mvNormalFront;
}
else {
  mvNormal = -mvNormalFront;
}
```

The vector `mvNormalFront` is the unit vector normal to the front side of the face; `mvNormal` is the vector normal to the side of the face visible to the viewer. The side visible to the viewer is determined by the variable `gl_FrontFacing`. [5]

IV.6 The Cook-Torrance lighting model*

The Cook-Torrance lighting model is an alternative to Phong lighting that can better capture reflectance properties of a wider range of surface materials. The Cook-Torrance lighting model was introduced by Cook and Torrance [29] based partly on a lighting model developed by Blinn [13]. The Cook-Torrance lighting model incorporates the physical properties of reflection more fully than the Phong lighting model, by using a microfacet model for rough surfaces and by incorporating the Fresnel equations in the calculation of reflection intensities. It thus can better handle rough surfaces and handle changes in reflection due to grazing view angles. In particular, the Cook-Torrance lighting model can be used to render metallic surfaces better than can be done with the Phong lighting model.

There are a number of other local lighting models besides the Phong and the Cook-Torrance models. He-Torrance-Sillion-Greenberg et al. [62] describes a model that extends the Cook-Torrance model to include more physical aspects of light reflection. Ashikhmin-Premože-Shirley [5] gives a different microfacet-based model. Ngan-Durand-Matusik [83] give comparison of several local lighting models against real-world measurements.

An earlier popular model by Schlick [97] incorporates most of the functionality of physically-based models, but is more efficient computationally. As discussed in Section IV.1.5, Schlick's approximation for Fresnel lighting is sometimes used in conjunction with Phong lighting.

IV.6.1 Bidirectional reflectivity

The central part of any local lighting model is to compute how light reflects off of a surface. To state this in a general form, we assume that a beam of light is shining on a point of the surface from the direction pointed to by a unit vector $\boldsymbol{\ell}$, and that we wish to compute the intensity of the light that

[5] The GLSL shader program using Gouraud shading (as compared to Phong shading) does not have access the variable `gl_FrontFacing` because it does the Phong lighting calculation in the vertex shader instead of the fragment shader. The best the vertex shader can do is to determine whether the normal at the vertex is facing towards or away from the viewer.

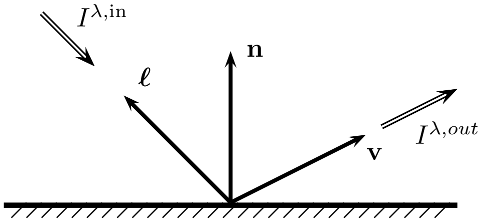

Figure IV.18: The *BRIDF* function relates the outgoing light intensity and the incoming light intensity according to $\mathit{BRIDF}(\boldsymbol{\ell},\mathbf{v},\lambda) \;=\; I^{\lambda,out}/I^{\lambda,\mathrm{in}}$.

is reflected in the direction of a unit vector $\mathbf{v}$. Thus, the light reflectance calculation can be reduced to computing a single *bidirectional reflectivity function*, *BRIDF*. The initials "BRIDF" actually stand for "bidirectional reflected intensity distribution function." The parameters to the *BRIDF* function are: (a) the incoming direction, $\boldsymbol{\ell}$; (b) the outgoing direction, $\mathbf{v}$; (c) the color or wavelength, λ, of the incoming light; and (d) the properties of the reflecting surface, including its normal and orientation. We write the *BRIDF* function as just

$$\mathit{BRIDF}(\boldsymbol{\ell},\mathbf{v},\lambda),$$

as a function of the light direction, view direction and wavelength, suppressing in the notation the dependence on the surface properties. The value $\mathit{BRIDF}(\boldsymbol{\ell},\mathbf{v},\lambda)$ is intended to be the ratio of the intensity of the outgoing light in the direction $\mathbf{v}$ to the intensity of the incoming light from the direction pointed to by $\boldsymbol{\ell}$.[6] As shown in Figure IV.18, the bidirectional reflectivity function is defined by

$$\mathit{BRIDF}(\boldsymbol{\ell},\mathbf{v},\lambda) \;=\; \frac{I^{\lambda,out}}{I^{\lambda,\mathrm{in}}}.$$

An important characteristic of the *BRIDF* function is that the incoming and outgoing directions are completely arbitrary, and in particular, the outgoing direction $\mathbf{v}$ does not have to be in the direction of perfect reflection. By expressing the *BRIDF* function in this general form, one can define *BRIDF* functions for *anisotropic* surfaces, where the reflectance function is not circularly symmetric around the perpendicular. An example of an anisotropic surface

[6] We are following [115] in using the *BRIDF* function, but many authors prefer to use a closely related function, $\mathit{BRDF}(\boldsymbol{\ell},\mathbf{v},\lambda)$ instead. The *BRDF* function is called the "bidirectional reflectivity distribution function." These two functions are related by

$$\mathit{BRIDF}(\boldsymbol{\ell},\mathbf{v},\lambda) \;=\; \mathit{BRDF}(\boldsymbol{\ell},\mathbf{v},\lambda)\cdot(\mathbf{n}\cdot\boldsymbol{\ell}).$$

Here, $\mathbf{n}$ is the unit surface normal, so $\mathbf{n}\cdot\boldsymbol{\ell}$ is the cosine of the angle between the surface normal and the incidence vector. Thus, the only difference between the two functions is that *BRIDF* takes into account the reduction in intensity (per unit surface area) due to the angle of incidence, whereas *BRDF* does not.

would be a brushed metal surface which has parallel grooves: light will reflect from such a surface differently depending on the orientation of the incoming direction relative to the orientation of the grooves. Other examples of anisotropic surfaces include some types of cloth, where the weave pattern may create directional dependencies in reflection. Still other examples include hair, feathers, and fur. We will not consider anisotropic surfaces, but the interested reader can consult Kajiya [72] for an early treatment of anisotropic surfaces in computer graphics.

The bidirectional reflectivity function can be computed in several ways. First, if one is trying to simulate the appearance of a physical, real-world surface, the most direct way would be to perform experiments measuring the reflectivity function. This would require shining light from various directions and of various wavelengths onto a sample of the material, and measuring the levels of reflected light in various directions. (Devices that perform these measurements are called goniometers.) Interpolation could then be used to fill in the values of the *BRIDF* function between the measured directions. In principle, this would give an accurate calculation of the bidirectional reflectivity function. In practice, the physical measurements are time consuming and inconvenient at best. And of course, physical measurements cannot be performed for materials that do not physically exist. There are published studies of reflectivity functions: these are typically performed at various wavelengths, but usually only from perpendicular illumination and viewing directions.

A second way to calculate bidirectional reflectivity functions is to create a mathematical model of the reflectivity of the surface. We have already seen one example of this, namely the Phong lighting model gives a simple and easy to compute bidirectional reflectivity function. The Cook-Torrance model, which we discuss in detail below, is another similar model, but takes more aspects of the physics of reflection into account, and thereby captures more features of reflectance.

The bidirectional reflectivity function is only an idealized model of reflection. To make physical sense of the way we have defined bidirectional reflectivity, one has to let the surface be an infinite flat surface, and let the distances to the light source and to the viewer tend to infinity. A number of more sophisticated local lighting models have been developed since the Cook-Torrance model. These models take into account more detailed aspects of the physics of reflectivity, such as subsurface scattering, polarization, and diffraction. To handle polarization, the *BRIDF* function needs to be redefined so as to incorporate polarization parameters (cf. [125]).

IV.6.2 Overview of Cook-Torrance lighting*

The Cook-Torrance model and the earlier Blinn model are based on a microfacet model for surface reflection. According to the microfacet model, a surface consists of small flat pieces called *facets*. A one dimensional cross section of a microfacet surface is shown in Figure IV.19 below. The assumption is then made that light hitting a microfacet can either be immediately reflected or can enter into the surface. The light that is immediately reflected is presumed to reflect off the microfacet in the direction of perfect reflection, that is, in the direction of reflection from a mirror parallel to the microfacet. Light that is refracted and enters into the surface through the microfacet is assumed to penetrate deeper into the material and to reflect around inside the surface several times before exiting the surface. This portion of the light that is refracted and undergoes multiple reflections inside the material will exit the surface in an unpredictable direction. Thus, this part of the light is treated as being diffusely reflected.

Just like the Phong model, the Cook-Torrance model treats reflection as being composed of separate ambient, diffuse, and specular components. The ambient and diffuse components are essentially the same in the Cook-Torrance model as in the Phong lighting model. Thus, in the Cook-Torrance model, reflected light at a given wavelength can be expressed by

$$\begin{aligned} I &= I_{\mathrm{a}} + I_{\mathrm{d}} + I_{\mathrm{s}} \\ &= \rho_{\mathrm{a}} I_{\mathrm{a}}^{\mathrm{in}} + \rho_{\mathrm{d}} I_{\mathrm{d}}^{\mathrm{in}} (\boldsymbol{\ell} \cdot \mathbf{n}) + I_{\mathrm{s}}. \end{aligned}$$

This is the same as in the Phong model (see Equation (IV.7)) except that now the specularly reflected light will be calculated differently.

The calculation for specular light has the form

$$I_{\mathrm{s}} \;=\; \frac{(\mathbf{n} \cdot \boldsymbol{\ell})}{(\mathbf{n} \cdot \mathbf{v})} \, s\, F\, G\, D \cdot I_{\mathrm{s}}^{\mathrm{in}},$$

where $\mathbf{n}$ is the unit vector normal to the surface, s is a scalar constant, and F, G, and D are scalar-valued functions that will be explained below. The constant s is used to scale the brightness of the specular reflection. Including the multiplicative factor $\mathbf{n} \cdot \boldsymbol{\ell}$ has the effect of converting the incoming light intensity into the incoming light energy flux per unit surface area; that is to say, the value $(\mathbf{n} \cdot \boldsymbol{\ell}) I^{\mathrm{in}}$ measures the amount of light energy hitting a unit area of the surface. Similarly, $(\mathbf{n} \cdot \mathbf{v}) I_{\mathrm{s}}$ measures the amount of light energy leaving a unit area of the surface, and for this reason we need to include the division by $\mathbf{n} \cdot \mathbf{v}$. Thus, the quantity $s \cdot F \cdot G \cdot D$ is the ratio of the energy hitting a unit area of the surface from the direction of $\boldsymbol{\ell}$ to the energy leaving the unit area in the direction of $\mathbf{v}$.

The function $D = D(\boldsymbol{\ell}, \mathbf{v})$ measures the distribution of the microfacets; namely, it equals the fraction of microfacets that are oriented correctly for specular reflection from the direction of $\boldsymbol{\ell}$ to the direction $\mathbf{v}$. Possible functions for D are discussed in Section IV.6.3 below. The $G = G(\boldsymbol{\ell}, \mathbf{v})$ function measures the diminution of reflected light due to shadowing and masking, where the roughness of the surface creates shadowing that prevents reflection. This geometric term will be discussed in Section IV.6.4. The function $F = F(\boldsymbol{\ell}, \mathbf{v}, \lambda)$ is the Fresnel coefficient. The Fresnel coefficient shows what percentage of the incidence light is reflected. The Fresnel term is discussed in Section IV.6.5 below.

The Fresnel coefficient is particularly important because it can be used to create the effect that light reflects more specularly at grazing angles than at

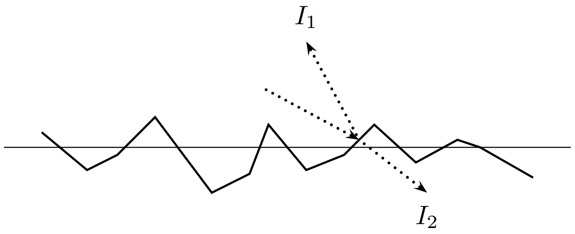

Figure IV.19: A microfacet surface consists of small flat pieces. The horizontal line shows the average level of a flat surface, and the microfacets show the microscopic shape of the surface. Dotted lines show the direction of light rays. The incoming light can either be reflected in the direction of perfect mirror-like reflection (I_1), or can enter the surface (I_2). In the second case, the light is modeled as possibly eventually exiting the material as diffusely reflected light.

angles near vertical. This kind of effect is easy to observe; for instance, a piece of white paper that usually reflects only diffusely will reflect specularly when viewed from a very oblique angle. An interesting additional effect is that the Fresnel term can cause the angle of greatest reflection to be different than the direction of perfect mirror-like reflection. The Fresnel term F, unlike the D and G functions, is dependent on the wavelength λ. This causes the color of specular reflections to vary with the angles of incidence and reflection.

In our description of the Cook-Torrance model, we have not followed exactly the conventions of Blinn [13] and Cook and Torrance [29]. They did not distinguish between diffuse and specular incoming light, but instead assumed that there is only one kind of incoming light. They then used a bidirectional reflectivity function of the form

$$BRIDF \;=\; d\cdot\rho_{\rm d}(\mathbf{n}\cdot\boldsymbol{\ell}) + s\cdot\frac{(\mathbf{n}\cdot\boldsymbol{\ell})}{(\mathbf{n}\cdot\mathbf{v})}\,F\,G\,D,$$

where d and s are scalars, with $d+s=1$, which control the fraction of diffuse versus specular reflection. We have changed this aspect of their model since it makes the model a little more general, and also for the practical reason that it allows Cook-Torrance lighting to coexist with Phong lighting in the ray tracing software described in Appendix **??**.

IV.6.3 The microfacet distribution term, $D^\star$

The microfacet model assumes that light incident from the direction of $\boldsymbol{\ell}$ is specularly reflected independently by each individual microfacet. Hence, the amount of light which is reflected in the direction $\mathbf{v}$ is deemed to be proportional to the fraction of microfacets which are correctly oriented to cause mirror-like reflection in that direction. To determine the direction of these microfacets, recall that the halfway vector was defined by

$$\mathbf{h} \;=\; \frac{\mathbf{v}+\boldsymbol{\ell}}{||\mathbf{v}+\boldsymbol{\ell}||}$$

(see Figure IV.11 on page 141). In order for a microfacet to be oriented properly for perfect reflection, the normal pointing outward from the microfacet must be equal to $\mathbf{h}$. We let ψ equal the angle between $\mathbf{h}$ and the overall surface normal $\mathbf{n}$, i.e., $\psi = \cos^{-1}(\mathbf{h}\cdot\mathbf{n})$. Then, we use the function $D = D(\psi)$ to equal the fraction of microfacets which are correctly oriented for perfect reflection. There are several functions that have been suggested for D. One possibility is the Gaussian distribution function

$$D(\psi) \;=\; ce^{-\psi^2/m^2}$$

where c and m are positive constants. Another possibility is the Beckmann distribution

$$D(\psi) \;=\; \frac{1}{\pi\, m^2 \cos^4 \psi} e^{-(\tan^2 \psi)/m^2},$$

where again m is a constant. The Beckmann distribution is based on a mathematical model for a rough one dimensional surface where the height of the surface is a normally distributed function, and where the auto-correlation of the surface makes the root mean value of the slope equal to $m/\sqrt{2}$. This sounds complicated, but what it means is that the constant m should be chosen to be approximately equal to the average slope of (microfacets of) the surface.[7] Bigger values of m correspond to rougher, more bumpy surfaces.

IV.6.4 The geometric surface occlusion term, $G^\star$

The geometric term G in the Cook-Torrance model computes the fraction of the illuminated portion of the surface which is visible to the viewer, or to be more precise, the geometric term computes the fraction of the light specularly reflected by the microfacets that is able to reach the viewer. Since the surface is rough and bumpy, it is probable that some of the illuminated area of the surface is not visible to the viewer, and this can reduce the amount of specularly reflected light which is visible.

In order to derive a formula for the geometric term, we make two simplifying assumptions. The first assumption is that the vectors $\boldsymbol{\ell}$, $\mathbf{n}$, and $\mathbf{v}$ are coplanar. We call this plane the *plane of reflection.* At the end of this section, we discuss how to remove this coplanarity assumption. The second, and more important, assumption is that the microfacets on the surface are arranged as symmetric “V”-shaped grooves. These grooves are treated as being at right angles to the plane of reflection. In effect, this means we are adopting a one dimensional model for the surface. We further assume that the tops of the grooves are all at the same height; i.e., that the surface is obtained from a perfectly flat surface

[7] See [7] for more details, including the details of the mathematical models.

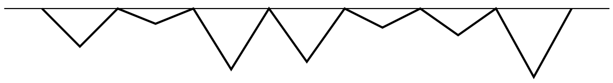

Figure IV.20: For the derivation of the geometric term, G, the microfacets are modeled as symmetric, "V"-shaped grooves with the tops of the grooves all at the same height. The horizontal line shows the overall plane of the surface.

by etching the grooves into the surface. A view of the grooves is shown in Figure IV.20.

The assumption about the microfacets being "V"-shaped may seem rather drastic and unjustified, but the reason for the assumption is that it turns the simplifies the calculation of the geometric factor G. In addition, it is hoped that the simplified model qualitatively matches the behavior of more complicated surfaces fairly well.

Some different kinds of occlusion of specularly reflected light are illustrated in Figure IV.21. Since the tops of the grooves are all at the same height, each groove may be considered independently. In Figure IV.21, light is shown coming in from the direction pointed to by $\boldsymbol{\ell}$, and is reflected specularly in the direction of $\mathbf{v}$. This means that the side of the groove must have normal vector equal to the halfway vector $\mathbf{h}$. In part (a) of the figure, the light falls fully onto the groove, and the entire groove is visible to the viewer. In part (b), the reflecting side of the groove is partly occluded by the other side, and thus some of the reflected light hits the opposite side of the groove and does not reach the viewer. In this case, we say that *masking* has occurred. In part (c), the reflecting side of the groove is partly shadowed by the other side of the groove, so that the reflecting side of the groove is not fully illuminated: we call this *shadowing*. Finally, in part (d), both shadowing and masking are occurring.

The usual formulation of the Cook-Torrance model calculates the percentage of light that is not shadowed and the percentage of the light that is not masked, and uses the minimum of these for the G term. However, this usual formulation is incorrect, because shadowing by itself should not cause any reduction in the intensity of reflected light. This is shown in Figure IV.22, where the incoming light is partially shadowed, but, nonetheless, all of the incoming light is reflected to the viewer. Figure IV.22 shows all the grooves having the same slope so as to make the situation clearer, but the same effect holds even if different grooves have different slopes (since the D term is used for the fraction of microfacets at a given slope, the G term does not need to take into account grooves that do not lead to perfect reflection).

Therefore, we present a version of the geometric term G that is different from the term used by Blinn [13] and Cook and Torrance [29] in that it uses a more correct treatment of shadowing. First, we need a geometric lemma due to Blinn [13]. This lemma will serve as the basis for calculating the fraction of the groove that is masked or shadowed. As stated with $\mathbf{v}$, the lemma computes the

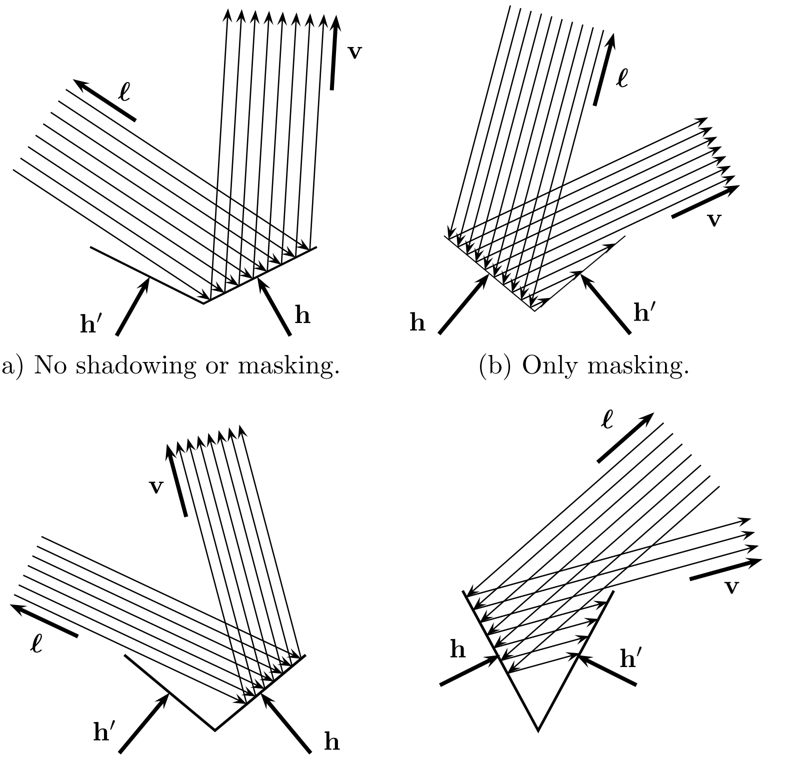

(a) No shadowing or masking.

(b) Only masking.

(c) Only shadowing.

(d) Both shadowing and masking.

Figure IV.21: Shadowing and masking inside a single groove. The "V"-shape represents a groove; the unit vector $\mathbf{h}$ is normal to the facet where specular reflection occurs. Light from the direction of $\boldsymbol{\ell}$ is specularly reflected in the direction $\mathbf{v}$.

fraction that is not masked (if there is any masking), but replacing $\mathbf{v}$ with $\boldsymbol{\ell}$ gives the formula for the fraction of the groove that is not shadowed (if there is any shadowing).

Lemma IV.4. *Consider the situation in Figure IV.23. Let $||AB||$ be the distance from A to B, etc. Then,*

$$\frac{||BC||}{||AC||} \;=\; \frac{2(\mathbf{n}\cdot\mathbf{h})(\mathbf{n}\cdot\mathbf{v})}{(\mathbf{h}\cdot\mathbf{v})}. \tag{IV.22}$$

In order to prove the lemma, and for subsequent algorithms, it will be useful to first define the vector $\mathbf{h}'$ to be the unit vector which is normal to the opposite side of the groove. By the symmetry of the groove, the vector $\mathbf{h}'$ is easily seen to equal

$$\mathbf{h}' \;=\; 2(\mathbf{n}\cdot\mathbf{h})\mathbf{n} - \mathbf{h}. \tag{IV.23}$$

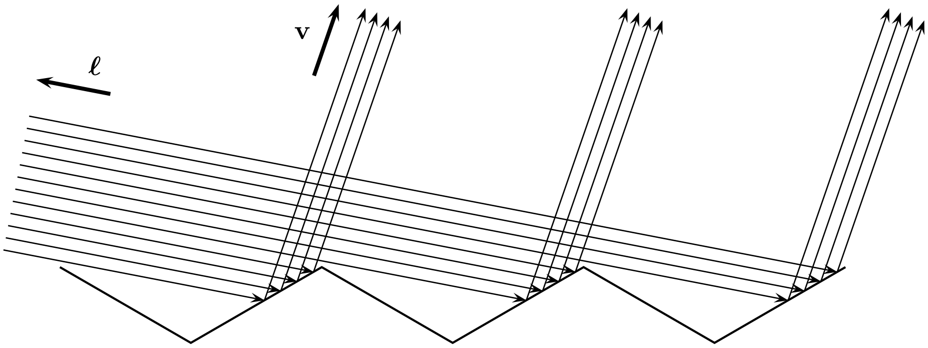

Figure IV.22: Shadowing without masking does not reduce the intensity of the reflected light.

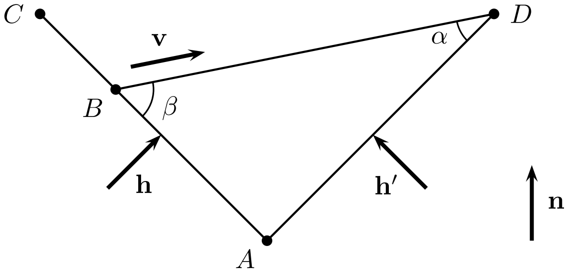

Figure IV.23: The situation for Lemma IV.4. The edges AC and AD form a symmetric groove, with AC and AD being of equal length. The vector $\mathbf{n}$ points upward from the overall surface. The vector $\mathbf{v}$ is in the direction from B to D. The vectors $\mathbf{h}$ and $\mathbf{h}'$ are normal to the sides of the groove. All four vectors are unit vectors. The ratio of $||BC||$ to $||AC||$ measures the fraction of the groove that is not masked.

We now prove the lemma.

Proof. From the symmetry of the groove and the law of sines, we have

$$\frac{||AB||}{||AC||} = \frac{||AB||}{||AD||} = \frac{\sin\alpha}{\sin\beta}.$$

Since $\mathbf{h}'$ is perpendicular to AD, we have $\sin\alpha = \cos(\frac{\pi}{2}-\alpha) = -\mathbf{v}\cdot\mathbf{h}'$. Similarly, we have $\sin\beta = \mathbf{v}\cdot\mathbf{h}$. From this, using Equation (IV.23), we get

$$\frac{||BC||}{||AC||} = 1 - \frac{||AB||}{||AC||} = 1 + \frac{\mathbf{v}\cdot(2(\mathbf{n}\cdot\mathbf{h})\mathbf{n}-\mathbf{h})}{\mathbf{v}\cdot\mathbf{h}},$$

and the lemma follows immediately. □

With the aid of the lemma, we can now give a formula for the geometric term that describes the reduction in reflection due to masking. First, we note that masking occurs if, and only if, $\mathbf{v}\cdot\mathbf{h}' < 0$. To see this, note that $\mathbf{v}\cdot\mathbf{h}'$ is positive only if the vector $\mathbf{h}'$ is facing towards the viewer. When masking occurs, the fraction of the side of the groove which is not masked is given by Equation (IV.22) of the lemma.

For similar reasons, shadowing occurs if and only if we have $\boldsymbol{\ell}\cdot\mathbf{h}' < 0$. By Lemma IV.4, with $\mathbf{v}$ replaced by $\boldsymbol{\ell}$, the fraction of the side of the groove which is not shadowed is equal to

$$\frac{2(\mathbf{n}\cdot\mathbf{h})(\mathbf{n}\cdot\boldsymbol{\ell})}{(\mathbf{h}\cdot\boldsymbol{\ell})}.$$

We can now describe how to compute the geometric factor G. In the case where there is neither masking nor shadowing, we set G equal to 1. When there is masking, but no shadowing, we set G equal to the fraction of the reflected light that is not masked, that is,

$$G \;=\; \frac{2(\mathbf{n}\cdot\mathbf{h})(\mathbf{n}\cdot\mathbf{v})}{(\mathbf{h}\cdot\mathbf{v})}.$$

In the case where both masking and shadowing occur together, as illustrated in Figure IV.21(d), we set G to equal the fraction of the reflected light which is not masked. This means that we set G equal to the ratio (note that $\mathbf{h}\cdot\mathbf{v} = \mathbf{h}\cdot\boldsymbol{\ell}$ by the definition of $\mathbf{h}$)

$$\left(\frac{2(\mathbf{n}\cdot\mathbf{h})(\mathbf{n}\cdot\mathbf{v})}{(\mathbf{h}\cdot\mathbf{v})}\right) \div \left(\frac{2(\mathbf{n}\cdot\mathbf{h})(\mathbf{n}\cdot\boldsymbol{\ell})}{(\mathbf{h}\cdot\boldsymbol{\ell})}\right) \;=\; \frac{\mathbf{n}\cdot\mathbf{v}}{\mathbf{n}\cdot\boldsymbol{\ell}}$$

if this value is less than 1. This is the case illustrated in part (d) of Figure IV.21(d), and we are setting G equal to the ratio of the non-masked amount to the non-shadowed amount. However, if the fraction is ≥ 1, then none of the non-shadowed part is masked, so we just set $G = 1$.

To summarize, the geometric term G is defined by

$$G \;=\; \begin{cases} 1 & \text{if } \mathbf{v}\cdot\mathbf{h}' \geq 0 \text{ or } \mathbf{n}\cdot\mathbf{v} \geq \mathbf{n}\cdot\boldsymbol{\ell} \\ \dfrac{2(\mathbf{n}\cdot\mathbf{h})(\mathbf{n}\cdot\mathbf{v})}{(\mathbf{h}\cdot\mathbf{v})} & \text{if } \mathbf{v}\cdot\mathbf{h}' < 0 \text{ and } \boldsymbol{\ell}\cdot\mathbf{h}' \geq 0 \\ \dfrac{\mathbf{n}\cdot\mathbf{v}}{\mathbf{n}\cdot\boldsymbol{\ell}} & \text{if } \mathbf{v}\cdot\mathbf{h}' < 0,\, \boldsymbol{\ell}\cdot\mathbf{h}' < 0, \text{ and } \mathbf{n}\cdot\mathbf{v} < \mathbf{n}\cdot\boldsymbol{\ell}. \end{cases}$$

The above formula for the geometric term was derived from a one dimensional model of “V”-shaped grooves. Although this assumption that the facets are arranged in grooves is unrealistic, it still works fairly well as long the vectors $\boldsymbol{\ell}$, $\mathbf{v}$, and $\mathbf{n}$ are coplanar. However, the above formula breaks down when these vectors are not coplanar, since the derivation of the formula for G made assumptions about how $\mathbf{h}$, $\mathbf{h}'$, and $\mathbf{n}$ interact which are no longer valid in the noncoplanar case. The coplanar case is actually quite common; for instance, these vectors are always coplanar in (non-distributed) ray tracing, as we shall in Chapter X, since basic ray tracing follows rays in the direction of perfect mirror-like reflection.

In the noncoplanar case, we suggest that the vector $\mathbf{n}$ be replaced by projecting (actually, rotating) it down to the plane containing $\boldsymbol{\ell}$ and $\mathbf{v}$. That is to say, instead of $\mathbf{n}$, we use a unit vector $\mathbf{m}$ which is parallel to the projection of $\mathbf{n}$ onto the plane containing $\boldsymbol{\ell}$ and $\mathbf{v}$. The vector $\mathbf{h}$ is still computed as usual, but now $\mathbf{h}'$ is computed using $\mathbf{m}$ instead of $\mathbf{n}$. It is not hard to see that the projection of $\mathbf{n}$ onto the plane is equal to

$$\mathbf{n}_0 \;=\; \frac{(\mathbf{n}\cdot\boldsymbol{\ell})\boldsymbol{\ell} + (\mathbf{n}\cdot\mathbf{v})\mathbf{v} - (\mathbf{v}\cdot\boldsymbol{\ell})(\mathbf{v}\cdot\mathbf{n})\boldsymbol{\ell} - (\mathbf{v}\cdot\boldsymbol{\ell})(\boldsymbol{\ell}\cdot\mathbf{n})\mathbf{v}}{1-(\mathbf{v}\cdot\boldsymbol{\ell})^2}. \qquad \text{(IV.24)}$$

Then, $\mathbf{m} = \mathbf{n}_0/||\mathbf{n}_0||$. In the extreme case where $\mathbf{v}$ and $\boldsymbol{\ell}$ are both perpendicular to $\mathbf{n}$, this gives a divide by zero, but this case can be handled by instead setting $\mathbf{n}_0 = \mathbf{v}+\boldsymbol{\ell}$.

Putting this together gives the following algorithm for the case where $\mathbf{v}$, $\boldsymbol{\ell}$, and $\mathbf{n}$ are not coplanar:

```
ComputeG( $\mathbf{n}$, $\boldsymbol{\ell}$, $\mathbf{v}$ ) {
    If ( $||\boldsymbol{\ell}+\mathbf{v}||$ == 0 ) {        // if $\mathbf{v}\cdot\boldsymbol{\ell} == -1$
        Set $G$ = 1;
        Return ( $G$ );
    }
    Set $\mathbf{h}$ = $(\boldsymbol{\ell}+\mathbf{v})/(||\boldsymbol{\ell}+\mathbf{v}||)$;
    Set $\mathbf{n}_0$ = $(\mathbf{n}\cdot\boldsymbol{\ell})\boldsymbol{\ell} + (\mathbf{n}\cdot\mathbf{v})\mathbf{v} - (\mathbf{v}\cdot\boldsymbol{\ell})(\mathbf{v}\cdot\mathbf{n})\boldsymbol{\ell} - (\mathbf{v}\cdot\boldsymbol{\ell})(\boldsymbol{\ell}\cdot\mathbf{n})\mathbf{v}$;
    If ( $||\mathbf{n}_0|| \neq 0$ ) {
        Set $\mathbf{m}$ = $\mathbf{n}_0/||\mathbf{n}_0||$;
    }
    Else {
        Set $\mathbf{m}$ = $\mathbf{h}$;
    }
    Set $\mathbf{h}'$ = $2(\mathbf{m}\cdot\mathbf{h})\mathbf{m} - \mathbf{h}$;
    Set $G$ = $\begin{cases} 1 & \texttt{if } \mathbf{v}\cdot\mathbf{h}' \ge 0 \texttt{ or } \mathbf{m}\cdot\mathbf{v} \ge \mathbf{m}\cdot\boldsymbol{\ell} \\ \dfrac{2(\mathbf{m}\cdot\mathbf{h})(\mathbf{m}\cdot\mathbf{v})}{(\mathbf{h}\cdot\mathbf{v})} & \texttt{if } \mathbf{v}\cdot\mathbf{h}' < 0 \texttt{ and } \boldsymbol{\ell}\cdot\mathbf{h}' \ge 0 \\ \dfrac{\mathbf{m}\cdot\mathbf{v}}{\mathbf{m}\cdot\boldsymbol{\ell}} & \texttt{otherwise.} \end{cases}$
    Return ( $G$ );
}
```

Although it is not part of the Cook-Torrance model, it is possible to use the geometric term to affect the diffuse part of the reflection too. Oren and Nayar [85, 86] use the same "V"-shaped groove model of surface roughness to compute masking and shadowing effects for diffuse lighting; this allows them to render non-Lambertian surfaces.

Exercise IV.8* Derive the formula (IV.24) for $\mathbf{n}_0$.

IV.6.5 The Fresnel term, $F^\star$

The Fresnel equations describe what fraction of incident light is specularly reflected from a flat surface. For a particular wavelength λ, this can be defined in terms of a function $\mathcal{F}$

$$F(\boldsymbol{\ell},\mathbf{v},\lambda) \;=\; \mathcal{F}(\varphi,\eta),$$

where $\varphi = \cos^{-1}(\boldsymbol{\ell}\cdot\mathbf{h})$ is the angle of incidence, and η is the index of refraction of the surface. Here, φ is the angle of incidence of the incoming light with respect to the surface of the microfacets, not with respect to the overall plane of the whole surface. The index of refraction is the ratio of the speed of light above the surface to the speed of light inside the surface material, and is discussed in more detail in Section X.1.2 in connection with Snell's law. For materials which are not electrically conducting, Fresnel's law states that the fraction of light intensity that is specularly reflected is equal to

$$\mathcal{F} \;=\; \frac{1}{2}\left(\frac{\sin^2(\varphi-\theta)}{\sin^2(\varphi+\theta)}+\frac{\tan^2(\varphi-\theta)}{\tan^2(\varphi+\theta)}\right), \qquad \text{(IV.25)}$$

where φ is the angle of incidence and θ is the angle of refraction. (We are not concerned with the portion of the light that is refracted, but the angle of refraction still appears in the Fresnel equation.) This form of the Fresnel equation applies to unpolarized light and is obtained by averaging the two forms of the Fresnel equations that apply to light polarized in two different orientations. The angles of incidence and refraction are related by Snell's law which states that

$$\frac{\sin\varphi}{\sin\theta} \;=\; \eta.$$

Let

$$c \;=\; \cos\varphi \qquad \text{and} \qquad g = \sqrt{\eta^2+c^2-1}\,. \qquad \text{(IV.26)}$$

The most common situation is that $\eta > 1$, and in this case $\eta^2+c^2-1>0$, so g is well defined.[8] A little work shows that $g = \eta\cos\theta$ and then using the trigonometric angle sum and difference formulas, it is not hard to see that

$$\frac{\sin(\varphi-\theta)}{\sin(\varphi+\theta)} \;=\; \frac{(g-c)}{(g+c)} \qquad \text{(IV.27)}$$

and

$$\frac{\cos(\varphi-\theta)}{\cos(\varphi+\theta)} \;=\; \frac{(c(g-c)+1)}{(c(g+c)-1)}. \qquad \text{(IV.28)}$$

[8] However, the $\eta < 1$ case can arise in ray tracing when transmission rays are used, as described in Chapter X. In that case, the condition $\eta^2+c^2-1\le 0$ corresponds to the case of total internal reflection. For total internal reflection, you should just set $\mathcal{F}$ equal to 1.

	Red	Green	Blue
Gold:	0.93	0.88	0.38
Iridium:	0.26	0.28	0.26
Iron:	0.44	0.435	0.43
Nickel:	0.50	0.47	0.36
Copper:	0.93	0.80	0.46
Platinum:	0.63	0.62	0.57
Silver:	0.97	0.97	0.96

Figure IV.24: Experimentally measured reflectances $\mathcal{F}_0$ for perpendicularly incident light. Values based on [112].

This lets us express the Fresnel equation (IV.25) in the following, easier to compute form:

$$\mathcal{F} \;=\; \frac{1}{2}\frac{(g-c)^2}{(g+c)^2}\left(1+\frac{[c(g+c)-1]^2}{[c(g-c)+1]^2}\right). \qquad \text{(IV.29)}$$

The above form of the Fresnel equation makes several simplifying assumptions. First, the incoming light is presumed to be unpolarized. Second, conducting materials such as metals need to use an index of refraction which has an imaginary component called the *extinction coefficient.* For simplicity, the Cook-Torrance model just sets the extinction coefficient to zero.

If the index of refraction η is known, then Equations (IV.26) and (IV.29) provide a good way to compute the reflectance $\mathcal{F}$. On the other hand, the Fresnel equation is sometimes used in the context of ray tracing, and, in that setting, a slightly more efficient method can be used. For this, refer ahead to Section X.1.2. That section has a vector $\mathbf{v}$ giving the direction from which the light arrives, and gives a method for computing the transmission direction $\mathbf{t}$. Then, we can calculate $c = \cos\varphi = \mathbf{v}\cdot\mathbf{n}$ and $g = \eta\cos\theta = -\eta\mathbf{t}\cdot\mathbf{n}$, instead of using Equation (IV.26).

Exercise IV.9* Prove that the reflectance $\mathcal{F}$ can also be computed by the formula

$$\mathcal{F} \;=\; \frac{1}{2}\left[\left(\frac{\eta\cos\theta-\cos\varphi}{\eta\cos\theta+\cos\varphi}\right)^2+\left(\frac{\eta\cos\varphi-\cos\theta}{\eta\cos\varphi+\cos\theta}\right)^2\right]. \qquad \text{(IV.30)}$$

[Hint: Use Equation (IV.27) and use trignometry identities to show

$$\frac{\tan(\varphi-\theta)}{\tan(\varphi+\theta)} \;=\; \frac{\eta\cos\varphi-\cos\theta}{\eta\cos\varphi+\cos\theta}. \quad] \qquad \text{(IV.31)}$$

This still leaves the question of how to find the value of η. Cook and Torrance suggested the following procedure for determining an index of refraction for metals. They first note that for perpendicularly incident light, $\varphi = \theta = 0$, so

$c = 1$, $g = \eta$. Then the Fresnel reflectivity $\mathcal{F}_0$ for perpendicularly incident light is equal to

$$\mathcal{F}_0 \;=\; \left(\frac{\eta-1}{\eta+1}\right)^2.$$

Solving for η in terms of $\mathcal{F}_0$ gives

$$\eta \;=\; \frac{1+\sqrt{\mathcal{F}_0}}{1-\sqrt{\mathcal{F}_0}}. \tag{IV.32}$$

Reflectance values $\mathcal{F}_0$ for perpendicularly incident light have been measured for many materials (see Touloukian et al. [112, 113, 114]). Given a reflectance value for perpendicularly incident light, Equation (IV.32) can be used to get an approximate value for the index of refraction. This value for η can then be used to calculate the Fresnel term for light incident at other angles. Figure IV.24 shows reflectance values $\mathcal{F}_0$ for a few metals. These reflectance values are estimated from the graphs in [112] at red, green, and blue color values that correspond roughly to the red, green, and blue colors used by standard monitors.

Figures IV.25 and VI.9 show some examples of roughened metals rendered with the Cook-Torrance model. As can be seen from the figures, the Cook-Torrance model can do a fairly good job of rendering a metallic appearance, although the colors are not very accurate (and in any event, the colors in these figures have not been properly calibrated). The Cook-Torrance model works less well on shiny metals with low roughness.

Schlick [97] suggested approximating the Fresnel reflectivity equation (IV.29) with

$$\mathcal{F} \;\approx\; \mathcal{F}_0 + (1-\mathcal{F}_0)(1-\boldsymbol{\ell}\cdot\mathbf{h})^5,$$

arguing that this is much easier to compute and introduces an error of most 1%. As discussed in Section IV.1.5, this is sometimes included with Phong lighting using Equation (IV.12), usually with $\boldsymbol{\ell}\cdot\mathbf{n}$ in place of $\boldsymbol{\ell}\cdot\mathbf{h}$.

IV.7 Additional exercises

Exercise IV.10. Let $h(r) = \cos r$ define a surface of revolution $f(r,\theta)$ by revolving the graph of h around the y-axis. Give the formula for a point $\mathbf{f}(r,\theta)$ on the surface of rotation. Also give a formula for a normal vector (not necessarily a unit vector) at that point on the surface of rotation. Your normal vector should be pointing generally upward.

Exercise IV.11. Repeat the previous exercise for the function $h(r) = (\sin r)/r$. (Include $r = 0$ in the domain of h. How is this possible?)

Exercise IV.12. Repeat Exercise IV.10 for the function $h(r) = 5 - r^2$.

Exercise IV.13. Let S be the paraboloid surface defined as a level set by

$$S \;=\; \{\langle x,y,z\rangle : y = 5 - x^2 - z^2\}. \tag{IV.33}$$

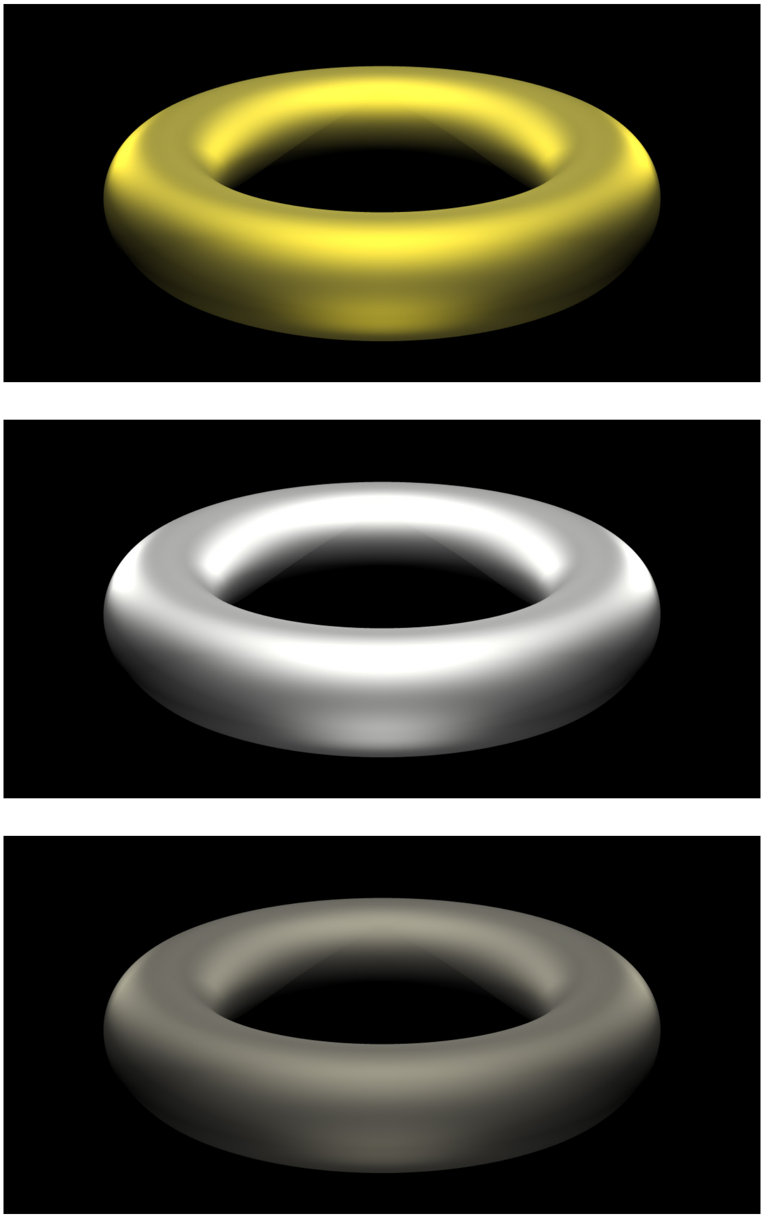

Figure IV.25: Metallic tori, with specular component computed using the Cook-Torrance model. The materials are, from top to bottom, gold, silver and platinum. The roughness is $m = 0.4$ for all three materials. The tori are each illuminated by five positional white lights. See color plate C.18.

Use the gradient method (for a level set surface) to give a formula $\mathbf{n} = \mathbf{n}(x, y, z)$ for a vector normal to S at a point $\langle x, y, z\rangle$ on S. The vector $\mathbf{n}$ should be pointing generally upward.

The surface S is the same as the surface of rotation in Exercise IV.12. Does your answer agree with the answer to Exercise IV.12? If so, how? If not, why not?

Exercise IV.14. Let S be a surface in $\mathbb{R}^2$. Suppose $\mathbf{0} = \langle 0, 0\rangle$ is on the surface S and the normal vector to the surface at this point is $\langle 1, 0\rangle$. Let A be the affine transformation of $\mathbb{R}^2$ defined by

$$A(\mathbf{x}) \;=\; \begin{pmatrix} 2 & 2 \\ 0 & 2 \end{pmatrix} \mathbf{x} \;+\; \begin{pmatrix} 3 \\ 5 \end{pmatrix}.$$

Thus A is the composition of a translation, a shearing transformation and the scaling S_2.

Let $A(S)$ be the surface as transformed by A. Give a vector perpendicular to $A(S)$ at the point $A(\mathbf{0}) = \langle 3, 5\rangle$. (It does not need to be a unit vector.)

Exercise IV.15. Let S be the paraboloid surface (IV.33) of Exercise IV.13. Let $A : \mathbb{R}^3 \to \mathbb{R}^3$ be the linear transformation with 3×3 matrix representation

$$M \;=\; \begin{pmatrix} 1 & 0 & -2 \\ 0 & 1 & 0 \\ 0 & 0 & 1 \end{pmatrix}.$$

Note that A is a shearing. What is $(M^{-1})^T$? Suppose $\langle x, y, z\rangle$ is a point on the surface S. Its normal vector $\mathbf{n}(x, y, z)$ was already computed in the previous exercise. Give a vector $\mathbf{m} = \mathbf{m}(x, y, z)$ normal to the transformed surface $A(S)$ at the transformed point $A(\langle x, y, z\rangle)$. Express your answer in terms of x, y and z.

Exercise IV.16. A smooth surface S in $\mathbb{R}^3$ is transformed by the linear transformation $f : \mathbb{R}^3 \to \mathbb{R}^3$ represented by the matrix

$$N \;=\; \begin{pmatrix} 2 & 0 & 0 \\ 0 & 0 & \frac{1}{2} \\ 0 & 4 & 0 \end{pmatrix}$$

to form the surface $f(S)$. Give a 3×3 matrix M such that whenever $\mathbf{n}$ is normal to S at a point $\mathbf{x}$ on S, then the vector $\mathbf{m} = M\mathbf{n}$ is normal to the point $f(\mathbf{x})$ on the surface $f(S)$. [Hint: It is not difficult to invert N.]

Exercise IV.17. The upper half of a hyperboloid $\mathcal{H}$ is specified by the equation $y = \sqrt{1 + x^2 + 2z^2}$. Equivalently, $\mathcal{H} = \{\langle x, y, z\rangle : y^2 = 1 + x^2 + 2z^2,\ y\geq 0\}$.

(a) Draw a rough sketch of the hyperboloid $\mathcal{H}$.

(b) This surface is expressed as a parametric function $y = y(x, z)$ of x and z. Give the formulas for its partial derivatives.

(c) Suppose $\langle x,y,z\rangle$ is a point on $\mathcal{H}$. Give a formula for a vector normal to $\mathcal{H}$ at the point $\langle x,y,z\rangle$, using Theorem IV.1 (cross products of partial derivatives). Your vector need not be a unit vector, but it should point downward from the surface (so as to be outward facing for a viewer placed at the origin). You may express the normal vector as either a function of x and z, or as a function of x, y and z.

(d) Now use the method of gradients to find a normal vector to the surface. Does your answer agree with the answer to part (c)? If so, why? If not, why not?

Exercise IV.18. A flattened ellipsoid $\mathcal{E}$ is defined by the equation $x^4 + 4y^2 + z^2 = 4$, so it has radii $2,1,2$.

(a) Draw a rough sketch of $\mathcal{E}$. Where does the ellipsoid intersect the three axes?

(b) Suppose $\langle x,y,z\rangle$ is a point on $\mathcal{E}$. Give a formula for an outward normal at the ellipsoid at this point.

(c) Give a parametric equation for $\mathcal{E}$; that is, a function $f(\theta,\varphi)$ so that $f(\theta,\varphi)$ gives the points on the ellipsoid as the parameters vary. What ranges do the parameters need to vary over? [Hint: Do this similarly to the parametric equation for a sphere in spherical coordinates.]

(d) Use the parametric equation for $\mathcal{E}$ to give a formula for an outward normal vector at a point on $\mathcal{E}$. Your formula for the normal vector should be in terms of θ and φ.

Exercise IV.19. Each part (a)-(e) asks when a task is done for Phong lighting with either Phong shading or Gouraud shading. Answer each part (a)-(e) with one of i.-v. indicating when the task is done.

i. Before the vertex shader is called.
ii. By the vertex shader.
iii. After the vertex shader is called, but before the fragment shader is called.
iv. By the fragment shader.
v. After the fragment shader is called.

Questions:

(a) Gouraud shading (averaging colors for Phong lighting) is done when?
(b) Phong shading (averaging normals for Phong lighting) is done when?
(c) When using Gouraud shading, when is the Phong lighting calculation (as in Equation IV.10 for example) done?
(d) When using Phong shading, when is the Phong lighting calculation done?
(e) When are material and light properties typically set?

Exercise IV.20. Answer questions (a) and (b).

(a) There are 12 assertions, i.-xii., below. With ***one*** exception these assertions are true, or true in most circumstances. Which of these assertions is false?

(b) Which of the 12 assertions best describes the reason that the Schlick-Fresnel term is sometimes used with Phong lighting?

The 12 assertions:

i. The halfway vector method works better than the Phong method when the specular exponent is equal to one.

ii. Many surfaces act like Lambertian surfaces under diffuse light.

iii. Some surfaces are non-Lambertian, such as the moon illuminated by the sun.

iv. Ambient light is viewed as arriving from all directions.

v. Diffuse and specular light are viewed as coming from a particular direction.

vi. Diffuse illumination depends on the light direction ($\boldsymbol{\ell}$) but not the view direction ($\mathbf{v}$).

vii. Specular highlights depend on the view direction ($\mathbf{v}$) but not the light direction ($\boldsymbol{\ell}$).

viii. The viewer might be very close to the light source, so the $\boldsymbol{\ell}$ and $\mathbf{v}$ vectors may be nearly equal.

ix. Specular light reflectivity is increased for light hitting the surface at a grazing angle.

x. Phong lighting is a local lighting model and does not model shadows.

xi. The ambient and diffuse material properties give the color of a material.

xii. Specular highlights should have the color of the light, not the color of the surface material.

Chapter V

Averaging and Interpolation

This is a ***preliminary*** *draft of a second edition of the book* 3-D Computer Graphics: A Mathematical Introduction with OpenGL. *So please read it cautiously and critically! Corrections are appreciated. Draft C.4.a*
Author: Sam Buss, `sbuss@ucsd.edu`

This chapter takes up the subject of interpolation. For the purposes of the present chapter, the term "interpolation" means the process of finding intermediate values of a function by averaging its values at extreme points. Interpolation was already discussed in Section III.3, where it was used for Gouraud and Phong interpolation to average colors or normals to create smooth lighting and shading effects. In Chapter VI, interpolation will be used to apply texture maps. More sophisticated kinds of interpolation will be important in the study of Bézier curves and B-splines in Chapters VIII and IX. Interpolation is also very important for animation, where both positions and orientations of objects may need to be interpolated.

The first three sections below study the simplest forms of interpolation; namely, linear interpolation on lines and triangles. This includes studying weighted averages, affine combinations, extrapolation, and barycentric coordinates. Then we turn to the topics of bilinear and trilinear interpolation, with an emphasis on bilinear interpolation, including an algorithm for inverting bilinear interpolation. The next section has a short, abstract discussion on convex sets, convex hulls, and the definition of convex hulls in terms of weighted averages. After that, we take up the topic of weighted averages performed on points represented in homogeneous coordinates. It is shown that the effect of the homogeneous coordinate is similar to an extra weighting coefficient, and as a corollary, we derive the formulas for hyperbolic interpolation which are important for accurate interpolation in screen space coordinates. The chapter concludes with a discussion of spherical linear interpolation ("slerping"), which will be used later for quaternion interpolation.

The reader may wish to skip many of the topics in this chapter on first reading, and return to them as needed for topics taken up in later chapters.

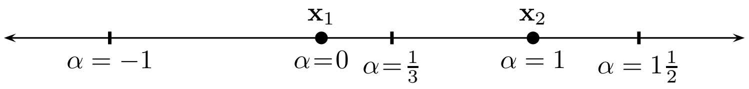

Figure V.1: Interpolated and extrapolated points for various values of α. When $\alpha < 0$, $\mathbf{x}(\alpha)$ is to the left of $\mathbf{x}_1$. When $\alpha > 1$, $\mathbf{x}(\alpha)$ is to the right of $\mathbf{x}_2$. When $0 < \alpha < 1$, $\mathbf{x}(\alpha)$ is between $\mathbf{x}_1$ and $\mathbf{x}_2$.

V.1 Linear interpolation

V.1.1 Interpolation between two points

Suppose that $\mathbf{x}_1$ and $\mathbf{x}_2$ are two distinct points, and consider the line segment joining them. We wish to parameterize the line segment between the two points, by using a function $\mathbf{x}(\alpha)$, which maps the scalar α to a point on the line segment $\overline{\mathbf{x}_1\mathbf{x}_2}$. We further want $\mathbf{x}(0) = \mathbf{x}_1$ and $\mathbf{x}(1) = \mathbf{x}_2$ and want $\mathbf{x}(\alpha)$ to linearly interpolate between $\mathbf{x}_1$ and $\mathbf{x}_2$ for values of α between 0 and 1. Therefore, the function is defined by

$$\mathbf{x}(\alpha) \;=\; (1-\alpha)\mathbf{x}_1 + \alpha\mathbf{x}_2. \tag{V.1}$$

Equivalently, we can also write

$$\mathbf{x}(\alpha) \;=\; \mathbf{x}_1 + \alpha(\mathbf{x}_2 - \mathbf{x}_1), \tag{V.2}$$

where, of course, $\mathbf{x}_2 - \mathbf{x}_1$ is the vector from $\mathbf{x}_1$ to $\mathbf{x}_2$. Equation (V.1) is a more elegant way to express linear interpolation, but the equivalent formulation (V.2) makes it clearer how linear interpolation works.

We can also obtain points by *extrapolation*, by letting α be outside the interval $[0,1]$. Equation (V.2) makes it clear how extrapolation works. When $\alpha > 1$, the point $\mathbf{x}(\alpha)$ lies past $\mathbf{x}_2$ on the line containing $\mathbf{x}_1$ and $\mathbf{x}_2$. And, when $\alpha < 0$, the point $\mathbf{x}(\alpha)$ lies before $\mathbf{x}_1$ on the line. All this is illustrated in Figure V.1.

Now we consider how to invert the process of linear interpolation. Suppose that the points $\mathbf{x}_1$, $\mathbf{x}_2$, and $\mathbf{u}$ are given, and we wish to find α such that $\mathbf{u} = \mathbf{x}(\alpha)$. Of course, this is possible only if $\mathbf{u}$ is on the line containing $\mathbf{x}_1$ and $\mathbf{x}_2$. Assuming that $\mathbf{u}$ is on this line, we solve for α as follows: From Equation (V.2), we have that

$$\mathbf{u} - \mathbf{x}_1 \;=\; \alpha(\mathbf{x}_2 - \mathbf{x}_1).$$

Taking the dot product of both sides of the equation with the vector $\mathbf{x}_2 - \mathbf{x}_1$ and solving for α, we get[1]

$$\alpha \;=\; \frac{(\mathbf{u}-\mathbf{x}_1)\cdot(\mathbf{x}_2-\mathbf{x}_1)}{(\mathbf{x}_2-\mathbf{x}_1)^2}. \tag{V.3}$$

[1] We write $\mathbf{v}^2$ for $\mathbf{v}\cdot\mathbf{v} = ||\mathbf{v}||^2$. So $(\mathbf{x}_2 - \mathbf{x}_1)^2$ means the same as $||\mathbf{x}_2 - \mathbf{x}_1||^2$.

This formula for α is reasonably robust, and will not have a divide-by-zero problem unless $\mathbf{x}_1 = \mathbf{x}_2$, in which case the problem was ill-posed. It is easy to see that if $\mathbf{u}$ is not on the line containing $\mathbf{x}_1$ and $\mathbf{x}_2$, then the effect of Formula (V.3) is equivalent to first projecting $\mathbf{u}$ onto the line and then solving for α.

Exercise V.1. Let $\mathbf{x}_1 = \langle -1, 0\rangle$ and $\mathbf{x}_2 = \langle 2, 1\rangle$. Let α control the linear interpolation (and linear extrapolation) from $\mathbf{x}_1$ to $\mathbf{x}_2$. What points are obtained with α equal to -2, -1, 0, $\frac{1}{10}$, $\frac{1}{3}$, $\frac{1}{2}$, 1, $1\frac{1}{2}$ and 2? What value of α gives the point $\langle 1, \frac{2}{3}\rangle$? The point $\langle 8, 3\rangle$? Graph your answers.

Now we extend the notion of linear interpolation to linearly interpolating a function on the line segment $\overline{\mathbf{x}_1\mathbf{x}_2}$. Let $f(\mathbf{u})$ be a function, and suppose that the values of $f(\mathbf{x}_1)$ and $f(\mathbf{x}_2)$ are known. To linearly interpolate the values of $f(\mathbf{u})$, we express $\mathbf{u}$ as $\mathbf{u} = (1-\alpha)\mathbf{x}_1 + \alpha\mathbf{x}_2$. Then linear interpolation for f gives

$$f(\mathbf{u}) \;=\; (1-\alpha)f(\mathbf{x}_1) + \alpha f(\mathbf{x}_2). \tag{V.4}$$

This method works equally well when the function f is vector-valued instead of scalar-valued. For instance, in Gouraud interpolation, this method was used to interpolate color values. However, it does not work quite so well for Phong interpolation, where normals are interpolated, since the interpolated vectors have to be renormalized.

Equation (V.4) can also be used when α is less than zero or greater than one to extrapolate values of f.

The process of interpolating a function's values according to Equation (V.4) is often referred to as "lerping". "Lerp" is short for "*L*inear int*ERP*olation." Occasionally, when we want to stress the use of interpolation, we shall use the notation

$$\mathit{lerp}(\mathbf{x}, \mathbf{y}, \alpha) \quad = \quad (1-\alpha)\mathbf{x} + \alpha\mathbf{y}.$$

So, (V.4) could be written as $f(\mathbf{u}) = \mathit{lerp}(f(\mathbf{x}_1), f(\mathbf{x}_2), \alpha)$.

Exercise V.2. Let $\mathbf{x}_1$ and $\mathbf{x}_2$ be the same as in the previous Exercise V.1. What point $\mathbf{u}$ on the line containing $\mathbf{x}_1$ and $\mathbf{x}_2$ is the closest to the origin? Find the value α such that $\mathbf{u} = \mathit{lerp}(\mathbf{x}_1, \mathbf{x}_2, \alpha)$. [Hint: Use Equation V.3.]

Exercise V.3. Let $\mathbf{x}_1$ and $\mathbf{x}_2$ be the same as in the previous two exercises. Suppose the values $f(\mathbf{x}_1) = -3$ and $f(\mathbf{x}_2) = 3$ have been set, and we wish to set other values for $f(\mathbf{z})$ by linear interpolation/extrapolation. What will this set $f(\langle 1, \frac{2}{3}\rangle)$ equal to?

V.1.2 Weighted averages and affine combinations

The next two definitions generalize interpolation to interpolating between more than two points.

Definition V.1. Let $\mathbf{x}_1, \mathbf{x}_2, \ldots, \mathbf{x}_k$ be points. Let $a_1, a_2, \ldots, a_k$ be real numbers. Then

$$a_1\mathbf{x}_1 + a_2\mathbf{x}_2 + \cdots + a_k\mathbf{x}_k \tag{V.5}$$

is called an *linear combination* of $\mathbf{x}_1, \ldots \mathbf{x}_k$.

If the coefficients sum to one, i.e., if $\sum_{i=1}^{k} a_i = 1$, then Equation (V.5) is called an *affine combination* of $\mathbf{x}_1, \ldots, \mathbf{x}_k$.

If $\sum_{i=1}^{k} a_i = 1$ and, in addition, each $a_i \geq 0$, then Equation (V.5) is called a *weighted average* of $\mathbf{x}_1, \ldots, \mathbf{x}_k$.

Theorem V.2. *Affine combinations are preserved under affine transformations. That is, if*

$$\mathbf{f}(\mathbf{x}_1, \ldots, \mathbf{x}_k) \;=\; a_1\mathbf{x}_1 + a_2\mathbf{x}_2 + \cdots + a_k\mathbf{x}_k$$

is an affine combination, and if A is an affine transformation, then

$$\mathbf{f}(A(\mathbf{x}_1), A(\mathbf{x}_2), \ldots, A(\mathbf{x}_k)) \;=\; A(\mathbf{f}(\mathbf{x}_1, \mathbf{x}_2, \ldots, \mathbf{x}_k)).$$

Theorem V.2 will turn out to be very important for Bézier curves and B-splines (as defined later in Chapters VIII and IX). Bézier curves and B-spline curves will be defined as affine combinations of points called “control points,” and Theorem V.2 tells us that arbitrary rotations and translations of the control points will rotate and translate the spline curves in exactly the same way.

Proof. Recall from Chapter II that the affine transformation A can be written as

$$A(\mathbf{x}) \;=\; B(\mathbf{x}) + A(\mathbf{0}),$$

where B is a linear transformation. Then,

$$\begin{aligned}
&A(a_1\mathbf{x}_1 + a_2\mathbf{x}_2 + \cdots + a_k\mathbf{x}_k)\\
&\quad= \;B(a_1\mathbf{x}_1 + a_2\mathbf{x}_2 + \cdots + a_k\mathbf{x}_k) + A(\mathbf{0})\\
&\quad= \;a_1B(\mathbf{x}_1) + a_2B(\mathbf{x}_2) + \cdots + a_kB(\mathbf{x}_k) + A(\mathbf{0})\\
&\quad= \;a_1B(\mathbf{x}_1) + a_2B(\mathbf{x}_2) + \cdots + a_kB(\mathbf{x}_k) + \sum_{i=1}^{k} a_iA(\mathbf{0})\\
&\quad= \;a_1B(\mathbf{x}_1) + a_1A(\mathbf{0}) + a_2B(\mathbf{x}_2) + a_2A(\mathbf{0}) + \cdots + a_kB(\mathbf{x}_k) + a_kA(\mathbf{0})\\
&\quad= \;a_1A(\mathbf{x}_1) + a_2A(\mathbf{x}_2) + \cdots + a_kA(\mathbf{x}_k).
\end{aligned}$$

The second equality above used the linearity of B and the third equality used the fact that the combination is affine. □

Exercise V.4$^\bigstar$ By definition, a function $\mathbf{f}(\mathbf{x})$ is *preserved under affine combinations* if and only if, for all α and all $\mathbf{x}_1$ and $\mathbf{x}_2$,

$$\mathbf{f}((1-\alpha)\mathbf{x}_1 + \alpha\mathbf{x}_2) \;=\; (1-\alpha)\mathbf{f}(\mathbf{x}_1) + \alpha\mathbf{f}(\mathbf{x}_2).$$

Show that any function which is preserved under affine combinations is an affine transformation. [Hint: Show that $\mathbf{f}(\mathbf{x}) - \mathbf{f}(\mathbf{0})$ is a linear transformation.]

Exercise V.5* Show that any vector-valued function $\mathbf{f}(\mathbf{x}_1, \mathbf{x}_2) : \mathbb{R}^m \times \mathbb{R}^m \to \mathbb{R}^m$ which is preserved under affine transformations is an affine combination of $\mathbf{x}_1$ and $\mathbf{x}_2$. [Hint: Any such function is fully determined by the value of $\mathbf{f}(\mathbf{0}, \mathbf{i})$.] Remark: this result holds also for functions $\mathbf{f}$ with more than two inputs as long as the number of inputs is at most one more than the dimension m of the underlying space.

Theorem V.2 states that affine transformations preserve affine combinations. On the other hand, *perspective* transformations do not in general preserve affine combinations. Indeed, if we try to apply affine combinations to points expressed in homogeneous coordinates, the problem arises that it makes a difference which homogeneous coordinates are chosen to represent the points. For example, working in $\mathbb{R}^3$, consider the homogeneous representations $\mathbf{v}_0 = \langle 0, 0, 0, 1\rangle$ and the point $\mathbf{v}_1 = \langle 1, 0, 0, 1\rangle$. The first homogeneous vector represents the origin and the second represents the vector $\mathbf{i}$. The second vector is also equivalent to $\mathbf{v}_1' = \langle 2, 0, 0, 2\rangle$. If we form the following linear combinations:

$$\tfrac{1}{2}\mathbf{v}_0 + \tfrac{1}{2}\mathbf{v}_1 \;=\; \langle \tfrac{1}{2}, 0, 0, 1\rangle \qquad \text{(V.6)}$$

and

$$\tfrac{1}{2}\mathbf{v}_0 + \tfrac{1}{2}\mathbf{v}_1' \;=\; \langle 1, 0, 0, \tfrac{3}{2}\rangle, \qquad \text{(V.7)}$$

then the resulting two homogeneous vectors represent *different* points in 3-space, even though they are weighted averages of representations of the same points! Thus, affine combinations of points in homogeneous coordinates have a different meaning than you might expect. We shall return to this topic in Section V.4, where it will be seen that the w-component of a homogeneous vector serves as an additional weighting term. We shall see later that affine transformations of homogeneous representations of points can be a powerful and flexible tool for rational Bézier curves and B-splines, since it allows them to define circles and other conic sections.

V.1.3 Interpolation on three points: barycentric coordinates

Section V.1.1 discussed linear interpolation (and extrapolation) on a line segment between points. In this section, the notion of interpolation is generalized to allow linear interpolation on a triangle.

Let $\mathbf{x}$, $\mathbf{y}$, and $\mathbf{z}$ be three noncollinear points, so they are the vertices of a triangle T. Recall that a point $\mathbf{u}$ is a weighted average of these three points if it is equal to

$$\mathbf{u} \;=\; \alpha\mathbf{x} + \beta\mathbf{y} + \gamma\mathbf{z} \qquad \text{(V.8)}$$

where $\alpha + \beta + \gamma = 1$ and α, β, and γ are all nonnegative. As shown below (Theorems V.3 and V.4), a weighted average $\mathbf{u}$ of the three vertices $\mathbf{x}, \mathbf{y}, \mathbf{z}$ will always be in or on the triangle T. Furthermore, for each $\mathbf{u}$ in the triangle, there are unique values for α, β, and γ such that Equation (V.8) holds. These values α, β, and γ are called the *barycentric coordinates* of $\mathbf{u}$.

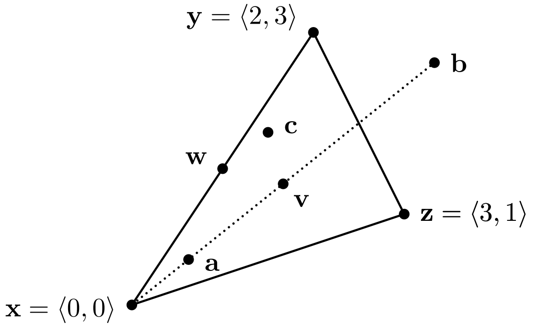
$\mathbf{y} = \langle 2, 3\rangle$
$\mathbf{b}$
$\mathbf{c}$
$\mathbf{w}$
$\mathbf{v}$
$\mathbf{z} = \langle 3, 1\rangle$
$\mathbf{a}$
$\mathbf{x} = \langle 0, 0\rangle$

Figure V.2: Some examples of barycentric coordinates. The point $\mathbf{w}$ is the midpoint of $\mathbf{x}$ and $\mathbf{y}$ and has barycentric coordinates $\alpha = \frac{1}{2}$, $\beta = \frac{1}{2}$ and $\gamma = 0$. Thus, $\mathbf{w} = \langle 1, \frac{3}{2}\rangle$. The point $\mathbf{v} = \langle \frac{5}{3}, \frac{4}{3}\rangle$ has barycentric coordinates $\alpha = \beta = \gamma = \frac{1}{3}$. The point $\mathbf{a} = \langle \frac{5}{8}, \frac{1}{2}\rangle$ has barycentric coordinates $\alpha = \frac{3}{4}$ and $\beta = \gamma = \frac{1}{8}$. The point $\mathbf{b} = \langle \frac{10}{3}, \frac{8}{3}\rangle$ has barycentric coordinates $\alpha = -\frac{1}{3}$ and $\beta = \gamma = \frac{2}{3}$. The point $\mathbf{c} = \langle \frac{3}{2}, \frac{19}{10}\rangle$ has barycentric coordinates $\alpha = \frac{3}{10}$, $\beta = \frac{6}{10}$ and $\gamma = \frac{1}{10}$.
In all cases, $\alpha + \beta + \gamma = 1$; so the barycentric equation (V.8) is an affine combination. Note that $\mathbf{x}$, $\mathbf{a}$, $\mathbf{v}$ and $\mathbf{b}$ are collinear. For instance, $\mathbf{b}$ can be expressed as $\mathbf{b} = \mathit{lerp}(\mathbf{x}, \mathbf{v}, 2)$.

More generally, any point $\mathbf{u}$ in the plane containing the triangle T can be expressed as an affine combination of $\mathbf{x}, \mathbf{y}, \mathbf{z}$ in the form of Equation (V.8) with $\alpha + \beta + \gamma = 1$, but with α, β, γ allowed to be negative.

Figure V.2 gives some examples of barycentric coordinates.

Theorem V.3. *Let* $\mathbf{x}$*,* $\mathbf{y}$*,* $\mathbf{z}$ *be noncollinear points and let* T *be the triangle formed by these three points.*

(a) *Let* $\mathbf{u}$ *be a point on* T *or in the interior of* T*. Then* $\mathbf{u}$ *can be expressed as a weighted average of the three vertices* $\mathbf{x}, \mathbf{y}, \mathbf{z}$ *as in Equation (V.8), with* $\alpha, \beta, \gamma \geq 0$ *and* $\alpha + \beta + \gamma = 1$*.*

(b) *Let* $\mathbf{u}$ *be any point in the plane containing* T*. Then* $\mathbf{u}$ *can be expressed as an affine combination of the three vertices, as in Equation (V.8), but with only the condition* $\alpha + \beta + \gamma = 1$*.*

Proof. (a) If $\mathbf{u}$ is on an edge of T, it is a weighted average of the two vertices on that edge. Suppose $\mathbf{u}$ is in the interior of T. Form the line containing $\mathbf{u}$ and $\mathbf{z}$. This line intersects the opposite edge, $\overline{\mathbf{xy}}$, of T at a point $\mathbf{w}$, as shown in Figure V.3. Since $\mathbf{w}$ is on the line segment between $\mathbf{x}$ and $\mathbf{y}$, it can be written as a weighted average

$$\mathbf{w} \;=\; a\mathbf{x} + b\mathbf{y},$$

where $a + b = 1$ and $a, b \geq 0$. Also, since $\mathbf{u}$ is on the line segment between $\mathbf{w}$ and $\mathbf{z}$, it can be written as a weighted average

$$\mathbf{u} = c\mathbf{w} + d\mathbf{z},$$

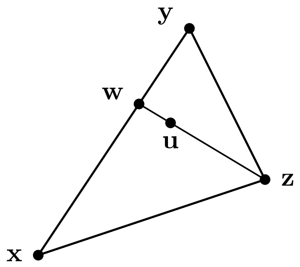

Figure V.3: The point **u** in the interior of the triangle is on the line segment from **w** to **z**. The point **w** is a weighted average of **x** and **y**. The point **u** is a weighted average of **w** and **z**.

where $c+d=1$ and $c,d \geq 0$. Therefore, **u** is equal to

$$\mathbf{u} \;=\; (ac)\mathbf{x} + (bc)\mathbf{y} + d\mathbf{z}.$$

This is easily seen to be a weighted average, since $ac+bc+d=1$ and all three coefficients are nonnegative. This proves (a).

Part (b) could be proved similarly to the proof of (a), but instead we give a proof based on linear independence. First, note that the vectors $\mathbf{y}-\mathbf{x}$ and $\mathbf{z}-\mathbf{x}$ are linearly independent, since they form two sides of a triangle and thus are noncollinear. Let P be the plane containing the triangle T: the plane P consists of the points **u** such that

$$\mathbf{u} \;=\; \mathbf{x} + \beta(\mathbf{y}-\mathbf{x}) + \gamma(\mathbf{z}-\mathbf{x}), \tag{V.9}$$

where $\beta, \gamma \in \mathbb{R}$. If we let $\alpha = (1-\beta-\gamma)$, then **u** is equal to the affine combination $\alpha\mathbf{x} + \beta\mathbf{y} + \gamma\mathbf{z}$. □

Exercise V.6. Let $\mathbf{x} = \langle 0,0 \rangle$, $\mathbf{y} = \langle 2,3 \rangle$, and $\mathbf{z} = \langle 3,1 \rangle$ in $\mathbb{R}^2$. Determine the points represented by the following sets of barycentric coordinates.

(a) $\alpha = 0$, $\beta = 1$, $\gamma = 0$.

(b) $\alpha = \frac{2}{3}$, $\beta = \frac{1}{3}$, $\gamma = 0$.

(c) $\alpha = \frac{1}{3}$, $\beta = \frac{1}{3}$, $\gamma = \frac{1}{3}$.

(d) $\alpha = \frac{4}{5}$, $\beta = \frac{1}{10}$, $\gamma = \frac{1}{10}$.

(e) $\alpha = \frac{4}{3}$, $\beta = \frac{2}{3}$, $\gamma = -1$.

Graph your answers along with the triangle formed by **x**, **y**, and **z**.

The proof of part (b) of Theorem V.3 constructed β and γ so that (V.9) holds. In fact, because $\mathbf{y}-\mathbf{x}$ and $\mathbf{z}-\mathbf{x}$ are linearly independent, the values of β and γ are uniquely determined by **u**. This implies that the barycentric coordinates of **u** are unique, so we have proved the following theorem.

Theorem V.4. *Let* $\mathbf{x}$*,* $\mathbf{y}$*,* $\mathbf{z}$*, and* T *be as in Theorem V.3. Let* $\mathbf{u}$ *be a point in the plane containing* T*. Then there are unique values for* α*,* β*, and* γ *such that* $\alpha+\beta+\gamma=1$ *and Equation (V.8) holds.*

One major application of barycentric coordinates and linear interpolation on three points is to extend the domain of a function f by linear interpolation. Suppose, as usual, that $\mathbf{x}$, $\mathbf{y}$, and $\mathbf{z}$ are the vertices of a triangle T and that f is a function for which we know the values of $f(\mathbf{x})$, $f(\mathbf{y})$ and $f(\mathbf{z})$. To extend f to be defined everywhere in the triangle by linear interpolation, we let

$$f(\mathbf{u}) \;=\; \alpha f(\mathbf{x}) + \beta f(\mathbf{y}) + \gamma f(\mathbf{z}),$$

where α, β, γ are the barycentric coordinates of $\mathbf{u}$. Mathematically, this is the same computation as used in Gouraud shading based on scan line interpolation. (At least, it gives the same results to within roundoff errors, which are due mostly to pixelization.) The same formula can be used to linearly extrapolate f to be defined for all points $\mathbf{u}$ in the plane containing the triangle.

Area interpretation of barycentric coordinates

There is a nice characterization of barycentric coordinates in terms of areas of triangles. Figure V.4 shows a triangle with vertices $\mathbf{x}$, $\mathbf{y}$, and $\mathbf{z}$. The point $\mathbf{u}$ divides the triangle into three subtriangles. The areas of these three smaller triangles are A, B, and C, so the area of the entire triangle is equal to $A+B+C$. As the next theorem states, the barycentric coordinates of $\mathbf{u}$ are proportional to the three areas A, B, and C.

Theorem V.5. *Suppose the situation shown in Figure V.4 holds. Then the barycentric coordinates of* $\mathbf{u}$ *are equal to*

$$\alpha = \frac{A}{A+B+C} \qquad \beta = \frac{B}{A+B+C} \qquad \gamma = \frac{C}{A+B+C}.$$

Proof. The proof is based on the construction used in the proof of part (a) of Theorem V.3. In particular, recall the way the scalars a, b, c, and d were used to define the barycentric coordinates of $\mathbf{u}$. You should also refer to Figure V.5, which shows additional areas D_1, D_2, E_1, and E_2.

As shown in part (a) of Figure V.5, the line $\overline{\mathbf{zw}}$ divides the triangle into two subtriangles, with areas D_1 and D_2. Let $D=A+B+C$ be the total area of the triangle, so $D=D_1+D_2$. By using the usual "one half base times height" formula for the area of a triangle, with the base along the line $\overline{\mathbf{xy}}$, we have that

$$D_1 \;=\; aD \qquad \text{and} \qquad D_2 = bD. \tag{V.10}$$

(Recall a and b are defined so that $\mathbf{w}=a\mathbf{x}+b\mathbf{y}$.)

Part (b) of the figure shows the triangle with area D_1 further divided into two subtriangles with areas E_1 and A, and the triangle with area D_2 divided

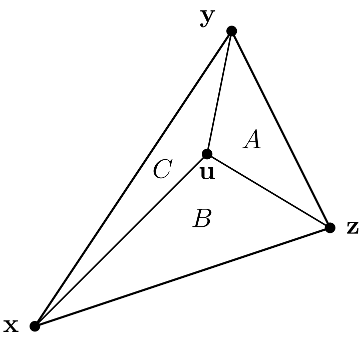

Figure V.4: The barycentric coordinates α, β and γ for the point $\mathbf{u}$ are proportional to the areas A, B and C.

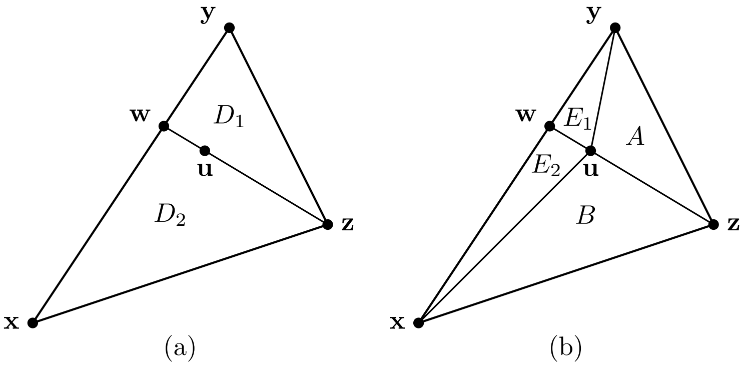

Figure V.5: The areas used in the proof of Theorem V.5.

into two subtriangles with areas E_2 and B. By exactly the same reasoning used for Equations (V.10), we have (recall that $\mathbf{u} = c\mathbf{w} + d\mathbf{z}$)

$$\begin{aligned} E_1 &= dD_1, \qquad A = cD_1, \\ E_2 &= dD_2, \qquad B = cD_2. \end{aligned} \tag{V.11}$$

Combining the Equations (V.10) and (V.11) and using $C = E_1 + E_2$ and $a + b = 1$ gives

$$A = acD, \qquad B = bcD, \quad \text{and} \quad C = dD.$$

This proves Theorem V.5, since $D = A + B + C$ and since $\alpha = ac = A/D$, $\beta = bc = B/D$, and $\gamma = d = C/D$. □

Calculating barycentric coordinates

Now we take up the problem of how to find the barycentric coordinates of a given point $\mathbf{u}$. First consider the simpler case of 2-space, where all points lie in the xy-plane. (The harder 3-space case will be considered afterwards.) The points $\mathbf{x} = \langle x_1, x_2 \rangle$, $\mathbf{y} = \langle y_1, y_2 \rangle$, $\mathbf{z} = \langle z_1, z_2 \rangle$, and $\mathbf{u} = \langle u_1, u_2 \rangle$ are presumed to be known points. We are seeking coefficients α, β, and γ which express $\mathbf{u}$ as an affine combination of the other three points.

Recall (see Appendix A.2.1), that in two dimensions, the (signed) area of a parallelogram with sides equal to the vectors $\mathbf{s} = \langle s_1, s_2 \rangle$ and $\mathbf{t} = \langle t_1, t_2 \rangle$ has area equal to the determinant

$$\mathit{det}(\mathbf{s}, \mathbf{t}) \;=\; \begin{vmatrix} s_1 & t_1 \\ s_2 & t_2 \end{vmatrix}.$$

Therefore, the area of the triangle shown in Figure V.4 is equal to

$$D \;=\; \tfrac{1}{2}\, \mathit{det}(\mathbf{z} - \mathbf{x},\, \mathbf{y} - \mathbf{x}).$$

Likewise, the area B is equal to

$$B \;=\; \tfrac{1}{2}\, \mathit{det}(\mathbf{z} - \mathbf{x},\, \mathbf{u} - \mathbf{x}).$$

Thus, by Theorem V.5,

$$\beta \;=\; \frac{B}{D} \;=\; \frac{\mathit{det}(\mathbf{z} - \mathbf{x},\, \mathbf{u} - \mathbf{x})}{\mathit{det}(\mathbf{z} - \mathbf{x},\, \mathbf{y} - \mathbf{x})}. \qquad \text{(V.12)}$$

Similarly,

$$\gamma \;=\; \frac{C}{D} \;=\; \frac{\mathit{det}(\mathbf{u} - \mathbf{x},\, \mathbf{y} - \mathbf{x})}{\mathit{det}(\mathbf{z} - \mathbf{x},\, \mathbf{y} - \mathbf{x})}. \qquad \text{(V.13)}$$

The barycentric coordinate α also can be computed as a ratio of determininants, but it is simpler to just let $\alpha = 1 - \beta - \gamma$.

The approach of Equations (V.12) and (V.13) can also be adapted for barycentric coordinates in 3-space, but you cannot use determinants. Instead, in 3-space, you can express the area of the parallelogram with edges $\mathbf{s}$ and $\mathbf{t}$ as the magnitude of the cross product $|\mathbf{s} \times \mathbf{t}|$. However, there is a simpler and faster method, presented below by Equations (V.14) through (V.16). This method works in any dimension ≥ 2, not just in 3-space.

To derive the better method, refer to Figure V.6. The two sides of the triangle are given by the vectors

$$\mathbf{e}_1 \;=\; \mathbf{y} - \mathbf{x} \qquad \text{and} \qquad \mathbf{e}_2 = \mathbf{z} - \mathbf{x}.$$

In addition, the vector from $\mathbf{x}$ to $\mathbf{u}$ is $\mathbf{f} = \mathbf{u} - \mathbf{x}$. The vector $\mathbf{n}$ is the unit vector perpendicular to the side $\mathbf{e}_2$, pointing into the triangle. The vector $\mathbf{n}$ is computed by letting $\mathbf{m}$ be the component of $\mathbf{e}_1$ perpendicular to $\mathbf{e}_2$,

$$\mathbf{m} \;=\; \mathbf{e}_1 - (\mathbf{e}_1 \cdot \mathbf{e}_2)\mathbf{e}_2/\mathbf{e}_2^2,$$

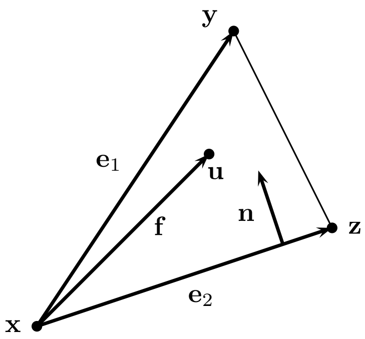

Figure V.6: Calculating barycentric coordinates in $\mathbb{R}^3$.

and setting $\mathbf{n} = \mathbf{m}/||\mathbf{m}||$. (The division by $\mathbf{e}_2^2$ is needed since $\mathbf{e}_2$ may not be a unit vector.)

Letting $\mathbf{e}_2$ be the base of the triangle with vertices $\mathbf{x}, \mathbf{y}, \mathbf{z}$, the height of the triangle is equal to $\mathbf{n} \cdot \mathbf{e}_1$. Thus, the area of the triangle is equal to

$$D \;=\; \tfrac{1}{2}(\mathbf{n} \cdot \mathbf{e}_1)||\mathbf{e}_2|| \;=\; \frac{(\mathbf{m} \cdot \mathbf{e}_1)||\mathbf{e}_2||}{2||\mathbf{m}||}.$$

Similarly, the area of the subtriangle B with vertices $\mathbf{x}, \mathbf{u}, \mathbf{z}$ is equal to

$$B \;=\; \tfrac{1}{2}(\mathbf{n} \cdot \mathbf{f})||\mathbf{e}_2|| \;=\; \frac{(\mathbf{m} \cdot \mathbf{f})||\mathbf{e}_2||}{2||\mathbf{m}||}.$$

Therefore, β is equal to

$$\beta \;=\; \frac{B}{D} \;=\; \frac{\mathbf{m} \cdot \mathbf{f}}{\mathbf{m} \cdot \mathbf{e}_1} \;=\; \frac{(\mathbf{e}_2^2\,\mathbf{e}_1 - (\mathbf{e}_1 \cdot \mathbf{e}_2)\mathbf{e}_2) \cdot \mathbf{f}}{\mathbf{e}_1^2\mathbf{e}_2^2 - (\mathbf{e}_1 \cdot \mathbf{e}_2)^2}. \tag{V.14}$$

A similar formula holds for γ, except with the roles of $\mathbf{e}_1$ and $\mathbf{e}_2$ reversed. We can preprocess the triangle by letting

$$\mathbf{u}_\beta \;=\; \frac{\mathbf{e}_2^2\mathbf{e}_1 - (\mathbf{e}_1 \cdot \mathbf{e}_2)\mathbf{e}_2}{\mathbf{e}_1^2\,\mathbf{e}_2^2 - (\mathbf{e}_1 \cdot \mathbf{e}_2)^2} \qquad \text{and} \qquad \mathbf{u}_\gamma \;=\; \frac{\mathbf{e}_1^2\mathbf{e}_2 - (\mathbf{e}_1 \cdot \mathbf{e}_2)\mathbf{e}_1}{\mathbf{e}_1^2\,\mathbf{e}_2^2 - (\mathbf{e}_1 \cdot \mathbf{e}_2)^2}. \tag{V.15}$$

So, the barycentric coordinates can be calculated by

$$\beta \;=\; \mathbf{u}_\beta \cdot \mathbf{f} \qquad \text{and} \qquad \gamma \;=\; \mathbf{u}_\gamma \cdot \mathbf{f}, \tag{V.16}$$

and of course $\alpha = 1 - \beta - \gamma$.

Note that the vectors $\mathbf{m}$ and $\mathbf{n}$ were used to derive the formulas for β and γ, but there is no need to actually compute them: instead, the vectors $\mathbf{u}_\beta$ and $\mathbf{u}_\gamma$ contain all the information needed to compute the barycentric coordinates of the point $\mathbf{u}$ from $\mathbf{f} = \mathbf{u} - \mathbf{x}$. This allows barycentric coordinates to be computed very efficiently. A further advantage is that Equations (V.15)

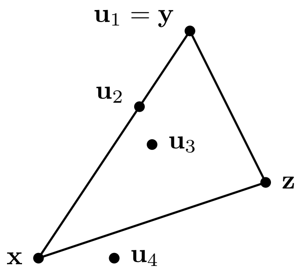

Figure V.7: The points from Exercise V.7.

and (V.16) work in any dimension, not just in $\mathbb{R}^3$. When the point $\mathbf{u}$ does not lie in the plane containing the triangle, then the effect of using Equations (V.15) and (V.16) is the same as projecting $\mathbf{u}$ onto the plane containing the triangle before computing the barycentric coordinates.

Exercise V.7. Let $\mathbf{x} = \langle 0,0 \rangle$, $\mathbf{y} = \langle 2,3 \rangle$, and $\mathbf{z} = \langle 3,1 \rangle$. Determine the barycentric coordinates of the following points (refer to Figure V.7). [Hint: The easier way to work the problem by hand is to use the determinant method to compute the areas B, C and D, and set $\beta = B/D$ and $\gamma = C/D$.]

a. $\mathbf{u}_1 = \langle 2,3 \rangle$.

b. $\mathbf{u}_2 = \langle 1\frac{1}{3}, 2 \rangle$.

c. $\mathbf{u}_3 = \langle \frac{3}{2}, \frac{3}{2} \rangle$.

d. $\mathbf{u}_4 = \langle 1,0 \rangle$.

Visualizing barycentric coordinates

The method for computing barycentric coordinates using $\mathbf{u}_\beta$ and $\mathbf{u}_\gamma$ also gives us an intuitive framework for visualizing barycentric coordinates. Indeed, the area interpretation of barycentric coordinates given by Theorem V.5 also lets us visualize barycentric coordinates.

The key observation is that $\mathbf{u}_\beta$ is equal to $\mathbf{m}/(\mathbf{m}\cdot\mathbf{e}_2)$ as defined in Equations (V.14) and (V.15). The vector $\mathbf{u}_\beta$ is perpendicular to the side $\mathbf{e}_2$ of the triangle containing $\mathbf{x}$ and $\mathbf{z}$ and is pointing from that side toward $\mathbf{y}$. Note also that $\mathbf{m}$ depends on only the original triangle vertices, $\mathbf{x}$, $\mathbf{y}$ and $\mathbf{z}$; not on $\mathbf{u}$. The value of the dot product $\mathbf{u}_\beta \cdot \mathbf{f}$ thus depends only on far $\mathbf{u}$ is displaced from the side containing $\mathbf{x}$ and $\mathbf{z}$ toward the parallel line containing $\mathbf{y}$. (See Figure V.6.)

Figure V.8 illustrates this, by showing the lines of points which have second barycentric coordinate β equal to one of the values $-\frac{1}{3}$, 0, $\frac{1}{3}$, $\frac{2}{3}$, 1 and $\frac{4}{3}$. For instance, the two points labelled $\mathbf{u}$ and $\mathbf{u}'$ both have their second barycentric coordinate β equal to $\frac{1}{3}$. This agrees with the area interpretation: if we form a first triangle with vertices $\mathbf{x}, \mathbf{z}, \mathbf{u}$ and and a second triangle with vertices $\mathbf{x}, \mathbf{z}, \mathbf{u}'$, then the two triangles have the same area B. This is because the

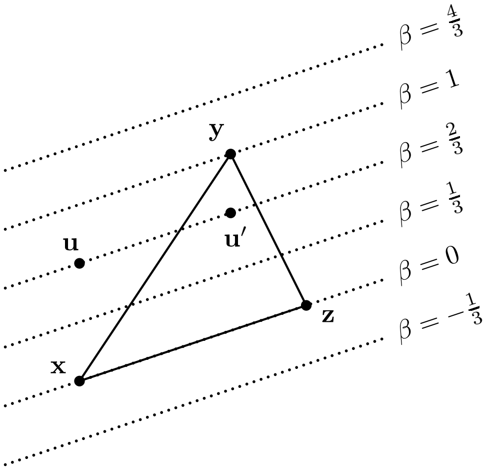

Figure V.8: Values of β.

triangles have the line segment $\overline{\mathbf{xy}}$ as a common base, amd they have the same perpendicular height above this base.

Exercise V.8. Redraw Figure V.8 to show where α and γ are equal to $-\frac{1}{3}$, 0, $\frac{1}{3}$, $\frac{2}{3}$, 1 and $\frac{4}{3}$.

V.2 Bilinear and trilinear interpolation

V.2.1 Bilinear interpolation

The last section discussed linear interpolation between three points. However, often we would prefer to interpolate between four points that lie in a plane or on a two dimensional surface, rather than between only three points. For example, a surface may be tiled by a mesh of four-sided polygons which are not rectangular (or even not planar), but we may wish to parameterize the polygonal patches with values α and β that range between 0 and 1. This frequently arises when using texture maps. Another common use is in computer games, for instance, in driving simulation games, where the player follows a curved race track consisting of a series of approximately rectangular patches. The game programmer can use coordinates $\alpha, \beta \in [0,1]$ to track the position within a given patch.

To interpolate four points, we use a method called *bilinear interpolation*. Suppose four points form a four-sided geometric patch, as pictured in Figure V.9. Bilinear interpolation will be used to define a smooth surface; the four straight-line boundaries of the surface will be the four sides of the patch. We wish to index points on the surface with two scalar values, α and β, both ranging from 0 to 1; essentially, we are seeking a smooth mapping which has domain the unit

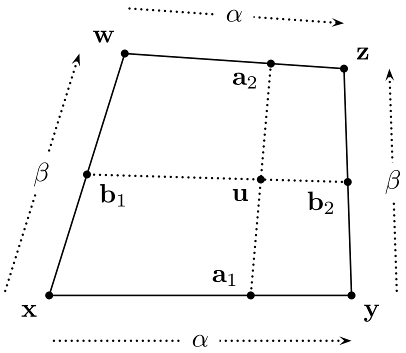

Figure V.9: The point $\mathbf{u} = \mathbf{u}(\alpha, \beta)$ is formed by bilinear interpolation with the scalar coordinates α and β. The points $\mathbf{a}_1$ and $\mathbf{a}_2$ are obtained by interpolating with α, and $\mathbf{b}_1$ and $\mathbf{b}_2$ are obtained by interpolating with β.

square $[0,1]^2 = [0,1] \times [0,1]$ and which maps the corners and the edges of the unit square to the vertices and the boundary edges of the patch. The value of α corresponds to the x-coordinate and β to the y-coordinate of a point $\mathbf{u}$ on the surface patch.

The definition of the bilinear interpolation function is:

$$\begin{aligned} \mathbf{u} &= (1-\beta)\cdot[(1-\alpha)\mathbf{x} + \alpha\mathbf{y}] + \beta\cdot[(1-\alpha)\mathbf{w} + \alpha\mathbf{z}] \\ &= (1-\alpha)\cdot[(1-\beta)\mathbf{x} + \beta\mathbf{w}] + \alpha\cdot[(1-\beta)\mathbf{y} + \beta\mathbf{z}] \qquad \text{(V.17)} \\ &= (1-\alpha)(1-\beta)\mathbf{x} + \alpha(1-\beta)\mathbf{y} + \alpha\beta\mathbf{z} + (1-\alpha)\beta\mathbf{w}. \end{aligned}$$

For $0 \le \alpha \le 1$ and $0 \le \beta \le 1$, this defines $\mathbf{u}$ as a weighted average of the vertices $\mathbf{x}$, $\mathbf{y}$, $\mathbf{z}$, and $\mathbf{w}$. We sometimes write $\mathbf{u}$ as $\mathbf{u}(\alpha, \beta)$ to indicate its dependence on α and β.

We defined bilinear interpolation with three equivalent equations in (V.17) so as to stress that bilinear interpolation can be viewed as linear interpolation with respect to α, followed by linear interpolation with respect to β; or vice-versa, as interpolation first with β and then with α. Thus, the first two lines of Equation (V.17) can be rewritten as

$$\begin{aligned} \mathbf{u} &= \mathit{lerp}(\,\mathit{lerp}(\mathbf{x},\mathbf{y},\alpha),\ \mathit{lerp}(\mathbf{w},\mathbf{z},\alpha),\ \beta) \qquad \text{(V.18)} \\ &= \mathit{lerp}(\,\mathit{lerp}(\mathbf{x},\mathbf{w},\beta),\ \mathit{lerp}(\mathbf{y},\mathbf{z},\beta),\ \alpha). \end{aligned}$$

Bilinear interpolation may be used to interpolate the values of a function f. If the values of f are fixed at the four vertices, then bilinear interpolation is used to set the value of f at the point $\mathbf{u}$ obtained by Equation (V.17) to

$$f(\mathbf{u}) \;=\; (1-\alpha)(1-\beta)f(\mathbf{x}) + \alpha(1-\beta)f(\mathbf{y}) + \alpha\beta f(\mathbf{z}) + (1-\alpha)\beta f(\mathbf{w}).$$

Exercise V.9. Let $\mathbf{x} = \langle 0,0\rangle$, $\mathbf{y} = \langle 4,0\rangle$, $\mathbf{z} = \langle 5,3\rangle$, and $\mathbf{w} = \langle 0,2\rangle$, as in Figure V.10. For each of the following values of α and β, what point is obtained by bilinear interpolation? Graph your answers.

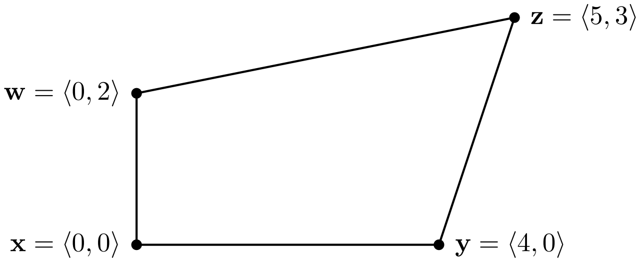
$\mathbf{z} = \langle 5, 3\rangle$
$\mathbf{w} = \langle 0, 2\rangle$
$\mathbf{x} = \langle 0, 0\rangle$
$\mathbf{y} = \langle 4, 0\rangle$

Figure V.10: Figure for Exercise V.9.

a. $\alpha = 1$ and $\beta = 0$.

b. $\alpha = \frac{1}{3}$ and $\beta = 1$.

c. $\alpha = \frac{1}{2}$ and $\beta = \frac{1}{4}$.

d. $\alpha = \frac{2}{3}$ and $\beta = \frac{1}{3}$.

The Equation (V.17) defining bilinear interpolation makes sense for an arbitrary set of vertices $\mathbf{x}$, $\mathbf{y}$, $\mathbf{z}$, $\mathbf{w}$. If the four vertices are coplanar and lie in a plane P, then the bilinearly interpolated points $\mathbf{u}(\alpha, \beta)$ clearly lie in the same plane, since they are weighted averages of the four vertices. If, on the other hand, the four vertices are not coplanar and are positioned arbitrarily in $\mathbb{R}^3$, then the points $\mathbf{u} = \mathbf{u}(\alpha, \beta)$ obtained by bilinear interpolation with $\alpha, \beta \in [0, 1]$ form a non-planar four-sided "patch," that is, a four-sided surface. The sides of the patch will be straight-line segments, but the interior of the patch may be curved.

Exercise V.10. Suppose a surface patch in $\mathbb{R}^3$ is defined by bilinearly interpolating from four vertices x, y, $z\,w$. Derive the following formulas for the partial derivatives of $\mathbf{u}$:

$$\begin{aligned} \frac{\partial \mathbf{u}}{\partial \alpha} &= (1-\beta)(\mathbf{y}-\mathbf{x}) + \beta(\mathbf{z}-\mathbf{w}) \qquad \text{(V.19)} \\ \frac{\partial \mathbf{u}}{\partial \beta} &= (1-\alpha)(\mathbf{w}-\mathbf{x}) + \alpha(\mathbf{z}-\mathbf{y}). \end{aligned}$$

Exercise V.11. From the previous exercise, we know that $\frac{\partial \mathbf{u}}{\partial \alpha} \times \frac{\partial \mathbf{u}}{\partial \beta}$ is a normal vector to the patch at a point $\mathbf{u} = \mathbf{u}(\alpha, \beta)$. (It may not be a unit vector however.) Prove that

$$\frac{\partial \mathbf{u}}{\partial \alpha} \times \frac{\partial \mathbf{u}}{\partial \beta} = \alpha(1-\beta)\mathbf{v}_1 \times \mathbf{v}_2 + \alpha\beta\mathbf{v}_2 \times \mathbf{v}_3 + (1-\alpha)\beta\mathbf{v}_3 \times \mathbf{v}_4 + (1-\alpha)(1-\beta)\mathbf{v}_4 \times \mathbf{v}_1. \qquad \text{(V.20)}$$

Therefore the cross product at an interior point of the patch can be obtained by bilinearly interpolation from the values of the cross products at the four vertices.

V.2.2 Properties of bilinear interpolation

Usually, bilinear interpolation uses vertices which are not coplanar, but which are not too far away from a planar, convex quadrilateral. A mathematical way to describe this is to say that there exists a plane P such that, when the four vertices are orthogonally projected onto the plane, the result is a convex, planar quadrilateral.[2] We call this condition the "Projected Convexity Condition":

Projected Convexity Condition: *The* Projected Convevity Condition *holds provided there exists a plane P such that the projection of the points $\mathbf{x}$, $\mathbf{y}$, $\mathbf{z}$, $\mathbf{w}$ onto the plane P are the vertices of a convex quadrilateral with the four vertices being in counter-clockwise or clockwise order.*

To check that the Projected Convexity Condition holds for a given plane, one can choose a unit vector $\mathbf{n}$ normal to the plane and assume, without loss of generality, that the plane contains the origin. Then project the four points onto the plane yielding four points $\mathbf{x}_P$, $\mathbf{y}_P$, $\mathbf{z}_P$, and $\mathbf{w}_P$, using the following formula (see Appendix A.2.2):

$$\mathbf{x}_P \;=\; \mathbf{x} - (\mathbf{n}\cdot\mathbf{x})\mathbf{n}.$$

Then one checks that the interior angles of the resulting quadrilateral are less than 180°. (We will discuss convexity more in Section V.3 below, but for now, we can take this test as being the definition of a convex quadrilateral.)

A mathematically equivalent method of checking whether the Projected Convexity Condition holds for a plane with unit normal $\mathbf{n}$ is as follows. First define the four edge vectors by

$$\begin{aligned} \mathbf{v}_1 &= \mathbf{y}-\mathbf{x} \\ \mathbf{v}_2 &= \mathbf{z}-\mathbf{y} \\ \mathbf{v}_3 &= \mathbf{w}-\mathbf{z} \\ \mathbf{v}_4 &= \mathbf{x}-\mathbf{w}. \end{aligned}$$

These give the edges in circular order around the quadrilateral, as shown Figure V.11. The condition that the interior angles of the projected quadrilateral are less than 180° is equivalent to the condition that the four values

$$\begin{array}{ll} (\mathbf{v}_1\times\mathbf{v}_2)\cdot\mathbf{n} & (\mathbf{v}_3\times\mathbf{v}_4)\cdot\mathbf{n} \\ (\mathbf{v}_2\times\mathbf{v}_3)\cdot\mathbf{n} & (\mathbf{v}_4\times\mathbf{v}_1)\cdot\mathbf{n} \end{array} \tag{V.21}$$

are either all positive or all negative. To verify this, suppose we view the plane down the normal vector $\mathbf{n}$. If the four values from (V.21) are all positive, then the projected vertices are in counter-clockwise order. When the four values are all negative, the projected vertices are in clockwise order.

[2] See Section V.3 for the definition of "convex".

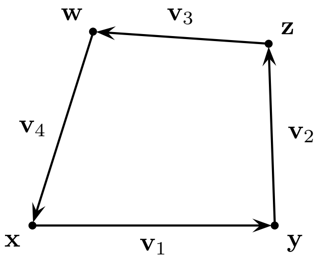

Figure V.11: The vectors $\mathbf{v}_i$ are the directed edges around the quadrilateral.

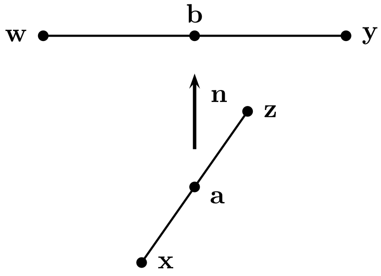

Figure V.12: The line segments $\overline{\mathbf{xz}}$ and $\overline{\mathbf{yw}}$ have midpoints $\mathbf{a}$ and $\mathbf{b}$. The vector $\mathbf{n}$ is the unit vector in the direction from $\mathbf{a}$ to $\mathbf{b}$.

Exercise V.12. Prove that the values $(\mathbf{v}_i \times \mathbf{v}_j) \cdot \mathbf{n}$ are equal to $\ell_i \cdot \ell_j \sin\theta$ where ℓ_i is the magnitude of the projection of $\mathbf{v}_i$ onto the plane P and where θ is the angle between the projections of $\mathbf{v}_i$ and $\mathbf{v}_j$.

The Projected Convexity Condition turns out to be very useful, for instance, in the proof of Corollary V.8 and for solving Exercise V.13. Thus, it is a pleasant surprise that the Projected Convexity Condition nearly always holds; indeed, it holds for *any* set of four noncoplanar vertices.

Theorem V.6. *Suppose that* $\mathbf{x}$, $\mathbf{y}$, $\mathbf{z}$, *and* $\mathbf{w}$ *are not coplanar. Then the Projected Convexity Condition is satisfied.*

Proof. We call the two line segments $\overline{\mathbf{xz}}$ and $\overline{\mathbf{yw}}$ the *diagonals*. Referring to Figure V.12, let $\mathbf{a}$ be the midpoint of the diagonal $\overline{\mathbf{xz}}$, so $\mathbf{a} = \frac{1}{2}(\mathbf{x}+\mathbf{z})$. Likewise, let $\mathbf{b}$ be the midpoint of the other diagonal. The points $\mathbf{a}$ and $\mathbf{b}$ must be distinct since otherwise the two diagonals would intersect, and the four vertices would all lie in the plane containing the diagonals, contradicting the hypothesis of the theorem.

Form the unit vector $\mathbf{n}$ in the direction from $\mathbf{a}$ to $\mathbf{b}$, i.e.,

$$\mathbf{n} = \frac{\mathbf{b}-\mathbf{a}}{||\mathbf{b}-\mathbf{a}||}.$$

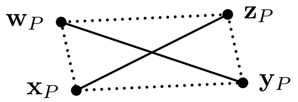

Figure V.13: The projections of the two diagonals onto the plane P are noncollinear and intersect at their midpoints, at the common projection of $\mathbf{a}$ and $\mathbf{b}$. The four projected vertices form a convex quadrilateral.

Let P be the plane containing the origin and perpendicular to $\mathbf{n}$, and consider the orthogonal projection of the four vertices onto P. The midpoints, $\mathbf{a}$ and $\mathbf{b}$, project onto the same point of P because of the way $\mathbf{n}$ was chosen. Also, the projections of the two diagonals cannot be collinear, since otherwise all four vertices would lie in the plane which contains the projections of the diagonals and is perpendicular to P. That is to say, the projections of the diagonals are two line segments which cross each other (intersect in their interiors), as shown in Figure V.13. In particular, neither diagonal projects onto a single point. The projections of the four vertices are the four endpoints of the projections of the diagonals. Clearly they form a convex quadrilateral with the vertices being in clockwise or counter-clockwise order. □

For convex, planar quadrilaterals, we have the following theorem.

Theorem V.7. *Let* $\mathbf{x}$*,* $\mathbf{y}$*,* $\mathbf{z}$*,* $\mathbf{w}$ *be the vertices of a non-degenerate, planar, convex quadrilateral, in counter-clockwise (or clockwise) order. Then the bilinear interpolation mapping*

$$\langle \alpha, \beta \rangle \mapsto \mathbf{u}(\alpha, \beta)$$

is a one-to-one map from $[0,1] \times [0,1]$ *onto the quadrilateral.*

Proof. We give a quick informal proof. If the value of β is fixed, then the second line in Equation (V.17) or (V.18) shows that the function $\mathbf{u}(\alpha, \beta)$ is just equal to the result of using α to linearly interpolate along the line segment L_β joining the two points

$$(1-\beta)\mathbf{x} + \beta\mathbf{w} \quad \text{and} \quad (1-\beta)\mathbf{y} + \beta\mathbf{z}.$$

These two points lie on opposite edges of the quadrilateral and thus are distinct. Furthermore, for $\beta \neq \beta'$, the two line segments L_β and $L_{\beta'}$ do not intersect, as may be seen by inspection of Figure V.14. This uses the fact that the interior angles of the quadrilateral measure less than 180°. Therefore, if $\beta \neq \beta'$, then $\mathbf{u}(\alpha, \beta) \neq \mathbf{u}(\alpha', \beta')$, since L_β and $L_{\beta'}$ are disjoint. On the other hand, if $\beta = \beta'$, but $\alpha \neq \alpha'$, then again $\mathbf{u}(\alpha, \beta) \neq \mathbf{u}(\alpha', \beta')$, since they are distinct points on the line L_β.

The fact that the map is onto can be verified by noting that the line segments L_β sweep across the quadrilateral as β varies from 0 to 1. Therefore any $\mathbf{u}$ in the quadrilateral lies on some L_β. □

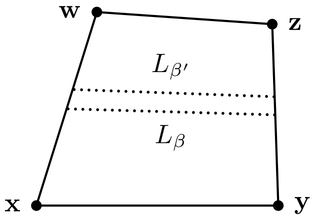

Figure V.14: Since the polygon is convex, distinct values β and β' give non-intersecting "horizontal" line segments.

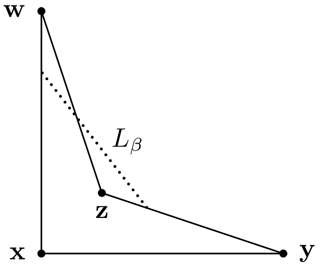

Figure V.15: An example of the failure of Theorem V.7 for non-convex, planar quadrilaterals.

Figure V.15 shows an example of how Theorem V.7 fails for planar quadrilaterals that are not convex. That figure shows a sample line L_β that is not entirely inside the quadrilateral; thus the range of the bilinear interpolation map is not contained inside the quadrilateral. Furthermore, the bilinear interpolation map is not one-to-one; for instance, the point where the segments L_β and $\overline{\mathbf{zw}}$ intersect has two sets of bilinear coordinates.

However, the next corollary states that Theorem V.7 does apply to any set of four noncoplanar points.

Corollary V.8. *Suppose* $\mathbf{x}$, $\mathbf{y}$, $\mathbf{z}$, *and* $\mathbf{w}$ *are not coplanar. Then the function* $\mathbf{u}(\alpha,\beta)$ *is a one-to-one map on the domain* $[0,1]\times[0,1]$.

Proof. By Theorem V.6, the Projected Convexity Condition holds for some plane P. Without loss of generality, the plane P is the xy-plane. The bilinear interpolation function $\mathbf{u}(\alpha,\beta)$ operates independently on the x-, y-, and z-components of the vertices. Therefore, by Theorem V.7, the projection of the values of $\mathbf{u}(\alpha,\beta)$ onto the xy-plane is a one-to-one function from $[0,1]^2$ into the xy-plane. It follows immediately that the function $\mathbf{u}(\alpha,\beta)$ is one-to-one. □

Exercise V.13* Let the vertices $\mathbf{x}$, $\mathbf{y}$, $\mathbf{z}$, $\mathbf{w}$ be four points in $\mathbb{R}^3$, and

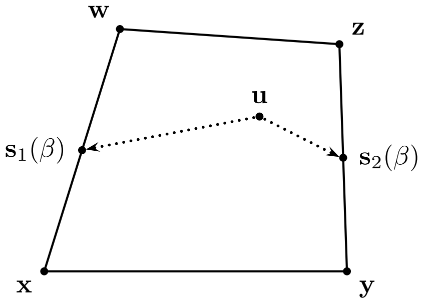

Figure V.16: The three points $\mathbf{s}_1(\beta)$, $\mathbf{u}$, and $\mathbf{s}_2(\beta)$ will be collinear for the correct value of β. The value of β shown in the figure is smaller than the correct β coordinate of $\mathbf{u}$.

suppose that the Projected Convexity Condition holds. Prove that

$$\frac{\partial \mathbf{u}}{\partial \alpha} \times \frac{\partial \mathbf{u}}{\partial \beta}$$

is nonzero for all $\alpha, \beta \in [0,1]$. Conclude that this defines a nonzero vector normal to the surface. [Hint: Refer back to Exercises V.10 and V.11. Use Equation V.20 and the fact that $(\mathbf{v}_i \times \mathbf{v}_j) \cdot \mathbf{n}$, for $j = i+1 \bmod 4$, all have the same sign, for $\mathbf{n}$ normal to the plane from the Projected Convexity Condition.]

V.2.3 Inverting bilinear interpolation

We now discuss how to invert bilinear interpolation. For this, we are given the four vertices $\mathbf{x}$, $\mathbf{y}$, $\mathbf{z}$, and $\mathbf{w}$ which are assumed to form a convex quadrilateral in a plane.[3] Without loss of generality, the points lie in $\mathbb{R}^2$, so $\mathbf{x} = \langle x_1, x_2 \rangle$, $\mathbf{y} = \langle y_1, y_2 \rangle$, etc. In addition, we are given a point $\mathbf{u} = \langle u_1, u_2 \rangle$ in the interior of the quadrilateral formed by these four points. The problem is to find the values of $\alpha, \beta \in [0,1]$ so that $\mathbf{u}$ satisfies the defining Equation (V.17) for bilinear interpolation.

Our algorithm for inverting bilinear interpolation will be based on vectors. Let $\mathbf{s}_1 = \mathbf{w} - \mathbf{x}$ and $\mathbf{s}_2 = \mathbf{z} - \mathbf{y}$. Then let

$$\mathbf{s}_1(\beta) = \mathbf{x} + \beta \mathbf{s}_1 \qquad \text{and} \qquad \mathbf{s}_2(\beta) = \mathbf{y} + \beta \mathbf{s}_2,$$

as shown in Figure V.16. To solve for the value of β, it is enough to find β such that $0 \le \beta \le 1$ and such that the three points $\mathbf{s}_1(\beta)$, $\mathbf{u}$, and $\mathbf{s}_2(\beta)$ are collinear.

Referring to Appendix A.2.1, recall that two vectors $\mathbf{a}, \mathbf{b}$ in $\mathbb{R}^2$ are collinear if and only if their determinant $\mathit{det}(\mathbf{a}, \mathbf{b})$ is equal to zero.[4] Thus, for the three

[3] At the end of this section, we discuss how to modify the algorithm to work in three dimensions.

[4] The notation $\mathit{det}(\mathbf{a}, \mathbf{b})$ means the determinant of the 2×2 matrix $(\mathbf{u}, \mathbf{v})$.

points to be collinear, we must have

$$\begin{aligned} 0 &= \mathit{det}(\mathbf{s}_1(\beta) - \mathbf{u},\, \mathbf{s}_2(\beta) - \mathbf{u}) \\ &= \mathit{det}(\beta\mathbf{s}_1 - (\mathbf{u} - \mathbf{x}),\, \beta\mathbf{s}_2 - (\mathbf{u} - \mathbf{y})) \qquad \text{(V.22)} \\ &= \mathit{det}(\mathbf{s}_1, \mathbf{s}_2)\beta^2 + [\mathit{det}(\mathbf{s}_2, \mathbf{u} - \mathbf{x}) - \mathit{det}(\mathbf{s}_1, \mathbf{u} - \mathbf{y})]\beta + \mathit{det}(\mathbf{u} - \mathbf{x}, \mathbf{u} - \mathbf{y}). \end{aligned}$$

This quadratic equation can be readily solved for the desired value of β. In general, there will be two roots of the quadratic equation. To find these, let A, B, and C be the coefficients of β^2, β, and 1 in Equation (V.22), namely,

$$\begin{aligned} A &= \mathit{det}(\mathbf{s}_1, \mathbf{s}_2) = \mathit{det}(\mathbf{w} - \mathbf{x},\, \mathbf{z} - \mathbf{y}) \\ B &= \mathit{det}(\mathbf{z} - \mathbf{y},\, \mathbf{u} - \mathbf{x}) - \mathit{det}(\mathbf{w} - \mathbf{x},\, \mathbf{u} - \mathbf{y}) \qquad \text{(V.23)} \\ C &= \mathit{det}(\mathbf{u} - \mathbf{x},\, \mathbf{u} - \mathbf{y}) \end{aligned}$$

The two roots of (V.22) are

$$\beta^+ = \frac{-B + \sqrt{B^2 - 4AC}}{2A} \qquad \text{and} \qquad \beta^- = \frac{-B - \sqrt{B^2 - 4AC}}{2A} \qquad \text{(V.24)}$$

There remains the question of which of the two roots is the right value for β. Of course, one way to decide this is to use the root which is between 0 and 1. But we can improve on this and avoid having to test the roots to see if they are between 0 and 1.[5] In fact, we shall see that the right root is *always* the root

$$\beta^- = \frac{-B - \sqrt{B^2 - 4AC}}{2A}. \qquad \text{(V.25)}$$

To prove this, consider the two cases $\mathit{det}(\mathbf{s}_1, \mathbf{s}_2) < 0$ and $\mathit{det}(\mathbf{s}_1, \mathbf{s}_2) > 0$ separately. (The case $\mathit{det}(\mathbf{s}_1, \mathbf{s}_2) = 0$ will be discussed later.) First, assume that $\mathit{det}(\mathbf{s}_1, \mathbf{s}_2) < 0$. This situation is shown in Figure V.17(a), where the two vectors $\mathbf{s}_1$ and $\mathbf{s}_2$ are diverging, or pointing away from each other, since the angle from $\mathbf{s}_1$ to $\mathbf{s}_2$ must be negative if the determinant is negative. As shown in Figure V.17(a), there are two values, β^- and β^+, where $\mathbf{s}_1(\beta)$, $\mathbf{u}$, and $\mathbf{s}_2(\beta)$ are collinear. The undesired root of Equation (V.22) occurs with a negative value of β, namely $\beta = \beta^+$ as shown in the figure. So in the case where $\mathit{det}(\mathbf{s}_1, \mathbf{s}_2) < 0$, the larger root of (V.24) is the correct one. Since the denominator $2A = 2\mathbf{s}_1 \times \mathbf{s}_2$ of (V.24) is negative, the larger root is obtained by taking the negative sign in the numerator.

Now assume that $\mathit{det}(\mathbf{s}_1, \mathbf{s}_2) > 0$. This case is shown in Figure V.17(b). In this case, the undesired root of Equation (V.22) is greater than 1; therefore, the desired root is the smaller of the two roots. Since the denominator $2A$ is positive in this case, we again need to choose the negative sign in the numerator of (V.24).

[5] The problem with testing for being between 0 and 1 is that roundoff error may cause the desired root to be slightly less than 0 or slightly greater than 1. In addition, if one is concerned about minor differences in computation time, then it can be good to avoid comparisons between floating point numbers.

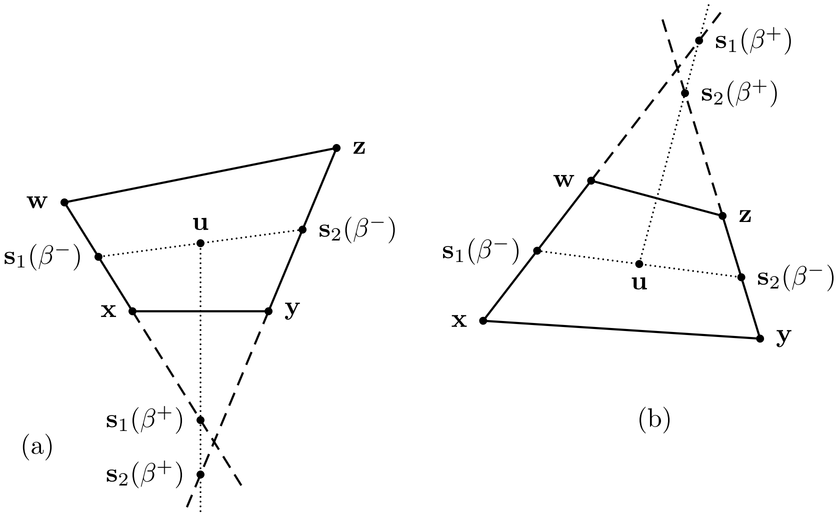

Figure V.17: The two possibilities for the sign of $det(\mathbf{s}_1, \mathbf{s}_2)$. In (a), $det(\mathbf{s}_1, \mathbf{s}_2) < 0$; in (b), $det(\mathbf{s}_1, \mathbf{s}_2) > 0$. In each case, there are two values for β where the points $\mathbf{s}_1(\beta)$, $\mathbf{s}_2(\beta)$, and $\mathbf{u}$ are collinear. The values β^+ and β^- are the solutions to Equation (V.24) obtained with the indicated choice of plus/minus sign. For both (a) and (b), $\beta = \beta^-$ is between 0 and 1 and is the desired root.

This almost completes the mathematical description of how to compute the value of β. However, there is one further modification to be made to make the computation more stable. It is well-known (c.f. [65]) that the usual formulation of the quadratic formula can be computationally unstable. This can happen to the formula (V.25) if value of B is negative and if B^2 is much larger than $4AC$, since the numerator will be computed as the difference of two large numbers that mostly cancel out to yield a value close to 0. In this case, a more stable computation can be performed by using the formula

$$\beta^- \ = \ \frac{2C}{-B + \sqrt{B^2 - 4AC}}. \tag{V.26}$$

This formula is equivalent to (V.25), as can be seen by multiplying both the numerator and denominator of (V.25) by $(-B + \sqrt{B^2 - 4AC})$, and it has the advantage of being computationally more stable when B is negative.

Once the value of $\beta = \beta^-$ has been obtained, it is straightforward to find the value of α, since $\mathbf{u}$ is now the weighted average of $\mathbf{s}_1(\beta)$ and $\mathbf{s}_2(\beta)$. This can be done by just setting

$$\alpha \ = \ \frac{(\mathbf{u} - \mathbf{s}_1(\beta)) \cdot (\mathbf{s}_2(\beta) - \mathbf{s}_1(\beta))}{(\mathbf{s}_2(\beta) - \mathbf{s}_1(\beta))^2},$$

since this is the ratio of the distance from $\mathbf{s}_1(\beta)$ to $\mathbf{u}$ to the distance from $\mathbf{s}_1(\beta)$ to $\mathbf{s}_2(\beta)$. (See also Equation (V.3) on page 184.)

We now can present the algorithm for inverting bilinear interpolation. The input to the algorithm is five points in $\mathbb{R}^2$. For reliable results, the points $\mathbf{x}$, $\mathbf{y}$, $\mathbf{z}$, $\mathbf{w}$ should be the vertices of a convex quadrilateral, and $\mathbf{u}$ should be on or inside the quadrilateral.

```
// $\mathbf{x}$, $\mathbf{y}$, $\mathbf{x}$, $\mathbf{w}$, $\mathbf{u}$ lie in the plane $R^2$
BilinearInvert( $\mathbf{u}$, $\mathbf{x}$, $\mathbf{y}$, $\mathbf{z}$, $\mathbf{w}$ ) {
    Set $A$ = $det(\mathbf{w}-\mathbf{x},\mathbf{z}-\mathbf{y})$;
    Set $B$ = $det(\mathbf{z}-\mathbf{y},\mathbf{u}-\mathbf{x}) - det(\mathbf{w}-\mathbf{x},\mathbf{u}-\mathbf{y})$;
    Set $C$ = $det(\mathbf{u}-\mathbf{x},\mathbf{u}-\mathbf{y})$;
    If ( $B > 0$ ) {
        Set $\beta$ = $\dfrac{-B-\sqrt{B^2-4AC}}{2A}$;
    }
    Else {
        Set $\beta$ = $\dfrac{2C}{-B+\sqrt{B^2-4AC}}$;
    }
    Set $\mathbf{s}_{1,\beta}$ = $(1-\beta)\mathbf{x}+\beta\mathbf{w}$;
    Set $\mathbf{s}_{2,\beta}$ = $(1-\beta)\mathbf{y}+\beta\mathbf{z}$;
    Set $\alpha$ = $\dfrac{(\mathbf{u}-\mathbf{s}_{1,\beta})\cdot(\mathbf{s}_{2,\beta}-\mathbf{s}_{1,\beta})}{(\mathbf{s}_{2,\beta}-\mathbf{s}_{1,\beta})^2}$;
    Return $\alpha$ and $\beta$ as the bilinear interpolation inverse.
}
```

We have omitted so far discussing the case where $A = det(\mathbf{s}_1, \mathbf{s}_2) = 0$: this happens whenever $\mathbf{s}_1$ and $\mathbf{s}_2$ are collinear, so the left and right sides of the quadrilateral are parallel. When A equals 0, the quadratic equation (V.22) becomes the linear equation $B\beta + C = 0$ with only one root, namely, $\beta = -C/B$. Thus, it would be fine to modify the above algorithm to test whether $A = 0$ and, if so, compute $\beta = -C/B$. However, the above algorithm will actually work correctly as written even when $A = 0$. To see this, note that if $A = 0$, the left and right sides are parallel, so $det(\mathbf{w}-\mathbf{x},\mathbf{u}-\mathbf{y}) \geq 0$ and $det(\mathbf{z}-\mathbf{y},\mathbf{u}-\mathbf{x}) \leq 0$ since $\mathbf{u}$ is in the polygon. Furthermore, for a proper polygon these determinants are not both zero. Therefore, $B < 0$ and the above algorithm computes β according to the second case using Equation (V.26). Since $A = 0$, this is mathematically equivalent to computing $-C/B$ and avoids the risk of a divide by zero.

Exercise V.14. Let $\mathbf{x} = \langle 0,0\rangle$, $\mathbf{y} = \langle 4,0\rangle$, $\mathbf{z} = \langle 5,3\rangle$, $\mathbf{w} = \langle 0,2\rangle$, and $\mathbf{u} = \langle \frac{3}{2}, \frac{7}{6}\rangle$, as in Figure V.18. What are the bilinear coordinates, α and β, of $\mathbf{u}$?

Now we generalize the bilinear inversion algorithm to work in three dimensions instead of two. The key idea is that we just need to choose

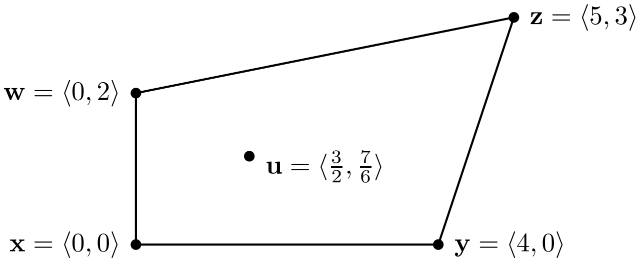
$\mathbf{z} = \langle 5, 3\rangle$
$\mathbf{w} = \langle 0, 2\rangle$
$\mathbf{u} = \langle \frac{3}{2}, \frac{7}{6}\rangle$
$\mathbf{x} = \langle 0, 0\rangle$
$\mathbf{y} = \langle 4, 0\rangle$

Figure V.18: Figure for Exercise V.14.

two orthogonal axes, and project the problem onto those two axes, reducing the problem back to the two dimensional case. For this, we start by choosing a unit vector $\mathbf{n}$ such that the Projected Convexity Condition holds for a plane perpendicular to $\mathbf{n}$. To choose $\mathbf{n}$, you should *not* use the vector from the proof of Theorem V.6, as this may give a poorly conditioned problem and lead to unstable computations. Indeed, this would give disastrous results if the points $\mathbf{x}$, $\mathbf{y}$, $\mathbf{z}$, and $\mathbf{w}$ are coplanar, and would give unstable results if they are close to coplanar. Instead, in most applications, a better choice for $\mathbf{n}$ would be the vector

$$\frac{(\mathbf{z}-\mathbf{x})\times(\mathbf{w}-\mathbf{y})}{||(\mathbf{z}-\mathbf{x})\times(\mathbf{w}-\mathbf{y})||}.$$

Actually, it will turn out that there is no need to make $\mathbf{n}$ a unit vector, so it is computationally easier to just set $\mathbf{n}$ to be the vector

$$\mathbf{n} \;=\; (\mathbf{z}-\mathbf{x})\times(\mathbf{w}-\mathbf{y}). \tag{V.27}$$

This choice for $\mathbf{n}$ is likely to work well in most applications. In particular, if this choice for $\mathbf{n}$ does not give a plane satisfying the Projected Convexity Condition, then the patches are probably poorly chosen and are certainly not very patch-like.

In many cases there are easier ways to choose $\mathbf{n}$. A common application of patches is to define a terrain, or more generally, a surface that does not vary too much from horizontal. In this case, the "up" direction vector, say $\mathbf{j}$, can be used for the vector $\mathbf{n}$.

Once we have chosen the vector $\mathbf{n}$, we can convert the problem into a two dimensional problem by projecting onto a plane P orthogonal to $\mathbf{n}$. Fortunately, it is unnecessary to actually choose coordinate axes for P and project the five points $\mathbf{u}$, $\mathbf{x}$, $\mathbf{y}$, $\mathbf{z}$, and $\mathbf{w}$ onto P. Instead, we only need the three scalar values A, B, and C, now based on areas of parallelograms projected onto the plane P. Let's first discuss how to compute A. Recall from Equation V.23 that, in $\mathbb{R}^2$, we had $A = \mathit{det}(\mathbf{s}_1, \mathbf{s}_2)$; this is equal to the area of the parallelogram with sides $\mathbf{s}_1$ and $\mathbf{s}_2$. Working now in $\mathbb{R}^3$, we want instead the area of the parallelogram after being projected onto the plane P. This is computed as $A = (\mathbf{s}_1 \times \mathbf{s}_2)\cdot\mathbf{n}$ (modulo scaling by the magnitude of $\mathbf{n}$ if is not a unit vector). Similarly, in Equation V.23, C was also the area of a parallelogram and B was the difference between the areas of two parallelograms. To compute these after projection to P, we use

$$\begin{aligned} B &= ((\mathbf{z}-\mathbf{y})\times(\mathbf{u}-\mathbf{x}) - (\mathbf{w}-\mathbf{x})\times(\mathbf{u}-\mathbf{y}))\cdot\mathbf{n} \\ C &= ((\mathbf{u}-\mathbf{x})\times(\mathbf{u}-\mathbf{y}))\cdot\mathbf{n}. \end{aligned}$$

routine, but then take the dot product with $\mathbf{n}$.

To summarize, the bilinear inversion algorithm for points in $\mathbb{R}^3$ is the same as the `BilinearInvert` program as given above, except that now $\mathbf{u}$, $\mathbf{x}$, $\mathbf{y}$, $\mathbf{z}$, and $\mathbf{w}$ are vectors in $\mathbb{R}^3$, and that the first three lines of the program are replaced by the following four lines.

```
Set $\mathbf{n} = (\mathbf{z}-\mathbf{x})\times(\mathbf{w}-\mathbf{y})$;
Set $A = \mathbf{n}\cdot((\mathbf{w}-\mathbf{x})\times(\mathbf{z}-\mathbf{y}))$;
Set $B = \mathbf{n}\cdot((\mathbf{z}-\mathbf{y})\times(\mathbf{u}-\mathbf{x}) - (\mathbf{w}-\mathbf{x})\times(\mathbf{u}-\mathbf{y}))$;
Set $C = \mathbf{n}\cdot((\mathbf{u}-\mathbf{x})\times(\mathbf{u}-\mathbf{y}))$;
```

The rest of `BilinearInvert` is unchanged. Other choices for $\mathbf{n}$ are possible too: the important point is that the Projected Convexity Condition should hold robustly.

V.2.4 Trilinear interpolation

Trilinear interpolation is a generalization of bilinear interpolation to three dimensions. For trilinear interpolation, we are given eight points $\mathbf{x}_{i,j,k}$ where $i,j,k \in \{0,1\}$. Our goal is to define a smooth map $\mathbf{u}(\alpha,\beta,\gamma)$ from the unit cube $[0,1]^3$ into 3-space so that $\mathbf{u}(i,j,k) = x_{i,j,k}$ for all $i,j,k\in\{0,1\}$. The intent is that the eight points $\mathbf{x}_{i,j,k}$ are roughly in the positions of the vertices of a rectangular prism, and that the map $\mathbf{u}(\alpha,\beta,\gamma)$ should be a smooth interpolation function.

For trilinear interpolation, we define

$$\mathbf{u}(\alpha,\beta,\gamma) \;=\; \sum_{i,j,k} w_i(\alpha)w_j(\beta)w_k(\gamma)\mathbf{x}_{i,j,k},$$

where the summation runs over all $i,j,k\in\{0,1\}$, and where the values $w_n(\delta)$, for $n\in\{0,1\}$, are defined by

$$w_n(\delta) \;=\; \begin{cases} 1-\delta & \text{if } n=0 \\ \delta & \text{if } n=1. \end{cases}$$

Trilinear interpolation can be used to interpolate the values of a function too. Suppose a function f has its values specified at the vertices, so that $f(\mathbf{x}_{i,j,k})$

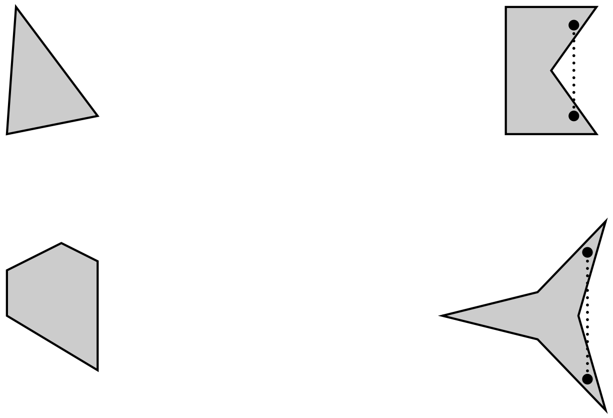

Figure V.19: The shaded regions represent sets. The two sets on the left are convex, and the two sets on the right are not convex. The dotted lines show line segments with endpoints in the set which are not entirely contained in the set.

is fixed for all eight vertices. Then, we extend f to the unit cube $[0,1]^3$ by trilinear interpolation by letting

$$f(\mathbf{u}(\alpha,\beta,\gamma)) \;=\; \sum_{i,j,k} w_i(\alpha)w_j(\beta)w_k(\gamma)f(\mathbf{x}_{i,j,k}).$$

To the best of our knowledge, there is no good way to invert trilinear interpolation in closed form. However, it is possible to use an iterative method based on Newton's method to quickly invert trilinear interpolation.

V.3 Convex sets and weighted averages

The notion of a convex quadrilateral has already been discussed in the sections above. This section introduces the definition of convexity for general sets of points and proves that a set is convex if and only if it is closed under the operation of taking weighted averages.

The intuitive notion of a convex set is that it is a fully "filled in" region with no "holes" or missing interior points, and that there are no places where the boundary bends inward and back outward. Figure V.19 shows examples of convex and non-convex sets in the plane. Non-convex sets have the property that it is possible to find a line segment that has both endpoints in the set but is not entirely contained in the set.

Definition V.9. Let A be a set of points (in R^d for some dimension d). The set A is *convex* if and only if the following condition holds: For any two points $\mathbf{x}$ and $\mathbf{y}$ in A, the line segment joining $\mathbf{x}$ and $\mathbf{y}$ is a subset of A.

Some simple examples of convex sets include: (a) any line segment, (b) any line or ray, (c) any plane or half-plane, (d) any half-space, (e) any linear subspace of $\mathbb{R}^d$, (f) the entire space $\mathbb{R}^d$, (g) any ball, where a "ball" consists of a circle or sphere plus its interior, (h) the interior of a triangle or parallelogram, etc. It is easy to check that the intersection of two convex sets must be convex. In fact, the intersection of an arbitrary collection of convex sets is convex. (You should supply a proof of this!) However, the union of two convex sets is not always convex.

Definition V.10. Let A be a set of points in $\mathbb{R}^d$. The *convex hull* of A is the smallest convex set containing A.

Every set A has a smallest enclosing convex set. In fact, if $\mathcal{S}$ is the set of convex sets containing A, then the intersection $\bigcap \mathcal{S}$ of these sets is convex and contains A. It is therefore the smallest convex set containing A. (Note the set $\mathcal{S}$ is nonempty since the whole space $\mathbb{R}^d$ is a convex set containing A.) Therefore, the notion of convex hull is well-defined and every set of points has a convex hull.

There is another, equivalent definition of *convex* that is sometimes used in place of the definition given above. Namely, a set is convex if and only if it is equal to the intersection of some set of half-spaces. In $\mathbb{R}^3$, a *half-space* is a set which lies on one-half of a plane; more generally, a half-space is a set of the form $\{\mathbf{x} : \mathbf{n} \cdot \mathbf{x} > a\}$ for some nonzero vector $\mathbf{n}$ and scalar a. With this definition of convex set, the convex hull of A is the set of points which lie in every half-space which contains A. Equivalently, a point $\mathbf{y}$ is *not* in the convex hull of A if and only if there is a half-space such that A lies entirely in the half-space and y is not in the half-space.

It should be intuitively clear that the definition of convex hulls in terms of intersections of half-spaces is equivalent to our definition of convex hulls in terms of line segments. However, giving a formal proof that these two definitions of convexity are equivalent is fairly difficult: the proof is beyond the scope of this book, but the reader can find a proof in the texts by Grünbaum [58] or Ziegler [129]. (You might want to try your hand at proving this equivalence in dimensions 2 and 3 to get a feel for what is involved in the proof.) We have adopted the definition based on line segments since it makes it easy to prove that the convex hull of a set A is precisely the set of points that can be expressed as weighted averages of points from A.

Definition V.11. Let A be a set and $\mathbf{x}$ a point. We say that $\mathbf{x}$ is a weighted average of points in A if and only if there is a *finite* set of points $\mathbf{y}_1, \ldots, \mathbf{y}_k$ in A such that $\mathbf{x}$ is equal to a weighted average of $\mathbf{y}_1, \ldots, \mathbf{y}_k$.

Theorem V.12. *Let A be a set of points. The convex hull of A is precisely the set of points which are weighted averages of points in A.*

Proof. Let $WA(A)$ be the set of points which are weighted averages of points in A. We first prove that $WA(A)$ is convex, and since $A \subseteq WA(A)$, this implies that the convex hull of A is a subset of $WA(A)$. Let $\mathbf{y}$ and $\mathbf{z}$ be points in $WA(A)$. We wish to prove that the line segment between these points is also contained in $WA(A)$. Since this line segment is just the set of points which are weighted averages of $\mathbf{y}$ and $\mathbf{z}$, it is enough to show that if $0 \le \alpha \le 1$ and $\mathbf{w} = (1-\alpha)\mathbf{y} + \alpha\mathbf{z}$, then $\mathbf{w}$ is in $WA(A)$. Since $\mathbf{y}$ and $\mathbf{z}$ are weighted averages of points in A, they are equal to

$$\mathbf{y} \;=\; \sum_{i=1}^{k} \beta_i \mathbf{x}_i \qquad \text{and} \qquad \mathbf{z} \;=\; \sum_{i=1}^{k} \gamma_i \mathbf{x}_i,$$

with each $\beta_i, \gamma_i \ge 0$ and $\sum_i \beta_i = 1$ and $\sum_i \gamma_i = 1$. We can assume the same k points $\mathbf{x}_1, \ldots, \mathbf{x}_k$ are used in both weighted averages, since we can freely add extra terms with coefficients 0 to a weighted average. Now

$$\mathbf{w} \;=\; \sum_{i=1}^{k} ((1-\alpha)\beta_i + \alpha\gamma_i)\mathbf{x}_i,$$

and the coefficients in the righthand side are clearly nonnegative and sum to 1. Therefore $\mathbf{w} \in WA(A)$. Thus, we have shown that $WA(A)$ is convex, and hence $WA(A)$ contains the convex hull of A.

For the second half of the proof, we need to show that every element of $WA(A)$ is in the convex hull of A. For this, we prove, by induction on k, that any weighted average of k points in A is in the convex hull. For $k = 1$, this is trivial since the convex hull of A contains A. For $k > 1$, let

$$\mathbf{w} \;=\; a_1\mathbf{x}_1 + a_2\mathbf{x}_2 + \cdots + a_k\mathbf{x}_k,$$

where $\alpha_k \neq 1$. This formula for $\mathbf{w}$ can be rewritten as

$$\mathbf{w} \;=\; (1-a_k)\left[\tfrac{a_1}{1-a_k}\mathbf{x}_1 + \tfrac{a_2}{1-a_k}\mathbf{x}_2 + \cdots + \tfrac{a_{k-1}}{1-a_k}\mathbf{x}_{k-1}\right] + a_k\mathbf{x}_k.$$

Letting $\mathbf{w}'$ be the vector in square brackets in this last formula, $\mathbf{w}'$ is a weighted average of $k-1$ points in A and thus, by the induction hypothesis, $\mathbf{w}'$ is in the convex hull of A. Now, $\mathbf{w}$ is a weighted average of the two points $\mathbf{w}'$ and $\mathbf{x}_k$; in other words, $\mathbf{w}$ is on the line segment from $\mathbf{w}'$ to $\mathbf{x}_k$. Since $\mathbf{w}'$ and $\mathbf{x}_k$ are both in the convex hull of A, so is $\mathbf{w}$. □

XXX ADD EXERCISE WITH ANSWER ABOUT CONVEX SETS.

V.4 Interpolation and homogeneous coordinates

This section takes up the question of what it means to form weighted averages of homogeneous vectors. The setting is that we have a set of homogeneous vectors (4-tuples) representing points in $\mathbb{R}^3$. We then form a weighted average of the four tuples by calculating the weighted averages of the x, y, z, and w-components independently. The question is, what point in $\mathbb{R}^3$ is represented by the weighted average obtained in this way?

A key observation is that a given point in $\mathbb{R}^3$ has many different homogeneous representations, and the weighted average may give different results depending on which homogeneous representation is used. An example of this was already given above on page 187. In that example, we set $\mathbf{v}_0 = \langle 0,0,0,1\rangle$ and $\mathbf{v}_1 = \langle 1,0,0,1\rangle$ and $\mathbf{v}_1' = 2\mathbf{v}_1$; so $\mathbf{v}_0$ is a homogeneous representation of $\mathbf{0}$, and $\mathbf{v}_1$ and $\mathbf{v}'$ are both homogeneous representations of $\mathbf{i}$. In Equation (V.6), the average $\frac{1}{2}\mathbf{v}_0 + \frac{1}{2}\mathbf{v}_1$ was seen to be $\langle \frac{1}{2},0,0,1\rangle$, which represents (not unexpectedly) the point midway between $\mathbf{0}$ and $\mathbf{i}$. On the other hand, the average $\frac{1}{2}\mathbf{v}_0 + \frac{1}{2}\mathbf{v}_1'$ is equal to $\langle 1,0,0,\frac{3}{2}\rangle$, which represents the point $\langle \frac{2}{3},0,0\rangle$: this is the point which is two-thirds of the way from $\mathbf{0}$ to $\mathbf{i}$. The intuitive reason for this is that the point $\mathbf{v}_1'$ has w-component equal to 2 and that the importance (or, weight) of the point $\mathbf{i}$ in the second weighted average has therefore been doubled.

We next give a mathematical derivation of this intuition about the effect of forming weighted averages of homogeneous coordinates. But first, to help increase readability of formulas, we introduce a new notation. Suppose $\mathbf{x} = \langle x_1, x_2, x_3\rangle$ is a point in $\mathbb{R}^3$ and w is a nonzero scalar. Then the notation $\langle \mathbf{x}, w\rangle$ will denote the 4-tuple $\langle x_1,x_2,x_3,w\rangle$. In particular, if $\mathbf{x}$ is a point in $\mathbb{R}^3$, then the homogeneous representations of $\mathbf{x}$ all have the form $\langle w\mathbf{x}, w\rangle$. For example, the point $\mathbf{v}_1' = 2\mathbf{v}$ above is equal to $\langle 2,0,0,2\rangle$. In our new notation, $\mathbf{v}_1'$ is written as $\langle 2\mathbf{u}, 2\rangle$, where $\mathbf{u} = \langle 1,0,0\rangle$. We may also say that $\mathbf{v}_1'$ is "$\mathbf{u}$ with weight 2". This terminology corresponds also to conventions often used by CAD/CAM programs. These programs will let the designer specify a vertex $\mathbf{x}$ with a weight w. This means the homogenous representation $\langle w\mathbf{x}, w\rangle$, but it allows the user to use the more intuitive notion of points with weights.

Now, suppose $\mathbf{x}_1, \mathbf{x}_2, \ldots, \mathbf{x}_k$ are points in $\mathbb{R}^3$, and $w_1, w_2, \ldots, w_k$ are positive scalars, so that the 4-tuples $\langle w_i\mathbf{x}_i, w_i\rangle$ are homogeneous representations of the points $\mathbf{x}_i$. Consider a weighted average of the homogeneous representations, i.e.,

$$\alpha_1\langle w_1\mathbf{x}_1, w_1\rangle + \alpha_2\langle w_2\mathbf{x}_2, w_2\rangle + \cdots + \alpha_k\langle w_k\mathbf{x}_k, w_k\rangle.$$

The result is a 4-tuple; but the question is, what point $\mathbf{y}$ in $\mathbb{R}^3$ has this 4-tuple as its homogeneous representation? To answer this, calculate as follows:

$$\begin{aligned}
&\alpha_1\langle w_1\mathbf{x}_1, w_1\rangle + \alpha_2\langle w_2\mathbf{x}_2, w_2\rangle + \cdots + \alpha_k\langle w_k\mathbf{x}_k, w_k\rangle \\
&\quad = \langle \alpha_1 w_1\mathbf{x}_1, \alpha_1 w_1\rangle + \langle \alpha_2 w_2\mathbf{x}_2, \alpha_2 w_2\rangle + \cdots + \langle \alpha_k w_k\mathbf{x}_k, \alpha_k w_k\rangle \\
&\quad = \langle \alpha_1 w_1\mathbf{x}_1 + \alpha_2 w_2\mathbf{x}_2 + \cdots + \alpha_k w_k\mathbf{x}_k,\ \alpha_1 w_1 + \alpha_2 w_2 + \cdots + \alpha_k w_k\rangle \\
&\quad \equiv \left\langle \frac{\alpha_1 w_1\mathbf{x}_1 + \alpha_2 w_2\mathbf{x}_2 + \cdots + \alpha_k w_k\mathbf{x}_k}{\alpha_1 w_1 + \alpha_2 w_2 + \cdots + \alpha_k w_k},\ 1\right\rangle,
\end{aligned}$$

where the last equality ($\equiv$) means only that the homogeneous coordinates represent the same point y in $\mathbb{R}^3$, namely the point

$$\mathbf{y} \ = \ \sum_{i=1}^{k} \frac{\alpha_i w_i}{\alpha_1 w_1 + \cdots + \alpha_k w_k} \cdot \mathbf{x}_i. \qquad \text{(V.28)}$$

It is obvious that the coefficients on the $\mathbf{x}_i$'s sum to 1, and thus (V.28) is an affine combination of the $\mathbf{x}_i$'s. Furthermore, the α_i's are nonnegative and at least one of them is positive. Therefore, each coefficient in (V.28) is in the interval [0,1], so (V.28) is a weighted average.[6]

Equation (V.28) shows that a weighted average

$$\alpha_1\langle w_1\mathbf{x}_1, w_1\rangle + \alpha_2\langle w_2\mathbf{x}_2, w_2\rangle + \cdots + \alpha_k\langle w_k\mathbf{x}_k, w_k\rangle$$

gives a homogeneous representation of a point $\mathbf{y}$ in $\mathbb{R}^3$ such that $\mathbf{y}$ is a weighted average of $\mathbf{x}_1, \ldots, \mathbf{x}_k$:

$$\mathbf{y} \;=\; \beta_1\mathbf{x}_1 + \beta_2\mathbf{x}_2 + \cdots + \beta_k\mathbf{x}_k.$$

The coefficients $\beta_1, \ldots, \beta_k$ have the property that they sum to 1, and the ratios

$$\beta_1 : \beta_2 : \beta_3 : \;\cdots\; : \beta_{k-1} : \beta_k$$

are equal to the ratios

$$\alpha_1 w_1 : \alpha_2 w_2 : \alpha_3 w_3 : \;\cdots\; : \alpha_{k-1}w_{k-1} : \alpha_k w_k.$$

Thus the w_i values serve as "weights" that adjust the relative importances of the $\mathbf{x}_i$'s in the weighted average.

The above discussion has established the following theorem:

Theorem V.13. *Let A be a set of points in $\mathbb{R}^3$ and A^{H} a set of 4-tuples so that each member of A^{H} is a homogeneous representation of a point in A. Further suppose that the fourth component (the w-component) of each member of A^{H} is positive. Then any weighted average of 4-tuples from A^{H} is a homogeneous representation of a point in the convex hull of A.*

As we mentioned earlier, using weighted averages of homogeneous representations can greatly extend the power of Bézier and B-spline curves — these are the so-called rational Bézier curves and rational B-spline curves. In fact, it is only with the use of weighted averages in homogeneous coordinates that these spline curves can define conic sections such as circles, ellipses, parabolas and hyperbolas.

A second big advantage of using weighted averages in homogeneous coordinates instead of in ordinary Euclidean coordinates is that weighted averages in homogeneous coordinates are preserved not only under affine transformations but also under perspective transformations. In fact, weighted averages (and more generally, linear combinations) of homogeneous representations are preserved under any transformation which is represented by a 4×4 homogeneous matrix. That is to say, for any 4×4 matrix M, any set of 4-tuples $\mathbf{u}_i$, and any set of scalars α_i,

$$M\left(\sum\nolimits_i \alpha_i\mathbf{u}_i\right) \;=\; \sum_i \alpha_i M(\mathbf{u}_i). \qquad \text{(V.29)}$$

[6] Recall that the weights w_i were assumed to be positive. If some of them were negative, then (V.28) would be an affine combination, not a weighted average.

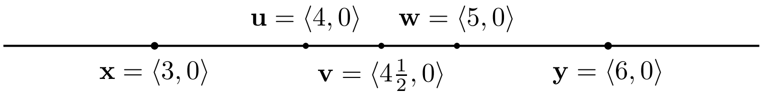
$\mathbf{u} = \langle 4, 0 \rangle$
$\mathbf{w} = \langle 5, 0 \rangle$
$\mathbf{x} = \langle 3, 0 \rangle$
$\mathbf{v} = \langle 4\frac{1}{2}, 0 \rangle$
$\mathbf{y} = \langle 6, 0 \rangle$

Figure V.20: Figure for Exercise V.17.

This fact will be useful later on when working with rational Bézier and B-spline curves since it means that a curve can be transformed by transforming its control points.

Exercise V.15. Work out the following example of how weighted averages of Euclidean points in $\mathbb{R}^3$ are not preserved under perspective transformations. Let the perspective transformation act on points in $\mathbb{R}^3$ by mapping $\langle x, y, z \rangle$ to $\langle x/z, y/z, 0 \rangle$. Give a 4×4 homogeneous matrix that represents this transformation (c.f. Section II.4.2). What are the values of the three points $\langle 0, 0, 3 \rangle$, $\langle 1, 0, 2 \rangle$, and $\langle 2, 0, 1 \rangle$ under this transformation? Explain how this shows that weighted averages are not preserved by the transformation.

Exercise V.16. Let $\mathbf{x}$ and $\mathbf{y}$ be distinct points in $\mathbb{R}^3$. Also let $\mathbf{x}' = \langle \mathbf{x}, 1 \rangle$ and $\mathbf{y}' = \langle 2\mathbf{y}, 2 \rangle$ be homogeneous representations of $\mathbf{x}$ and $\mathbf{y}$. Set $\mathbf{z}' = \mathit{lerp}(\mathbf{x}', \mathbf{y}', \frac{1}{2})$; this a homogeneous representation of a point $\mathbf{x} \in \mathbb{R}^3$. Is $\mathbf{z}$ closer to $\mathbf{x}$ or to $\mathbf{y}$? What the ratio of the distance from $\mathbf{x}$ to $\mathbf{z}$ and the distance from $\mathbf{y}$ to $\mathbf{z}$? What value of β makes $\mathit{lerp}(\mathbf{x}, \mathbf{y}, \beta) = \mathbf{z}$?

Exercise V.17. Let $\mathbf{x} = \langle 3, 0 \rangle$, $\mathbf{y} = \langle 6, 0 \rangle$, $\mathbf{u} = \langle 4, 0 \rangle$, $\mathbf{v} = \langle 4.5, 0 \rangle$, and $\mathbf{w} = \langle 5, 0 \rangle$. Note that $\mathit{lerp}(\mathbf{x}, \mathbf{y}, \frac{1}{3}) = \mathbf{u}$, $\mathit{lerp}(\mathbf{x}, \mathbf{y}, \frac{1}{2}) = \mathbf{v}$ and $\mathit{lerp}(\mathbf{x}, \mathbf{y}, \frac{2}{3}) = \mathbf{w}$. (See Figure V.20.)

Let $\mathbf{a} = \langle 3, 0, 1 \rangle$ and $\mathbf{b} = \langle 12, 0, 2 \rangle$. These are homogeneous representations of $\mathbf{x}$ and $\mathbf{y}$.

(a) What is $\mathit{lerp}(\mathbf{a}, \mathbf{b}, \frac{1}{2})$ equal to? (As a triple.) This triple is the homogeneous representation of what point in $\mathbb{R}^2$?

(b) For what value of β is $\mathit{lerp}(\mathbf{a}, \mathbf{b}, \beta)$ a homogeneous representation of $\mathbf{v}$?

(b) For what value of β is $\mathit{lerp}(\mathbf{a}, \mathbf{b}, \beta)$ a homogeneous representation of $\mathbf{w}$?

(b) For what value of β is $\mathit{lerp}(\mathbf{a}, \mathbf{b}, \beta)$ a homogeneous representation of $\mathbf{u}$?

V.5 Hyperbolic interpolation

The previous section discussed the effect of interpolation in homogeneous coordinates and what interpolation of homogeneous coordinates corresponds to in terms of Euclidean coordinates. Now we discuss the opposite direction: how to convert interpolation in Euclidean coordinates into interpolation in homogeneous coordinates. This process is called "hyperbolic interpolation" or sometimes "rational linear interpolation" (see Blinn [16] and Heckbert and Moreton [63]).

The situation is the following: we have points in Euclidean space specified with homogeneous coordinates $\langle w_i\mathbf{x}_i, w_i\rangle$, $i = 1, 2, \ldots, k$ (usually there are only two points, so $k = 2$). These correspond to Euclidean points $\mathbf{x}_i$. An affine combination of the points is given as

$$\mathbf{z} \;=\; \sum_i \alpha_i \mathbf{x}_i,$$

where $\sum_i \alpha_i = 1$. The problem is to find values β_i so that $\sum \beta_i = 1$ and so that the affine combination of homogeneous vectors

$$\sum_i \beta_i \langle w_i\mathbf{x}_i, w_i\rangle$$

is a homogeneous representation of the same point $\mathbf{z}$. From our work in the previous section, we know that the values β_i and α_i must satisfy the condition that the values α_i are proportional to the products $\beta_i w_i$. Therefore, we may choose

$$\beta_i \;=\; \frac{\alpha_i/w_i}{\sum_j \alpha_j/w_j}, \qquad \text{(V.30)}$$

for $i = 1, 2, \ldots, n$.

Hyperbolic interpolation is useful for interpolating values in stage 4 of the rendering pipeline (see Chapter II). In stage 4, perspective division has already been performed, so we are working with points lying in the two dimensional screen space. As described in Section III.3, linear interpolation is performed in screen space in order to fill in color, normal, and texture coordinate values for pixels inside a polygon. The linear interpolation along a line gives a weighted average

$$(1-\alpha)\mathbf{y}_1 + \alpha\mathbf{y}_2$$

specifying a point in screen coordinates in terms of the endpoints of a line segment. However, linear interpolation in screen coordinates is not really correct; it is often better to interpolate in spatial coordinates, because, after all, the object that is being modeled lies in 3-space, and interpolating in screen coordinates means that the viewed object will change as the viewpoint changes. This change in appearance can sometimes be very dramatic! For example, see Figure **??**.

Therefore, it is often desirable that values which are specified at the endpoints, such as color or texture coordinates, are interpolated using hyperbolic interpolation to take into account the depth component of the spatial coordinates. In this situation, $\mathbf{y}_1$ and $\mathbf{y}_2$ have homogeneous representations $\langle \mathbf{x}_1, w_1\rangle$ and $\langle \mathbf{x}_2, w_2\rangle$ where w_i is the depth (z) component from the perspective transformation. The hyperbolic interpolation uses weights $(1-\beta)$ and β so that $(1-\beta)\langle \mathbf{x}_1, w_1\rangle + \beta\langle \mathbf{x}_2, w_2\rangle$ is a homogeneous representation of $(1-\alpha)\mathbf{y}_1 + \alpha\mathbf{y}_2$. The weights $(1-\beta)$ and β are used to obtain the other interpolated values for values such as texture coordinates, color, etc.

The Bresenham algorithm described in Section III.3.1 computes the α values, but not the β values. From Equation (V.30), we get

$$\beta \;=\; \frac{\alpha/w_2}{(1-\alpha)/w_1+\alpha/w_2} \;=\; \frac{\alpha w_1}{(1-\alpha)w_2+\alpha w_1} \;=\; \frac{\alpha}{\mathit{lerp}(w_2/w_1,1,\alpha)}.$$

The denominator of this formula is a linear interpolation, and can be computed by a Bresenham-like algorithm. This makes it possible to use an extension of the Bresenham algorithm for hyperbolic interpolation between two points, but at the cost of an extra division at every pixel (c.f. [16, 63]).

Hyperbolic interpolation is most useful when a polygon is being viewed obliquely, with the near portion of the polygon much closer to the viewer than the far part. For examples of how hyperbolic interpolation can help with compensating for perspective distortion, see Figures VI.2 and **??**. XXXX UPDATE THIS FORWARD REFERENCE

XXXX ADD EXERCISE(S)

V.6 Spherical linear interpolation

This section discusses "spherical linear interpolation," also called "slerp"-ing, which is a method of interpolating between points on a sphere.[7] Fix a dimension $d > 1$, and consider the unit sphere in $\mathbb{R}^d$. This sphere consists of the unit vectors $\mathbf{x} \in \mathbb{R}^d$. In $\mathbb{R}^2$, the unit sphere is just the unit circle. In $\mathbb{R}^3$, the unit sphere is called S^2 or the "2-sphere," and is an ordinary sphere. In $\mathbb{R}^4$, it is called S^3 or the "3-sphere," and is a hypersphere.

Let $\mathbf{x}$ and $\mathbf{y}$ be points on the unit sphere, and further assume that they are not antipodal (i.e., are not directly opposite each other on the sphere). Then, there is a unique shortest path from $\mathbf{x}$ to $\mathbf{y}$ on the sphere. This shortest path is called a geodesic and lies on a great circle. A *great circle* is defined to be the intersection of a plane containing the origin (i.e., a two dimensional linear subspace of $\mathbb{R}^d$) and the unit sphere. Thus, a great circle is an ordinary circle of radius one.

Now suppose also that α is between 0 and 1. We wish to find the point $\mathbf{z}$ on the sphere which is fraction α of the distance from the point $\mathbf{x}$ to $\mathbf{y}$ along the geodesic, as shown in Figure V.21. This is sometimes called "slerp"-ing for "$\underline{S}$pherical $\underline{L}$inear int$\underline{ERP}$olation," and is denoted $\mathbf{z} = \mathit{slerp}(\mathbf{x},\mathbf{y},\alpha)$. The terminology comes from Shoemake [104] who used slerping in $\mathbb{R}^4$ for interpolating quaternions on the 3-sphere (see Section XIII.3.7).

An important aspect of spherical linear interpolation is that it is nonlinear: in particular, it is not good enough to form the interpolant by the formula

$$\frac{(1-\alpha)\mathbf{x}+\alpha\mathbf{y}}{||(1-\alpha)\mathbf{x}+\alpha\mathbf{y}||},$$

[7] The material in this section is not needed until the discussion of interpolation of quaternions in Section XIII.3.7.

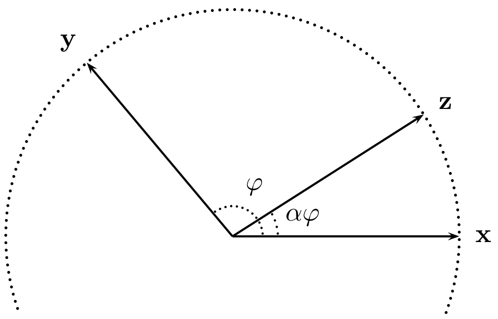

Figure V.21: The angle between $\mathbf{x}$ and $\mathbf{y}$ is φ. *slerp*$(\mathbf{x},\mathbf{y},\alpha)$ is the vector $\mathbf{z}$ which is obtained by rotating $\mathbf{x}$ a fraction α of the way towards $\mathbf{y}$. All vectors are unit vectors, as $\mathbf{x}$, $\mathbf{y}$, and $\mathbf{z}$ lie on the unit sphere.

since this will traverse the geodesic at a nonconstant rate with respect to α. Instead, we want to let $\mathbf{z}$ be the result of rotating the vector $\mathbf{x}$ a fraction α of the way towards $\mathbf{y}$. That is to say, if the angle between $\mathbf{x}$ and $\mathbf{y}$ is equal to φ, then $\mathbf{z}$ is the vector which is coplanar with $\mathbf{0}$, $\mathbf{x}$, and $\mathbf{y}$ and which is obtained by rotating $\mathbf{x}$ through an angle of $\alpha\varphi$ towards $\mathbf{y}$.

We now give a mathematical derivation of the formulas for spherical linear interpolation (slerping). Recall that φ is the angle between $\mathbf{x}$ and $\mathbf{y}$; hence $0 \le \varphi < 180^\circ$. If $\varphi = 180^\circ$, then slerping is undefined, since there is no unique direction or shortest geodesic from $\mathbf{x}$ to $\mathbf{y}$. Referring to Figure V.22, let $\mathbf{v}$ be the component of $\mathbf{y}$ which is perpendicular to $\mathbf{x}$, and let $\mathbf{w}$ be the unit vector in the same direction as $\mathbf{v}$.

$$\begin{aligned}\mathbf{v} &= \mathbf{y} - (\cos\varphi)\mathbf{x} \;=\; \mathbf{y} - (\mathbf{y}\cdot\mathbf{x})\mathbf{x},\\ \mathbf{w} &= \frac{\mathbf{v}}{\sin\varphi} \;=\; \frac{\mathbf{v}}{\sqrt{\mathbf{v}\cdot\mathbf{v}}}.\end{aligned}$$

Then we can define *slerp*$(\mathbf{x},\mathbf{y},\alpha)$ by

$$\mathit{slerp}(\mathbf{x},\mathbf{y},\alpha) \;=\; \cos(\alpha\varphi)\mathbf{x} + \sin(\alpha\varphi)\mathbf{w}, \qquad \text{(V.31)}$$

since this calculation rotates $\mathbf{x}$ through an angle of $\alpha\varphi$.

An alternative formulation of the formula for slerping can be given by the

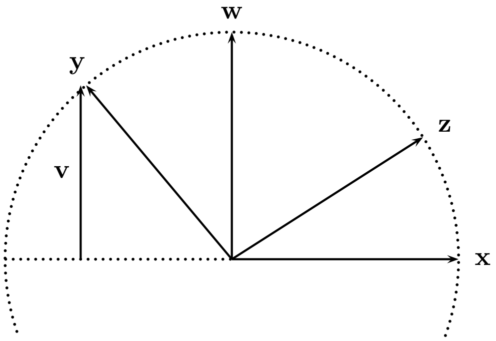

Figure V.22: $\mathbf{v}$ and $\mathbf{w}$ are used to derive the formula for spherical linear interpolation. The vector $\mathbf{v}$ is the component of $\mathbf{y}$ perpendicular to $\mathbf{x}$, and $\mathbf{w}$ is the unit vector in the same direction. The magnitude of $\mathbf{v}$ is $\sin\varphi$.

following derivation:

$$\begin{aligned}
\mathit{slerp}(\mathbf{x},\mathbf{y},\alpha) &= \cos(\alpha\varphi)\mathbf{x}+\sin(\alpha\varphi)\mathbf{w} \\
&= \cos(\alpha\varphi)\mathbf{x}+\sin(\alpha\varphi)\frac{\mathbf{y}-(\cos\varphi)\mathbf{x}}{\sin\varphi} \\
&= \left(\cos(\alpha\varphi)-\sin(\alpha\varphi)\frac{\cos\varphi}{\sin\varphi}\right)\mathbf{x}+\frac{\sin(\alpha\varphi)}{\sin\varphi}\mathbf{y} \\
&= \frac{\sin\varphi\cos(\alpha\varphi)-\sin(\alpha\varphi)\cos\varphi}{\sin\varphi}\mathbf{x}+\frac{\sin(\alpha\varphi)}{\sin\varphi}\mathbf{y} \\
&= \frac{\sin(\varphi-\alpha\varphi)}{\sin\varphi}\mathbf{x}+\frac{\sin(\alpha\varphi)}{\sin\varphi}\mathbf{y} \\
&= \frac{\sin((1-\alpha)\varphi)}{\sin\varphi}\mathbf{x}+\frac{\sin(\alpha\varphi)}{\sin\varphi}\mathbf{y}. \qquad \text{(V.32)}
\end{aligned}$$

The next-to-last equality was derived using the sine difference formula $\sin(a-b)=\sin a\cos b-\sin b\cos a$.

The usual method for computing spherical linear interpolation is based on Equation (V.32). Since typical applications of slerping require multiple uses of interpolation between the same two points $\mathbf{x}$ and $\mathbf{y}$, it makes sense to precompute the values of φ and $\mathtt{s}=\sin\varphi$. This is done by the following pseudo-code:

```
Precompute_for_Slerp(x, y) {
    Set c = $\mathbf{x}\cdot\mathbf{y}$;              // Cosine of $\varphi$
    Set $\varphi$ = acos(c);            // Compute $\varphi$ with arccos function
    Set s = sin($\varphi$);             // Sine of $\varphi$
}
```

An alternative method for precomputing φ and s can provide a little more accuracy for very small angles φ, without much extra computation:

```
Precompute_for_Slerp(x, y) {
    Set c = $\mathbf{x}\cdot\mathbf{y}$;                // Cosine of $\varphi$
    Set v = $\mathbf{y} - c\mathbf{x}$;
    Set s = $\sqrt{\mathbf{v}\cdot\mathbf{v}}$;             // Sine of $\varphi$
    Set $\varphi$ = atan2(s,c);          // Compute $\varphi = \arctan(s/c)$
}
```

Then, given any value for α, $0 \le \alpha \le 1$, compute $slerp(\mathbf{x},\mathbf{y},\alpha)$ by:

```
Slerp(x, y, $\alpha$) {
    // $\varphi$ and s=$\sin\varphi$ have already been precomputed.
    Set z = $\frac{\sin((1-\alpha)\varphi)}{\sin\varphi}\mathbf{x} + \frac{\sin(\alpha\varphi)}{\sin\varphi}\mathbf{y}$;
    Return z;
}
```

As written above, there will a divide-by-zero error when $\varphi = 0$, since then $\sin\varphi = 0$. In addition, for φ close to zero, the division by a near-zero value can cause numerical instability. To avoid this, you should use the following approximations when $\varphi \approx 0$:

$$\frac{\sin((1-\alpha)\varphi)}{\sin\varphi} \approx (1-\alpha) \qquad \text{and} \qquad \frac{\sin(\alpha\varphi)}{\sin\varphi} \approx \alpha.$$

These approximations are obtained by using $\sin\psi \approx \psi$ when $\psi \approx 0$. The error in these approximations can be estimated from the Taylor series expansion of $\sin\psi$; namely, $\sin\psi \approx \psi - \frac{1}{6}\psi^3$. The test of $\varphi \approx 0$ can be replaced by the condition that roundoff error makes $1 - \frac{1}{6}\varphi^2$ evaluate to the value 1. For single precision floating point, this condition can be replaced by the condition that $\varphi < 10^{-4}$. For double precision floating point, the condition $\varphi < 10^{-9}$ can be used.

Exercise V.18. Let $\mathbf{x} = \langle \frac{\sqrt{2}}{2}, 0, \frac{\sqrt{2}}{2} \rangle$ and $\mathbf{y} = \langle 0, 1, 0 \rangle$. What is the angle between the unit vectors $\mathbf{x}$ and $\mathbf{y}$? What is $lerp(\mathbf{x},\mathbf{y},\frac{1}{3})$? What is $slerp(\mathbf{x},\mathbf{y},\frac{1}{3})$? Which of these are unit vectors?

V.7 Interpolation with GLSL shaders

The OpenGL rendering pipeline supports three different modes of interpolation (also called "shading") for values output by the vertex or geometry shader. The most common mode (called "smooth") is hyperbolic barycentric (or linear) interpolation. The "flat" mode just propagates a fixed value. The much less common "noperspective" mode does barycentric (or linear) interpolation in Euclidean coordinates.

Suppose a shader program has only a vertex shader and a fragment shader, and is processing triangles. By default any output value will be smooth shaded. As an example, the simple vertex shader program on page 25 declared the variable

```
out vec3 theColor;
```

It could have equivalently declared it as

```
smooth out vec3 theColor;
```

The fragment shader (on page 26), has the corresponding declaration `in vec3 theColor;` which implies the default option of `smooth`. The effect of these declarations is to combine interpolation based on barycentric coordinates with hyperbolic interpolation as described in Section V.5. For this, the rasterization stage of the OpenGL pipeline identifies the three pixels corresponding to the vertices of the triangles. Then, each pixel in the interior has barycentric coordinates $\alpha_1, \alpha_2, \alpha_3$. From these, the $\beta_1, \beta_2, \beta_3$ are determined according to Equation V.30; the values w_1, w_2, w_3 come from the homogeneous representations for the three vertices. Then the `smooth out` value is interpolated from the its values using the coefficients $\beta_1, \beta_2, \beta_3$.

This use of smooth interpolation based on hyperbolic interpolation may sound complicated, but it is necessary to get good results. For more on this see XXXXX (NEXT CHAPTER).

Another interpolation mode is used when the vertex shader uses a declaration such as

```
flat out theColor;
```

In "flat" interpolation, the same value is used for all pixels in the triangle. This is usually the value in the final vertex in the triangle, but it can be changed using the OpenGL command `glProvokingIndex`.

The third interpolation mode is the "noperspective" mode. This is invoked with the declaration

```
noperspective out theColor;
```

This does barycentric interpolation in screen coordinates, based on the positions of the pixels on the screen. It does not take perspective into account. The noperspective interpolation mode is not so common. It gives correct results when using an orthographic viewing projection; however, with a perspective viewing transformation, it can give very bad visual results.

When the shader program has a geometry shader in addition to a vertex shader, rasterization and interpolation are performed only after values are output by the geometry shader. The geometry shader declares `out` values and they can be `smooth` (the default), `flat`, or `noperspective`.

V.8 Additional exercises

Exercise V.19. Let $\mathbf{x} = \langle 2, 0\rangle$ and $\mathbf{y} = \langle -4, 1\rangle$.

(a) What is $\mathbf{u} = \mathit{lerp}(\mathbf{x}, \mathbf{y}, \frac{1}{4})$? (Give $\mathbf{u}$ explicitly.)

(b) Is $\mathbf{u}$ closer to $\mathbf{x}$ or to $\mathbf{y}$?

(c) What is $\mathbf{v} = \mathit{lerp}(\mathbf{y}, \mathbf{x}, \frac{1}{4})$? Watch the order of the parameters!

(d) Suppose f is a function in $\mathbb{R}^2$ with $f(\mathbf{x}) = 1$ and $f(\mathbf{y}) = 10$. We wish to set other values for f by linear interpolation or extrapolation. What value does this give for $f(\langle 0, \frac{1}{3})$? For $f(\langle 5, -\frac{1}{2}\rangle)$?

Exercise V.20. Let L be the line continaing $\mathbf{x} = \langle 0, 2\rangle$ and $\mathbf{y} = \langle 3, 6\rangle$. What point $\mathbf{u}$ on L is closest to $\langle 2, 3\rangle$? Express $\mathbf{u}$ both in the form $\mathit{lerp}(\mathbf{x}, \mathbf{y}, \alpha)$ and explicitly as a point in RR.

Exercise V.21. Let $\mathbf{u} = \mathit{lerp}(\mathbf{x}, \mathbf{y}, \alpha)$.

(a) For what values of α must $\mathbf{u}$ be a linear combination of $\mathbf{x}$ and $\mathbf{y}$?

(b) For what values of α must $\mathbf{u}$ be an affine combination of $\mathbf{x}$ and $\mathbf{y}$?

(c) For what values of α must $\mathbf{u}$ be a weighted average of $\mathbf{x}$ and $\mathbf{y}$?

Exercise V.22. Refer to Figure V.23 for questions about barycentric coordinates $\alpha\mathbf{x} + \beta\mathbf{y} + \gamma\mathbf{z}$, where $\mathbf{x} = \langle -4, -2\rangle$, $\mathbf{y} = \langle -2, 1\rangle$ and $\mathbf{z} = \langle 0, 0\rangle$.

(a) Answer the following questions with the appropriate answer chosen from **a** through **z** (not a numeric answer!):

(i) Which point has barycentric coordinates $\alpha{=}0$, $\beta{=}0$, $\gamma{=}1$?

(ii) Which point has barycentric coordinates $\alpha{=}0$, $\beta{=}\frac{2}{3}$, $\gamma{=}\frac{1}{3}$?

(iii) Which point has barycentric coordinates $\alpha{=}\frac{1}{6}$, $\beta{=}\frac{2}{3}$, $\gamma{=}\frac{1}{6}$?

(iv) Which point has barycentric coordinates $\alpha{=}\frac{5}{7}$, $\beta{=}\frac{-1}{7}$, $\gamma{=}\frac{3}{7}$?

(b) The point $\mathbf{w}$ is outside the triangle: Let α, β, γ be its barycentric coordinates. Which of α, β, γ are positive? Which are negative?

(c) Answer the same questions for the point $\mathbf{v}$: Which of its barycentric coordinates are positive and which are negative?

Exercise V.23. What is the area of the triangle with vertices $\mathbf{x} = \langle -4, -2\rangle$, $\mathbf{y} = \langle -2, 1\rangle$ and $\mathbf{z} = \langle 0, 0\rangle$, as shown in Figure V.23?

Exercise V.24. Let $\mathbf{x} = \langle -1, 0\rangle$, $\mathbf{y} = \langle 0, 2\rangle$, and $\mathbf{z} = \langle 2, 0\rangle$.

(a) What point $\mathbf{u}$ has barycentric coordinates $\langle \frac{1}{2}, \frac{1}{3}, \frac{1}{6}\rangle$ with respect to these three points?

(b) Let $\mathbf{v} = \langle 0, 1\rangle$. Express $\mathbf{v}$ as an weighted average of $\mathbf{x}, \mathbf{y}, \mathbf{z}$, by finding its barycentric coordinates.

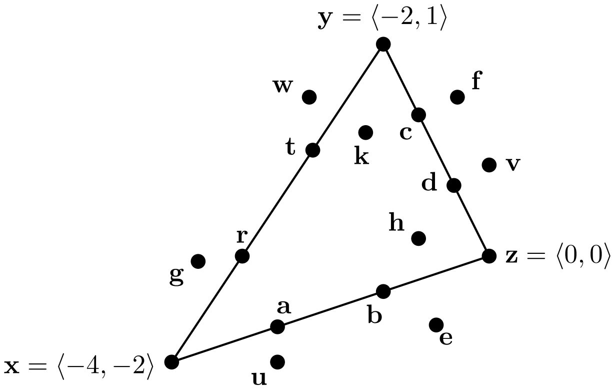

Figure V.23: Figure for Exercises V.22 and V.23.

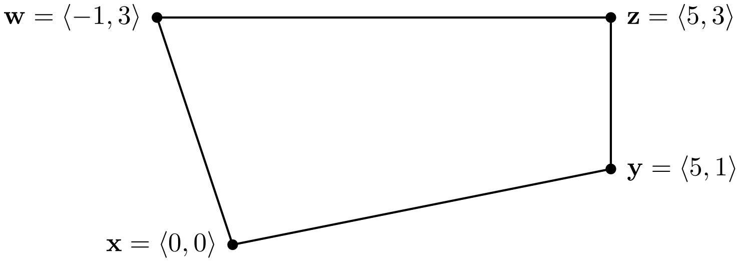
$\mathbf{w} = \langle -1, 3\rangle$
$\mathbf{z} = \langle 5, 3\rangle$
$\mathbf{y} = \langle 5, 1\rangle$
$\mathbf{x} = \langle 0, 0\rangle$

Figure V.24: Figure for Exercise V.25.

Exercise V.25. Let $\mathbf{x} = \langle 0, 0\rangle$, $\mathbf{y} = \langle 5, 1\rangle$, $\mathbf{z} = \langle 5, 3\rangle$, and $\mathbf{w} = \langle -1, 3\rangle$, as in Figure V.24. For each of the following values of α and β, what point is obtained by bilinear interpolation? Graph your answers.

a. $\alpha = 0$ and $\beta = 1$.

b. $\alpha = \frac{2}{3}$ and $\beta = 0$.

c. $\alpha = \frac{1}{2}$ and $\beta = \frac{3}{4}$.

d. $\alpha = \frac{1}{3}$ and $\beta = \frac{2}{3}$.

Exercise V.26. A function $\mathbf{p}(\alpha, \beta)$ is defined by letting $\mathbf{p}(\alpha, \beta)$ be the point with bilinear coordinates α and β for the the points $\mathbf{x} = \langle 0, 0\rangle$, $\mathbf{y} = \langle 4, -1\rangle$, $\mathbf{z} = \langle 5, 2\rangle$, and $\mathbf{w} = \langle -1, 3\rangle$ as shown in Figure V.25. So, $\mathbf{p}(0, 0) = \mathbf{x}$ and $\mathbf{p}(1, 0) = \mathbf{y}$, etc.

(a) Calculate $\mathbf{u} = \mathbf{p}(1, \frac{1}{3})$ (that is, calculate its x, y-coordinates).

(b) Make a copy of the figure and the approximate location of $\mathbf{u}$.

(c) Let $\mathbf{v} = \mathbf{p}(\frac{1}{2}, \frac{9}{10})$. Also show the *approximate* location of $\mathbf{v}$. (Do not calculates $\mathbf{v}$'s x, y-coordinates.)

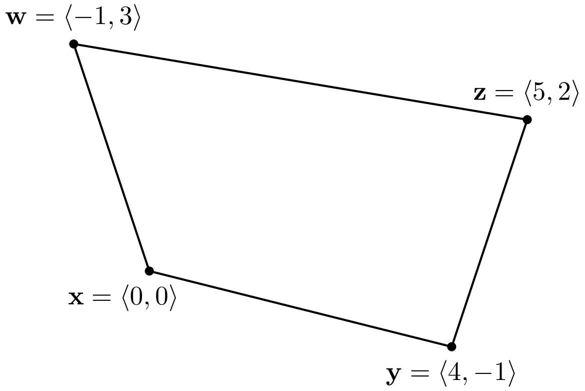
$\mathbf{w} = \langle -1, 3\rangle$
$\mathbf{z} = \langle 5, 2\rangle$
$\mathbf{x} = \langle 0, 0\rangle$
$\mathbf{y} = \langle 4, -1\rangle$

Figure V.25: The figure for Exercise V.26.

Exercise V.27. A function $\mathbf{g} : [0,1] \times [0,1] \to \mathbb{R}^3$ is defined by setting $\mathbf{g}(\langle 0,0\rangle) = \langle 2,0,0\rangle$, $\mathbf{g}(\langle 1,0\rangle) = \langle 0,1,0\rangle$, $\mathbf{g}(\langle 0,1\rangle) = \langle 0,2,4\rangle$, $\mathbf{g}(\langle 1,1\rangle) = \langle 2,2,0\rangle$, and then using bilinear interpolation to extend the domain of g to the square $[0,1] \times [0,1]$. What is $\mathbf{g}(\frac{1}{4}, 0)$? $\mathbf{g}(\frac{1}{4}, 1)$? $\mathbf{g}(\frac{1}{4}, \frac{1}{2})$?

Exercise V.28. Work with homogeneous coordinates representing points in $\mathbb{R}^2$. Let $\mathbf{x} = \langle -4, 0, 2\rangle$ and $\mathbf{y} = \langle 2, 0, 1\rangle$.

(a) What two points $\mathbf{u}$ and $\mathbf{v}$ in $\mathbb{R}^2$ are represented by the homogeneous coordinates $\mathbf{x}$ and $\mathbf{y}$?

(b) What is $\mathbf{z} = \mathit{lerp}(\mathbf{x}, \mathbf{y}, \frac{1}{2})$? Give your answer as a 3-vector.

(c) What point in $\mathbb{R}^2$ has $\mathbf{z}$ as a homogeneous representation? Is this the midpoint of $\mathbf{u}$ and $\mathbf{v}$?

(d) What value of β makes the 3-tuple $\mathit{lerp}(\mathbf{x}, \mathbf{y}, \beta)$ a homogeneous representation of the midpoint of $\mathbf{u}$ and $\mathbf{v}$.

Exercise V.29. This question is about points in $\mathbb{R}^2$, and their homogeneous representations; and how they act under linear combinations. Let

$$\mathbf{a} = \langle 4, 0, 4\rangle \quad \text{and} \quad \mathbf{b} = \langle 0, 8, 2\rangle$$

be homogeneous representations for the following two vectors in $\mathbb{R}^2$:

$$\mathbf{x} = \langle 1, 0\rangle \quad \text{and} \quad \mathbf{y} = \langle 0, 4\rangle.$$

(a) What point $\mathbf{u}$ in $\mathbb{R}^2$ is equal to $\mathit{lerp}(\mathbf{x}, \mathbf{y}, \frac{3}{4}) = \frac{1}{4}\mathbf{x} + \frac{3}{4}\mathbf{y}$?

(b) What point $\mathbf{w}$ in $\mathbb{R}^2$ is represented by (in homogeneous representation) $\mathit{lerp}(\mathbf{a}, \mathbf{b}, \frac{3}{4}) = \frac{1}{4}\mathbf{x} + \frac{3}{4}\mathbf{y}$? Is $\mathbf{w}$ equal to $\mathbf{u}$?

(c) Give a value α so that $\mathit{lerp}(\mathbf{a}, \mathbf{b}, \alpha) = (1-\alpha)\mathbf{a} + \alpha\mathbf{b}$ is an affine combination of $\mathbf{a}$ and $\mathbf{b}$ giving a homogeneous representation of the point $\mathbf{u}$ calculated in part (a).

(d) The answer to part (c) gives α equal to a fraction in $[0,1]$. Find two ***integers*** n and m so that $n\mathbf{a}+m\mathbf{b}$ is another homogeneous representation of the point $\mathbf{u}$.

Exercise V.30. Let $k \ge 1$ and let $\mathbf{x},\mathbf{y},\mathbf{z},\mathbf{w}$ be four distinct points in $\mathbb{R}^k$. Let $\mathbf{x}' = \langle \mathbf{x}, 1\rangle$, $\mathbf{y}' = \langle 2\mathbf{y}, 2\rangle$, $\mathbf{z}' = \langle 3\mathbf{z}, 3\rangle$, and $\mathbf{w}' = \langle 4\mathbf{w}, 4\rangle$ be homogeneous representations of these four points.

(a) Give values α_1, α_2, α_3, and α_4 so that $\alpha_1+\alpha_2+\alpha_3+\alpha_4=1$ and

$$\alpha_1\mathbf{x}+\alpha_2\mathbf{y}+\alpha_3\mathbf{z}+\alpha_4\mathbf{z}$$

is the point with homogeneous coordinates $\frac{1}{4}(\mathbf{x}'+\mathbf{y}'+\mathbf{z}'+\mathbf{w}')$.

(b) Give values α_1, α_2, α_3, and α_4 so that $\alpha_1+\alpha_2+\alpha_3+\alpha_4=1$ and

$$\alpha_1\mathbf{x}'+\alpha_2\mathbf{y}'+\alpha_3\mathbf{z}'+\alpha_4\mathbf{z}'$$

is a homogeneous representation of the point $\frac{1}{4}(\mathbf{x}+\mathbf{y}+\mathbf{z}+\mathbf{w})$.

(c) Give values α_1, α_2, α_3, and α_4 so that $\alpha_1+\alpha_2+\alpha_3+\alpha_4=1$ and

$$\alpha_1\mathbf{x}'+\alpha_2\mathbf{y}'+\alpha_3\mathbf{z}'+\alpha_4\mathbf{z}'$$

is a homogeneous representation of the point $\frac{1}{10}\mathbf{x}+\frac{2}{10}\mathbf{y}+\frac{3}{10}\mathbf{z}+\frac{4}{10}\mathbf{w}$.

Exercise V.31. Let $\mathbf{x} = \langle \frac{\sqrt{6}}{4}, -\frac{1}{2}, \frac{\sqrt{6}}{4}\rangle$ and $\mathbf{y} = \langle 0,1,0\rangle$. Confirm that $\mathbf{x}$ and $\mathbf{y}$ are unit vectors. What is the angle between $\mathbf{x}$ and $\mathbf{y}$? What is $\mathit{slerp}(\mathbf{x},\mathbf{y},\frac{3}{8})$ equal to?

Exercise V.32* Generalize the notions of linear interpolation and barycentric coordinates to allow interpolation between four noncoplanar points that lie in $\mathbb{R}^3$.

XXXXX NEED SEVERAL MORE EXERCISES, E.G. LIKE Exercise **??** IF NOT ALREADY PRESENT.

XXXXX Also CONVEX SETS and WEIGHTED AVERAGES and maybe another HYPERBOLIC INTERPOLATION.

XXXX EXERCISE ABOUT DERIVATIVE OF HYPERBOLIC INTERPOLATION (Compared with normal non-weighted interpolation.) Forward references Bezier section, appeoximately p 284, pdf 304.S

Chapter VI

Texture Mapping

This is a ***preliminary*** *draft of a second edition of the book* 3-D Computer Graphics: A Mathematical Introduction with OpenGL. *So please read it cautiously and critically! Corrections are appreciated. Draft C.4.a*
Author: Sam Buss, `sbuss@ucsd.edu`

VI.1 Texture mapping an image

Texture mapping, in its simplest form, consists of applying a graphics image, a picture, or a pattern to a surface. A texture map can apply an actual picture to a surface, such as a label on a can, or a picture on a billboard, etc.; or can apply semi-repetitive patterns such as wood grain or stone surfaces, etc. More generally, a texture map can hold any kind of information that affects the appearance of a surface: the texture map serves as a pre-computed table, and the texture mapping then consists simply of table lookup to get the information affecting a particular point on the surface as it is rendered. If you do not use texture maps, your surfaces will either be rendered as very smooth, uniform surfaces, or would need to be rendered with very small polygons so that you can explicitly specify surface properties on a fine scale.

Texture maps are often used to very good effect in real-time rendering settings, such as computer games, since it gives good results with a minimum of computational load. In addition, texture maps are widely supported by graphics hardware such as graphics boards for PCs, so that they can be used without needing much computation from a central processor.

Texture maps can be applied at essentially three different points in the graphics rendering process, which we list more-or-less in order of increasing generality and flexibility:

- A texture map can hold colors that are applied to a surface in "replace" or "decal" mode: the texture map colors just overwrite whatever surface colors are otherwise present. In this case, no lighting calculations should be performed, as the results of the lighting calculations would just be overwritten.

- A texture map can hold attributes such as color, brightness, or transparency, which affect the surface appearance after the lighting model calculations are completed. In this case, the texture map attributes are blended with, or modulate, the colors of the surface as calculated by the lighting model. This mode and the first mode are the most common modes for using texture maps.
- A texture map can hold attributes such as reflectivity coefficients, normal displacements, or other parameters for the Phong lighting model or the Cook-Torrance model. In this case, the texture map values modify the surface properties which are input to the lighting model. A prominent example of this is "bump mapping," which affects the surface normals by specifying virtual displacements to the surface.

Of course, there is no reason why you cannot combine various texture map techniques by applying more than one texture map to a single surface. For example, one might apply both an ordinary texture map that modulates the color of a surface, together with a bump map that perturbs the normal vector. In particular, one could apply texture maps both before and after the calculation of lighting.

A texture map typically consists of a two dimensional, rectangular array of data, indexed with two coordinates s and t, with both s and t varying from 0 to 1. The data values are usually colors, but could be any other useful value. The data in a texture map can be generated from an image such as a photograph, a drawing, or the output of a graphics program. The data can also be procedurally generated; for example, simple patterns like a checkerboard pattern can be easily computed. Procedurally generated data can either be pre-computed and stored in a two dimensional array or can be computed as needed. Finally, the texture map may be created during the rendering process itself; an example of this would be generating an environment map by pre-rendering the scene from one or more viewpoints, and using the results to build a texture map that is used for the final rendering stage.

This chapter will discuss the following aspects of texture mapping. First, as a surface is rendered, it is necessary to assign texture coordinates s and t to vertices, and then to pixels. These s and t values are used as coordinates to index into the texture and specify what position in the texture map is applied to the surface. Methods of assigning texture coordinates to vertices on a smooth surface are discussed in Section VI.1.2. Once texture coordinates are assigned to vertices on a polygon, it is necessary to interpolate them to assign texture coordinates to rendered pixels: the mathematics behind this is discussed in Section VI.1.1. Texture maps are very prone to bad visual effects from aliasing; this can be controlled by "mipmapping" and other techniques, as is discussed in Section VI.1.3. Section VI.2 discusses bump mapping, and Section VI.3 discusses environment mapping. The remaining sections in this

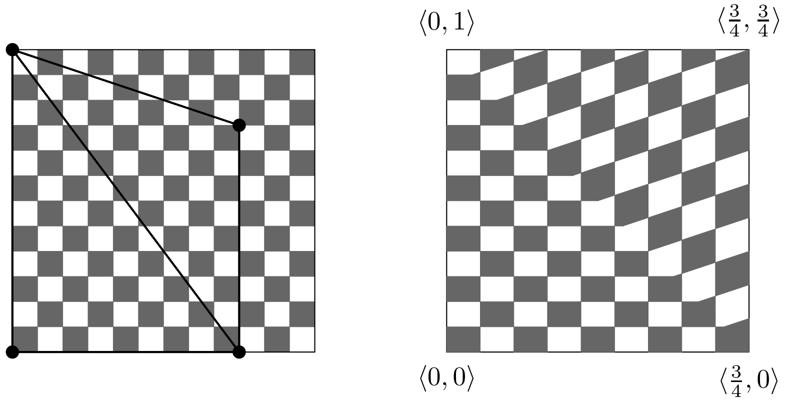
$\langle 0,1\rangle$
$\langle \frac{3}{4},\frac{3}{4}\rangle$
$\langle 0,0\rangle$
$\langle \frac{3}{4},0\rangle$

Figure VI.1: The square on the left is a texture map. The square on the right is filled with a quadrilateral region of this texture map. The coordinates labeling the corners of the square are s, t values indexing into the texture map. The subregion of the checkerboard texture map selected by the s and t coordinates is shown in the left square. This subregion of the texture map was converted to two triangles first, and each triangle was mapped by linear interpolation into the corresponding triangle in the square on the right: this caused the visible diagonal boundary between the triangles.

chapter cover applying a texture map in OpenGL and other practical aspects of texture mapping.

VI.1.1 Interpolating a texture to a surface

The first step in applying a two dimensional texture map to a polygonally modeled surface is to assign texture coordinates to the vertices of the polygons: that is to say, to assign s and t values to each vertex. Once this is done, texture coordinates for points in the interior of the polygon may be calculated by interpolation. If the polygon is a triangle (or is triangulated), then you may use barycentric coordinates to linearly interpolate the values of the s and t coordinates across the triangle. If the polygon is a quadrilateral, you may use bilinear interpolation to interpolate the values of s and t across the interior of the quadrilateral. The former process (barycentric coordinates is shown in Figure VI.1 where a quadrilateral is textured with a region of a checkerboard texture map; the distortion is caused by the fact that the s and t coordinates do not select a region of the texture map which is the same shape as the quadrilateral. The distortion is different in the upper right and the lower left halves of the quadrilateral: this is because the polygon was triangulated, and the linear interpolation of the texture coordinates was applied independently to the two triangles.

For either linear or bilinear interpolation of texture coordinates, it is almost always a good idea to include the hyperbolic interpolation correction which

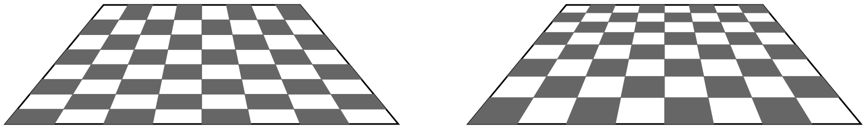

Without hyperbolic interpolation With hyperbolic interpolation

Figure VI.2: Rendering a checkerboard with perspective as a single quadrilateral using bilinear interpolation. The figure on the right uses hyperbolic interpolation to render the correct perspective foreshortening. The figure on the left does not.

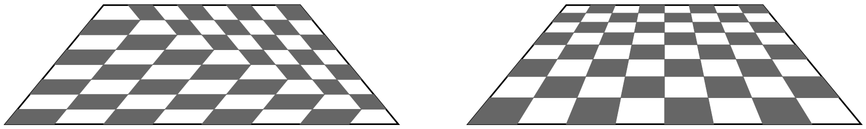

Without hyperbolic interpolation With hyperbolic interpolation

Figure VI.3: Rendering a checkerboard with perspective as two triangles using linear interpolation (barycentric cordinates). The figure on the right uses hyperbolic interpolation to render the correct perspective foreshortening. The figure on the left does not.

compensates for the change in distance affecting the rate of change of texture coordinates. When a perspective projection is used, hyperbolic interpolation corrects for the difference between interpolating in screen coordinates and interpolating in the coordinates of the 3-D model.

A subtle example of the advantage of hyperbolic interpolation is shown in Figure VI.2, where hyperbolic interpolation makes more distant squares be correctly foreshortened. Figure VI.2 uses bilinear interpolation to render the entire square region of a checkerboard as a single quadrilateral. For this reason, the errors introduced by not using hyperbolic interpolation (in the figure on the right) are hard to see at first glance. However, OpenGL does not render quadrilaterals; it only renders triangles. Rendering triangles without using hyperbolic interpolation can cause dramatically bad results; an example is shown in Figure VI.3.

The reason Figure VI.3 looks so bad without hyperbolic interpolation is that the square checkerboard has been split into two triangles, and each triangle has been separately texture mapped with out taking perspective into account. Note that the squares inside the two texture maps have edges parallel to the sides of the large triangles they are contained in. The C++ program *NoPerspective* at the book's web site provides interactive demonstration showing the checkerboard of Figure VI.3.

Clearly hyperbolic interpolation can give much better results than non-hyperbolic interpolation. For this reason, OpenGL uses hyperbolic interpolation by default; however, non-hyperbolic interpolation can be invoked using the `noperspective` qualifier. For more on this, see Section V.7. Refer to Section V.5 for the mathematics of hyperbolic interpolation.

VI.1.2 Assigning texture coordinates

We next discuss some of the issues involved in assigning texture coordinates to vertices on a surface. In many cases, the choice of texture coordinates is a little ad-hoc and depends greatly on the type of surface and the type of texture, etc. Since most surfaces are not flat, but we usually work with flat two dimensional textures, there is often no single best method of assigning texture coordinates. We will deal with only some of the simplest examples of how texture map coordinates are assigned: namely, for cylinders, for spheres, and for tori. We also discuss some of the common pitfalls in assigning texture coordinates. For more sophisticated mathematical tools that can aid the process of assigning texture coordinates to more complex surfaces, consult the article by Bier and Sloane [12] or the textbook [119].

First, consider the problem of mapping a texture map onto a shape whose faces are flat surfaces, for example, a cube. Since the faces are flat and a two dimensional texture map is flat, the process of mapping the texture map to one of the faces of the cube does not involve any nonlinear stretching or distortion of the texture map. For a simple situation such as a cube, one can usually just set the texture coordinates explicitly by hand. Of course, a single vertex on a cube belongs to three different faces of the cube, so it generally is necessary to draw the faces of the cube independently, so as to use the appropriate texture maps and different texture coordinates for each face.

To apply texture maps to surfaces other than individual flat faces, it is convenient if the surface can be parametrically defined by some function $\mathbf{p}(u,v)$, where $\langle u,v\rangle$ ranges over some region of $\mathbb{R}^2$. In most cases, one sets the texture coordinates s and t as functions of u and v, but more sophisticated applications might also let the texture coordinates depend on $\mathbf{p}(u,v)$ and/or the surface normal.

For the first example of a parametrically defined surface, consider how to map texture coordinates onto the surface of a cylinder. We will pay attention only to the problem of how to map a texture onto the side of the cylinder, not onto the top or bottom face. Suppose the cylinder has height h and radius r, and that we are trying to cover the side of the cylinder by a texture map that wraps around the cylinder, much as a label on a food can wraps around the can (see Figure VI.4). The cylinder's side surface can be parametrically defined with the variables θ and y with the function

$$\mathbf{p}(\theta,y) \;=\; \langle r\sin\theta, y, r\cos\theta\rangle,$$

which places the cylinder in "standard" position with its center at the origin

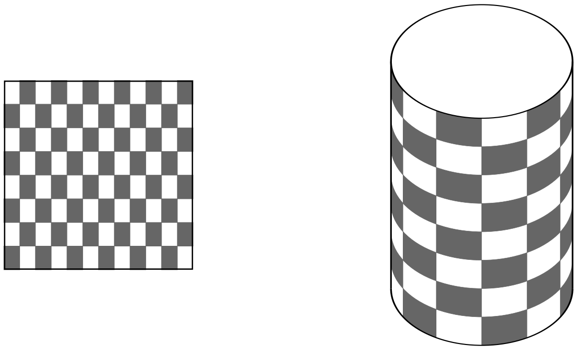

Figure VI.4: A texture map and its application to a cylinder.

and with the y-axis as the central axis of the cylinder. We let y range from $-h/2$ to $h/2$ so the cylinder has height h.

One of the most natural choices for assigning texture coordinates to the cylinder would be to use

$$s = \frac{\theta}{360} \qquad \text{and} \qquad t = \frac{y+h/2}{h}. \tag{VI.1}$$

This lets s vary linearly from 0 to 1 as θ varies from 0 to 360° (we are still using degrees to measure angles) and lets t vary from 0 to 1 as y varies from $-h/2$ to $h/2$. This has the effect of pasting the texture map onto the cylinder without any distortion beyond being scaled to cover the cylinder; the right and left boundaries meet at the front of the cylinder along the line where $x = 0$ and $z = r$.

Exercise VI.1. How should the cylinder texture coordinates be assigned to have the left and right boundaries of the texture map meet at the line at the rear of the cylinder where $x = 0$ and $z = -r$?

Although mapping texture coordinates to the cylinder is very straightforward, there is one potential pitfall that can arise when drawing a patch on the cylinder that spans the line where the texture boundaries meet. This is best explained with an example. Suppose we are drawing the patch shown in Figure VI.5, which has vertices $\mathbf{x}$, $\mathbf{y}$, $\mathbf{z}$, and $\mathbf{w}$. For $\mathbf{x}$ and $\mathbf{w}$, the value of θ is, say, $324° = 360° - 36°$, and, for $\mathbf{y}$ and $\mathbf{z}$, the value of θ is $36°$. Now if you compute the texture coordinates with $0 \le s \le 1$, then we get $s = 0.9$ for the texture coordinate of $\mathbf{x}$ and $\mathbf{w}$ and $s = 0.1$ for the points $\mathbf{y}$ and $\mathbf{z}$. This would have the unintended effect of mapping the long cross-hatched rectangular region of the texture map shown in Figure VI.5 into the patch on the cylinder.

In order to fix this problem, one should use a texture map that repeats, or "wraps around." A repeating texture map is an infinite texture map that covers the entire st-plane by tiling the plane with infinitely many copies of the

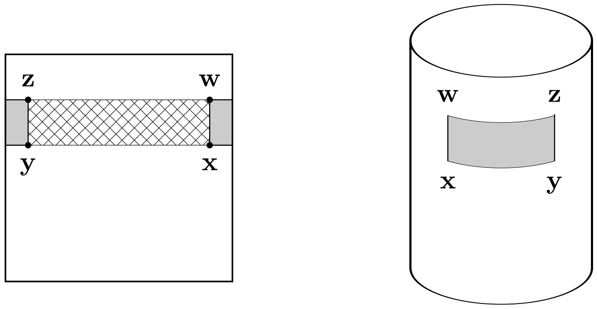

Figure VI.5: The quadrilateral $\mathbf{x}$, $\mathbf{y}$, $\mathbf{z}$, $\mathbf{w}$ selects a region of the texture map. The crosshatched region of the texture map is *not* the intended region of the texture map. The shaded area is the intended region.

texture map. Then, you can let $s = 0.9$ for $\mathbf{x}$ and $\mathbf{w}$, and $s = 1.1$ for $\mathbf{y}$ and $\mathbf{z}$. Or you can use $s = -0.1$ and $s = 0.1$, respectively, or, more generally, you can add on any integer amount to the s values. Of course this means that you need to use a certain amount of care in how you assign texture coordinates. Recall from Section III.3.2 that small roundoff errors in positioning a vertex can cause pixel-sized gaps in surfaces. Because of this, it is important that any point which is specified more than once by virtue of being part of more than one surface patch, always has its position specified with exactly the same θ and y value. The calculation of the θ and y values must be done in exactly the same method each time to avoid roundoff error. However, the same point may be drawn multiple times with different texture values. An example of this is the point $\mathbf{y}$ of Figure VI.5, which may need $s = 0.1$ sometimes and $s = 1.1$ sometimes. In particular, the texture coordinates s and t are not purely functions of θ and y; so you need to keep track of the 'winding number,' i.e., the number of times that the cylinder has been wound around.

There is still a residual risk that roundoff error may cause $s = 0.1$ and $s = 1.1$ to correspond to different pixels in the texture map. This would be expected to only rarely cause serious visible defects in the image.

We now turn to the problem of assigning texture coordinates to a sphere. Unlike the case of a cylinder, a sphere is *intrinsically curved*, which means that there is no way to cover (even part of) a sphere with a flat piece paper without causing the paper to stretch, fold, tear, or otherwise distort. This is also a problem faced by map makers, since it means there is no completely accurate, distortion-free way to represent the surface of the Earth on a flat map. (The Mercator map is an often used method to map a spherical surface to a flat map, but suffers from the problem of distorting relative sizes, as well as from the fact that it cannot be used to map all the way to the poles.)

The problem of assigning texture coordinates to points on a sphere is the problem faced by map makers, but in reverse: instead of mapping points on the sphere to a flat map, we are assigning points from a flat texture map onto a sphere. The sphere can be naturally parameterized in by variables θ and φ using the parametric function

$$\mathbf{p}(\theta,\varphi) \;=\; \langle r\sin\theta\cos\varphi, r\sin\varphi, r\cos\theta\cos\varphi\rangle.$$

Here, θ represents the heading angle (i.e., the rotation around the y-axis), and φ represents the azimuth or "pitch" angle. As the value of θ varies from 0° to 360°, and the value of φ ranges from -90° to 90°, the points $\mathbf{p}(\theta,\varphi)$ sweep out all of the sphere.

The first natural choice for assigning texture map coordinates would be

$$s \;=\; \frac{\theta}{360} \qquad \text{and} \qquad t \;=\; \frac{\varphi}{180}+\frac{1}{2}. \tag{VI.2}$$

This assignment works relatively well.

A second choice for assigning texture coordinates would be to use the y value in place of the φ value for t. Namely,

$$s \;=\; \frac{\theta}{360} \qquad \text{and} \qquad t \;=\; \frac{\sin\varphi}{2}+\frac{1}{2}. \tag{VI.3}$$

This assignment is called the "central cylindrical projections" and acts by mapping the sphere orthogonally outward to the surface of a cylinder and then unwrapping the cylinder to a flat rectangle. One advantage of this second map is that it is area preserving; but the disadvantage is that regions around the poles are badly distorted.

Figure VI.6 shows a checkerboard pattern applied to a sphere with the two texture coordinate assignment functions. Both methods of assigning texture coordinates suffer from the problem of bunching up at the poles of the sphere. Since the sphere is intrinsically curved, some kind of behavior of this type is unavoidable.

Finally, we consider the problem of how to apply texture coordinates to the surface of a torus. Like the sphere, the torus is intrinsically curved, so any method of assigning texture map coordinates on a torus must involve some distortion. Recall from Exercise IV.3 on page 152 that the torus has the parametric equation

$$\mathbf{p}(\theta,\varphi) \;=\; \langle (R+r\cos\varphi)\sin\theta, r\sin\varphi, (R+r\cos\varphi)\cos\theta\rangle,$$

where R is the major radius, r is the minor radius, and both θ and φ range from 0° to 360°. The most obvious way to assign texture coordinates to the torus would be

$$s \;=\; \frac{\theta}{360} \qquad \text{and} \qquad t \;=\; \frac{\varphi}{360}. \tag{VI.4}$$

Figure VI.7 illustrates the application of a checkerboard texture map to a torus.

Exercise VI.2. Where would the center of the texture map appear on the torus under the above assignment of texture coordinates to the torus? How would you change the assignment so as to make the center of the texture map appear at the front of the torus (on the positive z-axis)?

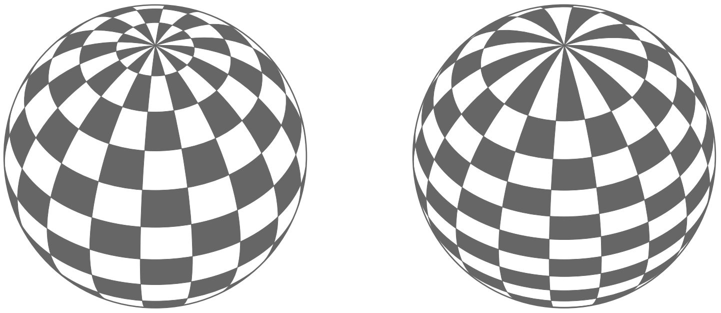

Figure VI.6: Two applications of a texture map to a sphere. The sphere on the left has a checkerboard texture applied with texture coordinates given by the spherical map of Equation (VI.2). The sphere on the right uses texture coordinates given by the cylindrical projection of Equation (VI.3). The spheres are drawn with a tilt and a small rotation.

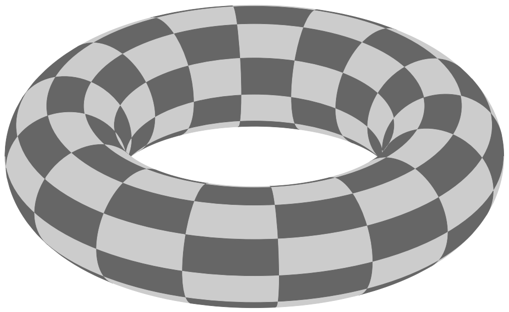

Figure VI.7: A checkerboard texture map applied to a torus.

VI.1.3 Mipmapping and anti-aliasing

Texture maps often suffer from problems with aliasing. The term 'aliasing' means, broadly speaking, any problem that results from conversion between digital and analog, or from conversion between differently sampled digital formats. In the case of texture maps, aliasing problems can occur whenever there is not a one-to-one correspondence between screen pixels and texture pixels. For the sake of discussion, we assume that texture coordinates are interpolated from the vertices of a triangle to give a texture coordinate to each individual pixel in the interior of the triangle. We then assume that the texture coordinates for a screen pixel are rounded to the nearest pixel position in the texture, and that the color of that texture map pixel is displayed on the screen in the given pixel location. In other words, each screen pixel holds the color from a single texture map pixel. We shall shortly discuss better ways to assign color to screen pixels from the texture map colors, but we make this assumption for the moment in order to discuss how this straightforward method of copying from a texture map to the screen leads to problems.

First, consider the case where the texture map resolution is less than the corresponding resolution of the screen. In this case, a single texture map pixel will correspond to a block of pixels on the screen. This will make each texture map pixel appear as a (probably more-or-less rectangularly shaped) region of the screen. The result is a blown-up version of the texture map which shows each pixel as a too-large block.

Second, consider the (potentially much worse) case where the screen pixel resolution is similar to or is less than the resolution of the texture map. At first thought, one might think that this is a good situation, since it means the texture map has plenty of resolution to be drawn on the screen. However, as it turns out, this case can lead to very bad visual effects such as interference and flashing. The problems arise from the fact that each screen pixel is assigned a color from only one texture map pixel. When the texture map pixel resolution is higher than the screen resolution, this means that only a fraction of the texture map pixels are chosen to be displayed on the screen. As a result, several kinds of problems may appear, including unwanted interference patterns, speckled appearance, graininess, or other artifacts. When rendering a *moving* texture map, different pixels from the texture map may be displayed in different frames; this can cause further unwanted visual effects such as strobing, flashing, or scintillating. Similar effects can occur when the screen resolution is slightly higher than the texture map resolution, due to the fact that different texture map pixels may correspond to different numbers of screen pixels.

There are several methods used to fix, or at least partially fix, the aliasing problems with texture maps. We will discuss three of the more common methods: bilinear interpolation, mipmapping, and stochastic supersampling.

Interpolating texture map pixels. One relatively easy way to smooth out the problems that occur when the screen resolution is about the same as the texture map resolution is to bilinearly interpolate the color values from several texture map pixels and use the resulting average color for the screen pixel. This is done by finding the exact s and t texture coordinates for the screen pixel and locating the four pixels in the texture map nearest to the $\langle s,t\rangle$ texture position by rounding s and t both up and down to the nearest integers. Then bilinearly interpolate the four color values in the texture map to set the color for the screen pixel as a weighted average of the four texture map values.

For the case where the texture map resolution is significantly greater (more than twice as great, say) than the screen resolution, then one could use more than just four pixels from the texture map to form an average color to display on the screen. Indeed, from a theoretical point of view, this is more-or-less exactly what you would wish to do: namely, find the region of the texture map which corresponds to a screen pixel and then calculate the average color of the pixels in that region, taking care to properly average in fractions of pixels that lie on the boundary of the region. This can be a potentially expensive process, however, so instead it is common to use ‘mipmapping’ to precompute some of the average colors.

Mipmapping. The term "mipmapping" was coined by Williams [123] who introduced it as a technique of precomputing texture maps of reduced resolution, in other words, as a "level of detail" (LOD) technique. The term "mip" is an acronym for a Latin phrase, *multum in parvo*, or "many in one." Mipmapping tries to avoid the problems that arise when displaying a texture map which has greater resolution than the screen by precomputing a family of lower resolution texture maps and always displaying a texture map whose resolution best matches the screen resolution.

The usual way to create mipmap textures is to start with a high resolution texture map of dimension $N \times M$. It is convenient to assume that N and M are powers of two. Then form a reduced resolution texture map of size $(N/2) \times (M/2)$ by letting the pixel in row i, column j in the reduced resolution texture map be given the average of the four pixels which are in rows $2i$ and $2i+1$ and in columns $2j$ and $2j+1$ of the original texture map. Then recursively apply this process as often as needed to get reduced resolution texture maps of arbitrarily low resolution.

When a screen pixel is to be drawn using a texture map, it can be drawn using a pixel from the mipmapped version of the texture map which has resolution not greater than the resolution of the screen. Thus, when the texture mapped object is viewed from a distance, a low resolution mipmap will be used; whereas, when viewed up close, a high resolution version will be used. This will get rid of many of the aliasing problems, including most problems with flashing and strobing. There can, however, be a problem when the distance from the viewer to the texture mapped surface is changing, since switching from one mipmap version to another can cause a visible "pop" or "jump" in the appearance of the texture map. This can be largely avoided by rendering pixels using the *two* mipmap versions which are closest to the screen resolution, and linearly interpolating between the results of the two texture maps.

A nice side benefit of the use of mipmaps is that it can greatly improve memory usage, provided the mipmap versions of texture maps are properly managed. Firstly, if each mipmap version is formed by halving the pixel dimensions of the previous mipmap, then the total space used by each successive mipmap is only one quarter the space of the previous mipmap. Since

$$1 + \frac{1}{4} + \frac{1}{16} + \frac{1}{64} + \cdots = 1\frac{1}{3},$$

this means that the use of mipmaps incurs only a 33% memory overhead. Even better, in any given scene, there are usually only relatively few texture maps being viewed from a close distance, whereas there may be many texture maps being viewed from a far distance. The more distant texture maps would be viewed at lower resolutions, so only the lower resolution mipmap versions of these need to be stored in the more accessible memory locations (e.g., in the GPU). This allows the possibility of more effectively using memory by keeping only the needed mipmap versions of texture maps available; of course, this may require sophisticated memory management.

One big drawback to mipmapping is that it does not fully address the problem that arises when surfaces are viewed obliquely. In this case, the ratio of the texture map resolution and the screen resolution may be quite different along different directions of the texture map, so no single mipmap version may be fully appropriate. Since the oblique view could come from any direction, there is no good way to generate enough mipmaps to accommodate all view directions.

VI.1.4 Stochastic supersampling

The term *supersampling* refers to rendering an image at a subpixel level of resolution, and then averaging over multiple subpixels to obtain the color value for a single pixel. This technique can be adapted to reduce aliasing with texture maps by combining it with a stochastic, or randomized, sampling method.

The basic idea of non-stochastic supersampling is as follows. First, we divide each pixel into subpixels; for the sake of discussion, we assume each pixel is divided into 9 sub-pixels, but other numbers of subpixels could be used instead. The nine subpixels are arranged in a 3×3 array of square subpixels. We render the image as usual into the subpixels, just as we would usually render the image for pixels, but using triple the resolution. Finally, we take the average of the results for the nine pixels and use this average for the overall pixel color.

Ninefold non-stochastic supersampling can be useful in reducing texture map aliasing problems, or at least in delaying their onset until the resolution of the texture map is about 3 times as high as the resolution of the screen pixels. However, if the texture map contains regular patterns of features or colors, then even with supersampling there can be significant interference effects.

The supersampling method can be further improved by using *stochastic supersampling*. In its simplest form, stochastic supersampling chooses points at random positions inside a pixel, computes the image color at the points, and then averages the colors to set the color value for the pixel. This can cause unrepresentative values for the average if the randomly placed points are clumped poorly, and better results can be obtained by using a *jitter* method to select the supersampling points. The jitter method works as follows: Initially, the supersample points are distributed evenly across the pixel. Then each supersample point is 'jittered', i.e., has its position perturbed slightly. A common way to compute the jitter on nine supersample points is to divide the pixel into a 3×3 array of square subpixels, and then place one supersample point randomly into each subpixel. This is illustrated in Figure VI.8.

It is important that the positions of the supersampling points be jittered independently for each pixel; otherwise, interference patterns can still form.

Jittering is not commonly used for ordinary texture mapping, but is often used for anti-aliasing in non-real-time environments, such as ray traced images. Figure X.9 on page 387 shows an example of jittering in ray tracing. It shows three pool balls on a checkerboard texture; part (a) does not use supersampling, whereas part (b) does. Note the differences in the checkerboard pattern off towards the horizon on the sides of the image.

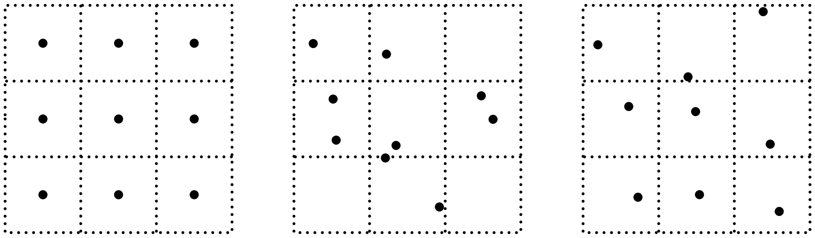

Figure VI.8: In the first figure, the nine supersample points are placed at the centers of the nine subpixels. In the second figure, the points are chosen at random. In the third figure, the points are jittered, namely, are chosen at random but constrained to stay inside their subpixel.

Jittering and other forms of stochastic supersampling decrease aliasing, but at the cost of increased noise in the resulting image. This noise generally manifests itself as a graininess similar to what is seen in a photograph taken at too low light levels. The noise can be reduced by using higher numbers of supersample points.

VI.2 Bump mapping

Bump mapping is used to give a smooth surface the appearance of having bumps or dents. It would usually be prohibitively expensive to model all the small dents and bumps on a surface with polygons since this would require a huge of number of very small polygons. Instead, bump mapping works by using a "height texture" which modifies surface normals. When used in conjunction with Phong lighting, or Cook-Torrance lighting, the changes in lighting caused by the perturbations in the surface normal will give the appearance of bumps or dents.

An example of bump mapping is shown in Figure VI.9. Looking at the silhouette of the torus, you can see that the silhouette is smooth, with no bumps. This shows that the geometric model for the surface is smooth: the bumps are instead an artifact of the lighting in conjunction with perturbed normals.

Bump mapping was first described by Blinn [14], and this section presents his approach to efficient implementation of bump mapping. Suppose we have a surface which is specified parametrically by a function $\mathbf{p}(u,v)$. We also assume that the partial derivatives,

$$\mathbf{p}_u = \frac{\partial \mathbf{p}}{\partial u} \qquad \text{and} \qquad \mathbf{p}_v = \frac{\partial \mathbf{p}}{\partial v},$$

are defined and nonzero everywhere, and that we are able to compute them. (All the points and vectors in our discussion are functions of u and v, even if we do not always indicate this explicitly.) As was discussed in Section IV.3, a

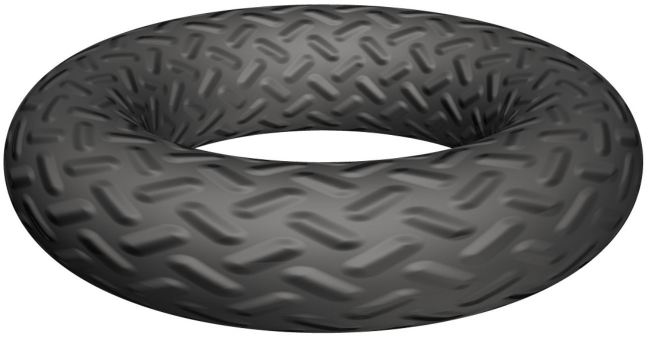

Figure VI.9: A bump mapped torus. Note the lack of bumps on the silhouette. There are four white lights shining on the scene, plus a low level of ambient illumination. This picture was generated with the ray tracing software described in Appendix **??**. See color plate C.8.

unit vector normal to the surface is given by

$$\mathbf{n}(u,v) \;=\; \frac{\mathbf{p}_u \times \mathbf{p}_v}{||\mathbf{p}_u \times \mathbf{p}_v||}.$$

The bump map is a texture map of scalar values $d(u,v)$ which represent displacements in the direction of the normal vector. That is to say, a point on the surface $\mathbf{p}(u,v)$ is intended to undergo a "virtual" displacement of distance $d(u,v)$ in the direction of the normal vector. This process is shown in Figure VI.10. However, remember that the surface is not actually displaced by the texture map, but rather we just imagine the surface as being displaced in order to adjust (only) the surface normals to match the normals of the displaced surface.

The formula for a point on the displaced surface is

$$\mathbf{p}^*(u,v) = \mathbf{p} + d\mathbf{n}.$$

The normals to the displaced surface can be calculated as follows. First, find the partial derivatives to the new surface by

$$\begin{aligned}\frac{\partial \mathbf{p}^*}{\partial u} &= \frac{\partial \mathbf{p}}{\partial u} + \frac{\partial d}{\partial u}\mathbf{n} + d\frac{\partial \mathbf{n}}{\partial u},\\ \frac{\partial \mathbf{p}^*}{\partial v} &= \frac{\partial \mathbf{p}}{\partial v} + \frac{\partial d}{\partial v}\mathbf{n} + d\frac{\partial \mathbf{n}}{\partial v}.\end{aligned}$$

By taking the cross product of these two partial derivatives, we can obtain the normal to the perturbed surface; however, first we simplify the partial

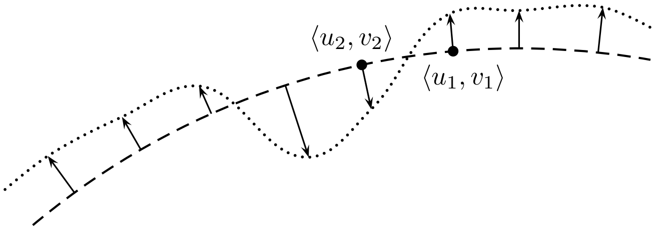

Figure VI.10: The dashed curve represents a cross section of a two dimensional surface. The surface is imagined to be displaced perpendicularly a distance $d(u, v)$ to form the dotted curve. The outward direction of the surface is upward, and thus the value $d(u_1, v_1)$ is positive and the value $d(u_2, v_2)$ is negative.

derivatives by dropping the last terms to obtain the approximations

$$\begin{aligned} \frac{\partial \mathbf{p}^*}{\partial u} &\approx \frac{\partial \mathbf{p}}{\partial u} + \frac{\partial d}{\partial u}\mathbf{n}, \\ \frac{\partial \mathbf{p}^*}{\partial v} &\approx \frac{\partial \mathbf{p}}{\partial v} + \frac{\partial d}{\partial v}\mathbf{n}. \end{aligned}$$

We can justify dropping the last term on the grounds that the displacement distances $d(u, v)$ are small since only small bumps and dents are being added to the surface, and that the partial derivatives of $\mathbf{n}$ are not too large if the underlying surface is relatively smooth. Note, however, that the partial derivatives $\partial d/\partial u$ and $\partial d/\partial v$ cannot be assumed to be small since the bumps and dents would be expected to have substantial slopes. With this approximation, we can approximate the normal of the displaced surface by calculating

$$\begin{aligned} \mathbf{m} &\approx \left(\frac{\partial \mathbf{p}}{\partial u} + \frac{\partial d}{\partial u}\mathbf{n}\right) \times \left(\frac{\partial \mathbf{p}}{\partial v} + \frac{\partial d}{\partial v}\mathbf{n}\right) \\ &= \left(\frac{\partial \mathbf{p}}{\partial u} \times \frac{\partial \mathbf{p}}{\partial v}\right) + \left(\frac{\partial d}{\partial u}\mathbf{n} \times \frac{\partial \mathbf{p}}{\partial v}\right) - \left(\frac{\partial d}{\partial v}\mathbf{n} \times \frac{\partial \mathbf{p}}{\partial u}\right). \qquad \text{(VI.5)} \end{aligned}$$

The vector $\mathbf{m}$ is perpendicular to the displaced surface, but is not normalized: the unit vector normal to the displaced surface is then just $\mathbf{n}^* = \mathbf{m}/||\mathbf{m}||$.

Note that equation (VI.5) uses only the partial derivatives of the displacement function $d(u, v)$; the values $d(u, v)$ are not directly needed at all. One way to compute the partial derivatives is to approximate them using finite differences. However, a simpler and more straightforward method is to not store the displacement function values themselves, but to instead save the partial derivatives as two scalar values in the texture map.

The algorithm for computing the perturbed normal $\mathbf{n}^*$ will fail when either of the partial derivatives $\partial\mathbf{p}/\partial u$ or $\partial\mathbf{p}/\partial v$ is equal to zero. This happens for exceptional points on many common surfaces; for instance, at the north and south poles of a sphere using either the spherical or the cylindrical parameterization. Thus, you need to be careful when applying a bump map in the neighborhood of a point where a partial derivative is zero.

The above discussion assumed that the bump map displacement distance d is given as a function of the variables u and v. It is sometimes more convenient to have a bump map displacement distance function $D(s,t)$ which is a function of the texture coordinates s and t. The texture coordinates are of course functions of u and v, i.e., we have $s = s(u,v)$ and $t = t(u,v)$, expressing s and t as either linear or bilinear functions of u and v. Then the bump map displacement function $d(u,v)$ is equal to $D(s(u,v),t(u,v))$. The chain rule then tells us that

$$\begin{aligned}\frac{\partial d}{\partial u} &= \frac{\partial D}{\partial s}\frac{\partial s}{\partial u} + \frac{\partial D}{\partial t}\frac{\partial t}{\partial u}\\ \frac{\partial d}{\partial v} &= \frac{\partial D}{\partial s}\frac{\partial s}{\partial v} + \frac{\partial D}{\partial t}\frac{\partial t}{\partial v}.\end{aligned}$$

The partial derivatives of s and t are either constant in a given u,v-patch in the case of linear interpolation, or can be found from Equation (V.19) on page 197 in the case of bilinear interpolation.

Bump mapped surfaces can have aliasing problems when viewed from a distance, particularly when the distance is far enough that the bumps are rendered at about the size of an image pixel or smaller. As usual, stochastic supersampling can reduce aliasing. A more ad hoc solution is to reduce the height of the bumps gradually based on the level of detail at which the bump map is being rendered; however, this does not accurately render the specular highlights from the bumps.

There is no built-in support for bump mapping in OpenGL, but it can be implemented in a shader program in the pixel shader.

XXX ADD A COMMENT THAT BUMP MAPPING IS USED IN CONJUNCTION WITH PHONE SHADING, NOT GOURAUD SHADING.

VI.3 Environment mapping

Environment mapping, also known as “reflection mapping,” is a method of rendering a shiny surface showing a reflection of a surrounding scene. Environment mapping is relatively cheap compared to the global ray tracing discussed later in Chapter X, but can still give good effects, at least for relatively compact shiny objects.

The general idea of environment mapping is as follows: We assume we have a relatively small, reflecting object. A small, flat mirror or spherical mirror (such as on a car’s passenger side door), or a compact object with a mirror-like surface such as a shiny teapot, chrome faucet, toaster, or silver goblet would be typical

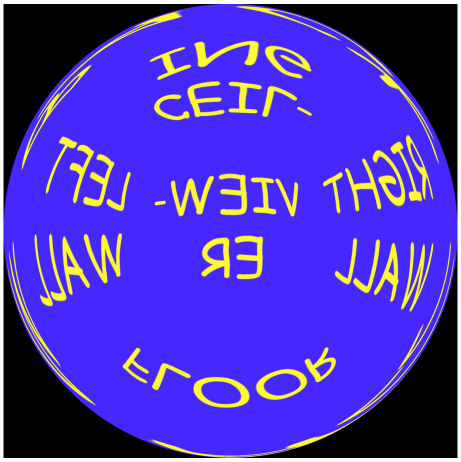

Figure VI.11: An environment map mapped into a sphere projection. This was the kind of environment map supported by "legacy" OpenGL. The scene is the same as is shown in Figure VI.12. Note that the front wall has the most fidelity, and the back wall the least. For this reason, spherical environment maps are best used when the view direction is close to the direction used to create the environment map. See color plate C.9.

examples. We then obtain, either from a photograph or by computer-rendering, a view of the world as seen from the center position of the mirror or object. From this view of the world, we create a texture map showing what is visible from the center position. Simple examples of such texture maps are shown in Figures VI.11 and VI.12.

When rendering a vertex on the reflecting object, one can use the viewpoint position, the vertex position, and surface normal to calculate a *view reflection direction*. The view reflection direction is the direction of perfect reflection from the viewpoint; i.e., a ray of light emanating from the viewer's position to the vertex on the reflecting object would reflect in the view reflection direction. From the view reflection direction, one calculates the point in the texture map which corresponds to the view reflection direction. This gives the texture coordinates for the vertex.

The two most common ways of representing environment maps are shown in Figures VI.11 and VI.12. The first figure shows the environment map holding the "view of the world" in a circular area. This is the same as you would see reflected from a perfectly mirror-like small sphere viewed orthogonally (from a point at infinity). The mathematics behind calculating the environment map texture coordinates is discussed a little more in Section VI.4.3 below.

The second figure shows the environment map comprising six square regions corresponding to the view seen through the six faces of a cube centered at the environment mapped object. This "box" environment map has a couple

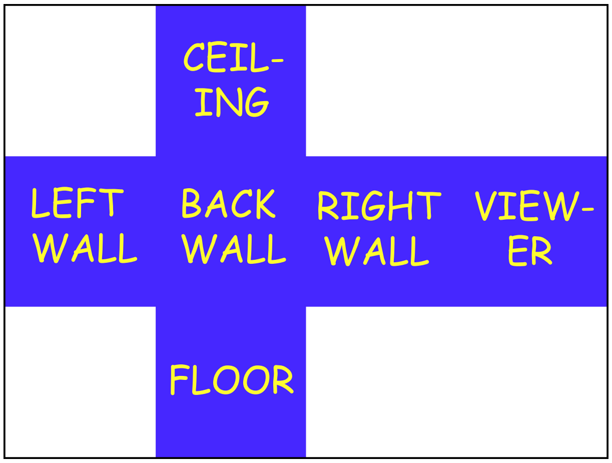

Figure VI.12: An environment map mapped into a box projection consists of the six views from a point, mapped to the faces of a cube and then unfolded to make a flat image. This scene shows the reflection map from the point at the center of a room. The room is solid blue, except for yellow writing on the walls, ceiling and floor. The rectangular white regions of the environment map are not used. See color plate C.10.

advantages over the former "sphere" environment map. Firstly, it can be generated for a computer rendered scene using standard rendering methods, by just rendering the scene six times from the viewpoint of the object, in the direction of the six faces of a cube. Secondly, the "box" environment map can be used effectively from any view direction, whereas the "sphere" environment map can be used only from view directions close to the direction from which the environment was formed.

Exercise VI.3. Derive formulas and an algorithm for converting the view reflection direction into texture coordinates for the "box" environment map. Make any assumptions necessary for your calculations.

An interesting, and fairly common, use of environment mapping is to add specular highlights to a surface. For this, one first creates an environment texture map which holds an image of the specular light levels in each reflection direction. The specular light from the environment map can then be added to the rendered image based on the reflection direction at each point. A big advantage of this approach is that the specular reflection levels from multiple lights can be precomputed and stored in the environment map: the specular light can then be added late in the graphics pipeline without needing to perform specular lighting calculations again.

VI.4 Texture mapping in OpenGL

We now discuss the most basic usages of texture mapping in OpenGL. There are three sample programs supplied, `TextureBMP`, `FourTextures`, and `TextureTorus`, that illustrate simple uses of texture mapping. You should refer to these programs and their accompanying online documentation as you read the descriptions of the OpenGL commands below.

VI.4.1 Loading a texture map

To use a texture map in OpenGL, you must first build an array holding the values of the texture map. This array will typically hold color values, but can also hold values such as luminance, intensity, or alpha (transparency) values. OpenGL allows you to use a number of different formats for the values of the texture map, but the most common formats are floating point numbers (ranging from 0 to 1) or unsigned 8-bit integers (ranging from 0 to 255).

Once you have loaded the texture map information into an array, you must call an OpenGL routine for OpenGL to load the texture map into a "texture object." The most basic method for this is to call the routine `glTexImage2D`. A typical use of `glTexImage2D` might have the following form, with `pixelArray` an array of `float`'s holding the texture map data:

```
glPixelStorei(GL_UNPACK_ALIGNMENT, 1);
glTexImage2D( GL_TEXTURE_2D, 0, GL_RGBA, textureWidth, textureHeight,
                0, GL_RGBA, GL_FLOAT, pixelArray );
```

Another typical usage, with the data in `pixelArray` stored in unsigned bytes (`unsigned char`'s), has the form

```
glPixelStorei(GL_UNPACK_ALIGNMENT, 1);
glTexImage2D( GL_TEXTURE_2D, 0, GL_RGB, textureWidth, textureHeight,
                0, GL_RGB, GL_UNSIGNED_BYTE, pixelArray );
```

The call to `glPixelStorei` tells OpenGL not to expect any particular alignment of the texture data in the pixel array. (This is actually needed only for data stored in byte formats rather than floating point format.)

The parameters to `glTexImage2D` have the following meanings: The first parameter, `GL_TEXTURE_2D`, specifies that a two dimensional texture is being loaded. The second parameter specifies the mipmapping level of the texture; the highest resolution image is level 0. The third parameter specifies what values are stored in the internal OpenGL texture map object: `GL_RGB` and `GL_RGBA` indicate that color (and alpha) values are stored. The next two parameters specify the width and height of the texture map in pixels; the minimum dimension of a texture map (for level 0) is 64×64. The sixth parameter is 0 or 1, indicating whether there is a border strip of pixels added to the texture map; the value 0 indicates no border. The seventh and eighth parameters indicate the format of the texture values as stored in the array of texture information. The last parameter is a pointer to the array of texture values.

There are a huge number of options for the `glTexImage2D` command, and you should refer to the OpenGL documentation for more information.

Frequently, one wants to also generate mipmap information for textures. Fortunately, OpenGL has a utility routine `gluBuild2DMipmaps` which does all the work of generating texture maps at multiple levels of resolution for you: this makes the use of mipmapping completely automatic. The mipmap textures are generated by calling (for example):

```
gluBuild2DMipmaps( GL_TEXTURE_2D, GL_RGBA, textureWidth,
                   textureHeight, GL_RGBA, GL_FLOAT, pixelArray );
```

The parameters to `gluBuild2DMipmaps` have the same meanings as the parameters to `glTexImage2D`, except that the level parameter is omitted, since the `gluBuild2DMipmaps` is creating all the levels for you, and borders are not supported. `gluBuild2DMipmaps` checks how much texture memory is available and decreases the resolution of the texture map if necessary; it also re-scales the texture map dimensions to the nearest powers of two. It then generates all the mipmap levels down to a 1×1 texture map. It is a very useful routine and is highly recommended, at least for casual users.

OpenGL texture maps are always accessed with s and t coordinates that range from 0 to 1. If texture coordinates outside the range $[0, 1]$ are used, then OpenGL has several options of how they are treated: first, in `GL_CLAMP` mode, values of s and t outside the interval $[0, 1]$ will index into a one pixel wide border of the texture map, or, if there is no border, then the pixels on the edge of the texture are used instead. Second, `GL_CLAMP_TO_EDGE` mode clamps s and t to lie in the range 0 to 1: this acts like `GL_CLAMP` except that if a border is present, it is ignored. Finally, `GL_REPEAT` makes the s and t wrap around; i.e., the fractional part of s or t is used; that is to say, $s - \lfloor s \rfloor$ and $t - \lfloor t \rfloor$ are used in "repeat" mode. The modes may be set independently for the s and t texture coordinates with the following command:

$$\texttt{glTexParameteri(GL\_TEXTURE\_2D, } \left\{\begin{matrix}\texttt{GL\_TEXTURE\_WRAP\_S}\\ \texttt{GL\_TEXTURE\_WRAP\_T}\end{matrix}\right\}\texttt{, } \left\{\begin{matrix}\texttt{GL\_REPEAT}\\ \texttt{GL\_CLAMP}\\ \texttt{GL\_CLAMP\_TO\_EDGE}\end{matrix}\right\}\texttt{);}$$

The default, and most useful, mode is the "repeat" mode for s and t values.

Section VI.1.3 above discussed the methods of averaging pixel values and of using mipmaps with multiple levels of detail to (partly) control aliasing problems and prevent interference effects and 'popping.' When only a single texture map level is used, with no mipmapping, the following OpenGL commands allow the averaging of neighboring pixels to be enabled or disabled:

$$\texttt{glTexParameteri(GL\_TEXTURE\_2D, }\left\{\begin{matrix}\texttt{GL\_TEXTURE\_MAG\_FILTER}\\ \texttt{GL\_TEXTURE\_MIN\_FILTER}\end{matrix}\right\}\texttt{, }\left\{\begin{matrix}\texttt{GL\_NEAREST}\\ \texttt{GL\_LINEAR}\end{matrix}\right\}\texttt{);}$$

The option `GL_NEAREST` instructs OpenGL to set a screen pixel color with just a single texture map pixel. The option `GL_LINEAR` instructs OpenGL to set the screen pixel by bilinearly interpolating from the immediately neighboring pixels in the texture map. The settings for "`GL_TEXTURE_MIN_FILTER`" apply when the screen pixel resolution is less than (that is, coarser than) the texture map resolution. The setting for "`GL_TEXTURE_MAG_FILTER`" applies when the screen resolution is higher than the texture map resolution.

When mipmapping is used, there is an additional option to set. OpenGL can be instructed either to use the "best" mipmap level, i.e., the one whose resolution is closest to the screen resolution, or to use linear interpolation between the two best mipmap levels. This is controlled with the following command:

$$\begin{array}{l}\texttt{glTexParameteri(GL\_TEXTURE\_2D,}\\ \qquad\qquad\qquad\texttt{GL\_TEXTURE\_MIN\_FILTER, }\left\{\begin{matrix}\texttt{GL\_NEAREST\_MIPMAP\_NEAREST}\\ \texttt{GL\_LINEAR\_MIPMAP\_NEAREST}\\ \texttt{GL\_NEAREST\_MIPMAP\_LINEAR}\\ \texttt{GL\_LINEAR\_MIPMAP\_LINEAR}\end{matrix}\right\}\texttt{);}\end{array}$$

This command is really setting two options at once. The first '`NEAREST`' or '`LINEAR`' controls whether only one pixel is used from a given mipmap level, or whether neighboring pixels on a given mipmap level are averaged. The second part, '`MIPMAP_NEAREST`' or '`MIPMAP_LINEAR`', controls whether only the best mipmap level is used, or whether the linear interpolation of two mipmap levels is used.

OpenGL has a number of additional advanced features that give you fine control over mipmapping; for documentation on these, you should again consult the OpenGL programming manual.

VI.4.2 Managing multiple texture maps

OpenGL provides a simple mechanism to manage multiple texture maps as "texture objects." This allows your program to load or create multiple texture maps, and give them to OpenGL to be stored in OpenGL's texture memory. We sketch below the basic functionality of texture objects in OpenGL; you should look at the `FourTextures` program supplied with this book to see an example of how to use multiple texture maps in OpenGL.

The OpenGL commands for handling multiple texture maps are `glGenTextures()`, `glBindTexture()`, and `glDeleteTextures()`. The `glGenTextures` command is used to get the names (actually, integer indices) for one or more new texture objects. This has the effect of reserving texture map names for future use. The `glBindTexture()` function takes a texture map name as input and makes that texture the currently active texture map. Subsequent uses of commands such as `glTexImage*()`, `glTexParameter*()`, `gluBuild2DMipmaps()`, `glTexCoord*()`, etc., will apply to the currently active texture map.

To reserve new names for texture objects, use commands such as

```
GLuint textureNameArray[N];
glGenTextures( N , textureNameArray );
```

where N is the integer number of texture names which are requested. The call to `glGenTextures()` returns N texture names in the array. Each texture name is a `GLuint`, an unsigned integer. The texture name 0 is never returned by `glGenTextures`; instead, 0 is the texture name reserved for the default texture object.

To select a 2-D texture object, use the command

```
glBindTexture( GL_TEXTURE_2D, textureName );
```

The second parameter, `textureName`, is a `GLuint` unsigned integer which names a texture. When `glBindTexture` is called as above for the first time with a given `textureName` value, it sets the texture type to 2-D and sets the various parameters. On subsequent calls, it merely selects the texture object as the current texture object. It is also possible to use `GL_TEXTURE_1D` or `GL_TEXTURE_3D`: refer to the OpenGL documentation for information on one dimensional and three dimensional texture maps.

A texture object is freed with the command

```
glDeleteTextures( N , textureNameArray );
```

which frees the N texture names in the array pointed to by the second parameter.

VI.4.3 Environment mapping in OpenGL

This section describes features of "legacy OpenGL" and is not applicable for "modern OpenGL".

Rewrite to (a) show how a fragment shader accesses a usual texture map. (b) how it accesses a box environment map.

XXXX Outline??

1. Accessing an ordinary texture map

2. Accessing an environment map. 2.a. Using surface normals for the direction. 2.b. Using reflection direction for the direction.

OpenGL supports the spherical projection version of environment maps (see Section VI.3). The OpenGL programming manual [126] suggests the following procedure for generating a texture map for environment mapping: take a photograph of a perfectly reflecting sphere with a camera placed an infinite distance away; then scan in the resulting photograph. This, of course, is not entirely practical, but it is mathematically equivalent to what should be done to generate the texture map for OpenGL environment mapping.

To turn on environment mapping in OpenGL, you need to give the following commands (in addition to enabling texture mapping and loading a texture map):

```
glTexGeni(GL_S, GL_TEXTURE_GEN_MODE, GL_SPHERE_MAP);
glTexGeni(GL_T, GL_TEXTURE_GEN_MODE, GL_SPHERE_MAP);
glEnable(GL_TEXTURE_GEN_S);
glEnable(GL_TEXTURE_GEN_T);
```

When rendering an object with an environment map, the surface normal direction, the viewpoint, and the view direction are used to determine the texture coordinates.

If the viewer is not local, i.e., if the view direction is fixed to be $\langle 0, 0, -1\rangle$ with the viewer positioned at a point at infinity, then texture coordinates are generated in the following way: If the normal to the surface is equal to the unit vector $\langle n_x, n_y, n_z\rangle$, then the s and t texture coordinates are set equal to

$$s \;=\; \frac{1}{2}n_x + \frac{1}{2} \qquad \text{and} \qquad t \;=\; \frac{1}{2}n_y + \frac{1}{2}. \tag{VI.6}$$

The effect is that the texture coordinates lie in the circle of radius $1/2$, centered at $\langle \frac{1}{2}, \frac{1}{2}\rangle$, so the values for s and t can range as low as 0 and as high as 1. For a sphere, this is the same as projecting the sphere orthogonally into a disk.

For a local viewer, the viewer is by convention placed at the origin, and the position and normal of the surface are used to compute the view reflection direction, i.e, the direction in which a ray of light from the view position would be specularly reflected by the surface. Given the view reflection direction, one then computes the unit vector $\mathbf{n}$ that would cause a *nonlocal* viewer to have the same view reflection direction. The s, t texture coordinates are then set by Equation (VI.6).

The overall effect is that the view reflection direction is used to compute the s, t values which are generated for a nonlocal viewer with the same view reflection direction. That is to say, the texture coordinates s, t are determined by the view reflection direction.

Exercise VI.4* As in the Phong lighting model, let $\mathbf{v}$ be the unit vector in the direction of the viewer and $\mathbf{n}$ be the surface normal. Show that the view reflection direction is in the direction of the unit vector

$$\mathbf{r}' \;=\; 2(\mathbf{n}\cdot\mathbf{v})\mathbf{n} - \mathbf{v}.$$

For a nonlocal viewer, $\mathbf{v}$ would be $\langle 0, 0, 1\rangle$; for a local viewer, the vector $\mathbf{v}$ is the normalization of the position of the point on the surface (since the local viewer is presumed to be positioned at the origin).

Let $\mathbf{r}' = \langle r'_1, r'_2, r'_3\rangle$ be a unit vector in the view reflection direction computed for a local viewer. Show that $\mathbf{n}' = \langle r'_1, r'_2, r'_3 + 1\rangle$ is perpendicular to the surface that gives the nonlocal viewer the same view reflection direction.

The vector $\mathbf{n}'$ of the exercise can be normalized, and then its first two components give the s and t coordinates by the calculation in Equation (VI.6).

Chapter VII

Color

*This is a **preliminary** draft of a second edition of the book* 3-D Computer Graphics: A Mathematical Introduction with OpenGL. *So please read it cautiously and critically! Corrections are appreciated. Draft C.4.a*

Author: Sam Buss, sbuss@ucsd.edu

This chapter briefly discusses some of the issues in color perception and color representation that are important for computer graphics. Color perception and color representation are both complicated topics, and more in-depth information can be found in references such as Berns, Billmeyer and Saltzman [9], Jackson, MacDonald and Freeman [68], Foley et al. [49], Volume I of Glassner [55], or Hall [59]. Also recommended is the short, readable introduction to the physics of color and the physiological aspects of color perception in Feynman [48]. Some more detailed recommendations for further reading are given at the end of this chapter.

The first section of this chapter discusses the physiology of color perception and its implications for computer graphics. The second, more applied section discusses some of the common methods for representing color in computers. The third section discusses gamma correction and the sRGB color space.

VII.1 Color perception

The basic theories of how humans perceive color were formulated already in the nineteenth century. There were two competing theories of color perception, the *trichromatic theory* and the *opponent color theory.* These two theories will appear contradictory at first glance, but in fact they are both correct in that they are grounded in different aspects of human color perception.

The trichromatic theory of vision. The trichromatic theory was formulated by G. Palmer in 1777 and then again by T. Young in 1801, and extended later by Helmholtz. This theory states that humans perceive color in three components: red, green, and blue. Namely, that we see independently the colors red, green, and blue, and that all other colors are formed from combinations of these three primary colors.

It was later discovered that the retina of the eye contains several kinds of light sensitive receptors, called cones and rods because of their shapes. Most people have three kinds of cones: one kind is most sensitive to red light, one to green light, and one to blue light. The fourth kind of light sensitive cell, rods, are mostly used for vision in very low light levels, and for peripheral vision, and do not have the ability to distinguish different colors (thus, in very dark settings, you are unable to see colors, but instead see only shades of gray and dark).

For direct viewing of objects in normal light levels, the cones are the primary color receptors, and, although the cones are each sensitive to a range of colors, the fact that the three different kinds are selectively sensitive more to red, to green, and to blue provides a physiological basis for the trichromatic theory.

The opponent theory of vision. The opponent theory was formulated by Ewald Hering in 1878. It states that humans perceive light in three opposing components: namely, light versus dark, red versus green, and blue versus yellow. This theory accounts for some aspects of our subjective perception of color, such as the fact that one cannot perceive mixtures of red and green or mixtures of blue and yellow (so there are no colors which are reddish green or blueish yellow, for instance). It also accounts for "afterimages"; for example, staring at a red image and then looking away will cause an afterimage in the opposing color, namely, green.

Although this theory would appear to be in conflict with the trichromatic theory, there is in fact a simple explanation of how both theories can be valid. The trichromatic theory applies to the different light sensitivities of cones in the retina, and the opponent color theory reflects the way the cells in the retina process color into signals sent to the brain. Namely, the neurons in the retina encode color in "channels," so that the neural signals from the eyes to the brain have different channels for encoding the amount of light versus dark, the amount of red versus green, and the amount of blue versus yellow.

The trichromatic theory is the main theoretical foundation for computer graphics, whereas the opponent theory seems to have little impact on computer graphics.[1] Indeed, the principal system of color representation is the RGB system, which is obviously based directly on the trichromatic theory. For applications in computer graphics, the main implications of the trichromatic theory are twofold. Firstly, the space of visible colors forms a three dimensional vector space, since colors are differentiated according to how much they stimulate the three kinds of cones.[2] Secondly, characterizing colors as being a

[1] One exception to this is that the opponent theory was used in the design of color encoding for television. In order to suitably compress the resolution of television signals and retain backward compatibility with black and white television transmissions, the opponent theory was used to aid the decision of what information to remove from the color channels.

[2] The opponent theory of color also predicts that the perceivable colors form a three dimensional space.

combination of red, green, and blue light is a fairly good choice, since these colors correspond to the light sensitivities of the different cones.

One consequence of the assumption that perceived colors form a three dimensional space is that there are light sources which have different spectral qualities (i.e., have different intensities of visible light at given wavelengths), but which are indistinguishable to the human eye. This is a consequence of the fact that the set of possible visible light spectra forms an infinite dimensional space. It follows that there must be different light spectra that are equivalent in the sense that the human eye cannot perceive any difference in their colors. This phenomenon is called metamerism.

There have been extensive experiments to determine how to represent different colors as combinations of red, green, and blue light. These experiments use the *tristimulus method* and proceed roughly as follows: Fixed reference light sources with colors red (R), green (G), and blue (B) are chosen as primary colors. Then, for a given color C, one tries to find a way to mix different intensities of the red, green, and blue lights to create a color which is equivalent to (i.e., visually indistinguishable from) the color C. The result is expressed by an equation

$$C \;=\; r_C R + g_C G + b_C B, \tag{VII.1}$$

where r_C, g_C, b_C are scalars indicating the intensities of the red, green, and blue lights. This means that when the three reference lights R, G, and B are combined at the relative intensities given by the three scalars, the resulting light looks identical in color to C. It has been experimentally verified that all colors can be expressed as linear combinations of red, green, and blue in this way.[3] Furthermore, when colors are combined, they act as a vector space. Thus, the combination of two colors C_1 and C_2 is equivalent to the color

$$(r_{C_1} + r_{C_2})R + (g_{C_1} + g_{C_2})G + (b_{C_1} + b_{C_2})B.$$

There is one big, and unfortunate, problem: sometimes the coefficients r_C, g_C, b_C are negative! The physical interpretation of a negative coefficient, say if $b_C < 0$, is that the reference color (blue, say) must be added to the color C to yield a color that is equivalent to a combination of red and green colors. That is to say, the interpretation of negative coefficients on colors is that the formula should be re-arranged by moving terms to the other side of the equality so as to make all coefficients positive.

The reason it is unfortunate that the tristimulus coefficients can be negative is that, since there is no way to make a screen or a drawing emit negative light intensities, it follows that there are some colors that cannot be rendered by a red-blue-green color scheme. That is to say, there are some colors which can be perceived by the human eye, but which cannot be rendered on a computer screen, even in principle, at least as long as the screen is rendering colors

[3] We are describing the standard, idealized model of color perception. The experiments only apply to colors at a constant level of intensity, and the experimental results are not as clear cut as we are making them sound. In addition, there is considerable variation in how different people distinguish colors.

using a system of three primary colors. The same considerations apply to any kind of color printing system based on three primary colors. For this reason, high-quality printing systems use more than three primary colors in order to achieve a broader range of perceptual colors.[4]

So far our discussion has concerned the color properties of light. The color properties of materials are a good deal more complicated. In Chapter IV, the Phong and Cook-Torrance illumination models treated each material as having reflectance properties for the colors red, green, and blue, with each color treated independently. However, a more physically accurate approach would treat every spectrally pure color independently; that is to say, for each wavelength of light, the material has reflectance properties, and these properties vary with the wavelength. This more physically accurate model would allow for *illuminant metamerism*, where two materials may appear to be the same color under one illumination source and to be a different color under another illumination source. There seems to be no way to easily extend the Phong and Cook-Torrance light models to allow for reflectance properties that vary with wavelength, except to use more than three primary colors. This is called *spectral sampling* and is sometimes used for high-quality, photorealistic renderings. For spectral sampling, each light source is treated as consisting of multiple pure components, and each surface has reflectance properties for each of the light components. The illumination equations are similar to what Chapter IV described, but carried out for more wavelengths. At the end, it is necessary to reduce back to three primary colors for printing or display purposes. The book [59] discusses algorithms for spectral sampling due to Hall and to Meyer .

VII.2 Representation of color values

This section discusses some of the principal ways in which colors are represented by computers. We discuss first the general theory of subtractive versus additive colors, then discuss how RGB values are typically encoded. Finally, we discuss alternate representations of color based on hue, saturation, and luminance.

[4] It is curious, to this author at least, that we are relatively unconcerned about the quality of color reproduction. Most people are perfectly happy with the rather low range of colors available from a CRT or a television. In contrast, systems for sound reproduction are widespread, with home stereo systems routinely providing high quality recording and reproduction of audio signals (music) accurately across the full audible spectrum. It is surprising that there has been no corresponding improvement in color reproduction systems for television over time, nor even any demand for such improvement, at least from the general consumer.

It is certainly conceivable that displays with improved color rendition could be developed; for instance, one could envision a display system where each pixel can emit a combination of two narrow spectrum wavelengths of light, with the two wavelengths individually tunable. Such a system would be able to render nearly every perceptual color.

VII.2.1 Additive and subtractive colors

The usual method of displaying red, green, and blue colors on a CRT monitor is called an *additive* system of colors. In an additive system of colors, the base or background color is black, and then varying amounts of three primary colors, usually red, green, and blue, are added. If all three colors are added at full intensity, the result is white. Additive colors are pictured in part (a) of Figure VII.1, where the three circles should be viewed as areas that generate or emit light of the appropriate color. Where two circles overlap, they combine to form a color: red and green together make yellow; green and blue make cyan; and blue and red make magenta. Where all three circles overlap, the color becomes white. The additive representation of color is appropriate for display systems, such as monitors, televisions, or projectors, where the background or default color is black, and where the primary colors are added in to form composite colors.

In the *subtractive* representation of light, the background or base color is white. Each primary color is subtractive, in that it removes a particular color from the light by absorption or filtering. The subtractive primary colors are usually chosen as magenta, cyan, and yellow. Yellow represents the filtering or removal of blue light, magenta the removal of green light, and cyan the removal of red light. Subtractive primaries are relevant for settings such as painting, printing, or film, where the background or default color is white, and where primary colors remove a single color from the white light. In painting, for instance, a primary color consists of a paint which absorbs one color from the light and reflects the rest of the colors in the light. Subtractive colors are illustrated in part (b) of Figure VII.1. You should think of these colors as being in front of a white light source and the three circles are filtering out components of the white light.

There can be confusion between the colors cyan and blue, or the colors magenta and red. Cyan is a light blue or greenish blue, whereas blue is a deep blue. Magenta is a purplish or blueish red; if red and magenta are viewed together, then the red frequently has an orangish appearance. Sometimes, cyan and magenta are referred to as blue and red, and this can lead to confusion over the additive and subtractive roles of the colors.

The letters RGB are frequently used to denote the additive red-green-blue primary colors, and CMY is frequently used for the subtractive cyan-magenta-yellow primary colors. Often, one uses these six letters to denote the intensity of the color on a scale 0 to 1. Then, the nominal way to convert from a RGB color representation to CMY is by the formulas

$$\begin{aligned} C &= 1-R \\ M &= 1-G \\ Y &= 1-B. \end{aligned}$$

We call this the 'nominal' way, because often this gives poor results. The usual purpose of converting from RGB to CMY is to convert an image displayed

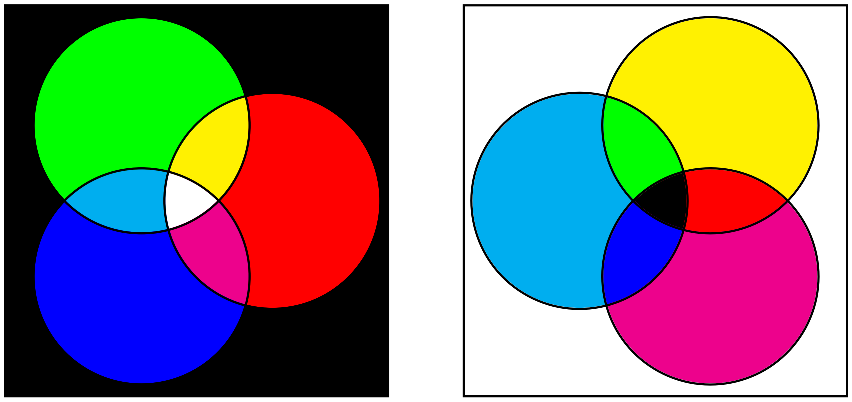
(a) (b)

Figure VII.1: (a) The additive colors are red, green, and blue. (b) The subtractive colors are cyan, magenta, and yellow. See color plate C.4.

on a screen into a printed image. It is, however, very difficult to properly match colors as they appear on the screen with printed colors, and to do this well requires knowing the detailed spectral properties (or color equivalence properties) of both the screen and the printing process. A further complication is that many printers use CMYK colors, which use a K channel in addition to C,M,Y. The value of K represents the level of black in the color, and is printed with a black ink, rather than a combination of primary colors. There are several advantages to using a fourth black color: firstly, black ink tends to be cheaper than combining three colored inks; secondly, less ink needs to be used, so the paper does not get so wet from ink, which saves drying time and prevents damage to the paper; thirdly, the black ink can give a truer black color than is obtained by combining three colored inks.

XXXX PROFESSSIONAL PRINTERS USE EVEN MORE COLORS

VII.2.2 Representation of RGB colors

This section discusses the common formats for representing RGB color values in computers. An RGB color value typically consists of integer values for each of the R, G, B values, these values being rescaled from the interval $[0,1]$ and discretized to the resolution of the color values.

The highest commonly used resolution for RGB values is the so-called 32 bit or 24 bit color. On a Macintosh, this is called “millions of colors,” and on a PC it is referred to variously as “32 bit color,” “16,777,216 colors,” or “true color.” The typical storage for such RGB values is in a 32 bit word: 8 bits are reserved for specifying the red intensity, 8 bits for green, and 8 bits for blue. Since $2^{24} = 16,777,216$, there are that many possible colors. The remaining 8 bits in the 32 bit word are either ignored or are used for an alpha (α) value. Typical uses of the alpha channel are for transparency or blending effects (OpenGL supports a wide range of transparency and blending effects). Since each color has 8 bits, each color value may range from 0 to 255.

The second highest resolution of the commonly used RGB color representations is the 16 bit color system. On a Macintosh, this is called "thousands of colors;" on a PC it will be called "high color," "32768 colors," or "16 bit color." In 16 bit color, there are, for each of red, green, and blue, five bits which represent the intensity of that color. The remaining one bit is sometimes used to represent transparency. Thus, each color is has its intensity represented by a number between 0 and 31, and altogether there are $2^{15} = 32768$ possible color combinations.

The lowest resolution which is still sometimes used by modern computers is 8 bit color. In 8 bit color, there are 256 possible colors. Usually, three of the bits are used to represent the red intensity, three bits represent the green intensity, and only two bits represent the blue intensity.

An alternative way to use eight bits per pixel for color representation is to use a *color lookup table*, often called a CLUT or a LUT, for short. This method is also called *indexed color*. A LUT is typically a table holding 256 distinct colors in 16 bit, 24 bit, or 32 bit format. Each pixel is then given an 8 bit color index. The color index specifies a position in the table, and the pixel is given the corresponding color. A big advantage of a LUT is that it can be changed depending on the contents of a window or image on the screen, so that the colors in the LUT can reflect the range of colors that are actually present in the image. For instance, if an image has a lot of reds, the lookup table might be loaded with many shades of reds, and with relatively few non-red colors. For this reason, using 8 bit indexed color can give much better color rendition of a particular image than just using the standard 8 bit color representation with $3+3+2$ bits for red, green, and blue intensities.

Color lookup tables are useful in situations where video memory is limited and there is only eight bits of memory per pixel available for storing color information. They are also useful for compressing files for transmission in bandwidth-limited or bandwidth-sensitive applications, such as when files are viewed over the internet. The widely used Compuserve GIF file format incorporates the use of indexed color: a GIF file uses a k bit index to specify the color of a pixel, where $1 \le k \le 8$. In addition, the GIF file contains a color lookup table of 2^k color values. Thus, with $k = 8$, there are 256 possible colors; however, smaller values for k can also be used to further reduce the file size at the cost of having fewer colors. This allows GIF files to be smaller than they would otherwise be and thereby faster to download, without sacrificing too much in image quality. To be honest, we should mention that there is a second reason that GIF files are so small: they use a sophisticated compression scheme, known as LZW after its inventors A. Lempel, J. Ziv, and T. Welch, which further compresses the file by removing certain kinds of redundant information.

Internet browsers, such as *Chrome* or *Safari*, support a standard color index scheme for "browser-safe" or "web-safe" colors. This scheme is based on colors which are restricted to six levels of intensity for red, for green, and for blue, which makes a total of $6^3 = 216$ web-safe colors. In theory at least, browsers should render these 216 colors identically on all hardware.

VII.2.3 Hue, saturation, and luminance

There are a number of methods for representing color other than in terms of its red, green, and blue components. These methods can be more intuitive and user-friendly for color specification and color blending.

We will discuss only one of the popular methods of this type, the "HSL" system which specifies a color in terms of its hue, saturation, and luminance. The *hue* (or *chromaticity*) of a light is the dominant color of the light. The *luminance* (also called *intensity*, or *value*, or *brightness*) specifies the overall brightness of the light. Finally, the *saturation* (also called *chroma* or *colorfulness*) of a color measures the extent to which the color consists of a pure color versus consists of white light. (These various terms with similar meanings are not precisely synonymous, but instead have different technical definitions in different settings. For other methods of color specification similar in spirit to HSL, you may consult Foley et al. [49], for instance.)

In the HSL system, hue is typically measured as an angle between 0 and 360 degrees. A pure red color has hue 0, a pure green color has hue equal to 120, and a pure blue color has hue equal to 240. Intermediate angles for the hue indicate the blending of two of the primary colors. Thus, a hue of 60 degrees indicates a color contains equal mixtures of red and green, i.e., the color yellow. Figure VII.2 shows the hues as a function of angle.

The luminance refers to the overall brightness of the color. In the HSL system, luminance is calculated from RGB values, by taking the average of the maximum and minimum intensities of the red, green, and blue colors.

The saturation is measured in a fairly complex fashion, but generally speaking, it measures the relative intensity of the brightest primary color versus the least bright primary color, and scales the result into the range $[0, 1]$.

The advantage of using HSL color specification is that it is a more intuitive method for defining colors. The disadvantage is that it does not correspond well the physical processes of displaying colors on a monitor or printing colors with ink or dyes. For this, it is necessary to have some way of converting between HSL values and either RGB or CMY values.

The most common algorithm for converting RGB values into HSL values is the following:

```
// Input:  R, G, B.  All in the range $[0,1]$.
// Output:  H, S, L.  H$\in [0,360]$, and S, L $\in [0,1]$.
   Set Max = $\max\{$R, G, B$\}$;
   Set Min = $\min\{$R, G, B$\}$;
   Set Delta = Max - Min;
   Set L = (Max+Min)/2;                    // Luminance
   If (Max==Min) $\{$
```

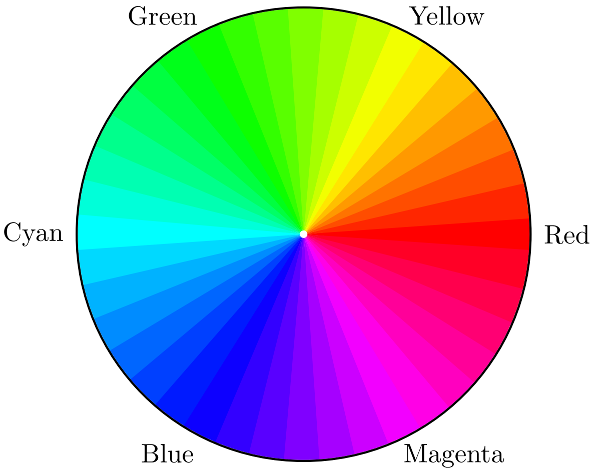

Figure VII.2: Hue is measured in degrees, representing an angle around the color wheel. Pure red has hue equal to 0, pure green has hue equal to 120, and pure blue has hue equal to 240. See color plate C.5.

```
    Set S = 0;          // Achromatic, unsaturated.
    Set H = 0;          // Hue is undefined.
}
Else {
    If ( L<1/2 ) {
        Set S = Delta/(Max+Min);      // Saturation
    }
    Else {
        Set S = Delta/(2-Max-Min);    // Saturation
    }
    If ( R == Max ) {
        Set H = 60*(G-B)/Delta;       // Hue
        If ( H<0 )
            Set H = 360+H;
    }
    Else if ( G == Max ) {
        Set H = 120 + 60*(B-R)/Delta; // Hue
    }
    Else {
        Set H = 240 + 60*(R-G)/Delta; // Hue
    }
}
```

The H, S, L values are often rescaled to be in the range 0 to 255.

In order to understand how the above algorithm works, consider the case where R is the dominant color, and B the least bright, so that $R > G > B$. Then the hue will be calculated by

$$H \;=\; 60 \cdot \frac{G-B}{R-B} \;=\; 60 \cdot \frac{G - \mathtt{Min}}{R - \mathtt{Min}}.$$

Thus, the hue will range from 0 to 60 degrees in proportion to $(G - \mathtt{Min})/(R - \mathtt{Min})$. If we think of the base intensity, Min, as the amount of white light, then $R - \mathtt{Min}$ is the amount of red in the color, and $G - \mathtt{Min}$ is the amount of green in the color. So, in this case, the hue measures the ratio of the amount of green in the color to the amount of red in the color.

On the other hand, the conversion from RGB into HSL does not seem to be completely ideal in the way it computes brightness: for instance, the color yellow, which has R,G,B values of 1,1,0, has luminance $L = 1/2$. Likewise the colors red and green, which have R,G,B values of 1,0,0 and of 0,1,0, respectively, also have luminance $L = 1/2$. However, the color yellow is usually a brighter color than either red or green. There seems to be no way of easily evading this problem.

The formulas for computing saturation from RGB values are perhaps a little mysterious. They are

$$S = \frac{\mathtt{Max} - \mathtt{Min}}{\mathtt{Max} + \mathtt{Min}} \qquad \text{and} \qquad S = \frac{\mathtt{Max} - \mathtt{Min}}{2 - (\mathtt{Max} + \mathtt{Min})}$$

where the formula on the left is used if $\mathtt{Max} + \mathtt{Min} \le 1$ and the otherwise the formula on the right is used. Note that when $\mathtt{Max} + \mathtt{Min} = 1$, then the two formulas give identical results, so the saturation is a continuous function. Also note that if $\mathtt{Max} = 1$, then $S = 1$. Finally, the formula on the right is obtained from the formula on the left by replacing Max by $1 - \mathtt{Min}$ and Min by $1 - \mathtt{Max}$.

It is not hard to see that the algorithm converting RGB into HSL can be inverted, and thus it is possible to calculate the RGB values from the HSL values. Or rather, the algorithm could be inverted if HSL values were stored as real numbers; however, the discretization to integer values means that the transformation from RGB to HSL is not one-to-one and cannot be exactly inverted.

Exercise VII.1. Give an algorithm for converting HSL values to RGB values. You may treat all numbers as real numbers, so you do not need to worry about discretization problems. [Hint: First compute Min and Max from L and S.]

The translation from RGB into HSL is a nonlinear function, thus a linear interpolation process such as Gouraud shading will give different results when applied to RGB values than to HSL values. Generally, Gouraud shading is applied to RGB values, but in some applications, it might give better results to interpolate in HSL space. There are potential problems with interpolating hue, however; for instance, how would one interpolate from a hue of 0 degrees to a hue of 180 degrees?

VII.3 Gamma correction and sRGB color

So far, we have discussed primarily RGB representations for colors; however, most digital images actually use a different "sRGB" encoding for colors. (The name "sRGB" stands for "standard RGB".) The usual RGB representation of color is a linear representation. This means that, in an RGB color value $\langle r, g, b\rangle$, the values r, g, b directly measure the intensity of the light; e.g., these values are proportional to the number of photons per second reaching the viewer. For instance, if two colors with RGB values $\langle r_1, g_1, b_1\rangle$ and $\langle r_2, g_2, b_2\rangle$ are combined, they are represented by $\langle r_1{+}r_2, g_1{+}g_2, b_1{+}b_2\rangle$.

The linear RGB representation is completely appropriate when doing physically-based modelling of lighting and color. In particular, the Phong and the Cook-Torrance lighting models are both physically-based and both based on the linear RGB representation for color. The linear RGB representation is also appropriate when averaging colors or lerping between colors, as is done by both Gouraud shading and mipmapping.

However, the linear RGB representation does not match the way humans perceive colors at different intensities. Instead, the perceived brightness of a color is related sublinearly to the intensity of a color. For instance, if the intensity of a color (measured in terms of photons per second) is doubled, then a human perceives the color's brightness as less than doubling.

Figure VII.3 shows a curve that approximates humans' perceived brightness as a function of light intensity. The two formulas most commonly used for this are the *gamma correction* function

$$\mathit{gamma}(x) \;=\; x^{1/2.2} \qquad \text{(VII.2)}$$

and especially the linear-to-sRGB conversion function

$$\mathit{linear\text{-}to\text{-}sRGB}(x) \;=\; \begin{cases} 12.92x & \text{if } 0 \le x < 0.0031308 \\ 1.055x^{1/2.4} - 0.055 & \text{if } 0.0031308 \le x \le 1. \end{cases} \qquad \text{(VII.3)}$$

The value 2.2 in Equation VII.2 for $\mathit{gamma}(x)$ is often called "gamma". The *linear-to-sRGB* function was picked to be approximately equal to the gamma correction function throughout the interval $[0,1]$ (the maximum difference is less than 0.033), while avoiding having infinite slope at $x = 0$. The constants were picked to make the *linear-to-sRGB* function continuous, and to make its first derivative have only a small discontinuity at 0.0031308.

The inverse of the gamma correction function *gamma* is just $x = y^{2.2}$. The inverse of the *linear-to-sRGB* function is generally computed as

$$\mathit{sRGB\text{-}to\text{-}linear}(x) \;=\; \begin{cases} x/12.92 & \text{if } 0 \le x < 0.04045 \\ \left(\frac{x+0.055}{1.055}\right)^{2.4} & \text{if } 0.04045 \le x \le 1. \end{cases}$$

If a color has RGB representation $\langle r, g, b\rangle$, then its sRGB representation $\langle r', g', b'\rangle$ is obtained by applying *linear-to-sRGB* to each RGB

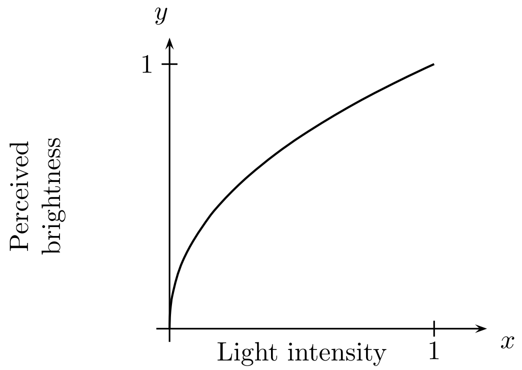

Figure VII.3: The gamma correction function *gamma* of Equation VII.2, or the *linear-to-sRGB* function of Equation VII.3. (The two functions are not quite equal, but they are so close that their graphs are nearly indistinguishable.) The x axis measures the light intensity. The y axis measures the brightness as perceived by a human.

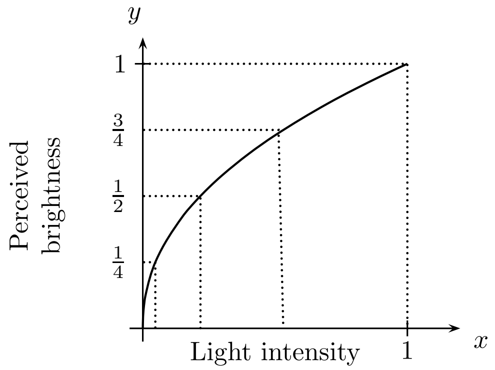

Figure VII.4: The vertical axis shows equally spaced perceived levels of brightness. These do not correspond to equally spaced levels of light intensity on the horizontal axis.

component; so that $r' = \textit{linear-to-sRGB}(r)$, $g' = \textit{linear-to-sRGB}(g)$ and $b' = \textit{linear-to-sRGB}(b)$. (If there is fourth *alpha* value for transparency, it is unchanged.)

The main advantage of sRGB color is when using 24-bit/32-bit color representations which have 8 bits for each of red, green and blue. These have only 256 distinct color settings for each of red, green and blue. The nonlinearity is humans' perception of brightness mean that the 24-bit linear

RGB representation, which has only 256 color settings for each of red, green and blue, lacks resolution for specifying darker colors as perceived by humans. This is illustrated in Figure VII.4, where the steep slope of the *gamma* function at dark colors means that small changes in light intensity cause large changes in the perceived brightness. On the other hand, in the sRGB color representation, the 256 color settings are spread more uniformly across the different brightness levels distinguishable by humans.[5]

VII.3.1 Using sRGB versus RGB

It is very common for digital images to use sRGB representations for colors. For example, digital cameras generally produce pictures with colors given in the sRGB encoding. Digital monitors typically are designed to take sRGB colors and display them correctly — in effect digital monitors are implicitly converting the sRGB colors back to RGB colors in order to display them. Since graphic artist and designer produce images to look good on monitors, this means they are in effect specifying colors with sRGB representations. In short, most digital images for texture maps will specify colors in the sRGB representation.

Shader programs in OpenGL can work with either linear (RGB) color values or sRGB color values. However, by default, color values should be RGB values. The main exception to this is the final color output by the fragment shader should generally use the sRGB representation, since the display monitors assume their input values are sRGB values. The reason shader programs work internally with RGB values is to allow to use linear operations on colors. For instance, physically-based lighting models such as Phong lighting and Cook-Torrance lighting combine light intensities linearly; namely, by adding up the illumination from multiple lights. Likewise, Gouraud shading uses linear interpolation on colors. Distance attenuation with an inverse square dropoff makes physical sense only for RGB colors. Finally, texture map methods such as mipmapping and supersampling combine colors linearly by default. All these operations work better with linear RGB values instead of the nonlinear sRGB values.

For these reasons, shader programs generally work with RGB color. In particular, a fragment shader receives color values from with the vertex shader or from a texture map that are in the RGB color space.[6] On the other hand, the final color value for a pixel, as output be a fragment shader, should use the sRGB encoding, since this is what display monitors expect.

OpenGL provides support for texture maps that use sRGB encoding. It has two texture map formats `GL_SRGB8` and `GL_SRGB8_ALPHA8` which are intended for sRGB encoded textures. `GL_SRGB8` is for 24-bit color with eight bits for each of red, green and blue. `GL_SRGB8_ALPHA8` uses 32 bits, adding eight bits

[5] If 16 bit color values are used instead of 8 bit values, then this loss of resolution is much less important. For this reason, sRGB representations are used primarily in conjunction with 24-bit/32-bit color representations.

[6] Technically, a texture map can contain *any* kind of values, and shader programs can be written to deal with them in custom ways. We are discussing just the most common usage.

for an alpha value, which is linearly encoded and is not affected by conversion between RGB and sRGB. Either of the formats `GL_SRGB8` and `GL_SRGB8_ALPHA8` can be used when creating a texture with `glTexImage2D`. For these textures, OpenGL will convert colors into linear RGB values whenever needed, such as for mipmapping. OpenGL in addition converts the texture values to RGB space when a fragment shader reads from an SRGB texture. In other words, when a fragment shader calls the GLSL `texture` function, it does not receive the actually stored in the shader; instead OpenGL converts the value to RGB and this is returned by the `texture` function.[7]

The *GammaCorrectTest* program. The program *GammaCorrectTest*, available on the book's web page, demonstrates how monitors expect sRGB values as input from the fragment shader, not RGB values. It creates the image shown in Figure VII.5. There are 10 rectangles in the figure, five on the left and five on the right. On the left, the five rectangles are intended to show five equally spaced levels of light intensity, that is, equally spaced in RGB space. The bottom rectangle is solid black (all pixels turned off). The next rectangle has 25% of its pixels turned on to full brightness, i.e., one out of every four pixels: the rest of its pixels are turned off. The middle rectangle has 50% of it pixels (two out of every four) turned on and the rest off. The next rectangle up has 75% of its pixels (three out of every four) turned on and the rest off. Thus, the brightness levels of these rectangles on the left are formed by equally spaced light intensities, as specified in the linear RGB representation.

On the righthand side, the rectangles are filled by setting all pixels to the same brightness value, with the value given by the *linear-to-sRGB* function. The second from the top rectangle on the right has every pixel with color $\langle\beta,\beta,\beta\rangle$ where $\beta = \textit{linear-to-sRGB}(0.25)$. The middle rectangle on the right uses $\beta = \textit{linear-to-sRGB}(0.5)$. The rectangle second from the bottom on the right uses $\beta = \textit{linear-to-sRGB}(0.25)$. On a well-calibrated display and, it is hoped, in this book if it has been printed with faithful color rendering, the five rectangles on the right should have the same overall perceived brightnesses as the five rectangles on the left.

The sRGB standard, and the conversion function *linear-to-sRGB* are designed with the goal that the brightness levels of the rectangles on the right side should match the brightness levels of the rectangles on the left side. You can also use the *GammaCorrectTest* program to interactively experiment with different gamma values for the *gamma* function.

Exercise VII.2. The function *linear-to-sRGB* defined in Equation VII.3 was claimed to be continuous at $x = 0.0031308$. If you check this, this is *almost* true. How big is the discontinuous jump at $x = 0.0031308$? The function was also claimed to have only a small discontinuity at the value. How big is the discontinuity?

[7] This automatic conversion to sRGB happens only for `GL_SRGB8` and `GL_SRGB8_ALPHA8` textures; all other texture formats are presumed to already be in RGB space.

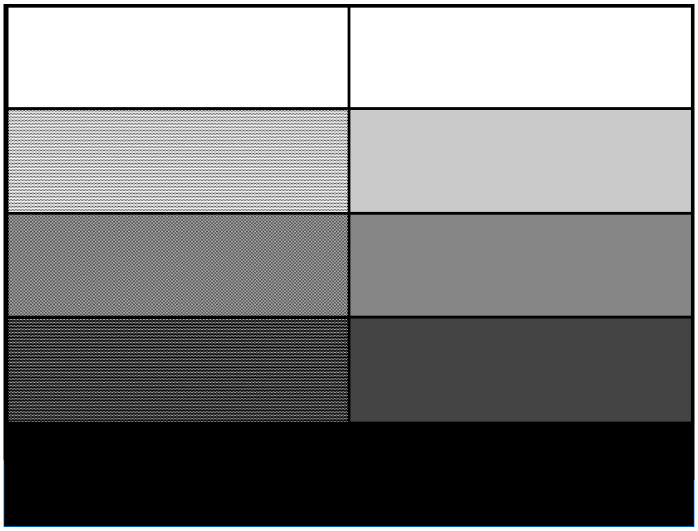

Figure VII.5: The middle three rectangles on the right use dithering of black and white to achieve an appearance of gray. The rectangles on the right are solid colors, with colors being set correctly in sRGB representation to get approximately the same level of gray. If you are viewing an electronic version of this image, you may be able to zoom in to see the individual pixels for the dithering on the right. If you zoom out, you should be able to see both the right and left as smooth gray colors. At intermediate resolutions, you may see interference patterns due to aliasing problems.

Exercise VII.3. A footnote on page 261 states that using 16 bit color values in the linear RGB representations gives sufficient precision for perceived colors, even for dark colors. Do a calculation to confirm this. What is *linear-to-sRGB*$(1/255)$? How many bits of precision are needed to specify a value this small? Is 16 bits enough?

Exercise VII.4. Why might it be important that the *linear-to-sRGB* function does not have infinite derivative at $x = 0$?

Further reading

Two highly recommended introductions to color and its use in computer graphics are the book by Jackson et al. [68] and the more advanced book of Berns at al. [9]; both are well-written with plenty of color illustrations. They also include discussion of human factors and good design techniques for using color in a user-friendly way.

For a discussion of humans' abilities to perceive and distinuish colors, you can consult Glassner [55], Wyszecki and Stiles [127], or Fairchild [40].

Discussions of monitor and display design, as well as color printing, are given by [55, 68, 59].

A major tool for using scientific and engineering use of color is the color representation standards supported by the Commission International d'Eclairage (CIE) organization. For computer applications, the 1931 CIE $(\bar{x}, \bar{y}, \bar{z})$ representation is the most relevant, but there are several other standards, including the 1964 10° observer standards, and the CIELAB and CIELUV color representations that better indicate human's abilities to discriminate colors. The CIE standards are described to some extent in all the above references. A particularly comprehensive mathematical explanation can be found in [127]; for a shorter mathematical introduction, see an appendix of [9]. Also, Fairman et al. [41] describe the the mathematical definition of the 1931 CIE color standard, and its historical motivations.

The early history of the development of the scientific theories of color is given by Bouma [21, chap. 12].

VII.4 Additional exercises

EXERCISES TO BE WRITTEN.

Chapter VIII

Bézier Curves

This is a ***preliminary*** *draft of a second edition of the book* 3-D Computer Graphics: A Mathematical Introduction with OpenGL. *So please read it cautiously and critically! Corrections are appreciated. Draft C.4.a*

Author: Sam Buss, sbuss@ucsd.edu

A spline curve is a smooth curve which is specified succinctly in terms of a few points. These two aspects of splines, that they are smooth and that they are specified succinctly in terms of only a few points, are both important. First, the ability to specify a curve with only a few points reduces storage requirements. In addition, it facilitates the computer-aided design of curves and surfaces, since the designer or artist can control an entire curve by varying only a few points. Second, the commonly used methods for generating splines give curves with good smoothness properties and without undesired oscillations. Furthermore, these splines also allow for isolated points where the curve is not smooth, such as points where the spline has a 'corner'. A third important property of splines is that there are simple algorithms for finding points on the spline curve or surface, and simple criteria for deciding how finely a spline must be approximated by linear segments to get a sufficiently faithful representation of the spline. The main classes of splines discussed in this book are the Bézier curves and the B-spline curves. Bézier curves and patches are covered in this chapter, and B-splines in the next chapter.

Historically, splines were mechanically specified by systems such as flexible strips of wood or metal that were tied into position to record a desired curve. These mechanical systems were awkward and difficult to work with, and they could not be used to give a permanent, reproducible description of a curve. Nowadays, mathematical descriptions are used instead of mechanical devices, since the mathematical descriptions are, of course, more useful and more permanent, not to mention more amenable to computerization. Nonetheless, some of the terminology of physical splines persists, such as the use of 'knots' in B-spline curves.

Bézier curves were first developed by automobile designers for the purpose of describing the shape of exterior car panels. Bézier curves are named after P. Bézier for his work at Renault in the 1960's [11, 10]. Slightly earlier, P. de Casteljau had already developed mathematically equivalent methods of defining spline curves at Citroën [37, 38].[1]

The present chapter discusses Bézier curves, which are a simple kind of spline. For sake of concreteness, the first five sections concentrate on the special case of degree three Bézier curves in detail. After that, we introduce Bézier curves of general degree. We then cover how to form Bézier surface patches, and how to use Bézier curves and surfaces in OpenGL. In addition, we describe rational Bézier curves and patches, and how to use them to form conic sections and surfaces of revolution. The last sections of the chapter describe how to form piecewise Bézier curves and surfaces that interpolate a desired set of points.

For a basic understanding of degree three Bézier curves, you should start by reading Sections VIII.1 through VIII.4. After that, you can skip around a little. Sections VIII.6-VIII.9 and VIII.12-VIII.14 discuss general degree Bézier curves and rational Bézier curves and are intended to be read in order. But it is possible to read Sections VIII.10 and VIII.11 about patches and about OpenGL immediately after Section VIII.4. Likewise, Sections VIII.15 and VIII.16 on interpolating splines can be read immediately after Section VIII.4. The mathematical proofs are not terribly difficult, but may be skipped if desired.

VIII.1 Bézier curves of degree three

The most common type of Bézier curves is the *degree three* polynomial curves, which are specified by four points, called *control points*. This is illustrated in Figure VIII.1, where a parametric curve $\mathbf{q} = \mathbf{q}(u)$ is defined by four control points $\mathbf{p}_0, \mathbf{p}_1, \mathbf{p}_2, \mathbf{p}_3$. The curve starts from $\mathbf{p}_0$ initially in the direction of $\mathbf{p}_1$, then curves generally towards $\mathbf{p}_2$, and ends up at $\mathbf{p}_3$ coming from the direction of $\mathbf{p}_2$. Only the first and last points, $\mathbf{p}_0$ and $\mathbf{p}_3$, lie on $\mathbf{q}$. The other two control points, $\mathbf{p}_1$ and $\mathbf{p}_2$, influence the curve: the intuition is that these two middle control points "pull" on the curve. You can think of $\mathbf{q}$ as being a flexible, stretchable curve that is constrained to start at $\mathbf{p}_0$ and end at $\mathbf{p}_3$, and in the middle is pulled by the two middle control points. Figure VIII.2 shows two more examples of degree three Bézier curves and their control points.

We say that a curve *interpolates* a control point if the control point lies on the curve. In general, Bézier curves do not interpolate their control points, except for the first and last points. For example, the degree three Bézier curves shown in Figures VIII.1 and VIII.2 interpolate the first and last control points $\mathbf{p}_0$ and $\mathbf{p}_3$, but not the middle control points.

[1] We do not attempt to give a proper discussion of the history of the development of Bézier curves and B-splines. The textbooks of Farin [42], Bartels et al. [6] and especially Rogers [94] and Schumaker [99] contain some historical material and many more references on the development of Bézier curves and B-splines.

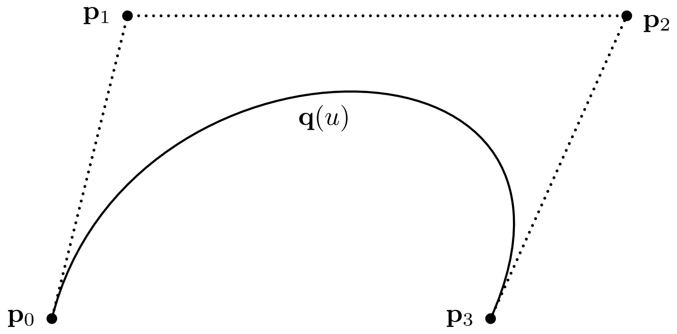

Figure VIII.1: A degree three Bézier curve $\mathbf{q}(u)$. The curve is parametrically defined with $0 \le u \le 1$, and it interpolates the first and last control points with $\mathbf{q}(0) = \mathbf{p}_0$ and $\mathbf{q}(1) = \mathbf{p}_3$. The curve is "pulled towards" the middle control points $\mathbf{p}_1$ and $\mathbf{p}_2$. At $\mathbf{p}_0$, the curve is tangent to the line segment joining $\mathbf{p}_0$ and $\mathbf{p}_1$. At $\mathbf{p}_3$, it is tangent to the line segment joining $\mathbf{p}_2$ and $\mathbf{p}_3$.

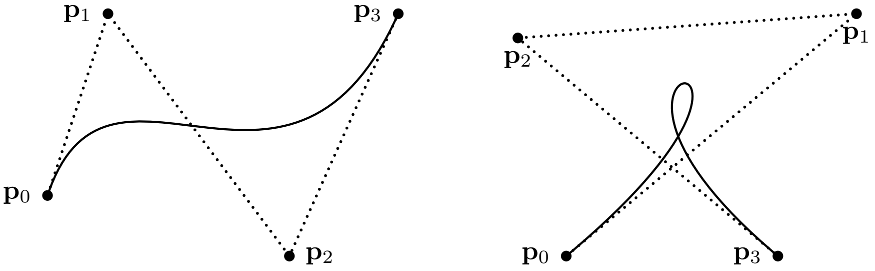

Figure VIII.2: Two degree three Bézier curves, each defined by four control points. The curves interpolate only their first and last control points, $\mathbf{p}_0$ and $\mathbf{p}_3$. Note that, just as in Figure VIII.1, the curves start off, and end up, tangent to line segments joining control points.

Definition VIII.1. Degree three Bézier curves are defined parametrically by a function $\mathbf{q}(u)$: as u varies from 0 to 1, the values of $\mathbf{q}(u)$ sweep out the curve. The formula for a degree three Bézier curve is

$$\mathbf{q}(u) \;=\; B_0(u)\mathbf{p}_0 + B_1(u)\mathbf{p}_1 + B_2(u)\mathbf{p}_2 + B_3(u)\mathbf{p}_3, \qquad \text{(VIII.1)}$$

where the four functions $B_i(u)$ are scalar-valued functions called blending functions, and are defined by

$$B_i(u) \;=\; \binom{3}{i} u^i (1-u)^{3-i}. \qquad \text{(VIII.2)}$$

The notation $\binom{n}{m}$ represents the "choice function" counting the number of subsets of size m of a set of size n, namely,

$$\binom{n}{m} \;=\; \frac{n!}{m!(n-m)!}.$$

Expanding the definitions gives

$$\begin{aligned} B_0(u) &= (1-u)^3 \;=\; 1-3u+3u^2-u^3 \\ B_1(u) &= 3u(1-u)^2 \;=\; 3u-6u^2+3u^3 \\ B_2(u) &= 3u^2(1-u) \;=\; 3u^2-3u^3 \\ B_3(u) &= u^3. \end{aligned}$$

Note that these are all degree three polynomials.

Much of the power and convenience of Bézier curves comes from their being defined in a uniform way independent of the dimension d of the space containing the curve. The control points $\mathbf{p}_i$ defining a Bézier curve lie in d-dimensional space $\mathbb{R}^d$ for some d. On the other hand, the blending functions $B_i(u)$ are scalar-valued functions. The Bézier curve itself is a parametrically defined curve $\mathbf{q}(u)$ lying in $\mathbb{R}^d$. Bézier curves can thus be curves in the plane $\mathbb{R}^2$ or in 3-space $\mathbb{R}^3$, and so forth. It is even permitted for d to equal 1, in which case a Bézier curve is a scalar-valued "curve." For instance, if u measures time and $d=1$, then the "curve" represents a time-varying scalar value.

The functions $B_i(u)$ are special cases of the *Bernstein polynomials*. When we define Bézier curves of arbitrary degree in Section VIII.6, the Bernstein polynomials of degree three will be denoted by B_i^3 instead of just B_i. But for now, we omit the superscript 3 in order to keep our notation from being overly cluttered.

The four blending functions $B_i(u)$ are graphed in Figure VIII.3. Obviously, the functions take on values in the interval $[0,1]$ for $0 \le u \le 1$. Less obviously, the sum of the four functions is always equal to one: this can be checked by summing the polynomials or, more elegantly, by the binomial theorem,

$$\sum_{i=0}^{3} B_i(u) \;=\; \sum_{i=0}^{3} \binom{3}{1} u^i(1-u)^{3-i} \;=\; (u+(1-u))^3 \;=\; 1.$$

In addition, $B_0(0)=1$ and $B_3(1)=1$. From this, we see immediately that $\mathbf{q}(u)$ is always computed as a weighted average of the four control points and that $\mathbf{q}(0)=\mathbf{p}_0$ and $\mathbf{q}(1)=\mathbf{p}_3$, confirming our observation that $\mathbf{q}(u)$ starts at $\mathbf{p}_0$ and ends at $\mathbf{p}_3$. The function $B_1(u)$ reaches its maximum value, namely $\frac{4}{9}$, at $u=\frac{1}{3}$: therefore, the control point $\mathbf{p}_1$ has the greatest influence over the curve at $u=\frac{1}{3}$. Symmetrically, $\mathbf{p}_2$ has the greatest influence over the curve at $u=\frac{2}{3}$. This coincides with the intuition that the control points $\mathbf{p}_1$ and $\mathbf{p}_2$ "pull" the hardest on the curve at $u=\frac{1}{3}$ and $u=\frac{2}{3}$.

If we calculate the derivatives of the four blending functions by hand, we of course find that their derivatives are degree two polynomials. If we then

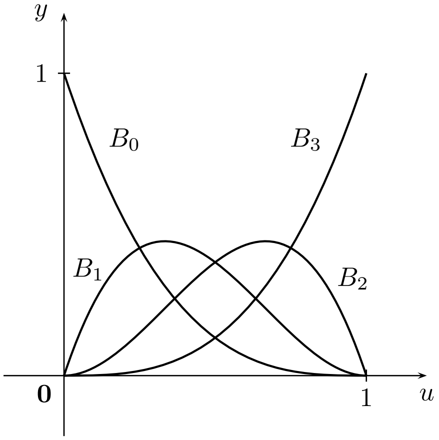

Figure VIII.3: The four blending functions for degree three Bézier curves. We are only interested in their values in the interval $[0, 1]$. Each $B_i(u)$ is a degree three polynomial.

evaluate these derivatives at $u = 0$ and $u = 1$, we find that

$$\begin{array}{llll} B_0'(0) = -3 & B_1'(0) = 3 & B_2'(0) = 0 & B_3'(0) = 0 \\ B_0'(1) = 0 & B_1'(1) = 0 & B_2'(1) = -3 & B_3'(1) = 3. \end{array}$$

The derivative of the function $\mathbf{q}(u)$ can be easily expressed in terms of the derivatives of the blending functions, namely,

$$\mathbf{q}'(u) \;=\; B_0'(u)\mathbf{p}_0 + B_1'(u)\mathbf{p}_1 + B_2'(u)\mathbf{p}_2 + B_3'(u)\mathbf{p}_3.$$

This is of course a vector-valued derivative since $\mathbf{q}$ is a vector-valued function. At the beginning and end of the curve, the values of the derivatives are

$$\begin{aligned} \mathbf{q}'(0) &= 3(\mathbf{p}_1 - \mathbf{p}_0) \qquad \text{(VIII.3)} \\ \mathbf{q}'(1) &= 3(\mathbf{p}_3 - \mathbf{p}_2). \end{aligned}$$

Graphically, this means that the curve $\mathbf{q}(u)$ starts at $u = 0$ traveling in the direction of the vector from $\mathbf{p}_0$ to $\mathbf{p}_1$. Similarly, at the end, where $u = 1$, the curve $\mathbf{q}(u)$ is tangent to the vector from $\mathbf{p}_2$ to $\mathbf{p}_3$. Referring back to Figures VIII.1 and VIII.2, this corresponds to the fact that the curve starts at $\mathbf{p}_0$ initially tangent to the line segment joining the first control point to the second control point, and ends at $\mathbf{p}_3$ tangent to the line segment joining the third and fourth control points.

Exercise VIII.1. A degree three Bézier curve in $\mathbb{R}^2$ satisfies $\mathbf{q}(0) = \langle 0, 1\rangle$, $\mathbf{q}(1) = \langle 3, 0\rangle$, $\mathbf{q}'(0) = \langle 3, 3\rangle$ and $\mathbf{q}'(1) = \langle -3, 0\rangle$. What are the control points for this curve? Give a rough freehand sketch of the curve, being sure to clearly show the slopes at the beginning and end of the curve.

Theorem VIII.9 below gives a formula for the derivative of a degree Bézier curve at an arbitrary value of u, expressed as a *degree two* Bézier curve.

VIII.2 De Casteljau's method

The qualitative methods described above allow you to make a reasonable freehand sketch of a degree three Bézier curve based on the positions of its control points. In particular, the curve starts at $\mathbf{p}_0$, ends at $\mathbf{p}_3$, and has initial and final directions given by the differences $\mathbf{p}_1 - \mathbf{p}_0$ and $\mathbf{p}_3 - \mathbf{p}_2$. Finding the exact values of $\mathbf{q}(u)$ for a given value of $\mathbf{u}$ can be done by using formulas (VIII.1) and (VIII.2) of course. However, an easier method, known as de Casteljau's method, can also be used to find values of $\mathbf{q}(u)$. De Casteljau's method is not only simpler for hand calculation, but is also more stable numerically for computer calculations.[2] In addition, de Casteljau's method will be important later on as the basis for recursive subdivision.

Let $\mathbf{p}_0, \mathbf{p}_1, \mathbf{p}_2, \mathbf{p}_3$ define a degree three Bézier curve $\mathbf{q}$. Fix $u \in [0,1]$ and suppose we want to compute $\mathbf{q}(u)$. The de Casteljau method for computing $\mathbf{q}(u)$ works as follows: First, form three points $\mathbf{r}_0$, $\mathbf{r}_1$, $\mathbf{r}_2$ by linear interpolation from the control points of $\mathbf{q}$ by

$$\mathbf{r}_i \;=\; (1-u)\cdot \mathbf{p}_i + u\cdot \mathbf{p}_{i+1}. \tag{VIII.4}$$

Recall from Section V.1.1 that this means that $\mathbf{r}_i$ lies between $\mathbf{p}_i$ and $\mathbf{p}_{i+1}$, with $\mathbf{r}_i$ at the point which is fraction u of the distance from $\mathbf{p}_i$ to $\mathbf{p}_{i+1}$. (This is illustrated below in Figures VIII.4 and VIII.5.) Then define $\mathbf{s}_0$ and $\mathbf{s}_1$ by linear interpolation from the $\mathbf{r}_i$'s by

$$\mathbf{s}_i \;=\; (1-u)\cdot \mathbf{r}_i + u\cdot \mathbf{r}_{i+1}. \tag{VIII.5}$$

Finally define $\mathbf{t}_0$ by linear interpolation from $\mathbf{s}_0$ and $\mathbf{s}_1$ by

$$\mathbf{t}_0 \;=\; (1-u)\cdot \mathbf{s}_0 + u\cdot \mathbf{s}_1. \tag{VIII.6}$$

Then, it turns out that $\mathbf{t}_0$ is equal to $\mathbf{q}(u)$. We shall prove a generalization of this fact as Theorem VIII.11 below; however, for the special case of degree three Bézier curves, the reader can easily verify that $\mathbf{t}_0 = \mathbf{q}(u)$ by expressing $\mathbf{t}_0$ as an explicit function of u and the four control points.

In the special case of $u = 1/2$, the de Casteljau method becomes particularly simple. Then,

$$\mathbf{r}_i = \frac{\mathbf{p}_i + \mathbf{p}_{i+1}}{2}, \qquad \mathbf{s}_i = \frac{\mathbf{r}_i + \mathbf{r}_{i+1}}{2}, \qquad \mathbf{t}_0 = \frac{\mathbf{s}_0 + \mathbf{s}_1}{2}. \tag{VIII.7}$$

That is to say, $\mathbf{q}(\frac{1}{2}) = \mathbf{t}_0 = \frac{1}{8}\mathbf{p}_0 + \frac{3}{8}\mathbf{p}_1 + \frac{3}{8}\mathbf{p}_2 + \frac{1}{8}\mathbf{p}_3$.

[2] See [44, 45, 34, 43] for technical discussions on the stability of the de Casteljau methods. They conclude that the de Castaljau method is preferable to conventional methods for polynomial representation and evaluation, including Horner's method.

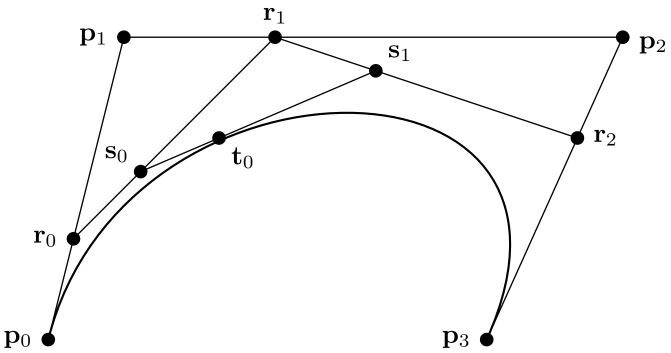

Figure VIII.4: The de Casteljau method for computing $\mathbf{q}(u)$ for $\mathbf{q}$ a degree three Bézier curve. This illustrates the $u = 1/3$ case.

Exercise VIII.2. Prove that $\mathbf{t}_0$, as computed by Equation (VIII.6), is equal to $\mathbf{q}(u)$.

Exercise VIII.3. Let $\mathbf{q}(u)$ be the curve from Exercise VIII.1. Use the de Casteljau method to compute $\mathbf{q}(1/2)$ and $\mathbf{q}(3/4)$. (Save your work for Exercise VIII.4.)

VIII.3 Recursive subdivision

Recursive subdivision is the term used to refer to the process of splitting a single Bézier curve into two subcurves. Recursive subdivision is important for several reasons, but the most important, perhaps, is for the approximation of a Bézier curve by straight-line segments. A curve that is divided into sufficiently many subcurves can be approximated by straight-line segments without too much error. As we discuss in the latter part of this section, this can help with rendering and other applications such as intersection testing.

Suppose we are given a Bézier curve $\mathbf{q}(u)$, with control points $\mathbf{p}_0, \mathbf{p}_1, \mathbf{p}_2, \mathbf{p}_3$. This is a cubic curve of course, and if we let

$$\mathbf{q}_1(u) \;=\; \mathbf{q}(u/2) \qquad \text{and} \qquad \mathbf{q}_2(u) \;=\; \mathbf{q}((u+1)/2), \tag{VIII.8}$$

then both $\mathbf{q}_1$ and $\mathbf{q}_2$ are also cubic curves. We restrict $\mathbf{q}_1$ and $\mathbf{q}_2$ to the domain $[0,1]$. Clearly, for $0 \le u \le 1$, $\mathbf{q}_1(u)$ is the curve which traces out the first half of the curve $\mathbf{q}(u)$, namely, the part of $\mathbf{q}(u)$ with $0 \le u \le 1/2$. Similarly, $\mathbf{q}_2(u)$ is the second half of $\mathbf{q}(u)$. The next theorem gives a simple way to express $\mathbf{q}_1$ and $\mathbf{q}_2$ as Bézier curves.

Theorem VIII.2. *Let $\mathbf{q}(u)$, $\mathbf{q}_1(u)$, and $\mathbf{q}_2(u)$ be as above. Let $\mathbf{r}_i$, $\mathbf{s}_i$, and $\mathbf{t}_0$ be defined as in Section VIII.2 for calculating $\mathbf{q}(u)$ with $u = 1/2$; that is to say,*

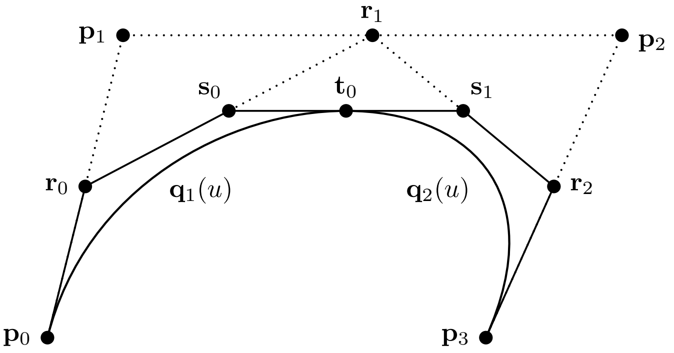

Figure VIII.5: The de Casteljau method for computing $\mathbf{q}(u)$ for $\mathbf{q}$ a degree three Bézier curve is the basis for finding the new points needed for recursive subdivision. Shown here is the $u = 1/2$ case. The points $\mathbf{p}_0, \mathbf{r}_0, \mathbf{s}_0, \mathbf{t}_0$ are the control points for the Bézier curve $\mathbf{q}_1(u)$ which is equal to the first half of the curve $\mathbf{q}(u)$, i.e., starting at $\mathbf{p}_0$ and ending at $\mathbf{t}_0$. The points $\mathbf{t}_0, \mathbf{s}_1, \mathbf{r}_2, \mathbf{p}_3$ are the control points for the curve $\mathbf{q}_2(u)$ equal to the second half of $\mathbf{q}(u)$, i.e., starting at $\mathbf{t}_0$ and ending at $\mathbf{p}_3$.

they are defined according to Equation (VIII.7). Then the curve $\mathbf{q}_1(u)$ is the same as the Bézier curve with control points $\mathbf{p}_0, \mathbf{r}_0, \mathbf{s}_0, \mathbf{t}_0$. And the curve $\mathbf{q}_2(u)$ is the same as the Bézier curve with control points $\mathbf{t}_0, \mathbf{s}_1, \mathbf{r}_2, \mathbf{p}_3$.

Theorem VIII.2 is illustrated in Figure VIII.5.

One way to prove Theorem VIII.2 is to just use a "brute force" evaluation of the definitions of $\mathbf{q}_1(u)$ and $\mathbf{q}_2(u)$. The two new Bézier curves are specified with control points $\mathbf{r}_i$, $\mathbf{s}_i$, and $\mathbf{t}_0$ that have been defined in terms of the $\mathbf{p}_i$'s. Likewise, from equations (VIII.8), we get equations for $\mathbf{q}_1(u)$ and $\mathbf{q}_2(u)$ in terms of the $\mathbf{p}_i$'s. From this, the theorem can be verified by straightforward calculation. This brute force proof is fairly tedious and uninteresting, so we omit it. The interested reader may work out the details or, better, wait until we give a proof of the more general Theorem VIII.12 below.

Theorem VIII.2 explained how to divide a Bézier curve into two halves, with the subdivision breaking the curve at the middle position $u = 1/2$. Sometimes, one wishes to divide a Bézier curve into two parts of unequal size, at a point $u = u_0$. That is to say, one wants curves $\mathbf{q}_1(u)$ and $\mathbf{q}_2(u)$, defined on $[0, 1]$, such that

$$\mathbf{q}_1(u) \;=\; \mathbf{q}(u_0 u) \qquad \text{and} \qquad \mathbf{q}_2(u) \;=\; \mathbf{q}(u_0 + (1 - u_0)u).$$

The next theorem explains how to calculate control points for the subcurves $\mathbf{q}_1(u)$ and $\mathbf{q}_2(u)$ in this case.

Theorem VIII.3. *Let $\mathbf{q}(u)$, $\mathbf{q}_1(u)$, and $\mathbf{q}_2(u)$ be as above. Let $0 < u_0 < 1$. Let $\mathbf{r}_i$, $\mathbf{s}_i$, and $\mathbf{t}_0$ be defined as in Section VIII.2 for calculating $\mathbf{q}(u)$ with $u = u_0$. That is, they are defined by Equations (VIII.4)-(VIII.6), so that*

$\mathbf{t}_0 = \mathbf{q}(u_0)$. *Then the curve* $\mathbf{q}_1(u)$ *is the same as the Bézier curve with control points* $\mathbf{p}_0, \mathbf{r}_0, \mathbf{s}_0, \mathbf{t}_0$. *Also, the curve* $\mathbf{q}_2(u)$ *is the same as the Bézier curve with control points* $\mathbf{t}_0, \mathbf{s}_1, \mathbf{r}_2, \mathbf{p}_3$.

For an illustration of Theorem VIII.3, refer to Figure VIII.4, which shows the $u = 1/3$ case. The curve from $\mathbf{p}_0$ to $\mathbf{t}_0$ is the same as the Bézier curve with control points $\mathbf{p}_0$, $\mathbf{r}_0$, $\mathbf{s}_0$, and $\mathbf{t}_0$. The curve from $\mathbf{t}_0$ to $\mathbf{p}_3$ is the same as the Bézier curve with control points $\mathbf{t}_0$, $\mathbf{s}_1$, $\mathbf{r}_2$, and $\mathbf{p}_3$.

Like Theorem VIII.2, Theorem VIII.3 may be proved by direct calculation. Instead, we shall prove a more general result later as Theorem VIII.12.

Exercise VIII.4. Consider the curve $\mathbf{q}(u)$ of Exercise VIII.1. Use recursive subdivision to split $\mathbf{q}(u)$ into two curves at $u_0 = 1/2$. Repeat with $u_0 = 3/4$.

Applications of recursive subdivision

There are several important applications of recursive subdivision. The first, most prominent application is for rendering a Bézier curve as a series of straight-line segments; this is often necessary since graphics hardware typically uses straight-line segments as primitives. For this, we need a way to break a Bézier curve into smaller and smaller subcurves until each subcurve is sufficiently close to being a straight line so that rendering the subcurves as straight lines gives adequate results. To carry out this subdivision, we need to have a criterion for "sufficiently close to being a straight line." Generally, this criterion should depend not just on the curvature of the curve, but also on the rendering context. For instance, when rendering to a rectangular array of pixels, there is probably no need to subdivide a curve which is so straight that the distance between the curve and a straight-line approximation is less than a single pixel.

A common way of testing whether a Bézier curve is "sufficiently close to a straight line" is to compare the total length of the control polygon to the distance between the first and last control points. For a degree three Bźier curve, the total length of the control polygon is $L = \sum_{i=0}^{2} ||\mathbf{p}_{i+1} - \mathbf{p}_i||$. Then, letting $\delta > 0$ be some small constant, a test such as $L \le ||\mathbf{p}_3 - \mathbf{p}_0||(1+\delta)$ can be used to decide if the curve is sufficiently close to a straight line. The value of δ should be fairly small; for example $\delta = 10^{-4}$ will would ensure that the curve does not deviate from a straight line by more than 2%.

A second important application of recursive subdivision involves combining it with convex hull tests to determine regions where the Bézier curve does *not* lie. For example, in Chapters X and XI, we shall be interested in determining when a ray (a half-line) intersects a surface, and we shall see that it will be particularly important to have efficient methods of determining when a line does not intersect the surface. As another example, suppose we are rendering a large scene of which only a small part is visible at any given time. In order to render the scene quickly, it is necessary to be able to decide quickly what objects are not visible, say by virtue of being outside the view frustum. A test for non-intersection or for non-visibility would be based on the following fact: for a Bézier curve defined with control points $\mathbf{p}_i$, the points $\mathbf{q}(u)$, for $0 \le u \le 1$, all lie in the convex hull of the control points. This fact is a consequence of the fact that the points on the Bézier curve are computed as weighted averages of the control points.

To illustrate the principle of recursive subdivision combined with convex hull testing, we consider the two dimensional analogue of the first example. The extension of these principles to three dimensional problems is straightforward. Suppose we are given a Bézier curve $\mathbf{q}(u)$ and a line or ray L, and want to decide whether the line intersects the Bézier curve and, if so, find where the line and the curve intersect. An algorithm based on recursive subdivision would work as follows: Begin by comparing the line L with the convex hull of the control points of $\mathbf{q}$.[3] Since the curve lies entirely in the convex hull of its control points, if L does not intersect the convex hull, then L does not intersect the Bézier curve: in this case the algorithm may return `false` to indicate no intersection occurs. If L does intersect the convex hull, then the algorithm performs recursive subdivision to divide the Bézier curve into two halves, $\mathbf{q}_1$ and $\mathbf{q}_2$. The algorithm then recursively calls itself to determine whether the line intersects either of the subcurves. However, before performing the recursive subdivision and recursive calls, the algorithm checks whether the Bézier curve is sufficiently close to a straight line and, if so, then the algorithm merely performs a check for whether the line L intersects the straight-line approximation to the Bézier curve. If so, this intersection, or non-intersection, is returned as the answer.

In order for algorithms using recursive subdivision for testing non-intersection or non-visibility to perform well, it is necessary for the convex hulls to decrease rapidly in size with each successive subdivision. One step of this process is illustrated in Figure VIII.6, which shows the convex hulls of the two subcurves, $\mathbf{q}_1$ and $\mathbf{q}_2$, obtained by recursive subdivision. Actually, the shrinkage of the convex hulls of subcurves proceeds even more rapidly than is apparent in the figure: the "width" of the convex hull will decrease quadratically with the "length" of the convex hull. This fact can be proved by elementary calculus, just from the fact that Bézier curves have continuous second derivatives.

VIII.4 Piecewise Bézier curves

There is only a limited range of shapes that can described by a single degree three Bézier curve. In fact, Figures VIII.1 and VIII.2 pretty much exhaust the types of shapes that can formed with a single Bézier curve. However, one frequently wants curves that are more complicated than can be formed with a single degree three Bézier curve. For instance, in Section VIII.15, we will define curves that interpolate an arbitrary set of points. One way to construct more complicated curves would be to use higher degree Bézier curves (look

[3] See Section XI.1.4 for an efficient algorithm for finding the intersection of a line and polygon.

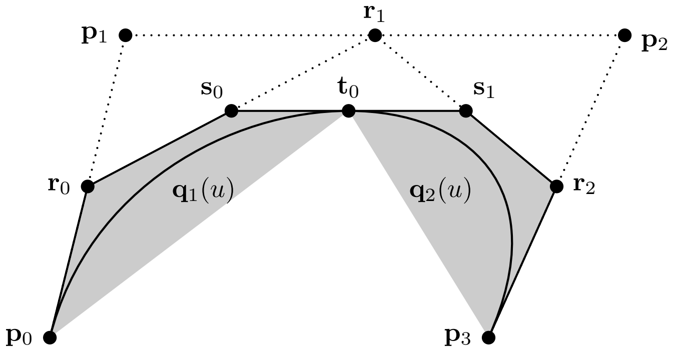

Figure VIII.6: The convex hull of the control points of the Bézier curves shrinks rapidly during the process of recursive subdivision. The whole curve is inside its convex hull, i.e., inside the quadrilateral $\mathbf{p}_0\mathbf{p}_1\mathbf{p}_2\mathbf{p}_3$. After one round of subdivision, the two subcurves are known to be constrained in the two convex shaded regions.

ahead to Figure VIII.9(c), for an example). However, higher degree Bézier curves are not particularly easy to work with. So, instead, it is often better to combine multiple Bézier curves to form a longer, more complicated curve, called a *piecewise Bézier curve*.

This section discusses how to join Bézier curves together, especially how to join them so as to preserve continuity and smoothness (i.e., continuity of the first derivative). For this, it is enough to show how to combine two Bézier curves to form a single smooth curve, as generalizing the construction to combine multiple Bézier curves is straightforward. We already saw the converse process above in the previous section, where recursive subdivision was used to split a Bézier curve into two curves.

Suppose we want to build a curve $\mathbf{q}(u)$ that consists of two constituent curves $\mathbf{q}_1(u)$ and $\mathbf{q}_2(u)$, with each of these two curves a degree three Bézier curve. That is to say, we want to have $\mathbf{q}(u)$ defined in terms of $\mathbf{q}_1(u)$ and $\mathbf{q}_2(u)$ so that Equation (VIII.8) holds. Two examples of this are illustrated in Figure VIII.7. Note that $\mathbf{q}(u)$ will generally not be a single Bézier curve; rather it is a union of two Bézier curves.

For $i = 1, 2$, let $\mathbf{p}_{i,0}$, $\mathbf{p}_{i,1}$, $\mathbf{p}_{i,2}$, and $\mathbf{p}_{i,3}$ be the control points for $\mathbf{q}_i(u)$. In order for $\mathbf{q}(u)$ to be a continuous curve, it is necessary for $\mathbf{q}_1(1)$ to equal $\mathbf{q}_2(0)$. Since Bézier curves begin and end at their first and last control points, this is equivalent to requiring that $\mathbf{p}_{1,3} = \mathbf{p}_{2,0}$. In order for $\mathbf{q}(u)$ to have continuous first derivative at $u = \frac{1}{2}$, it is necessary to have $\mathbf{q}_1'(1) = \mathbf{q}_2'(0)$, i.e., by Equation (VIII.3), to have

$$\mathbf{p}_{1,3} - \mathbf{p}_{1,2} \;=\; \mathbf{p}_{2,1} - \mathbf{p}_{2,0}.$$

If (and only if) these conditions are met, $\mathbf{q}(u)$ is continuous and has continuous first derivatives. In this case, we say that $\mathbf{q}(u)$ is C^1-*continuous.*

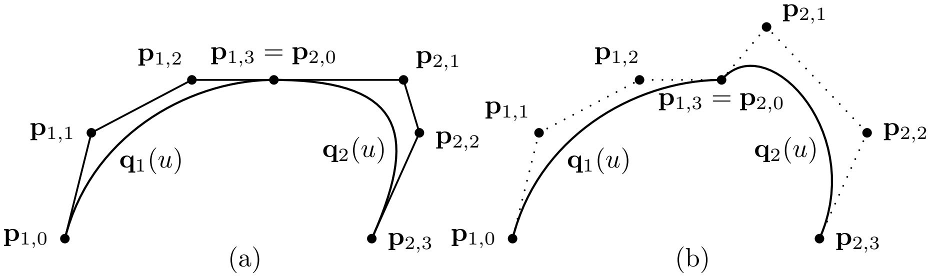

Figure VIII.7: Two curves, each formed from two Bézier curves, with control points as shown. The curve in part (a) is G^1-continuous, but not C^1-continuous. The curve in part (b) is neither C^1-continuous nor G^1-continuous. Compare these curves to the curves of Figures VIII.5 and VIII.6 which are both C^1-continuous and G^1-continuous.

Definition VIII.4. Let $k \geq 0$. A function $\mathbf{f}(u)$ is *C^k-continuous* if $\mathbf{f}$ has k-th derivative defined and continuous everywhere in the domain of $\mathbf{f}$. For $k = 0$, the convention is that the zeroth derivative of $\mathbf{f}$ is just $\mathbf{f}$ itself, so C^0-continuity is the same as continuity.

The function $\mathbf{f}(u)$ is *C^∞-continuous* if it is C^k-continuous for all $k \geq 0$.

In some situations, having continuous first derivatives is important. For example, if the curve $\mathbf{q}(u)$ will be used to parameterize motion as a function of u, with u measuring time, then the C^1-continuity of $\mathbf{q}(u)$ will ensure that the motion proceeds smoothly with no instantaneous changes in velocity or direction. However, in other cases, the requirement that the first derivative be continuous can be relaxed somewhat. For example, if the curve $\mathbf{q}(u)$ is being used to define a shape, then we do not really need the full strength of C^1-continuity. Instead, it is often enough to just have the slope of $\mathbf{q}(u)$ be continuous. That is, it is often enough if the slope of $\mathbf{q}_1(u)$ at $u = 1$ is equal to the slope of $\mathbf{q}_2(u)$ at $u = 0$. This condition is known as G^1-continuity, or *geometric continuity.* Intuitively, G^1-continuity means that when the curve is drawn as a static object, it "looks" smooth. A rather general definition of G^1-continuity can be given as follows.

Definition VIII.5. A function $\mathbf{f}(u)$ is *G^1-continuous* provided $\mathbf{f}$ is continuous, and provided there is a function $t = t(u)$ which is continuous and strictly increasing such that the function $\mathbf{g}(u) = \mathbf{f}(t(u))$ has continuous, nonzero first derivative everywhere in its domain.

In practice, one rarely uses the full power of this definition. Rather, a sufficient condition for the G^1-continuity of the curve $\mathbf{q}(u)$ is that $\mathbf{p}_{1,3} - \mathbf{p}_{1,2}$ and $\mathbf{p}_{2,1} - \mathbf{p}_{2,0}$ are both nonzero and that one can be expressed as a positive scalar multiple of the other.

Exercise VIII.5. Give an example of a curve which is C^1-continuous, but not G^1-continuous. [Hint: The derivative of the curve can be zero at some point.]

VIII.5 Hermite polynomials

Hermite polynomials provide an alternative to Bézier curves for representing cubic curves. Hermite polynomials allow a curve to be defined in terms its endpoints and its derivatives at its endpoints.

The degree three Hermite polynomials $H_0(u)$, $H_1(u)$, $H_2(u)$, and $H_3(u)$ are chosen so that

$$\begin{array}{llll} H_0(0)=1 & H_1(0)=0 & H_2(0)=0 & H_3(0)=0 \\ H_0'(0)=0 & H_1'(0)=1 & H_2'(0)=0 & H_3'(0)=0 \\ H_0'(1)=0 & H_1'(1)=0 & H_2'(1)=1 & H_3'(1)=0 \\ H_0(1)=0 & H_1(1)=0 & H_2(1)=0 & H_3(1)=1. \end{array}$$

The advantage of Hermite polynomials is that if we need a degree three polynomial $f(u)$ that has value equal to $\mathbf{a}$ at $u=0$ and equal to $\mathbf{d}$ at $u=1$ and has first derivative equal to $\mathbf{b}$ at $u=0$ and $\mathbf{c}$ at $u=1$, then we can just define

$$f(u) \;=\; \mathbf{a}H_0(u)+\mathbf{b}H_1(u)+\mathbf{c}H_2(u)+\mathbf{d}H_3(u).$$

Since a degree three polynomial is uniquely determined by its values and first derivatives at the two points $u=0$ and $u=1$, there is only way to define the Hermite polynomials H_i to satisfy the above conditions. Some simple calculus and algebra shows that the degree three Hermite polynomials are:[4]

$$\begin{aligned} H_0(u) &= (1+2u)(1-u)^2 \;=\; 2u^3-3u^2+1 \\ H_1(u) &= u(1-u)^2 \;=\; u^3-2u^2+u \\ H_2(u) &= -u^2(1-u) \;=\; u^3-u^2 \\ H_3(u) &= u^2(3-2u) \;=\; -2u^3+3u^2. \end{aligned}$$

The Hermite polynomials are scalar-valued functions, but can be used to define curves in $\mathbb{R}^k$ by using vectors as coefficients. This allows any degree three Bézier curve to be expressed in a Hermite form. In fact, it is easy to convert a Bézier curve $\mathbf{q}(u)$ with control points $\mathbf{p}_0$, $\mathbf{p}_1$, $\mathbf{p}_2$, and $\mathbf{p}_3$ in $\mathbb{R}^k$ into a Hermite representation: since the initial derivative is $\mathbf{q}'(0)=3(\mathbf{p}_1-\mathbf{p}_0)$ and the ending derivative is $\mathbf{q}'(1)=3(\mathbf{p}_3-\mathbf{p}_2)$, the Hermite representation must be

$$\mathbf{q}(u) \;=\; \mathbf{p}_0H_0(u)+3(\mathbf{p}_1-\mathbf{p}_0)H_1(u)+3(\mathbf{p}_3-\mathbf{p}_2)H_2(u)+\mathbf{p}_3H_3(u).$$

Unlike Bézier curves, the Hermite representation of a curve is not a weighted average, since the sum $H_1+H_2+H_3+H_4$ does not generally equal 1. The coefficients of H_0 and H_3 are points (the starting and end points of the curve), but the coefficients of H_1 and H_2 are vectors. As a consequence, the Hermite polynomials lack many of the nice properties of Bézier curves; their advantage,

[4] Another way to derive these formulas for the Hermite polynomials is to express them as Bézier curves that takes values in $\mathbb{R}$. This is simple enough, since we know the functions' values and derivatives at the endpoints $u=0$ and $u=1$.

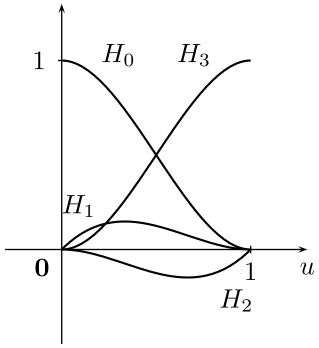

Figure VIII.8: The degree three Hermite polynomials.

however, is that sometimes it is more natural to define a curve in terms of its initial and ending positions and velocities than with control points.

For the opposite direction, converting a Hermite representation of a curve,

$$\mathbf{q}(u) \;=\; \mathbf{r}_0 H_0(u) + \mathbf{r}_1 H_1(u) + \mathbf{r}_2 H_2(u) + \mathbf{r}_3 H_3(u),$$

into a Bézier representation of the curve is also simple. Just let $\mathbf{p}_0 = \mathbf{r}_0$, let $\mathbf{p}_3 = \mathbf{r}_3$, let $\mathbf{p}_1 = \mathbf{p}_0 + \frac{1}{3}\mathbf{r}_1$, and let $\mathbf{p}_2 = \mathbf{p}_3 - \frac{1}{3}\mathbf{r}_2$.

Exercise VIII.6. Let $\mathbf{q}(u)$ be the curve of Exercise VIII.1. Express $\mathbf{q}(u)$ with Hermite polynomials.

VIII.6 Bézier curves of general degree

We now take up the topic of Bézier curves of arbitrary degree. So far we have considered only degree three Bézier curves, but it is useful to consider curves of other degrees. For instance, in Section VIII.13 we will use degree two, rational Bézier curves for rendering circles and other conic sections. As we shall see, the higher (and lower) degree Bézier curves behave analogously to the already studied degree three Bézier curves.

Definition VIII.6. Let $k \geq 0$. The *Bernstein polynomials of degree k* are defined by

$$B_i^k(u) \;=\; \binom{k}{i} u^i (1-u)^{k-i}.$$

When $k = 3$, the Bernstein polynomials $B_i^3(u)$ are identical to the Bernstein polynomials $B_i(u)$ defined in Section VIII.1. It is clear that the Bernstein polynomials $B_i^k(u)$ are degree k polynomials.

Definition VIII.7. Let $k \geq 1$. The *degree k Bézier curve* $\mathbf{q}(u)$ defined from $k+1$ control points $\mathbf{p}_0, \mathbf{p}_1, \ldots, \mathbf{p}_k$ is the parametrically defined curve given by

$$\mathbf{q}(u) \;=\; \sum_{i=0}^{k} B_i^k(u)\mathbf{p}_i,$$

on the domain $u \in [0,1]$.

For example, with $k = 1$, a degree one Bézier curve has two control points $\mathbf{p}_0$ and $\mathbf{p}_1$ and is defined by

$$\mathbf{q}(u) \;=\; (1-u)\mathbf{p}_0 + u\mathbf{p}_1 \;=\; \mathit{lerp}(\mathbf{p}_0, \mathbf{p}_1, u).$$

For $k = 2$, a degree two Bézier curve has three control points $\mathbf{p}_0$, $\mathbf{p}_1$ and $\mathbf{p}_2$ and equals

$$\mathbf{q}(u) \;=\; (1-u)^2\mathbf{p}_0 + 2u(1-u)\mathbf{p}_1 + u^2\mathbf{p}_2.$$

Section VIII.1 discussed degree three Bézier curves and their properties. The next two theorems and corollary generalize these properties to other degrees k.

Theorem VIII.8. *Let* $k \geq 1$.

a. $B_0^k(0) = 1 = B_k^k(1)$.

b. $\sum_{i=0}^{k} B_i^k(u) = 1$, *for all* u.

c. $B_i^k(u) \geq 0$ *for all* $0 \leq u \leq 1$.

Proof. Parts a. and c. are easily checked. To prove part b., use the binomial theorem:

$$\sum_{i=0}^{k} B_i^k(u) \;=\; \sum_{i=0}^{k} \binom{k}{i} u^i(1-u)^{k-i} \;=\; (u + (1-u))^k \;=\; 1. \qquad \square$$

The properties of Bernstein functions in Theorem VIII.8 immediately imply the corresponding properties of the curve $\mathbf{q}(u)$. By a., the curve starts at $\mathbf{q}(0) = \mathbf{p}_0$ and ends at $\mathbf{q}(1) = \mathbf{p}_k$. Properties b. and c. imply that each point $\mathbf{q}(u)$ is a weighted average of the control points. As an consequence, by Theorem V.12, a Bézier curve lies entirely in the convex hull of its control points.

We have already seen several examples of degree three Bézier curves in Figures VIII.1 and VIII.2. Figure VIII.9 shows some examples of Bézier curves of degrees 1, 2, and 8, along with their control points. The degree one Bézier curve is seen to have just two control points, and to consist of linear interpolation between the two control points. The degree two Bézier curve has three control points, and the degree eight Bézier curve has nine.

In all the examples, the Bézier curve is seen to be tangent to the first and last line segments joining its control points at $u = 0$ and $u = 1$. This general fact can be proved from the following theorem, which gives a formula for the derivative of a Bézier curve.

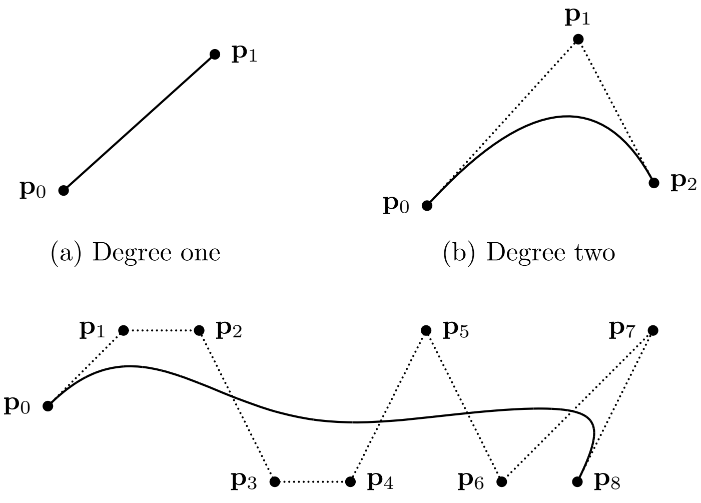

(a) Degree one

(b) Degree two

(c) Degree eight

Figure VIII.9: (a) A degree one Bézier curve is just a straight line interpolating the two control points. (b) A degree two Bézier curve has three control points. (c) A degree eight Bézier curve has nine control points. The dotted straight-line segments are called the *control polygon* of the Bézier curve.

Theorem VIII.9. *Let* $\mathbf{q}(u)$ *be a degree* k *Bézier curve, with control points* $\mathbf{p}_0, \ldots, \mathbf{p}_k$. *Then its first derivative is given by*

$$\mathbf{q}'(u) \;=\; k \cdot \sum_{i=0}^{k-1} B_i^{k-1}(u)(\mathbf{p}_{i+1} - \mathbf{p}_i).$$

Therefore, the derivative, $\mathbf{q}'(u)$, of a Bézier curve is itself a Bézier curve: the degree is decreased by one and the control points are $k(\mathbf{p}_{i+1} - \mathbf{p}_i)$. A special case of the theorem gives the following formulas for the derivatives of $\mathbf{q}(u)$ at its starting and end points:

Corollary VIII.10. *Let* $\mathbf{q}(u)$ *be a degree* k *Bézier curve. Then*

$$\mathbf{q}'(0) \;=\; k(\mathbf{p}_1 - \mathbf{p}_0) \qquad \textit{and} \qquad \mathbf{q}'(1) = k(\mathbf{p}_k - \mathbf{p}_{k-1}).$$

This corollary proves the observation that the beginning and ending directions of the Bézier curve are in the directions of $\mathbf{p}_1 - \mathbf{p}_0$ and of $\mathbf{p}_k - \mathbf{p}_{k-1}$.

Proof. The corollary is easily proved from Theorem VIII.9 with the aid of Theorem VIII.8. To prove Theorem VIII.9, one may either obtain it as a special case of Theorem IX.13 on page 355 which we will state and prove in the next chapter; or one can prove it directly by the following argument. Using the definition of the Bernstein polynomials, we have

$$\frac{d}{du}B_i^k(u) \;=\; \binom{k}{i} i u^{i-1}(1-u)^{k-i} - \binom{k}{i}(k-i)u^i(1-u)^{k-i-1}.$$

Note that the first term is zero if $i=0$ and the second is zero if $i=k$. Thus, the derivative of $\mathbf{q}(u)$ is equal to

$$\begin{aligned}
&\sum_{i=0}^{k}\binom{k}{i} i u^{i-1}(1-u)^{k-i}\mathbf{p}_i \;-\; \sum_{i=0}^{k}\binom{k}{i}(k-i)u^i(1-u)^{k-1-i}\mathbf{p}_i \\
&\quad= \sum_{i=1}^{k}\binom{k}{i} i u^{i-1}(1-u)^{k-i}\mathbf{p}_i \;-\; \sum_{i=0}^{k-1}\binom{k}{i}(k-i)u^i(1-u)^{k-1-i}\mathbf{p}_i \\
&\qquad\qquad\text{(Removing zero terms from the summations.)} \\
&\quad= \sum_{i=1}^{k} k\binom{k-1}{i-1}u^{i-1}(1-u)^{k-i}\mathbf{p}_i \;-\; \sum_{i=0}^{k-1} k\binom{k-1}{i}u^i(1-u)^{k-1-i}\mathbf{p}_i \\
&\qquad\qquad\text{(Using } \tbinom{k}{i}i = k\tbinom{k-1}{i-1} \text{ and } \tbinom{k}{i}(k-i) = k\tbinom{k-1}{i}.\text{)} \\
&\quad= \sum_{i=0}^{k-1} k\binom{k-1}{i}u^i(1-u)^{k-1-i}\mathbf{p}_{i+1} \;-\; \sum_{i=0}^{k-1} k\binom{k-1}{i}u^i(1-u)^{k-1-i}\mathbf{p}_i \\
&\qquad\qquad\text{(Change of variable in the first summation.)} \\
&\quad= \sum_{i=0}^{k-1} k\binom{k-1}{i}u^i(1-u)^{k-1-i}(\mathbf{p}_{i+1}-\mathbf{p}_i) \\
&\quad= k\sum_{i=0}^{k-1} B_i^{k-1}(u)(\mathbf{p}_{i+1}-\mathbf{p}_i),
\end{aligned}$$

and Theorem VIII.9 is proved. □

Bézier curves of arbitrary degree k have many of the properties which we discussed earlier in connection with degree three curves. These include the convex hull property which was mentioned above already. Another property is *invariance under affine transformations*; namely, if M is an affine transformation, then the result of applying M to a Bézier curve $\mathbf{q}(u)$ is identical to the result of applying M to the control points. In other words, the curve $M(\mathbf{q}(u))$ is equal to the Bézier curve formed from the control points $M(\mathbf{p}_i)$. The affine invariance property follows from the characterization of the point $\mathbf{q}(u)$ as a weighted average of the control points, using Theorem V.2.

An additional property of Bézier curves is the *variation diminishing property.* Define the *control polygon* to be the series of straight-line segments which connect the control points $\mathbf{p}_0, \mathbf{p}_1, \ldots, \mathbf{p}_k$ in sequential order (see Figure VIII.9). Then the *variation diminishing property* states that, for any line L in $\mathbb{R}^2$ (or, any plane P in $\mathbb{R}^3$), the number of times the curve $\mathbf{q}(u)$ crosses the line (or, the plane) is less than or equal to the number of times the control polygon crosses the line (or, the plane). A proof of the variation diminishing property may be found in [42]; this proof is also sketched below in Exercise VIII.42.

It is of course possible to create curves which are piecewise degree k Bézier curves, similarly to what was discussed in Section VIII.4 for degree three curves. Let $\mathbf{p}_{1,i}$ be the control points for the first curve and $\mathbf{p}_{2,i}$ be the control points for the second curve (where $0 \le i \le k$). A necessary and sufficient condition for continuity is that $\mathbf{p}_{1,k} = \mathbf{p}_{2,0}$ so that the second curve starts at the end of the first curve. A necessary and sufficient condition for C^1-continuity is that $\mathbf{p}_{1,k} - \mathbf{p}_{1,k-1}$ equals $\mathbf{p}_{2,1} - \mathbf{p}_{2,0}$ so that the first derivatives match up (see Corollary VIII.10). A sufficient condition for G^1-continuity is that $\mathbf{p}_{1,k} - \mathbf{p}_{1,k-1}$ and $\mathbf{p}_{2,1} - \mathbf{p}_{2,0}$ are both nonzero and are positive scalar multiples of each other. These conditions are equivalent to the conditions we encountered in the degree three case!

For the next exercise, we adopt the convention that two curves $\mathbf{q}_1(u)$ and $\mathbf{q}_2(u)$ are the same if and only if $\mathbf{q}_1(u) = \mathbf{q}_2(u)$ for all $u \in [0,1]$. Otherwise, the two curves are said to be *different*.

Exercise VIII.7. Prove that, for a given degree k Bézier curve, there is a *unique* set of control points $\mathbf{p}_0, \ldots, \mathbf{p}_k$ which defines that Bézier curve. I.e., two different sequences of $k+1$ control points define two different Bézier curves. [Hint: This should be clear for $\mathbf{p}_0$ and $\mathbf{p}_k$; for the rest of the control points, use induction on the degree and the formula for the derivative of a Bézier curve.]

A *degree k polynomial curve* is a curve of the form

$$\mathbf{q}(u) \;=\; \langle x(u), y(u), z(u) \rangle,$$

with $x(u)$, $y(u)$, and $z(u)$ polynomials of degree $\le k$. A degree two (respectively, degree three) polynomial curve is also called a *quadratic curve* (respectively, *cubic curve*). Note that every degree k Bézier curve is a degree k polynomial curve.

Exercise VIII.8. Let $\mathbf{q}(u)$ be a degree k polynomial curve. Prove that there are control points $\mathbf{p}_0, \ldots, \mathbf{p}_k$ which represent $\mathbf{q}(u)$ as a degree k Bézier curve for $u \in [0,1]$. [Hint: Prove that the dimension of the vector space of all degree k polynomial curves is equal to the dimension of the vector space of all degree k Bézier curves. You will need to use the previous exercise.]

VIII.7 De Casteljau's method, revisited

Recall from Section VIII.2 that de Casteljau gave a simple, and numerically stable, method for computing a point $\mathbf{q}(u)$ on a degree three Bézier curve for a particular value of u. As we show next, the de Casteljau method can be generalized to apply to Bézier curves of arbitrary degree, in the more-or-less obvious way.

Let a degree k Bézier curve $\mathbf{q}(u)$ have control points $\mathbf{p}_i$, $i = 0, \ldots, k$. Fix $u \in [0,1]$. We define points $\mathbf{p}_i^r(u)$ as follows. First, for $r = 0$, let $\mathbf{p}_i^0(u) = \mathbf{p}_i$. Second, for $r > 0$ and $0 \le i \le k - r$, let

$$\begin{aligned} \mathbf{p}_i^r(u) &= (1-u)\mathbf{p}_i^{r-1}(u) + u\mathbf{p}_{i+1}^{r-1}(u) \\ &= \mathit{lerp}(\mathbf{p}_i^{r-1}(u), \mathbf{p}_{i+1}^{r-1}(u), u). \end{aligned}$$

In Section VIII.2, for the degree $k = 3$ case, we used different names for the variables. Those variables can be translated into the new notation by $\mathbf{r}_i = \mathbf{p}_i^1$, and $\mathbf{s}_i = \mathbf{p}_i^2$, and $\mathbf{t}_0 = \mathbf{p}_0^3$.

The next theorem generalizes the de Casteljau method to the general degree case.

Theorem VIII.11. *Let $\mathbf{q}(u)$ and $\mathbf{p}_i^r(u)$ be as above. Then, for all u, $\mathbf{q}(u) = \mathbf{p}_0^k(u)$.*

As an example, suppose $k = 2$ and $\mathbf{q}(u)$ is a degree two Bézier curve with control points $\mathbf{p}_0$, $\mathbf{p}_1$ and $\mathbf{p}_2$. Then, for a fixed value u, $\mathbf{q}(u)$ can be computed by:

$$\begin{aligned} \mathbf{p}_0^1 &= \mathit{lerp}(\mathbf{p}_0, \mathbf{p}_1, u) &&= (1-u)\mathbf{p}_0 + u\mathbf{p}_1 \\ \mathbf{p}_1^1 &= \mathit{lerp}(\mathbf{p}_1, \mathbf{p}_2, u) &&= (1-u)\mathbf{p}_1 + u\mathbf{p}_2 \\ \mathbf{p}_1^2 &= \mathit{lerp}(\mathbf{p}_0^1, \mathbf{p}_1^1, u) &&= (1-u)\mathbf{p}_0^1 + u\mathbf{p}_1^1 \\ \mathbf{q}(u) &= \mathbf{p}_1^2. \end{aligned}$$

For $k = 3$, Theorem VIII.11 is illustrated by Equations (VIII.4)-(VIII.6) and Figure VIII.4.

Proof. The theorem is proved via a more general claim; and then the $r = k$ case of the claim immediately implies the theorem.

Claim *Let $0 \le r \le k$ and $0 \le i \le k - r$. Then*

$$\mathbf{p}_i^r(u) = \sum_{j=0}^{r} B_j^r(u)\mathbf{p}_{i+j}. \qquad \text{(VIII.9)}$$

The claim is proved by induction on r. The base case, $r = 0$, is obvious. Or, if you prefer to take $r = 1$ as the base case, the claim is also easily verified for $r = 1$. Now, suppose (VIII.9) holds for r: we wish to prove it holds for $r + 1$. We have

$$\begin{aligned} \mathbf{p}_i^{r+1}(u) &= (1-u)\mathbf{p}_i^r(u) + u\mathbf{p}_{i+1}^r(u) \\ &= \sum_{j=0}^{r}(1-u)B_j^r(u)\mathbf{p}_{i+j} + \sum_{j=0}^{r} uB_j^r(u)\mathbf{p}_{i+j+1} \\ &= \sum_{j=0}^{r+1}\left((1-u)B_j^r(u) + uB_{j-1}^r(u)\right)\mathbf{p}_{i+j}, \end{aligned}$$

where the last sum should interpreted by letting the quantities $\binom{r}{r+1}$ and $\binom{r}{-1}$, and thus $B^r_{-1}(u)$ and$B^r_{r+1}(u)$, be defined to equal zero. From the fact that $\binom{r}{j}+\binom{r}{j-1}=\binom{r+1}{j}$, it is easy to verify that

$$(1-u)B^r_j(u)+uB^r_{j-1}(u) \;=\; B^{r+1}_j(u),$$

from whence the claim, and thus Theorem VIII.11, are proved. □

VIII.8 Recursive subdivision, revisited

The recursive subdivision technique of Section VIII.3 can be generalized to Bézier curves of arbitrary degree. Let $\mathbf{q}(u)$ be a degree k Bézier curve, let $u_0 \in [0,1]$, and let $\mathbf{q}_1(u)$ and $\mathbf{q}_2(u)$ be the curves satisfying

$$\mathbf{q}_1(u) \;=\; \mathbf{q}(u_0u) \qquad \text{and} \qquad \mathbf{q}_2(u) \;=\; \mathbf{q}(u_0+(1-u_0)u).$$

So $\mathbf{q}_1(u)$ is the first u_0-fraction of $\mathbf{q}(u)$ and $\mathbf{q}_2(u)$ is the rest of $\mathbf{q}(u)$: both curves $\mathbf{q}_1(u)$ and $\mathbf{q}_2(u)$ have domain $[0,1]$. Also, let the points $\mathbf{p}^r_i=\mathbf{p}^r_i(u_0)$ be defined as in Section VIII.7 with $u=u_0$.

Theorem VIII.12. *Let $\mathbf{q}$, $\mathbf{q}_1$, $\mathbf{q}_2$, and $\mathbf{p}^r_i$ be as above.*

a. *The curve $\mathbf{q}_1(u)$ is equal to the degree k Bézier curve with control points $\mathbf{p}^0_0,\mathbf{p}^1_0,\mathbf{p}^2_0,\ldots,\mathbf{p}^k_0$.*

b. *The curve $\mathbf{q}_2(u)$ is equal to the degree k Bézier curve with control points $\mathbf{p}^k_0,\mathbf{p}^{k-1}_1,\mathbf{p}^{k-2}_2,\ldots,\mathbf{p}^0_k$.*

Proof. We will prove part a.; part b. is completely symmetric. In order to prove a., we need to show that

$$\mathbf{q}(u_0u) \;=\; \sum_{j=0}^{k} B^k_j(u)\mathbf{p}^j_0(u_0)$$

holds. Expanding the left-hand side with the definition of Bézier curves, and the righthand side with Equation (VIII.9) of the claim, this is equivalent to

$$\sum_{i=0}^{k} B^k_i(u_0u)\mathbf{p}_i \;=\; \sum_{j=0}^{k} B^k_j(u)\sum_{i=0}^{j} B^j_i(u_0)\mathbf{p}_i.$$

Reordering the summations, the righthand side of the equation is equal to

$$\sum_{i=0}^{k}\sum_{j=i}^{k} B^k_j(u)B^j_i(u_0)\mathbf{p}_i.$$

Therefore, equating coefficients of the $\mathbf{p}_i$'s, we need to show that

$$B_i^k(u_0u) \;=\; \sum_{j=i}^{k} B_j^k(u)B_i^j(u_0),$$

i.e.,

$$\binom{k}{i}(u_0u)^i(1-u_0u)^{k-i} \;=\; \sum_{j=i}^{k}\binom{k}{j}\binom{j}{i}u^ju_0^i(1-u)^{k-j}(1-u_0)^{j-i}.$$

Dividing both sides by $(u_0u)^i$, and using the fact that $\binom{k}{j}\binom{j}{i} = \binom{k}{i}\binom{k-i}{j-i}$, this reduces to showing that

$$(1-u_0u)^{k-i} \;=\; \sum_{j=i}^{k}\binom{k-i}{j-i}u^{j-i}(1-u)^{k-j}(1-u_0)^{j-i}.$$

By a change of variables from "j" to "$j+i$" in the summation, the righthand side is equal to

$$\begin{aligned}
&\sum_{j=0}^{k-i}\binom{k-i}{j}u^j(1-u_0)^j(1-u)^{k-i-j}\\
&\qquad= \sum_{j=0}^{k-i}\binom{k-i}{j}(u-u_0u)^j(1-u)^{k-i-j}\\
&\qquad= ((u-u_0u)+(1-u))^{k-i}\\
&\qquad= (1-u_0u)^{k-i},
\end{aligned}$$

where the second equality follows from the binomial theorem. This is what we needed to show in order to complete the proof of Theorem VIII.12. □

VIII.9 Degree elevation

The term "degree elevation" refers to the process of taking a Bézier curve of degree k and re-expressing the same curve as a higher degree Bézier curve. Degree elevation is useful for converting a low degree Bézier curve into a higher degree represention. For example, Section VIII.13 will describe several ways to represent a circle with degree two Bézier curves; and one may need to elevate their degree to three for use in a software program. The postscript language, for example, supports only degree three Bézier curves, not degree two.

Of course, it should not be surprising that degree elevation is possible. Indeed, any degree k polynomial can be viewed also as a degree $k+1$ polynomial by just treating it as having a leading term $0x^{k+1}$ with coefficient zero. It is not as simple to elevate the degree of Bézier curves, since we must define the curve in terms of its control points. To be completely explicit, the degree elevation problem is the following:

> We are given a degree k Bézier curve $\mathbf{q}(u)$ defined in terms of control points $\mathbf{p}_i$, $i = 0, \ldots, k$. We wish to find new control points $\widehat{\mathbf{p}}_i$, $i = 0, \ldots, k, k+1$ so that the degree $k+1$ Bézier curve $\widehat{\mathbf{q}}(u)$ defined by these control points is equal to $\mathbf{q}(u)$; i.e., $\widehat{\mathbf{q}}(u) = \mathbf{q}(u)$ for all u.

It turns out that the solution to this problem is fairly simple. However, before we present the general solution, we first do the $k = 2$ case as an example. (See Exercise VIII.16 on page 303 for an example of an application of this case.) In this case, we are given three control points, $\mathbf{p}_0, \mathbf{p}_1, \mathbf{p}_2$, of a degree two Bézier curve, $\mathbf{q}(u)$. Since $\mathbf{q}(0) = \mathbf{p}_0$ and $\mathbf{q}(1) = \mathbf{p}_2$, we must have $\widehat{\mathbf{p}}_0 = \mathbf{p}_0$ and $\widehat{\mathbf{p}}_3 = \mathbf{p}_2$ so that the degree three curve $\widehat{\mathbf{q}}(u)$ starts at $\mathbf{p}_0$ and ends at $\mathbf{p}_2$. Also, the derivatives at the beginning and end of the curve are equal to

$$\begin{aligned} \mathbf{q}'(0) &= 2(\mathbf{p}_1 - \mathbf{p}_0) \\ \mathbf{q}'(1) &= 2(\mathbf{p}_2 - \mathbf{p}_1). \end{aligned}$$

Therefore, by Equation (VIII.3) for the derivative of a degree three Bézier curve, we must have

$$\begin{aligned} \widehat{\mathbf{p}}_1 &= \widehat{\mathbf{p}}_0 + \frac{1}{3}\mathbf{q}'(0) = \tfrac{1}{3}\mathbf{p}_0 + \tfrac{2}{3}\mathbf{p}_1 \\ \widehat{\mathbf{p}}_2 &= \widehat{\mathbf{p}}_3 - \frac{1}{3}\mathbf{q}'(1) = \tfrac{2}{3}\mathbf{p}_1 + \tfrac{1}{3}\mathbf{p}_2, \end{aligned}$$

as shown in Figure VIII.10. These choices for control points give $\widehat{\mathbf{q}}(u)$ the right starting and ending derivatives. Since $\mathbf{q}(u)$ and $\widehat{\mathbf{q}}(u)$ both are polynomials of degree ≤ 3, it follows that $\widehat{\mathbf{q}}(u)$ is equal to $\mathbf{q}(u)$.

Now, we turn to the general case of degree elevation. Suppose $\mathbf{q}(u)$ is a degree k curve with control points $\mathbf{p}_0, \ldots, \mathbf{p}_k$: we wish to find $k+2$ control points $\widehat{\mathbf{p}}_0, \ldots, \widehat{\mathbf{p}}_{k+1}$ which define a degree $k+1$ Bézier curve $\widehat{\mathbf{q}}(u)$ which is identical to $\mathbf{q}(u)$. For this, the following definitions work:

$$\begin{aligned} \widehat{\mathbf{p}}_0 &= \mathbf{p}_0 \qquad\qquad \widehat{\mathbf{p}}_{k+1} = \mathbf{p}_k \\ \widehat{\mathbf{p}}_i &= \frac{i}{k+1}\mathbf{p}_{i-1} + \frac{k-i+1}{k+1}\mathbf{p}_i. \end{aligned}$$

Note that the first two equations, for $\widehat{\mathbf{p}}_0$ and $\widehat{\mathbf{p}}_{k+1}$, can be viewed as special cases of the third, by defining $\mathbf{p}_{-1}$ and $\mathbf{p}_{k+1}$ to be arbitrary points.

Theorem VIII.13. *Let $\mathbf{q}(u)$, $\widehat{\mathbf{q}}(u)$, $\mathbf{p}_i$, and $\widehat{\mathbf{p}}_i$ be as above. Then $\widehat{\mathbf{q}}(u) = \mathbf{q}(u)$ for all u.*

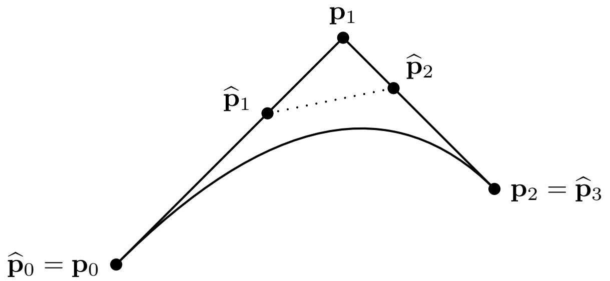
$\mathbf{p}_1$
$\widehat{\mathbf{p}}_2$
$\widehat{\mathbf{p}}_1$
$\mathbf{p}_2 = \widehat{\mathbf{p}}_3$
$\widehat{\mathbf{p}}_0 = \mathbf{p}_0$

Figure VIII.10: The curve $\mathbf{q}(u) = \widehat{\mathbf{q}}(u)$ is both a degree two Bézier curve with control points $\mathbf{p}_0$, $\mathbf{p}_1$, and $\mathbf{p}_2$, and a degree three Bézier curve with control points $\widehat{\mathbf{p}}_0$, $\widehat{\mathbf{p}}_1$, $\widehat{\mathbf{p}}_2$, and $\widehat{\mathbf{p}}_3$.

Proof. We need to show that

$$\sum_{i=0}^{k+1} \binom{k+1}{i} u^i(1-u)^{k-i+1}\widehat{\mathbf{p}}_i \;=\; \sum_{i=0}^{k} \binom{k}{i} u^i(1-u)^{k-i}\mathbf{p}_i. \qquad \text{(VIII.10)}$$

The left-hand side of this equation is also equal to

$$\sum_{i=0}^{k+1} \binom{k+1}{i} u^i(1-u)^{k-i+1}\left(\frac{i}{k+1}\mathbf{p}_{i-1} + \frac{k-i+1}{k+1}\mathbf{p}_i\right).$$

Regrouping the summation, we calculate the coefficient of $\mathbf{p}_i$ in this last equation to be equal to

$$\binom{k+1}{i+1}\frac{i+1}{k+1}u^{i+1}(1-u)^{k-i} + \binom{k+1}{i}\frac{k-i+1}{k+1}u^i(1-u)^{k-i+1}.$$

Using the identities $\binom{k+1}{i+1}\frac{i+1}{k+1} = \binom{k}{i} = \binom{k+1}{i}\frac{k-i+1}{k+1}$, this is further equal to

$$\binom{k}{i}(u+(1-u))u^i(1-u)^{k-i} \;=\; \binom{k}{i}u^i(1-u)^{k-i}.$$

Thus, we have shown that $\mathbf{p}_i$ has the same coefficient on both sides of Equation (VIII.10), which proves the desired equality. □

VIII.10 Bézier surface patches

This section extends the notion of Bézier curves to define Bézier patches. A Bézier curve was a one dimensional curve; a Bézier patch is a two dimensional parametric surface. Typically, a Bézier patch is parameterized by variables u and v which both range over the interval $[0,1]$. The patch is then the parametric surface $\mathbf{q}(u,v)$, where $\mathbf{q}$ is a vector-valued function defined on the unit square $[0,1]^2$.

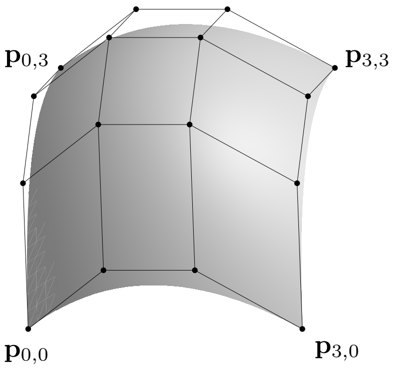

Figure VIII.11: A degree three Bézier patch and its control points. The control points are shown joined by straight-line segments.

VIII.10.1 Basic properties of Bézier patches

Bézier patches of degree three are defined using a 4×4 array of control points $\mathbf{p}_{i,j}$, where i, j take on values $0, 1, 2, 3$. The Bézier patch with these control points is given by the formula

$$\mathbf{q}(u,v) \;=\; \sum_{i=0}^{3}\sum_{j=0}^{3} B_i(u)B_j(v)\mathbf{p}_{i,j}. \qquad \text{(VIII.11)}$$

An example is shown in Figure VIII.11. Intuitively, the control points act similarly to the control points used for Bézier curves. The four corner control points, $\mathbf{p}_{0,0}$, $\mathbf{p}_{3,0}$, $\mathbf{p}_{0,3}$, and $\mathbf{p}_{3,3}$ form the four corners of the Bézier patch, and the remaining twelve control points influence the patch by "pulling" the patch towards them.

Equation (VIII.11) can be equivalently written in either of the forms

$$\mathbf{q}(u,v) \;=\; \sum_{i=0}^{3}\Bigl(B_i(u)\cdot\sum_{j=0}^{3} B_j(v)\mathbf{p}_{i,j}\Bigr) \qquad \text{(VIII.12)}$$

$$\mathbf{q}(u,v) \;=\; \sum_{j=0}^{3}\Bigl(B_j(v)\cdot\sum_{i=0}^{3} B_i(u)\mathbf{p}_{i,j}\Bigr). \qquad \text{(VIII.13)}$$

Consider the cross sections of $\mathbf{q}(u,v)$ obtained by holding the value of v fixed and varying u. Some of these cross sections are shown going from left to right in Figure VIII.12. Equation (VIII.12) shows that each such cross section is a degree three Bézier curve with control points $\mathbf{r}_i$ equal to the inner summation, i.e.,

$$\mathbf{r}_i \;=\; \sum_{j=0}^{3} B_j(v)\mathbf{p}_{i,j}.$$

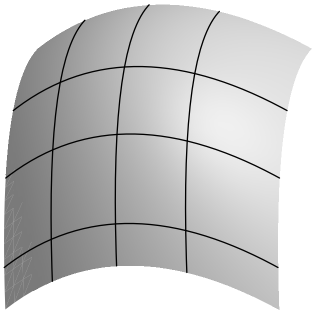

Figure VIII.12: A degree three Bézier patch and some cross sections. The cross sections are Bézier curves.

Thus, the cross sections of the Bézier patch obtained by holding v fixed and letting u vary are ordinary Bézier curves. The control points $\mathbf{r}_i$ for the cross section are functions of v of course, and are in fact given as Bézier curves of the control points $\mathbf{p}_{i,j}$.

Similarly, from Equation (VIII.13), if we hold u fixed and let v vary, then the cross sections are again Bézier curves, and the control points $\mathbf{s}_j$ of the Bézier curve cross sections are computed as functions of u as Bézier curve functions:

$$\mathbf{s}_j \;=\; \sum_{i=0}^{3} B_i(u)\mathbf{p}_{i,j}.$$

Now consider what the boundaries of the Bézier patch look like. The "front" boundary is where $v=0$ and $u \in [0,1]$. For this front cross section, the control points $\mathbf{r}_i$ are equal to $\mathbf{p}_{i,0}$. Thus, the front boundary is the degree three Bézier curve with control points $\mathbf{p}_{0,0}$, $\mathbf{p}_{1,0}$, $\mathbf{p}_{2,0}$, and $\mathbf{p}_{3,0}$. Similarly, the "left" boundary where $u=0$ is the Bézier curve with control points $\mathbf{p}_{0,0}$, $\mathbf{p}_{0,1}$, $\mathbf{p}_{0,2}$, and $\mathbf{p}_{0,3}$. Likewise, the other two boundaries are Bézier curves that have as control points the $\mathbf{p}_{i,j}$'s on the boundaries.

The first-order partial derivatives of the Bézier patch $\mathbf{q}(u,v)$ can be calculated with aid of Theorem VIII.9 along with Equations (VIII.12) and (VIII.13). This can be used to calculate the normal vector to the Bézier patch surface, via Theorem IV.1. Rather than carrying out the calculation of the general formula for partial derivatives here, we will instead consider only the partial derivatives at the boundary of the patches, since these will be useful below in the discussion about joining together Bézier patches with C^1- and G^1-continuity (see Section VIII.10.2). By using Equation (VIII.3) for the derivatives of a Bézier curve at its endpoints and Equations (VIII.12) and (VIII.13), we can calculate the partial derivatives of $\mathbf{q}(u,v)$ at its boundary points as

$$\begin{aligned}
\frac{\partial \mathbf{q}}{\partial v}(u,0) &= \sum_{i=0}^{3} 3B_i(u)(\mathbf{p}_{i,1} - \mathbf{p}_{i,0}) && \text{(VIII.14)}\\
\frac{\partial \mathbf{q}}{\partial v}(u,1) &= \sum_{i=0}^{3} 3B_i(u)(\mathbf{p}_{i,3} - \mathbf{p}_{i,2}) && \text{(VIII.15)}\\
\frac{\partial \mathbf{q}}{\partial u}(0,v) &= \sum_{j=0}^{3} 3B_j(v)(\mathbf{p}_{1,j} - \mathbf{p}_{0,j}) && \text{(VIII.16)}\\
\frac{\partial \mathbf{q}}{\partial u}(1,v) &= \sum_{j=0}^{3} 3B_j(v)(\mathbf{p}_{3,j} - \mathbf{p}_{2,j}). && \text{(VIII.17)}
\end{aligned}$$

These above four partial derivatives are the partial derivatives in the directions pointing perpendicular to the boundaries of the patch. The other partial derivatives at the boundary, such as $(\partial \mathbf{q}/\partial u)(u,0)$, can easily be calculated from the fact that the boundaries of the patch are Bézier curves.

Later, in Section VIII.16, we will need to know the formulas for the second-order mixed partial derivatives at the corners of the patch. Using Equation (VIII.3) or Corollary VIII.10, and Equation (VIII.14), we have

$$\frac{\partial^2 \mathbf{q}}{\partial u \partial v}(0,0) = 9 \cdot (\mathbf{p}_{1,1} - \mathbf{p}_{0,1} - \mathbf{p}_{1,0} + \mathbf{p}_{0,0}). \qquad \text{(VIII.18)}$$

Similarly, at the other three corners of the patch, we have

$$\begin{aligned}
\frac{\partial^2 \mathbf{q}}{\partial u \partial v}(0,1) &= 9 \cdot (\mathbf{p}_{1,3} - \mathbf{p}_{0,3} - \mathbf{p}_{1,2} + \mathbf{p}_{0,2})\\
\frac{\partial^2 \mathbf{q}}{\partial u \partial v}(1,0) &= 9 \cdot (\mathbf{p}_{3,1} - \mathbf{p}_{2,1} - \mathbf{p}_{3,0} + \mathbf{p}_{2,0}) \qquad \text{(VIII.19)}\\
\frac{\partial^2 \mathbf{q}}{\partial u \partial v}(1,1) &= 9 \cdot (\mathbf{p}_{3,3} - \mathbf{p}_{2,3} - \mathbf{p}_{3,2} + \mathbf{p}_{2,2}).
\end{aligned}$$

The second-order mixed partial derivatives at the corners are called *twist vectors.*

Exercise VIII.9* Use Theorem VIII.9 to work out the general formula for the first-order partial derivatives of a Bézier patch, $\partial \mathbf{q}(u,v)/\partial u$ and $\partial \mathbf{q}(u,v)/\partial v$.

Exercise VIII.10. Derive a recursive subdivision method for degree three Bézier patches, based on recursive subdivision for Bézier curves. Your method should either subdivide in the u direction or in the v direction, and split a patch into two patches (i.e., it should not subdivide in both directions at once).

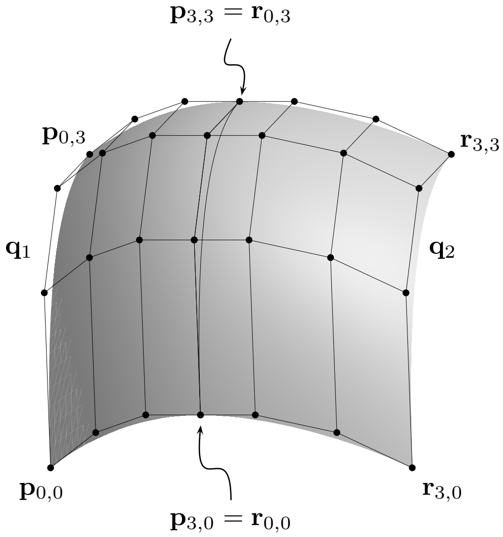

Figure VIII.13: Two Bézier patches join to form a single smooth surface. The two patches $\mathbf{q}_1$ and $\mathbf{q}_2$ each have sixteen control points. The four rightmost control points of $\mathbf{q}_1$ are the same as the four leftmost control points of $\mathbf{q}_2$. The patches are shown forming a C^1-continuous surface.

VIII.10.2 Joining Bézier patches

A common use of Bézier patches is to combine multiple patches together to make a smooth surface. With only 16 control points, a single Bézier patch can make only a limited range of surface shapes. However, by joining multiple patches, a wider range of surface shapes can be approximated. Let us start by considering how to join two patches together so as to make a continuous or C^1- or G^1-continuous surface. The situation is that we have two Bézier patches $\mathbf{q}_1(u,v)$ and $\mathbf{q}_2(u,v)$. The control points of $\mathbf{q}_1$ are $\mathbf{p}_{i,j}$ and those of $\mathbf{q}_2$ are the points $\mathbf{r}_{i,j}$. In addition, $\mathbf{q}_2$ has domain $[0,1]^2$ as usual, but the surface $\mathbf{q}_1$ has been translated to have domain $[-1,0] \times [0,1]$ (by use of the change of variables $u \mapsto u+1$). We wish to find conditions on the control points that will cause the two surfaces to join smoothly at their boundary where $u = 0$ and $0 \le v \le 1$, as shown in Figure VIII.13.

Recall that the right boundary of $\mathbf{q}_1$ (where $u = 0$) is the Bézier curve with control points $\mathbf{p}_{3,j}$, $j = 0,1,2,3$. Likewise, the left boundary of $\mathbf{q}_2$ is the Bézier curve with control points $\mathbf{r}_{0,j}$. Thus, in order for the two boundaries to match, it is necessary and sufficient that $\mathbf{p}_{3,j} = \mathbf{r}_{0,j}$ for $j = 0,1,2,3$.

Now let's assume that the patches are continuous at their boundary and consider continuity of the partial derivatives at the boundary between the patches. First, since the boundaries are equal, clearly the partials with respect to v are equal. For the partials with respect to u, it follows from Equations (VIII.16) and (VIII.17) that a necessary and sufficient condition for C^1-

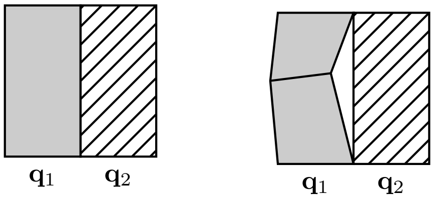

Figure VIII.14: Nonuniform subdivision can cause cracking. On the left, two Bézier patches share a common boundary. On the right, after subdivision of the left patch $\mathbf{q}_1$, the boundaries no longer match up.

continuity, i.e., for

$$\frac{\partial \mathbf{q}_2}{\partial u}(0,v) \;=\; \frac{\partial \mathbf{q}_1}{\partial u}(0,v)$$

to hold for all v, is that

$$\mathbf{p}_{3,j} - \mathbf{p}_{2,j} \;=\; \mathbf{r}_{1,j} - \mathbf{r}_{0,j} \qquad \text{for } j = 0,1,2,3. \tag{VIII.20}$$

For G^1-continuity, it is sufficient that these four vectors are nonzero and that there is a scalar $\alpha > 0$ so that

$$\mathbf{p}_{3,j} - \mathbf{p}_{2,j} \;=\; \alpha(\mathbf{r}_{1,j} - \mathbf{r}_{0,j}) \qquad \text{for } j = 0,1,2,3.$$

In Section VIII.16, we will use the condition (VIII.20) for C^1-continuity to help make surfaces that interpolate points specified on a rectangular grid.

Subdividing Bézier patches

In Exercise VIII.10, you were asked to give an algorithm for recursively subdividing degree three Bézier patches. As in the case of Bézier curves, recursive subdivision is often used to divide a surface until it consists of small patches which are essentially flat. Each flat patch can be approximated as a flat quadrilateral (or, more precisely, can be divided into two triangles, each of which is necessarily planar). These flat patches can then be rendered as usual. In the case of recursive subdivision of patches, there is a new problem: since some patches may need to be subdivided further than others, it can happen that a surface is subdivided and its neighbor is not. This is pictured in Figure VIII.14, where $\mathbf{q}_1$ and $\mathbf{q}_2$ are patches. After $\mathbf{q}_1$ is divided into two subpatches, there is a mismatch between the (formerly common) boundaries of $\mathbf{q}_1$ and $\mathbf{q}_2$. If this mismatch is allowed to persist, then we have a problem known as *cracking* where small gaps or small overlaps can appear in the surface.

One way to fix cracking is to replace the boundary by a straight line. Namely, once the decision has been made that $\mathbf{q}_2$ needs no further subdivision (and will be rendered as a flat patch), then replace the boundary between $\mathbf{q}_1$ and $\mathbf{q}_2$ with a straight line. This is done by redefining the two middle control

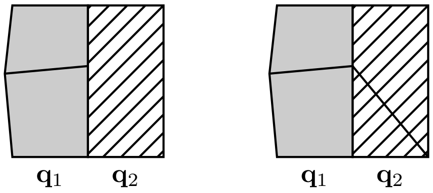

Figure VIII.15: Two solutions to the cracking problem. On the left, the subdivided $\mathbf{q}_1$ and the original $\mathbf{q}_2$ share a common, straight boundary. However, the lighting and shading calculations may cause the surface to be rendered discontinuously at the boundary. On the right, the patch $\mathbf{q}_2$ has been subdivided in an ad hoc way to allow the common boundary to have the same points and normals with respect to both patches.

points along the common boundary. This forces the boundary of $\mathbf{q}_1$ to also be straight and this straightness is preserved by subsequent subdivision.

Unfortunately, just replacing the boundary by a straight line is not enough completely fix the cracking problem. Firstly, as discussed at the end of Chapter II, there may be problems with pixel-size holes along the boundary (see the discussion accompanying Figure III.10 on page 129). Secondly, and more seriously, it is also important that the surface normals on the boundary between the two patches match up in order for lighting computations to be consistent. Still worse, being consistent about assigning surface normals to the vertices is not enough: this is because Gouraud interpolation is used to shade the results of the lighting calculation along the boundary between the patches. If the boundary is divided into two pieces in one patch, and left as one piece in the other patch, Gouraud interpolation will give different results in the two patches. This could happen if three quadrilaterals are rendered as shown on the left in Figure VIII.15, since the lighting calculated at the center vertex may not be consistent with the light values obtained by Gouraud interpolation when rendering patch $\mathbf{q}_2$. One possible fix to this problem is shown on the right in Figure VIII.15, where the quadrilateral patch $\mathbf{q}_2$ has been split into a triangle and another quadrilateral. With this fix, the boundary is rendered only in separate pieces, never as a single edge, and Gouraud interpolation yields consistent results on both sides of the boundary..

We have discussed only degree three Bézier patches above, but of course, Bézier patches can also be defined with other degrees. In addition, a Bézier patch may have a different degree in u than in v. In general, if the Bézier patch has degree k_u in u and degree k_v in v, then there are $(k_u+1)(k_v+1)$ control points $\mathbf{p}_{i,j}$, with $0 \le i \le k_u$ and $0 \le j \le k_v$. The Bézier patch is given by

$$\mathbf{q}(u,v) \;=\; \sum_{i=0}^{k_u}\sum_{j=0}^{k_v} B_i^{k_u}(u)B_j^{k_v}(v)\mathbf{p}_{i,j}.$$

We shall not develop the theory of Bézier patches of general degree any further; however, an example of a Bézier patch which is degree three in one direction and degree two in the other is shown in Section VIII.14 on page 308.

VIII.11 Bézier curves and surfaces in OpenGL

VIII.11.1 Bézier curves

OpenGL has several routines for automatic generation of Bézier curves of any degree. However, OpenGL does not have generic Bézier curve support; instead, its Bézier curve functions are linked directly to drawing routines. Unfortunately, this means that the OpenGL Bézier curve routines can be used only for drawing, so if you wish to use Bézier curves for other applications, such as animation, you cannot use the built-in OpenGL routines.

Instead of having a single command for generating Bézier curves, OpenGL has separate commands for defining or initializing a Bézier curve from its control points and for displaying part or all of the Bézier curve.

Defining Bézier curves. To define and enable (i.e., activate) a Bézier curve, the following two OpenGL commands are used:

```
glMap1f(GL_MAP1_VERTEX_3, float $u_{min}$, float $u_{max}$,
         int stride, int order, float* controlpointsptr );
glEnable(GL_MAP1_VERTEX_3);
```

The values of u_{min} and u_{max} give the range of u values over which the curve is defined. These are typically set to 0 and 1.

The last parameter points to an array of floats which contains the control points. A typical usage would define `controlpoints` as an array of x, y, z values:

```
float controlpoints[$M$][3];
```

and then the parameter `controlpointsptr` would be `&controlpoints[0][0]`. The `stride` value is the distance (in floats) from one control point to the next; i.e., the control point $\mathbf{p}_i$ is pointed to by `controlpointsptr+`i`*stride`. For the above definition of `controlpoints`, `stride` equals 3.

The value of `order` is equal to one plus the degree of the Bézier curve, thus it also equals the number of control points. Consequently, for the usual degree three Bézier curves, the order M equals 4.

As mentioned above, Bézier curves can be used only for drawing purposes. In fact, several Bézier curves can be active at one time to affect different aspects of the drawn curve, such as its location and color, etc. The first parameter to `glMap1f()` describes how the Bézier curve is used when the curve is drawn. The parameter `GL_MAP1_VERTEX_3` means that the Beziér curve is defining the x, y, z values of points in 3-space, as a function of u. There are several other useful constants that can be used for the first parameter. These include `GL_MAP1_VERTEX_4`, which means that we are specifying x, y, z, w values of a curve, i.e., a rational Bézier curve (see Sections VIII.12 and VIII.13 for information on rational curves). Also, one can use `GL_MAP1_COLOR_4` as the first parameter: this means that as the Bézier curve is being drawn (by the commands described below), the color values will be specified as a Bézier function of u. You should consult the OpenGL documentation for other permitted values for this first parameter. Finally, a reminder: don't forget to give the `glEnable` command for any of these parameters which you wish to activate!

Drawing Bézier curves. Once the Bézier curve has been specified with `glMap1f()`, the curve can be drawn with the following commands. The most basic way to specify a point on the curve is with the command:

```
glEvalCoord1f( float u );
```

which must be given between a `glBegin()` and `glEnd()`. The effect of this command is similar to specifying a point with `glVertex*` and, if the appropriate curves are enabled, with `glNormal*` and `glTexCoord*` commands. However, the currently active normal and texture coordinates are not changed by a call to `glEvalCoord1f()`.

When you use `glEvalCoord1f()`, you are explicitly drawing the points on the curve. However, frequently you want to draw an entire curve or a portion of a curve at once, instead of having to make multiple calls to `glEvalCoord1f`. For this, OpenGL has several commands that will automatically draw points at equally spaced intervals along the curve. To use these commands, after calling `glMap1f` and the corresponding `glEnable`, you must next tell OpenGL the "grid" or "mesh" of points on the curve to be drawn. This is done with the following command:

```
glMapGrid1f(int N, float u_start, float u_end);
```

which tells OpenGL that you want the curve to be discretized as $N+1$ equally spaced points starting with the value $u = u_{start}$ and ending with $u = u_{end}$. It is required that $u_{min} \le u_{start} \le u_{end} \le u_{max}$.

A call to `glMapGrid1f()` only sets a grid of u values. In order to actually draw the curve, you should then call

```
glEvalMesh1(GL_LINE, int p_start, int p_end);
```

This causes OpenGL to draw the curve at grid values, letting p range from p_{start} to p_{end} and drawing the points on the Bézier curve with coordinates

$$u \;=\; \left((N-p)u_{start} + p \cdot u_{end}\right)/N.$$

The first parameter, `GL_LINE`, tells OpenGL to draw the curve as a sequence of straight lines. This has the same functionality as drawing points after a call to `glBegin(GL_LINE_STRIP)`. To draw only the points on the curve without the connecting lines, use `GL_POINT` instead (similar in functionality to using `glBegin(GL_POINTS)`). The values of p_{start} and p_{end} should satisfy $0 \le p_{start} \le p_{end} \le N$.

You can also use `glEvalPoint1( int` p `)` to draw a single point from the grid. `glEvalPoint1` and `glEvalMesh1` are **not** called from inside `glBegin()` and `glEnd()`.

VIII.11.2 Bézier patches

THIS SECTION IS OUT-OF-DATE AND WILL BE REMOVED.

Bézier patches, or Bézier surfaces, can be drawn using OpenGL commands analogous to the commands described above for Bézier curves. Since the commands are very similar, only very brief descriptions are given of the OpenGL routines for Bézier patches. The `SimpleNurbs` program in the software accompanying this book shows an example of how to render a Bézier patch in OpenGL.

To specify a Bézier patch, one uses the `glMap2f()` routine:

```
glMap2f(GL_MAP2_VERTEX_3,
     float u_min , float u_max , int ustride, int uorder,
     float v_min , float v_max , int vstride, int vorder,
     float* controlpoints );
glEnable(GL_MAP2_VERTEX_3);
```

The `controlpoints` array is now a (`uorder`)×(`vorder`) array and would usually be specified by:

```
float controlpointsarray[M_u][M_v][3];
```

where M_u and M_v are the `uorder` and `vorder` values. In this case, the value `vstride` would equal 3, and `ustride` should equal $3M_v$. Note that the orders (which equal one plus the degrees) of the Bézier curves are allowed to be different for the u and v directions.

Other useful values for the first parameter to `glMap2f()` include `GL_MAP2_VERTEX_4` for rational Bézier patches, `GL_MAP2_COLOR_4` to specify colors, and `GL_MAP2_TEXTURE_COORD_2` to specify texture coordinates. Again, you must give the `glEnable` command to activate these settings for the parameter.

For many typical applications of texture coordinates to Bézier patches, one wants the texture coordinates s, t to just be equal to u and v. This is done by specifying a degree one (`order`$=2$) Bézier curve, for instance,

```
float texpts[8]={0,0, 0,1, 1,0, 1,1};
glMap2f(GL_MAP2_TEXTURE_COORD_2,0,1,4,2,0,1,2,2,&texpts[0]);
glEnable(GL_MAP2_TEXTURE_COORD_2);
```

The normals to the patch may be specified by a Bézier formula using GL_MAP2_NORMAL as the first parameter to glMap2f(). However, this is rarely useful since usually one wants the true normals to the Bézier surface. OpenGL will calculate these true normals for you (according to the formula (IV.17) if applicable), if you give the command

```
glEnable(GL_AUTO_NORMAL);
```

To display the Bézier patch, or a portion of the Bézier surface, the following OpenGL commands are available:

```
glEvalCoord2f(float u, float v);
glMapGrid2f(int N_u, float u_start, float u_end,
                int N_v, int v_start, int v_end);
glEvalMesh2(GL_FILL, int p_start, p_end, q_start, q_end);
glEvalPoint2(int p, int q);
```

The first parameter to glEvalMesh2() may be also GL_LINE or GL_POINT. These commands work analogously to the commands for one dimensional Bézier curves. The most direct method of drawing a Bézier patch is to call glMapGrid2f and then glEvalMesh2.

Exercise VIII.11. Build a figure such as a teapot, coffee pot, vase, or other shape of similar complexity. The techniques described in Blinn's article [15] on the famous Utah teapot can make this fairly straightforward. Make sure that normals are calculated so that lighting is applied correctly (OpenGL can compute the normal for you).

Optionally, refer ahead to Sections VIII.13 and VIII.14 to learn how to make surfaces of revolution with rational Bézier patches. Apply this to make the cross sections of your object perfectly circular.

One difficulty with completing the above exercise is that OpenGL does not always calculate normals on Bézier surfaces correctly. In particular, OpenGL has problems with normals when an edge of a Bézier patch consists of a single point. Remember that you should use glEnable(GL_NORMALIZE) when transforming illuminated objects. The sample program SimpleNurbs shows how to use OpenGL to render a Bézier patch with correct normals and illumination.

VIII.12 Rational Bézier curves

A Bézier curve is called *rational* if its control points are specified with homogeneous coordinates. Using homogeneous representations for control points may seem obscure or mystifying at first, but, in fact, there is nothing especially mysterious about the use of homogeneous coordinates for control points. In $\mathbb{R}^3$ (say), the control points are specified as 4-tuples $\mathbf{p}_i = \langle x, y, z, w\rangle$: the curve's values $\mathbf{q}(u)$ are expressed as weighted averages of the control points,

$$\mathbf{q}(u) \;=\; \sum\nolimits_i B_i^k(u)\mathbf{p}_i,$$

so the values of $\mathbf{q}(u)$ specify the points on the curve in homogeneous coordinates too.

There are several advantages to rational Bézier curves. These include:

a. The use of homogeneous coordinates allows the w-coordinate value to serve a weight factor that can be used to increase or decrease the relative weight of a control point. A higher weight for a control point causes the Bézier curve to be "pulled" harder by the control point.

b. The use of weights in this form allows rational Bézier curves to define circular arcs, ellipses, hyperbolas, and other conic curves.

c. Rational Bézier curves are preserved under perspective transformations, not just affine transformations. This is because the points on a Bézier curve are computed as weighted averages, and since affine combinations of homogeneous coordinates are preserved under perspective transformations (see Section V.4).

d. Control points can be placed at infinity, giving extra flexibility in the definition of a Bézier curve.

To understand a., recall from Section V.4 the notation $\langle w\mathbf{p}, w\rangle$, where $\mathbf{p} \in \mathbb{R}^3$ and $w \neq 0$, and where $\langle w\mathbf{p}, w\rangle$ is the 4-tuple which is the (unique) homogeneous representation of $\mathbf{p}$ which has w as its fourth component. Then a point on the curve $\mathbf{q}(u)$ is defined by a weighted average of homogeneous control points, namely

$$\mathbf{q}(u) \;=\; \sum\nolimits_i B_i^k(u)\langle w_i\mathbf{p}_i, w_i\rangle.$$

$\mathbf{q}(u)$ is also a 4-tuple, and thus is a homogeneous representation of a point in $\mathbb{R}^3$. By the earlier discussion in Section V.4, it represents the following point in $\mathbb{R}^3$:

$$\mathbf{r}(u) \;=\; \sum\nolimits_i \frac{w_i B_i^k(u)}{\sum_j w_j B_i^k(u)}\mathbf{p}_i. \qquad \text{(VIII.21)}$$

Thus, the w-components of the control points act like extra weighting factors. Figure VIII.16 shows an example of how weights can affect a Bézier curve.

We have used $\langle w\mathbf{p}, w\rangle$ for the homogeneous representation of $\mathbf{p}$ with last component w. That is to say, if $\mathbf{p} = \langle p_1, p_2, p_3\rangle \in \mathbb{R}^3$, then $\langle w\mathbf{p}, w\rangle$ is the 4-tuple $\langle wp_1, wp_2, wp_3, w\rangle$. This notation is a little confusing, and user unfriendly. Accordingly, drawing software or CAD programs usually use a different convention: they allow a user to set a control point at a position $\mathbf{p}$ with a weight w, but hide from the user the fact that the components of $\mathbf{p}$ are being multiplied by w. You can refer to Figure VIII.19 for an example of this convention, where the control points in $\mathbb{R}^2$ are given in terms of their non-homogeneous representation plus their weight.

If u measures time, then the rational Bézier curve $\mathbf{q}(u)$ can be used to define the motion of a particle with its position at time u given by $\mathbf{r}(u)$. The

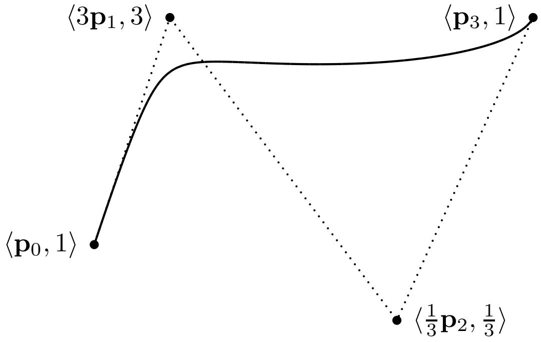
$\langle 3\mathbf{p}_1, 3\rangle$
$\langle \mathbf{p}_3, 1\rangle$
$\langle \mathbf{p}_0, 1\rangle$
$\langle \frac{1}{3}\mathbf{p}_2, \frac{1}{3}\rangle$

Figure VIII.16: A degree three, rational Bézier curve. The control points are the same as in the left-hand side of Figure VIII.2 on page 267, but now the control point $\mathbf{p}_1$ is weighted 3, and the control point $\mathbf{p}_2$ is weighted only $1/3$. The other two control points have weight 1. In comparison with the curve of Figure VIII.2, this curve more closely approaches $\mathbf{p}_1$, but does not approach $\mathbf{p}_2$ nearly as closely.

velocity of the point at time u is equal to the first derivative of $\mathbf{r}(u)$, not $\mathbf{q}(u)$. This can be calculated by differentiating Equation (VIII.21) for $\mathbf{r}(u)$, but this gives a messy formula. An easier way calculate $\mathbf{r}'(u)$ is to first calculate $\mathbf{q}'(u)$ and then use the quotient rule. To illustrate this in $\mathbb{R}^3$, suppose $\mathbf{q}(u)$ equals

$$\mathbf{q}(u) \;=\; \langle x, y, z, w\rangle,$$

where x, y, z, w are polynomial functions of u. Then its derivative

$$\mathbf{q}'(u) \;=\; \langle x', y', z', w'\rangle$$

can be calculated directly or by using Theorem VIII.9. Then $\mathbf{r}(u)$ equals

$$\mathbf{r}(u) \;=\; \left\langle \frac{x}{w}, \frac{y}{w}, \frac{z}{w} \right\rangle,$$

and the quotient rule gives

$$\mathbf{r}'(u) \;=\; \left\langle \frac{x'w - xw'}{w^2}, \frac{y'w - yw'}{w^2}, \frac{z'w - zw'}{w^2} \right\rangle. \qquad \text{(VIII.22)}$$

VIII.13 Conic sections with rational Bézier curves

A major advantage to using rational Bézier curves is that they allow the definition of conic sections as quadratic Bézier curves. We start with an example that includes a point at infinity.[5]

[5] Most of our examples of constructions of circular arcs by Bézier curves in this section and by B-spline curves in Section IX.11 can be found in the article of Piegl and Tiller [89].

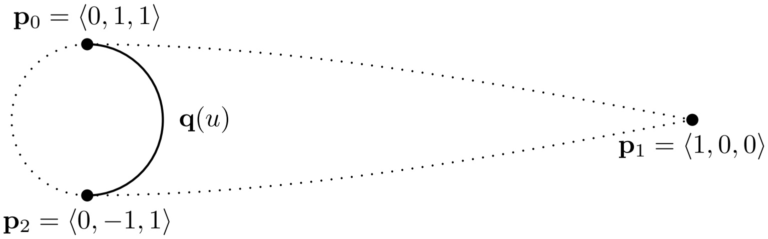
$\mathbf{p}_0 = \langle 0,1,1\rangle$
$\mathbf{q}(u)$
$\mathbf{p}_1 = \langle 1,0,0\rangle$
$\mathbf{p}_2 = \langle 0,-1,1\rangle$

Figure VIII.17: The situation of Theorem VIII.14. The middle control point is a point at infinity, and the dotted lines joining it to the other control points are actually straight and are tangent to the circle at $\mathbf{p}_0$ and $\mathbf{p}_2$.

Theorem VIII.14. *Let* $\mathbf{p}_0 = \langle 0,1,1\rangle$, $\mathbf{p}_1 = \langle 1,0,0\rangle$, *and* $\mathbf{p}_2 = \langle 0,-1,1\rangle$ *be homogeneous representations of points in* $\mathbb{R}^2$. *Let* $\mathbf{q}(u)$ *be the degree two Bézier curve defined with these control points. Then, the curve* $\mathbf{q}(u)$ *traces out the right half of the unit circle* $x^2+y^2=1$ *as* u *varies from 0 to 1.*

The situation of Theorem VIII.14 is shown in Figure VIII.17. Note that the middle control point is actually a point at infinity. However, we shall see that the points $\mathbf{q}(u)$ on the curve are always finite points, not points at infinity. These points $\mathbf{q}(u)$ are actually homogeneous representations of points in $\mathbb{R}^2$. That is to say, $\mathbf{q}(u)$ is a triple $\langle q_1(u), q_2(u), q_3(u)\rangle$ and is the homogeneous representation of the point $\mathbf{r}(u) := \langle q_1(u)/q_3(u), q_2(u)/q_3(u)\rangle$ in $\mathbb{R}^2$. The import of the theorem is that the points $\mathbf{q}(u)$, when interpreted as homogeneous representations of points $\mathbf{r}(u)$ in $\mathbb{R}^2$, trace out the right half of the unit circle.

We now prove Theorem VIII.14. From the definition of Bézier curves,

$$\begin{aligned}\mathbf{q}(u) &= (1-u)^2\mathbf{p}_0 + 2u(1-u)\mathbf{p}_1 + u^2\mathbf{p}_2\\ &= (1-u)^2\langle 0,1,1\rangle + 2u(1-u)\langle 1,0,0\rangle + u^2\langle 0,-1,1\rangle\\ &= \langle 2u(1-u), (1-u)^2-u^2, (1-u)^2+u^2\rangle.\end{aligned}$$

It is easy to check that the third component is nonzero for $0 \le u \le 1$. Thus, $\mathbf{q}(u)$ is the homogeneous representation of the point

$$\mathbf{r}(u) \;=\; \langle x(u), y(u)\rangle \;=\; \left\langle \frac{2u(1-u)}{(1-u)^2+u^2}, \frac{(1-u)^2-u^2}{(1-u)^2+u^2}\right\rangle.$$

We need to show two things. The first is that each point $\mathbf{q}(u)$ lies on the unit circle. This is proved by showing that $x(u)^2+y(u)^2=1$ for all u. For this, it is sufficient to prove that

$$[2u(1-u)]^2 + [(1-u)^2-u^2]^2 \;=\; [(1-u)^2+u^2]^2, \tag{VIII.23}$$

a fact which is almost immediate. The second thing to show is that $\mathbf{q}(u)$ actually traces out the correct portion of the unit circle: for this we need to check that $x(u) \geq 0$ for all $u \in [0,1]$ and that $y(u)$ is decreasing on the same interval $[0,1]$. Both these facts are readily checked and we leave this to the reader. □

If u measures time, the $\mathbf{q}(u)$ can be viewed the homogeneous representation of the position $\mathbf{r}(u)$ of a particle at time u. The particle's velocity at time u is $\mathbf{r}'(u)$. As an example, consider $u = 0$. Then

$$\mathbf{q}(0) \;=\; \mathbf{p}_0 \;=\; \langle 0,1,1\rangle,$$

and using Corollary VIII.10, its first derivative at $u = 0$ is

$$\mathbf{q}'(0) \;=\; 2(\mathbf{p}_1 - \mathbf{p}_0) \;=\; \langle 2,-2,-2\rangle.$$

Then $\mathbf{r}(0) = \langle 0,1\rangle$ and, using the method outlined in the last section for Equation (VIII.22),

$$\mathbf{r}'(0) \;=\; \left\langle \frac{2\cdot 1 - 0\cdot(-2)}{1^2}, \frac{(-2)\cdot 1 - 1\cdot(-2)}{1^2} \right\rangle \;=\; \langle 2,0\rangle.$$

Exercise VIII.12. The midpoint of the semicircle is at $\mathbf{q}(\frac{1}{2}) = \langle \frac{1}{2}, 0, \frac{1}{2}\rangle$ and $\mathbf{r}(\frac{1}{2}) = \langle 1,0\rangle$. What are $\mathbf{q}'(\frac{1}{2})$ and $\mathbf{r}'(\frac{1}{2})$ equal to? [Hint: Use the analogue of Equation (VIII.22) for $\mathbb{R}^2$.] Conclude that $\mathbf{r}(u)$ does not trace out the semicircle at a constant rate.

Now that we have proved Theorem VIII.14, the reader might reasonably ask how we knew to use the control point $\mathbf{p}_1 = \langle 1,0,0\rangle$ for the middle control point. The answer is that we first tried the control point $\langle h,0,0\rangle$ with h a to-be-determined constant. We then carried out the construction of the proof of the theorem, but using the value h where needed. The resulting analogue of Equation (VIII.23) then had its first term multiplied by h^2; from this we noted that equality holds only with $h = \pm 1$, and $h = +1$ was needed to get the right half of the curve.

This construction generalizes to a procedure that can be used to represent any finite segment of any conic section as a quadratic Bézier curve. Let C be a portion of a conic section (a line, parabola, circle, ellipse, or hyperbola) in $\mathbb{R}^2$. Let $\mathbf{p}_0$ and $\mathbf{p}_2$ be two points on (one branch of) the conic section. Our goal is to find a third control point $\mathbf{p}_1$ with appropriate weight w_1, so that the quadratic curve with these three control points is equal to the portion of the conic section between $\mathbf{p}_0$ and $\mathbf{p}_1$. (Refer to Figure VIII.18.)

Let T_0 and T_2 be the two lines tangent to the conic section at $\mathbf{p}_0$ and $\mathbf{p}_2$. Let $\mathbf{p}_1$ be the point in their intersection (or the appropriate point at infinity if the tangents are parallel, as in Theorem VIII.14). We further assume that the segment of the conic section between $\mathbf{p}_0$ and $\mathbf{p}_2$ lies in the triangle formed by $\mathbf{p}_0$, $\mathbf{p}_1$, and $\mathbf{p}_2$ — this rules out the case where the segment is more than 180° of a circle, for instance.

Theorem VIII.15. *Let C, $\mathbf{p}_0$, $\mathbf{p}_2$, T_0, T_2, and $\mathbf{p}_1$ be as above. Let $\mathbf{p}_0$ and $\mathbf{p}_2$ be given weight 1. Then there is a value $w_1 \geq 0$ such that when $\mathbf{p}_1$ is given*

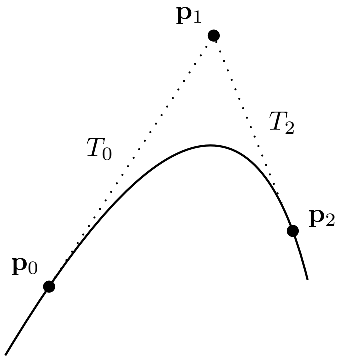

Figure VIII.18: A portion of a branch of a conic section C is equal to a rational quadratic Bézier curve. Control points $\mathbf{p}_0$ and $\mathbf{p}_2$ have weight 1 and $\mathbf{p}_1$ gets weight $w_1 \geq 0$.

weight w_1, the rational degree two Bézier curve $\mathbf{q}(u)$ with control points $\mathbf{p}_0$, $\mathbf{p}_1$, and $\mathbf{p}_2$ traces out the portion of C between $\mathbf{p}_0$ and $\mathbf{p}_2$.

Proof. This was originally proved by Lee [76]; we give here only a quick sketch of a proof. In the degenerate case where C is a line, take $\mathbf{p}_1$ to be any point between $\mathbf{p}_0$ and $\mathbf{p}_2$; then any value for $w_1 \geq 0$ will work. Otherwise, for each $h \geq 0$, let $\mathbf{q}_h(u)$ be the Bézier curve which is obtained when $w_1 = h$. At $h = 0$, $\mathbf{q}_h(1/2)$ lies on the line segment from $\mathbf{p}_0$ to $\mathbf{p}_2$. As $h \to \infty$, $\mathbf{q}_h(1/2)$ tends to $\mathbf{p}_1$. Thus, there must be a value $h > 0$ such that $\mathbf{q}_h(1/2)$ lies on the conic section. By Theorem VIII.16 below, the curve $\mathbf{q}_h(u)$ is a conic section. Furthermore, there is a unique conic section which (a) contains the three points $\mathbf{p}_0$, $\mathbf{q}_h(1/2)$, and $\mathbf{p}_2$, and (b) is tangent to T_0 and T_2 at $\mathbf{p}_0$ and $\mathbf{p}_2$. Therefore, with $w_1 = h$, the resulting Bézier curve must trace out C. □

Theorem VIII.15 gives the general framework for designing quadratic Bézier curves that form conic sections. Note that the fact that $\mathbf{p}_1$ lies at the intersection of the two tangent lines T_0 and T_2 is forced by the fact that the initial (respectively, the final) derivative of a Bézier curve points from the first (respectively, the second) control point towards the second point (respectively, the third point). It can be shown, using the equivalence of rational Bézier curves to Bézier curves with weighting, that this fact holds also for rational Bézier curves.

The next three exercises give some ways to form circles as quadratic Bézier curves that do not require the use of a point at infinity.

Exercise VIII.13. Let $\mathbf{q}(u)$ be the rational, degree two Bézier curve with homogeneous control points $\mathbf{p}_0 = \langle 1, 0, 1 \rangle$, $\mathbf{p}_1 = \langle \sqrt{2}/2, \sqrt{2}/2, \sqrt{2}/2 \rangle$ and $\mathbf{p}_2 = \langle 0, 1, 1 \rangle$. Prove that this Bézier curve traces out the 90° arc of the unit

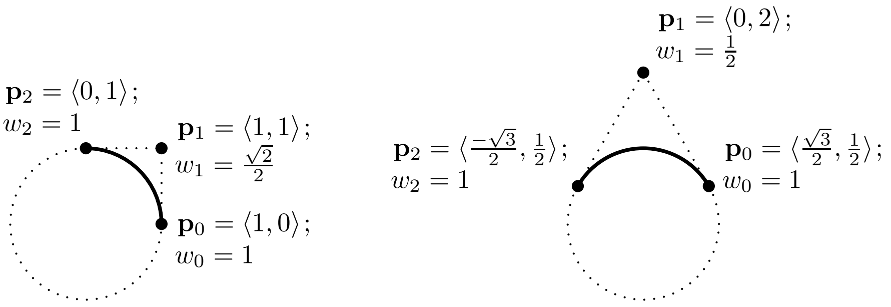
$\mathbf{p}_2 = \langle 0, 1\rangle$;
$w_2 = 1$
$\mathbf{p}_1 = \langle 1, 1\rangle$;
$w_1 = \frac{\sqrt{2}}{2}$
$\mathbf{p}_0 = \langle 1, 0\rangle$;
$w_0 = 1$
$\mathbf{p}_1 = \langle 0, 2\rangle$;
$w_1 = \frac{1}{2}$
$\mathbf{p}_2 = \langle \frac{-\sqrt{3}}{2}, \frac{1}{2}\rangle$;
$w_2 = 1$
$\mathbf{p}_0 = \langle \frac{\sqrt{3}}{2}, \frac{1}{2}\rangle$;
$w_0 = 1$

Figure VIII.19: Two ways to define circular arcs with rational Bézier curves without control points at infinity. Recall that saying a control point $\mathbf{p}_i$ has weight w_i means the control point has homogeneous representation $\langle w_i\mathbf{p}_i, w_i\rangle$.

circle in $\mathbb{R}^2$ from the point $\langle 1, 0\rangle$ to $\langle 0, 1\rangle$. See Figure VIII.19 for this and the next exercise.

Exercise VIII.14. Let $\mathbf{q}(u)$ be the rational, degree two Bézier curve defined with homogeneous control points $\mathbf{p}_0 = \langle\sqrt{3}/2, 1/2, 1\rangle$, $\mathbf{p}_1 = \langle 0, 1, 1/2\rangle$ and $\mathbf{p}_2 = \langle -\sqrt{3}/2, 1/2, 1\rangle$. Prove that this Bézier curve traces out the 120° arc of the unit circle in $\mathbb{R}^2$ from $\langle\sqrt{3}/2, 1/2\rangle$ to $\langle -\sqrt{3}/2, 1/2\rangle$. See Figure VIII.19, where these points are shown in $\mathbb{R}^2$ with their weights.

Exercise VIII.15* Generalize the constructions of the previous two exercises. Suppose that $\mathbf{p}_0$ and $\mathbf{p}_2$ lie on the unit circle, separated by an angle of θ, $0^\circ < \theta < 180^\circ$. Show that the arc from $\mathbf{p}_0$ to $\mathbf{p}_2$ can be represented by a degree two Bézier curve, where $\mathbf{p}_0$ and $\mathbf{p}_2$ are given weight 1, and $\mathbf{p}_1$ is given weight $w_1 = \cos(\theta/2)$. Also, give a formula expressing (or, if you prefer, an algorithm to compute) the position of $\mathbf{p}_1$ in terms of the positions of $\mathbf{p}_0$ and $\mathbf{p}_2$.

Sometimes it is desirable to use degree three instead of degree two curves for conic sections. There are many ways to define conic sections with degree three curves: the next exercise suggests that one general method is to first form the curve as a degree two conic section and then elevate the degree to degree three, using the method of Section VIII.9.

Exercise VIII.16. Apply degree elevation to the degree two Bézier curve of Theorem VIII.14 (Figure VIII.17) to prove that the following degree three Bézier curve traces out the right half of the unit circle: the degree three curve is defined with control points $\mathbf{p}_0 = \langle 0, 1\rangle$, $\mathbf{p}_1 = \langle 2, 1\rangle$, $\mathbf{p}_2 = \langle 2, -1\rangle$ and $\mathbf{p}_3 = \langle 0, -1\rangle$, with $\mathbf{p}_0$ and $\mathbf{p}_3$ having weight 1 and $\mathbf{p}_1$ and $\mathbf{p}_2$ having weight $1/3$. (See Figure VIII.20.)

The next exercise shows that it is also possible to use negatively weighted control points for rational Bézier curves. This is more of an oddity than a genuinely useful construction; in particular, the convex hull property is lost when negatively weighted points are allowed (see Theorem V.13).

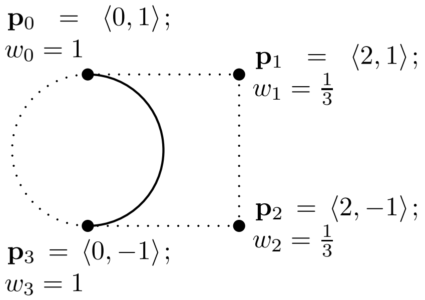
$\mathbf{p}_0 = \langle 0,1\rangle$;
$w_0 = 1$
$\mathbf{p}_1 = \langle 2,1\rangle$;
$w_1 = \frac{1}{3}$
$\mathbf{p}_2 = \langle 2,-1\rangle$;
$w_2 = \frac{1}{3}$
$\mathbf{p}_3 = \langle 0,-1\rangle$;
$w_3 = 1$

Figure VIII.20: A semicircle as a degree three Bézier curve. See Exercise VIII.16.

Exercise VIII.17. Investigate what happens with negatively weighted control points. For instance, investigate what happens to the Bézier curve of Exercise VIII.13 if the middle control point is redefined as $\mathbf{p}_1 = (-\sqrt{2}/2, -\sqrt{2}/2, -\sqrt{2}/2)$, i.e., is a homogeneous representation of the same point but now in negated form. [Answer: you obtain the other three quarters of the unit circle.]

Theorem VIII.15 showed that finite portions of conic sections can be represented by quadratic Bézier curves. Its proof depended on the next theorem, which asserts that conic sections are the only curves which can be represented by quadratic Bézier curves.

Theorem VIII.16. *Let $\mathbf{q}(u) = \langle x(u), y(u), w(u)\rangle$ be a rational quadratic curve in $\mathbb{R}^2$. Then there is a conic section such that every point of $\mathbf{q}(u)$ lies on the conic section.*

Proof. Recall that a conic section is defined as the set of points $\langle x, y\rangle \in \mathbb{R}^2$ which satisfy

$$Ax^2 + Bxy + Cy^2 + Dx + Ey + F = 0$$

for some constants A, B, C, D, E, F, not all zero. If we represent points with homogeneous coordinates $\langle x, y, w\rangle$, then this condition is equivalent to

$$Ax^2 + Bxy + Cy^2 + Dxw + Eyw + Fw^2 = 0. \qquad \text{(VIII.24)}$$

Namely, a conic section is the set of points whose homogeneous representations satisfy Equation (VIII.24).

Claim *Let $x = x(u)$, $y = y(u)$ and $w = w(u)$ be parametric functions of u. Let M be a transformation of $\mathbb{R}^2$ defined by an invertible 3×3 matrix that acts on homogeneous coordinates. Then, in $\mathbb{R}^2$, the curve $M(\mathbf{q}(u))$ lies on a conic section if and only if $\mathbf{q}(u)$ lies on a conic section.*

To prove the claim, let x_M, y_M, and w_M be the functions of u defined so that

$$\langle x_M, y_M, w_M\rangle \;=\; M\langle x, y, w\rangle.$$

Suppose that, for all u,

$$Ax_M^2 + Bx_M y_M + Cy_M^2 + Dx_M w_M + Ey_M w_M + Fw_M^2 = 0, \qquad \text{(VIII.25)}$$

with not all the coefficients zero (i.e., $M(\mathbf{q})$ lies on a conic section). Since each of x_M, y_M, and w_M is a linear combination of x, y, and w, Equation (VIII.25) can be rewritten in the form of Equation (VIII.24), but with different values for the coefficients. Since M is invertible, this process can be reversed, and therefore the coefficients of Equation (VIII.24) for x, y, w are not all zero. Therefore, we have shown that if $M(\mathbf{q})$ is a conic section, then so is $\mathbf{q}$. Since M is invertible, the converse implication holds as well and the claim is proved.

Returning to the proof of Theorem VIII.16, since $\mathbf{q}(u)$ is quadratic, it is equal to a Bézier curve (see Exercise VIII.8 on page 282). Let $\mathbf{p}_0$, $\mathbf{p}_1$, and $\mathbf{p}_2$ be the homogeneous control points of this Bézier curve. If these three control points represent points in $\mathbb{R}^2$ which are collinear, then the curve $\mathbf{q}(u)$ lies in the line containing the control points, and therefore lies on a (degenerate) conic section. Otherwise, since a line in $\mathbb{R}^2$ corresponds to a two dimensional linear subspace of homogeneous xyw-space, the three points $\mathbf{p}_0$, $\mathbf{p}_1$, and $\mathbf{p}_2$ are linearly independent in homogeneous space (see Section II.3.8). Therefore there is an invertible linear transformation M of homogeneous space, i.e., a nonsingular 3×3 matrix M, that sends the three points $\mathbf{p}_0$, $\mathbf{p}_1$, and $\mathbf{p}_2$ to the three control points $\langle 0, 1, 1\rangle$, $\langle 1, 0, 0\rangle$, and $\langle 0, -1, 1\rangle$ of Theorem VIII.14. That is to say, the projective transformation M maps the curve $\mathbf{q}(u)$ to a circle. Therefore, $M(\mathbf{q})$ lies on a conic section, so by the claim, $\mathbf{q}(u)$ lies on a conic section. □

The next two exercises show that we cannot avoid the use of homogeneous coordinates when representing conic sections.

Exercise VIII.18. Prove that there is no nonrational degree two Bézier curve which traces out a nontrivial part of a circle. [Hint: A quadratic curve consists of segments of the form $\langle x(u), y(u)\rangle$ with $x(u)$ and $y(u)$ degree two polynomials. To have only points on the unit circle, they must satisfy $(x(u))^2 + (y(u))^2 = 1$.]

Exercise VIII.19. Prove that there is no nonrational Bézier curve of any degree, which traces out a nontrivial part of a circle. [Hint: This is done by generalizing the proof of Exercise VIII.18.]

Lest one get the overly optimistic impression that rational Bézier curves are universally good for everything, we end this section with one last exercise showing a limitation on what curves can be defined with (piecewise) Bézier curves.

Exercise VIII.20★ (Requires advanced math.) Consider the helix spiraling around the z-axis, which is parametrically defined by $\mathbf{q}(u) = \langle \cos(u), \sin(u), u\rangle$. Prove that there is no rational Bézier curve which traces out a nontrivial portion of this spiral. [Hint: Suppose there is a rational curve $\mathbf{q}(u) =$

$\langle x(u), y(u), z(u), w(u)\rangle$ which traces out a nontrivial portion of the helix. Then we must have

$$\frac{x(u)}{w(u)} = \cos\left(\frac{z(u)}{w(u)}\right)$$

on some interval. But this is impossible because the lefthand side is a rational function and the righthand side is not.]

Another way to think about how to prove the exercise, at least for the quadratic case, is to note that if a nontrivial part of the helix is a Bézier curve, then its projection onto the xz-plane is a rational quadratic curve. But this projection is the graph of the function $z = \cos(x)$, which contradicts Theorem VIII.16 because the graph of $\cos(x)$ is not composed of portions of conic sections.

Farouki and Sakkalis [46] gave another approach to Exercise VIII.20. They proved that there is no rational polynomial curve $\mathbf{q}(u)$, of any degree, which gives a parametric definition of any curve other than a straight line, such that $\mathbf{q}(u)$ traverses the curve at a uniform speed with respect to the parameter u. In other words, it is not possible to parameterize any curve other than a straight-line segment by rational functions of its arclength. For the special case of the circle, this means that there is no way to parameterize circular motion with a Bézier curve that traverses the circle at a uniform speed. For the circle, the impossibility of a Bézier curve's traversing a circle at uniform speed is equivalent to Exercise VIII.20 because a Bézier curve tracing out the spiral could be reinterpreted with the z-value as time.

Another kind of curve that cannot be represented by a rational polynomial curve is the *clothoid*. A clothoid, also known as a Cornu spiral or Euler spiral. is a curve which has curvature varying linearly with arclength; it is extensively used for roads, railroad tracks, and even roller coaster tracks. (Clothoids were named somewhat whimsically after Clotho, one of the three Greek Fates.)

When we define B-splines in the next chapter, we shall see that B-spline curves are equivalent to piecewise Bézier curves (in Section IX.9). Therefore, the impossibility results from Exercises VIII.18-VIII.20 and of Farouki and Sakkalis, and for clothoids, also apply to B-splines curves.

VIII.14 Surface of revolution example

This section presents an example of how to form a surface of revolution using rational Bézier patches with control points at infinity.

Our point of departure is Theorem VIII.14, which showed how to form a semicircle with a single quadratic Bézier curve. We will extend this construction to form a surface of revolution using Bézier patches with quadratic cross sections. First, however, it useful to examine semicircles more closely; in particular, we want to understand how to translate, rotate, and scale circles.

Refer back to the semicircle shown in Figure VIII.17 on page 300. That semicircle was centered at the origin. Suppose we want to translate the

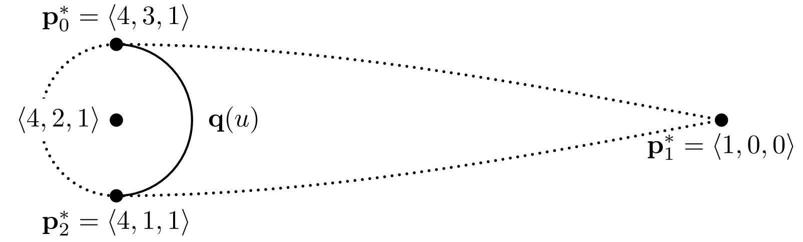
$\mathbf{p}_0^* = \langle 4,3,1\rangle$
$\langle 4,2,1\rangle$
$\mathbf{q}(u)$
$\mathbf{p}_1^* = \langle 1,0,0\rangle$
$\mathbf{p}_2^* = \langle 4,1,1\rangle$

Figure VIII.21: The semicircle of Figure VIII.17 translated by $\langle 4,2\rangle$.

semicircle, say to be centered at $\langle 4,2\rangle$. We want to express the the translated semicircle as a rational quadratic Bézier curve. Let $\mathbf{p}_0$, $\mathbf{p}_1$, and $\mathbf{p}_2$ be the control points shown in Figure VIII.17. The question is, what are the control points, $\mathbf{p}_i^*$, for the translated circle? Obviously, the first and last control points should now be $\mathbf{p}_0^* = \langle 4,3,1\rangle$ and $\mathbf{p}_2^* = \langle 4,1,1\rangle$, as obtained by direct translation. But what is the point $\mathbf{p}_1^*$ at infinity? Here, it does not make sense to translate the point at infinity; instead, the correct control point is $\mathbf{p}_1^* = \mathbf{p}_1 = \langle 1,0,0\rangle$. Intuitively, the reason for this is as follows: We chose the point $\mathbf{p}_1$ to be the point at infinity corresponding to the intersection of the two horizontal projective lines tangent to the circle at the top and bottom points (see Theorem VIII.15 above). When the circle is translated, the tangent lines remain horizontal, so they still contain the same point at infinity.

To be more systematic about translating the semicircle, we can work with the 3×3 homogeneous matrix that performs the translation, namely, the matrix

$$M = \begin{pmatrix} 1 & 0 & 4 \\ 0 & 1 & 2 \\ 0 & 0 & 1 \end{pmatrix}.$$

It is easy to check that

$$\mathbf{p}_0^* \;=\; M\mathbf{p}_0, \qquad \mathbf{p}_1^* \;=\; M\mathbf{p}_1, \qquad \text{and} \qquad \mathbf{p}_2^* \;=\; M\mathbf{p}_2.$$

This proves the correctness of the control points for the translated semicircle.

Exercise VIII.21. Consider the effect of rotating the semicircle from Figure VIII.17 through a counter-clockwise angle of 45 degrees around the origin. Prove that the result is the same as the quadratic rational Bézier curve with control points

$$\mathbf{p}_0^* \;=\; \langle -\tfrac{\sqrt{2}}{2}, \tfrac{\sqrt{2}}{2}, 1\rangle, \quad \mathbf{p}_0^* \;=\; \langle \tfrac{\sqrt{2}}{2}, \tfrac{\sqrt{2}}{2}, 0\rangle, \quad \text{and} \quad \mathbf{p}_2^* \;=\; \langle \tfrac{\sqrt{2}}{2}, -\tfrac{\sqrt{2}}{2}, 1\rangle.$$

[Hint: The rotation is performed by the homogeneous matrix

$$\begin{pmatrix} \frac{\sqrt{2}}{2} & -\frac{\sqrt{2}}{2} & 0 \\ \frac{\sqrt{2}}{2} & \frac{\sqrt{2}}{2} & 0 \\ 0 & 0 & 1 \end{pmatrix}. \qquad]$$

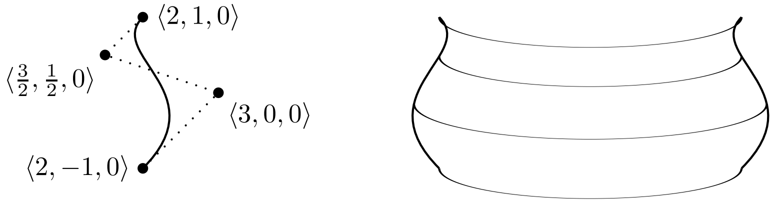

(a) (b)

Figure VIII.22: (a) A silhouette of a surface of revolution (the control points are in x, y, z-coordinates). (b) The front half of the surface of revolution. This example is implemented in the `SimpleNurbs` progam.

Exercise VIII.22. Consider the effect of scaling the semicircle from Figure VIII.17 by a factor of r, so that it has radius r. Prove that the result is the same as the quadratic rational Bézier curve with control points

$$\mathbf{p}_0^* \;=\; \langle 0,r,1\rangle, \quad \mathbf{p}_0^* \;=\; \langle r,0,0\rangle, \quad \text{and} \quad \mathbf{p}_2^* \;=\; \langle 0,-r,1\rangle.$$

[Hint: The scaling is performed by the homogeneous matrix

$$\begin{pmatrix} r & 0 & 0 \\ 0 & r & 0 \\ 0 & 0 & 1 \end{pmatrix}. \qquad]$$

We now give an example of how to form a surface of revolution. Figure VIII.22 shows an example of a surface of revolution. The silhouette of the surface is defined by a cubic (nonrational) Bézier curve; the silhouette is defined as a curve in the xy-plane, and the surface is formed by revolving around the y-axis. We will show how to define a 180 degree arc of the surface with a single Bézier patch using control points at infinity. The entire surface can be formed with two such patches.

Section VIII.10.1 discussed how the control points of a Bézier patch define the patch; most notably, each cross section is itself a Bézier curve and the control points of the cross sections are defined by Bézier curves. Considering the vertical cross sections (i.e., the cross sections that go up-and-down with the axis of revolution), it is clear that the control points of each vertical cross section must be obtained by revolving the control points shown in part (a) of Figure VIII.22. Now these revolved control points can therefore defined with Bézier curves that trace out semicircles.

These considerations let us define 180 degrees of the surface of revolution shown in Figure VIII.22(b) as a single rational Bézier patch that has order 4 in one direction and order 3 in the other direction. The control points for the patch are as follows:

$$\begin{array}{ccc}
\langle -2,-1,0,1\rangle & \langle 0,0,2,0\rangle & \langle 2,-1,0,1\rangle \\
\langle -3,0,0,1\rangle & \langle 0,0,3,0\rangle & \langle 3,0,0,1\rangle \\
\langle -\frac{3}{2},\frac{1}{2},0,1\rangle & \langle 0,0,\frac{3}{2},0\rangle & \langle \frac{3}{2},\frac{1}{2},0,1\rangle \\
\langle -2,1,0,1\rangle & \langle 0,0,2,0\rangle & \langle 2,1,0,1\rangle.
\end{array}$$

Each of the four rows of the table holds three control points that define a semicircular curve in $\mathbb{R}^3$. Taking vertical cross sections of the four semicircles gives the four control points for the corresponding vertical cross section of the surface of revolution.

VIII.15 Interpolating with Bézier curves

Frequently, one wishes to define a smooth curve that interpolates (i.e., passes through, or contains) a given set of points. For example, suppose we are given a set of points that define the positions of some object at different times; if we then find a smooth curve that interpolates these points, we can use the curve to define (or, estimate) the positions of the object at intermediate times.

The scenario is as follows. We are given a set of interpolation points $\mathbf{p}_0, \ldots, \mathbf{p}_m$, and a set of "knot values" $u_0, \ldots, u_m$. The problem is to define a piecewise (degree three) polynomial curve $\mathbf{q}(u)$, so that $\mathbf{q}(u_i) = \mathbf{p}_i$ for all i. There are several ways to define the interpolating curves as piecewise Bézier curves. The general idea is to define a series of Bézier curves connecting pairs of successive interpolation points. For each appropriate value of i, there will be a Bézier curve that starts at $\mathbf{p}_i$ and ends at $\mathbf{p}_{i+1}$. Putting these curves together forms the entire curve. This automatically makes a piecewise Bézier curve that interpolates the points $\mathbf{p}_i$, of course; but more work is needed to make the curve smooth at the points $\mathbf{p}_i$. For this, we need to use the methods of Section VIII.4 to make the curve C^1-continuous.

We describe three ways to define interpolating piecewise Bézier curves. The first is the Catmull-Rom splines, and the second is a generalization of Catmull-Rom splines called Overhauser splines. Catmull-Rom splines are used primarily when the points $\mathbf{p}_i$ are more-or-less evenly spaced, and with $u_i = i$. The Overhauser splines allow the use of more general values for u_i, as well as allow the use of chord-length parameterization in order to give better results when the distances between successive points $\mathbf{p}_i$ varies a lot. A more general variation on these splines is the Tension-Continuity-Bias interpolation methods, which allow a user to vary parameters to obtain a desirable curve.

VIII.15.1 Catmull-Rom splines

Catmull-Rom splines are specified by a list of $m+1$ interpolation points $\mathbf{p}_0, \ldots, \mathbf{p}_m$ and are piecewise degree three polynomial curves, of the type described in Section VIII.4, that interpolate all the points except the endpoints $\mathbf{p}_0$ and $\mathbf{p}_m$. For Catmull-Rom splines, $u_i = i$, so we want $\mathbf{q}(i) = \mathbf{p}_i$ for $1 \le i < m$. The Catmull-Rom spline will consist of $m-2$ Bézier curves, with

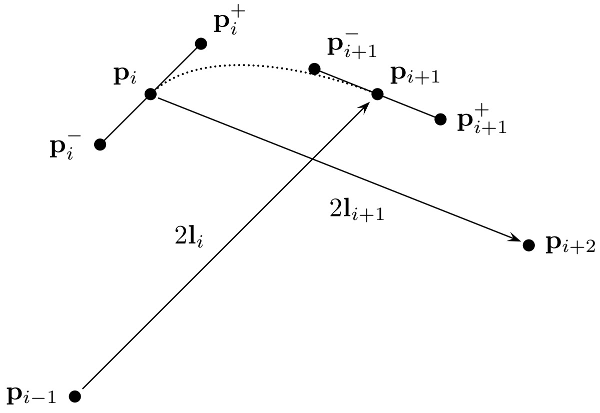

Figure VIII.23: Defining the Catmull-Rom spline segment from the point $\mathbf{p}_i$ to the point $\mathbf{p}_{i+1}$. The points $\mathbf{p}_i^-$, $\mathbf{p}_i$, and $\mathbf{p}_i^+$ are collinear and parallel to $\mathbf{p}_{i+1} - \mathbf{p}_{i-1}$. The points $\mathbf{p}_i$, $\mathbf{p}_i^+$, $\mathbf{p}_{i+1}^-$, and $\mathbf{p}_{i+1}$ form the control points of a degree three Bézier curve, which is shown as a dotted curve.

the i-th Bézier curve beginning at point $\mathbf{p}_i$ and ending at point $\mathbf{p}_{i+1}$. They are defined by making an estimate for the first derivative of the curve passing through $\mathbf{p}_i$. These first derivatives are used to define additional control points for the Bézier curves.

Figure VIII.23 illustrates the definition of a Catmull-Rom spline segment. Let

$$\mathbf{l}_i \;=\; \frac{1}{2}(\mathbf{p}_{i+1} - \mathbf{p}_{i-1})$$

and define

$$\mathbf{p}_i^+ \;=\; \mathbf{p}_i + \frac{1}{3}\mathbf{l}_i \qquad \text{and} \qquad \mathbf{p}_i^- \;=\; \mathbf{p}_i - \frac{1}{3}\mathbf{l}_i.$$

Then let $\mathbf{q}_i(u)$ be the Bézier curve — translated to have domain $i \le u \le i+1$ — which is defined with control points $\mathbf{p}_i, \mathbf{p}_i^+, \mathbf{p}_{i+1}^-, \mathbf{p}_{i+1}$. Define the entire Catmull-Rom spline, $\mathbf{q}(u)$, by piecing together these curves, so that $\mathbf{q}(u) = \mathbf{q}_i(u)$ for $i \le u \le i+1$.

Since Bézier curves interpolate their first and last control points, the curve $\mathbf{q}$ is continuous and $\mathbf{q}(i) = \mathbf{p}_i$ for all integers i such that $1 \le i \le m-1$. In addition, $\mathbf{q}$ has continuous first derivatives, with

$$\mathbf{q}'(i) \;=\; \mathbf{l}_i \;=\; (\mathbf{p}_{i+1} - \mathbf{p}_{i-1})/2.$$

It follows that $\mathbf{q}(u)$ is C^1-continuous. This formula for the first derivatives, $\mathbf{q}'(i)$, also explains the motivating idea behind the definition of Catmull-Rom splines. Namely, since $\mathbf{q}(i-1) = \mathbf{p}_{i-1}$ and $\mathbf{q}(i+1) = \mathbf{p}_{i+1}$, the *average* rate of change of $\mathbf{q}(u)$ between $u = i-1$ and $u = i+1$ must equal $(\mathbf{p}_{i+1} - \mathbf{p}_{i-1})/2$. Thus, the extra control points, $\mathbf{p}_i^+$ and $\mathbf{p}_i^-$, are chosen so as to make $\mathbf{q}'(i)$ equal to this average rate of change.

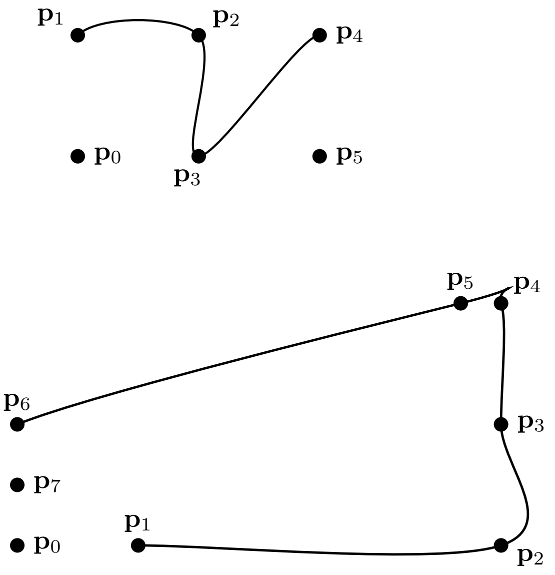

Figure VIII.24: Two examples of Catmull-Rom splines with uniformly spaced knots.

Figure VIII.24 shows two examples of Catmull-Rom splines.

VIII.15.2 Bessel-Overhauser splines

The second curve in Figure VIII.24(b) shows that bad effects can result when the interpolated points are not more or less equally spaced; bad "overshoot" can occur when two close control points are next to widely separated control points. One way to correct this problem is to use *chord-length* parameterization. For chord-length parameterization, the knots u_i are chosen so that $u_{i+1} - u_i$ is equal to $||\mathbf{p}_{i+1} - \mathbf{p}_i||$. The idea is that the arclength of the curve between $\mathbf{p}_i$ and $\mathbf{p}_{i+1}$ will be approximately proportional to the distance from $\mathbf{p}_i$ to $\mathbf{p}_{i+1}$ and therefore approximately proportional to $u_{i+1} - u_i$. If one views the parameter u as time, then, as u varies, the curve $\mathbf{q}(u)$ will be traversed at roughly a constant rate of speed.[6]

[6] Another common choice for knot parameterization is the *centripetal parameterization* where $u_{i+1} - u_i$ is set equal to $\sqrt{||\mathbf{p}_{i+1} - \mathbf{p}_i||}$. This presumably has an effect intermediate between uniform knot spacing and chord-length parameterization.

Of course, to use chord-length parameterization, we need to modify the formalization of Catmull-Rom splines to allow for nonuniform knot positions: in particular, it is necessary to find an alternative definition of the extra control points $\mathbf{p}_i^-$ and $\mathbf{p}_i^+$. More generally, to handle arbitrary nonuniform knot positions, we use a method called the *Bessel tangent* method or the *Overhauser* method [87]. Assume that we are given knot positions (not necessarily obtained from a chord-length parameterization) and that all knot positions are distinct with $u_i < u_{i+1}$. Define

$$\mathbf{v}_{i+\frac{1}{2}} \;=\; \frac{\mathbf{p}_{i+1} - \mathbf{p}_i}{u_{i+1} - u_i}.$$

The idea is that $\mathbf{v}_{i+\frac{1}{2}}$ is the average velocity at which the interpolating spline is traversed from $\mathbf{p}_i$ to $\mathbf{p}_{i+1}$. Of course, if we have defined the knot positions using a chord-length interpolation, then the velocities $\mathbf{v}_{i+\frac{1}{2}}$ will be unit vectors. Then we define a further velocity

$$\mathbf{v}_i = \frac{(u_{i+1} - u_i)\mathbf{v}_{i-\frac{1}{2}} + (u_i - u_{i-1})\mathbf{v}_{i+\frac{1}{2}}}{u_{i+1} - u_{i-1}},$$

which is a weighted average of the two velocities of the curve segments just before and just after the interpolated point $\mathbf{p}_i$. The weighted average is defined so that the velocities $\mathbf{v}_{i\pm\frac{1}{2}}$ are weighted more heavily when the elapsed time, $|u_{i\pm1} - u_i|$, between being at the control point $\mathbf{p}_{i\pm1}$ and being at the control point $\mathbf{p}_i$ is less. Finally, define

$$\begin{aligned} \mathbf{p}_i^- &= \mathbf{p}_i - \tfrac{1}{3}(u_i - u_{i-1})\mathbf{v}_i \\ \mathbf{p}_i^+ &= \mathbf{p}_i + \tfrac{1}{3}(u_{i+1} - u_i)\mathbf{v}_i. \end{aligned}$$

These points are then used to define Bézier curves in exactly the manner used for the uniform Catmull-Rom curves. The i-th segment, $\mathbf{q}_i(u)$, has control points $\mathbf{p}_i$, $\mathbf{p}_i^+$, $\mathbf{p}_{i+1}^-$, and $\mathbf{p}_{i+1}$, and is linearly transformed to be defined for u in the interval $[u_i, u_{i+1}]$. The entire piecewise Bézier curve $\mathbf{q}(u)$ is defined by patching these curves together, with $\mathbf{q}(u) = \mathbf{q}_i(u)$ for $u_i \le u \le u_{i+1}$.

Two examples of chord-length parameterization combined with the Overhauser method are shown in Figure VIII.25. These interpolate the same points as the Catmull-Rom splines in Figure VIII.24, but give a smoother and nicer curve, especially in the second example in the figures. Another example is given in Figure VIII.26.

Exercise VIII.23. Let $\mathbf{p}_0 = \mathbf{p}_1 = \langle 0, 0\rangle$, $\mathbf{p}_2 = \langle 10, 0\rangle$ and $\mathbf{p}_3 = \mathbf{p}_4 = \langle 10, 1\rangle$. Also, let $u_0 = 0$, $u_1 = 1$, $u_2 = 2$, $u_3 = 2.1$ and $u_4 = 3.1$. Find the control points for the corresponding Overhauser spline, $\mathbf{q}(u)$, with $\mathbf{q}(u_i) = \mathbf{p}_i$ for $i = 1, 2, 3$. Verify that your curve corresponds with the curve shown in Figure VIII.26.

Second, draw the Catmull-Rom curve defined by these same interpolation points. Qualitatively compare the Catmull-Rom curve with the Overhauser spline.

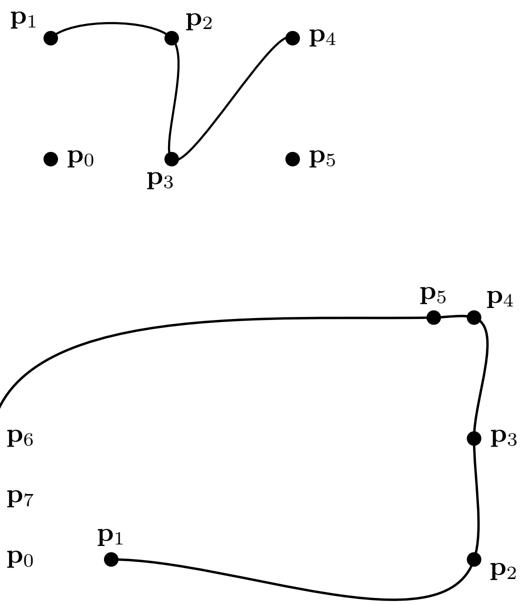

Figure VIII.25: Two examples of Overhauser spline curves. The knot positions were set by chord-length parameterization. These are defined from exactly the same control points as the Catmull-Rom curves in Figure VIII.24.

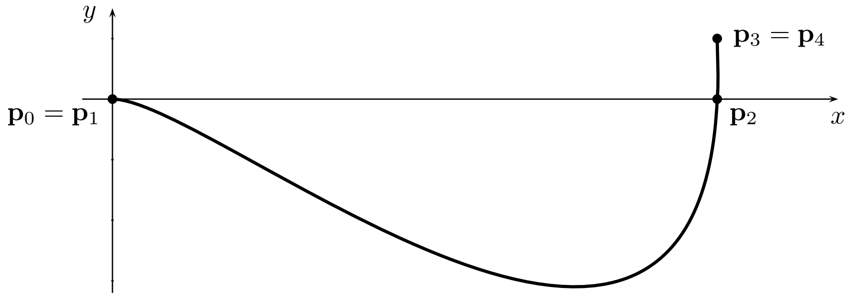

Figure VIII.26: The Overhauser spline which is the solution to Exercise VIII.23.

Exercise VIII.24. Investigate the chord-length parameterization Overhauser method curve from $\mathbf{p}_0$ to $\mathbf{p}_2$ when $\mathbf{p}_0, \mathbf{p}_1, \mathbf{p}_2$ are collinear. Apart from u_0 and u_4, this is a chord-length parameterization. What is the velocity at $\mathbf{p}_1$?

Consider separately the cases where $\mathbf{p}_1$ is, and is not, between $\mathbf{p}_0$ and $\mathbf{p}_2$.

Exercise VIII.25. It should be clear that the Overhauser method gives G^1-continuous curves. Prove that, in fact, the Overhauser method gives C^1-continuous curves. [Hint: Prove that $\mathbf{q}'(u_i) = \mathbf{v}_i$. You will need to take into account the fact that $\mathbf{q}_i(u)$ has domain $[u_i, u_{i+1}]$.]

There is another nice characterization of the Overhauser method in terms of blending two quadratic polynomials, which provides a second justification for its appropriateness. Define $\mathbf{f}_i(u)$ to be the (unique) quadratic polynomial such that $\mathbf{f}_i(u_{i-1}) = \mathbf{p}_{i-1}$, $\mathbf{f}_i(u_i) = \mathbf{p}_i$, and $\mathbf{f}_i(u_{i+1}) = \mathbf{p}_{i+1}$. Similarly define $\mathbf{f}_{i+1}(u)$ to be the quadratic polynomial with the values $\mathbf{p}_i, \mathbf{p}_{i+1}, \mathbf{p}_{i+2}$ at $u = u_i, u_{i+1}, u_{i+2}$. Then define

$$\mathbf{q}_i(u) \;=\; \frac{(u_{i+1}-u)\mathbf{f}_i(u) + (u-u_i)\mathbf{f}_{i+1}(u)}{u_{i+1}-u_i}. \qquad \text{(VIII.26)}$$

Clearly $\mathbf{q}_i(u)$ is a cubic polynomial and, further, for $u_i \le u \le u_{i+1}$, $\mathbf{q}_i(u)$ is equal to the curve $\mathbf{q}_i(u)$ obtained with the Overhauser method.

Exercise VIII.26* Prove the last assertion about the Overhauser method. [Suggestion: verify that $\mathbf{q}_i(u)$ has the correct values and derivatives at its endpoints u_i and u_{i+1}.]

Exercise VIII.27. Write a program that takes a series of positions specified with mouse clicks and draws a Catmull-Rom curve that interpolates them. Make the curve also interpolate the first and last point by doubling the first and last points (that is to say, treat the first and last points as if they occur twice). The supplied program `ConnectDots` can be used as a starting point; it accepts mouse clicks and joins the points with straight-line segments.

Exercise VIII.28. Extend the program from the previous exercise so that it also draws a Bessel-Overhauser spline curve that interpolates the points in the same fashion. Use keyboard commands to toggle between the Catmull-Rom and Bessel-Overhauser curves and visually compare the two kinds of curves.

VIII.15.3 Tension-continuity-bias splines

There are a variety of modified versions of Catmull-Rom interpolation schemes. Many of these are tools that let a curve designer specify a broader range of shapes for curves. For instance, someone may want to design a curve which is "tighter" at some points and "looser" at other points. One widely used method is the TCB (Tension-Continuity-Bias) method of Kochanek and Bartels [74], which uses three parameters of tension, continuity, and bias that affect the values of the tangents, and thereby the extra control points $\mathbf{p}_i^+$ and $\mathbf{p}_i^-$. The parameter of tension is used to control the tightness of curve, the continuity parameter controls the (dis)continuity of first derivatives, and the bias controls how the curve overshoots or undershoots an interpolation point.

The TCB method is a refinement of Catmull-Rom splines which adjusts the control points $\mathbf{p}_i^-$ and $\mathbf{p}_i^+$ according to the three new parameters. In order to describe how the TCB method works, we first reformulate the Catmull-Rom method slightly by introducing notations for the left and right first derivatives of the curve at an interpolation point $\mathbf{p}_i$.

$$\begin{aligned} D\mathbf{q}_i^- &= \lim_{u \to u_i^-} \frac{\mathbf{q}(u_i) - \mathbf{q}(u)}{u_i - u} = 3(\mathbf{p}_i - \mathbf{p}_i^-), \\ D\mathbf{q}_i^+ &= \lim_{u \to u_i^+} \frac{\mathbf{q}(u) - \mathbf{q}(u_i)}{u - u_i} = 3(\mathbf{p}_i^+ - \mathbf{p}_i). \end{aligned}$$

If we set values for $D\mathbf{q}_i^+$ and $D\mathbf{q}_i^-$, then this determines $\mathbf{p}_i^+$ and $\mathbf{p}_i^-$ by

$$\mathbf{p}_i^+ = \mathbf{p}_i + \tfrac{1}{3} D\mathbf{q}_i^+ \qquad \text{and} \qquad \mathbf{p}_i^- = \mathbf{p}_i - \tfrac{1}{3} D\mathbf{q}_i^-.$$

The basic Catmull-Rom splines can be defined by setting

$$D\mathbf{q}_i^- = D\mathbf{q}_i^+ = \frac{1}{2}\mathbf{v}_{i-\frac{1}{2}} + \frac{1}{2}\mathbf{v}_{i+\frac{1}{2}}, \tag{VIII.27}$$

where $\mathbf{v}_{i-\frac{1}{2}} = \mathbf{p}_i - \mathbf{p}_{i-1}$. The TCB splines work by modifying the Equation (VIII.27), but leaving the rest of the definition of the splines unchanged.

The tension parameter, denoted t, adjusts the tightness or looseness of the curve. The default value is $t = 0$; positive values should be less than 1 and make the curve tighter, and negative values make the curve looser. Mathematically, this has the effect of setting

$$D\mathbf{q}_i^- = D\mathbf{q}_i^+ = (1-t)\left(\frac{1}{2}\mathbf{v}_{i-\frac{1}{2}} + \frac{1}{2}\mathbf{v}_{i+\frac{1}{2}}\right),$$

i.e., of multiplying the derivative by $(1-t)$. Positive values of t make the derivative smaller: this has the effect of making the curve's segments between points $\mathbf{p}_i$ straighter, and making the velocity of the curve closer to zero at the points $\mathbf{p}_i$. Negative values of t make the curve looser, and can cause it to take bigger swings around interpolation points. The effect of setting tension to $1/2$ and to $-1/2$ is shown in Figure VIII.27.

The continuity parameter is denoted c. If $c = 0$, then the curve is C^1-continuous; otherwise, the curve has a corner at the control point $\mathbf{p}_i$, and thus discontinuous first derivative. Its mathematical effect is to set

$$\begin{aligned} D\mathbf{q}_i^- &= \frac{1-c}{2}\mathbf{v}_{i-\frac{1}{2}} + \frac{1+c}{2}\mathbf{v}_{i+\frac{1}{2}} \\ D\mathbf{q}_i^+ &= \frac{1+c}{2}\mathbf{v}_{i-\frac{1}{2}} + \frac{1-c}{2}\mathbf{v}_{i+\frac{1}{2}}. \end{aligned}$$

Typically, $-1 \le c \le 0$, and values $c < 0$ have the effect of turning the slope of the curve towards the straight-line segments joining the interpolation points.

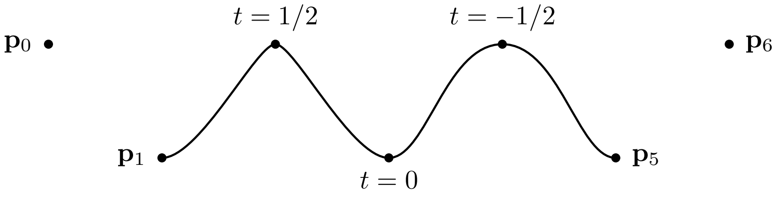

Figure VIII.27: The effects of the tension parameter.

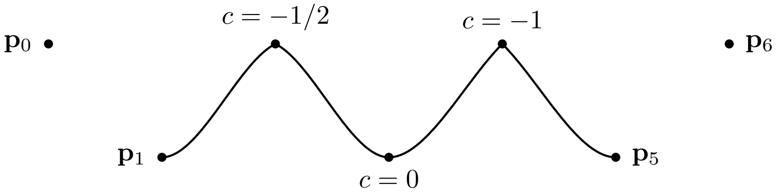

Figure VIII.28: The effects of the continuity parameter.

Setting $c = -1$ would make the curve's left and right first derivatives at $\mathbf{p}_i$ match the slopes of the line segments joining $\mathbf{p}_i$ to $\mathbf{p}_{i-1}$ and $\mathbf{p}_{i+1}$.

The effect of $c = -1/2$ and $c = -1$ is shown in Figure VIII.28. The effect of $c = -1/2$ in Figure VIII.28 looks very similar to the effect of tension $t = 1/2$ in Figure VIII.27; however, the effects are not as similar as they look. With $t = 1/2$, the curve still has continuous first derivative, and the velocity of a particle following the curve with u measuring time will be slower near the point where $t = 1/2$. On the other hand, with $c = -1/2$, the curve has a 'corner' where the first derivative is discontinuous, but there is no slowdown of velocity in the vicinity of the corner.

The bias parameter, b, weights the two average velocities $\mathbf{v}_{i-\frac{1}{2}}$ and $\mathbf{v}_{i+\frac{1}{2}}$ differently to cause either undershoot or overshoot. The mathematical effect is

$$D\mathbf{q}_i^- \ = \ D\mathbf{q}_i^+ \ = \ \frac{1+b}{2}\mathbf{v}_{i-\frac{1}{2}} + \frac{1-b}{2}\mathbf{v}_{i+\frac{1}{2}}.$$

The curve will have more tendency to overshoot $\mathbf{p}_i$ if $b > 0$, and to undershoot it if $b < 0$. The effect of bias $b = 1/2$ and bias $b = -1/2$ is shown in Figure VIII.29.

The tension, continuity, and bias parameters can be set independently to individual interpolation points or uniformly applied to an entire curve. This allows the curve designer to modify the curve either locally or globally. The effects of the three parameters can be applied together. This results in the

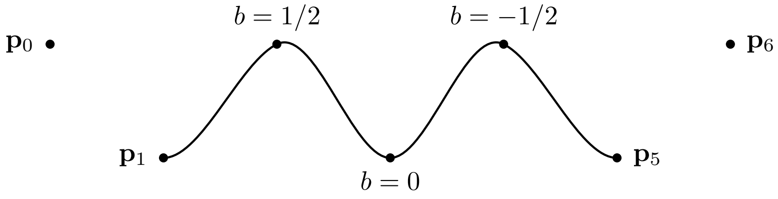

Figure VIII.29: The effects of the bias parameter.

following composite formula which replaces Equation (VIII.27):

$$\begin{aligned} D\mathbf{q}_i^- &= \frac{(1-t)(1-c)(1+b)}{2}\mathbf{v}_{i-\frac{1}{2}} + \frac{(1-t)(1+c)(1-b)}{2}\mathbf{v}_{i+\frac{1}{2}} \\ D\mathbf{q}_i^+ &= \frac{(1-t)(1+c)(1+b)}{2}\mathbf{v}_{i-\frac{1}{2}} + \frac{(1-t)(1-c)(1-b)}{2}\mathbf{v}_{i+\frac{1}{2}}. \end{aligned}$$

Exercise VIII.29* Extend the TCB parameters to apply to Overhauser splines instead of Catmull-Rom splines.

VIII.16 Interpolating with Bézier surfaces*

The previous sections have discussed methods of interpolating points with a series of Bézier curves that connects the interpolated points together with a smooth curve. The analogous problem for surfaces is to interpolate a two dimensional mesh of control points with a smooth surface formed from Bézier patches. For this, suppose we are given control points $\mathbf{p}_{i,j}$ for $i = 0, \ldots, m$ and $j = 0, \ldots, n$, and we want to find a smooth surface $\mathbf{q}(u, v)$ so that $\mathbf{q}(i, j) = \mathbf{p}_{i,j}$ for all appropriate i and j.

To formulate the problem a little more generally, let $\mathcal{I}$ and $\mathcal{J}$ be finite sets of real numbers,

$$\mathcal{I} = \{u_0, u_1, \ldots, u_m\} \qquad \text{and} \qquad \mathcal{J} = \{v_0, v_1, \ldots, v_n\},$$

where $u_i < u_{i+1}$ and $v_j < v_{j+1}$ for all i, j. For $0 \le i \le m$ and $0 \le j \le n$, let $\mathbf{p}_{i,j}$ be a point in $\mathbb{R}^3$. Then, we are seeking a smooth surface $\mathbf{q}(u, v)$ so that $\mathbf{q}(u_i, v_j) = \mathbf{p}_{i,j}$ for all $0 < i < m$ and $0 < j < n$.

We shall define the surface $\mathbf{q}(u, v)$ as a collection of Bézier patches, analogous to the Catmull-Rom and Bessel-Overhauser splines that were defined with multiple Bézier curves that interpolate a sequence of points. The corners of the Bézier patches comprising $\mathbf{q}(u, v)$ will meet at the interpolation points $\mathbf{p}_{i,j}$, and the Bézier patches will form a mesh of rectangular patches. One big advantage of this method is that the Bézier patches are defined locally; that is to say, each Bézier patch depends only on the nearby interpolation points.

We will discuss primarily the case where the interpolation positions u_i and v_j are equally spaced, with $u_i = i$ and $v_j = j$; but we will also discuss how to generalize to the non-equally-spaced case.

We will define degree three Bézier patches $Q_{i,j}(u,v)$ with domains the rectangles $[u_i, u_{i+1}] \times [v_j, v_{j+1}]$. The complete surface $\mathbf{q}(u,v)$ will be formed as the union of these patches $Q_{i,j}$. Of course, we will need to be sure that the patches have the right continuity and C^1-continuity properties. The control points for the Bézier patch $Q_{i,j}$ will be sixteen points, $\mathbf{p}_{\alpha,\beta}$, where $\alpha \in \{i, i+\frac{1}{3}, i+\frac{2}{3}, i+1\}$, and $\beta \in \{j, j+\frac{1}{3}, j+\frac{2}{3}, j+1\}$. Of course, this means that the patch $Q_{i,j}$ will interpolate the points $\mathbf{p}_{i,j}$, $\mathbf{p}_{i+1,j}$, $\mathbf{p}_{i,j+1}$ and $\mathbf{p}_{i+1,j+1}$, which is exactly what we want. It remains to define the other twelve control points of the patch.

As the first step towards defining the other twelve control points for each patch, we define the control points that lie on the boundary, i.e, the control points $\mathbf{p}_{\alpha,\beta}$ where either α or β is an integer. Fix, for the moment, the value of j and the value of v as $v = v_j$. Consider the cross section of the surface $\mathbf{q}(u,v)$ for this value of v, namely, the curve $\mathbf{q}_j(u) = \mathbf{q}(u, v_j)$. This cross section is piecewise degree three Bézier curves defined with control points $\mathbf{p}_{\alpha,j}$. It also interpolates the point $\mathbf{p}_{i,j}$ at $\alpha = u_i$. Thus, it seems natural to define the other control points $\mathbf{p}_{i\pm\frac{1}{3},j}$, for all values of i, using the Catmull-Rom or Bessel-Overhauser method. (Recall that the Catmull-Rom and Bessel-Overhauser methods are identical in the equally spaced case. The Bessel-Overhauser method should be used in the non-equally-spaced case.) The control points $\mathbf{p}_{i\pm\frac{1}{3},j}$ are chosen so that the curve $\mathbf{q}_j$ smoothly interpolates the points $\mathbf{p}_{i,j}$ for this fixed value of j.

Dually, by holding i fixed and fixing $u = u_i$, the cross sectional curves of $\mathbf{q}(u_i, v)$ are likewise piecewise degree three Bézier curves. Thus, the control points $\mathbf{p}_{i,\beta}$ can be defined using the Catmull-Rom or Bessel-Overhauser method to get a curve that interpolates the points $\mathbf{p}_{i,j}$ for a fixed value of i.

It now remains to pick the four interior control points for each patch $Q_{i,j}$, namely the control points $\mathbf{p}_{i+\frac{1}{3},j+\frac{1}{3}}$, $\mathbf{p}_{i+\frac{2}{3},j+\frac{1}{3}}$, $\mathbf{p}_{i+\frac{1}{3},j+\frac{2}{3}}$, and $\mathbf{p}_{i+\frac{2}{3},j+\frac{2}{3}}$. As we shall see, these four control points can be determined by choosing appropriate *twist vectors*. In order to simplify the details of how to set these control points, we now make the assumption that the interpolation positions u_i and v_j are equally spaced: in fact, we assume that $u_i = i$ and $v_j = j$ for all i and j.

The patches $Q_{i,j}$ and $Q_{i-1,j}$ share a common border. In order to have C^1-continuity between the two patches, it is necessary that the partial derivatives match up along the boundary. As was discussed in Section VIII.10.2, to match up partial derivatives, it is necessary and sufficient to ensure that

$$\mathbf{p}_{i,\beta} - \mathbf{p}_{i-\frac{1}{3},\beta} \;=\; \mathbf{p}_{i+\frac{1}{3},\beta} - \mathbf{p}_{i,\beta}, \tag{VIII.28}$$

for each $\beta \in \{j, j+\frac{1}{3}, j+\frac{2}{3}, j+1\}$. Likewise, in joining up patches $Q_{i,j}$ and $Q_{i,j-1}$, we must have

$$\mathbf{p}_{\alpha,j} - \mathbf{p}_{\alpha,j-\frac{1}{3}} \;=\; \mathbf{p}_{\alpha,j+\frac{1}{3}} - \mathbf{p}_{\alpha,j}, \tag{VIII.29}$$

for $\alpha \in \{i, i+\frac{1}{3}, i+\frac{2}{3}, i+1\}$. Equations (VIII.28) and (VIII.29) were derived for a particular patch $Q_{i,j}$, but since all the patches must join up smoothly, these equations actually hold for all values of i and j. We define the *twist vector* $\boldsymbol{\tau}_{i,j}$ by

$$\boldsymbol{\tau}_{i,j} \;=\; 9(\mathbf{p}_{i+\frac{1}{3},j+\frac{1}{3}} - \mathbf{p}_{i,j+\frac{1}{3}} - \mathbf{p}_{i+\frac{1}{3},j} + \mathbf{p}_{i,j}).$$

Then, by Equation (VIII.28), with $\beta = j$ and $\beta = j+\frac{1}{3}$, we get

$$\boldsymbol{\tau}_{i,j} \;=\; 9(\mathbf{p}_{i,j+\frac{1}{3}} - \mathbf{p}_{i-\frac{1}{3},j+\frac{1}{3}} - \mathbf{p}_{i,j} + \mathbf{p}_{i-\frac{1}{3},j}).$$

By similar reasoning, with Equation (VIII.29) for α equal to $i+\frac{1}{3}$, i and $i-\frac{1}{3}$, we have also

$$\begin{aligned}
\boldsymbol{\tau}_{i,j} &= 9(\mathbf{p}_{i+\frac{1}{3},j} - \mathbf{p}_{i,j} - \mathbf{p}_{i+\frac{1}{3},j-\frac{1}{3}} + \mathbf{p}_{i,j-\frac{1}{3}}) \\
\boldsymbol{\tau}_{i,j} &= 9(\mathbf{p}_{i,j} - \mathbf{p}_{i-\frac{1}{3},j} - \mathbf{p}_{i,j-\frac{1}{3}} + \mathbf{p}_{i-\frac{1}{3},j-\frac{1}{3}}).
\end{aligned}$$

Rewriting these four equations, we get formulas for the inner control points:

$$\begin{aligned}
\mathbf{p}_{i+\frac{1}{3},j+\frac{1}{3}} &= \frac{1}{9}\boldsymbol{\tau}_{i,j} + \mathbf{p}_{i,j+\frac{1}{3}} + \mathbf{p}_{i+\frac{1}{3},j} - \mathbf{p}_{i,j} \\
\mathbf{p}_{i-\frac{1}{3},j+\frac{1}{3}} &= -\frac{1}{9}\boldsymbol{\tau}_{i,j} + \mathbf{p}_{i,j+\frac{1}{3}} + \mathbf{p}_{i-\frac{1}{3},j} - \mathbf{p}_{i,j} \qquad \text{(VIII.30)} \\
\mathbf{p}_{i+\frac{1}{3},j-\frac{1}{3}} &= -\frac{1}{9}\boldsymbol{\tau}_{i,j} + \mathbf{p}_{i,j-\frac{1}{3}} + \mathbf{p}_{i+\frac{1}{3},j} - \mathbf{p}_{i,j} \\
\mathbf{p}_{i-\frac{1}{3},j-\frac{1}{3}} &= \frac{1}{9}\boldsymbol{\tau}_{i,j} + \mathbf{p}_{i,j-\frac{1}{3}} + \mathbf{p}_{i-\frac{1}{3},j} - \mathbf{p}_{i,j}.
\end{aligned}$$

Thus, once the twist vectors $\boldsymbol{\tau}_{i,j}$ have been fixed, the remaining control points for the Bézier patches are completely determined.

The twist vector has a simple geometric meaning as the second-order partial derivatives of the Bézier surfaces. Namely, by Equations (VIII.18) and (VIII.19) on page 290 and by the definition of the twist vector,

$$\frac{\partial^2 Q_{i,j}}{\partial u \partial v}(u_i, v_j) \;=\; \boldsymbol{\tau}_{i,j}.$$

Thus, the twist vector $\boldsymbol{\tau}_{i,j}$ is just the mixed partial derivative at the corners of the patches that meet at $\langle u_i, v_j \rangle$.

To finish specifying all the control points, it only remains to set the value of the twist vector. The simplest method is to just set the twist vectors $\boldsymbol{\tau}_{i,j}$ all equal to zero. This gives the so-called *Ferguson patches*, since it is equivalent to a construction from Ferguson [47]. The disadvantage of just setting the twist vector to zero is that it tends to make the surface $\mathbf{q}(u,v)$ too flat around the interpolation points. For specular surfaces in particular, this can make artifacts on the surface, known as "flats," where the surface is noticeably flattened around interpolation points.

It is better to set the twist vector by estimating the second-order mixed partial derivative of $\mathbf{q}(u,v)$ at an interpolation point $\langle u_i, v_j\rangle$. Here we are still making the assumption that interpolation positions are equally spaced, i.e, that $u_i = i$ and $v_j = j$. Then, a standard estimate for the partial derivative is

$$\begin{aligned}\frac{\partial^2\mathbf{q}}{\partial u\partial v}(i,j) &= \frac{1}{4}(\mathbf{q}(i+1,j+1) - \mathbf{q}(i-1,j+1) - \mathbf{q}(i+1,j-1) + \mathbf{q}(i-1,j-1)) \\ &= \frac{1}{4}(\mathbf{p}_{i+1,j+1} - \mathbf{p}_{i-1,j+1} - \mathbf{p}_{i+1,j-1} + \mathbf{p}_{i-1,j-1}). \qquad \text{(VIII.31)}\end{aligned}$$

Using this value as the value of $\boldsymbol{\tau}$ can give a better quality interpolating surface.

The estimate of Equation (VIII.31) is not entirely ad hoc: indeed, it can be justified as a generalization of the Bessel-Overhauser curve method. For surface interpolation, we refer to it as just the *Bessel twist method*, and the idea is as follows. Let $f_{i,j}(u,v)$ be the degree two polynomial ("degree two" means degree two in each of u and v separately) which interpolates the nine control points $\mathbf{p}_{\alpha,\beta}$ for $\alpha \in \{u_{i-1}, u_i, u_{i+1}\}$ and $\beta \in \{v_{j-1}, v_j, v_{j+1}\}$, so $f_{i,j}(\alpha,\beta) = \mathbf{p}_{\alpha,\beta}$ for these nine values of α and β. Then define the patch $Q_{i,j}$ by blending four of these functions, namely,

$$\begin{aligned}&Q_{i,j}(u,v) \qquad \text{(VIII.32)}\\ &= \frac{(u-u_i)(v-v_j)}{\Delta u_i \Delta v_j} f_{i+1,j+1}(u,v) + \frac{(u-u_i)(v_{j+1}-v)}{\Delta u_i \Delta v_j} f_{i+1,j}(u,v) \\ &\quad + \frac{(u_{i+1}-u)(v-v_j)}{\Delta u_i \Delta v_j} f_{i,j+1}(u,v) + \frac{(u_{i+1}-u)(v_{j+1}-v)}{\Delta u_i \Delta v_j} f_{i,j}(u,v),\end{aligned}$$

where $\Delta u_i = u_{i+1} - u_i$ and $\Delta v_j = v_{j+1} - v_j$. Note that this way of defining $Q_{i,j}$ is a direct generalization of the Bessel-Overhauser method of Equation (VIII.26). The patch $Q_{i,j}$ defined by Equation (VIII.32) is obviously a bicubic patch (i.e., is degree three in each of u and v separately). As a bicubic patch it can be expressed as a degree three Bézier patch. In view of Exercise VIII.26, the corners and boundary control points of $Q_{i,j}$ defined by (VIII.32) are equal to the control points defined using the first method. We claim that also the four interior control points of the patch $Q_{i,j}$ as defined by (VIII.32) are the same as the control points calculated by using Equation (VIII.30) with the twist vector estimate of Equation (VIII.31). To prove this for the case of equally spaced interpolation positions, we can evaluate the mixed partial derivatives of the righthand side of Equation (VIII.32), and use the fact that the four functions $f_{i+1,j+1}$, $f_{i,j+1}$, $f_{i+1,j}$ and $f_{i,j}$ are equal at $\langle u_i, v_j\rangle$ and the fact that $(\partial f_{i,j}/\partial u)(u_i,v_j) = (\partial f_{i,j+1}/\partial u)(u_i,v_j)$ and that $(\partial f_{i,j}/\partial v)(u_i,v_j) = (\partial f_{i+1,j}/\partial v)(u_i,v_j)$. We find that

$$\frac{\partial^2 Q_{i,j}}{\partial u\partial v}(u_i,v_j) = \frac{\partial^2 f_{i,j}}{\partial u\partial v}(u_i,v_j).$$

This holds even in the case of non-equally-spaced interpolation positions. We leave the details of the calculations to the reader.

Finally, we claim that

$$\frac{\partial^2 f_{i,j}}{\partial u \partial v}(u_i, v_j) \;=\; \frac{1}{4}(\mathbf{p}_{i+1,j+1} - \mathbf{p}_{i-1,j+1} - \mathbf{p}_{i+1,j-1} + \mathbf{p}_{i-1,j-1}), \qquad \text{(VIII.33)}$$

when the interpolation positions are equally spaced. This is straightforward to check, and we leave its verification to the reader, too. With this, the Bessel method is seen to be equivalent to the using the last formula of Equation (VIII.31) to calculate the twist vector.

We now generalize to the case of non-equally-spaced interpolation positions. We have already described how to set the corner and boundary control points of each patch $Q_{i,j}$. We still let the twist vector $\boldsymbol{\tau}_{i,j}$ be the mixed partial derivative at $\langle u_i, v_j \rangle$. Now the equations (VIII.30) become

$$\begin{aligned}
\mathbf{p}_{i+\frac{1}{3},j+\frac{1}{3}} &= \Delta u_i \Delta v_j \frac{\boldsymbol{\tau}_{i,j}}{9} + \mathbf{p}_{i,j+\frac{1}{3}} + \mathbf{p}_{i+\frac{1}{3},j} - \mathbf{p}_{i,j} \\
\mathbf{p}_{i-\frac{1}{3},j+\frac{1}{3}} &= -\Delta u_{i-1} \Delta v_j \frac{\boldsymbol{\tau}_{i,j}}{9} + \mathbf{p}_{i,j+\frac{1}{3}} + \mathbf{p}_{i-\frac{1}{3},j} - \mathbf{p}_{i,j} \qquad \text{(VIII.34)} \\
\mathbf{p}_{i+\frac{1}{3},j-\frac{1}{3}} &= -\Delta u_i \Delta v_{j-1} \frac{\boldsymbol{\tau}_{i,j}}{9} + \mathbf{p}_{i,j-\frac{1}{3}} + \mathbf{p}_{i+\frac{1}{3},j} - \mathbf{p}_{i,j} \\
\mathbf{p}_{i-\frac{1}{3},j-\frac{1}{3}} &= \Delta u_{i-1} \Delta v_{j-1} \frac{\boldsymbol{\tau}_{i,j}}{9} + \mathbf{p}_{i,j-\frac{1}{3}} + \mathbf{p}_{i-\frac{1}{3},j} - \mathbf{p}_{i,j}.
\end{aligned}$$

In addition, Equation (VIII.33) is no longer correct: instead, we let

$$T_{i,j} \;=\; \mathbf{p}_{i+1,j+1} - \mathbf{p}_{i+1,j} - \mathbf{p}_{i,j+1} + \mathbf{p}_{i,j},$$

and then we have

$$\begin{aligned}
&\frac{\partial^2 f_{i,j}}{\partial u \partial v}(u_i, v_j) \\
&\quad= \frac{\Delta u_i \Delta v_j T_{i-1,j-1} + \Delta u_i \Delta v_{j-1} T_{i-1,j} + \Delta u_{i-1} \Delta v_j T_{i,j-1} + \Delta u_{i-1} \Delta v_{j-1} T_{i,j}}{(\Delta u_i + \Delta u_{i-1})(\Delta v_j + \Delta v_{j-1})} \\
&\quad= \frac{\Delta u_i \Delta v_j T_{i-1,j-1} + \Delta u_i \Delta v_{j-1} T_{i-1,j} + \Delta u_{i-1} \Delta v_j T_{i,j-1} + \Delta u_{i-1} \Delta v_{j-1} T_{i,j}}{(u_{i+1} - u_{i-1})(v_{j+1} - v_{j-1})}.
\end{aligned}$$

Thus, for non-equally-spaced interpolation points, we recommend setting the twist vector $\boldsymbol{\tau}_{i,j}$ equal to this last equation, and setting the control points with equations (VIII.34).

There are a number of other ways of computing twist vectors: see [42] and the references cited therein.

Further reading. The discussion above has been limited to surfaces formed by regular patterns of retangular patches. Not all surfaces can be conveniently approximated by rectangular patches however; in fact, some cannot be approximated by a single array of rectangular patches at all. One alternative is to work with triangular patches; for example, the books [42] and [67] discuss

Bézier patches defined on triangles. More generally, it is desirable to be able to model surfaces containing an arbitrary topology of triangles, rectangles, and other polygons. There has been extensive work on *subdivision surfaces* for the purpose of modeling surfaces with a wide range of topologies. Subdivision surfaces are beyond the scope of this book, but for an introduction you can consult the Siggraph course notes of Schröder, Zorin, et al. [98] or the book by Warren and Weimer [117]

VIII.17 Additional exercises

Exercise VIII.30. Consider the curve consisting of the portion of the parabola $y = x^2$ between $\langle 0,0\rangle$ and $\langle 2,4\rangle$. First express this portion as a degree 2 Beźier curve by giving its three control points. Second, express this as a degree 3 Bézier curve by giving its four control points.

Exercise VIII.31. A particle moving in $\mathbb{R}^2$ is animated so that its position $\mathbf{p}(u)$ at time u is given by a degree 3 Bézier curve with control points $\mathbf{p}_0$, $\mathbf{p}_1$, $\mathbf{p}_2$, $\mathbf{p}_3$. At time $u = 0$, the particle is at $\langle 0,0\rangle$ and has velocity $\langle 6,0\rangle$. At time $u = 1$, the particle is at $\langle 0,4\rangle$ and has velocity $\langle -12,0\rangle$.

(a) What are the control points $\mathbf{p}_0$, $\mathbf{p}_1$, $\mathbf{p}_2$, and $\mathbf{p}_3$?

(b) Use the de Casteljau algorithm to calculate $\mathbf{p}(\frac{1}{2})$, the position at time $u = \frac{1}{2}$. Draw a graph that shows clearly the curve, and all intermediate steps of the de Casteljau algorithm.

(c) Consider the second half of the path of the particle, namely the path traced out when $\frac{1}{2} \le u \le 1$. This is also a degree three Bézier curve. What are its control points?

Exercise VIII.32. Let $\mathbf{p}_0 = \langle 0,-2\rangle$. $\mathbf{p}_1 = \langle 2,0\rangle$, $\mathbf{p}_2 = \langle 0,2\rangle$, $\mathbf{p}_3 = \langle -2,0\rangle$, and $\mathbf{p}_4 = \langle 0,0\rangle$, as shown in Figure VIII.30

(a) Draw the Catmull-Rom curve defined by these points. Be sure to show clearly the starting point, ending point, and the slopes of the curve at each point $\mathbf{p}_i$ on the curve.

(b) What are the control points for the first Bézier segment of the Catmull-Rom curve?

Exercise VIII.33. The next three problems use the control points $\mathbf{p}_0 = \langle -2,0\rangle$, $\mathbf{p}_1 = \langle -1,0\rangle$, $\mathbf{p}_2 = \langle 0,0\rangle$, $\mathbf{p}_3 = \langle 0,\frac{1}{4}\rangle$, $\mathbf{p}_4 = \langle 1,\frac{1}{4}\rangle$, and $\mathbf{p}_5 = \langle 2,\frac{1}{4}\rangle$. These are shown in Figure VIII.31. Let $\mathbf{q}(u)$ be the Catmull-Rom curve defined with these control points. Which points $\mathbf{p}_i$ must be interpolated by $\mathbf{q}(u)$? What is the slope of $\mathbf{q}(u)$ at each interpolated $\mathbf{p}_i$?

Exercise VIII.34. An Overhauser spline $\mathbf{q}(u)$ uses chord-length parameterization and has the same control points as the curve in Exercise VIII.33. What is the slope of $\mathbf{q}(u)$ at each interpolated point $\mathbf{p}_i$?

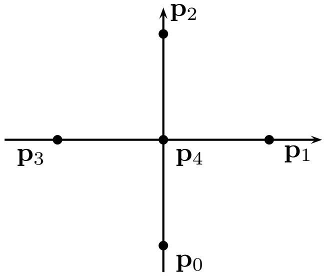

Figure VIII.30: The points for Exercise VIII.32.

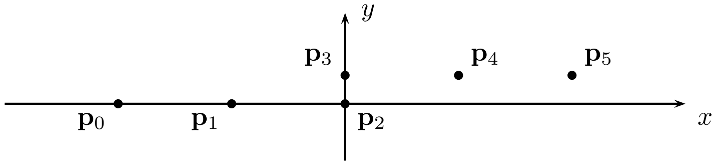

Figure VIII.31: The control points for Exercises VIII.33-VIII.35.

Exercise VIII.35. Repeat the previous exercise, but using centripetal parameterization instead of chord length parameterization.

Exercise VIII.36. An ellipse $\mathcal{E}$ in $\mathbb{R}^2$ is centered at the origin. It has major radius 2 extending horizontally from $\langle -2, 0\rangle$ to $\langle 2, 0\rangle$. It has minor radius 1 extending vertically from $\langle 0, -1\rangle$ to $\langle 0, 1\rangle$. Express the right half of $\mathcal{E}$ as a degree 2 Bézier curve. Do you need to use homogeneous coordinates? Do you need control points at infinity? Explain why or why not.

Exercise VIII.37. Now rotate $\mathcal{E}$ clockwise 45 degrees, i.e., forming the ellipse $\mathcal{E}' = R_{-\pi/2}$. This also rotates the Bézier curve from the previous exercise, namely the right half of $\mathcal{E}$. Express the rotated Bézier curve as a degree 2 Bézier curve by giving its control points.

Exercise VIII.38. Express the curve from Exercise VIII.36 as a degree 3 Bézier curve. [Hint: Use degree elevation.] Do you need control points at infinity? Do you need to use homogeneous coordinates?

Exercise VIII.39. The GLSL function `smoothstep` computes a generalized version of the degree 3 Hermite function H_3. Recall that H_3 is a cubic curve with $H_3(0) = H_3'(0) = H_3'(1) = 0$ and $H_3(1) = 1$. Express $H_3(u)$, for $u \in [0, 1]$, as a degree 3 Bézier curve in $\mathbb{R}$ by giving its four control points. (Note these control points lie in $\mathbb{R}$.)

Exercise VIII.40. Let $\mathcal{H}$ be the half-hyperbola in $\mathbb{R}^2$ defined as

$$\mathcal{H} \ = \ \{\langle x, y\rangle : xy = 1 \text{ and } x, y > 0\}.$$

Express $\mathcal{H}$ as a degree 2 Bézier curve $\mathbf{q}(u) = \langle x(u), y(u), z(u)\rangle$ over homogeneous coordinates. For this, use control points $\mathbf{p}_0$, $\mathbf{p}_1$, $\mathbf{p}_2$ where $\mathbf{p}_0 = \langle 0, 1, 0\rangle$ and $\mathbf{p}_2 = \langle 1, 0, 0$ are points at infinity. What should $\mathbf{p}_1$ equal? Prove that $\mathbf{q}(u)$ really does define $\mathcal{H}$ by proving that $x(u)y(u) = w(u)^2$.

Exercise VIII.41. (Reversing degree elevation.) Suppose you are given the control points $\mathbf{p}_0, \ldots, \mathbf{p}_3$ for a degree Bézier curve $\mathbf{q}(u)$ (working in ordinary coordinates, not homogeneous coordinates). Also suppose that it is promised that $\mathbf{q}(u)$ is actually a *degree 2* polynomial curve. How would you compute the control points representing $\mathbf{q}(u)$ as a degree 2 Bézier curve?

Suppose now that $\mathbf{q}(u)$ is only *close to* a degree 2 curve. How would you check that this holds? Suggest a robust method for converting $\mathbf{q}(u)$ into a degree 2 Bézier curve $\mathbf{q}^*(u)$ which is “close to” $\mathbf{q}(u)$. How would your method compute the control points for $\mathbf{q}^*(u)$? Can you give a reasonable and easy-to-compute upper bound on the maximum difference $||\mathbf{q}^*(u) - \mathbf{q}(u)||$ between the two curves for $u \in [0, 1]$?

Exercise VIII.42* Fill in the details of the following sketch of a proof of the variation diminishing property of Bézier curves. First, fix a line (or, in $\mathbb{R}^3$, a plane) and a continuous curve (the curve may consist of straight-line segments). Consider the following operation on the curve: choose two points on the curve and replace the part of the curve between the two points by the straight-line segment joining the two points. Prove that this does not increase the number of times the curve crosses the line. Second, show that the process of going from the control polygon of a Bézier curve to the two control polygons of the two subcurves obtained by using recursive subdivision to split the curve at $u = 1/2$ involves only a finite number of uses of the operation from the first step. Therefore, the total number of times the two new control polygons cross the line is less than or equal to the number of times the original control polygon crossed the curve. Third, prove that as the curve is repeatedly recursively subdivided, the control polygon approximates the curve. Fourth, argue that this suffices to prove the variation diminishing property (this last point is not entirely trivial).

Chapter IX

B-Splines

This is a ***preliminary*** *draft of a second edition of the book* 3-D Computer Graphics: A Mathematical Introduction with OpenGL. *So please read it cautiously and critically! Corrections are appreciated. Draft C.4.a*

Author: Sam Buss, sbuss@ucsd.edu

This chapter covers uniform and nonuniform B-splines, including rational B-splines (NURBS). B-splines are widely used in computer aided design and manufacturing, and are supported by OpenGL. B-splines are a powerful tool for generating curves with many control points, and provide many advantages over Bézier curves, especially in that a long complicated curve can be specified as a single B-spline. Furthermore, a curve designer has a lot of flexibility in adjusting the curvature of a B-spline curve, and B-splines can be designed with sharp bends and even "corners." In addition, it is possible to translate piecewise Bézier curves into B-splines and vice-versa. B-splines do not usually interpolate their control points, but it is possible to define interpolating B-splines. Our presentation of B-splines is based on the Cox-de Boor definition of blending functions, but the blossoming approach to B-splines is also presented.

The reader is warned that this chapter is a mix of introductory topics and more advanced, specialized topics. You should read at least the first parts of Chapter VIII before this chapter. Sections IX.1-IX.4 below give a basic introduction to B-splines. The next four sections cover the de Boor algorithm, blossoming, smoothness properties, and knot insertion; these sections are fairly mathematical and should be read in order. If you wish, you may skip these mathematical sections at first, as the remainder of the chapter can be read largely independently. Section IX.9 discusses how to convert a piecewise Bézier curves into a B-spline. The very short Section IX.10 discusses degree elevation. Section IX.11 covers rational B-splines. Section IX.12 gives a method for interpolating points with B-splines. You should feel free to skip most of the proofs if you find them confusing; most of the proofs, especially the more difficult ones, are not needed for practical use of splines.

Splines, especially interpolating splines, have a long history — and we do not try to describe it here. B-spline functions were defined by Shoenberg (and Curry) in 1946 [106, 33]. The name “B-spline”, with the “B” standing “basis”, was coined by Shoenberg [107] in 1967. The terminology “basis spline” refers to the fact that B-splines are defined in terms of “basis functions.” (We use the term “blending function” instead of “basis function.”) B-splines became popular after de Boor [36], Cox [30] and Mansfield discovered, in 1972, the fundamental Cox-de Boor formula for recursively defining the blending functions.

Figure IX.1 shows one of the simplest possible examples of how B-spline curves can be used. There are nine control points $\mathbf{p}_0, \ldots, \mathbf{p}_8$ which completely define the B-spline curves. The curve shown in part (a) is a uniform degree two B-spline curve; the curve in part (b) is a uniform degree three curve. (The mathematical definitions of these curves are in Sections IX.1 and IX.2.) Qualitatively, the curves are “pulled towards” the control points in much the same way that a Bézier curve is pulled towards its interior control points. Unlike Bézier curves, B-spline curves do not necessarily interpolate their first and last control points; rather, the degree two curve starts and ends midway between two control points, and the degree three curve starts and ends near the control points that are adjacent to the starting and ending points. However, there are ways of defining B-spline curves that ensure that the first and last control points are interpolated.

A big advantage of B-spline curves over Bézier curves is that they act more flexibly and intuitively with a large number of control points. Indeed, if you compare the curves of Figure IX.1 to the degree eight Bézier curve of Figure VIII.9(c) on page 280, you will see that the B-spline curves are pulled by the control points in a much more definite fashion. The Bézier curve seems to be barely affected by the placement of individual control points, whereas the B-spline curves are clearly affected in a direct fashion by the control points. This makes B-spline curves much more useful for designing curves.

We shall first treat the case of uniform B-splines, and then the more general case of nonuniform B-splines.

IX.1 Uniform B-splines of degree three

Before presenting the general definition of B-splines in Section IX.2, we first introduce one of the simplest and most useful cases of B-splines, namely the *uniform B-splines of degree three.* Such a B-spline is defined with a sequence $\mathbf{p}_0, \mathbf{p}_1, \mathbf{p}_2, \ldots, \mathbf{p}_n$ of *control points.* Together with a set of blending (or basis) functions $N_0(u), N_1(u), \ldots, N_n(u)$, this parametrically defines a curve $\mathbf{q}(u)$ by

$$\mathbf{q}(u) \;=\; \sum_{i=0}^{n} N_i(u) \cdot \mathbf{p}_i \qquad\qquad 3 \le u \le n+1\,. \tag{IX.1}$$

We define these blending functions below, but for the moment, just think of the blending functions N_i as having an effect analogous to the Bernstein polynomials B_i used in the definition of Bézier curves.

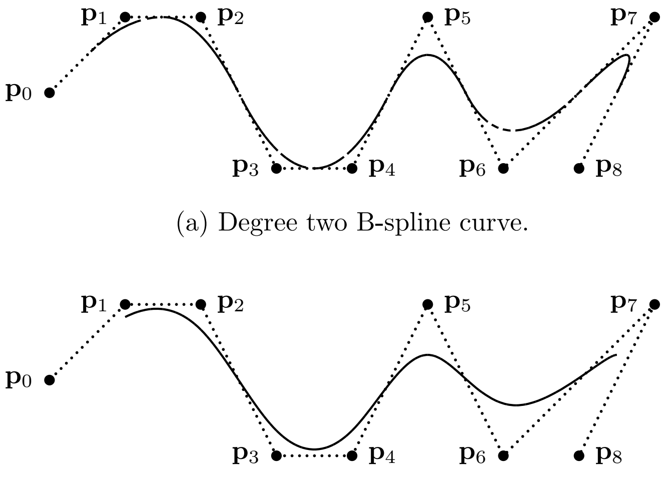

(a) Degree two B-spline curve.

(b) Degree three B-spline curve.

Figure IX.1: Degree two and degree three B-spline curves with uniformly spaced knots and nine control points. The degree three curve is smoother than the degree two curve, whereas, the degree two curve approaches the control points a little more closely. Compare with the degree eight Bézier curve of Figure VIII.9(c) on page 280.

An important property of the uniform degree three blending functions N_i is that $N_i(u)$ will equal zero if either $u \le i$ or $i + 4 \le u$. That is to say, the support of $N_i(u)$ is the open interval $(i, i+4)$. In particular, this means that we can rewrite the formula for $\mathbf{q}(u)$ as

$$\mathbf{q}(u) \;=\; \sum_{i=j-3}^{j} N_i(u) \cdot \mathbf{p}_i \qquad \text{provided } u \in [j, j+1],\ 3 \le j \le n, \qquad \text{(IX.2)}$$

since the terms omitted from the summation are all zero. This means that the B-spline has *local control*; namely, if a single control point $\mathbf{p}_i$ is moved, then only the portion of the curve $\mathbf{q}(u)$ with $i < u < i+4$ is changed and the rest of the B-spline remains fixed. Local control is an important feature enhancing the usefulness of B-spline curves: it allows a designer or artist to edit one portion of a curve without causing changes to other parts of the curve. In contrast, Bézier curves of higher degree do not have local control, since each control point affects the entire curve.

Figure IX.2 shows an example of a degree three B-spline curve $\mathbf{q}(u)$ defined with seven control points and defined for $3 \le u \le 7$. The curve $\mathbf{q}$ is split into four subcurves $\mathbf{q}_3, \ldots, \mathbf{q}_6$ where $\mathbf{q}_3$ is the portion of $\mathbf{q}(u)$ corresponding to $3 \le u \le 4$, $\mathbf{q}_4$ is the portion with $4 \le u \le 5$, etc. More generally, $\mathbf{q}_i(u) = \mathbf{q}(u)$ for $i \le u \le i+1$.

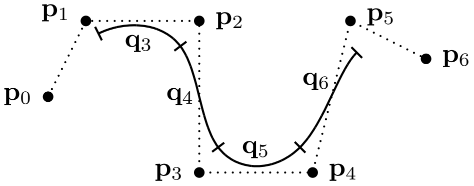

Figure IX.2: A degree three uniform B-spline curve with seven control points.

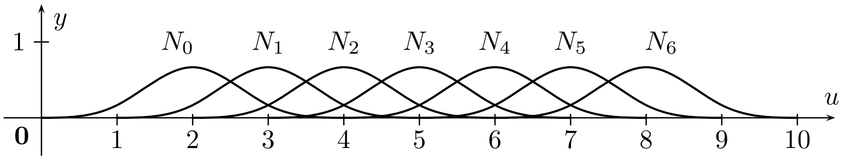

Figure IX.3: The blending functions for a uniform, degree three B-spline. Each function N_i has support $(i, i+4)$.

The intuition of how the curve $\mathbf{q}(u)$ behaves is as follows. The beginning point of $\mathbf{q}_3$, where $u = 3$, is being pulled strongly towards the point $\mathbf{p}_1$ and less strongly towards the points $\mathbf{p}_0$ and $\mathbf{p}_2$. The other points on $\mathbf{q}_3$ are calculated as a weighted average of $\mathbf{p}_0, \mathbf{p}_1, \mathbf{p}_2, \mathbf{p}_3$. The other segments are similar; namely, the beginning of $\mathbf{q}_i$ is being pulled strongly towards $\mathbf{p}_{i-2}$, the end of $\mathbf{q}_i$ is being pulled strongly towards $\mathbf{p}_{i-1}$, and the points interior to $\mathbf{q}_i$ are computed as a weighted average of the four control points $\mathbf{p}_{i-3}, \mathbf{p}_{i-2}, \mathbf{p}_{i-1}, \mathbf{p}_i$. Finally, the segments $\mathbf{q}_i(u)$ are degree three polynomial curves; thus, $\mathbf{q}(u)$ is piecewise a degree three polynomial curve. Furthermore, $\mathbf{q}(u)$ has continuous second derivatives everywhere it is defined.

These properties of the curve $\mathbf{q}(u)$ all depend on properties of the blending functions $N_i(u)$.[1] Figure IX.3 shows the graphs of the functions $N_i(u)$. At $u = 3$, we have $N_1(3) > N_0(3) = N_2(3) > 0$, and $N_i(3) = 0$ for all other values of i. In fact, we shall see that $N_1(3) = 2/3$ and $N_0(3) = N_2(3) = 1/6$. Therefore, $\mathbf{q}(3)$ is equal to the weighted average $(\mathbf{p}_0 + 4\mathbf{p}_1 + \mathbf{p}_2)/6$, which is consistent with what we earlier observed in Figure IX.2 about the beginning point of the curve $\mathbf{q}_3$. The other assertions we made about the curves $\mathbf{q}_3, \ldots, \mathbf{q}_6$ can likewise be seen to follow from the properties of the blending functions $N_i(u)$. Note that Equation (IX.2) is borne out by the behavior of the blending functions in Figure IX.3. Similarly, it is also clear that a control point $\mathbf{p}_i$ affects only the four segments $\mathbf{q}_i, \mathbf{q}_{i+1}, \mathbf{q}_{i+2}, \mathbf{q}_{i+3}$.

The blending functions should have the following properties:

[1] When we develop the theory of B-splines of arbitrary degree, these blending functions $N_i(u)$ will be denoted $N_{i,4}(u)$. Another mathematical derivation of these blending functions is given in the first example of Section IX.3.

(a) The blending functions are translates of each other, i.e.,

$$N_i(u) \ = \ N_0(u-i).$$

(b) The functions $N_i(u)$ are piecewise degree three polynomials. The breaks between the pieces occur only at integer values of u.

(c) The functions $N_i(u)$ have continuous second-derivatives, that is, they are C^2-continuous.

(d) The blending functions are a *partition of unity*, that is,

$$\sum_i N_i(u) \ = \ 1.$$

for $3 \le u \le 7$. (Or, for $3 \le u \le n+1$ when there are $n+1$ control points $\mathbf{p}_0, \ldots, \mathbf{p}_n$.) This property is necessary for points on the B-spline curve to be defined as weighted averages of the control points.

(e) $N_i(u) \ge 0$ for all u. Therefore, $N_i(u) \le 1$ for all u.

(f) $N_i(u) = 0$ for $u \le i$ and for $i+4 \le u$. This property of the blending functions gives the B-spline curves their local control properties.

Because of conditions (a) and (f), the blending functions will be fully specified once we specify the function $N_0(u)$ on the domain $[0,4]$. For this purpose, we will define four functions $R_0(u)$, $R_1(u)$, $R_2(u)$, $R_3(u)$ for $0 \le u \le 1$ by

$$\begin{aligned} R_0(u) &= N_0(u) & \qquad R_2(u) &= N_0(u+2) \\ R_1(u) &= N_0(u+1) & \qquad R_3(u) &= N_0(u+3). \end{aligned}$$

Thus, the functions $R_i(u)$ are the translates of the four segments of $N_0(u)$ to the interval $[0,1]$, and to finish the definition of $N_0(u)$ it suffices to define the four functions $R_i(u)$. These four functions are degree three polynomials by condition (b). In fact, we claim that the following choices for the R_i functions work (and this is the unique way to define these functions to satisfy the six conditions (a)-(f)):

$$\begin{aligned} R_0(u) &= \tfrac{1}{6}u^3 \\ R_1(u) &= \tfrac{1}{6}(-3u^3+3u^2+3u+1) \\ R_2(u) &= \tfrac{1}{6}(3u^3-6u^2+4) \\ R_3(u) &= \tfrac{1}{6}(1-u)^3. \end{aligned}$$

It takes a little work to verify that conditions (a)-(f) hold when $N_0(u)$ is defined from these choices for $R_0, \ldots, R_3$. Straightforward calculation shows that $\sum_i R_i(u) = 1$; thus, (d) holds. Also, it can be checked that $R_i(u) \ge 0$

for all $i = 0, 1, 2, 3$ and all $u \in [0, 1]$; hence (e) holds. For (c) to hold, $N_0(u)$ needs to have continuous second derivative. Of course, this also means $N_0(u)$ is continuous and has continuous first derivative. These facts are proved by noticing that when the R_i functions are pieced together, their values and their first and second derivatives match up. Namely,

$$\begin{array}{lll}
R_0(0)=0 & R_0'(0)=\ 0 & R_0''(0)=\ 0 \\
R_0(1)=\frac{1}{6}=R_1(0) & R_0'(1)=\ \frac{1}{2}\ =R_1'(0) & R_0''(1)=\ 1\ =R_1''(0) \\
R_1(1)=\frac{2}{3}=R_2(0) & R_1'(1)=\ 0\ =R_2'(0) & R_1''(1)=-2=R_2''(0) \\
R_2(1)=\frac{1}{6}=R_3(0) & R_2'(1)=\frac{-1}{2}=R_3'(0) & R_2''(1)=\ 1\ =R_3''(0) \\
R_3(1)=0 & R_3'(1)=\ 0 & R_3''(1)=\ 0
\end{array}$$

Exercise IX.1. Graph the four functions R_i on the interval $[0, 1]$. [Hint: These are portions of the blending functions shown in Figure IX.3.]

Exercise IX.2. Give formulas for the first and second derivatives of the R_i functions. Verify the 15 conditions needed for the C^2-continuity of the blending function $N_0(u)$.

Exercise IX.3. Verify that $\sum_i R_i(u) = 1$. Prove that $R_i(u) > 0$ for $i = 0, 1, 2, 3$ and for all $u \in (0, 1)$.

Exercise IX.4. Verify that $R_0(u) = R_3(1 - u)$ and that $R_1(u) = R_2(1 - u)$. Show that this means that uniform B-splines have left-right symmetry, in that if the order of the control points is reversed, then the curve $\mathbf{q}$ is unchanged except for being traversed in the opposite direction.

Exercise IX.5. Describe the effect of repeating control points in degree three uniform B-splines. Qualitatively describe the curve obtained if one control point is repeated, for instance, if $\mathbf{p}_3 = \mathbf{p}_4$.

Secondly, suppose $\mathbf{p}_2 \neq \mathbf{p}_3 = \mathbf{p}_4 = \mathbf{p}_5 \neq \mathbf{p}_6$. Show that the curve $\mathbf{q}$ interpolates the point $\mathbf{p}_3$ with $\mathbf{q}(6) = \mathbf{p}_3$. Further show that the segments $\mathbf{q}_5$ and $\mathbf{q}_6$ are straight lines.

IX.2 Nonuniform B-splines

The degree three uniform B-splines of the previous section were defined so that the curve $\mathbf{q}(u)$ was "pulled" by the control points in such way that $\mathbf{q}(i)$ is close to (or at least, strongly affected by) the control point $\mathbf{p}_{i-2}$. These splines are called "uniform" since the values u_i where the curve $\mathbf{q}(u)$ is most strongly affected by control points are evenly spaced at integer values $u_i = i$. These values u_i are called *knots*. A *nonuniform* spline is one where the knots u_i are not necessarily uniformly spaced. The ability to space knots nonuniformly makes it possible to define a wider range of curves, including curves with sharp bends or discontinuous derivatives. The uniform B-splines are just the special case of nonuniform B-splines where $u_i = i$.

NURBS "Cheat Sheet"

Degree k: The curve is piecewise degree k.

Order m: The order is $m = k + 1$.

Control points:
There are $n + 1$ control points, $\mathbf{p}_0, \mathbf{p}_1, \ldots, \mathbf{p}_{n-1}, \mathbf{p}_n$.

Knot positions:
There $\ell + 1$ knot positions, $u_0 \le u_1 \le \cdots \le u_{\ell-1} \le u_\ell$.
We have $\ell = n + k + 1 = n + m$.
So there are m more knots than control points.

Domain: The domain of $\mathbf{q}(u)$ is $[u_k, u_{n+1}]$.

Knots and control points:
The intuition is that $\mathbf{p}_i$ is "tied" to $\mathbf{q}(u)$ at $u = u_{i+m/2}$.

The curve $\mathbf{q}(u)$: The curve equals $\mathbf{q}(u) = \sum_{i=0}^{n} N_{i,m}(u)\mathbf{p}_i$.

Local control: The basis function $N_{i,m}$ has support $[u_i, u_{i+m})$.
Thus, for $u \in [u_j, u_{j+1}]$, $\mathbf{q}(u) = \sum_{i=j-k}^{j} N_{i,m}(u)\mathbf{p}_i$.

Multiplicity: The multiplicity of a knot is the number of times it appears in the knot vector.

Piecewise degree k: $\mathbf{q}(u)$ is a degree k polynomial for $u_i \le u < u_{i+1}$.

Continuity and multiplicity:
If u_i has multiplicity μ, then $q(u)$ is $C^{k-\mu}$-continuous at $u = u_i$.

Cox-de Boor formula:

$$N_{i,k+1}(u) \;=\; \frac{u - u_i}{u_{i+k} - u_i} N_{i,k}(u) + \frac{u_{i+k+1} - u}{u_{i+k+1} - u_{i+1}} N_{i+1,k}(u).$$

Properties: The basis functions form a partition of unity, with $\sum_i N_{i,m}(u) = 1$ for $u \in [u_3, u_{n+1}]$. Hence the convex hull property holds. In addition, the variation diminishing property holds.

Figure IX.4: The basic parameters and the usual conventions for nonuniform rational B-splines (NURBS)

We define a *knot vector* to be a sequence

$$[u_0, u_1, \ldots, u_{\ell-1}, u_\ell]$$

of real numbers $u_0 \le u_1 \le u_2 \le \cdots \le u_{\ell-1} \le u_\ell$ called *knots*. A knot vector is used with a sequence of $n+1$ control points $\mathbf{p}_0, \mathbf{p}_1, \ldots, \mathbf{p}_n$ to define a nonuniform B-spline curve. (When defining an order m B-spline curve, that is, a curve of degree $k = m-1$, we have $n = \ell - m$.) You should think of the spline curve as being a flexible and stretchable curve: the flexibility of the curve is limited and thus the curve resists being sharply bent. The curve is parameterized by the variable u and we can think of u as measuring the time spent traversing the length of the curve. The control points "pull" on parts of the curve; you should think of there being a stretchable string, or rubber band, attached to a point on the curve and tied also to the control point $\mathbf{p}_i$. These pull on the spline, and the spline settles down into a smooth curve.

Now, you might expect that the "rubber bands" tie the control point $\mathbf{p}_i$ to the point on the curve where $u = u_i$. This, however, is not correct. Instead, when defining a B-spline curve of order m, you should think of the control point $\mathbf{p}_i$ as being tied to the curve at the position $u = u_{i+m/2}$. If m is odd, we need to interpret the position $u_{i+m/2}$ as lying somewhere between the two knots $u_{i+(m-1)/2}$ and $u_{i+(m+1)/2}$. This corresponds to what we observed in the case of uniformly spaced knots defining a degree three curve, where $m = 4$: the curve $\mathbf{q}(u)$ is most strongly influenced by the control point $\mathbf{p}_i$ at the position with $u = u_{i+2}$.

It is possible for knots to be repeated multiple times. If a knot position has multiplicity two, i.e., if it occurs twice with $u_{i-1} < u_i = u_{i+1} < u_{i+2}$, then the curve will be affected more strongly by the corresponding control point. The curve will also lose some continuity properties for its derivatives. For instance, if $\mathbf{q}(u)$ is a degree three curve with a knot $u_i = u_{i+1}$ of multiplicity two, then $\mathbf{q}(u)$ will generally no longer have continuous second derivatives at u_i, although it will still have continuous first derivative at u_i. Further, if $\mathbf{q}(u)$ has a knot of multiplicity three, with $u_{i-1} < u_i = u_{i+1} = u_{i+2} < u_{i+3}$, then $\mathbf{q}(u)$ will interpolate the point $\mathbf{p}_{i-1}$ and will generally have a "corner" at $\mathbf{p}_{i-1}$ and thus not be C^1- or G^1-continuous at that point. However, unlike the situation in Exercise IX.5, the adjacent portions of the B-spline curve will not be straight-line segments. These behaviors are exhibited in Figures IX.5 and IX.6.

If a knot position occurs four times (in a degree three curve), then the curve can actually become discontinuous! Knots which repeat four times are usually used only at the beginning or end of the knot vector and thus do not cause a discontinuity in the curve.

Next, we give the Cox-de Boor mathematical definition of nonuniform B-spline blending functions. So far, all of our examples have been degree three splines, but it is now convenient to generalize to splines of degree $k = m-1$, which are also called *order m* splines. Assume the knot vector $u_0 \le u_1 \le \cdots \le u_\ell$ has been fixed. The blending functions $N_{i,m}(u)$ for order m

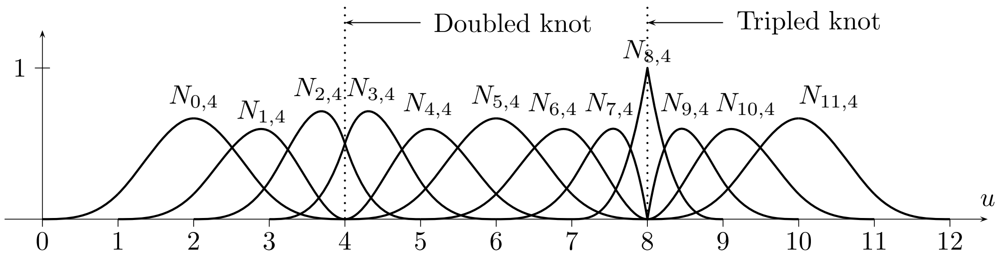

Figure IX.5: Example of order four (degree three) blending functions with repeated knots. The knot vector is $[0, 1, 2, 3, 4, 4, 5, 6, 7, 8, 8, 8, 9, 10, 11, 12]$ so that the knot 4 has multiplicity two and the knot 8 has multiplicity three.

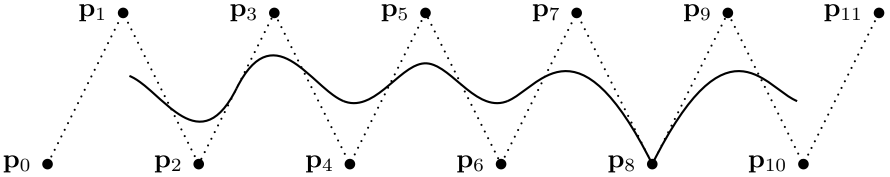

Figure IX.6: Example of an order four B-spline created with repeated knots. This curve is created with the knot vector and blending functions shown in Figure IX.5. It has domain $[3, 9]$.

splines depend only on the knot positions, not on the control points, and are defined by induction on $m \geq 1$ as follows. First, for $i = 0, \ldots, \ell - 1$, let

$$N_{i,1}(u) \; = \; \begin{cases} 1 & \text{if } u_i \leq u < u_{i+1} \\ 0 & \text{otherwise.} \end{cases}$$

There is one minor exception to the above definition, which is to include the very last point $u = u_\ell$ in the domain of the last nonzero function: namely, if $u_{i-1} < u_i = u_\ell$, then we let $N_{i-1,1}(u) = 1$ when $u_{i-1} \leq u \leq u_i$. In this way, the theorems stated below hold also for $u = u_\ell$. Second, for $m \geq 1$, letting $m = k + 1$, $N_{i,k+1}(u)$ is defined by the Cox-de Boor formula:

$$N_{i,k+1}(u) \; = \; \frac{u - u_i}{u_{i+k} - u_i} N_{i,k}(u) + \frac{u_{i+k+1} - u}{u_{i+k+1} - u_{i+1}} N_{i+1,k}(u)$$

The Cox-de Boor formula

When there are repeated knots, some of the denominators above may be zero: we adopt the convention that $0/0 = 0$ and $(a/0)0 = 0$. Since $N_{i,k}(u)$ will be identically zero when $u_{i+k} = u_i$ (see the next paragraph), this means that any term with denominator equal to zero may be ignored.

The form of the Cox-de Boor recursive formulas for the blending functions immediately implies that the functions $N_{i,m}(u)$ are piecewise degree $m-1$ polynomials and that the breaks between pieces occur at the knots u_i. Secondly, it is easy to prove, by induction on $m \geq 1$, that the function $N_{i,m}(u)$ has support in $[u_i, u_{i+m}]$. (I.e., $N_{i,m}(u) = 0$ for $u < u_i$ and for $u_{i+m} < u$.) From similar considerations, it is easy to see that the definition of the blending function $N_{i,m}(u)$ depends only on the knots $u_i, u_{i+1}, \ldots, u_{i+m}$.

The degree k B-spline curve $\mathbf{q}(u)$ is defined from the blending functions and control points by

$$\mathbf{q}(u) \;=\; \sum_{i=0}^{n} N_{i,k+1}(u)\cdot \mathbf{p}_i \qquad u_k \leq u \leq u_{n+1}. \tag{IX.3}$$

Note that the domain of $\mathbf{q}(u)$ is $[u_k, u_{n+1}]$. Since each $N_{i,k+1}$ has support in $[u_i, u_{i+k+1}]$, the curve can also be defined as

$$\mathbf{q}(u) \;=\; \sum_{i=j-k}^{j} N_{i,k+1}(u)\cdot \mathbf{p}_i \qquad \text{provided } u \in (u_j, u_{j+1}),\; k \leq j \leq n, \tag{IX.4}$$

by omitting terms which equal zero. Equation (IX.4) also holds for $u \in [u_j, u_{j+1}]$ provided $u_u < u_{j+1}$: for instance, when there are no repeated knots. It holds in addition for $j = n$ and $u = u_{n+1}$.

IX.3 Examples of nonuniform B-splines

To gain a qualitative understanding of how nonuniform B-splines work, it is helpful to do some simple examples.

Example: uniformly spaced knots

We start with what is perhaps the simplest example, namely the case where the knots are uniformly spaced, with the knot vector equal to just $[0, 1, 2, 3, \ldots, \ell]$. That is, the knots are $u_i = i$. Of course, we expect this case to give the same degree three results as the uniform B-splines discussed in Section IX.1, with the functions $N_{i,4}(u)$ equal to the functions $N_i(u)$ of that section.

In order to define the blending functions, $N_{i,m}(u)$, we start with the order $m = 1$ case, that is, the degree $k = 0$ case. For this we have merely the step functions, for $i = 0, \ldots, \ell - 1$,

$$N_{i,1}(u) \;=\; \begin{cases} 1 & \text{if } i \leq u < i+1 \\ 0 & \text{otherwise.} \end{cases}$$

These functions are piecewise degree zero (i.e., piecewise constant); of course, they are discontinuous at the knot positions $u_i = i$.

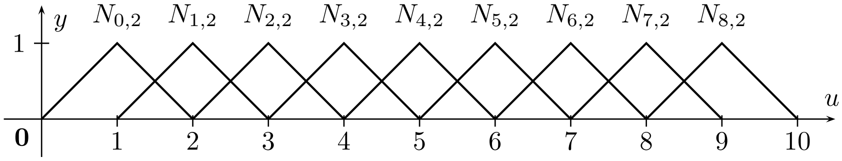

Figure IX.7: The order two (piecewise degree one) blending functions with uniformly spaced knots, $u_i = i$. Here $\ell = 10$, and there are $\ell + 1$ knots and $\ell - 1$ blending functions. The associated B-spline curve of Equation (IX.5) is defined for $1 \le u \le \ell - 1$.

Next, we compute the order two (piecewise degree one) blending functions $N_{i,2}(u)$. Using the fact that $u_i = i$, these are defined from the Cox-de Boor formula as

$$N_{i,2}(u) \;=\; \frac{u-i}{1} N_{i,1}(u) + \frac{i+2-u}{1} N_{i+1,1}(u),$$

for $i = 0, \ldots, \ell - 2$. Specializing to the case $i = 0$, we have

$$N_{0,2}(u) \;=\; uN_{0,1}(u) + (2-u)N_{1,1}(u),$$

and from the definitions of $N_{0,1}(u)$ and $N_{1,1}(u)$, this means that

$$N_{0,2}(u) \;=\; \begin{cases} u & \text{if } 0 \le u < 1 \\ 2-u & \text{if } 1 \le u < 2 \\ 0 & \text{otherwise.} \end{cases}$$

Because the knots are uniformly spaced, similar calculations apply to the rest of the order two blending functions $N_{i,2}(u)$, and these are all just translates of $N_{0,2}(u)$, with $N_{i,2}(u) = N_{0,2}(u - i)$. The order two blending functions are graphed in Figure IX.7.

Note that the order two blending functions are continuous (C^0-continuous) and piecewise linear. Since clearly $N_{i,2}(u) \ge 0$ and $\sum_i N_{i,2}(u) = 1$ for all $u \in [1, \ell - 1]$, we can define a 'curve' $\mathbf{q}(u)$ as

$$\mathbf{q}(u) \;=\; \sum_{i=0}^{\ell-2} N_{i,2}(u)\mathbf{p}_i, \qquad 1 \le u \le \ell - 1, \tag{IX.5}$$

with control points $\mathbf{p}_0, \ldots, \mathbf{p}_{\ell-2}$. By inspection, this 'curve' consists of straight-line segments connecting the control points $\mathbf{p}_0, \ldots, \mathbf{p}_{\ell-2}$ in a 'connect-the-dots' fashion, with $\mathbf{q}(u_{i+1}) = \mathbf{p}_i$ for $i = 0, \ldots, \ell - 2$.

Next, we compute the order three (piecewise degree two) blending functions, $N_{i,3}(u)$. From the Cox-de Boor formula with $m = 3$ or $k = 2$,

$$N_{i,3}(u) \;=\; \frac{u-i}{2} N_{i,2}(u) + \frac{i+3-u}{2} N_{i+1,2}(u).$$

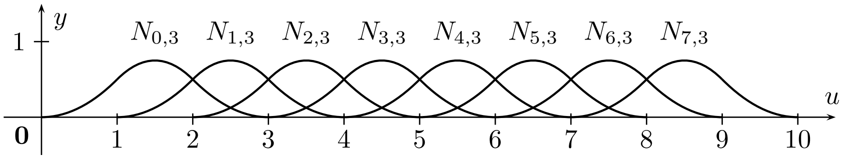

Figure IX.8: The order three (piecewise degree two) blending functions with uniform knot positions $u_i = i$. We still have $\ell = 10$; there are $\ell + 1$ knots and $\ell - 2$ blending functions. The associated B-spline curve of Equation (IX.6) is defined for $2 \le u \le \ell - 2$.

These are defined for $i = 0, \ldots, \ell - 3$. As before, we specialize to the case $i = 0$, and have

$$N_{0,3}(u) \;=\; \tfrac{1}{2}uN_{0,2}(u) + \tfrac{1}{2}(3-u)N_{1,2}(u).$$

Considering separately the cases $0 \le u < 1$ and $1 \le u < 2$ and $2 \le u < 3$, we have,

$$N_{0,3}(u) \;=\; \begin{cases} \frac{1}{2}u^2 & \text{if } 0 \le u < 1 \\ \frac{1}{2}u(2-u) + \frac{1}{2}(3-u)(u-1) = \frac{1}{2}(6u - 2u^2 - 3) & \text{if } 1 \le u < 2 \\ \frac{1}{2}(3-u)^2 & \text{if } 2 \le u < 3 \\ 0 & \text{otherwise.} \end{cases}$$

It is straightforward to check that $N_{0,3}(u)$ has continuous first-derivative. In addition, direct calculation shows that $N_{0,3}(u) \ge 0$ for all u. Because the knots are uniformly spaced, the rest of the order three blending functions, $N_{i,3}(u)$, are just translates of $N_{0,3}(u)$, with $N_{i,3}(u) = N_{0,3}(u-i)$: these functions are shown in Figure IX.8. It is also straightforward to check that $\sum_{i=0}^{\ell-3} N_{i,3}(u) = 1$ for $2 \le u \le \ell - 2$. Also note that the function $N_{i,3}(u)$ is maximized at $u = i + 3/2$, where it takes on the value $3/4$. A degree two B-spline curve can be defined with these blending functions as

$$\mathbf{q}(u) \;=\; \sum_{i=0}^{\ell-3} N_{i,3}(u)\mathbf{p}_i, \qquad 2 \le u \le \ell - 2. \tag{IX.6}$$

By using the Cox-de Boor formula again, we could define the order four (piecewise degree three) blending functions $N_{i,4}(u)$. We shall not carry out this computation; however, the results obtained would be identical to the blending functions $N_i(u)$ used in Section IX.1 and shown in Figure IX.3. We leave it as an exercise for the reader to verify this fact.

Example: Bézier curve as B-spline

For our second example, we let the knot vector be $[0, 0, 0, 0, 1, 1, 1, 1]$ and compute the order 1, 2, 3, and 4 blending functions for this knot vector. Here we have $u_i = 0$ for $i = 0,1,2,3$ and $u_i = 1$ for $i = 4,5,6,7$. The order one blending functions are just

$$N_{3,1}(u) \quad = \quad \begin{cases} 1 & \text{if } 0 \le u \le 1 \\ 0 & \text{otherwise} \end{cases}$$

and $N_{i,1}(u) = 0$ for $i \ne 3$.

The order two blending functions $N_{i,2}(u)$ are zero except for $i = 2,3$. Also, for every order $m \ge 1$, every blending function will be zero for $u < 0$ and $u > 1$. Both these facts use the conventions for the Cox-de Boor equations that $0/0 = 0$ and $(a/0) \cdot 0$. (The reader should verify all our assertions!) For $i = 2,3$ and $0 \le u \le 1$, the Cox-de Boor equations with $k = 1$ give

$$\begin{aligned} N_{2,2}(u) &= \frac{u-u_2}{u_3-u_2} \cdot N_{2,1}(u) + \frac{u_4-u}{u_4-u_3} \cdot N_{3,1}(u) \\ &= \frac{u-0}{0-0} \cdot 0 + \frac{1-u}{1-0} \cdot 1 \ = \ 1-u \\ N_{3,2}(u) &= \frac{u-u_3}{u_4-u_3} \cdot N_{3,1}(u) + \frac{u_5-u}{u_5-u_4} \cdot N_{4,1}(u) \\ &= \frac{u-0}{1-0} \cdot 1 + \frac{1-u}{1-1} \cdot 0 \ = \ u. \end{aligned}$$

The order three blending functions are zero except for $i = 1,2,3$, and $N_{1,3}(u)$, $N_{2,3}(u)$, and $N_{3,3}(u)$ are zero outside the domain $[0,1]$. Calculations from the Cox-de Boor equations, similar to the above, give, for $0 \le u \le 1$,

$$\begin{aligned} N_{1,3}(u) &= (1-u)^2 \\ N_{2,3}(u) &= 2u(1-u) \\ N_{3,3}(u) &= u^2. \end{aligned} \tag{IX.7}$$

Note that these three blending functions are equal to the Bernstein polynomials of degree two; namely, $B_i^2(u) = N_{i+1,4}(u)$. (The shift in the subscript from i to $i{+}1$ is caused by the fact that the first knot has multiplicity four instead of multiplicity three.)

The order four (piecewise degree three) blending functions $N_{i,4}(u)$ are nonzero for $i = 0,1,2,3$ and have support contained in $[0,1]$. Further calculations from the Cox-de Boor equations give

$$\begin{aligned} N_{0,4}(u) &= (1-u)^3 \\ N_{1,4}(u) &= 3u(1-u)^2 \\ N_{2,4}(u) &= 3u^2(1-u) \\ N_{3,4}(u) &= u^3, \end{aligned} \tag{IX.8}$$

for $0 \le u \le 1$. Surprisingly, these four blending functions are equal to the Bernstein polynomials of degree three; namely, $B_i^3(u) = N_{i,4}(u)$. Therefore, the B-spline curve defined with the four control points $\mathbf{p}_0, \mathbf{p}_1, \mathbf{p}_2, \mathbf{p}_3$ and knot vector $[0,0,0,0,1,1,1,1]$ is exactly the same as the degree three Bézier curve with the same control points.

Some generalizations of this example are given later in the first half of Section IX.9, where it is shown how to represent multiple Bézier curves as a single B-spline curve: see Theorem IX.17 on page 362.

Example: Nonuniformly spaced and repeated knots

Consider the nonuniform knot vector

$$[0,0,0,0,1,2,2\tfrac{4}{5},3\tfrac{1}{5},4,5,6,7,7,8,9,10,10,10,10].$$

This was obtained by starting with knots at integer values 0 through 10, quadrupling the first and last knots, doubling the knots at $u=3$ and $u=7$, and then separating the knots at 3 slightly to be at $2\frac{4}{5}$ and $3\frac{1}{5}$. As usual, for $i=0,\ldots,18$, u_i denotes the i-th knot, as shown:

i:	0	1	2	3	4	5	6	7	8	9	10	11	12	13	14	15	16	17	18
u_i:	0	0	0	0	1	2	$2\frac{4}{5}$	$3\frac{1}{5}$	4	5	6	7	7	8	9	10	10	10	10

The degree zero blending functions $N_{i,1}(u)$ are defined for $0 \le i \le 17$. These are the step functions defined to have value 1 on the half-open interval $[u_i, u_{i+1})$ and value 0 elsewhere. For values i such that $u_i = u_{i+1}$, this means that $N_{i,1}(u)$ is equal to zero for all u. This happens for i equal to $0,1,2,11,15,16,17$.

The degree one blending functions are $N_{i,2}(u)$, for $0 \le i \le 16$, and are shown in Figure IX.9. When u_i, u_{i+1}, and u_{i+2} are distinct, then the graph of the function $N_{i,2}(u)$ rises linearly from zero at u_i to one at u_{i+1}, and then decreases linearly back to zero at u_{i+2}. It is zero outside the interval (u_i, u_{i+2}). On the other hand, when $u_i = u_{i+1} \ne u_{i+2}$, then $N_{i,2}$ is discontinuous at u_i: it jumps from the value zero for $u < u_i$ to the value one at u_i. It then decreases linearly back to zero at u_{i+2}. The situation is dual when $u_i \ne u_{i+1} = u_{i+2}$. In the figure, $N_{10,2}$ and $N_{11,2}$ are both discontinuous at $u=7$. If $u_i = u_{i+2}$, as happens for $i = 0,1,15,16$, then $N_{i,2}(u)$ is equal to the constant zero everywhere.

The degree two blending functions are $N_{i,3}(u)$, for $0 \le i \le 15$, and are shown in part (b) of Figure IX.9. The functions $N_{i,3}(u)$ have support in the interval $[u_i, u_{i+3}]$. More than this is true: if $u_i \ne u_{i+1}$, then $N_{i,3}(u_i) = 0$, and similarly, if $u_{i+2} \ne u_{i+3}$, then $N_{i,3}(u_{i+3}) = 0$. Even further, if $u_i = u_{i+1} \ne u_{i+2}$, then $N_{i,3}(u_i) = 0$: this happens when $i = 2,11$. However, in this case, $N_{i,3}(u)$ has discontinuous first derivative at u_i. The symmetric case of $u_{i+1} \ne u_{i+2} = u_{i+3}$ can be seen with $i=9$ and $i=13$.

When there is a knot of multiplicity ≥ 3 and $u_i = u_{i+2} \ne u_{i+3}$, then we have $N_{i,3}(u_i) = 1$: in our example, this happens for $i=1$. Dually, when $u_i \ne u_{i+1} = u_{i+3}$, as happens with $u = 14$, then $N_{i,3}(u_{i+2}) = 1$. For $i = 0,15$, $N_{i,3}(u)$ is just the constant zero everywhere. At the doubled knot

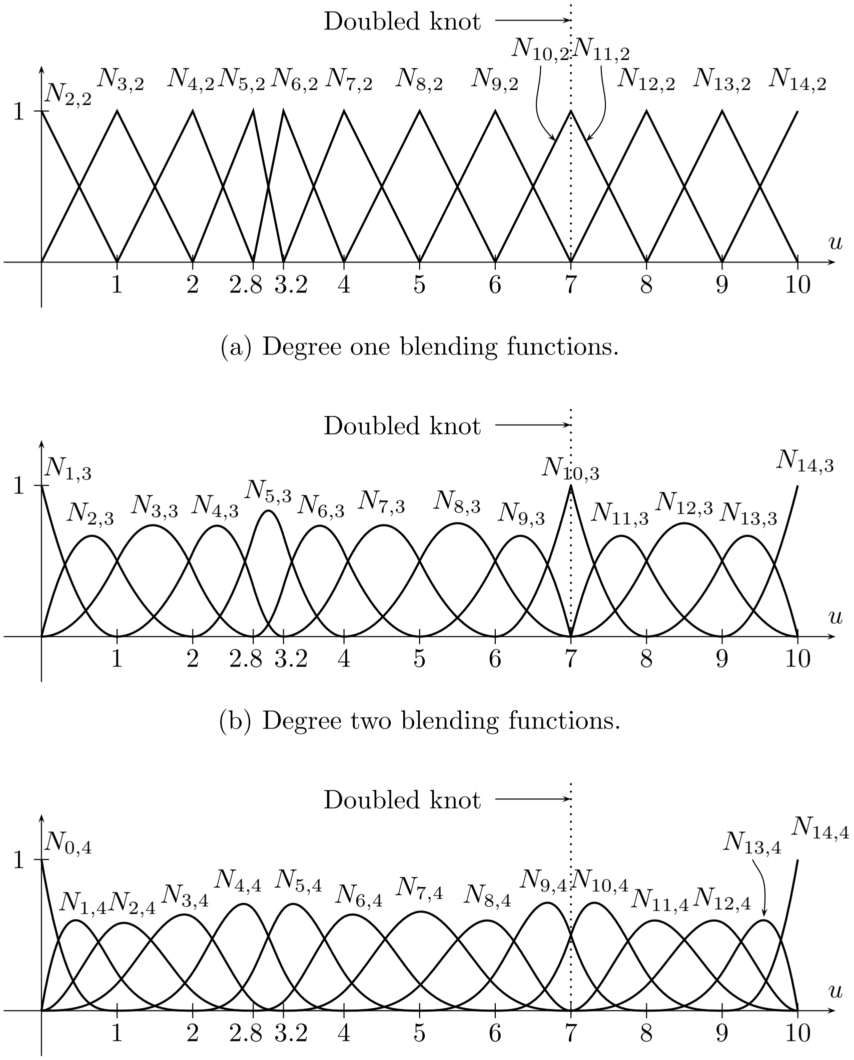

(a) Degree one blending functions.

(b) Degree two blending functions.

(c) Degree three blending functions.

Figure IX.9: Degree one, two, and three blending functions for a nonuniform knot sequence. The knot 7 has multiplicity two, and the knots 0 and 10 have multiplicity 4.

$u_{11} = u_{12} = 7$, the blending function $N_{10,3}(u)$ is continuous and equal to 1, but has discontinuous first derivative. A degree two B-spline curve formed with this knot vector will interpolate $\mathbf{p}_{10}$ at $u = 7$, but will, in general, have a corner there.

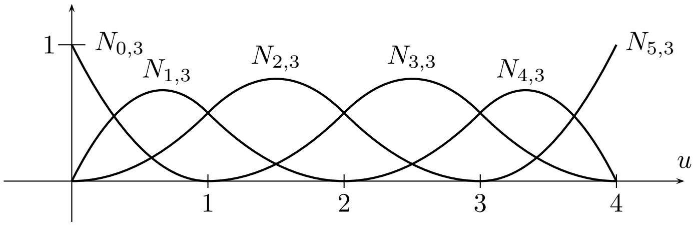

Figure IX.10: The degree two blending functions, $N_{i,3}(u)$, for the knot vector of Exercise IX.6.

The degree three blending functions, $N_{i,4}(u)$, are shown in part (c) of the figure. They are defined for $0 \le i \le 14$, and have support in the interval $[u_i, u_{i+4}]$. Where a knot has multiplicity ≥ 4, say if $u_i = u_{i+3} \ne u_{i+4}$, then the right limit $\lim_{u \to u_i^+} N_{i,4}(u)$ is equal to one. Likewise, if $u_i \ne u_{i+1} = u_{i+4}$, then the left limit $\lim_{u \to u_{i+1}^-} N_{i,4}(u)$ equals one. In this example, these situations happen only at the endpoints of the curve.

The degree three blending functions are C^2-continuous everywhere, *except* at the doubled knot position $u = 7$, where $N_{8,4}(u)$, $N_{9,4}(u)$, $N_{10,4}(u)$, and $N_{11,4}(u)$ are only C^1-continuous.

The next two exercises ask you to work out some details of the standard knot vectors for degree two and degree three. For general degree k, the standard knot vectors have the form

$$[0, 0, \ldots, 0, 1, 2, 3, \ldots, s-2, s-1, s, s, \ldots, s],$$

where the knots 0 and s have multiplicity $k+1$ and the rest of the knots have multiplicity 1. For these knot vectors the B-spline curve will interpolate the first and last control points: the exercises ask you to verify this for some particular examples. In Section IX.12, we will work again with the standard knot vector for degree three B-spline curves to interpolate a set of control points.

Exercise IX.6. Derive the formulas for the quadratic (order three, degree two) B-spline blending functions for the knot vector $[0, 0, 0, 1, 2, 3, 4, 4, 4]$. How many control points are needed for a quadratic B-spline curve with this knot vector? What is the domain of the B-spline curve? Show that the curve begins at the first control point and ends at the last control point. Check your formulas for the blending functions against Figure IX.10.

Exercise IX.7. Repeat the previous exercise, but with cubic B-spline curves with the knot vector $[0, 0, 0, 0, 1, 2, 3, 4, 5, 6, 6, 6, 6]$. The graph of the blending functions for this curve is shown in Figure IX.11. (If you actually do this exercise, you might wish to use a computer algebra program to derive the formulas to avoid excessive hand calculation.)

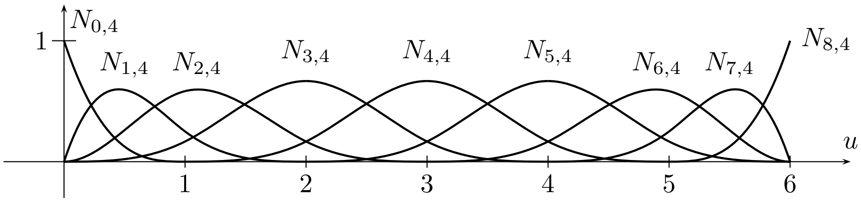

Figure IX.11: The degree three blending functions, $N_{i,4}(u)$, for the knot vector $[0,0,0,0,1,2,3,4,5,6,6,6,6]$ of Exercise IX.7.

IX.4 Properties of nonuniform B-splines

We now introduce some of the basic properties of the B-spline blending functions. Theorem IX.1 below describes the domain of definition of B-spline blending functions and shows they can be used to form weighted averages. Theorem IX.2 explains the continuity properties of derivatives of B-splines.

Throughout this section, we use m to denote the order of the blending functions, i.e., m is one plus the degree k of the blending functions.

Theorem IX.1. *Let $u_0 \le u_1 \le \cdots \le u_\ell$ be a knot vector. Then the blending functions $N_{i,m}(u)$, for $0 \le i \le \ell - m$, satisfy the following properties.*

(a) *$N_{i,m}$ has support in $[u_i, u_{i+m}]$ for all $m \ge 1$.*

(b) *$N_{i,m}(u) \ge 0$ for all u.*

(c) *$\sum_{i=0}^{\ell-m} N_{i,m}(u) = 1$, for all u such that $u_{m-1} \le u \le u_{\ell-m+1}$.*

It can get very confusing keeping track of all the precise values for subscripts, etc. Referring to Figures IX.3, IX.7, and IX.8 can help with this.

Proof. As discussed earlier, conditions (a) and (b) are readily proved by induction on m. Condition (c) is also proved by induction on m, by the following argument. The base case, with $m = 1$ is obviously true. For the induction step, we assume condition (c) holds, and then prove it with $m+1$ in place of m. Assume $u_m \le u \le u_{\ell-m}$:

$$\begin{aligned}
&\sum_{i=0}^{\ell-m-1} N_{i,m+1}(u) \\
&\quad= \sum_{i=0}^{\ell-m-1}\left(\frac{u-u_i}{u_{i+m}-u_i}N_{i,m}(u) + \frac{u_{i+m+1}-u}{u_{i+m+1}-u_{i+1}}N_{i+1,m}(u)\right) \\
&\quad= \frac{u-u_0}{u_m-u_0}N_{0,m}(u) \ + \ \sum_{i=1}^{\ell-m-1}\frac{(u-u_i)+(u_{i+m}-u)}{u_{i+m}-u_i}N_{i,m}(u) \\
&\qquad\qquad + \ \frac{u_\ell - u}{u_\ell - u_{\ell-m}}N_{\ell-m,m}(u) \\
&\quad= N_{0,m}(u) \ + \ \sum_{i=1}^{\ell-m-1} 1\cdot N_{i,m}(u) \ + \ N_{\ell-m,m}(u) \\
&\quad= \sum_{i=0}^{\ell-m} N_{i,m}(u) \ = \ 1.
\end{aligned}$$

The final equality follows from the induction hypothesis. The derivation of the next to last line needed the fact that $\frac{u-u_0}{u_m-u_0}N_{0,m}(u) = N_{0,m}(u)$. This holds since $u_m \le u$; in particular, if $u_m < u$ then $N_{0,m}(u) = 0$ by (a), and if $u_m = u$ then $\frac{u-u_0}{u_m-u_0} = 1$. Similarly, the fact that $\frac{u_\ell-u}{u_\ell-u_{\ell-m}}N_{\ell-m,m}(u) = N_{\ell-m,m}(u)$ is justified by the fact that $u \le u_{\ell-m}$. □

The importance of conditions (b) and (c) is that they allow the blending functions to be used as coefficients of control points to give a weighted average of control points. To define an order m (degree $m-1$) B-spline curve, one needs $n+m+1$ knot positions $u_0,\ldots,u_{n+m}$ and $n+1$ control points $\mathbf{p}_0,\ldots,\mathbf{p}_n$. Then $\ell = n+m$ and the B-spline curve equals

$$\mathbf{q}(u) \ = \ \sum_{i=0}^{n} N_{i,m}(u)\mathbf{p}_i$$

for $u_{m-1} \le u \le u_{\ell-m+1} = u_{n+1}$.

The bounded interval of support given in condition (a) means that

$$\mathbf{q}(u) \ = \ \sum_{i=j-m+1}^{j} N_{i,m}(u)\mathbf{p}_i$$

provided $u_j \le u < u_{j+1}$. Thus, the control points provide local control over the B-spline curve, since changing one control point only affects m segments of the B-spline curve.

The next theorem describes the smoothness properties of a B-spline curve. Since a B-spline consists of pieces which are degree $m-1$ polynomials, it is certainly C^∞-continuous at all values of u which are not knot positions. If there are no repeated knots and if $m > 1$ then, as we shall prove, the curve is in fact continuous everywhere in its domain and, even more, the curve is C^{m-2}-continuous everywhere in its domain. For instance, a degree three B-spline with no repeated knots has its second derivatives defined and continuous everywhere in its domain, including at the knot positions.

The case of repeated knots is more complicated. We say that a knot has *multiplicity* μ if it occurs μ times in the knot vector. Since the knots are linearly ordered, these μ occurrences must be consecutive values in the knot vector, i.e., we have

$$u_{i-1} < u_i = u_{i+1} = \cdots = u_{i+\mu-1} < u_{i+\mu}.$$

In this case, the curve will have its $(m-\mu-1)$-th derivative defined and continuous at $u = u_i$. For instance, a degree three B-spline will have continuous first derivative at a twice repeated knot position, but in general will be only continuous at a knot position of multiplicity three. In the latter case, the curve will generally have a "corner" or "bend" at that knot position. A B-spline curve of degree three can be discontinuous at a knot position of multiplicity four.

The ability to repeat knots and make the curve have fewer continuous derivatives is important for the usefulness of B-splines since it allows a single curve to include both smooth portions and sharply bending portions.

We combine the above assertions about the smoothness of B-splines into the next theorem.

Theorem IX.2. *Let* $\mathbf{q}(u)$ *be a B-spline curve of order* m*, and let the knot* u_i *have multiplicity* μ*. Then the curve* $\mathbf{q}(u)$ *has continuous* $(m-\mu-1)$*-th derivative at* $u = u_i$*.*

It is fairly difficult to give a direct proof of this theorem, so its proof is postponed until the end of Section IX.7, where we present a proof based on the use of the blossoms introduced in Section IX.6.

The last property of B-splines discussed in this section concerns the behavior of blending functions near repeated knots. In general, if a degree k B-spline curve has a knot of multiplicity $\geq k$, then there is a blending function $N_{i,k+1}(u)$ that goes to 1 at the knot. Examples of this are the blending functions shown in Figures IX.9-IX.11, where the first and last knots are repeated many times and the first and last blending functions reach the value one at the first and last knots, respectively. It can also happen that interior knot positions have multiplicity k as well, and at such knots the appropriate blending function(s) will reach the value one; see Figures IX.5 and IX.9(b) for examples of this.

The next theorem formalizes these facts. In addition to helping us understand the behavior of B-spline curves at their endpoints, the theorem will be useful in the next two sections for the development of the de Boor algorithm and for the proof of Theorem IX.2 about the continuity properties of B-splines.

Theorem IX.3. *Let $k \ge 1$.*

(a) *Suppose that $u_i = u_{i+k-1} < u_{i+k}$, so u_i has multiplicity at least k. Then*

$$\lim_{u \to u_i^+} N_{i-1,k+1}(u) \;=\; 1 \tag{IX.9}$$

and, for $j \neq i-1$,

$$\lim_{u \to u_i^+} N_{j,k+1}(u) \;=\; 0.$$

(b) *Dually, suppose $u_{i-1} < u_i = u_{i+k-1}$, so u_i has multiplicity at least k. Then*

$$\lim_{u \to u_i^-} N_{i-1,k+1}(u) \;=\; 1 \tag{IX.10}$$

and, for $j \neq i-1$,

$$\lim_{u \to u_i^-} N_{j,k+1}(u) \;=\; 0.$$

Proof. In order to prove both (a) and (b), it will suffice to prove that Equations (IX.9) and (IX.10) hold, since the fact that the other limits equal zero will then follow from the partition of unity property of Theorem IX.1(c).

We prove (IX.9) by induction on k. The base case is $k = 1$. (Refer to Figures IX.7 and IX.9(a).) Using the definitions of the $N_{j,1}(u)$ blending functions as step functions, the fact that $u_{i+1} - u_i \neq 0$, and the Cox-de Boor formula, we have

$$\begin{aligned}
\lim_{u \to u_i^+} N_{i-1,2}(u) &= \lim_{u \to u_i^+} \Big(\frac{u - u_{i-1}}{u_i - u_{i-1}} N_{i-1,1}(u) + \frac{u_{i+1} - u}{u_{i+1} - u_i} N_{i,1}(u) \Big) \\
&= 0 + 1 \cdot 1 \;=\; 1.
\end{aligned}$$

The induction step applies to $k \ge 2$. In this case, we have

$$\begin{aligned}
&\lim_{u \to u_i^+} N_{i-1,k+1}(u) \\
&\quad= \lim_{u \to u_i^+} \Big(\frac{u - u_{i-1}}{u_{i+k-1} - u_{i-1}} N_{i-1,k}(u) + \frac{u_{i+k} - u}{u_{i+k} - u_i} N_{i,k}(u) \Big) \\
&\quad= 1 \cdot 1 + 1 \cdot 0 \;=\; 1.
\end{aligned}$$

Here we have used the induction hypothesis and the fact that $u_i = u_{i+k-1}$.

The proof of (IX.10) is completely dual, and we omit it. □

Corollary IX.4. *Let $\mathbf{q}(u)$ be a degree k B-spline. Suppose that the knot u_i has multiplicity k with $u_{i-1} < u_i = u_{i+k-1} < u_{i+k}$. Then $\mathbf{q}(u)$ is continuous at $u = u_i$ and $\mathbf{q}(u_i) = p_{i-1}$.*

Proof. Theorem IX.3 implies that $\lim_{u=u_i} N_{i-1,k+1}(u) = 1$ and that $\lim_{u=u_i} N_{j,k+1}(u) = 0$ for all $j \neq i{-}1$. The corollary follows immediately from Equation (IX.3). □

Exercise IX.8. Use Theorem IX.3 to prove that B-splines defined with the standard knot vector interpolate their first and last control points. [Hint: Use $i = 0$ and $i = s + k - 1$.]

IX.5 The de Boor algorithm

The de Boor algorithm is a method for evaluating a B-spline curve $\mathbf{q}(u)$ at a single value of u. The de Boor algorithm is similar in spirit to the de Casteljau method for Bézier curves, in that it works by repeatedly linearly interpolating between pairs of points. This makes the de Boor algorithm stable and robust, and it is less prone to round-off errors than methods which work by calculating values of the blending functions $N_{i,m}(u)$. The de Boor algorithm is also an important construction for understanding the mathematical properties of B-spline curves, and it will be used to establish the "blossoming" method for B-splines in the next section.

Suppose that $\mathbf{q}(u)$ is a B-spline curve of degree $k \geq 1$, and is defined by the control points $\mathbf{p}_0, \mathbf{p}_1, \ldots, \mathbf{p}_n$ and the knot vector $[u_0, \ldots, u_{n+m}]$, where $m = k+1$ is the order of $\mathbf{q}(u)$. Therefore, the domain of definition of the curve is $[u_k, u_{n+1}]$. As usual, $\mathbf{q}(u)$ is defined by

$$\mathbf{q}(u) \;=\; \sum_{i=0}^{n} N_{i,k+1}(u)\mathbf{p}_i. \qquad \text{(IX.11)}$$

The next theorem provides the main tool needed to derive the de Boor algorithm.

Theorem IX.5. *Suppose $\mathbf{q}(u)$ is the curve given by Equation (IX.11). For all $u \in [u_k, u_{n+1}]$ (or, for all $u \in [u_k, u_{n+1})$ if $k = 1$),*

$$\mathbf{q}(u) \;=\; \sum_{i=1}^{n} N_{i,k}(u)\mathbf{p}_i^{(1)}(u), \qquad \text{(IX.12)}$$

where

$$\begin{aligned} \mathbf{p}_i^{(1)}(u) \;&=\; \frac{u_{i+k} - u}{u_{i+k} - u_i}\mathbf{p}_{i-1} + \frac{u - u_i}{u_{i+k} - u_i}\mathbf{p}_i \qquad \text{(IX.13)} \\ &=\; \mathit{lerp}\big(\mathbf{p}_{i-1},\, \mathbf{p}_i,\, \frac{u - u_i}{u_{i+k} - u_i}\big). \end{aligned}$$

If any knot has multiplicity $> k$, then we can have $u_i = u_{i+k}$ and the value $\mathbf{p}_i^{(1)}(u)$ is undefined. With our conventions on division by zero, the theorem still makes sense in this case, since then the function $N_{i,k}(u)$ is the constant zero function.

Proof of Theorem IX.5. Expanding Equation (IX.11) using the Cox-de Boor formula gives:

$$\begin{aligned}
\mathbf{q}(u) &= \sum_{i=0}^{n} N_{i,k+1}(u)\mathbf{p}_i \\
&= \sum_{i=0}^{n} \left(\frac{u-u_i}{u_{i+k}-u_i} N_{i,k}(u) + \frac{u_{i+k+1}-u}{u_{i+k+1}-u_{i+1}} N_{i+1,k}(u) \right) \mathbf{p}_i \\
&= \sum_{i=0}^{n} \frac{u-u_i}{u_{i+k}-u_i} N_{i,k}(u)\mathbf{p}_i + \sum_{i=1}^{n+1} \frac{u_{i+k}-u}{u_{i+k}-u_i} N_{i,k}(u)\mathbf{p}_{i-1} \\
&= \sum_{i=1}^{n} \frac{u-u_i}{u_{i+k}-u_i} N_{i,k}(u)\mathbf{p}_i + \sum_{i=1}^{n} \frac{u_{i+k}-u}{u_{i+k}-u_i} N_{i,k}(u)\mathbf{p}_{i-1} \\
&= \sum_{i=1}^{n} \left(\frac{u_{i+k}-u}{u_{i+k}-u_i} \mathbf{p}_{i-1} + \frac{u-u_i}{u_{i+k}-u_i} \mathbf{p}_i \right) N_{i,k}(u).
\end{aligned}$$

It is necessary to justify the fourth equality above, which reduced the domains of the summations, First note that, since $N_{0,k}(u)$ has support contained in $[u_0, u_k]$ and is right continuous at u_k, $N_{0,k}(u) = 0$ for $u \geq u_k$. This justifies dropping the $i = 0$ term from the first summation. For the second summation, we need to show that $N_{n+1,k}(u) = 0$. Note that $N_{n+1,k}(u)$ has support in $[u_{n+1}, u_{n+m}]$, so the desired equality $N_{n+1,k}(u) = 0$ certainly holds if $u < u_{n+1}$. It remains to consider the case where $k > 1$ and $u = u_{n+1}$. Now, if $u_{n+1} < u_{n+m}$, then $N_{n+1,k}(u_{n+1}) = 0$ by the Cox-de Boor formula. On the other hand, if $u_{n+1} = u_{n+m}$, then $N_{n+1,k}(u)$ is the constant zero function.

That suffices to prove the theorem. □

It is possible restate Theorem IX.5 without the special case for $k = 1$. For this, let the order k functions $N_{i,k}(u)$ be defined from the knot vector $[u_0, \ldots, u_{n+m-1}]$ instead of the knots $[u_0, \ldots, u_{n+m}]$. Then Equation (IX.12) holds for all $u \in [u_k, u_{n+1}]$, for all $k \geq 1$.

At first glance, Equation (IX.12) may appear to define $\mathbf{q}(u)$ as a degree $k-1$ B-spline curve. This is not quite correct however, since the new "control points" $\mathbf{p}_i^{(1)}(u)$ depend on u. Nonetheless, it is convenient to think of the theorem as providing a method of "degree lowering," and we can iterate the construction of the theorem to lower the degree all the way down to degree one. For this, we define

$$\mathbf{p}_i^{(0)}(u) = \mathbf{p}_i,$$

and, for $1 \leq j \leq k$, we generalize Equation (IX.13) to

$$\begin{aligned}
\mathbf{p}_i^{(j)}(u) &= \frac{u_{i+k-j+1}-u}{u_{i+k-j+1}-u_i} \mathbf{p}_{i-1}^{(j-1)} + \frac{u-u_i}{u_{i+k-j+1}-u_i} \mathbf{p}_i^{(j-1)} \qquad \text{(IX.14)} \\
&= \mathit{lerp}\Big(\mathbf{p}_{i-1}^{(j-1)}, \mathbf{p}_i^{(j-1)}, \frac{u-u_i}{u_{i+k-j+1}-u_i}\Big).
\end{aligned}$$

The following theorem shows that, for a particular value of j and a particular u, $\mathbf{q}(u)$ can be expressed in terms of a B-spline curve of degree $k-j$.

$$\begin{tikzcd}
 & & & & & \mathbf{p}^{(0)}_{s-k} \arrow[dl] & = & \mathbf{p}_{s-k} \\
 & & & & \mathbf{p}^{(1)}_{s-k+1} \arrow[dl] & \arrow[l] & & \\
 & & & \mathbf{p}^{(2)}_{s-k+2} & \arrow[l] & \vdots & & \vdots \\
 & & & & \vdots & & & \\
 & & \iddots & \vdots & & \arrow[dl] & & \\
 & & \arrow[dl] & & \mathbf{p}^{(1)}_{s-2} \arrow[dl] & \mathbf{p}^{(0)}_{s-2} \arrow[l] \arrow[dl] & = & \mathbf{p}_{s-2} \\
 & \mathbf{p}^{(k-1)}_{s-1} \arrow[dl] & \arrow[l] \arrow[dl] & \mathbf{p}^{(2)}_{s-1} \arrow[dl, phantom] & \mathbf{p}^{(1)}_{s-1} \arrow[l] \arrow[dl] & \mathbf{p}^{(0)}_{s-1} \arrow[l] \arrow[dl] & = & \mathbf{p}_{s-1} \\
\mathbf{p}^{(k)}_{s} & \mathbf{p}^{(k-1)}_{s} \arrow[l] & \cdots \arrow[l] & \mathbf{p}^{(2)}_{s} & \mathbf{p}^{(1)}_{s} \arrow[l] & \mathbf{p}^{(0)}_{s} \arrow[l] & = & \mathbf{p}_{s}
\end{tikzcd}$$

Figure IX.12: The control points obtained as $\mathbf{q}(u)$ is expressed as B-spline curves of lower degrees. For $j > 0$, the values $\mathbf{p}_i^{(j)}$ depend on u.

Theorem IX.6. *Let* $0 \le j \le k$. *Let* $u \in [u_k, u_{n+1}]$ *(or* $u \in [u_k, u_{n+1})$ *if* $j = k$*). Then*

$$\mathbf{q}(u) \;=\; \sum_{i=j}^{n} N_{i,k+1-j}(u)\mathbf{p}_i^{(j)}(u). \tag{IX.15}$$

This theorem is proved by induction on j, using Theorem IX.5. □

Corollary IX.7. *Suppose the hypotheses of Theorem IX.6 hold. Let* s *be the maximum value* $\le n$ *such that* $u_s \le u$. *This means that either we have* $u_s \le u < u_{s+1}$ *or we have* $s = n$ *and* $u = u_{n+1}$. *Then*

$$\mathbf{q}(u) \;=\; \mathbf{p}_s^{(k)}(u).$$

Proof. By Theorem IX.6, with $j = k$, we have $\mathbf{q}(u) = \sum_{i=j}^{n} N_{i,1}(u)\mathbf{p}_i^{(j)}(u)$. The order 1 blending functions $N_{i,1}$ were defined as step functions, equal to 1 on a finite interval and zero elsewhere. By the choice of s, the only $N_{i,1}$ which is non-zero on the interval containing u is $N_{i,s}$. Thus $\mathbf{q}(u) \;=\; \mathbf{p}_s^{(k)}(u)$. □

For the rest of this section, we suppose $\mathbf{q}(u)$ has degree k and that every knot position has multiplicity $\le k$, except that possibly the first and last knot positions have multiplicity $k+1$. It follows from Theorem IX.2 that $\mathbf{q}(u)$ is a continuous curve. These assumptions can be made without loss of generality, since the B-spline curve can be discontinuous at any knot with multiplicity $\ge k+1$, and if such knots do occur, the B-spline curve can be split into multiple B-spline curves.

We are now ready to describe the de Boor algorithm. Suppose we are given a value for u such that $u_s \le u < u_{s+1}$, and we wish to compute $\mathbf{q}(u)$. By Corollary IX.7, $\mathbf{q}(u) = \mathbf{p}_s^{(k)}(u)$. The de Boor algorithm thus consists of evaluating $\mathbf{p}_s^{(k)}(u)$ using Equation (IX.14) recursively. As shown in

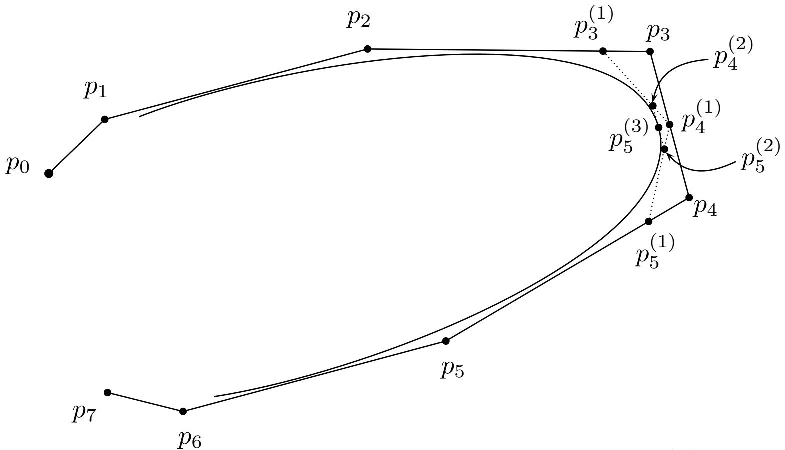

Figure IX.13: The use of the de Boor algorithm to compute $\mathbf{q}(u)$. The degree three spline has the uniform knot vector $u_i = i$ for $0 \le i \le 11$ and control points $\mathbf{p}_i$. The points $\mathbf{p}_i^{(j)}$ are computed by the de Boor algorithm with $u = 5\frac{1}{2}$, and $\mathbf{p}_5^{(3)} = \mathbf{q}(5\frac{1}{2})$.

Figure IX.12, $\mathbf{p}_s^{(k)}(u)$ does not in general depend on all of the original control points $\mathbf{p}_i$, but instead depends only on the control points $\mathbf{p}_i$ with $s-k \le i \le s$. The de Boor algorithm works by computing the control points $\mathbf{p}_i^{(j)}(u)$ which are shown in Figure IX.12. Namely, it computes $\mathbf{p}_i^{(j)}(u)$ for $j = 1, \ldots, k$ and for $i = s-k+j, \ldots, s$. In other words, for $u \in [u_s, u_{s-1})$, it computes:

- first, $\mathbf{p}_i^{(1)}(u)$ for $i = s-k+1, \ldots, s$,
- second, $\mathbf{p}_i^{(2)}(u)$ for $i = s-k+2, \ldots, s$,
- third, $\mathbf{p}_i^{(3)}(u)$ for $i = s-k+3, \ldots, s$,
- continuing similarly, until computing $\mathbf{p}_s^{(k)}$. This equals $\mathbf{q}(u)$.

An example of the de Boor algorithm for a degree three is illustrated in Figure IX.13. The next two examples are for a degree two curve with the uniform knot vector where $u_i = i$ for all i.

Example IX.8. First consider a degree $k = 2$ B-spline curve $\mathbf{q}(u)$ with the uniform knot vector. The domain of $\mathbf{q}(u)$ is $[u_2, u_{n+1}] = [2, n+1]$. As shown in Figure IX.1, $\mathbf{q}(2)$ should be the point midway between $\mathbf{p}_0$ and $\mathbf{p}_1$. We verify this with the Cox-de Boor algorithm.

We have $u \in [2,3) = [u_2, u_3)$, so the value s of Figure IX.12 equals 2. We

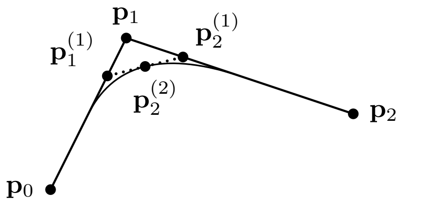

Figure IX.14: The computation of $\mathbf{q}(\frac{5}{2})$ in Example IX.9.

start by computing $\mathbf{p}_1^{(1)}(2)$ and $\mathbf{p}_2^{(1)}(2)$ by (using $u = 2$),

$$\begin{aligned}
\mathbf{p}_1^{(1)}(u) &= \frac{u_3 - u}{u_3 - u_1}\mathbf{p}_0 + \frac{u - u_1}{u_3 - u_1}\mathbf{p}_1 = \frac{3-2}{3-1}\mathbf{p}_0 + \frac{2-1}{3-1}\mathbf{p}_1 = \frac{1}{2}\mathbf{p}_0 + \frac{1}{2}\mathbf{p}_1 \\
\mathbf{p}_2^{(1)}(u) &= \frac{u_4 - u}{u_4 - u_2}\mathbf{p}_1 + \frac{u - u_1}{u_3 - u_1}\mathbf{p}_2 = \frac{4-2}{4-2}\mathbf{p}_1 + \frac{2-2}{4-2}\mathbf{p}_2 = \mathbf{p}_1
\end{aligned}$$

We then compute (still for $u = 2$)

$$\mathbf{p}_2^{(2)}(u) = \frac{u_3 - u}{u_3 - u_2}\mathbf{p}_1^{(1)}(u) + \frac{u - u_2}{u_3 - u_2}\mathbf{p}_2^{(1)}(u) = \frac{3-2}{3-2}\mathbf{p}_1^{(1)}(u) + \frac{2-2}{3-2}\mathbf{p}_2^{(1)}(u) = \mathbf{p}_1^{(1)}(u).$$

Finally, $\mathbf{q}(2) = \mathbf{p}_2^{(2)}(2)$. This equals $\frac{1}{2}\mathbf{p}_0 + \frac{1}{2}\mathbf{p}_1$ as expected.

Example IX.9. For a second example, again use the degree 2 B-spline curve with the uniform knot positions $u_i = i$. Now we evaulate $\mathbf{q}(\frac{5}{2})$. Proceeding similarly to the previous example, but with $u = \frac{5}{2}$,

$$\begin{aligned}
\mathbf{p}_1^{(1)}(\tfrac{5}{2}) &= \frac{u_3 - \frac{5}{2}}{u_3 - u_1}\mathbf{p}_0 + \frac{\frac{5}{2} - u_1}{u_3 - u_1}\mathbf{p}_1 = \frac{3 - \frac{5}{2}}{3-1}\mathbf{p}_0 + \frac{\frac{5}{2} - 1}{3-1}\mathbf{p}_1 = \frac{1}{4}\mathbf{p}_0 + \frac{3}{4}\mathbf{p}_1 \\
\mathbf{p}_2^{(1)}(\tfrac{5}{2}) &= \frac{u_4 - \frac{5}{2}}{u_4 - u_2}\mathbf{p}_1 + \frac{\frac{5}{2} - u_1}{u_3 - u_1}\mathbf{p}_2 = \frac{4 - \frac{5}{2}}{4-2}\mathbf{p}_1 + \frac{\frac{5}{2} - 2}{4-2}\mathbf{p}_2 = \frac{3}{4}\mathbf{p}_1 + \frac{1}{4}\mathbf{p}_2 \\
\mathbf{p}_2^{(2)}(\tfrac{5}{2}) &= \frac{u_3 - \frac{5}{2}}{u_3 - u_2}\mathbf{p}_1^{(1)}(\tfrac{5}{2}) + \frac{\frac{5}{2} - u_2}{u_3 - u_2}\mathbf{p}_2^{(1)}(\tfrac{3}{2}) = \frac{1}{2}\mathbf{p}_1^{(1)}(\tfrac{5}{2}) + \frac{1}{2}\mathbf{p}_2^{(1)}(\tfrac{5}{2}) \\
&= \frac{1}{8}\mathbf{p}_0 + \frac{3}{4}\mathbf{p}_1 + \frac{1}{8}\mathbf{p}_2.
\end{aligned}$$

These computations are shown in Figure IX.14. Thus $\mathbf{q}(\frac{5}{2}) = \frac{1}{8}\mathbf{p}_0 + \frac{3}{4}\mathbf{p}_1 + \frac{1}{8}\mathbf{p}_2$.

There is one special case where the de Boor algorithm can be made more efficient. When u is equal to the knot u_s, it is not necessary to iterate all the way to $j = k$. Instead, suppose the knot $u = u_s$ has multiplicity μ. Let $\delta = \min(k, \mu)$. Since $u_s < u_{s+1}$, we have $u_{s-\delta+1} = u_s$, and applying Theorem IX.3(b) with $i = s - \delta + 1$ gives

$$\mathbf{q}(u) = \mathbf{p}_{s-\delta}^{(k-\delta)}.$$

This was illustrated in Example IX.8 with $\delta = 1$, where $\mathbf{p}_1^{(1)}(u)$ was already equal to $\mathbf{q}(u)$ with $u = 2$.

Pseudo-code for the de Boor algorithm is presented below. The algorithm works by computing values $\mathbf{p}_i^{(j)}(u)$ for successive values of j up to $j = k - \mu$; these values are stored in an array `r[]`. For a given value of j, `r[`ℓ`]` is computed to equal $\mathbf{p}^{(j)}_{s-k+j+\ell}(u)$. To find the formula for computing successive values of `r[`ℓ`]`, make the change of variables $\ell = i - (s - k + j)$ in Equation (IX.14) to get

$$\mathbf{p}^{(j)}_{s-k+j+\ell}(u) \;=\; \frac{u_{s+\ell+1} - u}{u_{s+\ell+1} - u_{s-k+j+\ell}}\mathbf{p}^{(j-1)}_{s-k+j+\ell-1} + \frac{u - u_{s-k+j+\ell}}{u_{s+\ell+1} - u_{s-k+j+\ell}}\mathbf{p}^{(j-1)}_{s-k+j+\ell}. \tag{IX.16}$$

```
De Boor Algorithm
Input:  A degree $k$ B-spline curve $\mathbf{q}$ (thus of order $m = k+1$), given by:
            Control points $\mathbf{p}_0, \mathbf{p}_1, \ldots, \mathbf{p}_n$,
            Knot positions $u_0, u_1, \ldots, u_{n+m}$.
        A value $u$ such that $u_k \le u \le u_{n+1}$.
Result:  Return value is $\mathbf{q}(u)$.
Algorithm:
    If ( $u$==$u_{n+m}$ ) {        // If so, also $u = u_{n+1}$ holds.
            Return $\mathbf{p}_n$ ;
    }
    Set $s$ to be the value such that $u_s \le u < u_{s+1}$ ;
    Set $\delta$ = 0;
    // The next three lines are optional!  Letting $\delta = 0$ always works.
    If ( $u$==$u_s$ ) {
            Set $\delta$ = Min( $\delta$, the multiplicity of $u_s$);
    }
    // Initialize for $j$=0:
    For $\ell$ = 0, 1, ..., $k - \delta$ {
            Set r[$\ell$] = $\mathbf{p}_{s-k+\ell}$ ;
    }
    // Main loop:
    For j = 1,2,..., $k - \delta$ {
            For $\ell$ = 0, 1, ..., $k - \delta - j$ {
                Set $\alpha$ = $\frac{u - u_{s-k+j+\ell}}{u_{s+\ell+1} - u_{s-k+j+\ell}}$ ;
                Set r[$\ell$] = $lerp$(r[$\ell$],r[$\ell+1$],$\alpha$);
            }
    }
    Return r[0];
```

IX.6 Blossoms

Blossoms are a method of representing polynomial curves with symmetric, multiaffine functions. As such they provide an elegant tool for working with

B-splines. Apart from mathematical elegance, the most important aspect of blossoms is that they give a simple algorithm for computing the control points of a B-spline curve from the polynomial segments of the curve. Blossoms will be useful for obtaining formulas for the derivative of a B-spline. In addition, they give an easy method for deriving algorithms for knot insertion.

Suppose $\mathbf{q}(u)$ is a degree k B-spline curve and that $u_s < u_{s+1}$ are two knots. The curve $\mathbf{q}(u)$ consists of polynomial pieces; on the interval $[u_s, u_{s+1}]$, $\mathbf{q}(u)$ is defined by a (single) polynomial, which we call $\mathbf{q}_s(u)$. We shall find a new function $\mathbf{b}(x_1, x_2, \ldots, x_k)$ that takes k real numbers as arguments, but has the *diagonal* property that

$$\mathbf{b}(u, u, \ldots, u) \;=\; \mathbf{q}_s(u). \qquad \text{(IX.17)}$$

This function $\mathbf{b}(x_1, \ldots, x_k)$ is called the "blossom" of $\mathbf{q}_s$. The blossom $\mathbf{b}$ will also satisfy the following two properties:

Symmetric property: . Changing order of the inputs to $\mathbf{b}$ does not change the value of $\mathbf{b}$; namely, for any permutation π of $\{1, \ldots, k\}$ and for all values of $x_1, \ldots x_k$,

$$\mathbf{b}(x_{\pi(1)}, x_{\pi(2)}, \ldots, x_{\pi(k)}) \;=\; \mathbf{b}(x_1, x_2, \ldots, x_k).$$

A function with this property is called a *symmetric function.*

Multiaffine property: For any scalars α and β with $\alpha + \beta = 1$ and any $i = 1, \ldots, k$, the blossom satisfies

$$\begin{aligned}&\mathbf{b}(x_1, \ldots, x_{i-1}, \alpha x_i + \beta x'_i, x_{i+1}, \ldots, x_k)\\ &\quad = \;\; \alpha\mathbf{b}(x_1, \ldots, x_{i-1}, x_i, x_{i+1}, \ldots, x_k) + \beta\mathbf{b}(x_1, \ldots, x_{i-1}, x'_i, x_{i+1}, \ldots, x_k).\end{aligned}$$

A function with this property is called *multiaffine.*

The multiaffine property can be equivalently expressed using linear interpolation as

$$\begin{aligned}&\mathbf{b}(x_1, \ldots, x_{i-1}, \mathit{lerp}(x_i, x'_i, \beta), x_{i+1}, \ldots, x_k)\\ &\quad = \;\; \mathit{lerp}(\mathbf{b}(x_1, \ldots, x_{i-1}, x_i, x_{i+1}, \ldots, x_k), \mathbf{b}(x_1, \ldots, x_{i-1}, x'_i, x_{i+1}, \ldots, x_k), \beta).\end{aligned}$$

Many functions are symmetric. A simple example is the summation function $h(x_1, \ldots, x_k) = x_1 + \cdots + x_k$. Statistical functions such as mean, median, mode, and standard deviation are also symmetric since they do not depend on the order of the inputs. However, of these functions, only summation and mean are multiaffine. Another example of a multiaffine is a monomial such as $x_1x_2x_4$ in which no variable has exponent greater than one. Linear combinations of multiaffine functions are also multiaffine.

Normally, the term "affine" is used for a function of a single variable that is defined by a polynomial of degree one. Namely, a function $h : \mathbb{R} \to \mathbb{R}$ is *affine* if it is of the form $h(x) = ax + b$, for scalars a and b. (This is equivalent to how "affine" was defined in Chapter II, at least for functions mapping $\mathbb{R}$ to $\mathbb{R}$.) Such functions h are precisely the functions that satisfy $h(\alpha x+\beta y) = \alpha h(x)+\beta h(y)$ for all values of x, y, α, and β with $\alpha+\beta = 1$.

Multiaffine functions have domain $\mathbb{R}^k$ and range $\mathbb{R}$ for some $k \geq 1$. Since blossoms are affine in each input variable separately, they are called "multiaffine." For $k > 0$, we let $[k] = \{1, 2, \ldots, k\}$. For J a subset of $[k]$, we define the term x_J to be the product

$$x_J \ = \ \prod\nolimits_{j\in J} x_j.$$

For example, if $J = \{1, 3, 6\}$, then $x_J = x_1x_3x_6$. For the empty set, we define $x_\emptyset = 1$. It is easy to check that x_J is a multiaffine function. In fact, any multiaffine function $h(x_1, \ldots, x_k)$ can be expressed in the form

$$h(x_1, \ldots, x_k) \ = \ \sum_{J\subseteq[k]} \alpha_J x_J, \tag{IX.18}$$

where the α_J's are scalars (possibly equal to 0). It is easy to check that Equation (IX.18) defines a multiaffine function. The proof of the converse is left to Exercise IX.15.

We next define the blossom of a polynomial curve $\mathbf{q}(u)$ in $\mathbb{R}^d$.

Definition IX.10. Let $\mathbf{q}$ have degree $\leq k$, so that

$$\mathbf{q}(u) \ = \ \mathbf{r}_k u^k + \mathbf{r}_{k-1}u^{k-1} + \cdots + \mathbf{r}_2u^2 + \mathbf{r}_1u^1 + \mathbf{r}_0,$$

where the coefficients $\mathbf{r}_i$ are points from $\mathbb{R}^d$ for some d. (These coefficients $\mathbf{r}_i$ should not be confused with the control points of a B-spline curve.) We define the *degree k blossom* of $\mathbf{q}(u)$ to be the k variable polynomial

$$\mathbf{b}(x_1, \ldots, x_k) \ = \ \sum_{i=0}^{k} \sum_{\substack{J\subseteq[k]\\ |J|=i}} \binom{k}{i}^{-1} \mathbf{r}_i x_J, \tag{IX.19}$$

where $|J|$ denotes the cardinality of J.

We need to check that the definition of the blossom $\mathbf{b}$ satisfies the three properties described above. First, it is immediate, just from the form of the definition, that $\mathbf{b}$ is a symmetric function. Second, the terms in the polynomial defining $\mathbf{b}$ contain at most one occurrence of each variable; therefore, $\mathbf{b}$ is degree one in each variable separately and thus is affine in each variable. Finally, since there are $\binom{k}{i}$ many subsets J of k of size i, it is easy to see that $\mathbf{b}(u, u, \ldots, u) = \mathbf{q}(u)$.

As an example, let $\mathbf{q}(u)$ be the quadratic curve

$$\mathbf{q}(u) \ = \ \mathbf{a}u^2 + \mathbf{b}u + \mathbf{c}.$$

Then the degree two blossom of $\mathbf{q}(u)$ is the polynomial

$$\mathbf{b}(x_1, x_2) \ = \ \mathbf{a}x_1x_2 + \tfrac{1}{2}\mathbf{b}(x_1 + x_2) + \mathbf{c}.$$

There is also a degree three blossom for $\mathbf{q}(u)$. For this, we think of $\mathbf{q}(u)$ as a being a degree three polynomial, with leading coefficient zero. Then the degree three blossom of $\mathbf{q}(u)$ equals

$$\mathbf{b}(x_1, x_2, x_3) \;=\; \tfrac{1}{3}\mathbf{a}(x_1x_2 + x_1x_3 + x_2x_3) + \tfrac{1}{3}\mathbf{b}(x_1 + x_2 + x_3) + \mathbf{c}.$$

Exercise IX.9. Let $\mathbf{q}(u) = \mathbf{a}u^3 + \mathbf{b}u^2 + \mathbf{c}u + \mathbf{d}$. What is the degree three blossom of $\mathbf{q}(u)$?

The key reason that blossom functions are useful is that the blossom functions can be used to compute the control points of a B-spline curve from the polynomial equation of the curve. This is expressed by the next theorem.

Theorem IX.11. *Let $\mathbf{q}(u)$ be a degree k, order $m = k+1$ B-spline curve with knot vector $[u_0, \ldots, u_{n+m}]$ and control points $\mathbf{p}_0, \ldots, \mathbf{p}_n$. Suppose $u_s < u_{s+1}$ where $k \le s \le n$. Let $\mathbf{q}(u)$ be equal to the polynomial $\mathbf{q}_s(u)$ for $u \in [u_s, u_{s+1})$. Let $\mathbf{b}(x_1, \ldots, x_k)$ be the blossom of $\mathbf{q}_s(u)$.[2] Then the control points $\mathbf{p}_{s-k}, \ldots, \mathbf{p}_s$ are equal to*

$$\mathbf{p}_i \;=\; \mathbf{b}(u_{i+1}, u_{i+2}, \ldots, u_{i+k}), \qquad \text{(IX.20)}$$

for $i = s-k, \ldots, s$.

This theorem lets us obtain the control points that affect a single segment of a B-spline from the blossom of the segment. In particular, it means that $k+1$ consecutive control points can be calculated from just the one segment that they affect!

Proof. To prove Theorem IX.11, we relate the blossom's values to the intermediate values obtained in the de Boor algorithm. This is pictured in Figure IX.15 To save space, we have used two notational conveniences. First, the notation $u^{\langle i\rangle}$ is used to denote i occurrences of the parameter u; for example, the diagonal property (IX.17) can be re-expressed as $\mathbf{b}(u^{\langle k\rangle}) = \mathbf{q}_s(u)$. Second, for $i \le j$, the notation $u_{[i,j]}$ denotes the sequence of values $u_i, u_{i+1}, \ldots, u_j$.

Figure IX.15 looks very much like Figure IX.12, which described the de Boor algorithm. Indeed, the next lemma shows that it corresponds exactly to Figure IX.12.

Lemma IX.12. *Suppose (IX.20) holds for all $i = s-k, \ldots, s$. $\mathbf{p}_i^{(j)}(u)$ for Then, for $j = 0, \ldots, k$ and $i = s-k+j, \ldots, s$,*

$$\mathbf{p}_i^{(j)}(u) \;=\; \mathbf{b}(u_{[i+1,i+k-j]}, u^{\langle j\rangle}) \;=\; \mathbf{b}(u_{i+1}, \ldots, u_{i+k-j}, u, \ldots, u). \qquad \text{(IX.21)}$$

The second equality of (IX.21) is obtained by expanding our notational conventions.

[2] The B-spline curve $\mathbf{q}(u)$ is only piecewise polynomial, so it does not have a blossom. But, of course the subcurve $\mathbf{q}_s(u)$ does have a blossom.

$$\begin{tikzcd}
 & & & & \mathbf{b}(u_{[s-k+1,s]}) \arrow[dl] \\
 & & & \mathbf{b}(u_{[s-k+2,s]},u) \arrow[dl] & {} \arrow[l] \\
 & & \mathbf{b}(u_{[s-k+3,s]},u^{\langle 2\rangle}) & {} \arrow[l] & \vdots \\
 & & & \vdots & \\
 & & & & \mathbf{b}(u_{[s-2,s+k-3]}) \arrow[dl] \\
 & \iddots & \vdots & \mathbf{b}(u_{[s-1,s+k-3]},u) \arrow[dl] & \mathbf{b}(u_{[s-1,s+k-2]}) \arrow[l] \arrow[dl] \\
 & {} \arrow[dl] & \mathbf{b}(u_{[s,s+k-3]},u^{\langle 2\rangle}) & \mathbf{b}(u_{[s,s+k-2]},u) \arrow[l] \arrow[dl] & \mathbf{b}(u_{[s,s+k-1]}) \arrow[l] \arrow[dl] \\
\mathbf{b}(u^{\langle k\rangle}) & \cdots \arrow[l] & \mathbf{b}(u_{[s+1,s+k-2]},u^{\langle 2\rangle}) & \mathbf{b}(u_{[s+1,s+k-1]},u) \arrow[l] & \mathbf{b}(u_{[s+1,s+k]}) \arrow[l]
\end{tikzcd}$$

Figure IX.15: A table of blossom values. The value $\mathbf{b}(u^{\langle k\rangle})$ on the left is equal to $\mathbf{q}_s(u)$. The blossom values in the right column are equal to the control points of the B-spline curve. The symmetry and multiaffine properties of the blossom function mean that each blossom value is a weighted average of the two blossom values that point to it, as expressed in Equation (IX.22).

The lemma is proved by induction on j. The base case is $j=0$, and for this case, the lemma holds by the hypothesis that (IX.20) holds. For the induction step, let $j>0$ and $s-k+j \le i \le s$. The induction hypothesis tells us that

$$\begin{aligned}
\mathbf{p}_{i-1}^{(j-1)} &= \mathbf{b}(u_{[i,i+k-j]},u^{\langle j-1\rangle}) \\
\mathbf{p}_{i}^{(j-1)} &= \mathbf{b}(u_{[i+1,i+k-j+1]},u^{\langle j-1\rangle}).
\end{aligned}$$

The symmetry property of the blossom $\mathbf{b}$ thus gives

$$\begin{aligned}
\mathbf{p}_{i-1}^{(j-1)} &= \mathbf{b}(u_{[i+1,i+k-j]},u_i,u^{\langle j-1\rangle}) \\
\mathbf{p}_{i}^{(j-1)} &= \mathbf{b}(u_{[i+1,i+k-j]},u_{i+k-j+1},u^{\langle j-1\rangle}).
\end{aligned}$$

The multiaffine property implies that

$$\begin{aligned}
&\mathit{lerp}\Big(\mathbf{b}(u_{[i+1,i+k-j]},u_i,u^{\langle j-1\rangle}),\, \mathbf{b}(u_{[i+1,i+k-j]},u_{i+k-j+1},u^{\langle j-1\rangle}),\, \frac{u-u_i}{u_{i+k-j+1}-u_i}\Big) \\
&\quad = \mathbf{b}(u_{[i+1,i+k-j]},u,u^{\langle j-1\rangle}) \;=\; \mathbf{b}(u_{[i+1,i+k-j]},u^{\langle j\rangle}), \qquad \text{(IX.22)}
\end{aligned}$$

since $\mathit{lerp}(u_i,,u_{i+k-j+1},\frac{u-u_i}{u_{i+k-j+1}-u_i}) = u$. These equalities and the definition IX.14 of $\mathbf{p}_i^{(j)}$ imply that

$$\mathbf{p}_i^{(j)}(u) \;=\; \mathbf{b}(u_{[i+1,i+k-j]},u^{\langle j\rangle}).$$

That completes the induction step and thus the proof of the lemma.

In light of the de Boor algorithm, the lemma immediately implies that if the control points $\mathbf{p}_{s-k}, \ldots, \mathbf{p}_s$ satisfy Equation (IX.20), then the correct curve $\mathbf{q}_s(u)$ is obtained. That is to say, the values $\mathbf{b}(u_{i+1}, u_{i+2}, \ldots, u_{s+k})$ are a *possible* set of control points for $\mathbf{q}_s(u)$. On the other hand, vector space dimensionality considerations imply that there is most a single set of possible control points for $\mathbf{q}_s(u)$. Namely, for a curve lying in $\mathbb{R}^d$, the vector space of all degree k polynomials has dimension $(k+1)d$, and the space of possible control points $\mathbf{p}_{s-k}, \ldots, \mathbf{p}_s$ has the same dimension. Thus, Theorem IX.11 is proved. □

Exercise IX.10. Verify the following special case of Theorem IX.11. Let

$$\mathbf{q}(u) \;=\; (1-u)^2\mathbf{p}_0 + 2u(1-u)\mathbf{p}_1 + u^2\mathbf{p}_2$$

be the degree two B-spline with the knot vector $[0,0,0,1,1,1]$ and control points $\mathbf{p}_0, \mathbf{p}_1, \mathbf{p}_2$. (See equations (IX.7) on page 337.) Give the formula for the blossom $\mathbf{b}(x_1, x_2)$ of $\mathbf{q}$. What are the values of $\mathbf{b}(0,0)$, $\mathbf{b}(0,1)$, and $\mathbf{b}(1,1)$?

It is possible to develop the theory of Bézier curves and B-spline curves using the blossoms as the central concept. This alternate approach differs from our treatment in this book by using blossoms instead of blending functions $N_{i,m}$ as the main tool for defining B-splines. The textbook of Farin [42] describes this alternate approach. Two early papers describing the use of blossoms are those of Seidel [100, 101]; his work is based on the original developments by de Casteljau and Ramshaw.

IX.7 Derivatives and smoothness of B-spline curves

This section derives formulas for the derivative of a B-spline curve and proves Theorem IX.2 about the number of continuous derivatives of a B-spline. It is a pleasant discovery that the derivative of a degree k B-spline curve is itself a B-spline curve of degree $k-1$.

Theorem IX.13. *Let $\mathbf{q}(u)$ be a degree $k = m-1$ B-spline curve with control points $\mathbf{p}_0, \ldots, \mathbf{p}_n$. Then its first derivative is*

$$\mathbf{q}'(u) \;=\; \sum_{i=1}^{n} kN_{i,k}(u)\frac{\mathbf{p}_i - \mathbf{p}_{i-1}}{u_{i+k} - u_i}. \qquad \text{(IX.23)}$$

In particular, $\mathbf{q}'(u)$ is the degree $k-1$ B-spline curve with control points equal to

$$\mathbf{p}_i^* \;=\; \frac{k}{u_{i+k} - u_i}(\mathbf{p}_i - \mathbf{p}_{i-1}). \qquad \text{(IX.24)}$$

We prove Theorem IX.13 in stages. First, we prove that Equation (IX.23) is valid for all values of u that are not knots. We then use continuity considerations to conclude that Equation (IX.23) holds also for u a knot.[3] After proving Theorem IX.13, we use it to help prove Theorem IX.2.

The next lemma will be used for the first stage of the proof of Theorem IX.13. This lemma explains how to express the blossom of the first derivative of a function in terms of the blossom of the function.

Lemma IX.14. *Let* $\mathbf{f}(u)$ *be a polynomial curve of degree* $\le k$*, and let* $\mathbf{b}(x_1,\ldots,x_k)$ *be its degree* k *blossom.*

(a) *Let* $\mathbf{b}^*(x_1,\ldots,x_{k-1})$ *be the degree* $k-1$ *blossom of the first derivative* $\mathbf{f}'(u)$ *of* $\mathbf{f}(u)$*. Then,*

$$\mathbf{b}^*(x_1,\ldots,x_{k-1}) = k\cdot(\mathbf{b}(x_1,\ldots,x_{k-1},1)-\mathbf{b}(x_1,\ldots,x_{k-1},0)). \tag{IX.25}$$

(b) *More generally, for all* $s\neq t$*,*

$$\mathbf{b}^*(x_1,\ldots,x_{k-1}) = \frac{k}{t-s}(\mathbf{b}(x_1,\ldots,x_{k-1},t)-\mathbf{b}(x_1,\ldots,x_{k-1},s)). \tag{IX.26}$$

Proof. Let $\mathbf{f}(u)=\sum_{i=0}^k \mathbf{r}_i u^i$. The definition of the degree k blossom of $\mathbf{f}(u)$ given by Equation (IX.19) can be rewritten as

$$\mathbf{b}(x_1,\ldots,x_k) \;=\; \sum_{J\subseteq[k]} \binom{k}{|J|}^{-1} \mathbf{r}_{|J|}x_J. \tag{IX.27}$$

The first derivative of $\mathbf{f}(u)$ is $\mathbf{f}'(u)=\sum_{i=0}^{k-1}(i+1)\mathbf{r}_{i+1}u^i$, and its degree $k-1$ blossom is

$$\mathbf{b}^*(x_1,\ldots,x_{k-1}) \;=\; \sum_{J\subseteq[k-1]} \binom{k-1}{|J|}^{-1} (|J|+1)\mathbf{r}_{|J|+1}x_J. \tag{IX.28}$$

Now consider the difference $\mathbf{b}(x_1,\ldots,x_{k-1},1)-\mathbf{b}(x_1,\ldots,x_{k-1},0)$. Examining the formula (IX.27) for $\mathbf{b}$, we see that terms for subsets J's that do not contain x_k cancel out in the difference, and terms for J's that do contain x_k survive, but with the factor x_k removed. Thus,

$$\mathbf{b}(x_1,\ldots,x_{k-1},1)-\mathbf{b}(x_1,\ldots,x_{k-1},0) \;=\; \sum_{J\subseteq[k-1]} \binom{k}{|J|+1}^{-1} r_{|J|+1}x_J. \tag{IX.29}$$

[3] (For any practical use of splines, you can ignore this footnote.) To be completely rigorous, it is not quite true that $\mathbf{q}'(u)$ is always the degree $k-1$ B-spline curve with control points $\mathbf{p}_i^*$. Namely, at points where the degree $k-1$ curve is discontinuous, the first derivative of $\mathbf{q}$ is undefined. However, if the first derivative is extended to isolated points by taking right limits, we have equality. For similar reasons, Equation (IX.23) does not always hold either. A more correct way to say this is that Equation (IX.23) holds whenever the expression on the righthand side is continuous at u as well as whenever $\mathbf{q}'(u)$ is defined.

Now, (IX.25) follows immediately from (IX.28) and (IX.29), and the fact that $k \cdot \binom{k-1}{i} = (i+1) \cdot \binom{k}{i+1}$. So (a) is proved.

Part (b) is proved using (a). By the multiaffine property, since $s+(1-s) = 1$ and $s \cdot 1 + (1-s) \cdot 0 = s$,

$$\mathbf{b}(x_1, \ldots, x_{k-1}, s) \;=\; s \cdot \mathbf{b}(x_1, \ldots, x_{k-1}, 1) + (1-s) \cdot \mathbf{b}(x_1, \ldots, x_{k-1}, 0).$$

Therefore,

$$\mathbf{b}(x_1, \ldots, x_{k-1}, s) - \mathbf{b}(x_1, \ldots, x_{k-1}, 0) \;=\; s \cdot (\mathbf{b}(x_1, \ldots, x_{k-1}, 1) - \mathbf{b}(x_1, \ldots, x_{k-1}, 0)). \tag{IX.30}$$

Similarly, with t in place of s,

$$\mathbf{b}(x_1, \ldots, x_{k-1}, t) - \mathbf{b}(x_1, \ldots, x_{k-1}, 0) \;=\; t \cdot (\mathbf{b}(x_1, \ldots, x_{k-1}, 1) - \mathbf{b}(x_1, \ldots, x_{k-1}, 0)). \tag{IX.31}$$

Equation (IX.26) follows from Equations (IX.25), (IX.30), and (IX.31). □

Returning to the proof of Theorem IX.13, we can now show that $\mathbf{q}'(u)$ is the B-spline curve with control points $\mathbf{p}_i^*$. For this, by Theorem IX.11, it will suffice to prove the following: For two distinct adjacent knots, $u_s < u_{s+1}$, if $\mathbf{b}$ and $\mathbf{b}^*$ are the blossoms of $\mathbf{q}(u)$ and $\mathbf{q}'(u)$ on the interval (u_s, u_{s+1}), then $\mathbf{p}_i^* = \mathbf{b}^*(u_{i+1}, \ldots, u_{i+k-1})$ for all i such that $i \le s < i+k$. This is proved as follows using Lemma IX.14(b) with $s = u_i$ and $t = u_{i+k}$:

$$\begin{aligned}
&\mathbf{b}^*(u_{i+1}, \ldots, u_{i+k-1}) \\
&\quad= \frac{k}{u_{i+k} - u_i}(\mathbf{b}(u_{i+1}, \ldots, u_{i+k-1}, u_{i+k}) - \mathbf{b}(u_{i+1}, \ldots, u_{i+k-1}, u_i)) \\
&\quad= \frac{k}{u_{i+k} - u_i}(\mathbf{b}(u_{i+1}, \ldots, u_{i+k-1}, u_{i+k}) - \mathbf{b}(u_i, u_{i+1}, \ldots, u_{i+k-1})) \\
&\quad= \frac{k}{u_{i+k} - u_i}(\mathbf{p}_i - \mathbf{p}_{i-1}) \;=\; \mathbf{p}_i^*.
\end{aligned}$$

It follows from what we have proved so far that Equation (IX.23) holds for all values of u which are not knots. It remains to establish the appropriate continuity conditions. This will complete the proof of Theorem IX.13, since a function which is continuous and whose first derivative is equal to a continuous function except at isolated points has continuous first derivative. This is formalized by the following fact from real analysis. It can be proved by an ϵ-δ proof, but we we leave to the reader to prove.

Lemma IX.15. *Let f be a continuous function, whose first derivative is defined in a neighborhood of u_i such that the left and right limits of $f'(u)$ at $u = u_i$ satisfy $\lim_{u \to u_i^+} f'(u) = L = \lim_{u \to u_i^-} f'(u)$. Then $f'(u_i)$ exists and is equal to L.*

That concludes the proof of Theorem IX.13.

We are now ready to prove Theorem IX.2 relating the multiplicity of a knot to the number of continuous derivatives of the B-spline at that knot position.

It is certainly enough to prove the following statement: For all B-spline curves $\mathbf{q}(u)$ of degree k, if a knot u_i has multiplicity μ, then $\mathbf{q}(u)$ has continuous $(k-\mu)$-th derivative at $u = u_i$. We shall prove this statement by holding the knot vector and thus the multiplicity μ of u_i fixed, and using induction on k starting at $k = \mu$.

The base case, $k = \mu$, is a direct consequence of Theorem IX.3. Since $N_{i-1,k+1}(u)$ has limit 1 on both sides of u_i and thus value 1 at $u = u_i$. For $j \neq i-1$, $N_{j,k+1}(u)$ is continuous, and equal to zero, at u_i. So, in this case, $\mathbf{q}(u)$ is continuous at $u = u_i$ with $\mathbf{q}(u_i) = \mathbf{p}_{i-1}$.

The induction step uses the Cox-de Boor formula to establish continuity, and Theorem IX.13 and Lemma IX.15 to establish the continuity of the derivatives. Assume $k > \mu$. The induction hypothesis implies that, for all j, $N_{j,k}(u)$ is continuous and is $C^{k-\mu-1}$-continuous at u_i (the induction hypothesis applies to $N_{j,k}(u)$, since it is a real-valued, degree $k-1$ B-spline curve). The Cox-de Boor formula expresses each $N_{j,k+1}(u)$ in terms of $N_{j,k}(u)$ and $N_{j+1,k}(u)$, so the induction hypothesis applied to these two functions implies that, $N_{j,k+1}(u)$ has continuous $(k-\mu-1)$-th derivative at u_i. Thus, any degree k B-spline curve $\mathbf{q}(u)$ with this knot vector is $C^{k-\mu-1}$-continuous at u_i. Theorem IX.13 further implies that the first derivative of $\mathbf{q}(u)$ is equal to a degree $k-1$ B-spline curve, except possibly at knots. By the induction hypothesis, this degree $k-1$ curve is $C^{k-\mu-1}$-continuous at u_i. It follows that $\mathbf{q}(u)$ is has continuous $(k-\mu)$-th derivative, by using Lemma IX.15 with $\mathbf{f}(u)$ equal to the $(k-\mu-1)$-th derivative of $\mathbf{q}(u)$. □

IX.8 Knot insertion

An important tool for practical interactive use of B-spline curves is the technique of *knot insertion*, which allows one to add a new knot to a B-spline curve without changing the curve, or its degree. For instance, when editing a B-spline curve with a CAD program, one may wish to insert additional knots in order to be able to make further adjustments to a curve: having additional knots in the area of the curve that needs adjustment allows more flexibility in editing the curve. Knot insertion also allows the multiplicity of a knot to be increased, which allows more control over the smoothness of the curve at that point. A second use of knot insertion is to convert a B-spline curve into a series of Bézier curves, as we shall see in Section IX.9. A third use of knot insertion is that, by adding more knots and control points, the control polygon will more closely approximate the B-spline curve. This can be useful, for instance, in combination with the convex hull property, since the convex hull will be smaller and will more closely approximate the curve. This is similar to the way recursive subdivision can be used for Bézier curves. However, one complication is that, for B-spline curves with many knot positions, you should not work with the convex hull of the entire set of control points. Instead, you should use the local support property and define a sequence of convex hulls of $k+1$ consecutive control points, so that the union of these convex hulls contains the

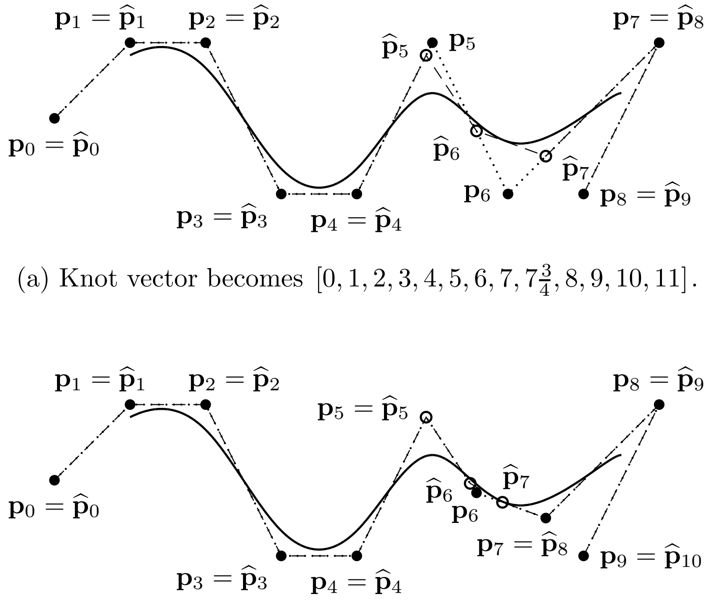
$\mathbf{p}_1 = \widehat{\mathbf{p}}_1$
$\mathbf{p}_2 = \widehat{\mathbf{p}}_2$
$\widehat{\mathbf{p}}_5$
$\mathbf{p}_5$
$\mathbf{p}_7 = \widehat{\mathbf{p}}_8$
$\mathbf{p}_0 = \widehat{\mathbf{p}}_0$
$\widehat{\mathbf{p}}_6$
$\widehat{\mathbf{p}}_7$
$\mathbf{p}_6$
$\mathbf{p}_8 = \widehat{\mathbf{p}}_9$
$\mathbf{p}_3 = \widehat{\mathbf{p}}_3$
$\mathbf{p}_4 = \widehat{\mathbf{p}}_4$
$\mathbf{p}_1 = \widehat{\mathbf{p}}_1$
$\mathbf{p}_2 = \widehat{\mathbf{p}}_2$
$\mathbf{p}_5 = \widehat{\mathbf{p}}_5$
$\mathbf{p}_8 = \widehat{\mathbf{p}}_9$
$\mathbf{p}_0 = \widehat{\mathbf{p}}_0$
$\widehat{\mathbf{p}}_6$
$\widehat{\mathbf{p}}_7$
$\mathbf{p}_6$
$\mathbf{p}_7 = \widehat{\mathbf{p}}_8$
$\mathbf{p}_9 = \widehat{\mathbf{p}}_{10}$
$\mathbf{p}_3 = \widehat{\mathbf{p}}_3$
$\mathbf{p}_4 = \widehat{\mathbf{p}}_4$

(a) Knot vector becomes $[0,1,2,3,4,5,6,7,7\frac{3}{4},8,9,10,11]$.

(b) Knot vector becomes $[0,1,2,3,4,5,6,7,7\frac{3}{4},7\frac{3}{4},8,9,10,11]$.

Figure IX.16: Showing the insertion of knots into a degree three curve. The original knot vector is the uniform knot vector $[0,1,2,3,4,5,6,7,8,9,10,11]$. We insert the value $7\frac{3}{4}$ into the curve twice, each time adding a new control point, and making the control polygon more closely approximate the curve near $7\frac{3}{4}$. The dotted straight lines show the control polygon before the insertion of the new knot position. The dashed straight lines are the control polygon after the insertion. (In (b), the dashed line from $\widehat{\mathbf{p}}_6$ to $\widehat{\mathbf{p}}_7$ is so close to the curve that it cannot be seen in the graph.) The filled circles are the original control point positions. The open circles are the changed control point positions. The control points $\widehat{\mathbf{p}}_i$ of (a) are renamed $\mathbf{p}_i$ in (b). In both figures, one new knot has been inserted and some of the control points have been moved, but the B-spline curve itself is unchanged. If we inserted $7\frac{3}{4}$ a third time, then the new control point $\widehat{\mathbf{p}}_7$ would be equal to the point on the curve at $u = 7\frac{3}{4}$.

B-spline curve. A fourth use of knot insertion is for knot refinement, whereby two curves with different knot vectors can each have new knot positions inserted until the two curves have the same knot vectors.

There are two commonly used methods for knot insertion. The Böhm method [19, 20] allows a single knot at time to be inserted into a curve, and the Oslo method [25, 91] allows multiple knots to be inserted at once. We shall discuss only the Böhm method; of course, multiple knots may be inserted by iterating the Böhm method. The proof of the correctness of the Böhm method will be based on blossoming. For other methods of knot insertion, the reader can consult Farin [42] and Piegl and Tiller [90] and the references cited therein.

Suppose $\mathbf{q}(u)$ is an order m, degree $k = m-1$, B-spline curve, defined with knot vector $[u_0, \ldots, u_{n+m}]$ and control points $\mathbf{p}_0, \ldots, \mathbf{p}_n$. We wish to insert a new knot position $\widehat{u}$ where $u_s \le \widehat{u} < u_{s+1}$, and then choose new control points so that the curve $\mathbf{q}(u)$ remains unchanged.

The new knot vector is denoted $[\widehat{u}_0, \ldots, \widehat{u}_{n+m+1}]$ where, of course,

$$\widehat{u}_i \;=\; \begin{cases} u_i & \text{if } i \le s \\ \widehat{u} & \text{if } i = s+1 \\ u_{i-1} & \text{if } i > s+1. \end{cases}$$

The method of choosing the new control points is less obvious, since we must be sure not to change the curve. The Böhm algorithm gives the following definition of the control points: (remember, $k = m-1$)

$$\widehat{\mathbf{p}}_i \;=\; \begin{cases} \mathbf{p}_i & \text{if } i \le s-k \\ \dfrac{u_{i+k} - \widehat{u}}{u_{i+k} - u_i}\mathbf{p}_{i-1} + \dfrac{\widehat{u} - u_i}{u_{i+k} - u_i}\mathbf{p}_i & \text{if } s-k < i \le s \\ \mathbf{p}_{i-1} & \text{if } s < i. \end{cases} \qquad \text{(IX.32)}$$

It is implicit in the definitions of the $\widehat{\mathbf{p}}_i$'s that $u_{s+1} > u_s$. This can always be arranged by inserting a new repeated knot at the end of a block of repeated knots, rather than the beginning or the middle of a block. The linear interpolation definition of $\widehat{\mathbf{p}}_i$ for $s-k < i \le s$ in Equation (IX.32) is equivalent to

$$\widehat{\mathbf{p}}_i \;=\; \frac{u_{i+k} - \widehat{u}}{u_{i+k} - u_i}\mathbf{p}_{i-1} + \frac{\widehat{u} - u_i}{u_{i+k} - u_i}\mathbf{p}_i,$$

and since $u_i \le u_s < u_{s+1} \le u_{i+k}$, the interpolation value $\frac{\widehat{u} - u_i}{u_{i+k} - u_i}$ is in the half-open interval $[0,1)$. This means that each new control point $\widehat{\mathbf{p}}_i$ is defined as a weighted average of the two old control points $\mathbf{p}_{i-1}$ and $\mathbf{p}_i$.

When $s-k < i \le s$, Equation (IX.32) for $\widehat{\mathbf{p}}_i$ is identical to $\mathbf{p}_i^{(}1)(\widehat{u})$ as defined by Equation IX.13 for the de Boor algorithm. It follows that the de Boor algorithm was essentially doing repeated knot insertion until the value u was a knot of multiplicity k.

The correctness of the Böhm algorithm for knot insertion is stated by the next theorem.

Theorem IX.16. *Suppose $k \ge 1$ and let $\widehat{\mathbf{q}}(u)$ be the degree k B-spline curve defined with the knot vector $[\widehat{u}_0, \ldots, \widehat{u}_{n+m+1}]$ and control points $\widehat{\mathbf{p}}_0, \ldots, \widehat{\mathbf{p}}_{n+1}$. Then, $\widehat{\mathbf{q}}(u) = \mathbf{q}(u)$ for all u.*

Proof. Fix s to be any index such that $\widehat{u}_s < \widehat{u}_{s+1}$. Because of the way blossoms determine control points, it will suffice to show that

$$\mathbf{q}(u) \;=\; \widehat{\mathbf{q}}(u) \qquad \text{for } u \in [u_s, u_{s+1}).$$

For this, it is enough to show that the blossom $\mathbf{b}$ of $\mathbf{q}$ on the interval $[u_s, u_{s+1})$ is also the blossom for $\widehat{\mathbf{q}}$ on the intervals $[u_s, \widehat{u})$ and $[\widehat{u}, u_{s+1})$. To prove this, it is necessary and sufficient to show that the blossom $\mathbf{b}$ has the properties given by Theorem IX.11 with respect to the knot positions and control points of $\widehat{\mathbf{q}}$; namely, that for all i such that $s-k \le i \le s+1$,

$$\widehat{\mathbf{p}}_i \;=\; \mathbf{b}(\widehat{u}_{i+1}, \widehat{u}_{i+2}, \ldots, \widehat{u}_{i+k}).$$

For $i = s-k$, this is easily shown by

$$\begin{aligned} \widehat{\mathbf{p}}_{s-k} &= \mathbf{p}_{s-k} \\ &= \mathbf{b}(u_{s-k+1}, u_{s-k+2}, \ldots, u_s) \\ &= \mathbf{b}(\widehat{u}_{s-k+1}, \widehat{u}_{s-k+2}, \ldots, \widehat{u}_s), \end{aligned}$$

since $u_j = \widehat{u}_j$ for $j \le s$. Likewise, for $i = s+1$,

$$\begin{aligned} \widehat{\mathbf{p}}_{s+1} &= \mathbf{p}_s \\ &= \mathbf{b}(u_{s+1}, u_{s+2}, \ldots, u_{s+k}) \\ &= \mathbf{b}(\widehat{u}_{s+2}, \widehat{u}_{s+3}, \ldots, \widehat{u}_{s+k+1}). \end{aligned}$$

It remains to consider the case where $s-k < i \le s$. Let

$$\alpha \;=\; \frac{u_{i+k} - \widehat{u}}{u_{i+k} - u_i} \qquad \text{and} \qquad \beta \;=\; \frac{\widehat{u} - u_i}{u_{i+k} - u_i}.$$

Then, by the definition of $\widehat{\mathbf{p}}_i$ and since $i \le s < i+k$,

$$\begin{aligned} \widehat{\mathbf{p}}_i &= \alpha\mathbf{p}_{i-1} + \beta\mathbf{p}_i \\ &= \alpha\mathbf{b}(u_i, u_{i+1}, \ldots, u_{i+k-1}) + \beta\mathbf{b}(u_{i+1}, u_{i+2}, \ldots, u_{i+k}) \\ &= \mathbf{b}(u_{i+1}, u_{i+2}, \ldots, u_s, \widehat{u}, u_{s+1}, \ldots, u_{i+k-1}) \\ &= \mathbf{b}(\widehat{u}_{i+1}, \widehat{u}_{i+2}, \ldots, \widehat{u}_{i+k}). \end{aligned}$$

The third equality above is justified by the symmetric and multiaffine properties of the blossom and the fact that $\alpha + \beta = 1$ and that $\alpha u_i + \beta u_{i+k} = \widehat{u}$. □

Exercise IX.11. In Exercise VIII.17 on page 300, a half circle is expressed as a quadratic rational Bézier curve. Rewrite this as a degree two rational B-spline with knot vector $[0,0,0,1,1,1]$. Insert $u = \frac{1}{2}$ as a new knot position. What are the new control points? Graph the curve and its new control polygon. Compare to Figure IX.19 on page 366.

Exercise IX.12* Prove that B-spline curves satisfy the variation diminishing property. [Hint: Combine the ideas of Exercise VIII.42 with the fact that repeatedly inserting knots in the correct sequence can make the control polygon approximate the B-spline curve arbitrarily well.]

IX.9 Bézier and B-spline curves

We now discuss methods for translating between Bézier curves and B-spline curves. These methods are degree preserving in that they will transform a degree k Bézier curve into a degree k B-spline, and vice-versa. Of course, there is a bit of a mismatch: a Bézier curve consists of a single degree k curve, specified by $k+1$ control points whereas a B-spline curve consists of a series of pieces, each piece a degree k polynomial. Accordingly, the translation between B-spline curves and Bézier curves will transform a series of degree k pieces that join together to make a single curve. Such a series of curve pieces can be viewed as either a single B-spline curve or as a collection of Bézier curves.

From Bézier curves to B-spline curves

First, we consider the problem of converting a single Bézier curve into a B-spline curve. Suppose we have a degree three Bézier curve $\mathbf{q}(u)$ defined with control points $\mathbf{p}_0, \mathbf{p}_1, \mathbf{p}_2, \mathbf{p}_3$, defined over the range $0 \le u \le 1$. In order to construct a definition of this curve as a B-spline curve with the same control points, we let $[0,0,0,0,1,1,1,1]$ be the knot vector and keep the control points as $\mathbf{p}_0, \mathbf{p}_1, \mathbf{p}_2, \mathbf{p}_3$. It can be verified by direct computation that the B-spline curve is in fact the same curve $\mathbf{q}(u)$ as the Bézier curve (see pages 336-338). In fact, we have the following general theorem.

Theorem IX.17. *Let $k \ge 1$ and $\mathbf{q}(u)$ be a degree k Bézier curve defined by control points $\mathbf{p}_0, \ldots, \mathbf{p}_k$. Then $\mathbf{q}(u)$ is identical to the degree k B-spline curve defined with the same control points over the knot vector consisting of the knot 0 with multiplicity $k+1$ followed by the knot 1 also with multiplicity $k+1$.*

In order to prove this theorem, let $N_{i,k+1}(u)$ be the basis functions for the B-spline with the knot vector $[0,\ldots,0,1,\ldots,1]$ containing $2k+2$ many knots. Then we claim that

$$N_{i,k+1}(u) \;=\; \binom{k}{i} u^i (1-u)^{k-i}. \qquad \text{(IX.33)}$$

The righthand side of this equation is just the same as the Bernstein polynomials used to define Bézier curves, so the theorem follows immediately from Equation (IX.33). Equation (IX.33) is easy to prove by induction on k, and we leave the proof to the reader. □

The most useful cases of the previous theorem are when $k=2$ and $k=3$. As we saw in Section VIII.13, the $k=2$ case is frequently used for defining conic sections, including circles, via Bézier curves. In the $k=2$ case, a degree two Bézier curve with the three control points $\mathbf{p}_0, \mathbf{p}_1, \mathbf{p}_2$ is equivalent to the degree two B-spline curve with the same three control points and with knot vector $[0,0,0,1,1,1]$.

Often one wants to combine two or more Bézier curves into a single B-spline curve. For instance, suppose one has degree two Bézier curves $\mathbf{q}_0(u)$ and $\mathbf{q}_1(u)$

defined with control points $\mathbf{p}_0, \mathbf{p}_1, \mathbf{p}_2$ and $\mathbf{p}'_0, \mathbf{p}'_1, \mathbf{p}'_2$. We wish to combine these curves into a single curve $\mathbf{q}(u)$ that consists of $\mathbf{q}_1(u)$ followed by $\mathbf{q}_2(u)$. That is, $\mathbf{q}(u) = \mathbf{q}_1(u)$ for $0 \le u \le 1$, and $\mathbf{q}(u) = \mathbf{q}_2(u-1)$ for $1 \le u \le 2$. By Theorem IX.17, $\mathbf{q}(u)$ is equivalent to the degree two B-spline curve with knot vector $[0,0,0,1,1,1,2,2,2]$ and with the six control points $\mathbf{p}_0, \ldots, \mathbf{p}'_2$. However, usually the two Bézier curves form a single continuous curve, i.e., $\mathbf{p}_2 = \mathbf{p}'_0$. In this case, $\mathbf{q}(u)$ is the same as the B-spline curve with knot vector $[0,0,0,1,1,2,2,2]$ and with five control points $\mathbf{p}_0, \mathbf{p}_1, \mathbf{p}_2, \mathbf{p}'_1, \mathbf{p}'_2$. Note that one knot position and the duplicate control point have been omitted. The fact that this construction works is proved by the calculation in the next exercise.

Exercise IX.13. Calculate the degree two blending functions for the knot vector $[0,0,0,1,1,2,2,2]$. Show that the results are the degree two Bernstein polynomials on the interval $[0,1$, followed by the same degree two Bernstein polynomials translated to the interval $[1,2]$. Conclude that a quadratic B-spline formed with this knot vector and control points $\mathbf{p}_0, \mathbf{p}_1, \mathbf{p}_2, \mathbf{p}_3, \mathbf{p}_4$ will be the concatenation of the two quadratic Bézier curves with control points $\mathbf{p}_0, \mathbf{p}_1, \mathbf{p}_2$ and with control points $\mathbf{p}_2, \mathbf{p}_3, \mathbf{p}_4$.

The construction in this exercise can be generalized in several ways. First, if one has three degree two Bézier curves which form a single continuous curve, then they are equivalent to a degree two B-spline curve with knot vector $[0,0,0,1,1,2,2,3,3,3]$. This generalizes to allow a continuous curve that consists of any number of quadratic Bézier curves to be expressed as a single B-spline curve. Second, the construction generalizes to other degrees: for instance, a continuous curve which consists of two degree three Bézier curves is the same as the degree three B-spline curve that has knot vector $[0,0,0,0,1,1,1,2,2,2,2]$ and has the same seven points as its control points. We leave the proofs of these statements to the reader.

Exercise IX.14. Prove that the de Casteljau algorithm for a Bézier curve is the same as the de Boor algorithm for the equivalent B-spline curve.

From B-spline curve to piecewise Bézier curve

We now discuss how to convert a general B-spline curve into constituent Bézier curves. A priori, it is always possible to convert a degree k B-spline curve into a series of degree k Bézier curves, merely because the B-spline curve is piecewise polynomials of degree k and since any finite segment of a degree k polynomial can be represented as a degree k Bézier curve (see Exercise VIII.8).

Here is an algorithm to convert a B-spline curve into multiple Bézier pieces: use repeated knot insertion to insert multiple occurrences of the knots until the first and last knots have multiplicity $k+1$ and each interior knot has multiplicity k. By the discussion about combining multiple Bézier curves into a B-spline curve, this means that the control points of the resulting B-spline curve (that is to say, the control points that result from the knot insertion) are also the control points for Bézier curves between the knot positions.

IX.10 Degree elevation

Section VIII.9 discussed degree elevation for Bézier curves. Degree elevation can also be applied to B-spline curves. In analogy to the situation with Bézier curves, suppose we are given a degree k B-spline curve $\mathbf{q}(u)$ and wish to find a way to describe the (same) curve as a degree $k+1$ B-spline curve.

The first thing to notice is that if a knot u has multiplicity μ in the degree k curve, then $\mathbf{q}(u)$ has continuous $(k-\mu)$-th derivative at u (by Theorem IX.2), but may well not have continuous $(k-\mu+1)$-th derivative at u. Thus, in order to represent $\mathbf{q}(u)$ as a degree $k+1$ curve, it is necessary for the knot position u to have multiplicity $\mu+1$. In other words, to elevate the degree of a curve, it will generally be necessary to increase the multiplicity of all the knots by one.

Because of the need to add so many (duplicate) knot positions, the algorithms for degree elevation are not particularly simple. We shall not cover them, but instead refer the reader to Farin [42] or Piegl-Tiller [90] for algorithms and references for other algorithms. Piegl and Tiller suggest the following algorithm: first, use knot insertion or knot refinement to make all knots multiplicity k in order to convert the curve into degree k Bézier curve segments; second, use the degree elevation algorithm for Bézier curves; and then, third, reduce the knot multiplicities by a process called "knot elimination." There are also other algorithms available which do not need to add excess knots, for example, based on blossoms.

IX.11 Rational B-splines and NURBS

A B-spline curve is called a *rational curve* if its control points are specified with homogeneous coordinates. These curves are sometimes called "NURBS," an acronym for "nonuniform, rational B-splines."

Rational Bézier curves were already discussed earlier in Sections VIII.12 and VIII.13; much of what was said about rational Bézier curves also applies to rational B-splines. A rational B-spline has 4-tuples $\langle x, y, z, w\rangle$ as control points; the curve's values $\mathbf{q}(u)$ are expressed as weighted averages of the control points,

$$\mathbf{q}(u) \;=\; \sum\nolimits_i N_{i,m}(u)\mathbf{p}_i,$$

so $\mathbf{q}(u)$ represents the points on the curve in homogeneous coordinates.

As with rational Bézier curves, the w component of a control point acts as a weight factor: a control point $\langle w\mathbf{p}_i, w\rangle$ weights the point $\mathbf{p}_i$ by a factor of w. This is illustrated in Figure IX.17. Also like rational Bézier curves, rational B-splines are preserved under perspective transformations and may have control points at infinity.

Section VIII.13 constructed Bézier curves that traced out a semicircle or, more generally, a portion of a conic section. B-splines can do better, in that a single B-spline can define an entire circle or an entire conic section. This is done by patching together several quadratic Bézier curves to form a quadratic

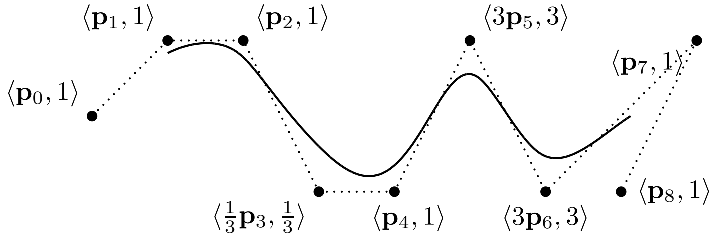
$\langle \mathbf{p}_1, 1\rangle$
$\langle \mathbf{p}_2, 1\rangle$
$\langle 3\mathbf{p}_5, 3\rangle$
$\langle \mathbf{p}_7, 1\rangle$
$\langle \mathbf{p}_0, 1\rangle$
$\langle \frac{1}{3}\mathbf{p}_3, \frac{1}{3}\rangle$
$\langle \mathbf{p}_4, 1\rangle$
$\langle 3\mathbf{p}_6, 3\rangle$
$\langle \mathbf{p}_8, 1\rangle$

Figure IX.17: A degree three, rational B-spline curve. The control points are the same as in Figure IX.1 on page 327, but now the control point $\mathbf{p}_3$ is weighted only $1/3$, and the two control points $\mathbf{p}_5$ and $\mathbf{p}_6$ are weighted 3. All other control points have weight 1. In comparison with the curve of Figure IX.1(b), this curve more closely approaches $\mathbf{p}_5$ and $\mathbf{p}_6$, but does not approach $\mathbf{p}_3$ as closely.

B-spline curve which traces out an entire circle or conic section. As was shown above in Section IX.9, two quadratic Bézier curves may be patched together into a single B-spline curve by using the knot vector $[0,0,0,1,1,2,2,2]$. Similarly, three quadratic Bézier curves can be combined into a single B-spline curve using the knot vector $[0,0,0,1,1,2,2,3,3,3]$; and a similar construction works for combining four Bézier curves into a single B-spline curve, etc. As an example, Theorem VIII.14 on page 300 implies that if we use the knot vector $[0,0,0,1,1,2,2,2]$ and the control points

$$\begin{aligned} \mathbf{p}_0 &= \langle 0,1,1\rangle & \qquad \mathbf{p}_3 &= \langle -1,0,0\rangle \\ \mathbf{p}_1 &= \langle 1,0,0\rangle & \qquad \mathbf{p}_4 &= \mathbf{p}_0, \\ \mathbf{p}_2 &= \langle 0,-1,1\rangle & & \end{aligned}$$

then the resulting B-spline will trace out the unit circle.

Similar constructions also give the unit circle as a B-spline consisting of either three or four Bézier segments, without using control points at infinity. These are based on the results from Exercises VIII.13 and VIII.14 and are pictured in Figure IX.18. Compare to Figure VIII.19 on page 303.

Another well-known construction of the unit circle by a degree two B-spline curve is shown in Figure IX.19; we leave the proof of its correctness to the reader (see Exercise IX.11 on page 361).

IX.12 Interpolating with B-splines

Frequently, one wishes to define a smooth curve that interpolates (i.e., passes through, or contains) a given set of points. Chapter VIII explained ways of forming interpolating curves using the Catmull-Rom and Overhauser splines, which consisted of piecewise Bézier curves. The Catmull-Rom and Overhauser curves are C^1-continuous, but generally do not have continuous second derivatives. On the other hand, we know (see Section IX.4) that degree

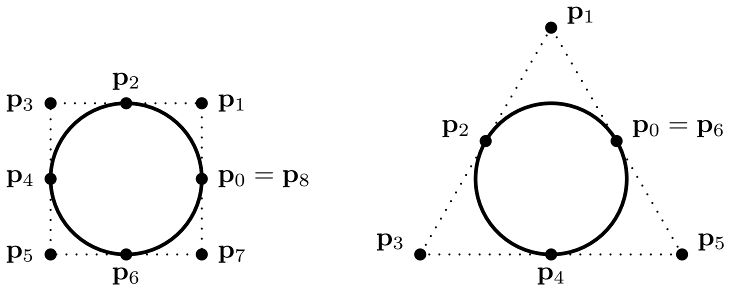

Figure IX.18: Two ways to form a complete circle with a quadratic B-spline curve. The first curve has knot vector $[0, 0, 0, 1, 1, 2, 2, 3, 3, 4, 4, 4]$ and the control points $\mathbf{p}_i$ have weight 1 when i is even and weight $\frac{\sqrt{2}}{2}$ when i is odd. The second curve has knot vector $[0, 0, 0, 1, 1, 2, 2, 3, 3, 3]$ and the control points $\mathbf{p}_i$ have weight 1 when i is even and weight $\frac{1}{2}$ when i is odd.

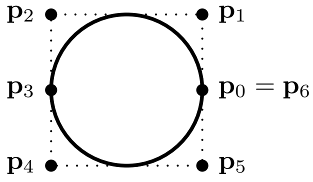

Figure IX.19: Another way to form a complete circle with a quadratic B-spline curve. The curve has knot vector $[0, 0, 0, 1, 2, 2, 3, 4, 4, 4]$ and the control points $\mathbf{p}_0$, $\mathbf{p}_3$, and $\mathbf{p}_6$ have weight 1, and the other control points $\mathbf{p}_1$, $\mathbf{p}_2$, $\mathbf{p}_4$, and $\mathbf{p}_5$ have weight $\frac{1}{2}$. Exercise IX.11 on page 361 shows a way to prove the correctness of this B-spline curve.

three splines can have continuous second derivatives, provided the knots have multiplicity one. Thus, we might hope to get better, smoother curves by using B-splines to interpolate a set of points.

Unfortunately, the B-spline curves that have been defined so far are not particularly convenient for this purpose; they have been defined from control points, and the control points merely influence the curve and usually are not interpolated, so the control points usually do not lie on the curve. When control points are interpolated, it is generally because of repeated knot values, but then the curve loses its good smoothness properties and may even have discontinuous first derivatives.

Our strategy for constructing interpolating B-spline curves with good smoothness properties will be to first choose knot positions and then solve for control points that will make the B-spline curve interpolate the desired points. The algorithm for finding the control points will be based on solving a system of linear equations. The linear equations will be tridiagonal, and thus easily solved.

Consider the following problem. We are given points $\mathbf{q}_0, \mathbf{q}_1, \mathbf{q}_2, \ldots, \mathbf{q}_n$, and positions $u_0, u_1, u_2, \ldots, u_n$, with $u_i < u_{i+1}$ for all i. The problem is to find a degree three B-spline curve $\mathbf{q}(u)$ so that $\mathbf{q}(u_i) = \mathbf{q}_i$ for all i. This still leaves too many possibilities, so we further make the rather arbitrary assumption that the B-spline curve is to be formed with the standard knot vector

$$[u_0, u_0, u_0, u_0, u_1, u_2, u_3, \ldots, u_{n-2}, u_{n-1}, u_n, u_n, u_n, u_n],$$

where the first and last knots have multiplicity 4 and the rest of the knots have multiplicity 1. (Refer to Exercises IX.6 and IX.7 for a qualitative understanding of the blending functions that are defined from this knot vector.) Note that there are $n+7$ knot positions, so there must be $n+3$ control points. The conditions are still not strong enough to fully determine the B-spline, as there are only $n+1$ conditions $\mathbf{q}(u_i) = \mathbf{q}_i$, but there are $n+3$ control points to be determined. Therefore, we make one more arbitrary assumption: namely, that the first derivative of $\mathbf{q}(u)$ at u_0 and at u_n is equal to zero. This means that the first two control points must be equal so that $\mathbf{q}'(u_0) = 0$, and the last two control points must be equal so that $\mathbf{q}'(u_n) = 0$.

The control points can thus be denoted

$$\mathbf{p}_0, \mathbf{p}_0, \mathbf{p}_1, \mathbf{p}_2, \ldots, \mathbf{p}_{n-2}, \mathbf{p}_{n-1}, \mathbf{p}_n, \mathbf{p}_n.$$

The equation for the curve $\mathbf{q}(u)$ based on these knot positions and control points is

$$\mathbf{q}(u) \;=\; (N_{0,4}(u) + N_{1,4}(u))\mathbf{p}_0 + \sum_{i=1}^{n-1} N_{i+1,4}(u)\mathbf{p}_i + (N_{n+1,4}(u) + N_{n+2,4}(u))\mathbf{p}_n.$$

Since the first and last knots have multiplicity 4, we have

$$\mathbf{q}(u_0) \;=\; \mathbf{p}_0 \qquad \text{and} \qquad \mathbf{q}(u_n) \;=\; \mathbf{p}_n,$$

and thus need $\mathbf{p}_0 = \mathbf{q}_0$ and $\mathbf{p}_n = \mathbf{q}_n$. Theorem IX.1 and the fact that the blending functions are continuous tell us where these blending functions are nonzero, so we have, for $1 \le i \le n-1$,

$$\mathbf{q}(u_i) \;=\; N_{i,4}(u_i)\mathbf{p}_{i-1} + N_{i+1,4}(u_i)\mathbf{p}_i + N_{i+2,4}(u_i)\mathbf{p}_{i+1}.$$

Of course, we want this value to equal $\mathbf{q}_i$. Letting $\alpha_i = N_{i,4}(u_i)$, $\beta_i = N_{i+1,4}(u_i)$, and $\gamma_i = N_{i+2,4}(u_i)$, this means we want

$$\mathbf{q}_i \;=\; \alpha_i \mathbf{p}_{i-1} + \beta_i \mathbf{p}_i + \gamma_i \mathbf{p}_{i+1}.$$

We can write the desired conditions as a single matrix equation:

$$\begin{pmatrix} 1 & 0 & 0 & \cdots & & \cdots & 0 \\ \alpha_1 & \beta_1 & \gamma_1 & 0 & \cdots & & \vdots \\ 0 & \alpha_2 & \beta_2 & \gamma_2 & 0 & \cdots & \\ 0 & 0 & \alpha_3 & \beta_3 & \gamma_3 & 0 & \cdots \\ \vdots & & & \ddots & \ddots & \ddots & \\ & & \cdots & 0 & \alpha_{n-1} & \beta_{n-1} & \gamma_{n-1} \\ 0 & & & \cdots & 0 & 0 & 1 \end{pmatrix} \begin{pmatrix} \mathbf{p}_0 \\ \mathbf{p}_1 \\ \mathbf{p}_2 \\ \mathbf{p}_3 \\ \vdots \\ \mathbf{p}_{n-1} \\ \mathbf{p}_n \end{pmatrix} = \begin{pmatrix} \mathbf{q}_0 \\ \mathbf{q}_1 \\ \mathbf{q}_2 \\ \mathbf{q}_3 \\ \vdots \\ \mathbf{q}_{n-1} \\ \mathbf{q}_n \end{pmatrix}.$$

We need to solve this matrix equation to find values for the control points $\mathbf{p}_i$. Since the matrix equation is tridiagonal, it is particularly easy to solve for the $\mathbf{p}_i$'s. The algorithm which calculates the $\mathbf{p}_i$'s uses two passes: first, we transform the matrix into an upper diagonal matrix by subtracting a multiple of the i-th row from the $(i+1)$-st row, for $i = 1, 2, \ldots, n-1$. This makes the matrix upper diagonal, and in the form

$$\begin{pmatrix} 1 & 0 & 0 & \cdots & & \cdots & 0 \\ 0 & \beta'_1 & \gamma_1 & 0 & \cdots & & \vdots \\ 0 & 0 & \beta'_2 & \gamma_2 & 0 & \cdots & \\ 0 & 0 & 0 & \beta'_3 & \gamma_3 & 0 & \cdots \\ \vdots & & & \ddots & \ddots & \ddots & \\ & & \cdots & 0 & 0 & \beta'_{n-1} & \gamma_{n-1} \\ 0 & & & \cdots & 0 & 0 & 1 \end{pmatrix} \begin{pmatrix} \mathbf{p}_0 \\ \mathbf{p}_1 \\ \mathbf{p}_2 \\ \mathbf{p}_3 \\ \vdots \\ \mathbf{p}_{n-1} \\ \mathbf{p}_n \end{pmatrix} = \begin{pmatrix} \mathbf{q}'_0 \\ \mathbf{q}'_1 \\ \mathbf{q}'_2 \\ \mathbf{q}'_3 \\ \vdots \\ \mathbf{q}'_{n-1} \\ \mathbf{q}'_n \end{pmatrix}.$$

Second, we can easily solve the upper diagonal matrix by setting $\mathbf{p}_n = \mathbf{q}'_n$ and $\mathbf{p}_i = (\mathbf{q}'_i - \gamma_i \mathbf{p}_{i+1})/\beta'_i$, for $i = n-1, n-2, \ldots, 0$.

The complete algorithm for calculating the $\mathbf{p}_i$'s is as follows:

```
// Pass One
Set $\beta'_0$ = 1;
Set $\gamma_0$ = 0;
Set $\mathbf{q}'_0$ = $\mathbf{q}_0$ ;
For $i$ = 1 , 2 , ..., $n-1$ {
    Set $m_i$ = $\alpha_i/\beta'_{i-1}$ ;
    Set $\beta'_i$ = $\beta_i - m_i\gamma_{i-1}$ ;
    Set $\mathbf{q}'_i$ = $\mathbf{q}_i - m_i\mathbf{q}'_{i-1}$ ;
}
Set $\mathbf{q}'_n$ = $\mathbf{q}_n$ ;
// Pass two
Set $\mathbf{p}_n$ = $\mathbf{q}'_n$ ;        // Same as $\mathbf{q}_n$ .
For $i$ = $n-1$ , $n-2$ , ..., 2 , 1 {
    Set $\mathbf{p}_i$ = $(\mathbf{q}'_i - \gamma_i\mathbf{p}_{i+1})/\beta'_i$ ;
}
```

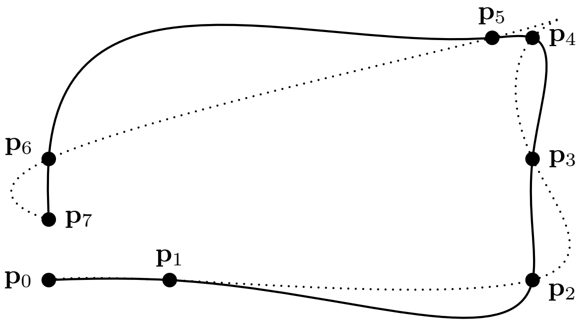

Figure IX.20: Degree three B-spline interpolating the points $\mathbf{p}_0, \ldots, \mathbf{p}_7$. The dotted curve uses uniform knot spacing. The solid curve uses chord-length parameterization. It is clear that chord-length parameterization gives much better results. The interpolation points are the same as used for the interpolating Catmull-Rom and Overhauser splines shown in Figures VIII.24 and VIII.25 on pages 311 and 313.

```
Set $\mathbf{p}_0$ = $\mathbf{q}_0'$;        // Same as $\mathbf{q}_0$.
```

It should be noted that the algorithm is only linear time, i.e., has runtime $O(n)$. This is possible because the matrix is in tridiagonal form. For general matrices, matrix inversion is much more difficult.

The B-spline interpolating curve does not enjoy local control properties: moving a single interpolation point $\mathbf{q}_i$ can affect the curve along its entire length. However, in usual cases, moving a control point has only a small effect on distant parts of the B-spline.

Figure IX.20 shows an example of an interpolating B-spline, and can be compared to the earlier examples of interpolating Catmull-Rom and Overhauser splines. The figure shows two curves. The dotted curve is based on uniformly spaced values for u_i, with $u_i = i$. The solid curve uses *chord-length parameterization*, with the values u_i chosen so that $u_i - u_{i-1} = ||\mathbf{p}_i - \mathbf{p}_{i-1}||$. The curves in Figure IX.20 should be compared with the Catmull-Rom and Overhauser splines shown in Figures VIII.24 and VIII.25. The Catmull-Rom and Overhauser splines were only C^1-continuous, whereas the interpolating B-splines of Figure IX.20 are C^2-continuous. It is evident that, just like the Overhauser splines, B-spline interpolation can benefit from the use of chord-length parameterization.

IX.13 Additional exercises

Exercise IX.15. Prove that every multiaffine function $h(x_1, \ldots, x_k)$ can be expressed in the form (IX.18). [Hint: Use induction on k. For the induction step, start by using the multiaffine property to prove that $h(x_1, \ldots, x_k)$ is equal to $x_k \cdot f(x_1, \ldots, x_{k-1}) + g(x_1, \ldots, x_{k-1})$ where f and g are multiaffine functions of $k-1$ variables.]

Exercise IX.16. Let $h(x) = 3x^2 + 4x + 5$. What is the degree 2 blossom of h? What is the degree 3 blossom of h? What is the degree 4 blossom of h?

Exercise IX.17. Let $h(x) = 2x^3 + 6x + 1$. What is the degree 3 blossom of h? What is the degree 4 blossom of h?

Exercise IX.18$^\bigstar$ Let $h(x) = x^3$. Prove that h does not have a degree 2 blossom.

Exercise IX.19. Let $\mathbf{q}(u)$ be the curve defined on the interval $[0, 2]$ by

$$\mathbf{q}(u) \;=\; \begin{cases} u^2 & \text{if } 0 \le u \le 1 \\ 4u - u^2 - 2 & \text{if } 1 < u \le 2 \end{cases}$$

(a) Verify that $\mathbf{q}(u)$ is C^1-continuous.

(b) We wish to express $\mathbf{q}(u)$ as a degree 2 B-spline curve with knot vector $[0, 0, 0, 1, 2, 2, 2]$. This requires finding four control points $\mathbf{p}_0, \mathbf{p}_1, \mathbf{p}_2, \mathbf{p}_3$. Use the method of blossoms on the interval $[0, 1]$ to determine $\mathbf{p}_0$, $\mathbf{p}_1$ and $\mathbf{p}_2$.

(c) Use the method of blossoms on the interval $[0, 2]$ to determine $\mathbf{p}_1$, $\mathbf{p}_2$ and $\mathbf{p}_3$. Your answers for $\mathbf{p}_1$ and $\mathbf{p}_2$ should agree with your answers in part (b).

(d) Express the derivative $\mathbf{q}'(u)$ of $\mathbf{q}(u)$ as a degree 1 B-spline curve. What is the domain of $\mathbf{q}'(u)$? What is the knot vector for $\mathbf{q}'(u)$? What are the control points for $\mathbf{q}'(u)$?

Chapter X

Ray Tracing

This is a ***preliminary*** *draft of a second edition of the book* 3-D Computer Graphics: A Mathematical Introduction with OpenGL. *So please read it cautiously and critically! Corrections are appreciated. Draft C.4.a*

Author: Sam Buss, sbuss@ucsd.edu

Ray tracing is a technique which performs, by a single unified technique, global calculations of lighting and shading, hidden surface elimination, reflection and transmission of light, casting of shadows, and other effects. As such, it extends significantly the local lighting models, such as the Phong and Cook-Torrance lighting models from Chapter IV. It also eliminates the use of a depth buffer for hidden surface determination. In addition, it allows for many special effects and can create images that are more realistic looking than what can easily be obtained by the methods we have discussed so far.

With all these advantages, ray tracing sounds too wonderful to be true; however, it has the big disadvantage of being computationally very expensive. Indeed, a single ray traced image may take minutes, hours, or occasionally even days to render. For example, modern computer-animated movies routinely use ray tracing to render scenes; it is not unusual for an *average* frame of a movie to require an hour of computation time to render, and individual frames might require 10 hours or more to render. A quick calculation shows that this means that a movie with 24 frames per second, lasting for 100 minutes, may require 6,000 CPU days to render, which is over 16 CPU years! It is fortunate that individual frames can be independently ray traced in parallel, and it is common for animated movies to be developed with the aid of hundreds of computers dedicated to rendering images. In spite of the high computational costs of ray tracing, it has become a widely used technique for generating high quality and photorealistic images, especially since computers are becoming cheaper and faster, and since ray tracing techniques are becoming more sophisticated.

The basic idea behind ray tracing is to follow the paths of light rays around a 3-D scene. Typically one follows the light rays' paths from the position of the viewer back to their source. When light rays hit objects in the 3-D scene, one computes the reflection direction for the light ray, and continues to follow the light ray in the reflection direction. Continuing this process, perhaps through multiple reflections (and/or transmissions through transparent media), one can trace the path of a light ray from its origination at a light source until it reaches the view position.

Ray tracing is generally combined with a local lighting model such as the Phong model or the Cook-Torrance model, but adds many global lighting effects that cannot be achieved with just these local lighting models. The global lighting phenomena that can be obtained with basic ray tracing include:

- Reflections — glossy or mirror-like reflections.
- Shadows — sharp shadows cast by lights.
- Transparency and refraction.

The basic form of ray tracing is covered in Section X.1. That section discusses the way rays are traced backwards from the view position to the light sources. It also discusses the mathematical models for transmission of light through semi-transparent materials. The basic ray tracing method can generate effects such as reflection, transparency, refraction, and shadows.

There are many more advanced models of ray tracing. Many of these go under the name of "distributed ray tracing," and involve tracing a multiplicity of rays. Applications of distributed ray tracing include anti-aliasing, depth of field, motion blur, and simulation of diffuse lighting. Distributed ray tracing is covered in Section X.2.1. Section X.2.2 covers the so-called "backwards" ray tracing, where light rays are traced starting from the positions of the lights.

OpenGL does not support ray tracing, so it is necessary to use custom code (such as the ray tracing code provided with this book) to perform all the rendering calculations from scratch. However, there are a variety of tricks, or "cheats," that can be used in OpenGL to give similar effects to ray tracing with substantially less computation. Some of these are surveyed in Section X.3.

Appendix **??** covers the features of a ray tracing software package developed for this book. The software package is freely available from the internet and may be used without restriction.

Radiosity is another global lighting method, which is complementary in many ways to ray tracing. Whereas ray tracing is good at handling specular lighting effects and less good at handling special diffuse lighting effects; radiosity is very good at diffuse lighting effects, but does not handle specularity. Radiosity will be covered later in Chapter XII.

X.1 Basic ray tracing

The basic idea behind ray tracing is to follow the paths taken by rays of light, or photons, as they travel from the light sources until they eventually reach the viewer's eye position. Of course, most light rays never reach the eye position at all, but instead either leave the scene or are absorbed into a material. Thus, from a computational point of view, it makes more sense to trace the paths traveled by rays of light from the eye, going backwards until eventually they reach a light source, since, in this way, we do not waste time on tracing rays that do not ever reach the viewer.[1]

The simplest kind of ray tracing is illustrated in Figure X.1. The figure shows, first, a 3-D scene containing two boxes and a sphere (which are represented by two rectangles and a circle); second, a single light source; and, third, a viewer. The viewer is looking at the scene through a virtual viewport rectangle, and our task is to render the scene as seen through the viewport. In order to determine the color of a pixel P in the viewport, a ray is sent from the eye through the center of the pixel, and then we determine the first point of intersection of the ray with the objects in the scene. In the figure, the ray would intersect both the lower rectangle and the circle. However, it intersects the rectangle first, so this is what is seen through the pixel. The point on the rectangle is shaded (colored) according to a local lighting model such as the Phong model, and the result is the contents of the pixel P.

In the simple form described so far, ray tracing would not achieve any new visual effects beyond what is already obtainable by a local lighting model and the depth buffer hidden surface algorithm. Indeed, so far all that has changed is that the depth buffer method of culling hidden surfaces has been replaced by a ray tracing method for determining visible surfaces. More interesting effects are obtained with ray tracing as we add reflection rays, transmission rays, and shadow feelers.

Shadow feelers

A *shadow feeler* is a ray sent from a point $\mathbf{u}$ on the surface of an object towards a light source to determine whether the light is visible from the point $\mathbf{u}$ or whether it is occluded by intervening objects. As you will recall from Chapter IV, the local lighting models (Phong or Cook-Torrance) do not form any shadows; instead, they assume that every light is visible at all times, and that there are no objects blocking the light and creating shadows. Examples of shadow feelers are shown in Figure X.2: four rays are traced from the eye, through the centers of four pixels in the viewport (not shown), until they hit points in the scene. From each of these four points, a ray, called a shadow feeler, is traced from the point to the light source. If the shadow feeler hits an object before reaching the light, then the light is presumed to be occluded by the object, so that the point is in a shadow and is not directly lit by the light. In the figure, two of the shadow feelers find intersections; these rays are marked with an "**X**" to show they are blocked. In one case, a point on the box surface

[1] In a confusing twist of terminology, the process of following rays from the eye position back to their point of origin from a light is sometimes called *forward ray tracing*, whereas, tracing paths from a light up to the viewpoint is called *backwards ray tracing.* To add to the confusion, many authors reverse the meaning of these terms. Section X.2.2 covers backwards ray tracing.

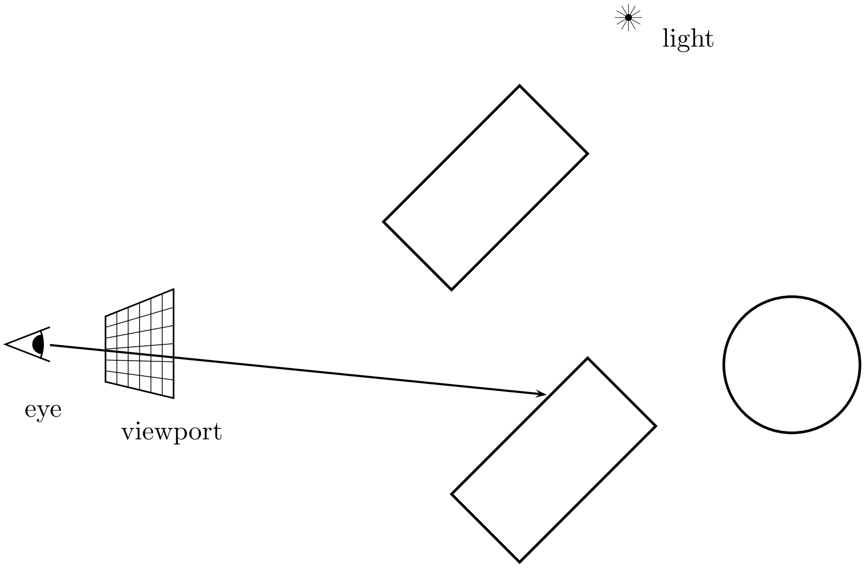

Figure X.1: The simplest kind of ray tracing, non-recursive ray tracing, involves casting rays of light from the view position through pixel positions. A local lighting model is used to calculate the illumination of the surface intersected by the ray.

is being shadowed by the box itself.

Reflection rays

What we have described so far accounts for light rays which originate from a point light, hit a surface, and then reflect from the surface to the eye. However, light can also travel more complicated paths, perhaps bouncing multiple times from surfaces before reaching the eye. This phenomenon can be partially simulated by adding reflection rays to the ray tracing algorithm. When a ray from the eye position hits a surface point, we generate a further *reflection ray* in the direction of perfect specular reflection. This reflection ray is handled similarly to the ray from the eye; namely, we find the first point where it hits an object in the scene, and calculate that point's illumination from all the light sources. This process can continue recursively, with reflection rays themselves spawning their own reflection rays.

This process is illustrated in Figure X.3, where a single ray from the eye hits an object, and from this point another ray is sent in the direction of perfect specular reflection. This second ray hits another object, then generates another reflection ray, etc.

Although it is not shown in Figure X.3, each time a ray hits an object, we

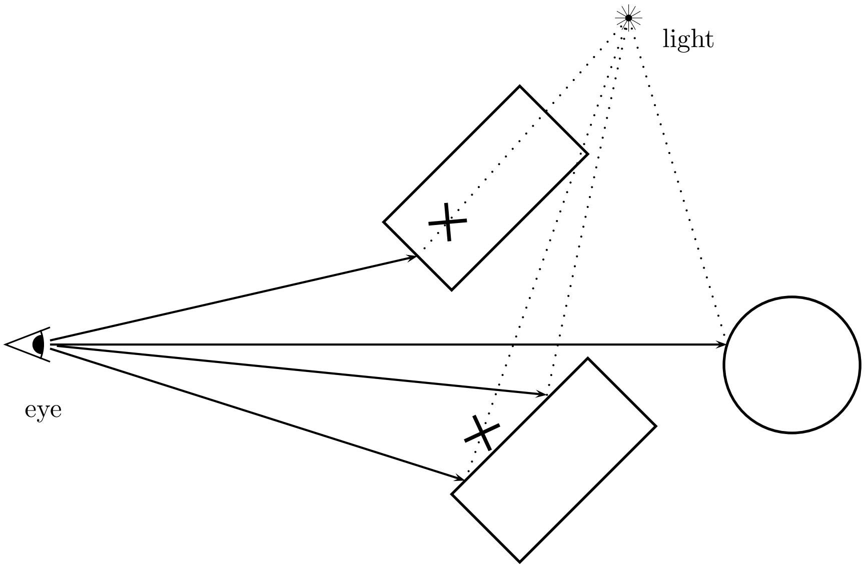

Figure X.2: Shadow feelers: Rays from the eye are traced to their intersections with objects in the scene. Shadow feeler rays, shown as dotted lines, are sent from the points in the scene to each light in order to determine whether the point is directly illuminated by the point light source or whether it is in a shadow. The two shadow feelers marked with an "**X**" show that the light is not directly visible from the point.

generate shadow feelers to all the light sources to determine which lights, if any, are illuminating the surface. In Figure X.3, the first and third points hit by the ray are directly illuminated by the light; the second point is not directly illuminated.

The purpose of tracing reflections is to determine the illumination of the point which is visible to the viewer (i.e., of the point hit by the ray from the eye through the pixel position). This is computed by a formula of the form

$$I \;=\; I_{\text{local}} \;+\; \rho_{rg} I_{\text{reflect}}. \tag{X.1}$$

Here, I_{local} is the lighting as computed by the local illumination model (Phong lighting, say), and I_{reflect} is the lighting of the point in the direction of the reflection ray. The scalar ρ_{rg} is a new material property: it is a factor specifying what fraction of the light from the reflection direction is reflected. Like the diffuse and specular material properties, the ρ_{rg} value is wavelength dependent, so there are separate reflection coefficients for red, green, and blue. The subscript "rg" stands for "reflection, global." The intensity of the incoming reflected light, I_{reflect}, is computed recursively by the same Equation (X.1).

Sections X.1.1 and X.1.3 give more details about how the local lighting is

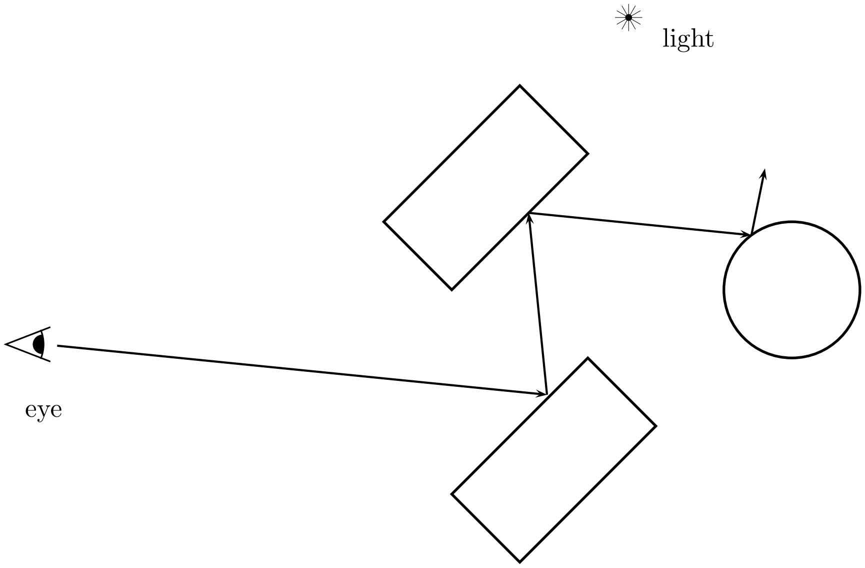

Figure X.3: Reflection rays: The path of the ray from the eye is traced through multiple reflections. This calculates approximations to the lighting effects of multiple reflections.

calculated, and about the recursive calculations.

Transmission rays

Ray tracing can also model transparency effects by using *transmission rays* in addition to reflection rays. Transmission rays can simulate *refraction*, the bending of light that occurs when light passes from one medium to another, for instance, from air into water.

A transmission ray is generated when a ray hits the surface of a transparent object: the transmission ray continues on through the surface. Refraction causes the direction of the transmitted ray to change. This change in direction is caused physically by the difference in the speed of light in the two media (air and water, for instance). The amount of refraction is calculated using the *index of refraction*, as discussed in Section X.1.2 below.

Transmitted rays are recursively traced in the same manner as reflected rays. Of course, the transmission rays may be inside an object, and their first intersection with the scene could be the boundary of an object hit from the inside. When the transmitted ray hits a point, it will again spawn a reflection ray and a transmission ray. This process continues recursively. Figure X.4 illustrates the generation of both reflection and transmission rays. In the figure, a single ray from the eye is traced through 3 bounces, spawning a total of twelve

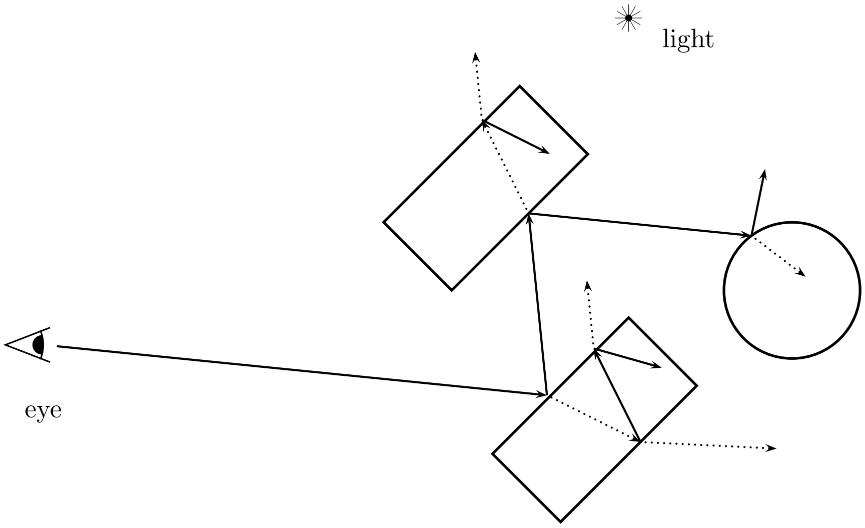

Figure X.4: Transmission and reflection rays: The path of the ray from the eye is traced through multiple reflections and transmissions. Reflection rays are shown as solid lines, transmission rays as dotted lines. The shadow feeler rays would still be used, but are not shown.

additional rays: the transmission rays are shown as dotted lines to distinguish them from reflection rays.

When transmission rays are used, the lighting formula has the form

$$I \;=\; I_{\text{local}} + \rho_{rg} I_{\text{reflect}} + \rho_{tg} I_{\text{xmit}}.$$

The new term $\rho_{tg} I_{\text{xmit}}$ includes the effect of recursively calculating the lighting in the transmission direction, scaled by the material property ρ_{tg}. The scalar ρ_{tg} is wavelength dependent and specifies the fraction of light which is transmitted through the surface. The subscript "tg" stand for "transmission, global."

X.1.1 Local lighting and reflection rays

We now give more details about the calculation of reflection rays and the lighting calculations for reflection rays. The basic setup is shown in Figure X.5, where we are tracing the path of a ray whose direction is determined by the vector $\mathbf{v}$. In keeping with our usual conventions that the vectors are pointing away from the point of intersection with the surface, the vector $\mathbf{v}$ is actually pointing in the opposite direction of the ray being traced. (The figure shows the traced ray as emanating from an eye position, but the ray could more generally emanate from another intersection point instead.) We assume $\mathbf{v}$ is a

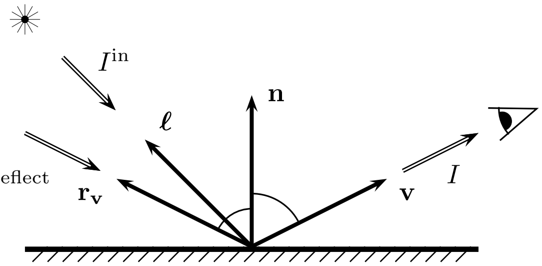

Figure X.5: The usual setup for reflection rays in basic recursive ray tracing. The vector $\mathbf{v}$ points in the direction opposite to the incoming ray. The direction of perfect reflection is shown by the vector $\mathbf{r_v}$. The vector $\boldsymbol{\ell}$ points to a point light source. I is the outgoing light intensity as seen from the direction given by $\mathbf{v}$. I_{reflect} is the incoming light from the reflection direction $\mathbf{r_v}$. I^{in} is the intensity of the light from the light source. (Compare this to Figure IV.8 on page 139.)

unit vector. Also, $\mathbf{n}$ is the unit vector normal to the surface at the point of intersection.

The direction of perfect reflection is shown as the vector $\mathbf{r_v}$. This is calculated according to the formula

$$\mathbf{r_v} \;=\; 2(\mathbf{v}\cdot\mathbf{n})\mathbf{n} - \mathbf{v}, \tag{X.2}$$

which is derived in the same way as the formula for the reflection vector in Section IV.1.2.[2]

The basic ray tracing algorithms depend on the use of a particular local lighting model: this would commonly be either the Phong lighting model or the Cook-Torrance lighting model; the discussion below will presume the use of the Phong lighting model (and it is straightforward to substitute the Cook-Torrance model in its place). The illumination of the point on the surface as seen from the ray trace direction $\mathbf{v}$ is given by the formula

$$I \;=\; I_{\text{local}} \;+\; \rho_{rg} I_{\text{reflect}}. \tag{X.3}$$

The I_{local} term is the lighting due to direct illumination by the lights which are visible from the intersection point.

For a given light i, let $\boldsymbol{\ell}_i$ be the unit vector in the direction of the light. Then let δ_i equal 1 if the light is above the surface and is directly illuminating the point as determined by a shadow feeler; otherwise, let δ_i equal 0. The value of δ_i is computed by checking whether the light is above the surface by

[2] The reflection vector is named $\mathbf{r_v}$ instead of $\mathbf{r}$ to avoid confusion with the reflection of the light vector $\boldsymbol{\ell}$ of Section IV.1.2.

checking whether $\boldsymbol{\ell}_i \cdot \mathbf{n} > 0$; if so, a shadow feeler is used to determine visibility of the light. The illumination due to the light i is defined as

$$I^i_{\text{local}} \;=\; \rho_{\text{a}} I^{\text{in},i}_{\text{a}} \;+\; \delta_i \cdot \Big(\rho_{\text{d}} I^{\text{in},i}_{\text{d}} (\boldsymbol{\ell}_i \cdot \mathbf{n}) + \rho_{\text{s}} I^{\text{in},i}_{\text{s}} (\mathbf{r}_{\mathbf{v}} \cdot \boldsymbol{\ell}_i)^f \Big). \qquad \text{(X.4)}$$

You should compare this to Equation (IV.7) on page 143. We are using here the notations $I^{\text{in},i}_{-}$ for the light coming from the i-th light. The term $\mathbf{r}\cdot\mathbf{v}$ has been replaced by $\mathbf{r}_{\mathbf{v}} \cdot \boldsymbol{\ell}_i$, which is clearly mathematically equivalent.

The net local lighting, due to all the lights which are above the surface, incorporating all the wavelengths, is obtained by summing the illumination from all the lights:

$$\mathbf{I}_{\text{local}} \;=\; \boldsymbol{\rho}_{\text{a}} * \mathbf{I}^{\text{in}}_{\text{a}} + \boldsymbol{\rho}_{\text{d}} * \sum_{i=1}^{k} \delta_i \mathbf{I}^{\text{in},i}_{\text{d}} (\boldsymbol{\ell}_i \cdot \mathbf{n}) + \boldsymbol{\rho}_{\text{s}} * \sum_{i=1}^{k} \delta_i \mathbf{I}^{\text{in},i}_{\text{s}} (\mathbf{r}_{\mathbf{v}} \cdot \boldsymbol{\ell}_i)^f + \mathbf{I}_{\text{e}},$$

which is similar to Equation (IV.10) on page 144. As before, the value $\boldsymbol{\rho}_{\text{a}}$, $\boldsymbol{\rho}_{\text{d}}$, $\boldsymbol{\rho}_{\text{s}}$ are tuples of coefficients, with one entry per color, and $*$ denotes component-wise product. The value of $\mathbf{I}^{\text{in}}_{\text{a}}$ is still given according to formula (IV.11).

The second term in Equation (X.3) contains the new material property ρ_{rg}: this coefficient is a scalar and can vary with wavelength (i.e., it is different for each color). The light intensity I_{reflect} is computed recursively by iterating the ray tracing algorithm.

X.1.2 Transmission rays

Now we turn to the details of how the ray tracing calculations work for transmission rays. First, we discuss how to compute the direction $\mathbf{t}$ of perfect transmission. The setup is shown in Figure X.6.

The direction of the transmission vector $\mathbf{t}$ is found using the incoming direction $\mathbf{v}$ and the surface normal $\mathbf{n}$, with the aid of Snell's law. Snell's law relates the angle of incidence with the angle of refraction by the formula

$$\frac{\sin\theta_v}{\sin\theta_t} \;=\; \eta.$$

Here, θ_v, the angle of incidence, is the angle between $\mathbf{v}$ and the normal $\mathbf{n}$; and θ_t, the angle of refraction, is the angle between the transmission direction $\mathbf{t}$ and the negated normal. The *index of refraction*, η, is the ratio of the speed of light in the medium above the surface (the side where $\mathbf{v}$ is) to the speed of light in the medium below the surface (where $\mathbf{t}$ is). Typical values for η are approximately equal to 1.3 for rays going from air to water, and approximately equal to 1.5 for rays going from air to glass. For the reverse direction, you need the reciprocal, so when traveling from water or glass to air, the index of refraction would be approximately $1/1.3$ or $1/1.5$. Snell's law can be derived from the wave model for light and can be found in many elementary physics books.

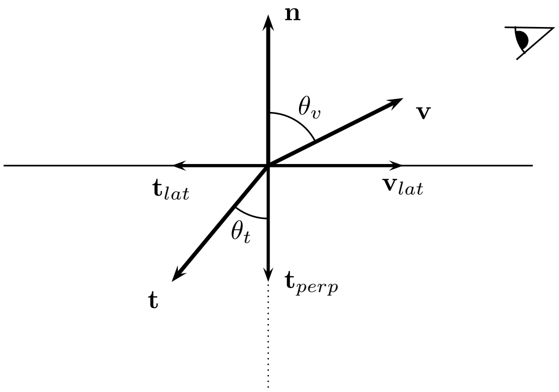

Figure X.6: Computing the transmission ray direction $\mathbf{t}$. The horizontal line represents the surface of a transmissive material; $\mathbf{n}$ is the unit vector normal to the surface. The vector $\mathbf{v}$ points in the direction opposite to the incoming ray. The direction of perfect transmission is shown by the vector $\mathbf{t}$. The vectors $\mathbf{v}_{lat}$ and $\mathbf{t}_{lat}$ are the projections of these vectors onto the plane tangent to the surface. And, $\mathbf{t}_{perp}$ is the projection of $\mathbf{t}$ onto the normal vector.

Snell's law can be rewritten as

$$\sin\theta_t \;=\; \eta^{-1}\sin\theta_v.$$

Now, if $\eta < 1$, it can happen that $\eta^{-1}\sin\theta_v$ is greater than 1. Of course in this case there is no possible angle θ_t which satisfies Snell's law. This corresponds to total internal reflection, where there is no transmission, only reflection. This happens only if $\eta < 1$, which is the case if light is traveling in a region of lower speed of light, e.g., inside a medium such as glass or water, and is exiting to a medium, such as air, with a higher speed of light. In addition, this happens only when the angle of incidence is sufficiently large, so that the quantity $\eta^{-1}\sin\theta_v$ is larger than 1.

We can derive a method of computing $\mathbf{t}$ from $\mathbf{n}$ and $\mathbf{v}$ as follows. Let $\mathbf{v}_{lat}$ be the component of $\mathbf{v}$ which is orthogonal to the normal vector, namely,

$$\mathbf{v}_{lat} \;=\; \mathbf{v} - (\mathbf{v}\cdot\mathbf{n})\mathbf{n}.$$

(The subscript *lat* stands for "lateral.") Note that $||\mathbf{v}_{lat}|| = \sin\theta_v$. Therefore, the component, $\mathbf{t}_{lat}$, of $\mathbf{t}$ orthogonal to $\mathbf{n}$ has magnitude equal to

$$||\mathbf{t}_{lat}|| \;=\; \sin\theta_t \;=\; \eta^{-1}\sin\theta_v \;=\; \eta^{-1}||\mathbf{v}_{lat}||.$$

If $||\mathbf{t}_{lat}|| \geq 1$, then total internal reflection occurs. Otherwise, if $||\mathbf{t}_{lat}|| < 1$, we can continue the computation of the transmission direction. Since $\mathbf{t}_{lat}$ points in the direction opposite to $\mathbf{v}_{lat}$, this means that

$$\mathbf{t}_{lat} \;=\; -\,\eta^{-1}\mathbf{v}_{lat}.$$

The component of $\mathbf{t}$ in the direction of the negation of the normal vector has magnitude equal to

$$\cos\theta_t \;=\; \sqrt{1-\sin^2\theta_t} \;=\; \sqrt{1-||\mathbf{t}_{lat}||^2},$$

and therefore is equal to

$$\mathbf{t}_{perp} \;=\; -\,\sqrt{1-||\mathbf{t}_{lat}||^2}\cdot\mathbf{n}.$$

Finally, we have

$$\mathbf{t} = \mathbf{t}_{lat} + \mathbf{t}_{perp},$$

which completes the calculation of the transmission direction.

Exercise X.1. An alternative calculation of the transmission vector uses

$$\mathbf{t}_{perp} \;=\; -\,\sqrt{1-\eta^{-2}(1-(\mathbf{v}\cdot\mathbf{n})^2)}\cdot\mathbf{n}.$$

Prove that this formula is correct too.

The exercise lets us give a closed form expression for $\mathbf{t}$:

$$\mathbf{t} \;=\; \eta^{-1}((\mathbf{v}\cdot\mathbf{n})\mathbf{n}-\mathbf{v}) - \sqrt{1-\eta^{-2}(1-(\mathbf{v}\cdot\mathbf{n})^2)}\cdot\mathbf{n}. \qquad \text{(X.5)}$$

provided the formula in the square root is nonnegative. If the value in the square root is negative, then there is no transmission ray at all, and we have total internal reflection.

To summarize, here is our preferred algorithm for computing the transmission ray.

```
CalcTransmissionDirection( $\mathbf{v}$ , $\mathbf{n}$ , $\eta$ ) {
    Set $\mathbf{t}_{lat}$ = $((\mathbf{v}\cdot\mathbf{n})\mathbf{n}-\mathbf{v})/\eta$ ;
    Set sinSq = $||\mathbf{t}_{lat}||^2$ ;                    // $\sin^2(\theta_t)$
    If ( sinSq>1 ) {
        Return(``No transmission --- total internal reflection!'');
    }
    Set $\mathbf{t}$ = $\mathbf{t}_{lat} - \sqrt{1-\mathtt{sinSq}}\cdot\mathbf{n}$ ;
    Return $\mathbf{t}$ ;
}
```

Next, we give details on how to extend the Phong lighting model to apply to transmission of light. (Cook-Torrance or other local lighting models could be used instead, but we shall only discuss the Phong-style lighting model.) The

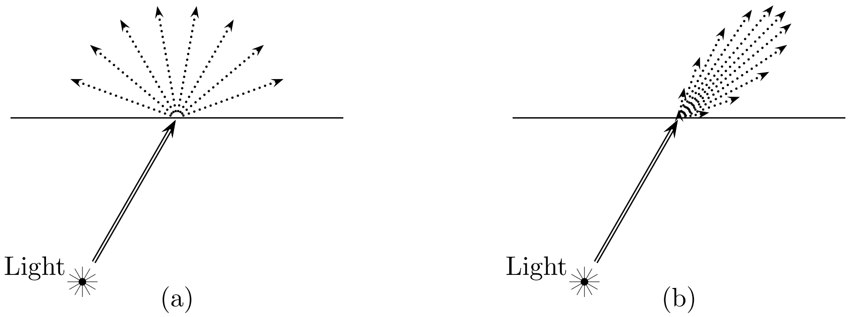

Figure X.7: (a) Diffusely transmitted light. (b) Specularly transmitted light. The specularly transmitted light is centered around the transmission direction from Snell's law.

new aspect of lighting is that a transparent surface may now be illuminated by a light that lies on the far side of the surface. That is to say, the light may be on the opposite side of the surface from the viewer, or incoming ray. Analogously to reflective illumination, transmitted illumination is modeled as having separate diffuse and specular components. These two kinds of illumination are shown in Figure X.7 — you should compare these to Figures IV.2 and IV.3 on pages 134 and 135. The diffusely transmitted light is reflected equally in all directions; the specularly transmitted light is transmitted primarily in the direction of perfect transmission.

The I_{local} term for the transmitted illumination from a light i which is on the opposite side of the surface is given by

$$I^i_{\mathrm{local}} \;=\; \rho_{\mathrm{a}} I^{\mathrm{in},i}_{\mathrm{a}} \;+\; \delta'_i \cdot \Big(\rho_{\mathrm{dt}} I^{\mathrm{in},i}_{\mathrm{d}} (\boldsymbol{\ell}_i \cdot (-\mathbf{n})) + \rho_{\mathrm{st}} I^{\mathrm{in},i}_{\mathrm{s}} (\mathbf{t} \cdot \boldsymbol{\ell}_i)^f \Big). \tag{X.6}$$

where ρ_{dt} and ρ_{st} are material properties for diffuse and specular transmitted light (these can reasonably be taken to just equal ρ_{d} and ρ_{s} in some cases). The value δ'_i is equal to 1 if the light is below the surface and the surface point is visible from the light as determined by a shadow feeler. Otherwise δ'_i is equal to zero. Equation (X.6) needs to be used only when the light is behind the surface and $\delta'_i = 1$, so $\boldsymbol{\ell}_i \cdot \mathbf{n} < 0$; otherwise, Equation (X.4) would be used instead. Figure X.8 shows the vectors used in the application of Equation (X.6).

The full local lighting formula, incorporating both reflected and transmitted illumination and incorporating all wavelengths, can be given as

$$\begin{aligned} \mathbf{I}_{\mathrm{local}} \;\;=\;\; & \boldsymbol{\rho}_{\mathrm{a}} * \mathbf{I}^{\mathrm{in}}_{\mathrm{a}} + \boldsymbol{\rho}_{\mathrm{d}} * \sum_{i=1}^{k} \delta_i \mathbf{I}^{\mathrm{in},i}_{\mathrm{d}} (\boldsymbol{\ell}_i \cdot \mathbf{n}) + \boldsymbol{\rho}_{\mathrm{s}} * \sum_{i=1}^{k} \delta_i \mathbf{I}^{\mathrm{in},i}_{\mathrm{s}} (\mathbf{r}_{\mathbf{v}} \cdot \boldsymbol{\ell}_i)^f \\ & + \boldsymbol{\rho}_{\mathrm{dt}} * \sum_{i=1}^{k} \delta'_i \mathbf{I}^{\mathrm{in},i}_{\mathrm{d}} (\boldsymbol{\ell}_i \cdot (-\mathbf{n})) + \boldsymbol{\rho}_{\mathrm{st}} * \sum_{i=1}^{k} \delta'_i \mathbf{I}^{\mathrm{in},i}_{\mathrm{s}} (\mathbf{t} \cdot \boldsymbol{\ell}_i)^f + \mathbf{I}_{\mathrm{e}}. \end{aligned} \tag{X.7}$$

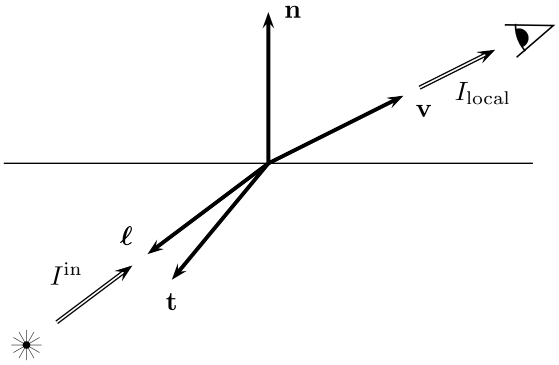

Figure X.8: The vectors used in the computation of transmitted light are $\mathbf{v}$, $\boldsymbol{\ell}$, $\mathbf{t}$, and $\mathbf{n}$. The vector $\mathbf{v}$ points in the direction opposite to the incoming ray. The direction of perfect transmission is shown by the vector $\mathbf{t}$. The direction opposite to the incoming light is given by $\boldsymbol{\ell}$.

For each particular light i, at most one of δ_i and δ_i' can be nonzero, since the light source cannot be both above and below the surface.

X.1.3 Putting it all together

We have finished the discussion of all the features of the basic form of recursive ray tracing. These are combined into a recursive routine for ray tracing. The main loop of the recursive routine loops over every pixel in the image, and forms the ray from the eye through that pixel. With that ray, a routine `RayTrace` is called. `RayTrace` does the following:

1. Finds the first place where the ray intersects the scene. If the ray does not hit any object in the scene, then a default "background color" is used for the illumination level.

2. Calculates the illumination of that point according to the local lighting model.

3. Spawns a reflection ray and a transmission ray, as appropriate.

4. Calls itself recursively with the reflection ray and with the transmission ray.

5. Combines the resulting illumination levels and returns.

In addition, a stopping criterion is needed to terminate the recursive calls to `RayTrace`: an easy, albeit rather arbitrary, stopping criterion is to just recursively trace to only a fixed number of levels, or "bounces." This is the approach we take in the pseudo-code below.

Here is the main program for basic recursive ray tracing:

```
RayTraceMain() {
    // Let $\mathbf{x}$ be the position of the viewer.
    // Let maxDepth be a positive integer.
    For each pixel $\mathbf{p}$ in the viewport, do {
        Set $\mathbf{u}$ = unit vector in the direction from $\mathbf{x}$ to $\mathbf{p}$.
        Call RayTrace( $\mathbf{x}$, $\mathbf{u}$, maxDepth );
        Assign pixel $\mathbf{p}$ the color returned by RayTrace.
    }
}
```

The recursive ray tracing routine is given next.

```
RayTrace( $\mathbf{s}$, $\mathbf{u}$, depth ) {
    // $\mathbf{s}$ is the starting position of the ray.
    // $\mathbf{u}$ is unit vector in the direction of the ray.
    // depth is the trace depth.
    // Return value is a 3-tuple of color values (R,G,B).
    // Part I - Non-recursive computations
    Check the ray with starting position $\mathbf{s}$ and direction $\mathbf{u}$
        against the surfaces of the objects in the scene.
        If it intersects any point, let $\mathbf{z}$ be the first intersection point
        and $\mathbf{n}$ be the surface normal at the intersection point.
    If no point was intersected {
        Return the background color.
    }
    For each light {
        Generate a shadow feeler from $\mathbf{z}$ to the light.
        Check if the shadow feeler intersects any object.
        Set $\delta_i$ and $\delta_i'$ appropriately.
    }
    Set color = $\mathbf{I}_{\mathrm{local}}$;                  // Use Equation (X.7)
    // Part II - Recursive computations
    If ( depth==0 ) {
        Return color;                        // Reached maximum trace depth.
    }
    // Calculate reflection direction & add in reflection color
    If ( $\boldsymbol{\rho}_{rg} \neq \mathbf{0}$ ) {        // if nonzero reflectivity
        Set $\mathbf{r} = \mathbf{u} - 2(\mathbf{u}\cdot\mathbf{n})\mathbf{n}$;          // Eq. (X.2) with $\mathbf{v} = -\mathbf{u}$.
        Set color = color + $\boldsymbol{\rho}_{rg}$*RayTrace($\mathbf{z}$, $\mathbf{r}$, depth-1);
    }
    // Calculate transmission direction (if any) & add in transmitted color
    If ( $\boldsymbol{\rho}_{tg} \neq \mathbf{0}$ ) {        // if has transparency
        // Let $\eta$ be the index of refraction.
        Set t = CalcTransmissionDirection($-\mathbf{u}$, $\mathbf{n}$, $\eta$);
        If t is defined {        // if not total internal reflection
            Set color = color + $\boldsymbol{\rho}_{tg}$*RayTrace(z, t, depth-1);
        }
    }
    Return color;
}
```

The basic recursive ray tracing algorithms have now been completely defined, with one notable exception; namely, we have not discussed how to find intersections of a ray with objects in the virtual scene. The basic idea is to model each object in the scene as a geometric object such a sphere, cylinder, cone, torus, etc., or as a polygonal object with surface comprising flat polygonal faces, or as being bounded by more general surfaces such as Bézier or B-spline patches. Then, one has to test the ray against each surface of each object for possible intersections. Further, it is important that the intersection testing algorithms be computationally efficient, since we have to perform the test for every ray and every shadow feeler. Indeed, it is typically the case that the computation time required for intersection testing is the major portion of the execution time in ray tracing.

The discussion of how to perform the intersection tests for rays against common surfaces is left to Chapter XI.

The basic ray tracing algorithm, with recursive calls and intersection testing, is much too slow for real-time rendering. Suppose, for instance, that the screen has approximately one million pixels, and that each ray is traced to a depth of six bounces (i.e., starting with `maxDepth` set equal to 5). In the worst case, each intersection spawns both a reflection ray and a transmission ray, so for each pixel, we trace a total of $1 + 2 + 4 + \cdots + 2^5 = 63$ rays. In the best case, there is no transmission, so each pixel requires us to trace six rays. In addition, for each light and each intersection point, we must intersect a shadow feeler against the scene. Thus, all in all, we may need to handle tens of millions, or even hundreds of millions, of rays: each ray needing to be tested for intersections with objects in the scene. It is common for this process to take several minutes on a modern-day personal computer. Given the amount of work being performed, one feels lucky that it takes only this long!

X.2 Advanced ray tracing techniques

X.2.1 Distributed ray tracing

Distributed ray tracing, first introduced by Cook et al. [28], is a collection of techniques used to extend the functionality of ray tracing by increasing the number of rays that are traced. Generally speaking, distributed ray tracing is significantly slower than basic recursive ray tracing; however, it can achieve a variety of additional effects. In this section, we describe some of the more common applications of distributed ray tracing.

Anti-aliasing with multiple eye-to-pixel rays

In the basic ray tracing model, only one ray is sent from the eye position to each pixel. This means that only a single ray determines the color of a given pixel. However, in actuality, a pixel covers a square region of the image, and sometimes one gets better visual effects if the pixel were colored as an average color of the region subtended by the pixel. This average color can be approximated by supersampling the pixel, namely, by tracing multiple rays through the pixel with the rays spread more-or-less evenly across the pixel and then assigning the pixel the average of the colors from the multiple rays.

Two prominent applications where forming an average pixel color can help with anti-aliasing are (a) removing the "jaggies," or pixel-sized bumps, from lines, edges, or other object boundaries; and (b) viewing texture maps. We already discussed two ad-hoc solutions to these problems: (a) smoothing lines can be achieved by the use of blending and transparency, and (b) texture map aliasing can be minimized by using mipmapping. Distributed ray tracing gives a more general solution to these and other related problems.

Supersampling and stochastic supersampling were discussed earlier in Section VI.1.4 in the context of texture maps. Supersampling consists of selecting multiple subpixel locations. Distributed ray tracing can trace separate rays from the eye to each subpixel location, and then average the results. The strategies described in Section VI.1.4 apply also to ray tracing; in particular, jittering is also a recommended method for selecting subpixel locations for distributed ray tracing (see Figure VI.8 on page 237).

Figures X.9 and X.10 show an example of anti-aliasing with jittered pixel supersampling.

Depth of field with jittered eye positions

Depth of field is caused by a lens focusing on objects at a given depth, thereby making objects that are either nearer or farther than the focus depth appear blurry and out of focus. This is particularly noticeable in movies when a camera switches from focusing up close to focusing far away, or vice-versa. Pinhole cameras and lenses with a very small aperture are not affected nearly so much by depth of field. Depth of field affects human eyes as well, however, your visual system compensates for this so that you do not notice it under normal circumstances. Computer graphics systems calculate images purely virtually and do not require physical focusing devices, so of course they are not affected by depth of field focusing problems. Nonetheless, it is sometimes desirable to simulate depth of field in computer graphics.

Ray tracing allows depth of field effects by jittering the eye position, while keeping the focal plane fixed. For this, you set up the virtual viewport in the

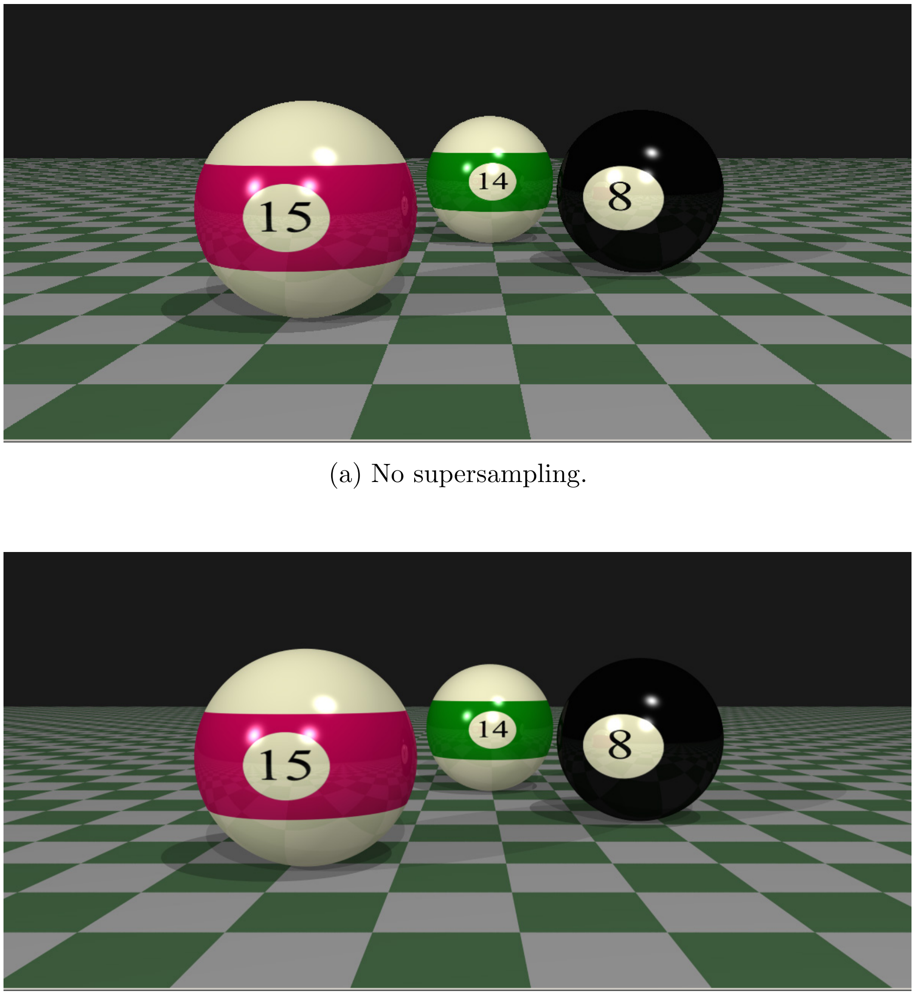

(a) No supersampling.

(b) Supersampling with jittered subpixel centers.

Figure X.9: An example of anti-aliasing using jittered subpixel centers. (a) shows the scene rendered without supersampling; note the “jaggies” on the silhouettes of the balls, for instance. (b) is the scene with pixels selectively supersampled up to a maximum of 40 times. See color plate C.11.

plane of the image you wish to have in focus. Then, for each pixel, you trace multiple rays from jittered eye positions to the center of the pixel (the pixel’s center being kept fixed in the focal plane). For instance, one possibility is to jitter the eye position to nine (or more) positions, with the jittered positions obtained by moving the eye position up or down, and left or right. Then, from

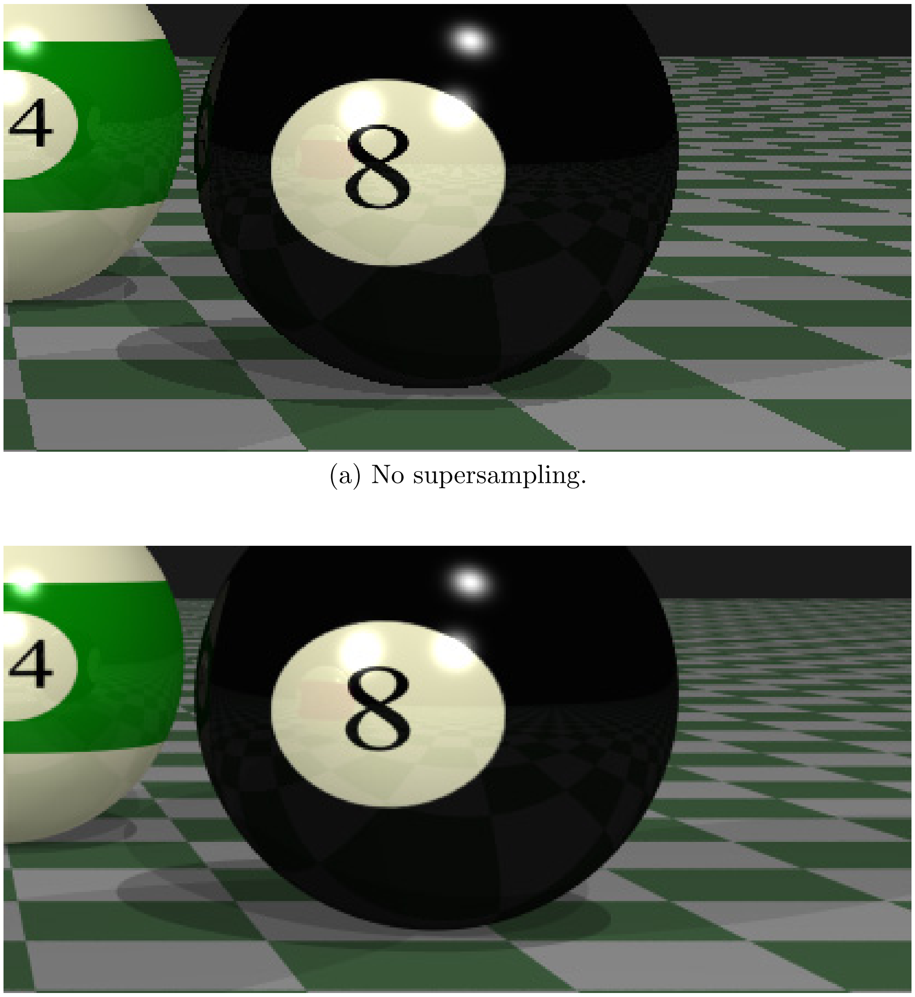

(a) No supersampling.

(b) Supersampling with jittered subpixel centers.

Figure X.10: Close up views of the images in Figure X.9. See color plate C.12.

each jittered position, perform ray tracing as usual: the final color of the pixel is the average of the results of the multiple ray traces.

The effect of jittering the eye position is that objects that lie in the focal plane (and are visible to the eye) are always hit exactly, and each of the multiple ray traces hit the same point and yield essentially the same results. On the other hand, objects which are either nearer or farther than the focal plane are hit differently from different jittered eye positions, and the averaging tends to blur them. Figure X.11 shows how the rays converge and diverge to focus objects in the focal plane and blur objects at other depths. Figure X.12 shows

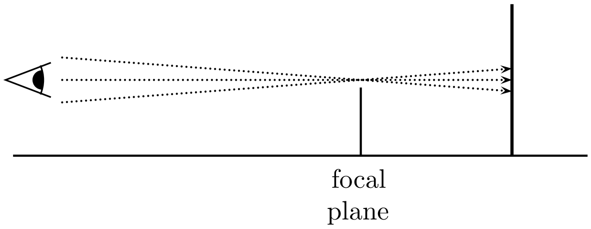

Figure X.11: The rays from the jittered viewpoints converge at the focal plane, but not at the back plane.

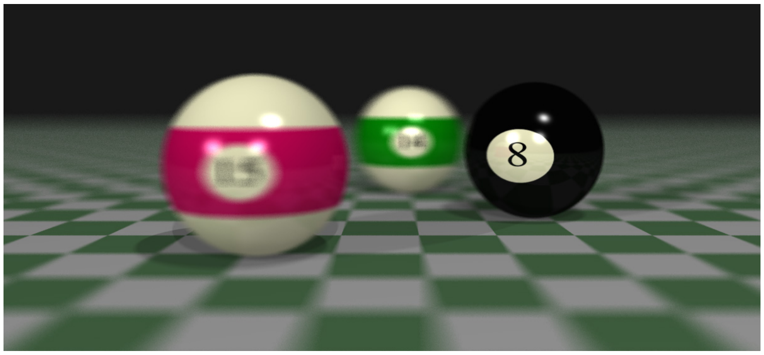

Figure X.12: An example of depth of field. The front of the eight ball is the focal plane. Note also the blurring of the checkerboard plane. In this image, each pixel is selectively supersampled up to 40 times. The eye positions and the subpixel positions were independently jittered as described on page 391. See color plate C.13.

an example of depth of field.

It is important that you choose the jittered positions for the eye separately for each pixel; i.e., do not use the same jittered eye positions for all the pixels, but instead use new jittered positions for each pixel. The problem with reusing the same jittered positions is that the result would be a composite of multiple copies of the scene from slightly different viewpoints, rather than an actual blurring of the scene.

Motion blur

Motion blur renders fast-moving objects as blurs or streaks to indicate their speed; an example is shown in Figure X.13. Motion blur can be accomplished by jittering objects' positions backwards in time. This can be down as follows: each time the high-level ray tracing routine begins tracing a ray from the eye position to a pixel, the moving object(s) are moved back to their position at

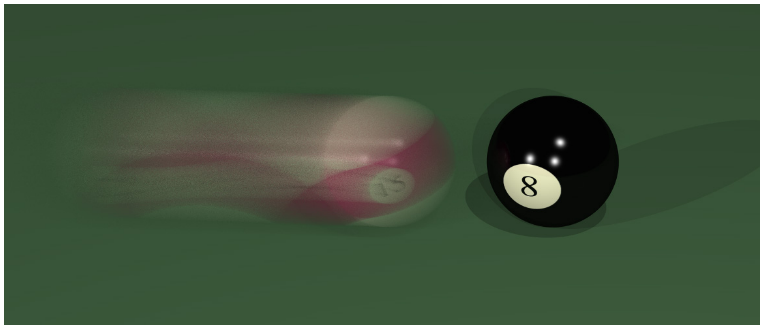

Figure X.13: An example of motion blur. Pixels were selectively supersampled up to 40 times. Both motion supersampling and subpixel supersampling were used. See color plate C.14.

a small time, δt, in the past. The δt values should be chosen at random and independently. You probably want to adjust the probabilities so that small δt values are more likely than large ones. For instance, you could use the following algorithm to choose k jittered values for δt: First choose values a_i randomly and independently from the intervals $[\frac{i}{k}, \frac{i+1}{k}]$, for $0 \le i < k$. Then set b_i by

$$b_i \;=\; a_i^2.$$

Finally, set the i-th jitter value δt equal to $b_i \Delta t$, where Δt is the time period over which the motion blur should extend. (That is, large Δt values make the motion blur trail longer.) Calculating the δt values using the b_i's instead of the a_i's has the effect of compressing them to be closer to zero: the intended visual effect is that the motion blur trail fades out smoothly.

Soft shadows with extended lights and jittered shadow rays

Up until now, we have discussed only point light sources. However, few light sources are modeled well by points. Most lights are either roundish or spherical (such as the sun, or light bulbs), or are rectangularly shaped (such as fluorescent lights in the ceiling behind a plastic cover). The term "extended light" refers to any non-point source.

Extended lights differ from point lights in several important ways. Mainly, an extended light source may be *partially* occluded. As a consequence, an extended light will not cast perfectly sharp shadows, and generally gives a softer, smoother lighting effect. Figure X.14 illustrates how soft shadows work: It shows a spherical light source shining on a wall, with an obstruction shadowing part of the wall. Where the obstruction blocks the entire light, the wall is completely in shadow. But there is a region, called the *penumbra*,

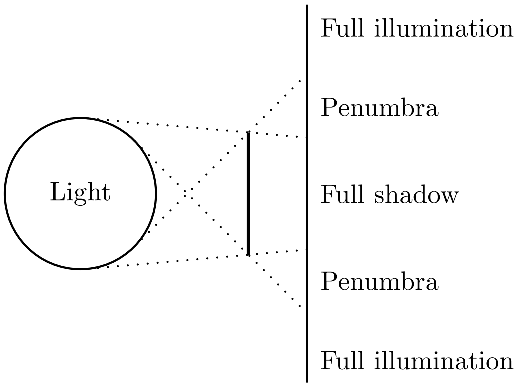

Figure X.14: The penumbra is the area where the light is only partly blocked.

where the obstruction blocks only part of the spherical light. In the penumbra, the shadowing transitions smoothly from completely shadowed to completely illuminated.

Ray tracing can be used to simulate penumbra effects by casting multiple shadow feelers instead of a single shadow feeler. The shadow feelers should be more-or-less evenly distributed across the extent of the light as seen from the point being illuminated. The fraction of shadow feelers that do not find an obstruction between the point of illumination and the light can be used as an estimate of the fraction by which the light is occluded. The lighting from the that light is then reduced correspondingly by the same fraction.

As usual, one gets better effects by randomly choosing positions on the light extent as seen by the point of illumination, and then casting shadow feelers to those positions on the light. If you were to pick fixed points on the light as the targets for shadow feelers, then the penumbra would show banding: there would be noticeable changes in the shading where each fixed light point vanished from view. Jittering can be used to good effect to help distribute the shadow feeler targets evenly over the extent of the light.

Using multiple techniques at once

It is possible to combine multiple distributed ray tracing techniques to achieve more than one effect at once. For instance, you can render an image that has both anti-aliasing and depth of field. To do this, you would jitter subpixel locations for anti-aliasing and jitter the eye position for depth of field. At first glance, this might seem to require tracing a lot more rays; namely, if each pixel has nine jittered subpixel locations and nine jittered eye positions, then one might try casting $9^2 = 81$ rays from the eye to the pixel, one for each choice of eye position and pixel position. Fortunately, this large increase in the number of rays is not necessary. We can instead cast rays from each eye position and to each subpixel position, but using only one ray for each eye position and choosing one jittered subpixel position for each eye position. For best results, you need to make sure that the choices of jittered subpixel positions are independent of the jittered eye positions. In particular, suppose the jittered subpixel positions are chosen from square subpixels, as shown in Figure VI.8 on page 237. Also suppose that the eye positions are chosen in a similar manner, by jittering the centers of an array of squares around the central view position. Then you should choose a random assignment of subpixel positions to eye positions (i.e., a random one-to-one correspondence between subpixel positions and eye positions), and then recursively trace one ray from each eye position to its corresponding pixel position. The point of using the random assignment is to avoid having a correlation between the jittered eye positions and jittered pixel positions that could cause unwanted visual effects.

The high-level algorithm for this is as follows.

```
Variables:
    Array p[$N$]:  An array for holding $N$ subpixel positions.
    Array e[$N$]:  An array for holding $N$ eye locations.
    Array $\pi$[$N$]:  An array that holds a permutation of $[0,\ldots,N-1]$
For each pixel: {
    Fill p[] with $N$ jittered subpixel locations.
    Fill e[] with $N$ jittered eye positions.
    Choose $\pi$ a random permutation of $[0,\ldots,N-1]$.
    For $i$ = $0,\ldots,N-1$ {
        Recursively ray trace with ray from e[$i$] to p[$\pi$[$i$]].
    }
}
```

To choose a random permutation of $[0,\ldots,N-1]$, you can use the following code.[3] We use the function RandInt(i) to compute a random integer in the range $0,\ldots,i$.

```
RandomPermutation($N$) {
    For $i = 0,\ldots,N-1$ {
        Set $\pi$[$i$] = $i$;
    }
    For $i = N-1, N-2,\ldots,1$ {
        Set $j$ = RandInt($i$);
        If $j < i$
            Swap values of $\pi$[$j$] and $\pi$[$i$];
    }
}
```

[3] This algorithm is the Durstenfeld modification of the Fisher-Yates shuffle algorithm. The original version of this algorithm, published in 1938 by Fisher and Yates, was intended for hand computation of random permutations.

Similar methods can be used to combine other distributed ray tracing methods.

Multiple colors

For greater realism, one can perform ray tracing for more colors than just the primary red, green, and blue colors. In addition, the speed of light in a medium typically depends on the wavelength of the light. For refraction, this means that the transmission direction varies with color: a good example of this is a prism splitting white light into a spectrum of wavelengths. In addition, in some local lighting models (such as Cook-Torrance, but not in the Phong model), the dominant reflection angle is also wavelength dependent. Thus, for more realistic results with multiple colors, one may wish to trace multiple reflection and transmission rays from a single ray-object intersection.

Path tracing. Tracing diffuse reflection and transmission

The basic ray tracing methods as described so far are a hybrid of (a) a local lighting model including ambient and diffuse lighting terms, and (b) ray tracing perfect reflection and perfect transmission directions. This hybrid is far from physically correct and contains a number of undesirable features. For example, the local lighting model has a term for ambient light, which is needed because of our inability to completely trace all rays of light. Similarly, the basic ray tracing model does not allow the illumination of a diffuse surface to illuminate other surfaces in the scene. For instance, in the real world, a diffusely lit red wall will itself illuminate nearby objects with reddish light; ray tracing, however, will not simulate this, since it only follows reflections in the direction of perfect, specular reflection.

It would be more physically realistic if we could completely subsume the ambient and diffuse lighting from the local lighting model into the global methods of ray tracing. In essence, this would mean trying to trace *all* the photons in the entire scene in order to track the entire flow of light throughout the scene. If this could be successfully done, then it would be possible to unify the local lighting models with the ray tracing model: for instance, one would use the same lighting models for both reflected and transmitted rays as for rays to light sources.

There are several techniques that are used to try to increase the realism of the ray tracing model to capture more effects of diffuse and ambient reflection. The main idea behind these techniques is to try to follow reflection (and perhaps transmission) rays in all possible directions, not just in the direction of perfect reflection. Unfortunately, this requires spawning a huge number of reflection rays in hundreds, or thousands, of directions. This is often done via a technique called *path tracing*. In path tracing, one generates a large number of rays starting at the eye position through a given pixel. At each intersection, the subsequent reflection direction is chosen by a random procedure. In this way, one attempts to sample a large number of representative paths by which light can reach the eye.

When tracing multiple reflection directions, one must also still trace shadow feelers to the lights and calculate direct illumination from the lights. Of course, this can be combined with extended lights and the use of multiple shadow feelers per light to create soft shadows.

The big drawback to tracing so many reflection directions is that it greatly increases the number of rays that must be traced, by a factor of a thousand-fold or more. These techniques are therefore very time consuming, and can take hours of computation time to trace a single image.

Path tracing can also be combined with so-called "backwards" ray tracing. Backwards ray tracing follows rays of light starting at the light source, through one or more bounces, and tracks the flow of light from the light source towards the eye. Backwards ray tracing is discussed briefly in the next section.

Another global lighting method, called *radiosity*, can also be used to simulate the flow of diffuse lighting through a scene. Radiosity is based on a method quite different from ray tracing, and we will cover it in Chapter XII.

X.2.2 Backwards ray tracing

Ray tracing as described so far has involved tracing paths of light starting at the eye position and ending at lights. It is also possible to trace light in the other direction, starting at light sources, and tracing the paths taken by light from the light sources. This process is called *backwards ray tracing.* The name is somewhat misleading, since backwards ray tracing involves tracing the forward movement of light from the light source; whereas, the usual ray tracing, sometimes called *forward ray tracing*, traces backwards from the eye along the paths taken by light.

The difficulty with backwards ray tracing is that most of the light leaving light sources never reaches the eye position at all, but instead either leaves the scene entirely, or is attenuated by multiple bounces until it is insignificant. Thus, a pure backwards ray tracing algorithm would be much more computationally intensive than forward ray tracing. For this reason, backwards ray tracing is generally used in conjunction with forward ray tracing.

The most common methods use backwards ray tracing to track the overall distribution of light throughout the scene, and then use forward ray tracing to view the lit scene. (Radiosity is another method with a similar idea.) The first such method was the method of *illumination maps*, introduced by Arvo [2]. For illumination maps, all the surfaces of objects in the scene are parameterized, and then gridded up into small patches. Then, a large number of light rays are traced forward from the light sources through multiple bounces. Each time a light ray hits a surface, one determines which surface patch is hit, and stores the color and intensity of the illuminating light. These color and intensity values are stored at the vertices of the patch, with the light color and intensity being distributed to each vertex roughly in proportion to the distance of the intersection point from the vertex (more precisely: by inverting linear or bilinear interpolation to get the weight coefficients). The corners of the surface patches are used as accumulators, and, at the end of the backwards ray tracing phase, they hold the sum of all the weighted illumination from all the light rays that hit neighboring patches. These vertices and their stored illumination values are together called an *illumination map.* After the illumination map has been created, forward ray tracing can be used to view the scene. For the forward ray tracing, the diffuse component of the lighting model is omitted; instead, the illumination map values are used for the diffuse lighting. More precisely, when a ray hits a patch, the intersection point is expressed as a weighted average of the corners of the patch, and the illumination levels at these vertices are combined using the corner weights to calculate the diffuse illumination at the intersection point.

A common visual effect which can be simulated well with illumination maps is the focusing of light through transparent objects. For example, light shining on a glass ball can create bright patterns on a surface under the glass ball, where the curvature of the ball has acted to focus many rays of light into a small area. Another visual effect that can be handled in this way is *caustics.* An example of caustics is seen in a pool of clear water, where small ripples on the surface of the water will bend light, creating rippling patterns of light on the bottom of the pool.

A more recent method, extending illumination maps, is the method of *photon maps*, introduced by Jensen and Christensen [70, 69]. Unlike illumination maps, which store aggregate illumination levels at vertices on a surface, a photon map stores information about each individual light ray (i.e. photon) that hits the surface, along with its color and intensity and possibly its direction. Photon maps were originally invented to avoid needing to parameterize surfaces, but when they include direction information they also can be used to model specular light. An example of how direction information can help is when light is reflected off a mirror and then strikes a surface at point $\mathbf{x}$. Then, a viewer looking at point $\mathbf{x}$, slightly off the direction of perfect specular reflection, will still be able to see the specular highlight, as it can be calculated from the photon map.

Using a photon map allows one to drop both the diffuse and specular terms from the local lighting model. In fact, if the backwards ray tracing is carried out sufficiently far, through enough bounces, then sometimes even the ambient light term can be omitted from the local lighting formula. Photon maps are also used for illumination of volumes, for light scattering, and for translucency, see [69].

Another form of backwards ray tracing is *bidirectional path tracing* [75, 116]. In bidirectional path tracing, paths are traced both from light sources and from the eye, and then are joined together.

Further reading

Our treatment of the more advanced topics in ray tracing has been quite cursory. Some of the topics we have completely skipped are (a) Monte-Carlo methods for choosing ray trace directions, importance sampling, and more sophisticated probability distributions than jittered samples; (b) Russian roulette methods for deciding when to stop tracing rays [3]; and (c) participating media, such as smoke, fog, or atmosphere, which scatter light.

There are several good sources for more information about these and other ray tracing topics. The book [54] has a collection of introductory articles about the techniques of ray tracing as developed prior to 1990. The textbook by Watt and Watt [119] has several chapters devoted to advanced topics in ray tracing, along with pointers to the literature. Shirley [103] has a nice overview of ray tracing, including a number of advanced topics. Glassner [55] covers a lot of advanced topics relevant for ray tracing. The online newsletter *Ray Tracing News*, also maintained by Glassner, has a huge amount of material on developments in ray tracing. Finally, many of the recent developments in ray tracing can be found in conference proceedings and journals; the annual proceedings of the ACM Siggraph conference and the Eurographics conferences are good places to search for this literature.

Ray tracing was first developed by Whitted [121]: this seminal paper is remarkably readable and still relevant.

X.3 Special effects without ray tracing

Ray tracing is too complicated and too experimental to be included in a standard graphics API such as OpenGL. Indeed, if you want to write a ray tracing application in OpenGL, you must completely rewrite all the lighting models yourself, including standard routines like the calculation of Phong lighting. (However, a ray tracing package is included with this book, and described in Appendix **??**.) On the other hand, there are a number of visual effects that are similar to what can be achieved with ray tracing which can also be obtained with much simpler and faster methods. We will discuss some of the more common such methods in this section. Most of these can be done efficiently in OpenGL; the rest can generally be done efficiently by modern graphics hardware. Low cost graphics boards for PCs are nowadays very sophisticated, have memory for computing and storing multiple textures, and even let the programmer download simple programs for remote real-time execution in the graphics pipeline. (Future releases of OpenGL are planned to allow the user to access these capabilities of graphics boards from OpenGL programs.)

Anti-aliasing lines with blending

OpenGL includes automatic use of blending to anti-alias lines, points, and polygons. These can be enabled by giving the commands

$$\texttt{glEnable(}\left\{\begin{array}{c}\texttt{GL\_POINT\_SMOOTH}\\ \texttt{GL\_LINE\_SMOOTH}\\ \texttt{GL\_POLYGON\_SMOOTH}\end{array}\right\}\texttt{);}$$

```
         ⎧  GL_POINT_SMOOTH_HINT  ⎫
glHint(  ⎨   GL_LINE_SMOOTH_HINT  ⎬ , GL_NICEST );
         ⎩ GL_POLYGON_SMOOTH_HINT ⎭
glEnable(GL_BLEND);
glBlendFunc(GL_SRC_ALPHA, GL_ONE_MINUS_SRC_ALPHA);
```

These commands cause OpenGL to render pixels that lie at the border of, and are partially covered by, a point or edge as partly transparent. This is done by giving the partially covered pixels an alpha value between 0 and 1 equal to the fraction of the pixel which is covered. As these pixels are drawn, the blending operation averages the drawn color (the source color) with the color already stored for the pixel (the destination color).

Anti-aliasing in this way works reasonably well for line and points, but does not work as well for filled polygons. You should see the OpenGL programming manual [126] for a more sophisticated way to anti-alias polygon edges, but that method requires performing your own depth calculations instead of using the depth buffer for hidden surface removal.

Motion blur and depth of field with the accumulation buffer

The OpenGL accumulation buffer is a memory region where you can temporarily store and combine images. It is possible to render a scene multiple times and combine the results into the accumulation buffer, and finally display the composite image. OpenGL allows you to scale the accumulation buffer contents, and the accumulation buffer can be loaded from, and saved to, the current frame buffer.

By taking multiple snapshots, and averaging them together into the frame buffer, you can obtain similar kinds of motion blur and depth of field that can be achieved with distributed ray tracing. For motion blur, you render the moving object several times at several intermediate positions in its motion. For depth of field, you render the complete scene from several different viewpoints. To get results comparable to distributed ray tracing, you may need to use a larger number of repeated images to avoid having the results look like several superimposed snapshots; but it is still substantially faster than ray tracing.

Finally, since a scene may have only a few fast moving objects, you can often render the more static background once and then repeatedly render the moving objects in front of the static background, and avoid the expense of repeatedly rendering the entire scene.

The OpenGL commands for manipulating the accumulation buffer are

```
glutInitDisplayMode( GLUT_ACCUM | other-options );
          ⎧  GL_ACCUM  ⎫
          ⎪  GL_LOAD   ⎪
glAccum(  ⎨ GL_RETURN  ⎬ , float factor );
          ⎪  GL_MULT   ⎪
          ⎩  GL_ADD    ⎭
glAccumClear( float red, float green, float blue, float alpha);
```

```
glClear(GL_ACCUM_BUFFER_BIT);
```

You must include the GLUT_ACCUM bit in the options to glutInitDisplayMode in order to request a rendering context with an accumulation buffer. The glAccumClear command sets the clear colors for the accumulator: the accumulator buffer is loaded with these values by the glClear command shown above. The call to glAccum with the GL_ACCUM operand adds into the accumulation buffer the contents of the current drawing buffer multiplied by the factor value. For superimposing multiple rendered images, you would use a loop of the following type:

```
glClear(GL_ACCUM_BUFFER_BIT);
For i = 1,...,n {
    glClear(GL_COLOR_BUFFER_BIT | GL_DEPTH_BUFFER_BIT);
    RenderScene( i );      // Render i-th version of scene
    glAccum(GL_ACCUM, 1.0/n);
}
glAccum(GL_RETURN, 1.0);
```

The subroutine RenderScene() must render the changing scene as usual, but should not swap buffers to display them. The last line uses the GL_RETURN option to glAccum to place the contents of the accumulation buffer back into the rendering buffer. The factor, which is equal to one here, specifies another scaling value.

See the OpenGL programming manual for documentation on the rest of the operands to glAccum.

Depth of field with z-buffer based blurring

The z-buffer contents contain the pseudo-distance, from which one can determine the actual distance of the object from the eye. This distance information can be used to create depth of field effects. To do this, any pixel whose depth does not approximately match the focal depth can be blurred by replacing it with a weighted average of the surrounding pixels. The radius of the area from which the surrounding pixels are taken should depend on the distance of the pixel from the focal plane.

Reflections with environment mapping

Shiny, specular objects with reflections of the surrounding scene can be rendered using environment maps. The environment map is created by rendering the scene from the viewpoint of the shiny object and then using this to create an environment map. Typically, this is done by rendering the scene from the viewpoint of the shiny object up to six times, and storing the environment map in the box projection format. Once an environment map is created from every shiny object, the final image can be rendered one further time from the eye position, with the environment maps applied as textures to the objects. It is also possible iterate this procedure to get multiple levels of reflection. Attenuated or blurry reflections can be handled by attenuating or blurring the environment map.

Environment maps were already discussed in more detail in Section VI.3.

Using environment maps in this way cannot fully simulate reflections. First there is some error in the calculation of reflection since the environment map is formed from the viewpoint of only a single position (usually the center point) of the object. Further, it doesn't handle self-reflections; for instance, a shiny teapot would not show the reflection of the spout on its body, or vice-versa, unless you treat the spout and the body as separate objects and calculate separate environment maps for them.

Mirror reflections with clones

Reflections from flat, mirrored surfaces can be created by rendering a mirror image of the world behind the mirror's plane. This involves first rendering the entire scene reflected across the plane of the mirror, then drawing the mirror as a transparent shape (using blending, see `glBlend` in the OpenGL programming manual) and then drawing the real scene. Attenuated reflections can be achieved by choosing blending value appropriately.

For small mirrors or for difficult geometric arrangements, you may need to use the OpenGL stencil buffer to automatically restrict the mirror image to be rendered only behind the mirror, since otherwise the mirror image of the world will be visible around the mirror too. For this, you set up the stencil buffer by drawing the mirror shape, then render the mirror image of the scene with the stencil buffer enabled, then disable the stencil buffer and render the mirror and then the rest of the scene again. The stencil buffer acts as a mask to prevent rendering outside of a defined area — for more details see the OpenGL programming manual.

Shadows

As we discussed already in Section II.4.5, shadows can be projected on a flat surface using projection transformations. For soft shadows, this process can be repeated with multiple light positions and blending.

Casting shadows on non-planar surfaces is harder, but there are variety of methods that can render shadows in real-time. Two of the most popular ways of rendering shadows in real-time without ray tracing are the *shadow volume* method and the *shadow map* method. We give only brief descriptions of these methods, but you can consult the references mentioned below for more information.

The shadow volume method works by determining what regions in 3-space are in shadow. For each point light source ℓ_i, and each polygonal object, we determine the solid region that lies in the shadow cast by the that object from light ℓ_i. This region is called a *shadow volume.* For positional lights, the shadow volume is a generalized truncated cone. For instance, if the object is a triangle, then its shadow volume is a three-sided, infinitely tall pyramid which is capped (truncated) by the triangle. For general polygonal objects instead of triangles, it suffices to find the "silhouette edges", and then the shadow volume is the infinite region bounded by the shadows cast by the silhouette edges and capped by the polygonal object. The side faces of the shadow volume are the boundaries of the shadow region as cast from the silhouette edges.

Standard implementations of shadow volumes proceed roughly as follows: First, the scene is rendered into the frame buffer as usual, with all depth buffer information, and either (a) with all lighting as usual, or (b) with ambient lighting only. Then, the shadow volumes' side faces are rendered, but instead of drawing them into the frame buffer, the (pseudo-)depths are compared to the depth buffer values in the frame buffer. By keeping track of the net number of front- and back-facing shadow volume faces which lie in front of a given pixel in the frame buffer, we can determine whether the pixel is in shadow. (The OpenGL stencil buffer can be used to keep track of the net number of front- and back-facing edges.) Third, once it is determined which pixels are in shadow, then either (a) all shadowed pixels are darkened to simulate shadows, or (b) Phong lighting is used to add diffuse and specular lighting to all non-shadowed pixels. These steps have to be repeated for each point light source.

The shadow volume method was first described by Crow [32]. It was generalized to more general shapes by Bergeron [8], and extended to handle soft shadows from extended lights by Brotman and Badler [22]. Heidmann [64] describes efficient implementation of shadow volumes with the stencil buffer. Everitt and Kilgard [39] also discuss implementations on modern graphics hardware, along with optimizations that avoid problems with clipping planes.

The second method is the method of shadow maps. A *shadow map* consists of the view of the scene as rendered from the viewpoint of a point light source (instead of from the viewpoint of the viewer). For each point light source, a shadow map is created with a depth buffer and with hidden surfaces removed. The shadow map can be used to determine the distance from the light source to the first object in the scene in any given direction (up the resolution of the shadow map). After the shadow maps are created, the scene is rendered as usual from the viewpoint of the viewer. Each pixel in the scene is rendered into screen space, with x and y coordinates and with a pseudo-depth value z. These screen space coordinates can be inverted to obtain the position of the pixel's contents in the scene in 3-space.[4] Then the distance from the light in 3-space can be compared to the corresponding distance from the shadow map. If the object is further away than the distance in the shadow map, then it is shadowed, otherwise it is not. (Usually, a bias value is added to the distance to avoid problems with self-shadowing caused by roundoff error.) Once it is known which pixels represent surfaces in shadow, then, as before, either shadowed pixels can be darkened, or non-shadowed pixels can be illuminated with Phong

[4] The OpenGL function `gluUnProject` can help with inverting the screen space coordinates.

lighting.

Shadow maps were introduced by Williams [122]. They can suffer from problems with aliasing and roundoff error; Reeves, Salesin, and Cook [93] use a method called "percentage closer filtering" than can reduce aliasing and make softer shadows. Agrawala et al. [1] and Chen and Williams [24] discuss ways to use shadow maps to render soft shadows with from jittered light sources.

McCool [79] describes a hybrid method that combines shadow volumes and shadow maps by extracting shadow volume information from a shadow map.

Transparency, blending, and fog

XXX THIS SECTION NEEDS TO BE REWRITTEN!

OpenGL includes a number of features that allow some aspects of transparency to be easily rendered. The OpenGL functions `glBlendFunc` and `glFog` control these features.

Blending allows transparent objects to modify the colors of object behind them. The alpha component of colors is used to control blending. To obtain good results with blending, it is often necessary to first render all non-transparent objects, and then render the transparent objects with the painter's algorithm, namely, to render the transparent objects sorted so that more distant objects are rendered first.

Fog allows more distant objects to "fade out," as from fog or other atmospheric interference. Fog has the advantage of providing "depth cueing," wherein the attenuation of images due to fog gives an indication of distance. In addition, fog can be used to obscure distant objects and thereby improve performance since obscured objects do not need to be rendered.

Chapter XI

Intersection Testing

This is a ***preliminary*** *draft of a second edition of the book* 3-D Computer Graphics: A Mathematical Introduction with OpenGL. *So please read it cautiously and critically! Corrections are appreciated. Draft C.4.a*

Author: Sam Buss, sbuss@ucsd.edu

This chapter discusses issues in intersection testing and describes algorithms for intersecting rays with geometric objects. Intersection testing is one of the fundamental algorithms used in ray tracing: ray tracing usually requires intersecting a large number of rays against a large set of geometric objects. For this reason, it is often the case that the bulk of the computational time required for ray tracing is spent on intersection testing. Intersection testing has other applications besides ray tracing, for instance, in motion planning and collision detection.

Intersection testing is a large and diverse field. In this chapter, we shall discuss only some of the first topics, namely, intersecting rays against simple geometric objects. We will only briefly discuss methods such as bounding boxes and bounding spheres, and global pruning methods such as octtrees and binary space partitioning. More information on intersection testing can be found in the book by Möller and Haines [80], which has two chapters devoted to this topic, including a large number of references to the literature. The *Graphics Gems* volumes also contain quite a few articles on intersection testing. For additional reading suggestions, see the end of this chapter.

There are two important goals to keep in mind when designing software for intersection testing. The first design goal is *accuracy* and *robustness.* Clearly, it is important that the algorithms be accurate; even more so, the algorithms need to free from occasional errors that may make visible artifacts, such as holes, or cause an occasional inconsistency in intersection status. For example, in ray tracing applications, it ought to be impossible for a path to be confused about being inside or outside a closed object such as a sphere. Similarly, for objects made up of multiple parts, say a cube made from six square faces, or a surface whose 'faces' are Bézier patches, it should not be possible for roundoff error to allow a ray to pass through a "crack" between two faces without hitting the surface.

The second design goal for intersection testing is *speed.* It is often the case that intersection testing is the most computationally intensive part of a program. In particular, in ray tracing, it is common for most of the computation time to be spent on intersection testing. The reason for this is that there are typically a large number of objects, hundreds, thousands, or perhaps many more, and one has to consider the possibility that each ray hits each object. Since the ray hits only one object, the time spent processing the actual hit is generally a lot less than the time spent determining which of the many objects is first hit. A subordinate principle is that what is really important is that one be able to very quickly determine when an intersection has *not* occurred. That is, it is often far more important to decide quickly when a ray does not hit an object than it is to decide quickly that a ray does hit an object.

If a ray is being intersection tested against a large number of objects, then it may be useful to preprocess the objects by arranging them hierarchically or by partitioning space with the use of octtrees or binary space partitioning trees. These are techniques that allow a quick rejection of many objects at once, so that intersection testing does not have to be performed against each individual object. We will discuss these briefly at the end of the chapter; however, the main emphasis of this chapter is on algorithms for testing whether a ray intersects an individual object.

XI.1 Fast intersections with rays

In this section, we discuss algorithms for intersecting rays with several common surfaces in $\mathbb{R}^3$. We do not try to be encyclopedic in our coverage of intersection testing with rays, but instead strive to show the issues and algorithms that arise in many common cases. We consider below intersections of rays against spheres, planes, triangles, convex polytopes, cylinders, quadrics, and Bézier patches.

XI.1.1 Ray versus sphere intersections

Assume that a ray and a sphere are fixed. The ray is specified by its starting position $\mathbf{p}$, and a unit vector $\mathbf{u}$ in the direction of the ray. That is to say, the ray is the set of points

$$\{\mathbf{p} + \alpha\mathbf{u} : \alpha \geq 0\}.$$

We will also talk about the *line* containing the ray, which we call the *ray-line.*

The sphere is specified by its center $\mathbf{c}$ and its radius $r > 0$, and is equal to the set of points at distance r from the center.

The ray-sphere intersection algorithm works by first finding the point $\mathbf{q}$ on the ray-line which is closest to the center of the sphere. (Refer to Figure XI.1.) The point $\mathbf{q}$ will be equal to $\mathbf{p} + \alpha\mathbf{u}$, where α is a scalar measuring how far

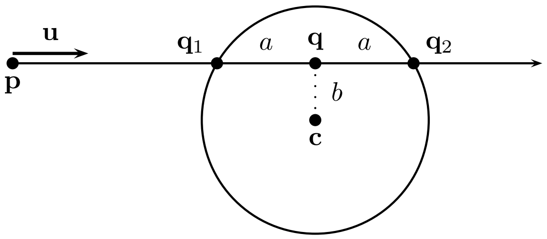

Figure XI.1: The ray from $\mathbf{p}$ in direction $\mathbf{u}$ reaches its closest point to the center $\mathbf{c}$ of the sphere at $\mathbf{q}$. The points $\mathbf{q}_1$ and $\mathbf{q}_2$ are the two places where the line intersects the sphere.

$\mathbf{q}$ is from $\mathbf{p}$ along the ray. A point $\mathbf{q}$ will be the closest point on the ray-line to the point $\mathbf{c}$ provided that the line from $\mathbf{q}$ to $\mathbf{c}$ is perpendicular to the ray; that is to say, the point $\mathbf{q}$ can be defined by

$$0 \;=\; (\mathbf{q}-\mathbf{c})\cdot\mathbf{u} \;=\; (\mathbf{p}+\alpha\mathbf{u}-\mathbf{c})\cdot\mathbf{u}.$$

Solving for α, using the fact that $\mathbf{u}\cdot\mathbf{u}=1$, gives

$$\alpha = -(\mathbf{p}-\mathbf{c})\cdot\mathbf{u}.$$

Therefore $\mathbf{q} = \mathbf{p} - ((\mathbf{p}-\mathbf{c})\cdot\mathbf{u})\mathbf{u}$.

Once we have found $\mathbf{q}$, we can check whether $\mathbf{q}$ lies inside the sphere by checking whether $||\mathbf{q}-\mathbf{c}|| \le r$. Finding the norm of a vector involves calculating a square root, so it is actually more efficient to check whether $||\mathbf{q}-\mathbf{c}||^2 \le r^2$. The calculation of the square of the magnitude of a vector, say of $||\mathbf{w}||^2$, can be done with only 3 multiplies and 2 additions, so this is significantly more efficient than also using a square root. If $\mathbf{q}$ does not lie inside the sphere, then obviously the ray does not intersect the sphere.

When $\mathbf{q}$ does lie inside the sphere, let $b = ||\mathbf{q}-\mathbf{c}||$ and set $a = \sqrt{r^2-b^2}$. Note that only the square of b is needed; however, a square root is needed to compute a. Then the ray-line intersects the sphere at the two points

$$\mathbf{q}_1 = \mathbf{p} + (\alpha - a)\mathbf{u} \qquad \text{and} \qquad \mathbf{q}_2 = \mathbf{p} + (\alpha + a)\mathbf{u}.$$

(See Figure XI.1.) Now, if $\alpha - a \ge 0$, then the ray does actually hit the sphere at $\mathbf{q}_1$, and this is its first intersection with the sphere. However, if $\alpha < a$, then the point $\mathbf{q}_1$ lies in the wrong direction along the ray-line, i.e., behind $\mathbf{p}$ on the line. In this latter case, we then check whether $\alpha + a > 0$; if so, then the point $\mathbf{p}$ lies inside the sphere, and $\mathbf{q}_2$ is the point where the ray first hits the sphere.

Putting this together gives the following algorithm for ray-sphere intersection testing.

```
Ray-Sphere Intersection:
Input:  $\mathbf{p}$ and $\mathbf{u}$ describe a ray. $\mathbf{u}$ a unit vector.
        A sphere specified by center $\mathbf{c}$ and radius $r$.
Algorithm:
    Set $\alpha = -(\mathbf{p}-\mathbf{c})\cdot\mathbf{u}$;
    Set $\mathbf{q} = \mathbf{p}+\alpha\mathbf{u}$;
    Set bSq = $||\mathbf{q}-\mathbf{c}||^2$;
    If ( bSq > $r^2$ ) {
        Return "No intersection";
    }
    Set $a = \sqrt{r^2 - \mathrm{bSq}}$;
    If ( $\alpha \ge a$ ) {
        Set $\mathbf{q}_1 = \mathbf{q} - a\mathbf{u}$;
        Return $\mathbf{q}_1$;
    }
    If ( $\alpha + a > 0$ ) {
        Set $\mathbf{q}_2 = \mathbf{q} + a\mathbf{u}$;
        Return $\mathbf{q}_2$;
    }
    Return "No intersection";
```

As discussed in the introduction, the most important aspect of the computational speed of the algorithm is how fast it detects non-intersections. In the algorithm above, to get to the rejection test of $b^2 > r^2$ on line 4 of the algorithm, one performs 9 multiplications, 11 additions, and one comparison, assuming that the radius squared, r^2, has been precomputed.

If you know that the ray's beginning point $\mathbf{p}$ is never inside the sphere, it could be worthwhile to add a check for whether $\alpha > 0$, since $\alpha \le 0$ means that the ray is not pointing towards the sphere at all. In ray tracing, this may be the case if the sphere is not transmissive. This extra test for non-intersection doesn't work so easily when it is possible for $\mathbf{p}$ to be inside the sphere. For that, you need to check both $\alpha > 0$ and $||\mathbf{p}-\mathbf{c}||^2 > r^2$, i.e., check that $\mathbf{p}$ is outside the sphere and that the ray is pointing away from the sphere. This test then requires three extra multiplications, two extra additions and two extra comparisons, so it is generally only marginally useful to perform this extra test.

Intersection tests for complicated geometric objects can be speeded up by giving the object a bounding sphere. The bounding sphere must completely enclose the object. To test whether a ray intersects the complicated object, you can first test whether the ray intersects the bounding sphere. If not, then it also does not intersect the geometric object. However, if the ray does intersect the bounding sphere, you must further test for intersection with the geometric object. The advantage of the bounding sphere is that it allows you to *quickly* detect many cases of non-intersection.

Exercise XI.1. Write an efficient pseudo-code algorithm for bounding sphere testing. [Hint: Use the first part of the ray-sphere intersection algorithm, namely the part through line 6 ending with the test for $b^2 > r^2$. Finish up by testing the condition “$\alpha > 0$ or $\alpha^2 \le a^2$.”]

Exercise XI.2* An ellipsoid is specified by its center, three orthogonal axes, and three radii. The three orthognal axes and radii can be specified by three orthogonal vectors $\mathbf{v}_1$, $\mathbf{v}_2$, and $\mathbf{v}_3$, with each norm $||\mathbf{v}_i||$ equal to the inverse of the radius in the direction of $\mathbf{v}_i$: the ellipsoid is the set of points $\mathbf{x}$ such that $\sum_i((\mathbf{x}-\mathbf{c})\cdot\mathbf{v}_i)^2 = 1$. Formulate an efficient ray versus ellipsoid intersection algorithm.

XI.1.2 Ray versus plane intersections

A plane is specified by a normal vector $\mathbf{n}$ perpendicular to the plane and a scalar d. The plane is the set of points $\mathbf{x}$ satisfying $\mathbf{x}\cdot\mathbf{n} = d$.

If $\mathbf{p}$ and $\mathbf{u}$ specify a ray as usual, then, to intersect the ray with the plane, we first calculate the point $\mathbf{q}$ (if it exists) which is the intersection of the ray-line with the plane. This $\mathbf{q}$ will equal $\mathbf{p} + \alpha\mathbf{u}$ for α a scalar. To lie in the plane, it must satisfy

$$d \;=\; \mathbf{q}\cdot\mathbf{n} \;=\; \mathbf{p}\cdot\mathbf{n} + \alpha\mathbf{u}\cdot\mathbf{n}.$$

Solving for α yields

$$\alpha \;=\; \frac{d - \mathbf{p}\cdot\mathbf{n}}{\mathbf{u}\cdot\mathbf{n}}.$$

The quantities in this formula for α all have geometric meaning. If $\mathbf{n}$ is a unit vector, then the value $d - \mathbf{p}\cdot\mathbf{n}$ is the negative of the distance of $\mathbf{p}$ above the plane, where “above” means in the direction of $\mathbf{n}$. For non-unit $\mathbf{n}$, $(d - \mathbf{p}\cdot\mathbf{n})/||\mathbf{n}||$ is the negative of the distance of $\mathbf{p}$ above the plane. In particular, $\mathbf{p}$ is above (respectively, below) the plane if and only if $d - \mathbf{p}\cdot\mathbf{n}$ is negative (respectively, positive).

The dot product $\mathbf{u}\cdot\mathbf{n}$ is negative if the ray’s direction is downward relative to the plane (with $\mathbf{n}$ defining the notions of “down” and “up”). If $\mathbf{u}\cdot\mathbf{n} = 0$, then the ray is parallel to the plane, and the usual convention is that in this case the ray does not intersect the plane at all. Even if the ray lies in the plane, it is usually desirable for applications to treat this as not intersecting the plane. The value of α is the signed distance of $\mathbf{q}$ from $\mathbf{p}$. If $\alpha < 0$, then the ray does not intersect the plane.

These considerations give the following ray versus plane intersection algorithm.

```
Ray-Plane Intersection:
Input:  $\mathbf{p}$ and unit vector $\mathbf{u}$ defining a ray.
        $\mathbf{n}$ and $d$ defining a plane.
Algorithm:
    Set $c$ = $\mathbf{u}\cdot\mathbf{n}$;
```

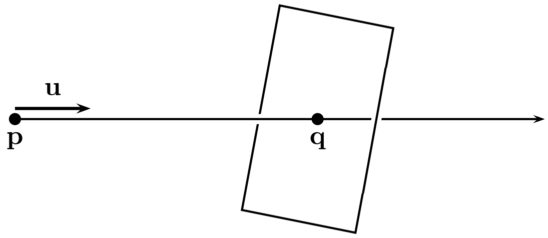

Figure XI.2: The ray specified by its start position **p** and direction **u** intersects the plane at the point **q**.

```
    If ( $c == 0$ ) {
        Return "No intersection (parallel)";
    }
    Set $\alpha$ = $(d - \mathbf{p} \cdot \mathbf{n})/c$;
    If ( $\alpha < 0$ ) {
        Return "No intersection";
    }
    Set $\mathbf{q}$ = $\mathbf{p} + \alpha\mathbf{u}$;
    Return $\mathbf{q}$;
```

Sometimes we want to intersect the ray-line against the plane instead, for instance in the ray versus convex polytope intersection algorithm in Section XI.1.4. This is even simpler than above, as we just omit the test for $\alpha \geq 0$:

```
Line-Plane Intersection:
Input:  $\mathbf{p}$ and unit vector $\mathbf{u}$ defining a line.
        $\mathbf{n}$ and $d$ defining a plane.
Algorithm:
    Set $c$ = $\mathbf{u} \cdot \mathbf{n}$;
    If ( $c == 0$ ) {
        Return "No intersection (parallel)";
    }
    Set $\alpha$ = $(d - \mathbf{p} \cdot \mathbf{n})/c$;
    Set $\mathbf{q}$ = $\mathbf{p} + \alpha\mathbf{u}$;
    Return $\mathbf{q}$;
```

Exercise XI.3. What would happen if we drop the requirement that the vector **u** be a unit vector? Show that the above algorithms would still compute the intersection point **q** correctly, but not the distance α.

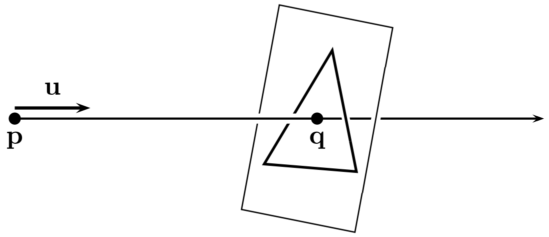

Figure XI.3: Intersecting a ray with a triangle. The first step is to find the intersection $\mathbf{q}$ with the plane containing the triangle.

XI.1.3 Ray versus triangle intersections

We next take up the intersection of a ray with a triangle. In principle, this can be taken as the fundamental intersection operation, since all surfaces can be approximated by planar patches, indeed by triangles.

A ray is, as usual, specified by its starting position $\mathbf{p}$ and direction $\mathbf{u}$, with $\mathbf{u}$ a unit vector. A triangle can be represented by its three vertices $\mathbf{v}_0$, $\mathbf{v}_1$, and $\mathbf{v}_2$, which are presumed to be noncollinear.

The first step in intersecting a ray with the triangle is to intersect it with the plane containing the triangle. Let $\mathbf{n}$ be a vector normal to the plane, and let d be the scalar so that the plane consists of those points $\mathbf{x}$ such that $\mathbf{n}\cdot\mathbf{x} = d$. By convention, the vector $\mathbf{n}$ is taken to be the "upward" direction, and we presume the triangle's vertices are ordered in the counter-clockwise direction when the plane is viewed from above. Values for $\mathbf{n}$ and d can be computed by the following formulas.

$$\begin{aligned} \mathbf{n} &= (\mathbf{v}_1 - \mathbf{v}_0) \times (\mathbf{v}_2 - \mathbf{v}_0) \\ d &= \mathbf{n}\cdot\mathbf{v}_0. \end{aligned}$$

The point $\mathbf{q}$ where the ray intersects the plane is found using the ray-plane intersection test of the previous section. This also gives the signed distance α from $\mathbf{p}$ to $\mathbf{q}$; if this test finds that $\alpha < 0$, then there is no intersection. By further examining the sign of either $\mathbf{u}\cdot\mathbf{n}$ or $d-\mathbf{p}\cdot\mathbf{n}$, one can determine whether the point $\mathbf{p}$ lies above or below the surface.

Once the point $\mathbf{q}$ has been found, we still need to determine whether $\mathbf{q}$ is inside or outside the triangle. One way to do this is by computing the barycentric coordinates of $\mathbf{q}$ relative to the triangle. The barycentric coordinates can be found using Equations (V.15) and (V.16) on page 193. To translate these equations to our present setting, we let $\mathbf{x} = \mathbf{v}_0$, let $\mathbf{y} = \mathbf{v}_1$, let $\mathbf{z} = \mathbf{v}_2$, and let $\mathbf{u} = \mathbf{q}$. To find the barycentric coordinates of $\mathbf{q}$, we first calculate

$$\begin{aligned} \mathbf{e}_1 &= \mathbf{v}_1 - \mathbf{v}_0 \\ \mathbf{e}_2 &= \mathbf{v}_2 - \mathbf{v}_0 \\ a &= \mathbf{e}_1^2 \\ b &= \mathbf{e}_1 \cdot \mathbf{e}_2 \\ c &= \mathbf{e}_2^2. \end{aligned}$$

Here $\mathbf{e}_1$ and $\mathbf{e}_2$ are two of the edge vectors for the triangle. Then, calculate

$$\begin{aligned} D &= ac - b^2 \\ A &= a/D \\ B &= b/D \\ C &= c/D \end{aligned}$$

Then let

$$\mathbf{u}_\beta = C\mathbf{e}_1 - B\mathbf{e}_2 \qquad \text{and} \qquad \mathbf{u}_\gamma = A\mathbf{e}_2 - B\mathbf{e}_1.$$

The barycentric coordinates, α, β, γ, which represent $\mathbf{q}$ as $\mathbf{q} = \alpha\mathbf{v}_0 + \beta\mathbf{v}_1 + \gamma\mathbf{v}_2$ are found by

$$\begin{aligned} \beta &= \mathbf{u}_\beta \cdot (\mathbf{q} - \mathbf{v}_0) \\ \gamma &= \mathbf{u}_\gamma \cdot (\mathbf{q} - \mathbf{v}_0) \\ \alpha &= 1 - \beta - \gamma. \end{aligned}$$

The point $\mathbf{q}$ lies in or on the triangle provided that α, β, and γ are all nonnegative.

Putting this together gives the following algorithm. The algorithm is split into two phases. The precomputation calculates values that depend on the triangle only, and these values can be computed once and saved.

```
Ray-Triangle Intersection Algorithm
Input:  $\mathbf{p}$ and unit vector $\mathbf{u}$ specifying a ray.
        $\mathbf{v}_0$, $\mathbf{v}_1$, $\mathbf{v}_2$ specifying a triangle.
Precompute $\mathbf{n}$, $d$, $\mathbf{u}_\beta$, $\mathbf{u}_\gamma$:
    Set $\mathbf{e}_1$ = $\mathbf{v}_1 - \mathbf{v}_0$;
    Set $\mathbf{e}_2$ = $\mathbf{v}_2 - \mathbf{v}_0$;
    Set $\mathbf{n}$ = $\mathbf{e}_1 \times \mathbf{e}_2$;
    Set $d$ = $\mathbf{n} \cdot \mathbf{v}_0$;
    Set $a$ = $\mathbf{e}_1 \cdot \mathbf{e}_1$;
    Set $b$ = $\mathbf{e}_1 \cdot \mathbf{e}_2$;
    Set $c$ = $\mathbf{e}_2 \cdot \mathbf{e}_2$;
    Set $D$ = $ac - b^2$;
    Set $A$ = $a/D$;
    Set $B$ = $b/D$;
    Set $C$ = $c/D$ ;
    Set $\mathbf{u}_\beta$ = $C\mathbf{e}_1 - B\mathbf{e}_2$ ;
    Set $\mathbf{u}_\gamma$ = $A\mathbf{e}_2 - B\mathbf{e}_1$ ;
Main algorithm:
    Invoke Ray-Plane intersection algorithm to calculate $\mathbf{q}$ .
    If ( No ray-plane intersection exists ) {
        Return "No intersection" ;
    }
    Set $\mathbf{r}$ = $\mathbf{q} - \mathbf{v}_0$ ;
    Set $\beta$ = $\mathbf{u}_\beta \cdot \mathbf{r}$ ;
    If ( $\beta < 0$ ) {
        Return "No intersection" ;
    }
    Set $\gamma$ = $\mathbf{u}_\gamma \cdot \mathbf{r}$ ;
    If ( $\gamma < 0$ ) {
        Return "No intersection" ;
    }
    Set $\alpha$ = $1 - \beta - \gamma$ ;
    If ( $\alpha < 0$ ) {
        Return "No intersection" ;
    }
    Return $\mathbf{q}$ ;
```

The algorithm above has been optimized for speed, not memory usage. Examination of the algorithm shows that for each triangle we need to have the values $\mathbf{v}_0$, $\mathbf{n}$, d, $\mathbf{u}_\beta$, and $\mathbf{u}_\gamma$; this is four floating point numbers more than would be needed to store just the three vertices (but most applications would need to keep $\mathbf{v}_1$ and $\mathbf{v}_2$ too). There are several algorithms which use fewer precomputed numbers; see especially [81, 80] for an algorithm which skips the stage of calculating $\mathbf{q}$. Those algorithms have the advantage of needing less memory, which can be important if there are a large number of triangles; however, without storing the plane normal and scalar values, it is not possible to have such a quick intersection rejection test.

XI.1.4 Ray versus convex polytope intersections

A convex polytope in $\mathbb{R}^3$ is a region which is bounded by a finite number of planes.[1] In 3-space, convex polytopes are also called convex polyhedra, and examples include cubes, rectangular prisms (boxes), pyramids, etc. In 2-space, the bounding planes are replaced by bounding lines, and so a convex polytope is the same as a convex polygon. The concept of polytope is easily extended to arbitrary dimension (in $\mathbb{R}^d$, the bounding planes are replaced by $(d-1)$-dimensional affine subspaces), and the algorithms we develop below

[1] Generally, it is also required that the polytope be bounded, i.e., not infinite in size; however, the algorithm we present does not require polytopes to be bounded.

apply equally well to all dimensions. However, to avoid confusion, we will just discuss the case of polytopes in $\mathbb{R}^3$.

Since we never consider non-convex polytopes, we simplify terminology by omitting the adjective "convex" and using "polytope" to mean convex polytope.

After working out the rather complex algorithm for ray-triangle intersection in the previous section, one might fear that ray-polytope intersection algorithms are even more complex. Surprisingly, and fortunately, this does not happen, and the algorithm for ray-polytope intersection is not particularly complicated.

Consider a fixed polytope. If there are k faces for the polytope, then the k planes bounding the polytope have normals $\mathbf{n}_i$ and scalars d_i for $1 \le i \le k$. By convention, the normals face outward from the polytope. Therefore, the polytope is the set of points $\mathbf{x}$ satisfying

$$\mathbf{x}\cdot\mathbf{n}_i \;\le\; d_i \qquad\qquad \text{for all } i = 0, 1, 2, \ldots k.$$

That is to say, the polytope is the intersection of the k closed half-spaces which are bounded by the k planes.

To intersect a ray with a convex polytope, we first intersect the ray with each of the k bounding planes. For each plane i, we compute the intersection $\mathbf{q}_i$ of the ray-line with that plane, along with the signed distance α_i from the originating point $\mathbf{p}$ to $\mathbf{q}_i$. In addition, we compute whether the ray-line hits the bounding plane from above or from below. By "from above," we mean that $\mathbf{u}\cdot\mathbf{n}_i < 0$ and that the ray direction vector $\mathbf{u}$ is pointing in the plane's downward direction. By "from below," we mean that $\mathbf{u}\cdot\mathbf{n}_i > 0$ and that the ray direction is pointing in the upwards direction.

An intersection from above is also called a "front intersection," meaning that the ray-line has hit the plane from its front face and is entering the half-space bounded by the plane. An intersection from below is also called a "back intersection," and the ray-line is hitting the back face and is exiting the half-space. The intersections are categorized as front or back intersections based on the dot product $\mathbf{u}\cdot\mathbf{n}_i$ according to the following table.

Test	Meaning
$\mathbf{u}\cdot\mathbf{n}_i < 0$	Front intersection: ray-line entering half-space
$\mathbf{u}\cdot\mathbf{n}_i > 0$	Back intersection: ray-line exiting half-space
$\mathbf{u}\cdot\mathbf{n}_i = 0$ & $\mathbf{p}\cdot\mathbf{n}_i \le d_i$	Parallel ray below face: front intersection, $\alpha_i = -\infty$.
$\mathbf{u}\cdot\mathbf{n}_i = 0$ & $\mathbf{p}\cdot\mathbf{n}_i > d_i$	Parallel ray above face: back intersection, $\alpha_i = -\infty$.

The degenerate case of the ray being parallel to the plane is treated by the convention that it hits the plane at $\alpha = -\infty$. However, in this case, it may be treated as either a front or a back intersection. This is consistent with the treatment of other front and back intersections in that it makes the following property hold:

Lemma XI.1. *Let $\mathbf{q}_i$ and α_i be set for the i-th plane as above. Let $\mathbf{p}(\beta) = \mathbf{p} + \beta\mathbf{u}$. Then,*

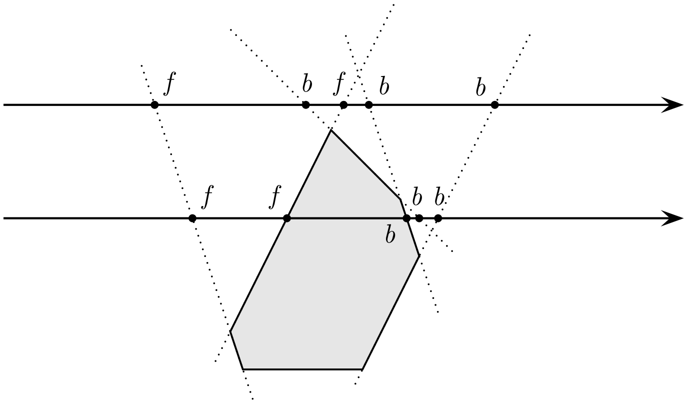

Figure XI.4: The two rays are shown intersecting the bounding planes of the shaded polytope. Front intersections are labeled "f" and back intersections are labeled "b". The upper ray hits some back intersections before some front intersections and thus does not intersect the polytope. The lower ray hits all the front intersections before all the back intersections and thus does intersect the polytope.

a. *If the intersection with the i-th plane is a front intersection then* $\mathbf{p}(\beta)$ *is in the half-space bounded by the i-th plane if and only if $\beta \ge \alpha_i$.*

b. *If the intersection with the i-th plane is a back intersection then* $\mathbf{p}(\beta)$ *is in the half-space bounded by the i-th plane if and only if $\beta \le \alpha_i$.*

The proof of the lemma is immediate from the definitions.

The property of the lemma is the crucial idea behind the algorithm for intersecting a ray and a convex polytope. The algorithm calculates all the α_i and $\mathbf{q}_i$ values and categorizes them as either front or back intersections. It then lets

$$\begin{aligned} \texttt{fMax} &= \max\{\alpha_i : \text{the } i\text{-th intersection is a front intersection}\} \\ \texttt{bMin} &= \min\{\alpha_i : \text{the } i\text{-th intersection is a back intersection}\}. \end{aligned}$$

The ray-line then intersects the polytope if and only if $\texttt{fMax} \le \texttt{bMin}$. If $\texttt{fMax} \ge 0$, then the ray intersects the polytope boundary first at $\mathbf{p}(\texttt{fMax})$, and it is entering the polytope at this point. If $\texttt{fMax} < 0 \le \texttt{bMin}$, then $\mathbf{p}$ is inside the polytope, and the ray first hits the polytope boundary at $\mathbf{p}(\texttt{bMin})$; it is exiting the polytope at this point. If however, $\texttt{bMin} < 0$ or $\texttt{bMin} < \texttt{fMax}$, then the ray does not intersect the polytope. Figure XI.4 illustrates the idea for this intersection testing algorithm.

To verify all the assertions of the last paragraph, you simply note that, in order to be in the polytope, it is necessary and sufficient to be inside all the half-spaces simultaneously. The front intersections give the point where the line enters a half-space, and the back intersections are where the line exits a half-space.

We can now give the intersection algorithm based on the above constructions. We use ±∞ only as a shorthand notation for very large (in absolute value) positive and negative numbers.

```
Input:  A ray specified by $\mathbf{p}$ and a unit vector $\mathbf{u}$
        $k$ planes specified by normals $\mathbf{n}_i$ and scalars $d_i$.
Algorithm:
    Set fMax = $-\infty$;
    Set bMin = $+\infty$;
    For $i$ = $1, 2, ..., k$ {
        // Ray to plane intersection
        Set $s$ = $\mathbf{u} \cdot \mathbf{n}_i$;
        If ($s == 0$) {                        // If parallel to plane
            If ( $\mathbf{p} \cdot \mathbf{n}_i > d_i$ ) {
                Return "No intersection";
            }
            Else {
                Continue loop with next value of $i$;
            }
        }
        // If not parallel to plane
        Set $\alpha$ = $(d_i - \mathbf{p} \cdot \mathbf{n}_i)/s$;
        If ( $\mathbf{u} \cdot \mathbf{n}_i < 0$ ) {                   // If front intersection
            If ( $\alpha >$ fMax ) {
                If ( $\alpha >$ bMin ) {
                    Return "No intersection";
                }
                Set fMax = $\alpha$;
            }
        }
        Else {                                 // Else, back intersection
            If ( $\alpha <$ bMin ) {
                If ( $\alpha < 0$ or $\alpha <$ fMax ) {
                    Return "No intersection";
                }
                Set bMin = $\alpha$;
            }
        }
    }                                          // End of for loop
    If ( fMax > 0 ) {
        Set $\alpha$ = fMax;
    }
    else {
        Set $\alpha$ = bMin;
    }
    Return $\mathbf{q} = \mathbf{p} + \alpha\mathbf{u}$;
```

There are some notable special cases where the above algorithm can be sped up. In particular, a number of common shapes like cubes, rectangular prisms, parallelepipeds, and k-DOP's (see Section XI.2) have bounding planes that come in pairs with opposite faces parallel. For these, it is possible to speed up the algorithm by treating pairs of parallel faces simultaneously.

XI.1.5 Ray versus cylinder intersections

The intersection of a ray with a cylinder can be done by combining the techniques for intersecting rays with spheres and polytopes. We will consider only the case of right, circular, finite cylinders: such a cylinder is specified by a radius r, an axis $\mathbf{v}$, a center point $\mathbf{c}$, and a height $\mathbf{h}$. It is convenient to assume that $\mathbf{v}$ is a unit vector. The cylinder consists of the points that both lie within distance r of the line through $\mathbf{c}$ in the direction $\mathbf{v}$ and are between the two planes perpendicular to $\mathbf{v}$ that are distance $h/2$ away from the center $\mathbf{c}$. That is to say, the cylinder is the set of points

$$\{\mathbf{x} : ||\mathbf{x} - ((\mathbf{x}-\mathbf{c})\cdot\mathbf{v})\mathbf{v} - \mathbf{c}||^2 \le r^2\} \cap \{\mathbf{x} : ((\mathbf{x}-\mathbf{c})\cdot\mathbf{v})^2 \le (h/2)^2\}.$$

The cylinder is expressed as the intersection of two sets of points: the first set is the infinite height cylinder, and the second set is the region bounded between two parallel planes. Clearly, a cylinder is convex.

The algorithm to intersect a ray with this cylinder proceeds as follows. First, use essentially the method of Section XI.1.1 to find where the ray-line intersects the infinite height cylinder: this gives zero, one, or two intersections. (Handle the case of the ray being parallel to the cylinder's axis as a special case.) If there is only one intersection, it is a glancing intersection and should be treated as being either zero or two intersections. If there are two intersections, categorize them as being front and back intersections, much like what was done in the algorithm for ray-polytope intersection; the front intersection will always precede the back intersection. Otherwise, if the ray does not intersect the infinite cylinder, it also does not intersect the finite cylinder. Second, intersect the ray with the two parallel planes, getting its front and back intersections (the degenerate case of the ray parallel to the planes is best treated as a separate special case). Again, the front intersection will always precede the back intersection. Third, combine the (up to) four intersections in the same manner as was used for ray-polytope intersections. Figure XI.5 illustrates the idea for this intersection testing algorithm.

Exercise XI.4. Fill in the details of the above paragraph and write an algorithm for ray-cylinder intersections.

The `RayTrace` software package described in Appendix **??** includes more general cylinders, allowing them to have elliptical cross section and to have bounding planes that are not perpendicular to the central axis. We leave it to the reader as an exercise to work out efficient intersection algorithms for these.

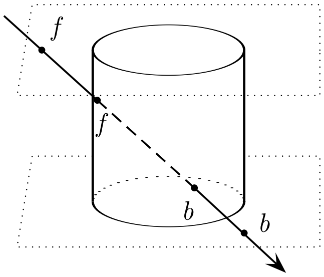

Figure XI.5: A cylinder is the intersection of an infinite cylinder and the area between two parallel planes. The ray is shown hitting the top plane, then entering the (infinite) cylinder, then exiting the cylinder, and finally hitting the bottom plane. All the front intersections come before all the back intersections, so the ray does intersect the cylinder.

XI.1.6 Ray versus quadric intersections

A *quadric* is a surface in 3-space which consists of the points satisfying a polynomial of degree 2. That is to say, a quadric is a surface which consists of all points $\langle x, y, z\rangle$ satisfying a identity $f = 0$, where f is a function of the form

$$f(\langle x, y, z\rangle) \;=\; Ax^2 + By^2 + Cz^2 + Dxy + Exz + Fyz + Gx + Hy + Jz + K.$$

Examples of quadrics include spheres, ellipsoids, cylinders, paraboloids, and hyperboloids.

To intersect a ray with a quadric, let $\mathbf{p}$ and $\mathbf{u}$ specify the starting point and the direction of the ray as usual. Let $\mathbf{p}(\alpha)$ equal $\mathbf{p} + \alpha\mathbf{u}$. To find the points $\mathbf{p}(\alpha)$ that lie on the quadric, we need to find the values for $\alpha \geq 0$ such that $f(\mathbf{p}(\alpha)) = 0$. Since f is a polynomial of total degree two, the value of $f(\mathbf{p}(\alpha))$ is a polynomial of degree two,

$$f(\mathbf{p}(\alpha)) \;=\; a\alpha^2 + b\alpha + c.$$

Solving for values of α such that $f(\mathbf{p}(\alpha)) = 0$ can easily be done with the quadratic formula, and yields 0, 1, or 2 solutions. The least nonnegative solution, if any, gives the first intersection of the ray with the quadric.

For ray tracing applications, you want to know not only the point of intersection, but also the normal vector to the surface at that point. For a quadric, the normal vector can be found by using the method of Theorem IV.2 on page 153, using the gradient of f. Except in degenerate cases, the gradient, ∇f, will be nonzero.

XI.1.7 Ray versus Bézier patch intersections

Testing the intersection of a ray and Bézier patch can be a daunting task. In fact, there is no way to give a closed form solution to the problem, and one must instead use iterative methods to find the intersection approximately.

There are several approaches to algorithms that perform ray versus Bézier patch intersection testing. These basically fall into two categories: (a) Newton and quasi-Newton methods and (b) recursive subdivision methods.

Let a Bézier patch be given by a function $\mathbf{q}(u,v)$ which is, say, degree three in each of u and v, and let a ray be specified as usual by $\mathbf{p}$ and $\mathbf{u}$. Finding an intersection is the same as finding values for u, v, and α so that $||\mathbf{q}(u,v)-\mathbf{p}+\alpha\mathbf{u}|| = 0$. Alternatively, one can define $d(\mathbf{q})$ to equal the distance from $\mathbf{q}$ to the ray-line. In this case, we are seeking values for u and v such that $d(\mathbf{q}(u,v)) = 0$. In both approaches, we are seeking the zeros of a function. Newton methods and quasi-Newton methods are methods that, at least in ideal situations, will iteratively compute points that converge rapidly to a solution. Papers that discuss (quasi-)Newton methods include Toth [111] and Joy et al. [71].

Recursive subdivision algorithms are more straightforward, but do not hold out the promise of fast quadratic convergence of the type that can be obtained from (quasi-)Newton methods. For this, a surface patch is given a bounding volume such as bounding sphere or a bounding box. The ray is checked for intersections against the bounding volume. If an intersection occurs, then the Bézier patch is split into two subpatches using the de Casteljau subdivision algorithm, and the ray is recursively checked against both patches. The `RayTrace` software performs ray versus Bézier patch intersections in this way, using a bounding parallelepiped. The bounding parallelepiped is chosen so as to enclose the control points of the patch. This is sufficient, since the convex hull property guarantees that the entire Bézier patch lies in the convex hull of its control points.

A recursive subdivision algorithm for ray versus bicubic surface patch intersection was used already in the original publication on ray tracing by Whitted [121]. A more sophisticated, recursive subdivision algorithm is suggested by Nishita et al. [84], who subdivide Bézier patches into sizes smaller than half the size of the whole patch when this can be justified by convexity considerations: this allows for much faster convergence, particularly in cases where the ray is hitting the patch at an angle significantly away from parallel to the surface.

XI.2 Pruning intersection tests

We next discuss "pruning" methods that let us avoid having to perform so many intersection tests. For space reasons, we shall not cover these in depth, but instead give an overview of some of the more common techniques and give some references at the end for further reading.

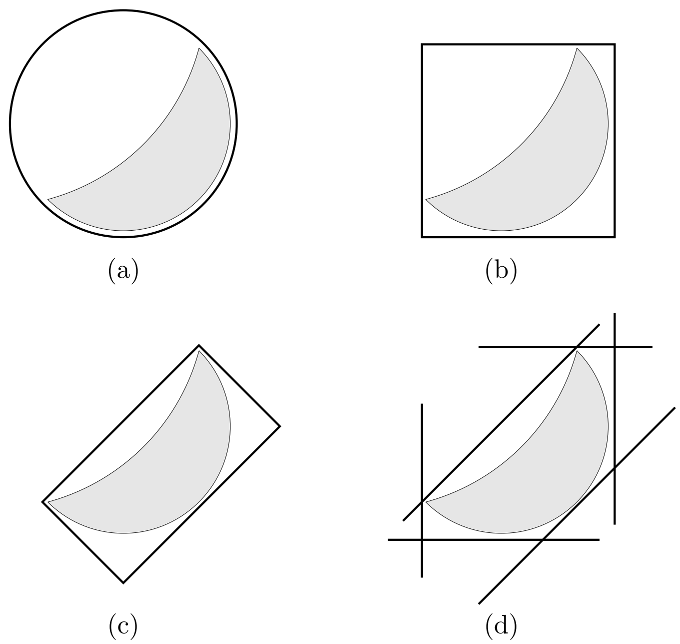

Figure XI.6: Various kinds of two dimensional bounding volumes enclosing a crescent shape. (a) is a bounding sphere. (b) is an axis aligned bounded box (AABB). (c) is an oriented bounding box (OBB). (d) is a discrete oriented polygon (k-DOP) with $k = 3$.

There are several standard approaches used to prune intersection tests. The first is to use bounding volumes to enclose objects. The bounding volumes are picked to be much simpler than the enclosed object and must completely enclose the object. If there is no intersection with the bounding volume, then there is also no intersection with the enclosed object. Common bounding volumes include bounding spheres, bounding boxes called AABB's and OBB's, and k-DOP's. Figure XI.6 shows examples of these different types of bounding volumes. A bounding sphere is a sphere that completely encloses an object. An AABB is an *axis-aligned bounding box* and is a bounding box whose edges are parallel to the standard x, y, z-axes. An OBB is an *oriented bounding box*: this is a box placed at an arbitrary orientation. Computing intersections against OBB's is more complex than against AABB's, but OBB's can sometimes more closely enclose an object, plus have the flexibility to move with an object as it changes orientation. A k-DOP, is a *discrete oriented polygon*: it is a convex polytope bounded by k planes, where the k-planes come in pairs so that opposite faces of the polytope are parallel (it is permitted for some planes to be extraneous and intersect the k-DOP in only a single point).

The second approach to pruning intersection tests involves partitioning

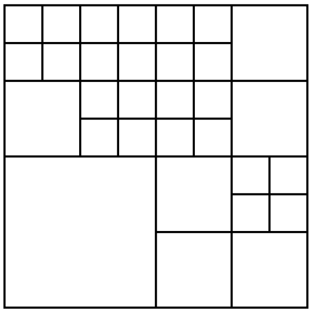

Figure XI.7: A quadtree.

space into regions. Each object lies in one or more regions. When a ray is tested for intersections with the set of all objects, the regions that the ray intersects are traversed one at a time: for each region that the ray enters, the ray intersection tests are performed for each object which intersects the region. There are a wide variety of ways to partition space: representative methods include (a) room or cell based methods, (b) quadtrees or octtrees, (c) k-d trees, and (d) BSP trees.

Room or cell based partitions apply well to situations where space is partitioned into rooms or regions: typical applications that could use room based partitions are 3-D models of houses or buildings, and computer games where the player traverses rooms or other discrete regions. In a room based partition, the extents of the rooms would usually be explicitly set by the designer of the 3-D model.

Quadtrees are used to partition 2-space hierarchically into square regions, as shown in Figure XI.7. The root of a quadtree is an axis-aligned square containing the entire region of interest. It is split into the four subsquares obtained by dividing it into half horizontally and vertically. Each of these subsquares may themselves be split into four subsquares, and so on, recursively. The decision of whether to split a square into four sub-subsquares depends usually on how many objects intersect the region. The entire quadtree is stored as a tree structure, including pointers to allow traversal of the quadtree. Octtrees are the generalization of quadtrees to three dimensions: each node of an octtree is a cube, and can be split into eight sub-cubes.

k-d trees are a generalization of quadtrees. k-d trees partition space (of any dimension) by using axis-aligned planes, as shown in Figure XI.8. The root of a k-d tree is a rectangular box containing the region of interest. Each non-leaf node N in a k-d tree has two children, i.e., is split into two subregions. The two subregions are defined by choosing an axis and dividing the node N with a plane perpendicular to that axis. The most common way to choose the two subregions is by choosing a vertex $\mathbf{v}$ from an object in the region covered by N, choosing one axis, and splitting the region into two subregions based on $\mathbf{v}$'s coordinate for that axis. In 2-space this means choosing a vertical or horizontal

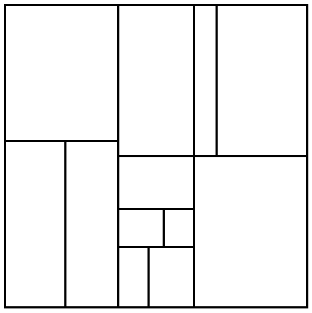

Figure XI.8: A k-d tree in two dimensions. A region in a k-d tree can be subdivided by either a vertical or a horizontal line.

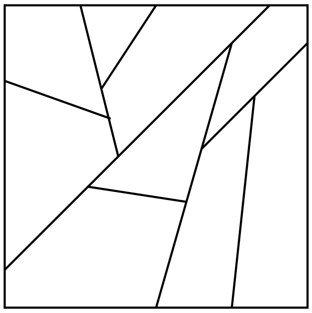

Figure XI.9: A BSP tree in two dimensions.

line through $\mathbf{v}$; in 3-space this means splitting the region with an axis-aligned plane through $\mathbf{v}$. The advantage of k-d trees over quadtrees is that one can intelligently pick the vertex $\mathbf{v}$ and axis direction so as to try to divide into sub-regions that partition the objects into sets of approximately equal size. The hope is that the tree will have lower depth and be faster to traverse.

Binary Space Partitioning trees, known as BSP trees, generalize k-d trees by allowing the regions to be partitioned by an arbitrary plane, rather than only axis-aligned planes. (See Figure XI.9.) Typically, the plane that divides a region is chosen so that it contains one of the faces of one of the objects in the region. BSP trees were first introduced by Fuchs et al. [51, 50], see also the references in the "Further reading" section below.

The third approach to pruning intersection tests is the use of hierarchical bounding volumes. This is actually a hybrid of the first two approaches. Typically, they work by first enclosing each individual object with a bounding volume, then enclosing pairs or small clusters of bounding volumes by another bounding volume, and recursively iterating this procedure until the entire scene in enclosed in a bounding volume. OBB's are a popular choice for these bounding volumes, see Gottschalk, Lin and Manocha [56], but other types of bounding volumes can be used as well.

Further Reading: Some good textbooks which cover octtrees, BSP's, and related spatial data structures are Samet [96, 95] and de Berg et al. [35]. Möller and Haines [80] describe many algorithms for AABB's, OBB's, k-DOP's, and hierarchical methods.

This chapter has discussed only intersecting rays against three dimensional objects. For many applications, one also wants to perform intersection tests on pairs of three dimensional objects to determine if they have collided or interpenetrated: this is a much harder task in general. For an overview of intersecting three dimensional objects, see Möller and Haines [80], who discuss algorithms for intersecting simple objects such as spheres, boxes, and k-DOP's. Exact algorithms for intersection testing between general convex objects have been given by Lin and Canny [77, 78] and Gilbert, Johnson and Keerthi [52]. As of this writing, at the University of North Carolina, the Geometry Group's web site, `http://www.cs.unc.edu/∼geom`, has a large number of related papers and resources, including extensive downloadable software.

Chapter XII

Radiosity

*This is a **preliminary** draft of a second edition of the book* 3-D Computer Graphics: A Mathematical Introduction with OpenGL. *So please read it cautiously and critically! Corrections are appreciated. Draft C.4.a*
Author: Sam Buss, `sbuss@ucsd.edu`

Radiosity is a global lighting method that tracks the spread of diffuse light around a scene. As a *global* lighting method, it attempts to simulate the effect of multiple light reflection. Unlike basic ray tracing, which tracks only the specular transport of light, radiosity tracks only the diffuse transport of light.

The goal of a radiosity algorithm is to calculate the illumination levels and brightness of every surface in a scene. As an example, consider a scene of a classroom with fluorescent light fixtures, painted walls, a non-shiny tile floor, and desks and other furniture. We assume that there are no shiny surfaces, and thus no significant amount of specular light reflection. All the light in the room emanates originally from the ceiling lights; it then reflects diffusely from objects in the room, especially from the walls and floor, providing indirect illumination of the entire room. For instance, portions of the floor underneath the desk may have no direct illumination from any of the lights; however, these parts of the floor are only partly shadowed. Likewise, the ceiling of the room receives no direct illumination from the overhead lights, but still is not completely dark. As a more extreme case, the bottom sides of the desk tops are partly shadowed, but are certainly not completely dark: they are illuminated by light reflecting off the floor.

Another common example of a scene with diffuse lighting is a room lit by indirect light, such as by a torchiere. A torchiere is a vertically standing, bright white light that shines up onto the ceiling of the room. The light reflects diffusely from the ceiling to illuminate the entire room, even though essentially none of the room is directly visible to the light. Radiosity can also model a room lit by indirect outdoor light.

Radiosity methods are, in many ways, complementary to ray tracing methods. Basic ray tracing tracks the global transport of specularly reflected light, whereas radiosity tracks the global transport of diffusely reflected light. Thus, radiosity is much better at softly lit scenes with subtle color shading, whereas ray tracing is better at rendering sharp shadows. Radiosity methods usually track the diffusely reflected light by starting at the light source and tracking the movement of illumination forward. Ray tracing generally starts at the view point position and tracks rays of light backwards (in the so-called *forward* ray tracing). For this reason, the results of ray tracing are view dependent, whereas the results of radiosity are view independent. Thus, radiosity can be used to preprocess a scene ahead of time, and once the radiosity algorithm is completed, the scene can be traversed in realtime without expensive computation. This means that radiosity is well suited to interactive walkthrough applications. By comparison, ray tracing cannot generally be viewed by a moving viewer in realtime, since the entire ray tracing procedure must be repeated for each change in the view position.

This chapter describes radiosity algorithms in some detail. However, before starting into the detailed mathematical algorithms, we give a high-level overview of radiosity algorithms.

Radiosity algorithms typically begin by breaking the scene into a set of flat polygons called "patches;" for an example, see Figure XII.1. The main goal of the radiosity algorithm will be to compute an illumination level, or brightness, of each patch. For this, the radiosity algorithm assumes that each patch is uniformly lit. In addition, it is assumed that all light is reflected only diffusely; that is to say, it is only the total illumination of a given patch that is important, and the direction of the incoming illumination can be ignored. Some of the patches are light sources: these are called emissive patches. For the other polygons, we wish to determine their illumination levels. This will be done by tracing the flow of all the light, from the light sources, through multiple bounces, to determine the overall light levels for each patch.

After breaking the scene into patches, the radiosity algorithm computes "form factors." The form factors will be used to describe how much light reflects diffusely from one patch to another. For each pair of patches, their form factor measures the fraction of the light that leaves the first patch which directly illuminates the second patch. For instance, if the first patch lies on the wall of the classroom, and the second patch corresponds to one tile on the floor, then the form factor would be equal to the percentage of the light leaving the wall's patch that goes directly to the tile.

Once the form factors have been determined, we set up equations that relate the patch illuminations and the form factors. These equations can be conveniently set up as a large system of linear equations. The remainder of the radiosity algorithm solves the system of equations to determine the level of illumination of each patch. Figure XII.2 shows an example of a scene with each patch illuminated according to the radiosity algorithm. In the figure, each patch is flat shaded, so the scene does not look realistic. But, as the final step of the radiosity algorthm, an averaging procedure is applied to make each patch smoothly shaded. Figure XII.3 shows the result of smoothly shading the patches.

Although we will describe the radiosity algorithm as computing a single brightness value for each patch, in fact, we really mean for it to compute a different brightness level at each wavelength (typically, red, green, and blue). As a general rule, the same patches and the same form factors are used for all wavelengths.

XII.1 The radiosity equations

XII.1.1 Patches, light levels, and form factors

The first step in rendering a scene in the radiosity algorithm is to break the surfaces in the scene into a set of small flat patches. The main part of the radiosity algorithm will treat each patch as being uniformly illuminated, but in the end, shading will be used to render the patches with smoothly varying illumination levels. It is important to choose the patches small enough so that the assumption that each patch is uniformly illuminated will not cause too much error in the calculation. Thus, the illumination levels should not change very much between adjacent patches or within a single patch; otherwise, the radiosity algorithm may give poor results.

An example of a scene broken into patches is shown in Figure XII.1, which shows a table and a box sitting in a room, with the whole scene drawn as wireframe quadrilaterals. This is a particularly simple example of a scene to break into patches, since all the surfaces are already rectangular. However, complications arise even here, since the changes in illumination levels are more pronounced near corners, and thus it helps to use smaller patches near corners.

There are a number of important issues involved in making a good choice for the patches. The smaller the patches, the more likely it is that the radiosity algorithm will succeed in calculating lighting levels well. On the other hand, the radiosity algorithm takes time at least $O(n^2)$, where n is the number of patches, so the running time increases quadratically with the number of patches. Even worse, the memory usage is also $O(n^2)$. Thus, it is common to use some kind of adaptive meshing, where some patches are large and some patches are small. In Figures XII.1-XII.3, we used smaller patches near the sides of the room, near the box and under the table: the idea is that patches should be smaller where the illumination levels are changing more rapidly.

We shall not discuss further issues in how to choose patches (see [27, 108] for a discussion of good tactics for choosing patches). Instead, we henceforth assume that patches have already been chosen. We label the patches $P_1, P_2, \ldots, P_n$. We let A_i denote the area of patch P_i.

The central goal of the radiosity algorithm is to determine the average brightness of each patch P_i. For this, we define B_i to equal the light intensity leaving patch P_i, divided by the area of P_i. Thus, the brightness B_i measures the light intensity per unit area, averaged over patch P_i. Note that the B_i values are different from the intensity levels, denoted I, discussed

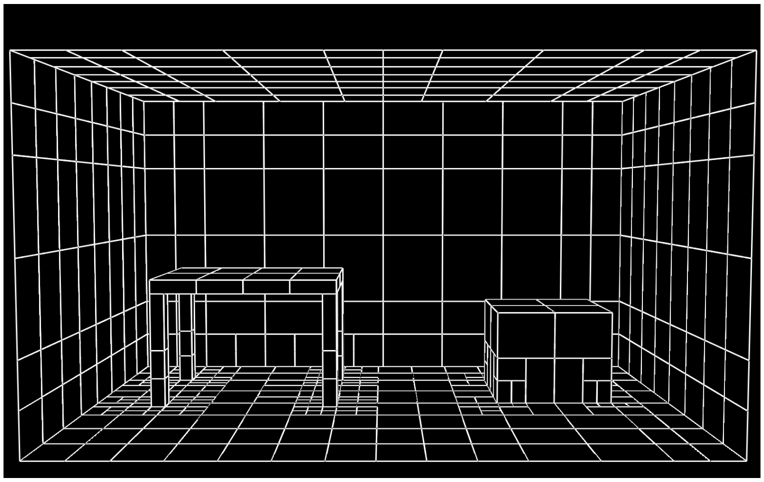

Figure XII.1: The patches used to render the radiosity scene of Figures XII.2 and XII.3. See color plate C.15.

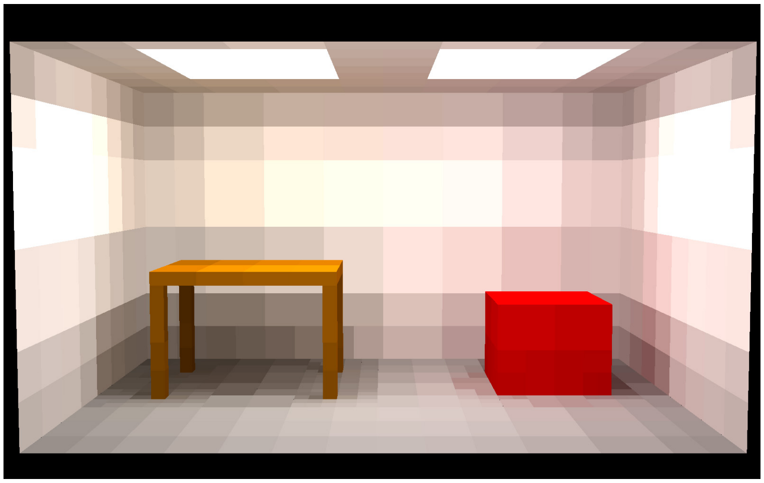

Figure XII.2: A radiosity rendered figure, with flat shading. It is evident that this image is based on the patches shown in Figure XII.1. See color plate C.16.

in Chapter IV. The intensities I were defined as light flux per unit area perpendicular to the direction of light propagation, whereas B_i equals light flux per unit of surface area. The reason for using brightness values instead of intensity levels is that we now are interested in the illumination levels for each individual patch, rather than (at least for the moment) in the illumination that reaches a viewer. However, the assumption that the surfaces are Lambertian

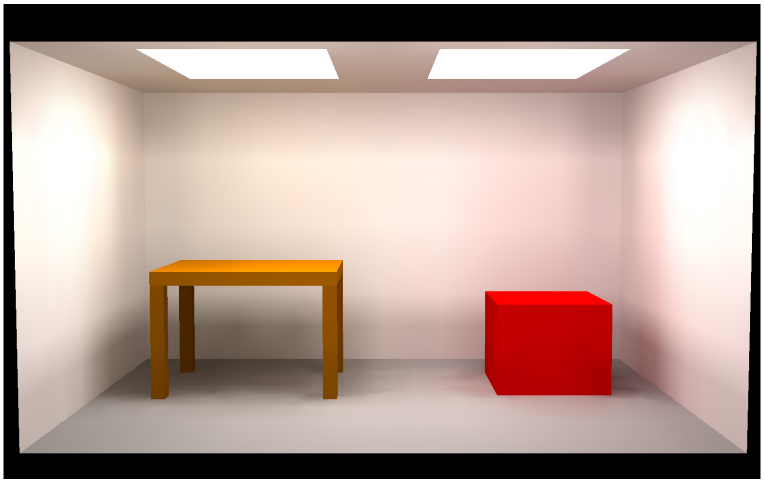

Figure XII.3: A radiosity rendered figure, with smooth shading of illumination. The red color of the box is reflected onto the nearby walls, giving them a slight reddish hue. This is based on the patches shown in Figure XII.1. See color plate C.17.

means the perceived brightness of a patch is proportional to its B_i value, and independent of the viewing angle.

Often, the term "radiosity" is used for the values B_i, but we will use the more intuitive term "brightness".

We write $B_i^{\rm in}$ to denote the brightness of the total light shining onto patch P_i. The equation relating the incoming and outgoing brightnesses is

$$B_i \;=\; E_i + R_i \cdot B_i^{\rm in}, \tag{XII.1}$$

where E_i is the emissiveness of the patch and R_i is the reflectivity of the patch. Like the brightness values B_i and $B_i^{\rm in}$, the emissiveness E_i is measured in terms of light energy per unit area. E_i represents the amount of light being generated by the surface (as compared to being reflected by the surface). Positive values of E_i are used for patches which are light sources. For ordinary surfaces other than lights, E_i should equal zero. The reflectivity value R_i specifies the color of the patch. Since we are considering only a single wavelength, R_i is a scalar and equals the fraction of incoming light that is (diffusely) reflected by the patch. We require that $0 \le R_i < 1$. If $R_i = 0$, the patch is not reflective at all, and values of R_i close to 1 mean that the patch is highly reflective. Values of R_i close to 0 are appropriate for black surfaces, and values near 1 are appropriate for white surfaces.

Equation (XII.1) gives a formula for the light leaving a patch in terms of the light incident on the patch. We also want to express the light incident to a patch in terms of the outgoing brightnesses of the rest of the patches. The light incident on a patch P_i should be equal to the total light leaving the other patches which directly illuminates patch P_i. To express this mathematically, let $F_{i,j}$ be the fraction of the light leaving patch P_i which shines directly onto patch P_j without reflecting off any intermediate patches. To handle the case of $i = j$, we let $F_{i,i} = 0$. The values $F_{i,j}$ are called *form factors*.

Since brightness is measured in terms of light intensity per unit area, the total light leaving patch P_j is equal to $A_j B_j$. Likewise, the total light entering patch P_i is equal to $A_i B_i^{\rm in}$. Therefore, the definition of form factors gives us

$$A_i B_i^{\rm in} \;=\; \sum_{j=1}^{n} F_{j,i} A_j B_j. \tag{XII.2}$$

We shall see later that the form factors satisfy the following *reciprocity* equation:

$$A_i F_{i,j} \;=\; A_j F_{j,i}.$$

With this, Equation (XII.2) may be rewritten as

$$B_i^{\rm in} \;=\; \sum_{j=1}^{n} F_{i,j} B_j. \tag{XII.3}$$

Combining Equations (XII.1) and (XII.3) gives the *radiosity equation*:

$$B_i \;=\; E_i + R_i \sum_{j=1}^{n} F_{i,j} B_j. \tag{XII.4}$$

The radiosity equation can be rewritten in matrix form by letting

$$\mathbf{B} \;=\; \begin{pmatrix} B_1 \\ \vdots \\ B_n \end{pmatrix} \qquad \text{and} \qquad \mathbf{E} \;=\; \begin{pmatrix} E_1 \\ \vdots \\ E_n \end{pmatrix},$$

and letting M be the $n \times n$ matrix, $M = (R_i F_{i,j})_{i,j}$. Then, the matrix form of the radiosity equation is

$$\mathbf{B} \;=\; \mathbf{E} + M\mathbf{B}. \tag{XII.5}$$

Letting I equal the $n \times n$ identity matrix, this can be rewritten as

$$(I - M)\mathbf{B} \;=\; \mathbf{E}.$$

The vector $\mathbf{E}$ of emissivities and the reflectivity values R_i are presumed to be known, and we shall see how to compute the form factors $F_{i,j}$. It will then remain to compute the value of the brightness vector $\mathbf{B}$. One way to do this would be to invert the matrix $(I - M)$. However, matrix inversion is relatively time consuming and difficult, so we discuss alternate, iterative methods of computing $\mathbf{B}$ in Section XII.3.

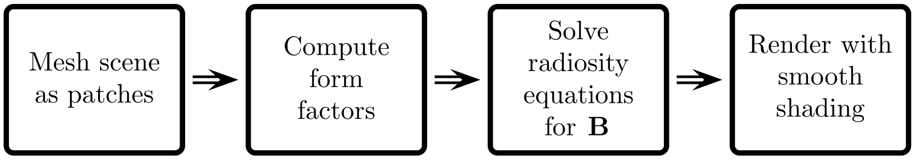
Mesh scene as patches
Compute form factors
Solve radiosity equations for **B**
Render with smooth shading

Figure XII.4: The four stages of the radiosity algorithm

XII.1.2 High-level description of the radiosity algorithm

We can now describe the major steps in the basic radiosity algorithm. These are illustrated in Figure XII.4. The first step is to model the scene and break it into patches P_i. We presume that the emissivities E_i and the reflectivities R_i are given ahead of time.

The second step is to compute the form factors $F_{i,j}$. This typically is the computationally difficult part of the radiosity algorithm and consumes most of the time needed for the radiosity computation. We shall discuss a couple methods for computing form factors in Section XII.2. Once the form factors are computed, it is easy to compute the entries in the matrix M and set up the Radiosity Equation (XII.5).

The third step is to solve the radiosity equation for the brightness levels $\mathbf{B}$. Several methods for solving this are presented in Section XII.3: these are iterative methods that mostly work by chasing light around the scene from the light sources (i.e., patches with nonzero emissivity values) and calculating better and better estimates for the brightness levels of all the patches.

The fourth step is to render the scene. Each patch has been assigned a brightness (or, color); but we do not want to merely render each patch as a flat color, instead we want to use interpolation to render the surfaces with smooth shading. (Figures XII.2 and XII.3 illustrate the difference between flat and smooth shading.) To obtain smooth shading, we first use the brightness levels for each patch to set the brightness levels for each patch vertex. For instance, each patch vertex can be assigned a brightness equal to a weighted average of the brightness levels of the adjacent patches. Once the brightness level is set for each vertex, then the patches can be rendered by standard means, using Gouraud interpolation. The use of interpolation and shading helps to smooth out the lighting and hide the fact that we computed a uniform average brightness level for each patch.

There are several complications that arise in the fourth step. First, the lighting levels will generally be only continuous — but not C^1-continuous — across patch boundaries, which can sometimes cause visible edges due to “Mach banding”. The human eye is fairly sensitive to discontinuities in the first-order derivative of lighting levels, and this tends to make boundaries between patches more visible than expected. Second, if the patches are not uniform in size, then one must be careful with adjacent patches which share an edge. This was already discussed at the end of Chapter II, as well as on page 293 with Figure VIII.15. If a larger patch shares part of an edge with another smaller patch, then the common edge should be split for rendering the larger patch too.

The first three stages of the radiosity algorithm in Figure XII.4 are *view independent*. The final, fourth state is view dependent of course, but this stage is computationally easy and efficient. For this reason, radiosity lends itself well to precomputation of lighting and allows interactive walkthroughs.

Figure XII.4 shows the most basic form of the radiosity algorithm. Frequently, one wishes to use adaptive methods to form patches: that is to say, based on the quality of the solution obtained in the third stage, one may wish to refine the patches in areas where light levels are changing rapidly or where the solution otherwise needs more accuracy. Thus, sophisticated algorithms may alternate between solving the radiosity equations, and adding more patches and computing new form factors.

XII.2 Calculation of form factors

Recall that $F_{i,j}$ is equal to the fraction of the light leaving patch P_i which goes directly to patch P_j. Clearly, the values of $F_{i,j}$ are always in the interval $[0,1]$. We assume that we have an enclosed environment, so that all light leaving a patch hits some other patch; in other words,

$$\sum_{j=1}^{n} F_{i,j} \;=\; 1.$$

This holds without loss of generality, since if necessary, we can add completely non-reflective black patches surrounding the environment.

To aid our intuition about the values of $F_{i,j}$, consider the situation shown in Figure XII.5. Here, a small patch P_2 is facing upward, and centered above it is a large patch P_1 facing downward. We expect the value of $F_{1,2}$ to be small, since only a relatively small fraction of the light leaving the upper patch hits the small lower patch. Conversely, we expect the value of $F_{2,1}$ to be large since the larger patch P_1 fills much of the field of view of the smaller patch.

Now consider two small patches P_i and P_j obliquely facing each other, as shown in Figure XII.6. The distance between the centers of the patches is equal to d, and the normal vectors to the two patches make angles $\varphi_{i,j}$ and $\varphi_{j,i}$ with the line joining the centers of the two patches. Here we assume that $\varphi_{i,j}$ and $\varphi_{j,i}$ are both less than 90°, since otherwise the two patches are not facing each other and the form factors are zero, $F_{i,j} = 0 = F_{j,i}$.

We further make the assumption that the patches are infinitesimally small, so as to make it easier to estimate the form factors. The patches have areas A_i and A_j. Consider the field of view of patch P_i. The other patch P_j has area A_j, but is turned away at an angle of $\varphi_{j,i}$ and is a distance d away.

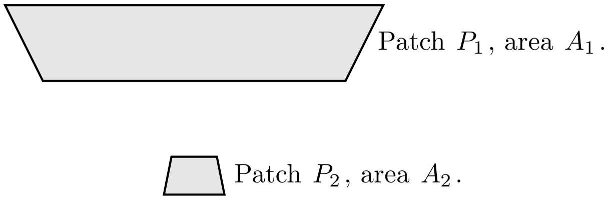

Figure XII.5: A large patch and small patch.

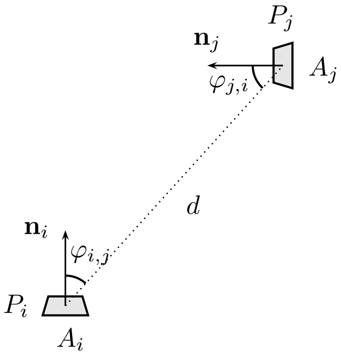

Figure XII.6: Two infinitesimally small patches P_i and P_j with areas A_i and A_j. The normals to the patches are $\mathbf{n}_i$ and $\mathbf{n}_j$.

Consider what happens when patch P_j is projected towards P_i onto the unit sphere centered around P_i. The area that the projection of patch P_j occupies on that unit sphere is equal to $(\cos\varphi_{j,i})A_j/d^2$. The area of the upper half of the unit sphere is equal to 2π; hence the fraction of P_i's field of view that is occupied by patch P_j is

$$\frac{(\cos\varphi_{j,i})A_j}{2\pi d^2}.$$

The surface of patch P_i is assumed to be Lambertian. A large Lambertian surface has the same apparent brightness from any viewing angle. But, as we remarked already on page 138, because of the foreshortening of areas when viewed obliquely, this means that the fraction of light that leaves the patch P_i in a direction at an angle $\varphi_{i,j}$ from the normal is proportional to $\cos\varphi_{i,j}$. Therefore, the fraction $F_{i,j}$ of the light energy that leaves P_i in the direction of P_j is *proportional* to

$$\cos\varphi_{i,j}\frac{(\cos\varphi_{j,i})A_j}{2\pi d^2}. \qquad \text{(XII.6)}$$

The constant of proportionality is set from the condition that the total light leaving patch P_i should of course be fraction 1 of the light. For this, we let S^{2+} denote the upper half of the unit sphere and, thinking of the patches A_j constituting the unit sphere around P_i, evaluate the integral

$$\int_{S^{2+}} \cos\varphi \, dA \;=\; \int_{\varphi=0}^{\pi/2} (\cos\varphi)(2\pi \sin\varphi)\, d\varphi \;=\; \pi.$$

Therefore, we need to drop the factor of 2 from Equation (XII.6), and the form factor $F_{i,j}$ is equal to

$$F_{i,j} \;=\; \frac{(\cos\varphi_{i,j})(\cos\varphi_{j,i})A_j}{\pi d^2}. \tag{XII.7}$$

One convenient property of the form factors is the reciprocity property that

$$F_{i,j}A_i \;=\; F_{j,i}A_j.$$

The reciprocity property is an immediate consequence of Equation (XII.7). In some cases, the reciprocity property can effectively cut the work of computing form factors in half. Usually, the areas are known, so once the form factors $F_{i,j}$ with $i<j$ have been computed, then the rest can be computed by using $F_{j,i} = F_{i,j}A_i/A_j$.

The above derivation of the formula XII.7 for the form factor is simple enough, but there are two potentially serious pitfalls. First, the formula was derived under the assumption that the two patches are infinitesimal in size, but are separated by a non-infinitesimal distance d. Often this assumption does not hold, and, in this case, the actual form factor may be quite different from the value given by formula (XII.7). As a general rule, if the sizes of the patches are small compared to the distance d, then Equation (XII.7) will be close enough to the correct value for practical purposes. Define the *diameter* of a patch to be the diameter of the smallest circle that contains the patch. Then if the distance d between the patches is at least five times the diameters of the patches, then Equation (XII.7) is likely to be sufficiently accurate.

One might wish to have a better formula for the form factors that could be applied to (say) arbitrary rectangles. Such formulas can be derived for important special cases, but even in simple cases, such as two patches that share a common edge and meet at right angles, the formulas are quite complicated. Thus, if you want more accurate calculation for form factors, then you must perform a double integral over the surfaces of the two patches. In practice, this means that the two patches are divided into multiple, sufficiently small subpatches, and the form factors between each subpatch of P_i and subpatch of P_j are computed using (XII.7). These form factors are then combined to obtain the overall form factor $F_{i,j}$ for P_i and P_j.

The second pitfall in using Equation (XII.7) concerns visibility. In other words, if there are other patches between P_i and P_j, then they can obstruct the light from P_i to P_j. Now, if the light from P_i to P_j is completely blocked, then $F_{i,j}$ is just equal to 0. On the other hand, if the light is only partially blocked, then the form factor needs to be reduced by multiplying by the fraction of light from P_i which can reach P_j.

XII.2.1 The ray tracing method

One method for computing the visibility between functions is to use ray tracing. We sketch a simple, and fairly robust, way to compute form factors with the aid of ray tracing.

The computation of the form factors will be based on Equation (XII.7), but with an additional visibility term $V_{i,j}$, which is an estimate for the fraction of patch P_i which is visible from patch P_j. Note that we will have $V_{i,j} = V_{j,i}$. One way to compute $V_{i,j}$ is to cast rays from k positions on patch P_i towards k positions on patch P_j. Ray tracing is then used to determine if these rays intersect any intermediate objects. We then set $V_{i,j}$ equal to the fraction of rays that were not obstructed by intersections with intermediate objects.

A good way to choose the k rays is to use the method of jittering discussed in Chapters VI and X. You can choose k jittered subpixel positions on each of P_i and P_j, then choose a random one-to-one correspondence between jittered positions in P_i and jittered positions in P_j, and cast rays between the corresponding points.

The rest of the form factor calculation is unchanged. We let $\mathbf{c}_i$ and $\mathbf{c}_j$ be the centers of P_i and P_j, let d be the distance from $\mathbf{c}_i$ to $\mathbf{c}_j$, and let $\varphi_{i,j}$ and $\varphi_{j,i}$ be the angles that the patches' normals make with the vector $\mathbf{c}_j - \mathbf{c}_i$. Then the form factor can be estimated by

$$F_{i,j} \;=\; V_{i,j}\frac{(\cos\varphi_{i,j})(\cos\varphi_{j,i})A_j}{\pi d^2}.$$

XII.2.2 The hemicube method

The hemicube method, introduced by Cohen and Greenberg [26], is a method for computing form factors which takes advantage of hardware acceleration using the depth buffer algorithms present in most graphics chips. The hemicube algorithm computes the form factors for a particular patch P_i by rendering a view of the world from the viewpoint of patch P_i. For every other patch P_j, this rendered view can be used to determine what fraction of P_i's field of view is occupied by patch P_j. After compensating for distance and for the cosine factors, this gives the form factor $F_{i,j}$.

The basic idea of the hemicube algorithm is illustrated in Figure XII.7. Here a virtual hemicube is placed over the center of patch P_i. The hemicube is the top half of a cube with sides of length 2. The field of view occupied by patch P_j is projected towards P_i onto the hemicube. Clearly, the form factor $F_{i,j}$ is the same as the form factor from P_i to the projection of P_j.

This does not yet take visibility or occlusion into account. Now, for each of the five faces of the hemicube, the top and the four sides, we render a view of the scene from the center of P_i as seen through that face. This maps every other patch onto a (possibly empty) set of pixels of the viewscreen, and the depth buffer algorithm keeps track of which patches are visible in the direction of any given pixel. At the end of rendering the scene from the point of view

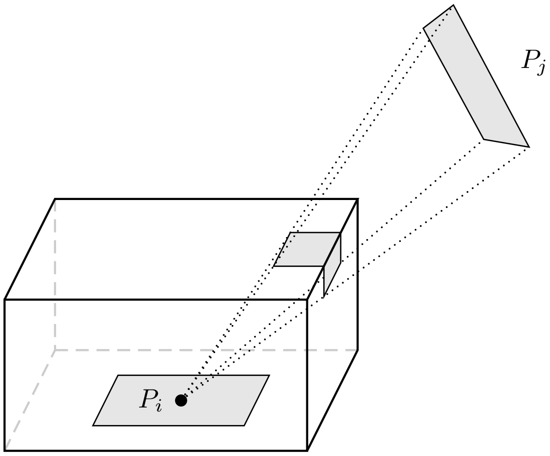

Figure XII.7: Projection onto a hemicube.

of P_i, we do not display the rendered scene as usual, but instead read the contents of the image buffer to determine which patch was visible at each pixel position.

We use a trick to determine which patch is visible in each pixel position. We do not render the patches in their correct color, but instead, we assign to each patch P_j a distinct color, C_j. Then, P_j is visible at a given pixel position if and only if the pixel has been rendered with color C_j. Since there are typically $(256)^3$ many distinct colors, there will be plenty of colors available to give each patch a distinct color.

The hemicube algorithm estimates the form factor $F_{i,j}$ as the sum of the form factors from P_i to the pixels showing P_j, namely as

$$F_{i,j} \;=\; \sum_{\substack{\text{Pixels}\\ \text{showing } P_j}} (\text{fraction of } P_i\text{'s light that reaches pixel}). \qquad \text{(XII.8)}$$

Figure XII.8 shows the situation for a pixel in the top surface of the hemicube. Here a pixel containing the color of P_j is at coordinates $\langle x, y, 1\rangle$ on the top surface of the hemicube, where the coordinates refer to the natural coordinatization of the hemicube relative to placing the origin at the center $\mathbf{c}_i$ of patch P_i. The distance from $\mathbf{c}_i$ to the pixel is $d = \sqrt{x^2+y^2+1}$. The angles $\varphi_{i,j}$ and $\varphi_{j,i}$ are equal, and the cosine of this angle is equal to $1/d$. Thus, referring back to Equation (XII.7), the contribution to the summation (XII.8)

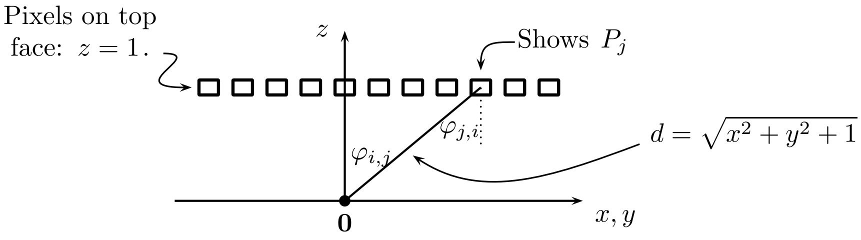

Figure XII.8: A row of pixels along the top of the hemicube. One pixel shows patch P_j. The origin is placed at the center of patch P_i. The top of the cube is the $z = 1$ plane.

from pixels on the top of the hemicube is

$$\sum_{\substack{\text{Pixels on top} \\ \text{showing } P_j}} \frac{(1/d)(1/d)(PixelArea)}{\pi d^2} = \sum_{\substack{\text{Pixels on top} \\ \text{showing } P_j}} \frac{(PixelArea)}{\pi d^4},$$

where $d^4 = (x^2 + y^2 + 1)^2$. The "$PixelArea$" value is equal to the area occupied by a single pixel on the top of the cube. Since the top of the cube is a 2×2 square, the pixel area will be $4/(w\,h)$ where h and w stand for "height" and "width," and are the dimensions of the image buffer measured in pixels.

Pixels from the view through the side faces of the hemicube contribute similarly to the form factor $F_{i,j}$. For instance, pixels on any of the four side faces of the hemicube, as shown in Figure XII.9, contribute the following amount to $F_{i,j}$:

$$\sum_{\substack{\text{Pixels on side} \\ \text{showing } P_j}} \frac{z(PixelArea)}{\pi d^4},$$

where z is the z-component of the side face pixel.

There are some odd side effects that can arise when using the hemicube method. One phenomenon is that patches are treated asymmetrically when computing form factors. That is to say, when computing $F_{i,j}$ for i fixed and for all j's, we are essentially treating patch P_i as a single point, whereas we are treating the other patches as extended areas. Therefore, the reciprocity condition may no longer hold. On the other hand, it is still guaranteed that $\sum_j F_{i,j} = 1$; this is important, since the convergence of the algorithms discussed in the next section for solving the radiosity equations depends on this fact. Finally, like any method based on discretization into pixels, the hemicube method is subject to errors involving aliasing.

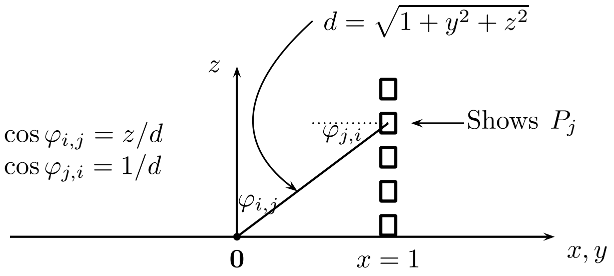

Figure XII.9: A row of pixels along the $x=1$ side of the hemicube.

XII.3 Solving the radiosity equations

We now assume that all patch geometry has been set and the form factors have all been computed; this means that the matrix M is completely known, and it remains to solve the Radiosity Equation (XII.5) for the value of the brightness vector $\mathbf{B}$. The first section below will discuss theoretical issues, especially iterative methods that can obtain approximate values for $\mathbf{B}$. The basic iterative method, called Jacobi iteration, works by solving a fixed point equation by iterating a function. However, there are various ways to improve on this basic iteration. We give sketches of proofs that these various methods are guaranteed to converge. The remaining three sections describe the details of implementing successively better iterative methods for solving the radiosity equations.

XII.3.1 Iterative methods

Recall that the matrix form of the radiosity equations is

$$(I-M)\mathbf{B} \;=\; \mathbf{E}.$$

The vectors $\mathbf{B}$ and $\mathbf{E}$ have n entries and M is an $n \times n$ matrix. I is the $n \times n$ identity matrix and we assume that $\mathbf{E}$ and M are known. We wish to solve for the brightness vector $\mathbf{B}$.

Of course, one way to solve for $\mathbf{B}$ would be to invert the matrix $I-M$ and just set

$$\mathbf{B} \;=\; (I-M)^{-1}\mathbf{E}.$$

The problem with this is that inverting a large matrix can be computationally expensive and difficult to implement robustly. Since n is the number of patches in the scene, the matrix is indeed quite large, say on the order of $n = 10,000$ for moderately complex scenes. It is not hard to verify that the straightforward algorithms for matrix inversion require running time of $O(n^3)$, so it would be prohibitively difficult to invert such a large matrix.

On the other hand, the matrix M enjoys a number of special properties, and there are iterative methods that can exploit these properties to get better and better approximations to the correct solution to the radiosity equation. These special properties of M are captured by the next lemma.

Definition XII.1. The entry in the i-th row and j-th column of M is denoted $m_{i,j}$. We denote this by $M = (m_{i,j})_{i,j}$. Let $\max(M)$ be the maximum entry of M. Let $\mathit{RowSum}_i(M)$ be the sum of the entries in the i-th row of M, i.e.,

$$\mathit{RowSum}_i(M) \;=\; \sum_{j=1}^{n} m_{i,j}.$$

Finally, let $\mathit{MaxRowSum}(M) = \max\{\mathit{RowSum}_i(M) : i = 1, \ldots, n\}$.

Lemma XII.2. *Let $M = (m_{i,j})_{i,j}$ be the matrix for the radiosity equation.*
(a) *For all i, j, $m_{i,j} \geq 0$.*
(b) $0 \leq \mathit{MaxRowSum}(M) < 1$.
(c) *Let $\alpha = \mathit{MaxRowSum}(M)$. For all $k \geq 0$,*

$$\mathit{MaxRowSum}(\,M^k\,) \;\leq \alpha^k.$$

In particular, $\max(M^k) \leq \alpha^k$.

Proof. The fact that (a) and (b) hold follows immediately from the definition of M. Each diagonal entry of M is zero, and each off-diagonal entry is equal to $m_{i,j} = R_i F_{i,j}$ which is certainly nonnegative. Thus, (a) holds. To prove (b), note that the sum of the entries in the i-th row is equal to

$$\sum_{j=1}^{n} m_{i,j} \;=\; R_i \sum_{j=1}^{n} F_{i,j} \;=\; R_i.$$

As mentioned in Section XII.1.1, the reflectances are strictly less than one for any realistic situation. Thus, each row sum is less than one, and as there are finitely many rows, the maximum row sum exists and is less than one.

Now we prove (c). For k equal to 0 or 1, (c) is trivially true. The general case is proved by induction on k. First note that every entry in M^k is nonnegative. In order to prove the induction step, we need the following fact:

Claim *If $N = (n_{i,j})_{i,j}$ and $P = (p_{i,j})_{i,j}$ are arbitrary matrices containing only nonnegative entries, and if $\nu = \mathit{MaxRowSum}(N)$ and $\rho = \mathit{MaxRowSum}(P)$, then*

$$\mathit{MaxRowSum}(NP) \leq \nu\rho.$$

To prove the claim, note that the entry in row i and column k of the product NP is equal to

$$\sum_{j=1}^{n} n_{i,j} p_{j,k}.$$

Thus, $\mathit{RowSum}_i(NP)$ can be bounded by

$$\begin{aligned}\mathit{RowSum}_i(NP) &= \sum_k \sum_j n_{i,j} p_{j,k} \;=\; \sum_j n_{i,j} \sum_k p_{j,k} \\ &\le \sum_j n_{i,j}\rho \;\le\; \nu\rho.\end{aligned}$$

That proves the claim, and now part (c) follows easily using induction on k. □

In particular, part (c) of the lemma implies that every entry in M^k is $\le \alpha^k$. Thus, since $\alpha < 1$, the matrices M^k converge quickly to zero as k tends to infinity. With part (c) of the lemma proved, are now able to establish that the matrix $I - M$ is invertible. One motivation for the next theorem comes from the Taylor series for the function $f(x) = 1/(1-x)$. It is not hard to show, using the formula for Taylor series, that

$$\frac{1}{1-x} \;=\; 1 + x + x^2 + x^3 + x^4 + \cdots,$$

for all x such that $|x| < 1$. Thus, one might guess that a similar fact holds for the matrix $I - M$, namely,

$$(I-M)^{-1} \;=\; I + M + M^2 + M^3 + M^4 + \cdots,$$

where the role of the condition that $|x| < 1$ is now played by the property that $\mathit{MaxRowSum}(M) < 1$. This formula for matrix inverse does indeed hold, as the next theorem states.

Theorem XII.3. *Let M satisfy the properties of parts (a) and (b) of Lemma XII.2. Then $I - M$ is invertible and its inverse is equal to the infinite sum*

$$I + M + M^2 + M^3 + M^4 + \cdots. \tag{XII.9}$$

Proof. We give a sketch of the proof. The first observation is that the summation (XII.9) converges to a matrix N, where the limit N is a matrix in which all entries are finite. This is because each entry in M^k is in the range $[0, \alpha^k]$, and because the geometric series $\sum_k \alpha^k$ has a finite limit.

Let N_k be the matrix equal to the first $k+1$ terms in the series:

$$N_k \;=\; I + M + M^2 + M^3 + \cdots + M^k.$$

As $k \to \infty$, $N_k \to N$, where N is the matrix given by (XII.9). Now,

$$\begin{aligned}(I-M)N_k &= (I-M)(I + M + \cdots + M^{k-1} + M^k) \\ &= (I + M + \cdots + M^{k-1} + M^k) - (M + M^2 \cdots + M^k + M^{k+1}) \\ &= I - M^{k+1}.\end{aligned}$$

Since $M^{k+1} \to 0$, we have $(I-M)N_k \to I$ as $k \to \infty$. By the continuity of matrix product, this means that $(I-M)N = I$. This proves the theorem. □

An important consequence of Theorem XII.3 is that there is a unique solution $\mathbf{B}$ to the radiosity equation, namely, $\mathbf{B} = (I - M)^{-1}\mathbf{E}$. The theorem also suggests one method for approximating $\mathbf{B}$: First, choose a value of k large enough so that M^k is expected to be sufficiently close to zero. Then, compute N_k, the first $k+1$ terms of the power series. Then set $\mathbf{B} = N^k\mathbf{E}$, so

$$\mathbf{B} \ = \ (I + M + M^2 + M^3 + \cdots + M^k)\mathbf{E}.$$

This would indeed work, but the runtime would still be much slower than we would like, since computing powers M^i of M requires iterated matrix multiplication and since the usual algorithms for matrix multiplication have a fairly poor cubic runtime of $O(n^3)$ for $n \times n$ matrices. There are better algorithms for matrix multiplication, but even those are still not as good as we would like.

To find a faster algorithm, we cast the radiosity equation back into its original form $\mathbf{B} = \mathbf{E} + M\mathbf{B}$. We think of this as a *fixed point problem* by defining an operator Ω that acts on matrices by

$$\Omega(\mathbf{B}) = \mathbf{E} + M\mathbf{B}.$$

Then we are seeking a $\mathbf{B}$ (in fact, the unique $\mathbf{B}$) such that

$$\Omega(\mathbf{B}) \ = \ \mathbf{B}.$$

We call such a $\mathbf{B}$ a *fixed point* of Ω. A standard way to solve fixed point problems is to choose an initial guess for the value of $\mathbf{B}$, and then repeatedly apply the operator Ω. If we are lucky (and we will be lucky in the present situation), then repeatedly applying Ω yields a sequence of matrices that converge to a finite limit. In that case, the limit of the sequence will be a fixed point of Ω.

To make this more concrete, define a sequence of vectors $\mathbf{B}_0, \mathbf{B}_1, \mathbf{B}_2, \ldots$ by

$$\begin{aligned} \mathbf{B}_0 \ &= \ \mathbf{0} \quad \text{(the zero vector)} \\ \mathbf{B}_{k+1} \ &= \ \mathbf{E} + M\mathbf{B}_k, \end{aligned}$$

for all $k \geq 0$. Thus, $\mathbf{B}_1 = \mathbf{E}$ and $\mathbf{B}_2 = \mathbf{E} + M\mathbf{E} = (I + M)\mathbf{E}$ and $\mathbf{B}_3 = \mathbf{E} + M\mathbf{E} + M^2\mathbf{E} = (I + M + M^2)\mathbf{E}$. For general k,

$$\mathbf{B}_{k+1} \ = \ (I + M + M^2 + \cdots + M^k)\mathbf{E}.$$

Therefore, by the earlier theorem and proofs, $\mathbf{B}_k$ converges to the solution of the radiosity equation as k increases.

The fixed point algorithm for approximating the solution $\mathbf{B}$ of the radiosity equation is mathematically equivalent to the power series algorithm. However, in the fixed point algorithm, each iteration uses only one matrix-vector product and one matrix addition. This takes time only $O(n^2 + n) = O(n^2)$ and is considerably faster than the power series algorithm, which required matrix multiplications.

There is a simple physical intuition for the meaning of the intermediate brightness vectors $\mathbf{B}_k$ obtained by the fixed point iteration method. The first nonzero one, $\mathbf{B}_1 = \mathbf{E}$, is just the directly emitted light. The second one, $\mathbf{B}_2 = \mathbf{E} + M\mathbf{E}$, is equal to the emitted light, plus the illumination from a single bounce of the emitted light. The k-th one, $\mathbf{B}_k$, is equal the lighting that results after $k-1$ bounces of reflected light.

A useful property of the $\mathbf{B}_i$ vectors is that they are increasing. Let the notation $B_{k,i}$ represent the i-entry of $\mathbf{B}_k$. Then the increasing property states that, for all i, k, we have $B_{k,i} \le B_{k+1,i}$. This is easy to prove by induction on k, using the fact that every entry in the matrix M is nonnegative. Intuitively, this corresponds to the fact that the more reflection bounces that are taken into account, the brighter the scene gets.

The proof of Theorem XII.3 and Lemma XII.2 gives an estimate for the rate of convergence of the fixed point iterative algorithm. Namely, the errors of the entries N_k are bounded by $\sum_{i>k} \alpha^i = \alpha^{k+1}/(1-\alpha)$ where α is the maximum reflectivity of the patches. Actually, the error tends to zero more like β^k, where β is the *average* of the reflectivities. Thus, not surprisingly, the lower the reflectivity values, the fewer iterations are needed to achieve a good accuracy. That is, the lower the reflectivities, the smaller the number of "bounces" that need to be followed.

The iterative fixed point method described above is the same as the Jacobi iteration given in more detail in the next section.

XII.3.2 Jacobi iteration

The Jacobi method for solving the radiosity equation is just the iterative method described in the previous section. This algorithm computes successively $\mathbf{B}_1, \mathbf{B}_2, \mathbf{B}_3, \ldots$. Here is the algorithm expressed in terms of individual entries, rather than in terms of vectors.

```
JacobiIteration.
    // B[], E[] and Bnew[] are arrays.  E[] is already set.
    // m[i,j] denotes $m_{i,j}$.
    // Initialization set $\mathbf{B} = \mathbf{E}$.
    For i = 1 to n {
        Set B[i] = E[i];
    }
    // Main loop.
    While (not converged enough) {
        For i = 1 to n {
            Set Bnew[i] = E[i] + $\sum_{j=1}^{n}$ m[i,j]*B[j];
        }
        For i = 1 to n {
            Set B[i] = Bnew[i];
        }
    }
```

The algorithm uses the emissivity array $\mathbf{E}$ instead of the zero vector $\mathbf{0}$ for its initial brightness vector: this saves one iteration of the loop. The array `Bnew[]` is used to save a separate copy of `B[]`, so that the previous values can be remembered long enough to compute the new values. Strictly speaking, there is no need to copy back the array values; instead, the two arrays could alternate roles on each iteration of the loop.

We have not shown any explicit test for whether the solution has converged sufficiently. Usually, this would just involve checking whether the change in value of `B[`i`]` is sufficiently small for all i. This can be tested by checking the values of `Bnew[i]-B[i]`.

XII.3.3 Gauss-Seidel iteration

The Gauss-Seidel method is an improvement of the Jacobi method which is easier to implement and converges to the solution faster. The new feature of the Gauss-Seidel method is that it does not save a copy of the old values of `B[]`, but instead updates them immediately.

```
Gauss-Seidel Iteration.
    // B[] and E[] are arrays.  E[] is already set.
    // m[i,j] denotes $m_{i,j}$.
    // Initialization set $\mathbf{B} = \mathbf{E}$.
    For i = 1 to n {
        Set B[i] = E[i];
    }
    // Main loop.
    While (not converged enough) {
        For i = 1 to n {
            Set B[i] = E[i] + $\sum_{j=1}^{n}$m[i,j]*B[j];
        }
    }
```

The Gauss-Seidel method is sometimes called the *gathering method.* The reason for the name "gathering method" is that you can think of the computation updating the brightness B_i of patch P_i (that is, of `B[i]`) by setting[1]

$$B_i \ = \ E_i + \sum_j m_{i,j} B_j,$$

as gathering together all the light from other patches to calculate the brightness of patch P_i. The difference with the Jacobi method is that we apply the update

[1] This B_i should not be confused with the vector $\mathbf{B}_i$ (note the difference in font).

to B_i immediately, instead of waiting until the next loop iteration for the new value to take effect. Thus, the new value of B_i affects the updated values of B_j for $j > i$ in the same loop iteration.

It is not hard to show that the Gauss-Seidel algorithm converges to the correct solution of the radiosity equation. In fact, it is easy to prove, by induction on the number of gathering calculations, that the brightness values in the array `B[]` computed by the Gauss-Seidel method are less than or equal to the correct brightness values. In addition, if $\mathbf{B}_k$ denotes the brightness vector obtained after $k-1$ iterations of the Jacobi algorithm loop, and $\mathbf{B}_k^{GS}$ the brightness vector obtained by $k-1$ iterations of the Gauss-Seidel loop, then the entries in the vector $\mathbf{B}_k^{GS}$ are greater than or equal to the corresponding entries in $\mathbf{B}_k$. This fact is also easily proved by induction on k, again using the fact that the entries of M are nonnegative. Therefore, the Gauss-Seidel results are sandwiched between the results of the Jacobi iteration and the correct solution. Since the Jacobi algorithm converges to the correct solution, the Gauss-Seidel algorithm must also converge to the correct solution. In practice, the Gauss-Seidel method tends to converge noticeably faster than the Jacobi method.

XII.3.4 The shooting method

The shooting method, also known as the Southwell iteration method or "progressive refinement", is another iterative method for solving the radiosity equations. For both the Gauss-Seidel and Jacobi methods, a basic update step consisted of choosing a single patch, and updating its brightness level based on the brightnesses of all the other patches. The shooting method operates rather differently: the basic update step now chooses a single patch, and sends (or "shoots") its brightness out to all the other patches. That is to say, instead of concentrating on a single receiving patch at a time, the shooting method concentrates on a single transmitting patch. To make this work, the shooting method must track, for each patch P_j, how much of its brightness level has not yet been taken into account by the brightness levels of the other patches P_i.

The shooting algorithm maintains two brightness values for each patch, B_i and ΔB_i. Both B_i and ΔB_i will always be nonnegative and the overall brightness of the patch is equal to the sum $B_i + \Delta B_i$. ΔB_i represents the "unshot" part of the brightness of patch P_i, namely the brightness that has not yet been transmitted on to the other patches. The update loop consists of choosing a value for i, and "shooting" the ΔB_i value to all the other patches; thereby updating the values of all the other patches to take into account the brightness due to ΔB_i.

The shooting algorithm is as follows.

```
Shooting_Method
    // B[] and ΔB[] and E[] are arrays.
    // Initialization.
```

```
For i = 1 to n {
    Set B[i] = 0;
    Set ΔB[i] = E[i];
}
// Main loop
While (not converged enough) {
    Choose j so that ΔB[j]*$A_j$ is maximized;      // $A_j$ = area of $P_j$
    Set B[j] = B[j] + ΔB[j];
    For i = 1 to n {
        Set ΔB[i] = ΔB[i] + m[i,j]*ΔB[j];
    }
    Set ΔB[j] = 0;
}
// Finish up
For i = 1 to n {
    Set B[i] = B[i]+ΔB[i];
}
```

The choice of j was made so as to find the patch which has the largest amount of outgoing light energy that has not been accounted for. Since the brightness values B[] are measured in terms of light intensity per unit surface area, we multiply the unshot brightness value ΔB[i] times the patch area in order to measure the total outgoing light energy. Thus, this choice for j attempts to "shoot" the largest amount of light energy possible. Other choices for j could work well too, but it is important that every j value which still has unshot brightness get picked eventually.

The runtime of a single shooting operation is clearly just $O(n)$. For comparison, a single gather operation is also $O(n)$; the advantage of the shooting algorithm lies in the possibility that fewer shooting operations may be needed, because the shooting algorithm concentrates its efforts on the patches with the most unshot light.

The test in the while loop for sufficient convergence could be based on a threshold value for the largest ΔB[i]*A_i value. The code written above assumes that the diagonal entries m[j,j] in the matrix are equal to zero.

Exercise XII.1. Prove that, under the assumptions we have been making about the matrix M, the shooting method is guaranteed to converge to the correct answer. [Hint: Prove bounds on how fast the summation $\sum_i A_i \Delta B_i$ is decreasing. Use the reciprocity condition.]

Further reading. This chapter has covered only the most basic aspects of radiosity. Good sources for information on more advanced topics in radiosity are the books of Cohen and Wallace [27] and Sillion and Puech [108]. There is a hierarchical method of calculating form factors which can greatly reduce the computational work in very large scenes [60]. Advanced work in global lighting often combines techniques from radiosity and ray tracing.

Ashdown [4] gives a theoretical description and complete code for a radiosity renderer.

Chapter XIII

Animation and Kinematics

This is a ***preliminary*** *draft of a second edition of the book* 3-D Computer Graphics: A Mathematical Introduction with OpenGL. *So please read it cautiously and critically! Corrections are appreciated. Draft C.4.a*

Author: Sam Buss, sbuss@ucsd.edu

XIII.1 Overview

The term *animation* refers to the process of specifying or controlling the movement of objects. Of particular concern to us in this chapter is the use of mathematical techniques to aid in the programming of animation.

Traditional animation techniques, used notably in movies, substantially predate computerized animation. Traditionally, animation requires drawing a series of pictures, each picture showing an instantaneous snapshot of objects in motion. These are then displayed in rapid succession, giving the visual effect of smooth motion. The same general idea applies to computer animation: a software program repeatedly renders a three dimensional scene, with each scene showing the objects at a particular point in time. These scenes are then displayed at a sufficiently fast frame rate to give the visual illusion of motion.

Nowadays, much of the work of animation is being taken over by computers. An artist will create objects, people, creatures, etc., as three dimensional models in a CAD program. These models can include information about the formation and permissible motions of the objects. For instance, an object may have a skeleton of rigid links connected by joints, and the joints can be given characteristics that control the motion of the joints. The rest of the object can be controlled to move in sync with the skeleton. One such technique is called *skinning* and permits the "skin," or surface, of a creature to move in conjunction with the movement of the skeleton. Once a model has been properly created and once the appropriate software is written, the task of an animator is greatly simplified: he or she only needs to control the motion of the skeleton to control the motion of the entire model. Furthermore, techniques such as *inverse kinematics* (IK) allow an even simpler interface for the animator; inverse kinematics allows the animator to set the positions or orientations of only a few selected portions of the skeleton and the software can automatically control the rest of the skeleton.

The outline of this chapter is as follows. First, there is some general introductory discussion about topics including keyframing, motion capture, and applications of animation and of forward and inverse kinematics. Next, we discuss some problems in animation of position, including "ease-in" algorithms. Animation of orientation is covered next, including yaw, pitch, and roll, and an in-depth treatment of quaternions. The chapter concludes with forward and inverse kinematics for articulated rigid bodies (multibodies).

XIII.1.1 Techniques evolved from traditional animation

There are a number of techniques from traditional animation that are useful for computer animation. Space (and lack of knowledge) prevents us from covering very much traditional animation, but you can find a lot of information on techniques traditionally used in animation in the books by Thomas and Johnston [110] and by White [120]. (The former book has a thorough discussion of animation at Disney.) Traditional animation is certainly more of an art than a science, and a great deal of experience and talent was needed to devise styles of animation that produce visually pleasing results. Of course, using computers for animation is no less of an art than traditional animation.

There are several mathematical aspects of computer animation that are direct extensions of techniques used in traditional animation: two prominent examples are keyframing and motion capture.

Keyframing. *Keyframing* refers to the process of creating animated motion by specifying the positions of objects at *keyframes*, and then filling in the motion in intermediate frames by interpolation. For traditional animation of movies, the keyframes, also called *keys*, are drawn by a senior animator. Other artists, *inbetweeners* and *inkers*, draw the intermediate frames and flesh out the complete detailed drawings. The keyframes typically show the extreme poses, or most critical poses. Initially, the keyframes can be in only rough form without complete details. The job of the inbetweener would be to draw the intermediate poses, being sure to make the motion look fluid and natural.

Keyframing is particularly important to the animation of full-length movies. A movie shows 24 frames per second, and thus there are too many frames for a single artist to draw all the frames in a movie. On the other hand, if multiple artists draw different parts of the movie, then consistency of style is lost. By employing a few senior animators to draw the keyframes, and a larger number of inbetweeners and inkers, a movie can be drawn with a smaller number of senior animators. A single senior animator can handle the drawing of all keyframes for a particular character in the movie, providing more consistency of style.

The computerized analogue of keyframing and inbetweening is the use of splines for interpolating points. At keyframes, the positions, orientations, and shapes of objects in the scene are specified. Then, by using interpolating curves, one can obtain positions, orientations, and shapes of the objects as smooth functions of time. This often can be done fully automatically with Catmull-Rom or Overhauser splines, but also can be manually edited, e.g., using tension-continuity-bias splines.

Motion capture. *Motion capture* is the measurement of the motion of (real-world) objects and using this to guide animated motion. In early animated movies, motion capture consisted of filming live action. The filmed live-action could be traced over to generate animated motion. For instance, in order to animate a fight scene, one might first film a movie of a two actors mock fighting. This could be translated into an animated fight by using the motion and timing of the filmed fight as the basis for the animated motion. Of course, the filmed motion capture does not need to be followed too slavishly. For instance, if one is animating a fight involving Daffy Duck, then one certainly does not want the movements of Daffy Duck to exactly follow the motion of the actor. Rather, the motions would be modified to reflect Daffy's physiology, and some aspects of the motion would be exaggerated for better artistic results. This kind of motion capture, when properly used, can greatly increase the fluidity and naturalness of the animated motion.

Modern versions of motion capture involve attaching sensors to actors that allow measurement of the three dimensional motion of the actors. There are various types of motion capture sensors. Some motion capture systems work by using small devices (called diodes) which sense motion through electrical or magnetic fields; these magnetic sensors can provide both position and orientation data in real-time. Optical motion capture systems work by attaching bright reflective spheres to the actors, and tracking the spheres with multiple cameras: the multiple camera views can be combined to give three dimensional positional information. Other systems work by attaching mechanical sensors to the actor's body that directly measure joint angles or bending, etc. A small-scale example of this is the *data glove*, which can capture precise finger movements.

All approaches provide for measurement of the position of each sensor as a function of time. The motion capture data usually needs (often significant) processing to remove noise and/or distortion. After the motion capture data has been cleaned up, it can be translated into information about positions and joint angles. This detailed information about positions of parts of the bodies as a function of time can be used to control animated motion that is highly realistic. Typical applications include capturing the motion of actors performing movements such as walking, running, fighting, etc., or of acrobats or athletes performing movements. These animated movements can be approximated by spline curves and played back to reproduce the captured motion as an animation.

XIII.1.2 Computerized animation

The kinds of systems that can be animated with the aid of computers include:

Particle systems. Particle systems are collections of particles moving as a group. These can be used to simulate a wide range of phenomena, including smoke, fluids, and the flocking behavior of large crowds or large groups of creatures.

Rigid bodies. A rigid body does not change shape as it moves, but does change position and orientation. It may be controlled directly in terms of its position and orientation, or indirectly in terms of velocity and angular velocity.

Articulated rigid bodies. Articulated rigid bodies, also called *multibodies*, are hierarchically connected assemblages of rigid bodies, called *links*. The connections between the rigid bodies are generally joints. The joints may be rotational or translational; more complicated joints, such as screw joints, are also possible. Examples of objects that can be modeled as multibodies include skeletons of humans or other creatures; for this, the links are the bones of the skeletons. Other examples include robot arms and other mechanical linkages.

Flexible objects. Flexible objects include objects such as cloth or rope. They also include "squishy" or bendable objects.

Camera viewpoint. An important element in many computer games is the use of a camera that follows the player around as he or she navigates an environment. The camera needs to follow the viewpoint of the player, without having excessive jerkiness, oscillation, or other jitter.

Other, specialized phenomena. Other applications of animation are diverse, including topics such as lightning, clouds, galaxy collisions, and many more.

The rest of the present chapter will be concerned with the animation of rigid bodies and of articulated rigid bodies.

The motion of rigid bodies can be completely described in terms of position and orientation. The specification of position is, at least from a mathematical viewpoint, quite straightforward. The position of an object is usually given by specifying the position of its center of mass, and the position consists of a single point in $\mathbb{R}^3$. Similarly, the velocity of an object (the velocity of the center of mass of the object, for instance) is just a single vector. Of course, both position and velocity will generally be functions of time. Section XIII.2 will cover some simple topics in controlling the position of objects.

Specifying and controlling the orientation of a rigid body is more problematic. There are several possible ways to represent orientation, including rotation matrices, yaw-pitch-roll angles, and quaternions. Section XIII.3 discusses these ways of representing rotation, with particular attention paid to the theory of quaternions. It also discusses spherical linear interpolation (slerping) for interpolation between two quaternion specifications of orientation.

Articulated rigid bodies are taken up in Section XIII.4. Techniques for animating articulated bodies can be divided roughly into two categories. The first category, *kinematics*, concerns the relationship between joint angles, or more generally, joint settings, and the positions of the links. Typical concerns of kinematics include the relationships between, on the one hand, the joint angles and their rate of motion and, on the other hand, the positions and velocities of the links. The second category is *dynamics* and is concerned with physical properties such as forces, accelerations, energy, etc. It is often convenient to further subdivide techniques for animation of articulated objects into four categories:

Forward kinematics. The forward kinematics problem is as follows: Given settings for all the joint angles, determine the positions of all the links in the articulated structure.

Inverse kinematics. The inverse kinematics, or IK, problem is as follows: Given a desired position for one or more links of an articulated object, determine settings for the joint angles that will achieve the desired position. For example, we set the position of one or more of the hands or feet of an animated person, and then solve the IK problem to determine good settings for all the joints in the body which give the hands or feet the desired positions. IK allows an animator to set only the position of a small number of links; for instance, to simulate a person reaching for an object, the animator could specify the trajectory of the hand as a function of time, and let the IK algorithm automatically determine the position of the joints, and thereby the position of the rest of the body. Not surprisingly, the inverse kinematics problem is much more difficult than the forward kinematics problem.

Forward dynamics. Forward dynamics is the same as physical simulation. If we are given the initial positions, orientations, velocities, angular velocities (or essentially equivalently, if we are given the initial joint angles and rates of change of joint angles), and, if one is furthermore given information about all external forces and torques, then we want to compute the movement of the articulated object as a function of time. This usually requires a physical simulation of the motion of the object.

Inverse dynamics. The inverse dynamics problem is usually considerably simpler than forward dynamics. Here, we are given the motions of all the links (or, equivalently, the motions of all the joint angles). The problem is to determine what forces must be applied, firstly at the joints and secondly from external sources, in order to obtain this motion.

Section XIII.4 will treat the mathematical theory of forward and inverse kinematics. We will not discuss dynamics at all.

XIII.2 Animation of position

The position of an object at time u can be given by a single vector $\mathbf{q}(u)$. We have several tools for describing curves $\mathbf{q}(u)$, namely, Bézier curves and B-splines. To animate position using keyframing, one picks times $u_0, u_1, \ldots, u_n$, and corresponding values for $\mathbf{q}(u_i)$ for each i. Then, Bézier or B-spline interpolation as described in Sections VIII.15 and IX.12 can be used to describe the curve at arbitrary instances in time u, for $u_0 \le u \le u_n$.

Often, one wants to animate non-preprogrammed motion. By "non-preprogrammed" we mean that the motion is not following a path determined in advance, but is instead following a path in response to changing circumstances. A notable example of this is in interactive applications such as computer games. However, non-preprogrammed motion also can be useful in non-interactive situations. A prime example of non-preprogrammed motion is the motion of the camera, or viewpoint, in a computer game which must follow the movement of a player around a virtual world. The player could be a character moving on foot, or could be a vehicle in a driving game, etc. The camera then needs to follow behind the character, keeping the character and the environs in view. In addition, the camera needs to move smoothly without jerkiness.

One way to control a camera position is with techniques known as "ease-in". Ease-in refers to moving from a starting position to a desired position in a smooth, non-jerky fashion, with no sudden changes in position or velocity, and perhaps with an additional constraint of no sudden changes in acceleration. A real world example of ease-in is the motion of a subway train or an airport tram as it stops at a station. The tram needs to stop smoothly with no sudden changes in acceleration which would jerk passengers, but it also needs to end up a precise location so that the automatic doors line up correctly. The ease-in problem in computer graphics is much simpler to solve than the ease-in problem for trams, since we do not have to deal with real world considerations like brakes, or with needing feedback to measure current velocity and position accurately.

XIII.2.1 Ease in: fixed target

The *fixed target ease-in* problem is as follows. At some time u_0, an object has position $\mathbf{p}_0$ and velocity $\mathbf{v}_0$. It is desired that at some future time, u_1, the object has position $\mathbf{p}_1$ and stays there with velocity $\mathbf{0}$. The airport tram mentioned above is an example of the fixed target ease-in problem.

A simple solution to this fixed-target ease-in problem can be given using degree three Hermite polynomials. (Hermite polynomials were defined in Section VIII.5.) First, if $u_0 = 0$ and $u_1 = 1$, then we can let

$$\mathbf{q}(u) \;=\; \mathbf{p}_0 H_0(u) + \mathbf{v}_0 H_1(u) + \mathbf{p}_1 H_3(u),$$

and let $\mathbf{q}(u)$ specify the position at time u, $0 \le u \le 1$. It is easy to verify that this meets all the requirements of the ease-in problem. In addition, the position curve $\mathbf{q}(u)$ is a degree three polynomial, and thus has constant third derivative, so the acceleration of the object is changing at a constant rate throughout the movement.[1]

For general $u_0 < u_1$, we need to make a change of variables, by setting

$$J_i(u) \;=\; H_i\left(\frac{u-u_0}{u_1-u_0}\right).$$

The functions J_i have properties similar to the Hermite functions, but on the domain $[u_0, u_1]$ instead of on $[0,1]$. Note, however, that the change of variables affects the first derivatives, so that

$$J_1'(u_0) \;=\; \frac{1}{u_1-u_0}.$$

The curve $\mathbf{q}(u)$ can then be defined for $u_0 \le u \le u_1$ by

$$\mathbf{q}(u) \;=\; \mathbf{p}_0 J_0(u) + (u_1-u_0)\mathbf{v}_0 J_1(u) + \mathbf{p}_1 J_3(u).$$

Exercise XIII.1. The *fixed target ease out* problem is similar to the fixed target ease in problem, but has initial position $\mathbf{p}_0$ and velocity $\mathbf{0}$ at time u_0 and needs to reach a target position $\mathbf{p}_1$ and velocity $\mathbf{v}_1$ at time u_1. Give a solution to the fixed target ease out problem based on Hermite polynomials.

XIII.2.2 Ease in: moving target

The moving target version of the ease-in problem is the problem of making an object both move smoothly and track a moving target. An example of this would be a camera position in a computer game; in a first-person exploration game, or in a driving game, the camera position needs to smoothly follow behind the player position. In this case, it is desirable for the camera to stay at a more-or-less fixed distance behind the player, but it is also important for the camera to not move too jerkily.

We will use the term "target position" to indicate the position we wish to track or approximate. The term "current position" means the current position of the object which is trying to track the target position. We assume that the animation is being updated in fixed time steps, each time step being of duration Δt. Let $\mathbf{t}_i$ denote the target position at time step i, i.e., at time step $i \cdot \Delta t$. Let $\mathbf{c}_i$ be the current position of the tracking object at time step i. In each time step, we are given the target positions up through $\mathbf{t}_{i+1}$ and wish to compute $\mathbf{c}_{i+1}$.

We will discuss two versions of the moving target ease-in problem. In the first case, suppose that the target does not have any inherent velocity, and that, likewise, the object does not have any inherent velocity. By "have inherent velocity," we mean that the object has enough mass or inertia that it should

[1] This solution would not be good enough for the above-mentioned tram example, since the acceleration does not go smoothly to zero at $u = 1$.

not change velocity abruptly. In the case where neither the target nor the tracking device has inherent velocity, a very simple update is to set

$$\mathbf{c}_{i+1} \;=\; (1-\alpha)\mathbf{c}_i + \alpha\mathbf{t}_{i+1},$$

for some fixed scalar α between 0 and 1. This defines the next position $\mathbf{c}_{i+1}$ as a weighted average of the current position $\mathbf{c}_i$ and the target position. The higher α is, the faster the object's position responds to changes in the target position, but the greater the possibility of jumpy or jerky movement. The best value for α would depend on the time step Δt and on the particular application.

For the second case, suppose the target does not have a velocity, but the tracking object does. The current velocity of the tracking object can be approximated as

$$\mathbf{v}_i \;=\; \frac{\mathbf{c}_i - \mathbf{c}_{i-1}}{\Delta t}.$$

If the object were to keep moving at this velocity, then its next position would be

$$\mathbf{c}_i + \frac{\mathbf{c}_i - \mathbf{c}_{i-1}}{\Delta t}\Delta t \;=\; 2\mathbf{c}_i - \mathbf{c}_{i-1}.$$

However, we want to also incorporate the new target position, so we can set

$$\mathbf{c}_{i+1} \;=\; (1-\alpha)\cdot(2\mathbf{c}_i - \mathbf{c}_{i-1}) + \alpha\cdot\mathbf{t}_{i+1}.$$

This sets $\mathbf{c}_{i+1}$ to be an average of the target position and the position the object would reach if there was no change in velocity.

In both cases, the closer the value of α is to 1, the more tightly the object tracks the target; the closer α is to 0, the smoother, and less jerky, the motion of the object is.

XIII.3 Representations of orientations

We now turn to the problem of animating the orientation of objects. A rigid body's position in space can be completely specified in terms of the position of its center (its center of mass, say) and in terms of its orientation. The position of the center of the rigid body is specified by a single vector $\mathbf{q} \in \mathbb{R}^3$, and is readily amenable to keyframing and interpolation. Specifying the orientation of a rigid body is more problematic. There are several ways to represent orientations, and the best choice of representation depends on the application at hand.

Let us consider two examples of applications of orientation. As a first example, consider the orientation of a camera or viewpoint. The camera is given a position as usual, and then its orientation can specified by a view direction and an "up" direction, as was used by the `gluLookAt` command. Cameras usually have a preferred up direction, namely pointing up along the y-axis as much as possible. As a second example, consider the orientation of a spacecraft traveling in deep space, away from any planets or suns. There is no preferred "up" direction in space, and so the orientation of the spacecraft is essentially arbitrary when it is not moving. If the spacecraft is accelerating, or has nonzero velocity relative to its surroundings, then the spacecraft has a preferred forward orientation direction; but even in this case, it would generally not have a preferred axial rotation (or roll amount).

This lack of a preferred up direction for spacecraft is somewhat counterintuitive to us, since we are so used to living on the surface of a planet. Indeed, in popular shows such as *Star Trek*, spacecraft always have an up direction and, furthermore, whenever two spacecraft meet in an episode of *Star Trek*, they always miraculously share the same up direction. That is to say, they never meet turned axially, or meet facing each other upside down, etc. Of course, this common up direction is unrealistic, since there is no reason that there should be a shared "up" direction out in deep space. On the other hand, for spacecraft near a planet, there is of course a preferred up direction, namely away from (or towards) the planet. For instance, the US space shuttle frequently oriented itself so that its top side faced the earth.

When animating orientation, the decision of how to represent orientation is crucial. For applications that have a preferred up direction (such as cameras), it is probably useful to use the yaw, pitch, and roll representation. For applications which do not have a preferred up direction, and where it is necessary to blend or interpolate orientations, quaternions provide a good representation. We will discuss these representations, along with rotation matrices, in the next sections.

XIII.3.1 Rotation matrices

Specifying an orientation is essentially identical to specifying a rotation; namely, if we choose an initial orientation Ω_0, then any other orientation Ω can be specified in terms of the rotation which takes the body from Ω_0 to Ω. As was discussed in Chapter II, an orientation in 3-space can be described by an orthonormal 3×3 matrix which represents a rigid, orientation preserving transformation.

A big drawback to using rotation matrices for animating orientation is that they cannot be interpolated or averaged in a straightforward manner. For instance, consider the following two rotation matrices:

$$\begin{pmatrix} 0 & 0 & 1 \\ 0 & 1 & 0 \\ -1 & 0 & 0 \end{pmatrix} \qquad \text{and} \qquad \begin{pmatrix} 0 & -1 & 0 \\ 1 & 0 & 0 \\ 0 & 0 & 1 \end{pmatrix}. \tag{XIII.1}$$

The first matrix represents a 90° rotation around the y-axis, and the second represents a 90° rotation around the z-axis. If you attempt to take the average of these two rotations by just adding the matrices and dividing by two, then you get the matrix

$$\begin{pmatrix} 0 & -1/2 & 1/2 \\ 1/2 & 1/2 & 0 \\ -1/2 & 0 & 1/2 \end{pmatrix}.$$

The resulting matrix is not even orthonormal and certainly does not represent a rotation midway between the two initial rotations.

XIII.3.2 Yaw, pitch, and roll

Yaw, pitch, and roll specify an orientation in terms of three successive rotations around the x-, y-, and z-axes. This is particularly useful for orientations in settings where there is a preferred up direction, such as for cameras or for airplane navigation.

Actually, yaw, pitch, and roll is only one example of a more general class of methods called *Euler angles.* Euler angles specify a rotation in terms of three rotations around three axes: there are many different forms of Euler angles depending (a) on the order in which the rotations are performed (i.e., on the order in which the axes x, y, and z are chosen for rotations), and (b) on whether the axes move with the object or whether the axes remain fixed in global coordinates. Yaw, pitch, and roll performs rotation first around the y-axis (yaw), then around the x-axis (pitch), and finally around the z-axis (roll). The second and third rotations (pitch and roll) are around the local x- and z-axes which move with the object, not around the fixed x-, z-axes in world coordinates.[2] Figure XIII.1 shows the effects of yaw, pitch, and roll on the orientation of an airplane.

So far, we have described the axes of rotations for yaw, pitch, and roll as being local axes that move with the object being rotated. An equivalent way to describe the rotations is as being made around the fixed x-, y-, and z-axes. By "fixed", we mean that the axes do not move with the object. However, as discussed in Section II.2.7, if fixed rotation axes are used, then the rotations must be performed in the opposite order: first roll around the z-axis, then pitch around the x-axis, and finally yaw around the y-axis. This representation of yaw, pitch, and roll around fixed axes lets us give a formula for yaw, pitch, and roll. Let θ_y, θ_p, and θ_r be the yaw, pitch, and roll angles, with directions of rotation determined by the righthand rule. Then the effect of the yaw, pitch, and roll is the transformation

$$R_{\theta_y,\mathbf{j}} \circ R_{\theta_p,\mathbf{i}} \circ R_{\theta_r,\mathbf{k}}. \tag{XIII.2}$$

Exercise XIII.2. The methods of Chapter II let you express the rotations $R_{\theta_y,\mathbf{j}}$, $R_{\theta_p,\mathbf{i}}$, and $R_{\theta_r,\mathbf{k}}$ as 3×3 matrices. Use these to derive the formula for the rotation matrix of formula (XIII.2) in terms of the sines and cosines of the three angles. Your answer should have the form

$$\begin{pmatrix} s_y s_p s_r + c_y c_r & s_y s_p c_r - c_y s_r & s_y c_p \\ c_p s_r & c_p c_r & -s_p \\ c_y s_p s_r - s_y c_r & c_y s_p c_r + s_y s_r & c_y c_p \end{pmatrix},$$

[2] Our conventions for the names "yaw," "pitch," and "roll" and for the order in which the rotations occur are based on the assumption that the z-axis is the forward direction, the x-axis is the leftward direction, and the y-axis is the upwards direction. The reader is warned that other conventions are often used.

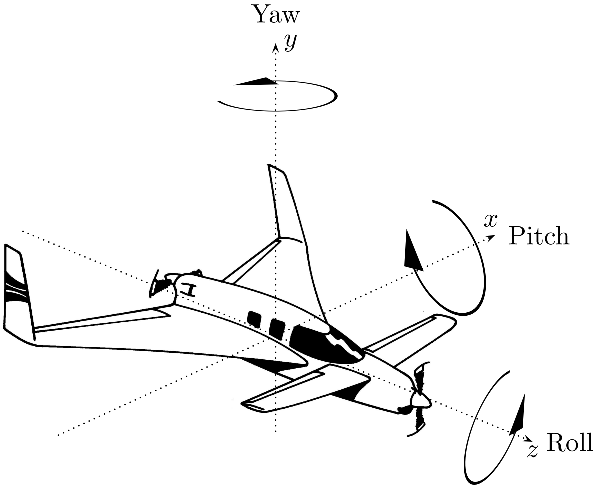

Figure XIII.1: Yaw, pitch, and roll represent rotations around the y-axis, the x-axis and the z-axis. If the axes move with the object, then the rotations are performed in the order yaw, then pitch, and finally roll. If the axes are taken as fixed, then the rotations are performed in the opposite order: roll, then pitch, then yaw. Rotation directions are determined by the righthand rule. The reader is warned that the rotation directions for pitch and yaw that are shown in the figure are opposite to customary usage in aviation. For us, a positive pitch means the nose dips down and a positive yaw steers to the left. However, aviation conventions are that a positive pitch means the nose moves up, and a positive yaw means turning to the right. It is customary for positive roll to mean that the right wing dips, which agrees with the our convention. In aviation conventions, the directions of the x and y axes are reversed, with the x-axis pointing rightward and the y-axis pointing downward.

where $c_y = \cos\theta_y$, $s_y = \sin\theta_y$, etc.

As we discuss below, yaw, pitch, and roll can sometimes lead to bad behavior of interpolation. On the other hand, yaw, pitch, and roll have the advantage of being intuitive. For instance, yaw, pitch, and roll are commonly used for airplane navigation since they correspond well to the controls available to a pilot. Yaw, pitch, and roll also work well for a camera. Actually, cameras usually do not use roll, and instead keep roll equal to zero. The orientation for a camera can be given in terms of just yaw and pitch, and interpolating yaw and pitch values usually works well for interpolating camera orientation.

There are three ways in which the use of yaw, pitch, and roll can cause problems with interpolation. The first two are easy to circumvent, but the third one (gimbal lock) is more serious. First, when interpolating yaw, pitch, and roll, you need to keep in mind that if angles are changed by 360° the orientation is unchanged. For instance, when interpolating from a yaw angle of 170°, to a yaw angle of $-170°$ (with pitch and roll both held fixed, say equal to zero), it is usually intended that the yaw varies by only 20° rather than rotating the other direction through 340°. This is easily handled by adding 360° to the second angle and interpolating the yaw from 170° to 190°. (The interpolated yaw values which are greater than 180° can of course have 360° subtracted back off if desired.)

The second potential pitfall with interpolating yaw, pitch, and roll is that every orientation has two distinct representations. Namely, the orientation represented by the angles θ_y, θ_p and θ_r is identical to the orientation represented by the following yaw, pitch, and roll angles:

$$\begin{aligned} \theta'_y &= \theta_y \pm 180^\circ \\ \theta'_p &= -\theta_p \pm 180^\circ \\ \theta'_r &= \theta_r \pm 180^\circ, \end{aligned} \tag{XIII.3}$$

where any combination of plus/minus signs may be used. Thus, care must be taken when interpolating yaw, pitch, and roll angles to properly decide whether to transform the angles according to equations (XIII.3) before performing the interpolations.

The third, and most serious, problem with interpolation of yaw, pitch, and roll involves *gimbal lock*. Gimbal lock occurs when a degree of freedom is lost at particular angle settings (to be precise, at pitch equal to ±90°). As an example, consider interpolation between the following two orientations: Ω_1 is the "standard position" orientation given with yaw, pitch, and roll all equal to zero. Let Ω_2 be the orientation with yaw equal to 90°, pitch equal to −90° and roll equal to −90°. (You should visualize this! The airplane of Figure XIII.1 in orientation Ω_2 would have its nose pointing up the y-axis and its bottom facing the positive z-axis.) The orientation Ω_2 suffers from gimbal lock, since a degree of freedom has been lost: in particular, the yaw and roll axes have become effectively identical, so changing either yaw or roll has the same effect on the orientation Ω_2. Now suppose we try to use averaging to obtain an orientation midway between Ω_1 and Ω_2; straightforward averaging will give yaw equal to 45°, pitch equal to −45°, and roll equal to −45°. This orientation is by no means intuitively midway between Ω_1 and Ω_2: indeed, the intuitive midway position would be obtained by rotating around the (global, fixed) x-axis. One could complain that this example is unfair, since it involved a pitch of 90° and was in gimbal lock; however, one could use instead a pitch very close to 90°, say a pitch of 89°, and then there would still be the same kinds of problems with interpolation.

Exercise XIII.3. Prove that yaw, pitch, and roll angles θ'_y, θ'_p and θ'_r of equations (XIII.3) represent the same orientation as θ_y, θ_p, and θ_r.

XIII.3.3 Quaternions

Quaternions provide a method of representing rotations by 4-tuples. Recall from Euler's theorem in Section II.3.7 that an arbitrary rigid, orientation preserving, linear transformation can be expressed as a rotation around some fixed axis. Such a rotation is specified by a rotation angle θ and a rotation axis $\mathbf{u}$, where $\mathbf{u}$ is a unit vector: recall that this rotation was denoted $R_{\theta,\mathbf{u}}$. To represent $R_{\theta,\mathbf{u}}$ with a quaternion, let $c = \cos(\theta/2)$, $s = \sin(\theta/2)$, and $\mathbf{u} = \langle u_1, u_2, u_3 \rangle$. Then the 4-tuple q defined by

$$q \;=\; \langle c, su_1, su_2, su_3 \rangle$$

is called a *quaternion,* and represents the rotation $R_{\theta,\mathbf{u}}$. We shall see that quaternions provide a useful method of representing rotations in situations where there is no preferred up direction.

Most of our discussion below will give a theoretical development of quaternions. But before starting the theoretical treatment, we point out a couple practical issues.

Note that the magnitude of the quaternion q as defined above is equal to one (strictly speaking, this is not necessary, and we can also deal with non-unit quaternions; but, in practice, it is common to use only magnitude 1 quaternions). Conversely, suppose we are given an arbitrary 4-tuple of magnitude 1, say

$$r \;=\; \langle r_1, r_2, r_3, r_4 \rangle,$$

such that $r_1^2 + r_2^2 + r_3^2 + r_4^2 = 1$. Then, since $-1 \le r_1 \le 1$, we can set $\varphi = \cos^{-1}(r_1)$. Also, let $\mathbf{v} = \langle r_2, r_3, r_4 \rangle$, so that $||\mathbf{v}|| = \sqrt{1 - r_1^2}$. Since $\sin\varphi = \pm\sqrt{1 - r_1^2}$, the vector

$$\mathbf{u} \;=\; \frac{\mathbf{v}}{\sin\varphi}$$

is a unit vector. Finally, let $\theta = 2\varphi$. Then we have

$$r \;=\; \langle \cos(\theta/2), \sin(\theta/2)u_1, \sin(\theta/2)u_2, \sin(\theta/2)u_3 \rangle,$$

so r is a quaternion representing the rotation $R_{\theta,\mathbf{u}}$. By this method, any unit 4-tuple represents a rotation. Non-unit 4-tuples can be normalized in order to also represent rotations.

Quaternions have the unexpected property that $-q$ represents the same rotation as q. This is because adding 360 degrees to a rotation angle does not change the ending orientation. That is to say, $R_{\theta+360^\circ,\mathbf{u}}$ is the same transformation as $R_{\theta,\mathbf{u}}$. Letting c, s, and q be defined from θ and $\mathbf{u}$ as above, we have $-c = \cos(\theta/2 + 180^\circ)$ and $-s = \sin(\theta/2 + 180^\circ)$. Thus, $-q$ is the quaternion that corresponds to the transformation $R_{\theta+360^\circ,\mathbf{u}}$, so $-q$ represents the same rotation as q.

We shall next take up the theoretical development of quaternions. The theoretical discussion culminates with practical considerations of how quaternions represent rotations and how to perform interpolation (slerping) with quaternions. For more discussion of how quaternions represent rotations, the reader can also consult [61].

XIII.3.4 Theoretical development of quaternions

Quaternions were developed by the mathematician W.R. Hamilton in 1843 for the purpose of representing rotations in 3-space. The quaternions were invented (or, discovered?) as a generalization of complex numbers. The complex numbers are of course obtained from the real numbers by including the number i, which is a square root of -1. Quaternions further extend the complex numbers by including a total of *three* square roots of -1, which are represented by i, j, and k. Thus, we have $i^2 = j^2 = k^2 = -1$. We wish to be able to multiply quaternions, and for this, we need to define how the three new symbols i, j, k multiply with each other, namely,

$$\begin{array}{rclcrclcrcl} i^2 & = & -1 & \qquad & j^2 & = & -1 & \qquad & k^2 & = & -1 \\ ij & = & k & & jk & = & i & & ki & = & j \\ ji & = & -k & & kj & = & -i & & ik & = & -j. \end{array} \qquad \text{(XIII.4)}$$

Note that this multiplication is not commutative; for example, $ij \neq ji$.

A quaternion q is defined to equal an expression of the form

$$d + ai + bj + ck,$$

where d, a, b, c are all scalars from $\mathbb{R}$. We also represent this quaternion by the 4-tuple $q = \langle d, a, b, c \rangle$.[3]

Two quaternions are defined to be *equal* if and only if they have exactly the same four components. (Two unequal quaternions may still represent the same rotation.) Addition of quaternions is defined component-wise, namely

$$(d+ai+bj+ck)+(d'+a'i+b'j+c'k) \;=\; (d+d')+(a+a')i+(b+b')j+(c+c')k.$$

The product of a scalar and quaternion is defined also as expected, namely,

$$\alpha(d + ai + bj + ck) \;=\; (\alpha d) + (\alpha a)i + (\alpha b)j + (\alpha c)k,$$

where $\alpha \in \mathbb{R}$. The product of two quaternions q_1 and q_2 is denoted $q_1 q_2$ (we reserve the dot product notation $q_1 \cdot q_2$ for the usual dot product). The definition of multiplication is more complicated than the definition of addition, and is defined from the identities (XIII.4) using the associative and distributive laws. This gives

$$\begin{aligned} &(d + ai + bj + ck)(d' + a'i + b'j + c'k) \\ &\quad = \; dd' + da'i + db'j + dc'k + ad'i + aa'i^2 + ab'ij + ac'ik \\ &\qquad\; + bd'j + ba'ji + bb'j^2 + bc'jk + cd'k + ca'ki + cb'kj + cc'k^2 \\ &\quad = \; (dd' - aa' - bb' - cc') + (da' + ad' + bc' - cb')i \\ &\qquad\qquad + (db' + bd' + ca' - ac')j + (dc' + cd' + ab' - ba')k. \end{aligned} \qquad \text{(XIII.5)}$$

[3] There are various conventions on representing quaternions, and many authors put the scalar component last in the 4-tuple and might prefer the notation $\langle a, b, c, d \rangle$ for $d + ai + bj + ck$. Similarly, we later introduce the notation $\langle d; \mathbf{u} \rangle$, and these authors would typically prefer $\langle \mathbf{u}, d \rangle$ instead. We prefer to put the scalar component, d, first since it corresponds better to the way one treats complex numbers.

This formula for multiplication is fairly messy, but can be expressed more clearly with vector notation. Let $\mathbf{u}$ be the vector $\mathbf{u} = \langle a, b, c\rangle$. Then the notation $\langle d; \mathbf{u}\rangle$ is used as a shorthand notation for the quaternion $\langle d, a, b, c\rangle$. Letting also $\mathbf{u}' = \langle a', b', c'\rangle$, we can rewrite Equation (XIII.5) as

$$(\langle d; \mathbf{u}\rangle)(\langle d'; \mathbf{u}'\rangle) \;=\; \langle dd' - \mathbf{u}\cdot\mathbf{u}'; d\mathbf{u}' + d'\mathbf{u} + \mathbf{u}\times\mathbf{u}'\rangle. \qquad \text{(XIII.6)}$$

Thus, for $q = \langle d; \mathbf{u}\rangle$ and $q' = \langle d'; \mathbf{u}'\rangle$, the scalar component of the quaternion product qq' is equal to $dd' - \mathbf{u}\cdot\mathbf{u}'$ and the vector component is $d\mathbf{u}' + d'\mathbf{u} + \mathbf{u}\times\mathbf{u}'$.

Theorem XIII.1. *Quaternion addition is commutative and associative. Quaternion multiplication is associative. The left and right distributive laws hold for quaternions, i.e., for all quaternions q, r, s,*

$$q(r+s) = qr + qs \qquad \textit{and} \qquad (r+s)q = rq + sq.$$

The theorem is proved by simple calculations and we leave the proof to the reader.

On the other hand, we already mentioned that quaternion multiplication is not commutative; in Equation (XIII.6) the noncommutativity arises from the fact that $\mathbf{u}\times\mathbf{u}'$ is not generally equal to $\mathbf{u}'\times\mathbf{u}$. The noncommutativity may seem strange at first; however, you are already quite familiar with a couple other noncommutative systems. First, matrices (2×2 matrices, for instance) have addition and multiplication operations which satisfy properties similar to quaternions, and matrix multiplication is not commutative. As a second example, consider vectors over $\mathbb{R}^3$ with the usual vector addition and with cross product as the multiplication operation. Vector addition is of course associative and commutative. Furthermore, cross products are distributive over vector addition. However, the vector cross product is neither commutative nor associative.

The *norm*, or *magnitude*, of a quaternion $q = \langle d, a, b, c\rangle$ is defined to equal

$$||q|| \;=\; \sqrt{d^2 + a^2 + b^2 + c^2}.$$

We define the *conjugate*, q^*, of q to equal $q^* = \langle d, -a, -b, -c\rangle$. If $q = \langle d; \mathbf{u}\rangle$, then $||q|| = \sqrt{d^2 + \mathbf{u}^2}$, where $\mathbf{u}^2 = \mathbf{u}\cdot\mathbf{u}$. Also, $q^* = \langle d; -\mathbf{u}\rangle$. It is easily verified, from the definition of quaternion multiplication, that

$$qq^* \;=\; q^*q \;=\; \langle d^2 + \mathbf{u}^2; \mathbf{0}\rangle \;=\; ||q||^2. \qquad \text{(XIII.7)}$$

A *unit quaternion* is a quaternion with norm equal to 1.

Exercise XIII.4. Let $q_1 = \langle \frac{\sqrt{2}}{2}, 0, \frac{\sqrt{2}}{2}, 0\rangle$, $q_2 = \langle \frac{\sqrt{2}}{2}, 0, 0, \frac{\sqrt{2}}{2}\rangle$, and $q_3 = \langle 2, 0, 0, 0\rangle$.

(a) Calculate $q_1 + q_2$, $q_1 - q_2$, and $q_1 + q_3$.

(b) Calculate the products q_1q_2, q_2q_1, q_1q_3, q_3q_1, and $q_1(q_2 + q_3)$.

(c) Calculate q_1^*, q_2^*, and q_3^*.

(d) Calculate $||q_1||$, $||q_2||$, $||q_3||$, $||q_1q_2||$, and $||q_1q_3||$.

Exercise XIII.5. Give examples showing that vector cross product is not commutative and not associative.

A quaternion $\langle d; \mathbf{0}\rangle$ with zero vector component will be identified with the scalar $d \in \mathbb{R}$. This is compatible with the earlier definitions, since the product dq is the same whether d is interpreted as a quaternion or as a scalar. Similarly, a vector $\mathbf{u} \in \mathbb{R}^3$ will be identified with the quaternion $\langle 0; \mathbf{u}\rangle$ with zero scalar component. Care should be taken when vectors are interpreted as quaternions, since vector cross product is *not* the same as quaternion product. (Indeed, they could not be the same, since quaternion products are associative, but vector cross products are not associative.) As an example, we have

$$(\mathbf{i}+\mathbf{j})\times\mathbf{j} \;=\; \mathbf{k},$$

but,

$$(i+j)j \;=\; (\langle 0,1,1,0\rangle)(\langle 0,0,1,0\rangle) \;=\; \langle -1,0,0,1\rangle \;\neq\; \langle 0,0,0,1\rangle \;=\; k.$$

The next theorem discusses the scalar multiplication and multiplicative inverse properties for quaternions.

Theorem XIII.2.

a. *The scalar* $1 = \langle 1; \mathbf{0}\rangle$ *is the multiplicative identity, i.e.,* $q = 1q = q1$ *for all quaternions* q.

b. *Let* $s = \langle s; \mathbf{0}\rangle$ *be a scalar. Then* $sq = qs$ *for all quaternions* q.

c. *Let* q *be a nonzero quaternion. Then*

$$q^{-1} \;=\; \frac{1}{||q||^2}q^*$$

is the multiplicative inverse of q, *i.e.,* $qq^{-1} = q^{-1}q = 1$.

The proof of the theorem is by straightforward calculation; use Equation (XIII.7) to help prove part c. Note that if $q = \langle d; \mathbf{u}\rangle$ is a unit quaternion, then q^{-1} is very simply computable as $q^{-1} = \langle d; -\mathbf{u}\rangle$.

Exercise XIII.6. Let q_1, q_2, and q_3 be as in Exercise XIII.4. Also, let $q_4 = \langle 1, 0, 1, 0\rangle$. Calculate q_1^{-1}, q_2^{-1}, q_3^{-1}, and q_4^{-1}.

Exercise XIII.7. Let q_1 and q_2 be arbitrary quaternions. Prove that $(q_1q_2)^* = q_2^*q_1^*$ and that $(q_1q_2)^{-1} = q_2^{-1}q_1^{-1}$.

Exercise XIII.8. Let q_1 and q_2 be arbitrary quaternions. Prove that $||q_1q_2|| = ||q_1||\cdot||q_2||$. [Hint: This can be proved with straightforward but messy algebraic manipulation; alternatively, a slick proof can be given using the previous exercise and Equation (XIII.7).]

XIII.3.5 Representing rotations with quaternions

We are now ready to (re)state the method by which quaternions represent rotations. Fix a unit vector $\mathbf{u}$ and a rotation angle θ. Recall that $R_{\theta,\mathbf{u}}$ is the rotation around axis $\mathbf{u}$ through angle θ, with the rotation direction given by the righthand rule. Let $c = \cos(\theta/2)$ and $s = \sin(\theta/2)$, and let q be the quaternion

$$q \;=\; \langle c, s\mathbf{u}\rangle \;=\; \langle c, su_1, su_2, su_3\rangle.$$

The next theorem explains the basic method by which quaternions represent rotations, namely, to rotate a vector $\mathbf{v}$, you multiply on the left by q and on the right by q^{-1}.

Theorem XIII.3. *Let* $\mathbf{u}$*,* θ*, and* q *be as above. Let* $\mathbf{v}$ *be any vector in* $\mathbb{R}^3$*, and set* $\mathbf{w} = R_{\theta,\mathbf{u}}\mathbf{v}$*. Then,*

$$q\mathbf{v}q^{-1} \;=\; \mathbf{w}. \tag{XIII.8}$$

Some comments are in order before we prove the theorem. First note that q, as defined above, is a unit quaternion, so $q^{-1} = q^*$. So for unit quaternions, we have $q\mathbf{v}q^* = \mathbf{w}$. Second, Equation (XIII.8) uses our convention on treating vectors as quaternions, so another way of stating (XIII.8) is

$$q\langle 0; \mathbf{v}\rangle q^{-1} \;=\; \langle 0; \mathbf{w}\rangle.$$

Third, Equation (XIII.8) can also be used for non-unit quaternions. To see this, let α be a nonzero scalar and let $r = \alpha q$. Then $r^{-1} = (1/\alpha)q^{-1}$, and thus

$$r\mathbf{v}r^{-1} \;=\; (\alpha q)\mathbf{v}(\alpha^{-1}q^{-1}) \;=\; q\mathbf{v}q^{-1} \;=\; \mathbf{w}.$$

In other words, multiplying a quaternion by a nonzero scalar does not change the value of $q\mathbf{v}q^{-1}$. In this way, quaternions act very much like homogeneous coordinates, since, if we are interested only in what rotation is represented by the formula $q\mathbf{v}q^{-1}$, then multiplication by nonzero scalars has no effect. In most applications, it is best to work with unit quaternions; unit quaternions can be viewed as 4-tuples which lie on the unit sphere S^3 in $\mathbb{R}^4$. Conversely, each point on the unit sphere S^3 can be viewed as a quaternion.[4] Antipodal points on the sphere represent the same rotation, since q and $-q$ differ by a nonzero scalar factor.

In abstract algebra, a mapping of the form

$$\mathbf{v} \;\mapsto\; q\mathbf{v}q^{-1},$$

computed by multiplying on the left by a fixed element and on the right by its inverse, is called an *inner automorphism.*

We now prove Theorem XIII.3.

[4] The unit sphere S^3 is the set of points $\{\langle x, y, z, w\rangle : x^2 + y^2 + z^2 + w^2 = 1\}$. The superscript 3 means that the surface of the sphere is a three dimensional manifold.

Proof. (of Theorem XIII.3.) Let $\mathbf{u}$, θ, and q be as in the statement of the theorem: in particular, $\mathbf{u}$ is a unit vector and q is a unit quaternion. Referring back to Figure II.22 on page 78, we write the vector $\mathbf{v}$ as a sum of two vectors $\mathbf{v} = \mathbf{v}_1 + \mathbf{v}_2$ such that $\mathbf{v}_1$ is parallel to $\mathbf{u}$ and $\mathbf{v}_2$ is perpendicular to $\mathbf{u}$. By the distributive law, the map $\mathbf{v} \mapsto q\mathbf{v}q^{-1}$ is linear, i.e.,

$$q\mathbf{v}q^{-1} \;=\; q\mathbf{v}_1q^{-1} + q\mathbf{v}_2q^{-1} \;=\; ||\mathbf{v}_1||(q\mathbf{u}q^{-1}) + q\mathbf{v}_2q^{-1}.$$

Therefore, it will suffice to prove

a. $q\mathbf{u}q^{-1} = \mathbf{u}$, and

b. $q\mathbf{v}_2q^{-1} = R_{\theta,\mathbf{u}}\mathbf{v}_2$, for $\mathbf{v}_2$ perpendicular to $\mathbf{u}$.

First we prove a., by direct calculation:

$$\begin{aligned}
q\mathbf{u}q^{-1} &= [(\langle c; s\mathbf{u}\rangle)(\langle 0; \mathbf{u}\rangle)]q^{-1} \\
&= (\langle 0 - s\mathbf{u}\cdot\mathbf{u}; c\mathbf{u} + s\mathbf{u}\times\mathbf{u}\rangle)q^{-1} \\
&= (\langle -s; c\mathbf{u}\rangle)q^{-1} \\
&= (\langle -s; c\mathbf{u}\rangle)(\langle c; -s\mathbf{u}\rangle) \\
&= \langle -cs + cs\mathbf{u}\cdot\mathbf{u}; s^2\mathbf{u} + c^2\mathbf{u} - cs\mathbf{u}\times\mathbf{u}\rangle \\
&= \langle -cs + cs; (s^2 + c^2)\mathbf{u}\rangle \\
&= \langle 0; \mathbf{u}\rangle \;=\; \mathbf{u}.
\end{aligned}$$

These calculations used the fact that $\mathbf{u}$ is a unit vector, so $\mathbf{u}\cdot\mathbf{u} = 1$. In addition, $c^2 + s^2 = 1$, since $c = \cos(\theta/2)$ and $s = \sin(\theta/2)$.

We now prove b. We have $\mathbf{v}_3 = \mathbf{u}\times\mathbf{v}_2$ and $\mathbf{v}_3\times\mathbf{u} = \mathbf{v}_2$, where $\mathbf{v}_3$ is defined as in Section II.3.6 (again, see Figure II.22 on page 78). We shall explicitly compute $q\mathbf{v}_2q^{-1}$. First,

$$\begin{aligned}
q\mathbf{v}_2 &= (\langle c; s\mathbf{u}\rangle)(\langle 0; \mathbf{v}_2\rangle) \\
&= \langle 0 - s\mathbf{u}\cdot\mathbf{v}_2; c\mathbf{v}_2 + s\mathbf{u}\times\mathbf{v}_2\rangle \\
&= \langle 0; c\mathbf{v}_2 + s\mathbf{v}_3\rangle.
\end{aligned}$$

Then,

$$\begin{aligned}
q\mathbf{v}_2q^{-1} &= (\langle 0; c\mathbf{v}_2 + s\mathbf{v}_3\rangle)(\langle c; -s\mathbf{u}\rangle) \\
&= \langle 0 + sc\mathbf{v}_2\cdot\mathbf{u} + s^2\mathbf{v}_3\cdot\mathbf{u}; 0 + c^2\mathbf{v}_2 + cs\mathbf{v}_3 - cs\mathbf{v}_2\times\mathbf{u} - s^2\mathbf{v}_3\times\mathbf{u}\rangle \\
&= \langle 0; c^2\mathbf{v}_2 + cs\mathbf{v}_3 + cs\mathbf{v}_3 - s^2\mathbf{v}_2\rangle \\
&= \langle 0; (c^2 - s^2)\mathbf{v}_2 + (2cs)\mathbf{v}_3\rangle. \\
&= \langle 0; (\cos\theta)\mathbf{v}_2 + (\sin\theta)\mathbf{v}_3\rangle \\
&= R_{\theta,\mathbf{u}}\mathbf{v}_2.
\end{aligned}$$

The last equality follows from Equation (II.12) on page 79. The next-to-last equality follows from the sine and cosine double angle formulas:

$$\cos(2\varphi) \;=\; \cos^2\varphi - \sin^2\varphi \qquad \text{and} \qquad \sin(2\varphi) \;=\; 2\cos\varphi\sin\varphi,$$

with $\varphi = \theta/2$. We have thus completed the proof of Theorem XIII.3. □

Using quaternions to represent rotations makes it easy to calculate the composition of two rotations. Indeed, if the quaternion q_1 represents the rotation $R_{\theta_1,\mathbf{u}_1}$ and if q_2 represents $R_{\theta_2,\mathbf{u}_2}$, then the product q_1q_2 represents the composition $R_{\theta_1,\mathbf{u}_1}R_{\theta_2,\mathbf{u}_2}$. To prove this, note that

$$R_{\theta_1,\mathbf{u}_1}R_{\theta_2,\mathbf{u}_2}\mathbf{v} \;=\; q_1(q_2\mathbf{v}q_2^{-1})q_1^{-1} \;=\; (q_1q_2)\mathbf{v}(q_2^{-1}q_1^{-1}) \;=\; (q_1q_2)\mathbf{v}(q_1q_2)^{-1}$$

holds by associativity of multiplication and by Exercise XIII.7.

Exercise XIII.9. Let R_1 and R_2 be the two rotations with matrix representations given in the formulas (XIII.1) on page 453.

(a) What are the two unit quaternions that represent R_1? What are the two unit quaternions that represent R_2?

(b) Let $\mathbf{v} = \langle 1,3,2\rangle$. Compute $R_1\mathbf{v}$ and $R_2\mathbf{v}$ using the quaternion representations from part (a) by the method of Theorem XIII.3. Check your answers by multiplying by the matrices in (XIII.1).

XIII.3.6 Quaternion and rotation matrix conversions

Since a quaternion represents a rotation, its action on $\mathbb{R}^3$ can be represented by a 3×3 matrix. We now show how to convert a quaternion q into a 3×3 matrix. Recall from the discussion on page 64 that a transformation $A(\mathbf{v})$ is represented by the matrix $(\mathbf{w}_1\ \mathbf{w}_2\ \mathbf{w}_3)$, where the columns $\mathbf{w}_i$ are equal to $A(\mathbf{v}_i)$. Thus, to represent a quaternion q by a matrix, we shall set

$$\mathbf{w}_1 \;=\; q\mathbf{i}q^{-1}, \qquad \mathbf{w}_2 \;=\; q\mathbf{j}q^{-1}, \qquad \textit{and}\quad \mathbf{w}_3 \;=\; q\mathbf{k}q^{-1},$$

and then the matrix representation will be $(\mathbf{w}_1\ \mathbf{w}_2\ \mathbf{w}_3)$.

Let $q = \langle d,a,b,c\rangle$ be a unit quaternion. To compute $q\mathbf{i}q^{-1}$, first compute

$$(\langle d,a,b,c\rangle)(\langle 0,1,0,0\rangle) \;=\; \langle -a,d,c,-b\rangle.$$

Then, since $q^{-1} = \langle d,-a,-b,-c\rangle$, compute $q\mathbf{i}q^{-1}$ by:

$$(\langle -a,d,c,-b\rangle)(\langle d,-a,-b,-c\rangle) \;=\; \langle 0, d^2+a^2-b^2-c^2, 2ab+2cd, 2ac-2bd\rangle.$$

Similar computations give

$$\begin{aligned} q\mathbf{j}q^{-1} \;&=\; \langle 0, 2ab-2cd, d^2-a^2+b^2-c^2, 2bc+2ad\rangle \\ q\mathbf{k}q^{-1} \;&=\; \langle 0, 2ac+2bd, 2bc-2ad, d^2-a^2-b^2+c^2\rangle. \end{aligned}$$

Thus, the matrix which represents the same rotation as the quaternion $\langle d,a,b,c\rangle$ is

$$\begin{pmatrix} d^2+a^2-b^2-c^2 & 2ab-2cd & 2ac+2bd \\ 2ab+2cd & d^2-a^2+b^2-c^2 & 2bc-2ad \\ 2ac-2bd & 2bc+2ad & d^2-a^2-b^2+c^2 \end{pmatrix}. \tag{XIII.9}$$

A 3×3 matrix which represents a rotation can also be transformed into a quaternion. For this, we are given a matrix $M = (m_{i,j})$, and want to find a quaternion $q = \langle d, a, b, c \rangle$ such that M is equal to (XIII.9). Furthermore, the quaternion will be a unit quaternion, with $d^2 + a^2 + b^2 + c^2 = 1$. Since q and $-q$ represent the same rotation, there are two possible answers.

There are several methods for converting M into a quaternion (see [73, 109, 102]). We shall follow the algorithm of Shepperd [102]. The algorithm is also similar to the one given in Section II.3.6 to convert a rotation matrix into a rotation axis and rotation angle.

The first step in the derivation of a quaternion from a matrix is to note the following identities

$$\begin{array}{lll} m_{2,1} + m_{1,2} = 4ab & m_{1,3} + m_{3,1} = 4ac & m_{3,2} + m_{2,3} = 4bc \\ m_{2,1} - m_{1,2} = 4cd & m_{1,3} - m_{3,1} = 4bd & m_{3,2} - m_{2,3} = 4ad. \end{array} \tag{XIII.10}$$

If we know one of the values of d, a, b, c, and if this value is nonzero, then we can solve for the other three values by using the appropriate three of these six equations. For instance, if we have the value for d, then we can solve for a, b, c by using the bottom three equations; note this requires dividing by d, and thus works only if d is nonzero.

The *trace* of M is equal to the sum of its diagonal elements:

$$T \;=\; m_{1,1} + m_{2,2} + m_{3,3} \;=\; 3d^2 - a^2 - b^2 - c^2 \;=\; 4d^2 - 1,$$

where the last step used $d^2 + a^2 + b^2 + c^2 = 1$. It is convenient to also use the notation $m_{0,0}$ for the trace, i.e., set $m_{0,0} = T$. Then, we have

$$\begin{array}{rcl} 2m_{0,0} - T & = & T \;=\; 3d^2 - a^2 - b^2 - c^2 \;=\; 4d^2 - 1 \\ 2m_{1,1} - T & = & -d^2 + 3a^2 - b^2 - c^2 \;=\; 4a^2 - 1 \\ 2m_{2,2} - T & = & -d^2 - a^2 + 3b^2 - c^2 \;=\; 4b^2 - 1 \\ 2m_{3,3} - T & = & -d^2 - a^2 - b^2 + 3c^2 \;=\; 4c^2 - 1. \end{array}$$

We can use any of these four equations to solve for values of any of a, b, c, d, for instance,

$$a \;=\; \pm\frac{1}{2}\sqrt{2m_{1,1} - T + 1}.$$

However, there is the complication that we would not be able to determine the proper signs for a, b, c, and d in this way. In addition, this would require the computational expense of four square roots. Therefore, instead of using all four equations, we use just one of them to calculate one of a, b, c, or d : this value may arbitrarily be set to be either positive or negative, since it will affect only the overall sign of the quaternion. Then we can use the appropriate equations from (XIII.10) to solve for the other three variables. To choose which of a, b, c, d to solve for first, recall that we want to avoid division by zero. Further, to avoid division by a value near zero, we can choose to solve for the one of a, b, c, d which has the largest absolute value. It is evident from the four equations that this is done by choosing the largest $m_{i,i}$, for $0 \le i \le 3$, and using the corresponding equation.

We can write out the complete algorithm as follows:

```
Input:  A rotation matrix $M$ .
        $M$ has entries $m_{i,j}$ , for $i = 1,2,3$ and $j = 1,2,3$ .
Output:  A quaternion $\langle d, a, b, c \rangle$
Algorithm:
    Set $m_{0,0}$ = $m_{1,1} + m_{2,2} + m_{3,3}$ ;                    // Trace
    Set $i$ so that $m_{i,i} = \max\{m_{0,0}, m_{1,1}, m_{2,2}, m_{3,3}\}$ ;
    Switch ( $i$ ) {
    Case 0:                                                 // i == 0
        Set $d$ = $\frac{1}{2}\sqrt{m_{0,0}+1}$ ;
        Set $a$ = $(m_{3,2} - m_{2,3})/(4d)$ ;
        Set $b$ = $(m_{1,3} - m_{3,1})/(4d)$ ;
        Set $c$ = $(m_{2,1} - m_{1,2})/(4d)$ ;
        Return;
    Case 1:                                                 // i == 1
        Set $a$ = $\frac{1}{2}\sqrt{2m_{1,1} - m_{0,0} + 1}$ ;
        Set $d$ = $(m_{3,2} - m_{2,3})/(4a)$ ;
        Set $b$ = $(m_{2,1} + m_{1,2})/(4a)$ ;
        Set $c$ = $(m_{1,3} + m_{3,1})/(4a)$ ;
        Return;
    Case 2:                                                 // i == 2
        Set $b$ = $\frac{1}{2}\sqrt{2m_{2,2} - m_{0,0} + 1}$ ;
        Set $d$ = $(m_{1,3} - m_{3,1})/(4b)$ ;
        Set $a$ = $(m_{2,1} + m_{1,2})/(4b)$ ;
        Set $c$ = $(m_{3,2} + m_{2,3})/(4b)$ ;
        Return;
    Case 3:                                                 // i == 3
        Set $c$ = $\frac{1}{2}\sqrt{2m_{3,3} - m_{0,0} + 1}$ ;
        Set $d$ = $(m_{2,1} - m_{1,2})/(4c)$ ;
        Set $a$ = $(m_{1,3} + m_{3,1})/(4c)$ ;
        Set $b$ = $(m_{3,2} + m_{2,3})/(4c)$ ;
        Return;
    }
```

The algorithm returns a single quaternion $q = \langle d, a, b, c \rangle$, however, recall that $-q$ represents the same rotation. Depending on how you use the quaternion, you may need to determine which of q or $-q$ is more appropriate.

XIII.3.7 Interpolation of quaternions

Interpolation of quaternions is best done with the spherical linear interpolation introduced earlier in Section V.6. Since every rotation is represented by a unit

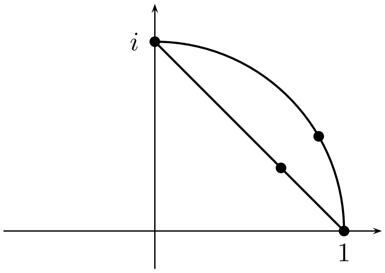

Figure XIII.2: Lerping moves from 1 to i at a constant rate along the secant line. Slerping moves from 1 to i at a constant rate along the great circle. The points drawn on the secant line and on the great circle are obtained by lerping and slerping with $\alpha = \frac{1}{3}$. They do not correspond to the same rotation.

quaternion, we restrict our attention to unit quaternions. Recall that unit quaternions can be viewed as points on the unit sphere S^3 in $\mathbb{R}^4$. The only catch is that antipodal points on the sphere represent the same rotation; thus each rotation has two possible representations as a unit quaternion. It is often important in applications to choose the most appropriate of the quarternion represention.

Suppose we are given two unit quaternions q_1 and q_2 and a scalar $\alpha \in [0,1]$, and wish to interpolate between q_1 and q_2. Because the quaternions lie on the unit sphere, it is better to use spherical linear interpolation instead of ordinary linear interpolation. Namely, one can interpolate with

$$q(\alpha) \;=\; \mathit{slerp}(q_1, q_2, \alpha).$$

The *slerp* function is computed by the method of Section V.6.

What would go wrong if we used linear interpolation (lerping) instead of spherical linear interpolation (slerping)? First, of course, the results would not lie on the sphere and would need to be renormalized. Even more importantly, linear interpolation would not result in a constant rate of rotation. For example, in Figure XIII.2, the two quaternions $1 = \langle 1,0,0,0\rangle$ and $i = \langle 0,1,0,0\rangle$ are shown. The latter quaternion corresponds to a 180° rotation around the x-axis. Both slerping and lerping can be used to move smoothly from the quaternion 1 to the quaternion i. However, using linear interpolation and computing $q(\alpha) = \mathit{lerp}(1,i)$ causes the quaternion $q(\alpha)$ to move along the straight-line segment from 1 to i at a constant rate. On the other hand, setting $q(\alpha) = \mathit{slerp}(1,i,\alpha)$ causes $q(\alpha)$ to move along the great circle from 1 to i at a constant rate. So only slerping makes the orientation vary at a constant rate.

Recall from Equation (V.32) on page 217 that the formula for spherical linear interpolation is

$$\mathit{slerp}(q_1, q_2, \alpha) \;=\; \frac{\sin((1-\alpha)\varphi)}{\sin\varphi} q_1 + \frac{\sin(\alpha\varphi)}{\sin\varphi} q_2.$$

Here φ is the angle between q_1 and q_2. This angle can be computed by using the dot product $q_1 \cdot q_2$, which is equal to $\cos\varphi$. (You treat q_1 and q_2 as ordinary vectors in $\mathbb{R}^4$ for the purpose of computing the dot product.) Alternately, you may also compute the sine of φ and then take the arctangent, as was done on page 218 in the second version of the `Precompute_for_Slerp`.

One typically is really interested in interpolating between rotations, rather than between quaternions. That is say, one is typically given two orientations and is asked to interpolate between them. The orientations can be converted to quaternions by the method of the previous section, but then one has the choice of negating one of the quaternions to get a second quaternion representation of the same orientation. The question then is, should one use

$$\mathit{slerp}(q_1, q_2, \alpha) \qquad \text{or} \qquad \mathit{slerp}(q_1, -q_2, \alpha)$$

for the interpolation? (Negating both quaternions just negates the results of the slerp function, so these are really the only two choices.) The usual way to resolve this question is to consider the angle between q_1 and q_2. If this is less than or equal to 90°, then slerp between q_1 and q_2. If it is greater than 90°, then slerp between q_1 and $-q_2$. Physically, the corresponds to rotating in the shortest direction between the two orientations. To determine whether the angle is greater than 90°, form the dot product $q_1 \cdot q_2$; the dot product is negative if and only if the angle is greater than 90°.

Interpolation between quaternions can be used to create spline-like curves which take on quaternion values. The importance of this is that it allows orientation to be smoothly animated by a spline function in terms of control points. The main remaining technical difficulty is that slerping only interpolates between two quaternions at a time, but the usual definitions of Bézier and B-spline curve in terms of blending functions require taking a weighted average of multiple control points at a time. This problem can be circumvented by using de Casteljau and de Boor methods, which allow calculating the value of a Bézier curve or B-spline curve by a series of interpolations of two control points at a time. Shoemake [104, 105] uses this as the basis for some methods of using Catmull-Rom style curves which interpolate given quaternions, and a number of other authors have made similar suggestions. We have also proposed a method of forming the weighted average of multiple quaternions at a time in Buss-Fillmore [23].

XIII.4 Kinematics

The term "kinematics" refers to motion or movement without regard to physical properties such as mass or momentum. Instead, kinematics refers to the purely geometric properties of motion such as position, orientation, velocity, rotational velocity, etc.

We shall focus on the kinematics of hierarchies of simple, rigid, three dimensional objects linked with perfect joints; such assemblages are also called *articulated objects* or *multibodies*. Applications include the animation of humans and other creatures by controlling their skeletal movement. These techniques can also be used for simulating chains or ropes by approximating them as a series of short rigid segments. Much of the theory of kinematics was developed for the analysis and control of mechanical linkages, as well as for motion planning and control of robots.

The outline of the rest of this chapter is as follows. We first set up a framework for discussing rigid, articulated objects. This involves creating a tree structure of links, with each link connected to its parent by a single degree of freedom (1-DOF) joint. Next we examine *forward kinematics*: this involves methods for calculating positions and orientations of the rigid objects as functions of the joint positions. The final section will take up the harder topic of *inverse kinematics*; inverse kinematics provides methods to control the positions of the joints so as to achieve a desired motion.

XIII.4.1 Rigid links and joints

We wish to model simple arrangements of rigid bodies, called links, connected by joints. We shall make several simplifying assumptions. The first assumption is that the joints are purely rotational and have a single degree of freedom (that is, they are 1-DOF joints). This assumption is not so crucial in that it can be relaxed significantly without seriously affecting the difficulty of either forward kinematics or inverse kinematics. The second assumption is that the links are hooked up in a tree-like fashion; i.e., there is no loop or closed chain of links. This second assumption is crucial for our discussion of kinematics: Indeed any loop or closed chain would imply dependencies among joint positions, and we would have no meaningful way to deal with these dependencies kinematically (as compared to dealing with the dynamics or physics of the bodies).

We assume therefore that we have a set L of links (rigid objects) which are connected by rotational joints (see Figure XIII.3). The links are organized as a tree; the nodes of the tree are the set of links from L. One of the links is identified as the *root link*, and the leaves of the tree (i.e., links which do not have any children), are called *end links.* Each link is joined to its parent and its children in the tree by 1-DOF rotational joints. A joint is attached to fixed positions on two links and has a single axis of rotation — this is similar in effect to a door hinge, for example. The axis of rotation of the 1-DOF joint is fixed relative to the two links that it joins. End links are also called *end effectors.* For each end effector, we pick a fixed point on the link which is called an *end effector point.* The end effector points are the points which we are trying to control with inverse kinematics. For example, for a robot arm, the end effector point could be the position of the hand or other tool at the end of the robot arm, and we would like to control the position and/or orientation of the end effector.

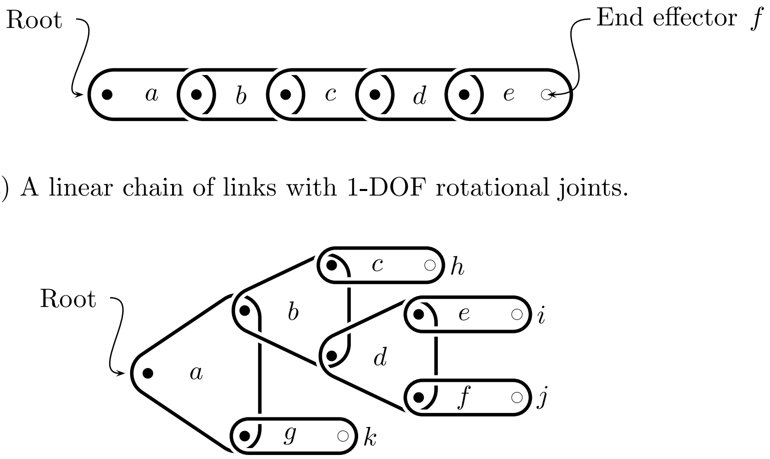

(a) A linear chain of links with 1-DOF rotational joints.

(b) A tree-like arrangement of links and 1-DOF joints. The points h-k are end effector points.

Figure XIII.3: Two examples of tree-like arrangements of links. The black dots represent 1-DOF rotational joints. The small circles are end effector points.

XIII.4.2 Forward kinematics

To mathematically describe the positions of links, we need to set up a scheme for naming joints and effectors, and their positions and orientations, etc. Each link $x \in L$ has an *attachment point*, which is the place where link x is attached to its parent. The root link also has an attachment point, called the *base position*, where it is attached to a fixed point. We assume each attachment point consists of a 1-DOF joint. A 1-DOF joint rotates around a single axis. This axis is fixed relative to the two adjacent links, but of course may depend on other joint angles. We use the variable θ_x to denote the angle of the 1-DOF joint connecting link x to its parent.

The *relative positions* of the links (other than the root link) will be specified with variables $\mathbf{r}_x$. The relative position vectors $\mathbf{r}_x$ are *fixed* and are not functions of the joint angles. The relative positions $\mathbf{r}_x$ for x a link are defined as follows: if y is the parent link of link x, and if all the joint angles are set equal to zero, then $\mathbf{r}_x$ is equal the vector from the attachment point of y to the attachment point of x. This is illustrated in Figure XIII.4. We also define $\mathbf{r}_x$ when x is an end effector point, instead of a link. In this case, if x lies on link y, then $\mathbf{r}_x$ is defined to be the vector from the attachment point of y to the end effector point x. Examples of this in Figure XIII.4 are $\mathbf{r}_f$ in the first figure and $\mathbf{r}_h$ through $\mathbf{r}_k$ in the second figure.

As discussed above, the angle θ_x is measured in terms of the *relative orientation* of joint x to its parent. This means that if the parent link is

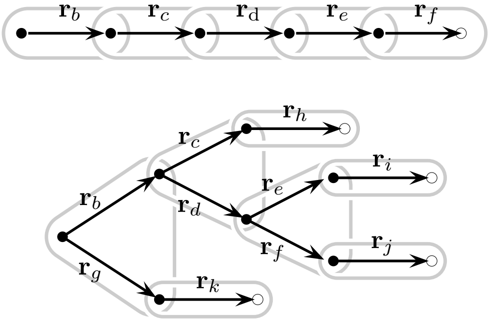

Figure XIII.4: The relative position vectors $\mathbf{r}_x$ measure the relative rest positions of the links. $\mathbf{r}_a = \mathbf{0}$ and the other relative position vectors are as shown.

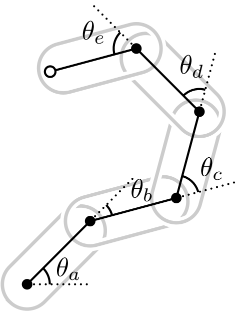

Figure XIII.5: The angles of joints are measured relative to the two links it joins.

rotated, and θ_x is held fixed, then x moves and changes orientation with its parent. (See Figure XIII.5.) We will use vectors $\mathbf{v}_x$ to denote the rotation axis for the 1-DOF joint attaching x to its parent link (or, if x is the root link, attaching x to the base position). The vector $\mathbf{v}_x$ is equal to the unit vector along the axis of rotation of the joint when all the joint angles equal zero. Of course, as the joint angles θ_x vary, the joints' actual axes of rotation can change (we will denote these changing axes by $\mathbf{w}_x$ below).

The vectors $\mathbf{r}_x$ and $\mathbf{v}_x$ give a description of the mechanical functionality of the links. These vectors are fixed and do not vary with the joint angles θ_x; in other words, they are static. We shall shortly define values $\mathbf{s}_x$ and $\mathbf{w}_x$ that give the positions of the joints' attachment points and the joints' rotational axes as functions of the joint angles θ_x.

The basic problem of forward kinematics is to obtain a formula for end effector point positions as functions of the angles θ_x. We shall solve this problem by defining vectors $\mathbf{s}_x$ which equal the position of the attachment point of a link x, or equal the position of an end effector x, with $\mathbf{s}_x$ being a function of the joint angles. A good way to define the vectors $\mathbf{s}_x$ is to traverse the tree of links starting from the end effectors up to the root. We shall give formulas for intermediate vectors $\mathbf{s}_x^y$, where x is either a link or an end effector point, and where the link y is an ancestor of x in the tree. The meaning of $\mathbf{s}_x^y$ is as follows (also, refer to Figure XIII.6). Let T_y be the set containing the link y and all the links z which are descendants of y in the tree, i.e., T_y is the subtree rooted at y. Then $\mathbf{s}_x^y$ is a function of the angles θ_z such that $z \in T_y$. For x a link, $\mathbf{s}_x^y$ is the vector from the attachment point of y to the attachment point of x, assuming the joint positions are set according to the values of the angles θ_z and assuming that $\theta_{z'} = 0$ for all other links $z' \notin T_y$. For x an end effector point, $\mathbf{s}_x^y$ is the vector from the attachment point of y to the point x again assuming the joint positions are set according to the values of the angles θ_z and that $\theta_{z'} = 0$ for all $z' \notin T_y$.

For x a link in the subtree T_y, we also define a vector $\mathbf{w}_x^y$ which describes the rotation axis for the joint attaching x. The vector $\mathbf{w}_x^y$ will be a function of the angles θ_z such that $z \in T_y$. The value of $\mathbf{w}_x^y$ is defined to be the unit vector along the axis of rotation for 1-DOF joint connecting x to its parent, based on the angles θ_z, $z \in T_y$, under the same assumption that $\theta_{z'} = 0$ for $z' \notin T_y$.

It is fairly easy to give recursive formulas for $\mathbf{s}_x^y$ and $\mathbf{w}_x^y$. For $y = x$, we have

$$\mathbf{s}_x^x \;=\; \mathbf{0} \qquad\text{and}\qquad \mathbf{w}_x^x \;=\; \mathbf{v}_x.$$

And, for x an end effector position on the link y,

$$\mathbf{s}_x^y \;=\; \mathbf{r}_x.$$

Then, for y equal to the parent link of w and for x in T_w, we have

$$\begin{aligned} \mathbf{s}_x^y &= R_{\theta_y,\mathbf{v}_y}(\mathbf{r}_w + \mathbf{s}_x^w), \\ \mathbf{w}_x^y &= R_{\theta_y,\mathbf{v}_y}(\mathbf{w}_x^w). \end{aligned}$$

As you should recall from Section II.3.6, $R_{\theta,\mathbf{u}}$ represents the linear transformation that performs a rotation of θ degrees around the axis $\mathbf{u}$.

These formulas for $\mathbf{s}_x^y$ and $\mathbf{w}_x^y$ suffice to solve the forward kinematics problem. For instance, the position of end effector f is given as a function of the joint angles by $\mathbf{s}_f^a$, where a is the root link.

To avoid excessive superscripts, we henceforth let $\mathbf{s}_x$ and $\mathbf{w}_x$ equal

$$\mathbf{s}_x \;=\; \mathbf{s}_x^a \qquad\text{and}\qquad \mathbf{w}_x \;=\; \mathbf{w}_x^a,$$

where a is the root link. Thus, $\mathbf{s}_x$ gives the position of the link or end effector point x as a function of the joint angles. Likewise, $\mathbf{w}_x$ gives the rotation axis for the joint at link x.

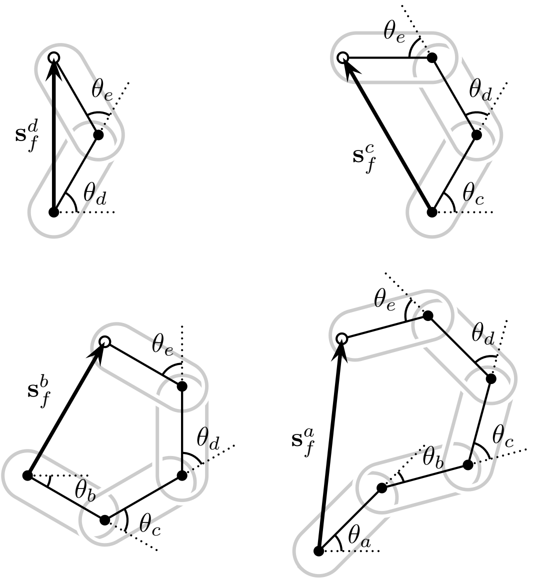

Figure XIII.6: The definitions of $\mathbf{s}_f^y$ for the end effector f and the links $y = a, b, c, d$ of the linear chain shown in Figure XIII.3.

We now turn to the inverse kinematics problem, which is to find joint angles that will produce desired values for the end effector positions.

XIII.4.3 Inverse kinematics, setting it up

The inverse kinematics problem is the problem of, given desired positions for some of the links, finding appropriate joint angles that will place the links in these positions. Applications of inverse kinematics include motion planning in real world applications such as in robotics, and also include animation in graphical environments, especially of articulated figures such as humans or other creatures.

Our discussion of inverse kinematics is based loosely on the paper of Girard and Maciejewski [53], who used inverse kinematics to animate the walking motion of legged creatures. See also the later paper of Zhao and Badler [128] for more advanced methods of inverse kinematics, applications to human figures, and references to related work.

In computer graphics, a typical application of inverse kinematics is animation of a creature. An animator may specify the desired positions of the hand and feet of a person (say), and then the inverse kinematics problem will be solved to find good positions for the joints of the entire body. If this works well, then the job of the animator can be significantly simplified, since it can spare the animator the work of manually setting all the joint angles in a skeleton. Other applications include motion planning, either for robotics or in a virtual reality application. For instance, if it is desired to make an arm and hand reach out to grasp an object, then inverse kinematics can be used to find possible solutions for the movement. Of course, these possible solutions may need to take into account issues such as collision detection and avoidance, or joint forces and joint limits.

We will discuss only the "pure" form of inverse kinematics: in particular, we will not consider issues like collision avoidance or limits on joint angles. Rather, we will discuss solutions to the following problem: Given a set of joint angles, and thereby, from forward kinematics, given the positions and orientations of all the links, and given a set of desired new positions for *some* of the links, then we want to find a way to change the joint angles so as to move the links' positions closer to the desired positions. This process can be iterated in such a way that each iteration moves the links' positions closer to their target positions until eventually new joint positions are reached that place the links close enough to their desired positions. The reason for using an iterative procedure is that it is usually too complicated to actually solve for joint angles, $\vec{\theta}$, in terms of the desired link positions. The iterative procedure will be easier to implement and, if it converges sufficiently well, can provide values for the joint angles that put the links arbitrarily close to their desired positions.

For a single step of the iterative procedure, we shall consider the function telling us how links' positions depend on joint angles (this function is obtainable from the forward kinematics of the last section). We shall then evaluate the partial derivatives of this function to find a linear approximation to the function. That is to say, we shall compute the rates of changes in links' positions with respect to the rates of changes in joint angles. These will give a *Jacobian* matrix of partial derivatives. With some assumptions about the non-singularity of the Jacobian matrix, we can then find a way to change the joints' angles so as to move the links' positions closer to the desired positions. Since the Jacobian gives only a linear approximation to the function, we have to iterate the process until it converges (we hope!) to a good solution.

Suppose that x is an end effector position or an attachment point of a link, and that we are seeking to set the joint angles so as to set the position $\mathbf{s}_x$ of x equal to a target value $\mathbf{s}'_x$. More generally, we may have more than one x and be trying to make each x reach its target position $\mathbf{s}'_x$. We assume the links are already placed in some initial configuration with known joint angles $\vec{\theta}$, where $\vec{\theta}$ represents the vector of all the joint angles. The discussion in the previous section on forward kinematics gives us a formula for $\mathbf{s}_x$ in terms of the angles $\vec{\theta}$.

The first step in setting up the inverse kinematics problem is to define the Jacobian matrix. The Jacobian matrix will tell us how the position of x changes with respect to small changes in the angles $\vec{\theta}$; in other words, will contain the partial derivatives of $\mathbf{s}_x$ with respect to the variables $\vec{\theta}$.

To define the Jacobian matrix, we must define the partial derivatives of the functions $\mathbf{s}_x$ giving the link positions. We have $\mathbf{s}_x$ as a function of $\vec{\theta}$,

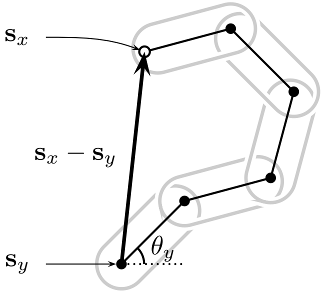

Figure XIII.7: The rate of change of the position $\mathbf{s}_x$ of point x with respect to the joint angle θ_y is calculated in terms of rotation around the axis $\mathbf{w}_y$ of the joint y as $\mathbf{w}_y \times (\mathbf{s}_x - \mathbf{s}_y)$. The axis $\mathbf{w}_y$ is pointing out of the page, so $\mathbf{w}_y \times (\mathbf{s}_x - \mathbf{s}_y)$ has the right direction for the partial derivative. Since $\mathbf{w}_y$ is a unit vector, $\mathbf{w}_y \times (\mathbf{s}_x - \mathbf{s}_y)$ also has the right magnitude. This calculation works for any x and y, not for just end effectors and the root link.

i.e., $\mathbf{s}_x = \mathbf{s}_x(\vec{\theta})$. For particular links x and y, we can define $\partial\mathbf{s}_x/\partial\theta_y$ as follows:

$$\frac{\partial\mathbf{s}_x}{\partial\theta_y} = \begin{cases} \mathbf{0} & \text{if } y = x \text{ or } x \notin T_y \\ \mathbf{w}_y \times (\mathbf{s}_x - \mathbf{s}_y) & \text{otherwise} \end{cases}$$

To see that this correctly defines the partial derivative, note the following: (a) If x is not a proper descendent of y, then the rotation of y's joint does not affect the position of x, so $\partial\mathbf{s}_x/\partial\theta_y = \mathbf{0}$. (b) Otherwise, the vector from point y to point x is equal to $\mathbf{s}_x - \mathbf{s}_y$ and the rotation axis for angle θ_y is the axis $\mathbf{w}_y$. An infinitesimal rotation φ radians around the axis $\mathbf{w}_y$ centered at $\mathbf{s}_y$ will move the point x an infinitesimal distance given by the vector $\varphi\mathbf{w}_y \times (\mathbf{s}_x - \mathbf{s}_y)$. From this observation, the second part of the definition of $\partial\mathbf{s}_x/\partial\theta_y$ is obtained immediately. Figure XIII.7 shows how to visualize the derivation of the formula for the partial derivative.[5]

The vector version of the Jacobian matrix is then defined to equal the $m \times n$ matrix

$$\left(\frac{\partial\mathbf{s}_x}{\partial\theta_y}\right)_{x,y}$$

where the rows of the matrix are indexed by the m many links x whose position we are trying to set (often, x ranges over the set of end effectors, for instance), and where the columns of the matrix are indexed by the set of all joints y.

The entries in the above matrix are 3-vectors; to convert the matrix into an ordinary matrix with real numbers as entries, we replace each vector-valued entry by its column form. This gives a matrix of dimension $(3m) \times n$. We call

[5] The formula for $\partial\mathbf{s}_x/\partial\theta_y$ is only correct if angles are measured in radians. If the angle θ is measured in units of α radians, then the equation for the partial derivative becomes $\alpha\mathbf{w}_y \times (\mathbf{s}_x - \mathbf{s}_y)$. For example, if angles are measured in degrees, then $\alpha = \pi/180$.

this $(3m) \times n$ matrix the *Jacobian matrix* and denote it J. Each row in J has length n and consists of partial derivatives of one of the x, y, or z coordinates of one of the $\mathbf{s}_x$ values with respect to the n angles θ_y.

To finish setting up the inverse kinematics problem, we assume we are given current values for the angles $\vec{\theta}$. This gives values $\mathbf{s}_x$, and we denote the sequence of all these by $\vec{\mathbf{s}}$ (so $\vec{\mathbf{s}}$ is a sequence of m vectors, and thus a sequence of $3m$ scalars). We also let $\mathbf{s}'_x$ be the desired values for these positions, and let $\vec{\mathbf{s}'}$ denote the sequence of all these. Finally, let $\Delta\vec{\mathbf{s}}$ equal

$$\Delta\vec{\mathbf{s}} \ = \ \vec{\mathbf{s}'} - \vec{\mathbf{s}},$$

which equals the desired change in the links' positions.

In order to solve the inverse kinematics problem, we want to solve the following equation for $\Delta\vec{\theta}$:

$$\Delta\vec{\mathbf{s}} \ = \ J(\Delta\vec{\theta}). \tag{XIII.11}$$

This will give $\Delta\vec{\theta}$ as a first-order approximation to the change in values of $\vec{\theta}$ necessary to effect the desired change $\Delta\vec{\mathbf{s}}$ in positions.

The next section will describe an algorithm to find a solution $\Delta\vec{\theta}$ to Equation (XIII.11). Once we have this solution, we might be tempted to set $\vec{\theta}$ equal to $\vec{\theta} + \Delta\vec{\theta}$. This however, will not work so easily and is likely to lead to unstable performance. The Jacobian matrix gives only a first-order approximation to the change in angles, and unfortunately, the partial derivatives can change very rapidly with changes in the angles $\vec{\theta}$. A second problem is that when the links and joints are positioned badly, Equation (XIII.11) can be unstable; in particular, the matrix J may have rank less than n, or be close to having rank less than n, and this can cause instability and overshoot problems.

To keep these problems under control, it is recommended that you choose a small positive scalar $\epsilon < 1$, and update the joint angles $\vec{\theta}$ by adding $\epsilon\Delta\vec{\theta}$. Then proceed iteratively by recomputing the Jacobian based on the updated angles and positions, finding new values for $\Delta\vec{\theta}$, and again updating with a small fraction ϵ. This is repeated until the links x are sufficiently close to the desired positions. The question of how small ϵ needs to chosen depends on the geometry of the links; it would be a good idea to keep ϵ small enough so that the angles are updated by at most 5 or 10 degrees at a time.

XIII.4.4 Inverse kinematics, finding a local solution

The previous section reduced the inverse kinematics problem to the problem of solving Equation (XIII.11) for $\Delta\vec{\theta}$ in terms of $\Delta\vec{\mathbf{s}}$ and J. Of course, if we are very lucky, then J is a square matrix and is invertible. In that case, we can solve for $\Delta\vec{\theta}$ as

$$\Delta\vec{\theta} \ = \ J^{-1}(\Delta\vec{\mathbf{s}}).$$

However, we are not usually so lucky. First of all, J may well not be square. For example, if there is only one end effector, so $m = 1$, and there are $n > 3$ joints, then J is a $3 \times n$ matrix with more columns than rows. In this case, the rank of J is ≤ 3, and thus the columns cannot be linearly independent. A second way that things can go wrong is when the rows of J are not linearly independent, i.e., the rank of J is $< 3m$. A simple example of this is seen in Figure XIII.3(a) on page 469: suppose the joints are all straight as shown in the figure and that the end effector is at the point f at the right end of the rightmost link. Let f_x measure the x-coordinate (horizontal position) of the end effector f. Then $\partial f_x / \partial \theta = 0$ for all the joint angles θ: in other words, the corresponding row of J is zero. Physically, this means that no infinitesimal change in joint angles can effect a change in the horizontal position of the end effector.

Since J is not invertible, we will use the *pseudo-inverse* of J instead of the inverse of J. The pseudo-inverse is also sometimes called the *Moore-Penrose inverse*. Before defining the pseudo-inverse of J, we need to develop some background from linear algebra. (See Appendix A.3.3 for related background material.)

We define the *kernel* of J to be the set of vectors $\mathbf{v} \in \mathbb{R}^n$ such that $J\mathbf{v} = \mathbf{0}$. We define the *rowspan* of J to be the subspace of $\mathbb{R}^n$ spanned by the rows of J (i.e., the subspace of vectors that can be expressed as linear combinations of the rows of J). Then $\mathbb{R}^n$ is the direct sum of *kernel*(J) and *rowspan*(J); that is, every vector $\mathbf{v}$ in $\mathbb{R}^n$ can be written uniquely in the form

$$\mathbf{v} = \mathbf{k} + \mathbf{r} \qquad \text{with } \mathbf{k} \in \textit{kernel}(J) \text{ and } \mathbf{r} \in \textit{rowspan}(J). \qquad \text{(XIII.12)}$$

Furthermore, the dot product $\mathbf{k} \cdot \mathbf{r}$ is equal to zero for all $\mathbf{k} \in \textit{kernel}(J)$ and $\mathbf{r} \in \textit{rowspan}(J)$. Since these conditions hold, *kernel*(J) and *rowspan*(J) are called *orthogonal complements*. It is an elementary fact from linear algebra that any subspace of $\mathbb{R}^n$ has a unique orthogonal complement.

Similarly, we let *colspan*(J) be the column span of J, and its orthogonal complement is $\textit{kernel}(J^{\mathrm{T}})$.[6] It is easy to check that *colspan*(J) is the same as the range of the linear map represented by J.

We henceforth let $k = 3m$ be the number of rows of J.

Definition XIII.4. Let J be a $k \times n$ matrix. Then the *pseudo-inverse* of J, denoted $J^\dagger$, is the $n \times k$ matrix such that,

(a) For every $\mathbf{v} \in \textit{kernel}(J^{\mathrm{T}})$, $J^\dagger \mathbf{v} = \mathbf{0}$.

(b) For every $\mathbf{v} \in \textit{colspan}(J)$, $J^\dagger \mathbf{v} \in \textit{rowspan}(J)$.

(c) For every $\mathbf{v} \in \textit{colspan}(J)$, $JJ^\dagger \mathbf{v} = \mathbf{v}$.

A crucial property of the pseudo-inverse is that $J^\dagger J$ is the projection mapping onto the subspace *rowspan*(J); namely, if Equation (XIII.12) holds, then $J^\dagger J \mathbf{v} = \mathbf{r}$. To prove this, note that applying condition (b) with $\mathbf{v}$ replaced by $J\mathbf{v}$, shows that $J^\dagger J \mathbf{v}$ is in *rowspan*(J). Further, by (c), $JJ^\dagger J\mathbf{v} = J\mathbf{v} = J\mathbf{r}$. These two facts imply $J(J^\dagger J\mathbf{v} - \mathbf{r}) = \mathbf{0}$, so $J^\dagger J \mathbf{v} - \mathbf{r} \in \textit{kernel}(J)$. But also, $J^\dagger J\mathbf{v} - \mathbf{r} \in \textit{rowspan}(J)$, so $J^\dagger J \mathbf{v} - \mathbf{r} = \mathbf{0}$, i.e., $J^\dagger J \mathbf{v} = \mathbf{r}$.

[6] J^{T} is the transpose of J.

By similar reasoning, it can also be shown that $JJ^\dagger$ is the projection mapping onto $\mathit{colspan}(J)$. By (a), $JJ^\dagger$ maps $\mathit{kernel}(J^{\mathrm{T}})$, the orthogonal complement of $\mathit{colspan}(J)$, to zero. For $\mathbf{v} \in \mathit{colspan}(J)$, $JJ^\dagger\mathbf{v} = \mathbf{v}$, by (c). Thus, $JJ^\dagger$ is the projection mapping onto $\mathit{colspan}(J)$.

To see that conditions (a)-(c) determine a unique matrix $J^\dagger$, note that for all $\mathbf{v} \in \mathit{colspan}(J)$, there is a unique $\mathbf{w} \in \mathit{rowspan}(J)$ such that $J\mathbf{w} = \mathbf{v}$. Thus, (a)-(c) uniquely determine $J^\dagger(\mathbf{v})$ for $\mathbf{v}$ in $\mathit{kernel}(J^{\mathrm{T}}) \cup \mathit{colspan}(J)$. These are orthogonal complements, so the linear map $J^\dagger$ is thereby uniquely specified for all vectors $\mathbf{v}$.

An alternative, and equivalent, definition of the pseudo-inverse of J is as follows: for any vector $\mathbf{v} \in \mathbb{R}^k$, $J^\dagger\mathbf{v} = \mathbf{w}$, where $\mathbf{w} \in \mathbb{R}^n$ is the vector such that

(a') $||\mathbf{v} - J\mathbf{w}||$ is minimized, and

(b') $||\mathbf{w}||$ is the minimum among all $\mathbf{w}$ satisfying (a').

To see this equivalence, first note that since the range of J is $\mathit{colspan}(J)$, the quantity $||\mathbf{v} - J\mathbf{w}||$ will be minimized if $J\mathbf{w}$ is the projection of $\mathbf{v}$ onto $\mathit{colspan}(J)$. As just proved above, $JJ^\dagger$ is the projection mapping onto $\mathit{colspan}(J)$, and thus condition (a') holds. Condition (b') now follows from (b).

Conditions (a') and (b') can be equivalently expressed in terms of minimizing the squares of the magnitudes, i.e., minimizing $||\mathbf{v} - J\mathbf{w}||^2$ and $||\mathbf{w}||^2$. The square magnitude of a vector is, of course, the sum of the squares of the components of the vector. Therefore, (a') and (b') show that the pseudo-inverse $J^\dagger$ finds a solution which is as good as possible, where "good" is measured in terms of the sum of the squares. In other words, it solves the least squares minimization problem.

Exercise XIII.10* Suppose that $J^\dagger$ satisfies conditions (a') and (b'). Prove that it also satisfies conditions (a), (b), and (c).

Now that we have defined the pseudo-inverse, we can give a solution for Equation (XIII.11), namely,

$$\Delta\vec{\theta} \;=\; J^\dagger(\Delta\vec{\mathbf{s}}). \tag{XIII.13}$$

By the characterization of pseudo-inverses by conditions (a') and (b'), we see that this is a reasonably good choice for $\Delta\vec{\theta}$.

It remains to explain how to compute $J^\dagger$. The next theorem gives a formula for finding $J^\dagger$ in the case where J has at least as many columns as rows and where the rows are linearly independent.

Theorem XIII.5. *Suppose J is a $k \times n$ matrix and that J has rank k. Then JJ^{T} is nonsingular, and the pseudo-inverse $J^\dagger$ of J is*

$$J^\dagger \;=\; J^{\mathrm{T}}(JJ^{\mathrm{T}})^{-1}. \tag{XIII.14}$$

Proof. We start by just assuming that JJ^{T} is nonsingular, so $(JJ^{\mathrm{T}})^{-1}$ exists. Let $J^\dagger$ be the matrix given by the righthand side of Equation (XIII.14).

Since J has rank k, the rows of J are linearly independent. Also, *colspan*(J) has dimension k. Thus, *colspan*(J) is equal to all of $\mathbb{R}^k$, and *kernel*$(J^{\mathrm{T}}) = \{\mathbf{0}\}$. Therefore, condition (a) of the definition of the pseudo-inverse automatically holds for $J^\dagger$, without even using Equation (XIII.14). In addition, the range of J^{T} equals *colspan*(J^{T}), and therefore the range of $J^{\mathrm{T}}(JJ^{\mathrm{T}})^{-1}$ is certainly a subset of *colspan*(J^{T}). Since *colspan*(J^{T}) equals *rowspan*(J), condition (b) must hold for $J^\dagger$ defined by Equation (XIII.14). Finally, condition (c) holds since

$$JJ^\dagger \;=\; J(J^{\mathrm{T}}(JJ^{\mathrm{T}})^{-1}) \;=\; JJ^{\mathrm{T}}(JJ^{\mathrm{T}})^{-1} \;=\; \mathit{Identity}.$$

We have shown that if $J^\dagger$ is defined by Equation (XIII.14), then conditions (a)-(c) hold, so it remains only to prove the assumption that $Z = JJ^{\mathrm{T}}$ is invertible. Note that Z is a $k \times k$ matrix and that the entries of Z are equal to

$$z_{i,j} = \mathbf{r}_i \cdot \mathbf{r}_j,$$

where $\mathbf{r}_i$ is the i-th row of J and where '$\cdot$' denotes vector dot product. Suppose Z has rank $< k$, so there is a linear dependence among the rows of Z. This means there are scalars α_i, not all zero, such that

$$0 \;=\; \sum_i \alpha_i z_{i,j} \;=\; \sum_i \alpha_i \mathbf{r}_i \cdot \mathbf{r}_j \qquad \text{for all } j = 1, 2, \ldots, k.$$

Then, for all j,

$$\left(\textstyle\sum_i \alpha_i \mathbf{r}_i\right) \cdot \mathbf{r}_j \;=\; 0.$$

The vector in the parentheses is in the span of the rows of J and also has dot product equal to zero with each of the rows $\mathbf{r}_j$. Therefore the quantity in parentheses must be zero. This however contradicts the hypothesis that the rows of J are linearly independent. □

Very frequently, the Jacobian J does not have full row rank, that is, its rank is $< k$. In this case, Theorem XIII.5 does not apply and we must find another way to compute the pseudo-inverse $J^\dagger$. Let ℓ equal the rank of J. We wish to express J in the form

$$J \;=\; J_1 J_2 \tag{XIII.15}$$

where J_1 is a $k \times \ell$ a matrix, J_2 is an $\ell \times n$ matrix, and both J_1 and J_2 have rank ℓ. When these conditions hold, the product $J = J_1 J_2$ is called the *full rank factorization* of J.

To find J_1 and J_2, first find ℓ rows of J which are linearly independent. Let $\mathbf{r}_{s_1}, \ldots, \mathbf{r}_{s_\ell}$ be these ℓ rows. Then, express all the rows of R as

$$\mathbf{r}_i \;=\; \sum_{j=1}^{\ell} \alpha_{i,j} \mathbf{r}_{s_j}.$$

The linearly independent rows $\mathbf{r}_{s_j}$ and the coefficients $\alpha_{i,j}$ can be found by a Gaussian elimination type procedure. Care should be taken here to have good criteria for deciding when a given row is the span of another set of rows, since roundoff errors and/or matrices that are near-singular mean that one has to allow a row that is nearly equal to a linear combination of other rows to be treated as being a linear combination.

Once the values $\alpha_{i,j}$ have been found, let J_1 be the matrix with entries $\alpha_{i,j}$, and let J_2 be the matrix obtained from J by keeping the ℓ rows $\mathbf{r}_{s_1}$ through $\mathbf{r}_{s_\ell}$ and discarding the rest of the rows. Then by inspection, $J = J_1 J_2$.

Theorem XIII.6. *Let $J = J_1 J_2$ be such that J_1 is $k \times \ell$ and J_2 is $\ell \times n$ and suppose J (and thus J_1 and J_2) are rank ℓ. Then*

$$J^\dagger \;=\; J_2^{\mathrm{T}}(J_2 J_2^{\mathrm{T}})^{-1}(J_1^{\mathrm{T}} J_1)^{-1} J_1^{\mathrm{T}}. \tag{XIII.16}$$

Proof. We already proved that $J_2 J_2^{\mathrm{T}}$ is invertible in the proof of Theorem XIII.5. A similar argument shows that $J_1^{\mathrm{T}} J_1$ is invertible. Let $J^\dagger$ be the matrix defined by Equation (XIII.16): we must show that conditions (a)-(c) hold. Since $J^{\mathrm{T}} = J_2^{\mathrm{T}} J_1^{\mathrm{T}}$ and since $\mathit{kernel}(J_2^{\mathrm{T}}) = \{\mathbf{0}\}$, we have $\mathit{kernel}(J^{\mathrm{T}}) = \mathit{kernel}(J_1^{\mathrm{T}})$. Therefore, condition (a) certainly holds. Similarly, since $\mathit{kernel}(J_1) = \{\mathbf{0}\}$, J and J_2 have the same kernel, so $\mathit{rowspan}(J_2) = \mathit{rowspan}(J)$. Clearly, the range of $J^\dagger$ is a subset of $\mathit{colspan}(J_2^{\mathrm{T}}) = \mathit{rowspan}(J_2)$. Therefore, the range of $J^\dagger$ is a subset of $\mathit{rowspan}(J)$, so condition (b) holds. Finally, suppose $\mathbf{v}$ is in $\mathit{colspan}(J)$, i.e., $\mathbf{v}$ is in the range of J, so that $\mathbf{v} = J(\mathbf{w})$ for some w. From this,

$$\begin{aligned}
JJ^\dagger\mathbf{v} &= JJ^\dagger J\mathbf{w}\\
&= JJ_2^{\mathrm{T}}(J_2J_2^{\mathrm{T}})^{-1}(J_1^{\mathrm{T}}J_1)^{-1}J_1^{\mathrm{T}}J\mathbf{w}\\
&= (J_1J_2)J_2^{\mathrm{T}}(J_2J_2^{\mathrm{T}})^{-1}(J_1^{\mathrm{T}}J_1)^{-1}J_1^{\mathrm{T}}(J_1J_2)\mathbf{w}\\
&= J_1(J_2J_2^{\mathrm{T}})(J_2J_2^{\mathrm{T}})^{-1}(J_1^{\mathrm{T}}J_1)^{-1}(J_1^{\mathrm{T}}J_1)J_2\mathbf{w}\\
&= J_1J_2\mathbf{w}\\
&= J\mathbf{w}\\
&= \mathbf{v},
\end{aligned}$$

and condition (c) is proved. □

Theorems XIII.5 and XIII.6 imply algorithms for finding the pseudo-inverse that are fairly efficient as long as k is small; that is to say, as long as the total number of links were are trying to force to a specified position is small. There are other, iterative methods that find the pseudo-inverse by computing a singular value decomposition (c.f., [92]). Quasi-Newton methods have also been used to solve the inverse kinematics problem, c.f., [128].

There are many important issues we have glossed over that are important for writing a functioning inverse kinematics system based on pseudo-inverse calculations. Perhaps the most significant such issues are how to handle extra constraints such as joint limits, and how to avoid unnecessarily reaching configurations of the links where where the Jacobian has reduced row rank. One way to help avoid these problems was suggested by Girard and Maciejewski [53]. For each joint angle, we choose a "rest position", which is a desired value for the joint angle; preferably, this rest position would be in a partially flexed position, away from any joint limits and away from configurations which lead to reduced row rank in the Jacobian. In a given configuration of the links, let $\Delta\vec{H}$ denote the change in the values of the joint angles $\vec{\theta}$ which would suffice to bring all the joints back to their rest positions. Then, after performing the pseudo-inverse calculation of $\Delta\vec{\theta}$, update the joint positions by

$$\epsilon[\Delta\vec{\theta} + (I - J^\dagger J)(\Delta\vec{H})]. \tag{XIII.17}$$

As mentioned above, $J^\dagger J$ is the projection mapping onto *rowspan* of J. Therefore, $(I - J^\dagger J)$ is the projection map onto the kernel of J, and we have

$$J(\Delta\vec{\theta} + (I - J^\dagger J)(\Delta\vec{H})) \;=\; J(\Delta\vec{\theta}).$$

Updating the joint positions by (XIII.17) thus tends to move the joint angles back to their rest positions as best as can be done without worsening the progress made towards the target positions of the links.

Weighting joint angles. Often, it is useful to weight joint angle changes to allow some joints to rotate more readily than others. For example, in a robot arm, it can be much easier to rotate a joint angle near an end link than a joint angle near the root. Analogously, for a human arm, it is generally much easer to rotate a finger joint through an angle of φ degrees than to move a shoulder joint through the same angle φ. Indeed, it is generally preferable to change a finger joint by a relatively large angle, rather than a shoulder joint through a relatively small angle.

The above described pseudo-inverse method does not incorporate any weighting of the costs of rotating different joints; however, it is fairly simple to modify it to do so. Let $\vec{\theta} = \langle\theta_1, \ldots, \theta_m\rangle^{\mathrm{T}}$ be the joint angles (which are now indexed by integers instead of by links). We assign positive weights α_i, for $i = 1, \ldots, m$, to these joint angles, choosing the values α_i to be proportional to the cost of changing the angle θ_i. That is to say, the cost of changing angle θ_i by a small angle φ is equal to α_i/α_j times the cost of changing angle θ_j by the same amount φ. For instance, in the shoulder/finger example, the value of weight α would be much higher for the shoulder joint than for the finger joint. Another way to state the property satisfied by the weights α_i is that if $\alpha_i\Delta\theta_i = \alpha_j\Delta\theta_j$, then the costs of the changes to the two angles θ_i and θ_j are equal.

We introduce new variables $\psi_i = \alpha_i\theta_i$, and let $\vec{\psi}$ be the vector of values ψ_i. Note that $\theta_i = \psi_i/\alpha_i$, and $\Delta\theta_i = (\Delta\psi_i)/\alpha_i$, etc. We now define a new Jacobian matrix $\widehat{J}$ using the variables $\vec{\psi}$, namely, $\widehat{J}$ is the Jacobian matrix whose entries are equal to

$$\frac{\partial \mathbf{s}_x}{\partial \psi_i}.$$

Since $(d\theta_i/d\psi_i) = 1/\alpha_i$, we have

$$\frac{\partial \mathbf{s}_x}{\partial \psi_i} \;=\; \frac{1}{\alpha_i}\frac{\partial \mathbf{s}_x}{\partial \theta_i}.$$

Therefore, the matrix $\widehat{J}$ can be obtained from the original Jacobian J by dividing the entries in each column i by α_i. Then we solve the least squares problem, but using the variables $\vec{\psi}$. To do this, form the pseudo-inverse $\widehat{J}^\dagger$ and set

$$\Delta\vec{\psi} \;=\; \widehat{J}^\dagger(\Delta\vec{\mathbf{s}}).$$

Finish by letting $\Delta\theta_i = (\Delta\psi_i)/\alpha_i$ and then proceed as before, choosing a small ϵ and incrementally updating the joint angles.

As seen above, weighting joint angle costs corresponds to a very simple change of variables. Now, one should wonder why it is appropriate to use the multipliers α_i instead of some other value. This choice can be justified by the following simple example.

Suppose we want to solve

$$\theta_1 + \theta_2 \;=\; 1,$$

subject to minimizing the quantity

$$(\alpha_1\theta_1)^2 + (\alpha_2\theta_2)^2.$$

That is, we are trying to minimize the sum of the squares of the costs of the angles, with α_1 and α_2 specifying the relative costs. When we change to the variables ψ_1 and ψ_2, this is the same as solving for

$$\frac{\psi_1}{\alpha_1} + \frac{\psi_2}{\alpha_2} \;=\; 1,$$

subject to minimizing the quantity

$$\psi_1^2 + \psi_2^2.$$

In other words, the problem becomes an ordinary least squares problem with all weights equal to 1. Thus, the transformation from the variables θ_i to the variables ψ_i converts the weighted least squares minimization problem into an unweighted least squares minimization problem.

Appendix A

Mathematics Background

This appendix quickly reviews a lot of the mathematical prerequisites for this book. This material is mostly from a first year calculus course, with particular emphasis on vectors. The first section covers some preliminaries. Section A.2 covers vectors in $\mathbb{R}^2$ and then in $\mathbb{R}^3$, including dot products and cross products. The next section introduces 3×3 matrices and their connections to vector dot product and cross product. Matrix determinants and inverses and adjoints in $\mathbb{R}^3$ are covered after that. After that, there is a review of fundamental properties of linear spaces and dimension. The concluding sections discuss some of the basic concepts from multivariable calculus, including partial derivatives, gradients, vector-valued functions, and Jacobians.

Other prerequisites, not covered in this appendix, include basic topics from discrete math, most notably proofs by induction and simple facts about trees. There a few places where we presume knowledge of big-O notation, of the choice function $\binom{n}{k}$, and of geometric series. The reader is also expected to already have knowledge of trigonometry and of the basics of single-variable calculus.

A.1 Preliminaries

The set $\mathbb{R}$ is the set of real numbers. For $k \geq 1$ an integer, $\mathbb{R}^k$ is the set of k-tuples of real numbers; these k-tuples are also called k-vectors when we want to emphasize the fact that $\mathbb{R}^k$ is a vector space (vector spaces are discussed more below). A k-tuple is a sequence of length k, and is represented by the notation

$$\langle a_1, a_2, \ldots, a_k \rangle,$$

using angle brackets.

For $a < b$, the set $[a,b]$ is the closed interval containing all points x such that $a \leq x \leq b$. The square brackets indicate the inclusion of the endpoints a and b. We use parentheses instead of square brackets when the endpoints are omitted, for example,

$$[a,b) \;=\; \{x \in \mathbb{R} : a \leq x < b\}$$

is a half-open interval. Exponent notation is used for tuples of elements from intervals too, for example,

$$[0,1]^2 \;=\; [0,1]\times[0,1] \;=\; \{\langle a,b\rangle : a,b\in[0,1]\}$$

is the unit square containing pairs of reals from $[0,1]$.

The notation

$$f : A \to B$$

indicates that f is a function with domain A and with range contained in B. A function is also called a *mapping*. The *range* of f is the set of values $f(a)$ for a in the domain A; the set B is sometimes called the *codomain* of f. For example, the function $g:\mathbb{R}\to\mathbb{R}$ defined by $g(x)=\sin(x)$ has domain $\mathbb{R}$ and range $[-1,1]$. The function $f:A\to B$ is *one-to-one* provided that for each $b\in B$, there is at most one $a\in A$ such that $f(a)=b$. The function is *onto* provided that the range of f is equal to all of B.

When the codomain B is $\mathbb{R}$, we define the *support* of f to be the set of elements a such that $f(a)$ is non-zero.

A.2 Vectors and vector products

A k-vector $\mathbf{u}$ is a sequence of k real numbers,

$$\mathbf{u} \;=\; \langle u_1, u_2, \ldots, u_k\rangle.$$

Our conventions are to use bold face letters, like $\mathbf{u}$, to denote vectors, and italic symbols, like u or u_i, for scalar values.

In computer graphics, we are mostly concerned with vectors with 2, 3, or 4 components. For $k=2$, a 2-vector represents a point in $\mathbb{R}^2$, the real plane. Going up a dimension, a 3-vector represents a point in $\mathbb{R}^3$, that is, in three dimensional space. We use 4-vectors mostly to represent points in homogeneous coordinates (see Chapter II for information on homogeneous coordinates).

The space of all k-vectors is the k-dimensional vector space, sometimes called Euclidean space, and is denoted $\mathbb{R}^k$.

A.2.1 Vectors in $\mathbb{R}^2$

A vector in $\mathbb{R}^2$ is a pair of real numbers (also called *scalars*), written $\mathbf{u}=\langle u_1,u_2\rangle$. As an ordered pair, a vector can be viewed either as a point in the usual xy-plane, or as a displacement between two points. (See Figure A.1.) It is sometimes useful to make a distinction between points and vectors since they are often used in different ways. However, they are both represented by a pair of scalars, and their similarities greatly outweigh their differences. Thus, we find it convenient to treat vectors and points as being the same kind of object, namely, as a pair of scalars.

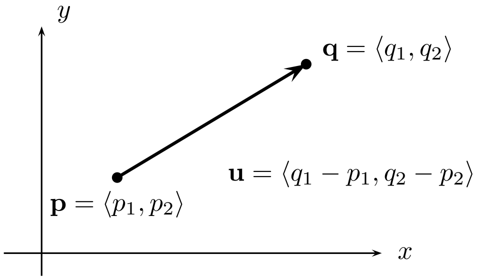
y
$\mathbf{q} = \langle q_1, q_2 \rangle$
$\mathbf{u} = \langle q_1 - p_1, q_2 - p_2 \rangle$
$\mathbf{p} = \langle p_1, p_2 \rangle$
x

Figure A.1: Two points $\mathbf{p}$ and $\mathbf{q}$ and the vector $\mathbf{u} = \mathbf{q} - \mathbf{p}$.

The length of a vector, also called the *magnitude* or *norm* of the vector, can be defined in terms of the Euclidean distance function:

$$||\mathbf{u}|| \;=\; \sqrt{u_1^2 + u_2^2}.$$

A *unit vector* is a vector with magnitude equal to 1.

The unit circle in $\mathbb{R}^2$, also called the 1-sphere, is the set of vectors with magnitude 1.

Vector addition and vector subtraction are defined to act component-wise:

$$\begin{aligned} \mathbf{u} + \mathbf{v} &= \langle u_1, u_2 \rangle + \langle v_1, v_2 \rangle \;=\; \langle u_1 + v_1, u_2 + v_2 \rangle, \\ \mathbf{u} - \mathbf{v} &= \langle u_1, u_2 \rangle - \langle v_1, v_2 \rangle \;=\; \langle u_1 - v_1, u_2 - v_2 \rangle. \end{aligned}$$

One could define a component-wise multiplication operation on vectors, but this turns out not to be a very useful operation. Instead, there are two much more useful ways to define scalar-valued multiplication on vectors, the dot product and the determinant:

$$\mathbf{u} \cdot \mathbf{v} \;=\; u_1 v_1 + u_2 v_2 \qquad \text{Dot product} \tag{A.1}$$

$$det(\mathbf{u}\,\mathbf{v}) \;=\; \begin{vmatrix} u_1 & v_1 \\ u_2 & v_2 \end{vmatrix} \;=\; u_1 v_2 - u_2 v_1 \qquad \text{Determinant} \tag{A.2}$$

Note that both the dot product and the determinant (in $\mathbb{R}^2$) take two vectors and produce a scalar as the result. The dot product is sometimes called the *inner product.*

Dot products in $\mathbb{R}^2$

The dot product was defined above with the formula $u_1 v_1 + u_2 v_2$. An alternate definition can be given in terms of the magnitudes of $\mathbf{u}$ and $\mathbf{v}$ and the angle φ between the two vectors. Namely, referring to Figure A.2,

$$\mathbf{u} \cdot \mathbf{v} \;=\; ||\mathbf{u}|| \cdot ||\mathbf{v}|| \cos \varphi. \tag{A.3}$$

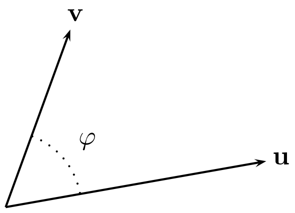

Figure A.2: The angle between $\mathbf{u}$ and $\mathbf{v}$ equals φ, and is used for computing the dot product. Since $\cos\varphi = \cos(-\varphi) = \cos(360^\circ - \varphi)$ it makes no difference which way the angle is measured for the purposes of computing the dot product.

It is fine to take Equation (A.3) on faith, but if you wish to see a proof you may work the next exercise.

Exercise A.1* Prove the correctness of Equation (A.3). [Hint: Let $\mathbf{u}$ make angle ψ with the x-axis. Therefore, $\mathbf{v}$ makes angle $\psi + \varphi$ with the x-axis. Express the vectors $\mathbf{u}$ and $\mathbf{v}$ component-wise with sines and cosines. Then compute the dot product according to the definition in Equation (A.1), and transform it using the sine or cosine angle sum formulas (or the angle difference formulas). Show that Equation (A.3) results.]

Suppose $\mathbf{u}$ and $\mathbf{v}$ are nonzero. Then Equation (A.3) shows that $\mathbf{u} \cdot \mathbf{v}$ is equal to zero if and only if $\cos\theta$ equals zero. This happens if and only if the angle between $\mathbf{u}$ and $\mathbf{v}$ is a right angle. In this case, the two vectors are said to be *perpendicular*, or *orthogonal*.

When $\mathbf{u}$ is a unit vector, the dot product formula reduces to just $\mathbf{u} \cdot \mathbf{v} = ||\mathbf{v}|| \cos\varphi$. Referring to Figure A.3, this implies that, when $\mathbf{u}$ is a unit vector, $\mathbf{u} \cdot \mathbf{v}$ is the (signed) length of the *projection* of $\mathbf{v}$ onto the line in the direction of $\mathbf{u}$. The *projection of* $\mathbf{v}$ *onto* $\mathbf{u}$ is defined to equal

$$(\mathbf{u} \cdot \mathbf{v})\mathbf{u},$$

which is the component of $\mathbf{v}$ parallel to the vector $\mathbf{u}$. (This formula for projection is correct only if $\mathbf{u}$ is a unit vector.) Note that the projection is a vector parallel to $\mathbf{u}$.

We can also find a formula for the component of $\mathbf{v}$ which is perpendicular to $\mathbf{u}$. Namely, if we subtract off the projection, the remaining part is perpendicular to $\mathbf{u}$. Thus, for $\mathbf{u}$ a unit vector, the component of $\mathbf{v}$ perpendicular to $\mathbf{u}$ is equal to

$$\mathbf{v} - (\mathbf{u} \cdot \mathbf{v})\mathbf{u}.$$

It is easy to check that $\mathbf{u} \cdot \mathbf{u} = ||\mathbf{u}||^2$. Thus the magnitude of $\mathbf{u}$ is $\sqrt{\mathbf{u} \cdot \mathbf{u}}$. We use $\mathbf{u}^2$ as a shorthand notation for $\mathbf{u} \cdot \mathbf{u} = ||\mathbf{u}||^2$.

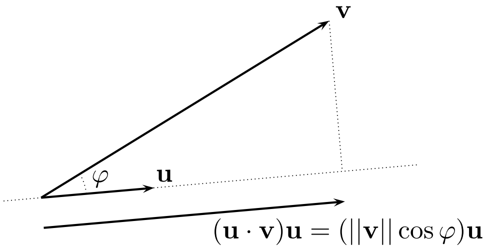
$\mathbf{v}$
φ
$\mathbf{u}$
$(\mathbf{u}\cdot\mathbf{v})\mathbf{u} = (||\mathbf{v}||\cos\varphi)\mathbf{u}$

Figure A.3: The projection of $\mathbf{v}$ onto the line parallel to a unit vector $\mathbf{u}$. φ is the angle between $\mathbf{u}$ and $\mathbf{v}$. How would the picture look if φ were between 90° and 180°?

Determinants in $\mathbb{R}^2$

The determinant of two vectors $\mathbf{u}$ and $\mathbf{v}$ in $\mathbb{R}^2$ was defined as $det(\mathbf{u}\,\mathbf{v}) = u_1v_2 - u_2v_1$. This is actually the determinant of the 2×2 matrix which has $\mathbf{u}$ and $\mathbf{v}$ as column vectors. There are several useful ways to think about determinants:

(a) If you are familiar with cross products in three dimensions, we can restate the two dimensional determinant in terms of the three dimensional cross product. For this, we pad $\mathbf{u}$ and $\mathbf{v}$ with a third entry equal to zero, and take the cross product in three dimensions. This yields

$$\langle u_1, u_2, 0\rangle \times \langle v_1, v_2, 0\rangle \;=\; \langle 0, 0, u_1v_2 - u_2v_1\rangle.$$

Thus, the two dimensional determinant is equal to the z-component of the cross product obtained by embedding $\mathbf{u}$ and $\mathbf{v}$ into three dimensions. The advantage of thinking about two dimensional determinants in this way is that properties (c) and (d) below may already be quite familiar.

(b) In the two dimensional setting, the determinantt can be expressed as a dot product with a rotated vector. To explain, let, as usual, $\mathbf{u} = \langle u_1, u_2\rangle$, and let $\mathbf{u}^{\text{rot}}$ be the vector $\mathbf{u}$ rotated counter-clockwise 90°. By referring to Figure A.4, we see that $\mathbf{u}^{\text{rot}}$ is equal to

$$\mathbf{u}^{\text{rot}} \;=\; \langle -u_2, u_1\rangle.$$

It is immediate from the definitions of the determinant and the dot product, that $det(\mathbf{u},\,\mathbf{v}) = \mathbf{u}^{\text{rot}}\cdot\mathbf{v}$. That is to say, the determinant $det(\mathbf{u},\,\mathbf{v})$ can be calculated by rotating $\mathbf{u}$ through a right angle and then forming the dot product with $\mathbf{v}$.

This tells us that $det(\mathbf{u},\,\mathbf{v})$ is equal to zero if and only if $\mathbf{u}$ and $\mathbf{v}$ are parallel (i.e., collinear). In other words, $det(\mathbf{u},\,\mathbf{v}) = 0$ if and only if $\mathbf{u} = \alpha\mathbf{v}$ (or $\mathbf{v} = \alpha\mathbf{u}$) for some scalar α; or equivalently, if the angle between the vectors is equal to either zero or 180°.

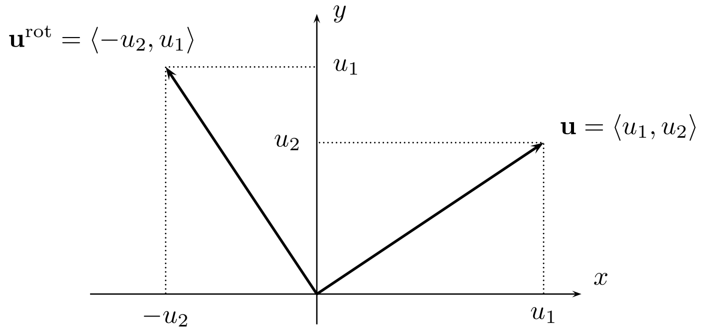
$\mathbf{u}^{\mathrm{rot}} = \langle -u_2, u_1 \rangle$
y
u_1
u_2
$\mathbf{u} = \langle u_1, u_2 \rangle$
x
$-u_2$
u_1

Figure A.4: The effect of rotating a vector 90 degrees counter-clockwise.

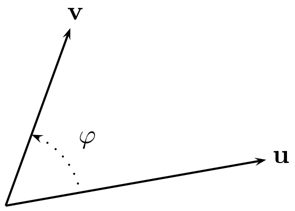

Figure A.5: The angle between $\mathbf{u}$ and $\mathbf{v}$ equals φ, and is used for computing the determinant. The direction (sign) of the angle is important for the determinant.

(c) Let φ be the angle between $\mathbf{u}$ and $\mathbf{v}$, with the angle φ measured in the counter-clockwise direction from $\mathbf{u}$ to $\mathbf{v}$ as shown in Figure A.5. Then the determinant is equal to

$$\mathit{det}(\mathbf{u},\, \mathbf{v}) \;=\; ||\mathbf{u}|| \cdot ||\mathbf{v}|| \sin\varphi.$$

(This fact can be easily proved from Equation (A.3) and the fact that $\mathit{det}(\mathbf{u},\, \mathbf{v})$ is equal to $\mathbf{u}^{\mathrm{rot}} \cdot \mathbf{v}$.) Note that it is important that the angle φ be measured in the correct direction, since $\sin(-\varphi) = -\sin\varphi$. Indeed, the determinant is antisymmetric with respect to interchanging columns:

$$\mathit{det}(\mathbf{u},\, \mathbf{v}) \;=\; -\,\mathit{det}(\mathbf{v},\, \mathbf{u}).$$

(d) There is an elegant interpretation of determinant in $\mathbb{R}^2$ in terms of area. Consider the parallelogram with sides equal to the vectors $\mathbf{u}$ and $\mathbf{v}$, as shown in Figure A.6. Then the (signed) area of the parallelogram is equal to

$$\mathit{Area} \;=\; \mathit{det}(\mathbf{u},\, \mathbf{v}).$$

To prove this, use the formula $(\mathit{base}) \cdot (\mathit{height})$. If the base length is measured along $\mathbf{u}$, it is just equal to $||\mathbf{u}||$. Then, the height must be measured perpendicularly to $\mathbf{u}$, and is equal to $||\mathbf{v}|| \sin\varphi$.

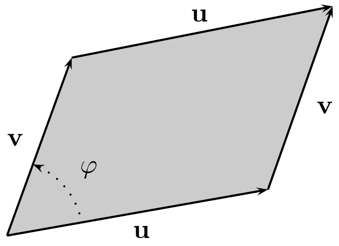

Figure A.6: In $\mathbb{R}^2$, the (signed) area of the parallelogram is equal to the determinant $det(\mathbf{u}, \mathbf{v})$. In $\mathbb{R}^3$, the area of the parallelogram is equal to the magnitude of $\mathbf{u} \times \mathbf{v}$.

When the angle φ is greater than 180° and less than 360°, then the determinant $det(\mathbf{u}, \mathbf{v})$ is negative. In this case, the parallelogram can be thought of as having "negative height," and hence negative area.

A.2.2 Vectors in $\mathbb{R}^3$

$\mathbb{R}^3$ is the three dimensional Euclidean space. A point or a vector $\mathbf{u}$ in $\mathbb{R}^3$ is specified by a triple of values, $\mathbf{u} = \langle u_1, u_2, u_3 \rangle$. In computer graphics, it is common to use x, y, z-axes that are oriented as shown in Figure I.4 on page 7: as shown there, the x-axis points rightward, the y-axis points upwards, and the z-axis points towards the viewer. This is different from the usual conventions that you probably learned in calculus class, but is still a righthanded coordinate system. (The main reason to work with a righthanded coordinate system rather than a lefthanded coordinate system is that it makes the cross product obey the usual "righthand rule.")

The length (usually called *magnitude* or *norm*) of a vector in $\mathbb{R}^3$ is given by the Euclidean distance formula

$$||\mathbf{u}|| = \sqrt{u_1^2 + u_2^2 + u_3^2}.$$

$\mathbf{u}$ is a *unit vector* provided $||\mathbf{u}|| = 1$. The unit sphere in $\mathbb{R}^2$, also called the 2-sphere or S^2, is the set of vectors with magnitude 1.

A non-unit vector $\mathbf{u}$ is *normalized* by the process of replacing it with a unit vector pointing in the same direction. That is to say, $\mathbf{u}$ is normalized by calculating $\mathbf{u}/||\mathbf{u}||$. The terminology is a little confusing, because the term "normal vector" is used to mean a non-zero vector that is perpendicular (that is, normal) to a surface. By definition, normal vectors are *not* required to be unit vectors. In other words, normal vectors do not always need to be normalized. Nonetheless, it is frequently helpful to use unit normal vectors, particularly in Chapter IV for lighting applications.

Addition and subtraction of vectors in $\mathbb{R}^3$ is defined component-wise, similar to their definition in $\mathbb{R}^2$. Dot product and cross product are discussed in the next two sections.

Dot products in $\mathbb{R}^3$

The dot product of two vectors in $\mathbb{R}^3$ is defined by

$$\mathbf{u}\cdot\mathbf{v} \;=\; u_1v_1 + u_2v_2 + u_3v_3.$$

This means that the dot product of two 3-vectors is a scalar.

If φ is the angle between the vectors $\mathbf{u}$ and $\mathbf{v}$, then

$$\mathbf{u}\cdot\mathbf{v} \;=\; ||\mathbf{u}||\cdot||\mathbf{v}||\cos\varphi.$$

Suppose that $\mathbf{u}$ is a unit vector. Then the *projection* of the vector $\mathbf{v}$ onto the line containing the vector $\mathbf{u}$ has signed length equal to $\mathbf{u}\cdot\mathbf{v}$. (This can be proved in the way used for $\mathbb{R}^2$, using the characterization of dot product in terms of $\cos\varphi$.) The *projection of* $\mathbf{v}$ *onto the unit vector* $\mathbf{u}$ is thus equal to the vector

$$(\mathbf{u}\cdot\mathbf{v})\mathbf{u}.$$

This is the component of $\mathbf{v}$ in the direction of $\mathbf{u}$.

The component of $\mathbf{v}$ perpendicular to $\mathbf{u}$ is equal to

$$\mathbf{v}-(\mathbf{u}\cdot\mathbf{v})\mathbf{u}.$$

The magnitude or *norm* of a vector $\mathbf{u}$ is equal to $\sqrt{\mathbf{u}^2}=\sqrt{\mathbf{u}\cdot\mathbf{u}}$.

Cross products in $\mathbb{R}^3$

The cross product of two vectors in $\mathbb{R}^3$ is the vector defined by

$$\mathbf{u}\times\mathbf{v} \;=\; \langle u_2v_3-u_3v_2,\, u_3v_1-u_1v_3,\, u_1v_2-u_2v_1\rangle.$$

To describe the definition of $\mathbf{u}\times\mathbf{v}$ in an alternate, geometric way, let φ be the angle from $\mathbf{u}$ to $\mathbf{v}$ measured in a direction such that $0\le\varphi\le 180^\circ$ (the direction to measure φ is unique for noncollinear $\mathbf{u}$ and $\mathbf{v}$). Then, $\mathbf{u}\times\mathbf{v}$ has magnitude

$$||\mathbf{u}||\cdot||\mathbf{v}||\sin\varphi,$$

and is perpendicular to both $\mathbf{u}$ and $\mathbf{v}$ with its direction given by the *righthand rule*. The righthand rule states that if you use the palm of your right hand to push $\mathbf{u}$ towards $\mathbf{v}$, with your thumb extended out at right angles, then your thumb will point in the direction of $\mathbf{u}\times\mathbf{v}$.

An equivalent way to state the geometric definition of the cross product is as follows. Let $\mathbf{u}$ and $\mathbf{v}$ both lie in a plane P. The plane P divides $\mathbb{R}^3$ into two half-spaces. Arbitrarily choose one of these half-spaces as being "above" the plane. Viewing the two vectors from above, let ψ be the angle from $\mathbf{u}$ to $\mathbf{v}$ measured in the counter-clockwise direction. Then $\mathbf{u}\times\mathbf{v}$ is the vector with *signed* magnitude equal to

$$||\mathbf{u}||\cdot||\mathbf{v}||\sin\psi, \tag{A.4}$$

and $\mathbf{u} \times \mathbf{v}$ is pointing up perpendicularly to P. We called the value (A.4) the signed magnitude since, if this value is negative, then the cross product is pointing downwards from P.

Evidently, for nonzero $\mathbf{u}$ and $\mathbf{v}$, the cross product is equal to zero if and only if $\mathbf{u}$ and $\mathbf{v}$ are collinear.

Recall that property (d) described how th The parallelogram area property (d) of determinants in $\mathbb{R}^2$ still holds in $\mathbb{R}^3$. Referring to Figure A.6, the vectors $\mathbf{u}$ and $\mathbf{v}$ now lie in $\mathbb{R}^3$. The area of the parallelogram is equal to the length of $\mathbf{u} \times \mathbf{v}$.

A.3 Matrices

A matrix $M = (m_{i,j})_{i,j}$ is a rectangular array of scalars,

$$M = \begin{pmatrix} m_{1,1} & \cdots & m_{1,s} \\ \vdots & \ddots & \vdots \\ m_{r,1} & \cdots & m_{r,s} \end{pmatrix}.$$

Here M is $r \times s$ matrix, and $m_{i,j}$ is the entry in row i and column j.

If N is further an $s \times t$ matrix, then the matrix product of M times N is the $r \times t$ matrix P whose entries $p_{i,k}$ are obtained by taking the inner product of the i-th row of M with the k-th column of N, namely,

$$p_{i,k} = \sum_{j=1}^{s} m_{i,j} n_{j,k}.$$

The $r \times r$ identity matrix is the matrix I which has diagonal entries equal to one, $I_{i,i} = 1$, and off-diagonal entries equal to zero. There is a different identity matrix for each $r \geq 1$, but we use the same notation I for all of them since it should always be clear from the context what the dimension is.

The identity matrices have the property that

$$IM = M \qquad \text{and} \qquad MI = M.$$

The inverse of M is the matrix M^{-1} such that $MM^{-1} = M^{-1}M = I$. Only square matrices can have inverses, and not even all of them do. A matrix which is invertible is also said to be *nonsingular*.

The *transpose* of M is the matrix M^{T} obtained by swapping elements of M across the diagonal: for $M = (m_{i,j})_{i,j}$ an $r \times s$ matrix, its transpose $M^{\mathrm{T}} = (m_{j,i})_{i,j}$ is an $s \times r$ matrix. (Note the subscripts in reverse order!)

The following identities are easy to check:

$$M^{\mathrm{T}} N^{\mathrm{T}} = (NM)^{\mathrm{T}} \qquad \text{and} \qquad I^{\mathrm{T}} = I.$$

In addition, for invertible M, $(M^{\mathrm{T}})^{-1} = (M^{-1})^{\mathrm{T}}$.

The matrices used in the early chapters of this book are primarily small, of dimensions 2×2 through 4×4. Frequently, we are interested in how these matrices act on points or vectors. For this, points and vectors will be treated as being column vectors: namely, a 2-vector is a 2×1 matrix, and a 3-vector is a 3×1 matrix. For instance, our convention is that a 3-vector $\mathbf{u} = \langle u_1, u_2, u_3 \rangle$ is the same as the column vector

$$\begin{pmatrix} u_1 \\ u_2 \\ u_3 \end{pmatrix}.$$

In this way, we can take the product of a matrix and a vector and get a vector as a result. You should refer to Chapter II for more information on matrices and vectors in $\mathbb{R}^2$ and $\mathbb{R}^3$. As discussed in Chapter II, matrices are used extensively in computer graphics to transform vectors by multiplication.

A.3.1 Matrices and vector products in $\mathbb{R}^3$

It is possible to re-express dot and cross products in terms of matrix products. As we just said, a vector $\mathbf{u} = \langle u_1, u_2, u_3 \rangle$ is, by convention, the same as a column vector (i.e., a 3×1 matrix). Therefore, the transpose of a vector is a 1×3 matrix, or a row vector. That is,

$$\mathbf{u}^{\mathrm{T}} \;=\; (u_1 \;\; u_2 \;\; u_3).$$

It is easy to check that a dot product can be expressed as

$$\mathbf{u} \cdot \mathbf{v} \;=\; \mathbf{u}^{\mathrm{T}}\mathbf{v}.$$

Or, to write it out fully,

$$\langle u_1, u_2, u_3 \rangle \cdot \langle v_1, v_2, v_3 \rangle \;=\; (u_1 \;\; u_2 \;\; u_3) \begin{pmatrix} v_1 \\ v_2 \\ v_3 \end{pmatrix}.$$

To interpret this correctly, the left-hand side of each of the above two equalities is a dot product, and the righthand side is a matrix product. (If one wanted to be overly precise, one could note that the righthand side really denotes a 1×1 matrix, not a scalar, but it does no harm to treat a 1×1 matrix as being the same as a scalar.)

We just described how to re-express a dot product as a matrix product using a 1×3 matrix. Similarly, a cross product operation can be expressed as a matrix product, but now using a 3×3 matrix. Namely, let $M_{\mathbf{u}\times}$ be the matrix

$$M_{\mathbf{u}\times} \;=\; \begin{pmatrix} 0 & -u_3 & u_2 \\ u_3 & 0 & -u_1 \\ -u_2 & u_1 & 0 \end{pmatrix}.$$

Then it is easy to check that

$$(M_{\mathbf{u}\times})\mathbf{v} \;=\; \mathbf{u}\times\mathbf{v}$$

using the first definition of cross product in $\mathbb{R}^3$.

The matrix version of dot product allows us to express the projection operator as a matrix. Let $\mathbf{u}$ be a unit vector, and recall that the projection of $\mathbf{v}$ onto $\mathbf{u}$ is equal to $(\mathbf{u}\cdot\mathbf{v})\mathbf{u}$. This can be rewritten as

$$(\mathbf{u}\cdot\mathbf{v})\mathbf{u} \;=\; \mathbf{u}(\mathbf{u}\cdot\mathbf{v}) \;=\; \mathbf{u}(\mathbf{u}^{\mathrm{T}}\mathbf{v}) \;=\; (\mathbf{u}\mathbf{u}^{\mathrm{T}})\mathbf{v}.$$

(The last equality used the associativity of matrix multiplication.) Thus, letting Proj_u be the matrix

$$\mathit{Proj}_u \;=\; \mathbf{u}\mathbf{u}^{\mathrm{T}} \;=\; \begin{pmatrix} u_1 \\ u_2 \\ u_3 \end{pmatrix} (u_1 \;\; u_2 \;\; u_3) \;=\; \begin{pmatrix} u_1^2 & u_1u_2 & u_1u_3 \\ u_1u_2 & u_2^2 & u_2u_3 \\ u_1u_3 & u_2u_3 & u_3^2 \end{pmatrix},$$

we have that $(\mathit{Proj}_u)\mathbf{v}$ is equal to the projection of $\mathbf{v}$ onto $\mathbf{u}$.

A.3.2 Determinants, inverses, and adjoints

Let M be a square $n\times n$ matrix. For $i,j\in\{1,\ldots,n\}$, the matrix $M_{i,j}$ is defined to be the $(n-1)\times(n-1)$ matrix obtained by deleting the i-th row and the j-th column from M.

We now define the *determinant* $\mathit{det}(M)$ of M. The definition of the determinant proceeds by induction on the dimension of M. When $n=1$, M is just a 1×1 matrix, and $\mathit{det}(M)$ is equal to its sole entry $m_{1,1}$. For $n>1$, the determinant of M is equal to

$$\begin{aligned} \mathit{det}(M) \;&=\; m_{1,1}\,\mathit{det}(M_{1,1}) - m_{1,2}\,\mathit{det}(M_{1,2}) + m_{1,3}\,\mathit{det}(M_{1,3}) \\ &\qquad -m_{1,4}\,\mathit{det}(M_{1,4}) + \;\cdots\; \pm\, m_{1,n}\,\mathit{det}(M_{1,n}) \\ &=\; \sum_{j=1}^{n}(-1)^{1+j}m_{1,j}\,\mathit{det}(M_{1,j}). \qquad \text{(A.5)} \end{aligned}$$

The definition (A.5) defines the determinant in terms of its expansion along the first row of the matrix. More generally, the determinant can also be defined with an expansion along any row i as

$$\mathit{det}(M) \;=\; \sum_{j=1}^{n}(-1)^{i+j}m_{i,j}\,\mathit{det}(M_{i,j}),$$

as well as in terms of an expansion along any column j:

$$\mathit{det}(M) \;=\; \sum_{i=1}^{n}(-1)^{i+j}m_{i,j}\,\mathit{det}(M_{i,j}).$$

The value $(-1)^{i+j}\,det(M_{i,j})$ is called the *cofactor of M at (i,j)*. Thus, the determinant is expressed in terms of an inner product of the entries in a given row (or column) of the matrix and its cofactors along the same row (or column).

The *adjoint* of M is the matrix N which is the transpose of the cofactors of M. Namely, N is the matrix with entries

$$n_{i,j} \;=\; (-1)^{i+j}\,det(M_{j,i}).$$

It is always the case that

$$MN \;=\; NM \;=\; det(M)I,$$

for N the adjoint of M. Therefore, if $det(M) \neq 0$, then M is invertible and

$$M^{-1} \;=\; \frac{1}{det(M)}N.$$

This gives a formula for inverting any invertible matrix, since a matrix M is invertible if and only if its determinant is nonzero.

A.3.3 Linear subspaces*

(Knowledge of linear subspaces is needed only for the discussion of inverse kinematics in Chapter XIII, and, to a lesser extent, for the material on projective geometry in Chapter II.)

Let $k \geq 1$ and consider $\mathbb{R}^k$. A subset $A \subseteq \mathbb{R}^k$ is called a *linear subspace* provided that A is closed under addition and under scalar multiplication.[1] That is, A is a linear subspace if and only if, for all $\mathbf{x}$ and $\mathbf{y}$ in A and for all scalars α, $\mathbf{x}+\mathbf{y}$ and $\alpha\mathbf{x}$ are also in A.

The vectors $\mathbf{x}_1, \mathbf{x}_2, \ldots, \mathbf{x}_n$ said to be *linearly independent* provided there is no sequence of scalars $\alpha_1, \ldots, \alpha_n$, not all zero, such that

$$\alpha_1\mathbf{x}_1 + \alpha_2\mathbf{x}_2 + \cdots + \alpha_n\mathbf{x}_n \;=\; \mathbf{0}.$$

(Here, $\mathbf{0}$ is the zero vector.) The *dimension* of a linear subspace A is the largest value n for which A contains n linearly independent vectors. When $A \subseteq \mathbb{R}^k$, the dimension of A can be at most k.

Let $\mathbf{x}_1, \ldots, \mathbf{x}_n$ be vectors in $\mathbb{R}$. The *span* of these vectors is the linear subspace that contains all linear combinations of the vectors $\mathbf{x}_i$. In other words, the span of $\mathbf{x}_1, \ldots, \mathbf{x}_n$ is the following subspace:

$$span(\vec{\mathbf{x}}) \;=\; \{\alpha_1\mathbf{x}_1 + \cdots + \alpha_n\mathbf{x}_n : \alpha_1, \ldots, \alpha_n \in \mathbb{R}\}.$$

It is easy to check that this is closed under addition and scalar multiplication, and thus is indeed a linear subspace. If $\mathbf{x}_1, \ldots, \mathbf{x}_n$ are linearly independent, then every vector in their span can be expressed as a linear combination of $\mathbf{x}_1, \ldots, \mathbf{x}_n$ in a unique way.

[1] Vector spaces are usually defined in a very general fashion. However, we shall only use vector spaces which are subsets of $\mathbb{R}^k$ for some k, and therefore make the corresponding simplifications in the discussion of linear subspaces.

Theorem A.1. *Let $A \subseteq \mathbb{R}^k$ have dimension n. Suppose $\mathbf{x}_1, \ldots, \mathbf{x}_n$ are in A and are linearly independent. Then $span(\vec{\mathbf{x}})$ is equal to A.*

Let A and B be linear subspaces of $\mathbb{R}^k$. We say that A and B are *orthogonal* if and only if, for all $\mathbf{x} \in A$ and all $\mathbf{y} \in B$, $\mathbf{x} \cdot \mathbf{y} = 0$. We say that A and B are *orthogonal complements* if they are orthogonal and if for every $\mathbf{u} \in \mathbb{R}^k$ there are $\mathbf{x} \in A$ and $\mathbf{y} \in B$ such that $\mathbf{u} = \mathbf{x} + \mathbf{y}$. In this case, $\mathbf{x}$ and $\mathbf{y}$ are uniquely determined by $\mathbf{u}$; in fact, $\mathbf{x}$ and $\mathbf{y}$ are the orthogonal projections of $\mathbf{u}$ onto the subspaces A and B.

Theorem A.2. *Let A be a linear subspace of $\mathbb{R}^k$. Then there is a unique subspace B such that A and B are orthogonal complements. In fact,*

$$B \ = \ \{\mathbf{y} : \textit{for all } \mathbf{x} \in A,\ \mathbf{x} \cdot \mathbf{y} = 0\}.$$

We use $A^\perp$ to denote the orthogonal complement of A.

Now, we return to matrices. Let M be an $r \times s$ matrix. If $\mathbf{x}$ is an s-vector, then $M\mathbf{x}$ is an r-vector. Therefore, the mapping

$$f_M : \mathbf{x} \mapsto M\mathbf{x}$$

is a function with domain $\mathbb{R}^s$ and codomain R^r. We shall often conflate the matrix M with the mapping f_M and use "M" to refer both the matrix and the mapping. It is easily seen that the range of M is exactly equal to the span of the columns of M. That is, let M have as columns the r-vectors $\mathbf{u}_1, \ldots, \mathbf{u}_s$; then the range of M is equal to $span(\vec{\mathbf{u}})$.

The *kernel* of M (or of f_M, to be more proper), is the set of vectors $\mathbf{x} \in \mathbb{R}^s$ such that $M\mathbf{x} = \mathbf{0}$. Let the rows of M be the s-vectors $\mathbf{v}_1, \ldots, \mathbf{v}_r$. Clearly, the kernel of M is the set of vectors $\mathbf{x}$ such that $\mathbf{x} \cdot \mathbf{v}_i = 0$ for all $i = 1, \ldots, r$. From the previous theorem, it follows easily that the kernel of M is the linear subspace which is the orthogonal complement of the span of the rows of M; namely, the kernel of M is equal to $(span(\vec{\mathbf{v}}))^\perp$.

We call $span(\vec{\mathbf{u}})$ the *column span* of M, and $span(\vec{\mathbf{v}})$ the *row span* of M. These are also denoted $colspan(M)$ and $rowspan(M)$.

The *rank* of the matrix M is defined to be the dimension of $rowspan(M)$ and of $colspan(M)$. (It is a theorem that these both have the same dimension.) The rank can also defined as be equal to the maximum number of linearly independent rows (or, columns) of M.

A.4 Multivariable calculus

A.4.1 Multivariable functions

A *multivariable* function is a function with multiple inputs. For now, we consider only real-valued multivariable functions, that is, functions with domain $\mathbb{R}^k$ and codomain $\mathbb{R}$. Simple examples of such functions include things like

$$f(x, y) = x^2 + y^2,$$

which can be visualized as a paraboloid surface, as well as functions of three variables, such as $f(x,y,z) = x^2 + y^2 + z^2$. The latter function is hard to visualize, since it would require four dimensions to graph it properly.

In addition, functions that take vectors as inputs can be viewed as multivariable functions. For example, the vector magnitude function $\mathbf{u} \mapsto ||\mathbf{u}||$ can be viewed as a function of the three scalar values u_1, u_2, u_3. Likewise, the distance function $f(\mathbf{u}, \mathbf{v}) = ||\mathbf{u} - \mathbf{v}||$ can be viewed as a function with domain $\mathbb{R}^6$, taking six scalar inputs.

Fix some function $f = f(x_1, \ldots, x_k)$ with k inputs. We sometimes slightly abuse notation and also write f as $f(\mathbf{x})$, where $\mathbf{x} = \langle x_1, \ldots, x_k \rangle$. The *partial derivative* of f with respect to x_i is the multi-variable function

$$\frac{\partial f}{\partial x_i}(x_1, \ldots, x_k)$$

that equals the rate of change in values of f with respect to changes in the value of x_i while keeping the rest of the input values fixed. To express this formally with limits, the partial derivative is the function satisfying

$$\frac{\partial f}{\partial x_i}(x_1, \ldots, x_k) \;=\; \lim_{h \to 0} \frac{f(x_1, \ldots, x_{i-1}, x_i + h, x_{i+1}, \ldots x_k) - f(x_1, \ldots, x_i, \ldots x_k)}{h}.$$

The partial derivative is undefined where this limit does not exist.

The *total derivative* of f is given by the expression

$$df \;=\; \frac{\partial f}{\partial x_1} dx_1 + \frac{\partial f}{\partial x_2} dx_2 + \cdots + \frac{\partial f}{\partial x_k} dx_k.$$

A good way to visualize what the total derivative means is to think of it as providing a way to approximate f in the neighborhood of a point $\langle x_1, \ldots, x_k \rangle$:

$$f(x_1 + \Delta x_1, \ldots, x_k + \Delta x_k) - f(x_1, \ldots, x_k) \;\approx\; \frac{\partial f}{\partial x_1} \Delta x_1 + \cdots + \frac{\partial f}{\partial x_k} \Delta x_k. \quad \text{(A.6)}$$

We can write this more suggestively as

$$\Delta f \;\approx\; \frac{\partial f}{\partial x_1} \Delta x_1 + \cdots + \frac{\partial f}{\partial x_k} \Delta x_k.$$

For well-behaved functions, this approximation is first-order accurate, which is to say that the error in the approximation is only $O(\Delta x_1^2 + \cdots + \Delta x_k^2)$. Therefore, the approximation is very accurate for sufficiently small values of Δx_i.

The *gradient* of $f(x_1, \ldots, x_k)$ is the vector-valued function

$$(\nabla f)(\mathbf{x}) \;=\; \left\langle \frac{\partial f}{\partial x_1}(\mathbf{x}), \frac{\partial f}{\partial x_2}(\mathbf{x}), \ldots, \frac{\partial f}{\partial x_k}(\mathbf{x}) \right\rangle.$$

The gradient function has k scalar inputs, and its value is a k-vector.

The motivation for the definition of the gradient is that it plays the role of the first derivative of $f(\mathbf{x})$. Indeed, using the gradient function, we can rewrite the first-order approximation of Equation (A.6) in vector notation as

$$f(\mathbf{x}+\Delta\mathbf{x}) - f(\mathbf{x}) \;\approx\; (\nabla f)\cdot(\Delta\mathbf{x}).$$

The righthand side of this approximation is a vector dot product.

A *level set* of a function f is a set of the points $\langle x_1, \dots x_k\rangle$ satisfying $f(x_1,\dots,x_k) = c$ for some fixed constant c. In this book, we only work with level sets of functions of three variables (i.e., $k = 3$). Such sets are also called *implicitly defined surfaces*. For example, the equation $x^2 + y^2 + z^2 - 1 = 0$ is an implicit definition of the unit sphere in $\mathbb{R}^3$.

In "nice" situations, an implicitly defined surface is a two dimensional surface lying inside $\mathbb{R}^3$ (think of the unit sphere, for instance). Of course, there are pathological cases of surfaces that have cusps, discontinuities, or self-intersections; however, in most cases that are of interest to us, an implicitly defined surface is (at least locally) a smooth, well-behaved surface.

Let S be an implicitly defined surface in $\mathbb{R}^3$ and $\mathbf{x}$ be a point on S. A vector $\mathbf{n}$ is said to be normal to the surface S at the point $\mathbf{x}$ provided that $\mathbf{n}$ is perpendicular to the surface at that point. If the gradient vector $\nabla f(\mathbf{x})$ is nonzero, then it is normal to the surface at $\mathbf{x}$. In this case,

$$\mathbf{n} \;=\; \frac{(\nabla f)(\mathbf{x})}{||(\nabla f)(\mathbf{x})||}$$

is a unit normal for the surface. It is harder to compute a normal vector when the gradient vector is zero; in fact, the surface may have a cusp or other strange behavior, and may not have any normal vector at all.

As an example of computing $\mathbf{n}$, consider the implicit definition of a flattened ellipsoid by $4x^2 + y^2 + 4z^2 = 4$. Here, $\nabla f(x,y,z) = \langle 8x, 2y, 8z\rangle$ is nonzero for any point $\langle x,y,z\rangle$ on the ellipsoid, and hence is normal to the ellipsoid at that point.

A.4.2 Vector-valued functions

A vector-valued function is a function whose values are vectors. We often use the convention of writing vector-valued functions in bold face, for instance $\mathbf{f}(x)$, to distinguish them from scalar-valued functions. (Less commonly, we also use upper case, such as $P(x)$, for the same purpose.) An example of a vector-valued function is a function $\mathbf{p}(t)$ which gives the position of a point at time t. For a point moving in the xy-plane, $\mathbf{p}(t)$ would be in $\mathbb{R}^2$; for a point moving in $\mathbb{R}^3$, $\mathbf{p}(t)$ would be in $\mathbb{R}^3$.

The components of a vector-valued function $\mathbf{f}$ are scalar-valued functions, $f_1(x),\dots,f_n(x)$. Thus,

$$\mathbf{f}(x) \;=\; \langle f_1(x), f_2(x), \dots, f_n(x)\rangle.$$

The first derivative of $\mathbf{f}$ is calculated component-wise. Namely, the first derivative is equal to

$$\mathbf{f}'(x) \;=\; \langle f_1'(x), f_2'(x), \ldots, f_n'(x)\rangle.$$

For example, the derivative of a position function $\mathbf{p}(t)$ is the velocity function $\mathbf{v}(t) = \mathbf{p}'(t)$. The second derivative of $\mathbf{p}(t)$ is the acceleration function.

A *parametric curve* is defined by a vector-valued function $\mathbf{f}(x)$. The curve is the set of points $\{\mathbf{f}(x) : x \in \mathbb{R}\}$. If the values of the function $\mathbf{f}$ are k-vectors, then the parametric curve lies in $\mathbb{R}^k$. The first derivative $\mathbf{f}'(x)$ will be tangent to the curve at the point $\mathbf{f}(x)$, provided it is nonzero.

A.4.3 Multivariable vector-valued functions

A vector-valued multivariable function is a function which has as input a sequence of reals, and which produces a vector as its value.

Let $\mathbf{f} : \mathbb{R}^k \to \mathbb{R}^n$. Then we can write $\mathbf{f}$ in terms of its n components as

$$\mathbf{f}(\mathbf{x}) \;=\; \langle f_1(\mathbf{x}), f_2(\mathbf{x}), \ldots, f_n(\mathbf{x})\rangle,$$

where $\mathbf{x} = \langle x_1, \ldots, x_k\rangle$. Note that each f_i is a scalar-valued, multivariable function.

The first derivative of $\mathbf{f}$ is called the *Jacobian* of $\mathbf{f}$. Intuitively, the first derivative of $\mathbf{f}$ should be the vector of first derivatives of its n components. However, from Section A.4.1, the first derivative of a component f_i is actually the gradient function ∇f_i, which is a k-vector valued function. Thus, the first derivative of $\mathbf{f}(\mathbf{x})$ becomes an $n \times k$ matrix, called the Jacobian matrix.

The Jacobian matrix is defined to be the matrix whose i-th row is equal to the gradient of $f_i(\mathbf{x})$. This can be written explicitly as

$$J(\mathbf{x}) \;=\; \left(\frac{\partial f_i}{\partial x_j}\right)_{i,j} \;=\; \begin{pmatrix} \dfrac{\partial f_1}{\partial x_1} & \cdots & \dfrac{\partial f_1}{\partial x_k} \\ \vdots & \ddots & \vdots \\ \dfrac{\partial f_n}{\partial x_1} & \cdots & \dfrac{\partial f_n}{\partial x_k} \end{pmatrix}.$$

The first-order approximation formula for values of $\mathbf{f}$ in a neighborhood of $\mathbf{x}$ is then

$$\mathbf{f}(\mathbf{x}+\Delta\mathbf{x}) - \mathbf{f}(\mathbf{x}) \;\approx\; J\,\Delta\mathbf{x}.$$

Appendix B

Answers to Selected Exercises

This appendix gives sketches of answers for a selection of the exercises stated inline in the chapters.

Chapter I

Exercise I.3 (page 15). There are seven possible answers for each part, depending on which vertex is used to start. For starting with vertex $\mathbf{u}_0$, the answers must be:
(a) Triangle fan: $\mathbf{u}_0, \mathbf{u}_1, \mathbf{u}_2, \mathbf{u}_3, \mathbf{u}_4, \mathbf{u}_5, \mathbf{u}_6$.
(b) Triangle strip: $\mathbf{u}_0, \mathbf{u}_1, \mathbf{u}_6, \mathbf{u}_2, \mathbf{u}_5, \mathbf{u}_3, \mathbf{u}_4$.
The triangulations are:

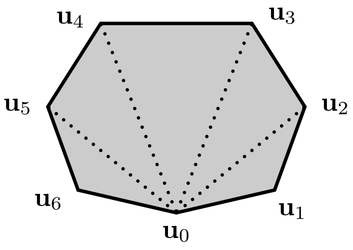

and

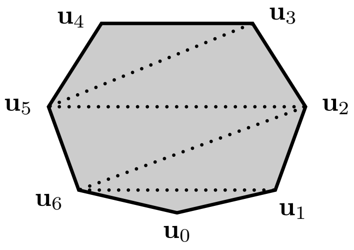

Exercise I.4 (page 19). Reordering the vertices as $\mathbf{u}_1, \mathbf{u}_0, \mathbf{u}_3, \mathbf{u}_2, \mathbf{u}_5, \mathbf{u}_4, \mathbf{u}_7, \mathbf{u}_6, \mathbf{u}_9, \mathbf{u}_8$ will change which triangles are rendered. With this vertex ordering, Figure I.12 would change so that the triangles' edges will have the dotted lines sloping downward instead of upward. It will also cause the front faces to be facing away from the viewer.

Reordering as $\mathbf{u}_9, \mathbf{u}_8, \mathbf{u}_7, \mathbf{u}_6, \mathbf{u}_5, \mathbf{u}_4, \mathbf{u}_3, \mathbf{u}_2, \mathbf{u}_1, \mathbf{u}_0$ will render the same triangles, with the same front faces, as the order $\mathbf{u}_0, \mathbf{u}_1, \mathbf{u}_2, \mathbf{u}_3, \mathbf{u}_4, \mathbf{u}_5, \mathbf{u}_6, \mathbf{u}_7, \mathbf{u}_8, \mathbf{u}_9$.

Chapter II

Exercise II.1 (page 39).

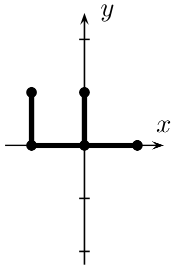

$A_1 : \langle x, y\rangle \mapsto \langle -y, x\rangle$

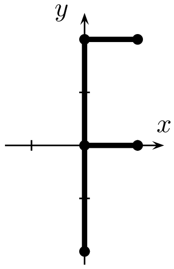

$A_2 : \langle x, y\rangle \mapsto \langle x, 2y\rangle$

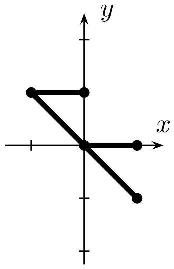

$A_3 : \langle x, y\rangle \mapsto \langle x - y, y\rangle$

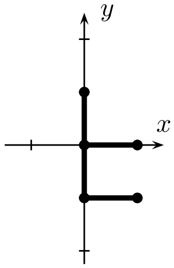

$A_4 : \langle x, y\rangle \mapsto \langle x, -y\rangle$

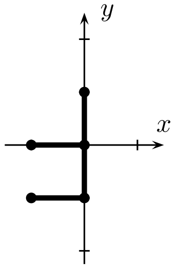

$A_5 : \langle x, y\rangle \mapsto \langle -x, -y\rangle$

Exercise II.2 (page 44).
(a) $\begin{pmatrix}1 & 0\\ 0 & 1\end{pmatrix}$ (b) $\begin{pmatrix}\frac{1}{2} & 0\\ 0 & \frac{1}{2}\end{pmatrix}$ (c) $\begin{pmatrix}\frac{3}{2} & 0\\ 0 & \frac{1}{2}\end{pmatrix}$ (d) $\begin{pmatrix}0 & -1\\ 1 & 0\end{pmatrix}$ (e) $\begin{pmatrix}1 & 1\\ 0 & 1\end{pmatrix}$ (f) $\begin{pmatrix}0 & -1\\ -1 & 0\end{pmatrix}$

Exercise II.3 (page 45). (a) It is not linear since it does not map $\mathbf{0}$ to $\mathbf{0}$.
(b) $M = \begin{pmatrix}-1 & 0\\ 1 & -1\end{pmatrix}$ and $\mathbf{u} = \langle 1, 0\rangle$.

Exercise II.4 (page 45). (a) It is not linear.
(b) $N = \begin{pmatrix}-1 & 0\\ -1 & -1\end{pmatrix}$ and $\mathbf{v} = \langle 1, 1\rangle$.

Exercise II.5 (page 47). A_1, A_4 and A_5 are rigid. A_1, A_2, A_3 and A_5 are orientation preserving. A_1 and A_5 are both rigid and orientation preserving.

Exercise II.7 (page 48). Since $M\mathbf{i} = \mathbf{u}$ and $M\mathbf{j} = \mathbf{v}$, the conditions that $||\mathbf{u}_{|}| = 1$ and $||\mathbf{v}_{|}| = 1$ express that $M\mathbf{i}$ and $M\mathbf{j}$ are unit vectors. The condition $\mathbf{u} \cdot \mathbf{v} = 0$ states that $M\mathbf{i}$ and $M\mathbf{j}$ are orthogonal. This proves the "only if" part of the equivalence.

For the converse, let $\mathbf{x} = \langle x_1, x_2\rangle$, Then

$$\begin{aligned} ||M\mathbf{x}|| &= ||x_1\mathbf{u} + x_2\mathbf{v}|| = \sqrt{(x_1\mathbf{u} + x_2\mathbf{v}) \cdot (x_1\mathbf{u} + x_2\mathbf{v})} \\ &= \sqrt{x_1^2\mathbf{u} \cdot \mathbf{u} + 2x_1x_2\mathbf{u} \cdot \mathbf{v} + x_2\mathbf{v} \cdot \mathbf{v}} \\ &= \sqrt{x_1^2 + x_2^2} = ||\mathbf{x}||. \end{aligned}$$

Linearity then gives, for all $\mathbf{x}$ and $\mathbf{y}$, $||M\mathbf{x} - M\mathbf{y}|| = ||\mathbf{x} - \mathbf{y}||$. Hence distances are preserved. Since distances are preserved, angles are also preserved.

Exercise II.8 (page 48). This follows immediately from the properties of Exercise II.7.

Exercise II.9 (page 48). For a conceptual geometric proof, first note that $det M$ is equal to $\mathbf{u}' \cdot \mathbf{v}$ where $\mathbf{u}'$ is $\mathbf{u}$ rotated 90° counter-clockwise. Second show that, since $\mathbf{u}$ and $\mathbf{v}$ are perpendicular unit vectors, $\mathbf{u}' \cdot \mathbf{v} = \pm 1$.

An algebraic proof can be given by showing that $(u_1v_2 - u_2v_1)^2 = 1$ follows from $\mathbf{u} \cdot \mathbf{u} = \mathbf{v} \cdot \mathbf{v} = 1$ and $\mathbf{u} \cdot \mathbf{v} = 0$.

Exercise II.11 (page 50). $R_\theta^{\mathbf{u}}(\mathbf{x}) = T_{\mathbf{u}}(R_\theta(T_{-\mathbf{u}}(\mathbf{x}))) = R_\theta(\mathbf{x} - \mathbf{u}) + \mathbf{u} = R_\theta(\mathbf{x}) - R(\mathbf{u}) + \mathbf{u}$.

Exercise II.12 (page 52). $R_{-90^\circ}^{\langle 1/2, -1/2 \rangle}$ (or $R_{-\pi/2}^{\langle 1/2, -1/2 \rangle}$ in radians).

Exercise II.13 (page 53). Examples include $\langle -1, \frac{1}{2}, 1 \rangle$, $\langle -2, 1, 2 \rangle$, $\langle -\frac{1}{2}, \frac{1}{4}, \frac{1}{2} \rangle$, $\langle 1, -\frac{1}{2}, -1 \rangle$, $\langle 2, -1, -2 \rangle$ and $\langle \frac{1}{2}, -\frac{1}{4}, -\frac{1}{2} \rangle$.

Exercise II.14 (page 54). It is not linear, since $\mathbf{0}$ is not mapped to $\mathbf{0}$. A 3×3 matrix is $\begin{pmatrix} 0 & -\frac{1}{2} & \frac{1}{2} \\ 1 & 1 & 0 \\ 0 & 0 & 1 \end{pmatrix}$. Any non-zero constant multiple of this matrix can be used instead.

Exercise II.15 (page 54). $\begin{pmatrix} 2 & 1 & -1 \\ -2 & 0 & 1 \\ 0 & 0 & 1 \end{pmatrix}$.

Exercise II.16 (page 55). The matrix of Exercise II.14 represents the same mapping as $\begin{pmatrix} 0 & -1 & 1 \\ 2 & 2 & 0 \\ 0 & 0 & 2 \end{pmatrix}$, for instance. Any other non-zero constant multiple of this matrix also works.

Exercise II.17 (page 59). (a)

```
Set $M_0$ = $T_{\langle 0,2 \rangle}$;
Set $M$ = $M \cdot R_{\pi/2}$;
Render $M_0$(F);
```

(b) $\begin{pmatrix} 0 & -1 & 2 \\ 1 & 0 & 0 \\ 0 & 0 & 1 \end{pmatrix}$.

Exercise II.18 (page 60). From Equation (II.7, the lower "F" shape shape is rendered using the matrix $R_\theta \circ T_{\langle \ell, 0 \rangle} \circ R_\pi \circ T_{\langle 0, r+1 \rangle}$.

The four associated local coordinate systems can be pictured as:

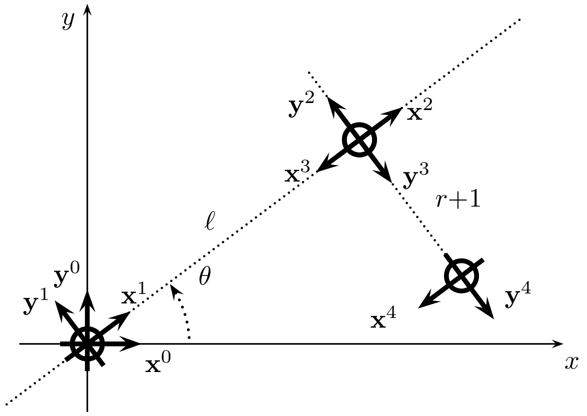

Exercise II.21 (page 67).

$$\begin{pmatrix} 1 & 0 & 0 & 0 \\ 0 & \frac{1}{2} & -\frac{\sqrt{3}}{2} & 0 \\ 0 & \frac{\sqrt{3}}{2} & \frac{1}{2} & 0 \\ 0 & 0 & 0 & 1 \end{pmatrix} \text{ and } \begin{pmatrix} -\frac{1}{2} & \frac{\sqrt{3}}{2} & 0 & 0 \\ -\frac{\sqrt{3}}{2} & -\frac{1}{2} & 0 & 0 \\ 0 & 0 & 1 & 0 \\ 0 & 0 & 0 & 1 \end{pmatrix} \text{ and } \begin{pmatrix} \frac{\sqrt{2}}{2} & 0 & -\frac{\sqrt{2}}{2} & 0 \\ 0 & 1 & 0 & 0 \\ \frac{\sqrt{2}}{2} & 0 & \frac{\sqrt{2}}{2} & 0 \\ 0 & 0 & 0 & 1 \end{pmatrix}.$$

Exercise II.22 (page 73). The two lines

```
viewMatrix.Set_glTranslate(0.0, 0.0, -CameraDistance);
viewMatrix.Mult_glRotate(viewAzimuth, 1.0, 0.0, 0.0);
```

can be replaced with

```
VectorR3 eyePos(0.0, CameraDistance * sin(viewAzimuth),
                     CameraDistance * cos(viewAzimuth));
VectorR3 lookAtPos(0.0, 0.0, 0.0);
VectorR3 upDir(0.0, 0.0, 1.0);
viewMatrix.Set_gluLookAt(eyePos, lookAtPos, upDir);
```

Exercise II.24 (page 79). Substituting into Equation II.14 with $c = \cos\theta$ and $s = \sin\theta$ and with $\mathit{Proj}_{\mathbf{u}}$ and $M_{\mathbf{u}\times}$ given by Equations II.11 and II.13 yields Equation II.10.

Exercise II.29 (page 87). Verify these by multiplying the 4×4 matrix (II.17) by the two 4-vectors.

Exercise II.30 (page 94). (a) $\begin{pmatrix} 1 & 0 & 0 \\ 0 & 1 & -1 \\ 1 & -1 & -2 \end{pmatrix}$ (b) $\begin{pmatrix} 0 & 0 & 1 & 0 \\ 0 & 1 & 1 & 1 \\ 0 & 0 & 3 & 6 \\ 0 & 0 & 1 & 2 \end{pmatrix}$.

Exercise II.31 (page 96). Since the two triangles shown in Figure II.29 are similar, we have $\frac{y_0}{x'} = \frac{y}{x'-x}$. Solving for x' gives $x' = x/(1 - y/y_0)$. A similar calculation works for z'. This yields Equation (II.28). To prove the correctness of the 4×4 matrix, first reexpresss Equation (II.28) in the following form for homogeneous coordinates:

$$\langle x, y, z, w\rangle \;\mapsto\; \langle x,\, 0,\, z,\, w - y/y_0\rangle.$$

Exercise II.32 (page 96). (a) $\langle x', y', z'\rangle$ is obtained by $x' = 9x/(10-y)$, $y' = 1$, and $z' = 9z/(10-y)$.
(b) In homogeneous coordinates, the mapping can be described as sending $\langle x, y, z, 1\rangle$ to $\langle 9x, 10-y, 9x, 10-y\rangle$. This is represented by the matrix

$$\begin{pmatrix} 9 & 0 & 0 & 0 \\ 0 & -1 & 0 & 10 \\ 0 & 0 & 9 & 0 \\ 0 & -1 & 0 & 10 \end{pmatrix}.$$

Exercise II.33 (page 99). To prove the first assertions, multiply the matrix S and the homogeneous representations $\langle \ell, b, -n, 1\rangle$ and $\langle r, t, -n, 1\rangle$: this yields $\langle -1, -1, -1, 1\rangle$ and $\langle 1, 1, -1, 1\rangle$, respectively. The front center point of the frustum is at $\langle \frac{(\ell+r)}{2}, \frac{(b+t)}{2}, -n\rangle$; multiplying through by f/n gives the back center point as $\langle \frac{f(\ell+r)}{2n}, \frac{f(b+t)}{2n}, -f\rangle$. Its homogeneous representation is $\langle \frac{f(\ell+r)}{2n}, \frac{f(b+t)}{2n}, -f, 1\rangle, 1$. Multiplying by S and simplifing yields $\langle 0, 0, f, f\rangle$, which is a homogeneous representation of $\langle 0, 0, 1\rangle$ as desired.

Chapter III

Exercise III.1 (page 113).
a. Answer: iv, exactly once per triangle containing v. If the "same" vertex appears twice in the VBO, the rendering pipeline treats them as being different vertices, even if the instance ID is not used in the vertex shader.
b. Answer: iii, one or more times. A vertex in a triangle strip will occur in up to two triangles. There is no need for the rendering pipeline to call the vertex shader twice for the same vertex in adjacent triangles in a triangle strip. However if the "same" vertex appears again later in the triangle strip, it will be at a different location in the VBO, and the vertex shader will be called again.
c. Answer: iii, one or more times. This for similar reasons as part b. However, since `glDrawElements` is used, vertices are referred to by their index in the VBO. Thus, it is possible that a vertex can be used for non-adjacent triangles in a triangle strip; for instance a triangle strips that makes a closed loop of triangles. This case, it possible this will be detected via the vertex cache, and an extra call to the vertex shader will be avoided.

Exercise III.2 (page 118). The geometry shader needs to know the positions of the vertices in world coordinates in order to be able to compute the other ends of vectors representing the normal vectors. This would be impossible to compute from just device independent coordinates. (Or, to be more precise, it would require recovering the world coordinates from the device independent coordinates.)

Exercise III.3 (page 118). a. True. **b.** True. **c.** True. (With the exception that a triangle fan of length 1 or 2 can be output as a single triangle strip.) **d.** False. **e.** False. **f.** False. **g.** False.

Chapter IV

Exercise IV.1 (page 144). If the specular exponent were different for different wavelengths, then the size of the specular highlight would be different for different wavelenths. For example, if $f^{\mathrm{red}} < f^{\mathrm{green}} < f^{\mathrm{blue}}$, so that the specular highlights are largest for red and smallest for green, then a specular highlight might render with white center (combining red, green and blue), surrounded by a yellow ring (combining red and green), and with an outermost red ring.

Exercise IV.4 (page 153). The function $\mathbf{f}(\theta,\phi)$ of Equation (IV.18) defines a torus as a parametric surface. Then

$$\begin{aligned}
\frac{\partial \mathbf{f}}{\partial \theta} &= \langle\, (R + r\cos\varphi)\cos\theta, 0, -(R+r\cos\varphi)\sin\theta\,\rangle \\
\frac{\partial \mathbf{f}}{\partial \varphi} &= \langle\, -r\sin\varphi\sin\theta, r\cos\varphi, -r\sin\varphi\cos\theta\,\rangle \\
\frac{\partial \mathbf{f}}{\partial \theta}\times\frac{\partial \mathbf{f}}{\partial \varphi} &= \langle (R+r\cos\varphi)\sin\theta\sin\varphi, \\
&\qquad (R+r\cos\varphi)r\sin\varphi\cos^2\theta + (R+r\cos\varphi)r\sin\varphi\sin^2\theta, \\
&\qquad (R+r\cos\varphi)\cos\theta\sin\varphi\,\rangle \\
&= (R+r\cos\varphi)\langle\, \sin\theta\cos\varphi, \sin\varphi, \cos\theta\sin\varphi\,\rangle.
\end{aligned}$$

Direct calculation, using $\sin^2 + \cos^2 = 1$ gives $||\frac{\partial \mathbf{f}}{\partial \theta}\times\frac{\partial \mathbf{f}}{\partial \varphi}|| = R{+}r\cos\varphi$. Dividing by this gives the formula (IV.19).

To verify the normal is pointing outwards instead of inwards, you can check a single point such as $\theta = \varphi = 0$.

Exercise IV.5 (page 154). (Part of answer.) The three partial derivatives of f are

$$\begin{aligned}
f_x(x,y,z) &= \frac{x}{\sqrt{x^2+z^2-R}} \\
f_y(x,y,z) &= 2y \\
f_z(x,y,z) &= \frac{z}{\sqrt{x^2+z^2-R}}.
\end{aligned}$$

This is non-zero for $\langle x,y,z\rangle$ on the surface of the torus, so a (not necessarily unit) normal vector is $\langle x/\sqrt{x^2+z^2-R}, 2y, z/\sqrt{x^2+z^2-R}\rangle$. Another possible answer is $\langle x, 2y\sqrt{x^2+z^2-R}, z\rangle$.

Exercise IV.6 (page 154). We have $\mathbf{f}(\theta,t) = \langle t\sin\theta, h(t), t\cos\theta\rangle$. A vector perpendicular to the surface at $\mathbf{f}(\theta,t)$, and pointing upwards, is

$$\mathbf{n}_f(\theta,t) \;=\; \langle -h'(t)\sin\theta, 1, -h'(t)\cos\theta\rangle.$$

Note that we know $\mathbf{n}_f(\theta,t)$ is pointing generally upwards since its y component is positive. This is not generally a unit vector, but its magnitude is $\sqrt{1+(h'(t))^2}$. Thus the unit normal vector perpendicular to $\mathbf{f}$, and pointing upwards, is

$$\frac{\langle -h'(t)\sin\theta, 1, -h'(t)\cos\theta\rangle}{\sqrt{1+(h'(t))^2}}.$$

To have a well-defined normal when $t=0$, we need $h'(0)=0$.

Exercise IV.7 (page 156). The adjoint of M is $\begin{pmatrix}1 & 0\\ 0 & 1/2\end{pmatrix}$, the determinant of M is $1/2$, and the inverse of M is $\begin{pmatrix}2 & 0\\ 0 & 1\end{pmatrix}$. The adjoint and inverse matrices are symmetric and thus are equal to their transposes.

If a line L has slope s, then the vector $\langle -s, 1\rangle$ has slope $-1/s$ and is perpendicular to L. The line $M(L)$ has slope $2s$. The matrix $(M^{-1})^{\mathrm{T}} = \begin{pmatrix}2 & 0\\ 0 & 1\end{pmatrix}$ maps $\langle -s, 1\rangle$ to $\langle -2s, 1\rangle$. This vector has slope $-1/(2s)$ and is perpendicular to $M(L)$.

Chapter V

Exercise V.1 (page 185).

α:	-2	-1	0	$\frac{1}{10}$	$\frac{1}{3}$	$\frac{1}{2}$	1	$1\frac{1}{2}$	2
$\mathbf{x}(\alpha)$:	$\langle -7,-2\rangle$	$\langle -4,-1\rangle$	$\langle -1,0\rangle$	$\langle -\frac{7}{10},\frac{1}{10}\rangle$	$\langle 0,\frac{1}{3}\rangle$	$\langle \frac{1}{2},\frac{1}{2}\rangle$	$\langle 2,1\rangle$	$\langle 3\frac{1}{2},1\frac{1}{2}\rangle$	$\langle 5,2\rangle$

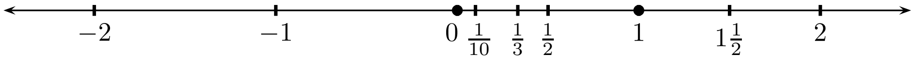

$\alpha = \frac{2}{3}$ gives $\langle 1, \frac{2}{3}\rangle$ and $\alpha = 3$ gives $\langle 8, 3\rangle$.

Exercise V.2 (page 185). $\alpha = \frac{(\mathbf{x}_2-\mathbf{x}_1)\cdot(\mathbf{0}-\mathbf{x}_1)}{||\mathbf{x}_2-\mathbf{x}_1||^2} = \frac{3}{10}$ and $\mathit{lerp}(\mathbf{x}_1, \mathbf{x}_2, \frac{3}{10}) = \langle -\frac{1}{10}, \frac{3}{10}\rangle$

Exercise V.3 (page 185). It will set $f(\langle 1, \frac{2}{3}\rangle)$ equal to 1.

Exercise V.6 (page 189).

Barycentric coordinates	Point
$\alpha = 0$, $\beta = 1$, $\gamma = 0$	$\mathbf{a} = \mathbf{y} = \langle 2, 3\rangle$
$\alpha = \frac{2}{3}$, $\beta = \frac{1}{3}$, $\gamma = 0$	$\mathbf{b} = \langle \frac{2}{3}, 1\rangle$
$\alpha = \frac{1}{3}$, $\beta = \frac{1}{3}$, $\gamma = \frac{1}{3}$	$\mathbf{c} = \langle \frac{5}{3}, \frac{4}{3}\rangle$
$\alpha = \frac{4}{5}$, $\beta = \frac{1}{10}$, $\gamma = \frac{1}{10}$	$\mathbf{d} = \langle \frac{1}{2}, \frac{2}{5}\rangle$
$\alpha = \frac{4}{3}$, $\beta = \frac{2}{3}$, $\gamma = -1$	$\mathbf{e} = \langle -\frac{5}{3}, -1\rangle$

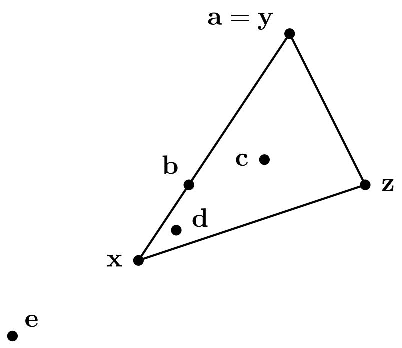

Exercise V.7 (page 194). Solve for α, β, γ using Equations (V.12) and (V.13). Check your answer by computing $\alpha\mathbf{x} + \beta\mathbf{y} + \gamma\mathbf{z}$.

a. For $\mathbf{u}_1 = \langle 2, 3\rangle$: $\alpha = 0$, $\beta = 1$, $\gamma = 0$.

b. $\mathbf{u}_2 = \langle 1\frac{1}{3}, 2\rangle$: $\alpha = \frac{1}{3}$, $\beta = \frac{2}{3}$, $\gamma = 0$.

c. $\mathbf{u}_3 = \langle \frac{3}{2}, \frac{3}{2}\rangle$: $\alpha = \frac{5}{14}$, $\beta = \frac{3}{7}$, $\gamma = \frac{3}{14}$.

d. $\mathbf{u}_4 = \langle 1, 0\rangle$: $\alpha = \frac{5}{7}$, $\beta = -\frac{1}{7}$, $\gamma = \frac{3}{7}$.

Exercise V.9 (page 196). Answers: a. $\langle 4, 0\rangle$. b. $\langle \frac{5}{3}, \frac{7}{3}\rangle$. c. $\langle \frac{17}{8}, \frac{5}{8}\rangle$. d. $\langle \frac{26}{9}, \frac{8}{9}\rangle$.

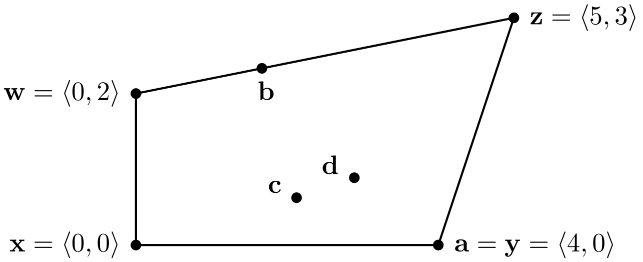

Exercise V.14 (page 205). Answer: $\alpha = \frac{1}{2}$ and $\beta = \frac{1}{3}$. Intermediate calculations: $A = -2$ and $B = -\frac{25}{3}$ and $C = \frac{14}{3}$ and $\sqrt{B^2 - 4AC} = \frac{31}{3}$.

Exercise V.15 (page 213).

$$M = \begin{pmatrix} 1 & 0 & 0 & 0 \\ 0 & 1 & 0 & 0 \\ 0 & 0 & 0 & 0 \\ 0 & 0 & 1 & 0 \end{pmatrix}.$$

The three points can be represented with the homogeneous vectors $\mathbf{a} = \langle 0, 0, 3, 1\rangle$, $\mathbf{b} = \langle 2, 0, 1, 1\rangle$, and $\mathbf{c} = \langle 1, 0, 2, 1\rangle$. Transforming these with M yields $M\mathbf{a} = \langle 0, 0, 0, 3\rangle$, $M\mathbf{b} = \langle 2, 0, 0, 1\rangle$, and $M\mathbf{c} = \langle 1, 0, 0, 2\rangle$. These represent the points $\mathbf{u} = \mathbf{0}$, $\mathbf{v} = \langle 2, 0, 0\rangle$, and $\mathbf{w} = \langle \frac{1}{2}, 0, 0\rangle$ in $\mathbb{R}^3$. We have $\mathbf{c} = (\mathbf{a}+\mathbf{b})/2$, but $\mathbf{w} \neq (\mathbf{u}+\mathbf{v})/2$, and this shows that the mapping represented (over homogeneous coordinates) by M does not preserve weighted averages.

Exercise V.16 (page 213). $\mathbf{z}$ is twice as far away from $\mathbf{x}$ and as it is from $\mathbf{y}$.

Exercise V.17 (page 213). (a) $\mathit{lerp}(\mathbf{a},\mathbf{b},\frac{1}{2}) = \langle \frac{15}{2}, 0, \frac{3}{2} \rangle$ is a homogeneous representation of $\mathbf{w} = \langle 5, 0 \rangle$.
(b) $\beta = \frac{1}{3}$. (c) $\beta = \frac{1}{2}$. (d) $\beta = \frac{1}{5}$.

Exercise V.18 (page 218). $\mathit{lerp}(\mathbf{x},\mathbf{y},\frac{1}{3}) = \langle \frac{\sqrt{2}}{3}, \frac{1}{3}, \frac{\sqrt{2}}{3} \langle$ and $\mathit{slerp}(\mathbf{x},\mathbf{y},\frac{1}{3}) = \langle \frac{\sqrt{6}}{4}, \frac{1}{2}, \frac{\sqrt{6}}{4} \rangle$. $\mathit{slerp}(\mathbf{x},\mathbf{y},\frac{1}{3})$ is a unit vector; $\mathit{lerp}(\mathbf{x},\mathbf{y},\frac{1}{3})$ is not.

Chapter VI

Exercise VI.1 (page 230). Assuming θ is between $-180°$ and $180°$,

$$s = \frac{\theta}{360} + \frac{1}{2}.$$

Values of s outside the range $[-180, 180]$ should be first adjusted to be in that range by adding a multiple of 360. The t texture coordinate is still equal to $(y + h/2)/h$.

Exercise VI.2 (page 232). Using Equation (VI.4 for the texture coordinates places the center of the texture map at the back inside point on the torus where it intersects the negative z-axis at $z = -R + r$. To place the center of the texture map at the front of the torus, use

$$s = \frac{\theta}{360} + \frac{1}{2} \qquad \text{and} \qquad t = \frac{\varphi}{360} + \frac{1}{2},$$

Exercise VI.3 (page 242). If $z \geq |x|$ and $z \geq |y|$, then the reflection direction hits the front face of the "box" environment map. The texture coordinates for this point are $s = (x/z + 1)/2$ and $t = (y/z + 1)/2$. This maps s and t to be in the range $[0, 1]$. The bottom left corner of the front face is $s = t = 0$. The upper right corner is $s = t = 1$.

Similar formulas work for the other four faces.

Chapter VII

Exercise VII.2 (page 262). The discontinuous jump is approximately equal to 2.8×10^{-8}. The left and right derivatives differ by almost 0.22.

Exercise VII.3 (page 263). Twelve bits of precision are enough to capture this level of resolution for perceived brightness. A 16 bit color encoding provides another 4 bits of accuracy.

Exercise VII.4 (page 263). A commonly given reason is to avoid numerical instability. Bounding a signal-to-noise ratio may require dividing by the derivative of the *linear-to-sRGB* function.

Chapter VIII

Exercise VIII.1 (page 269). The four control points are $\mathbf{p}_0 = \langle 0, 1 \rangle$, $\mathbf{p}_1 = \langle 1, 2 \rangle$, $\mathbf{p}_2 = \langle 4, 0 \rangle$ and $\mathbf{p}_3 = \langle 3, 0 \rangle$.

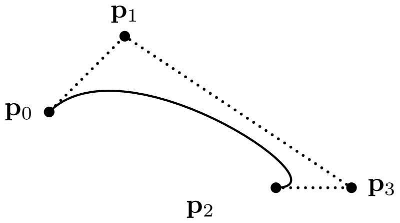

Exercise VIII.3 (page 271). For $u = \frac{1}{2}$, we have $\mathbf{r}_0(\frac{1}{2}) = \langle \frac{1}{2}, \frac{3}{2} \rangle$, $\mathbf{r}_1(\frac{1}{2}) = \langle \frac{5}{2}, 1 \rangle$, $\mathbf{r}_2(\frac{1}{2}) = \langle \frac{7}{2}, 0 \rangle$, $\mathbf{s}_0(\frac{1}{2}) = \langle \frac{3}{2}, \frac{5}{4} \rangle$, $\mathbf{s}_1(\frac{1}{2}) = \langle 3, \frac{1}{2} \rangle$, $\mathbf{t}_0(\frac{1}{2}) = \langle \frac{9}{4}, \frac{7}{8} \rangle$. Hence $\mathbf{q}(\frac{1}{2}) = \langle \frac{9}{4}, \frac{7}{8} \rangle$.

For $u = \frac{3}{4}$, we have $\mathbf{r}_0(\frac{3}{4}) = \langle \frac{3}{4}, \frac{7}{4} \rangle$, $\mathbf{r}_1(\frac{3}{4}) = \langle \frac{13}{4}, \frac{1}{2} \rangle$, $\mathbf{r}_2(\frac{3}{4}) = \langle \frac{13}{4}, 0 \rangle$, $\mathbf{s}_0(\frac{3}{4}) = \langle \frac{21}{8}, \frac{13}{16} \rangle$, $\mathbf{s}_1(\frac{3}{4}) = \langle \frac{13}{4}, \frac{1}{8} \rangle$, $\mathbf{t}_0(\frac{3}{4}) = \langle \frac{99}{32}, \frac{19}{64} \rangle$. Hence $\mathbf{q}(\frac{3}{4}) = \langle \frac{99}{32}, \frac{19}{64} \rangle$.

Exercise VIII.23 (page 312). Intermediate results are that

$$\mathbf{v}_{\frac{1}{2}} = \mathbf{0},\ \mathbf{v}_{1\frac{1}{2}} = \langle 10, 0 \rangle,\ \mathbf{v}_{2\frac{1}{2}3} = \langle 0, 10 \rangle \text{ and } \mathbf{v}_{3\frac{1}{2}} = \mathbf{0},$$

so

$$\mathbf{v}_1 = \langle 5, 0 \rangle,\ \mathbf{v}_2 = \langle \tfrac{10}{11}, \tfrac{100}{11} \rangle \text{ and } \mathbf{v}_3 = \langle 0, \tfrac{100}{11} \rangle.$$

From this, the control points include:

$$\mathbf{p}_1^+ = \langle \tfrac{5}{3}, 0 \rangle,\ \mathbf{p}_2^- = \langle 9\tfrac{23}{33}, -3\tfrac{1}{33} \rangle,\ \mathbf{p}_2^+ = \langle 10\tfrac{1}{33}, \tfrac{10}{33} \rangle \text{ and } \mathbf{p}_3^- = \langle 10, \tfrac{23}{33} \rangle.$$

ZZZ

Bibliography

[1] M. Agrawala, R. Ramamoorthi, A. Heirich, and L. Moll, *Efficient image-based methods for rendering soft shadows*, in Computer Graphics Proceedings, ACM, 2000, pp. 375–384. SIGGRAPH'2000.

[2] J. Arvo, *Backwards ray tracing*, in Developments in Ray Tracing, 1986. SIGGRAPH'86 Course Notes, Volume 12.

[3] J. Arvo and D. Kirk, *Particle transport and image synthesis*, Computer Graphics, 24 (1990). SIGGRAPH'90.

[4] I. Ashdown, *Radiosity: A Programmer's Perspective*, John Wiley, New York, 1994.

[5] M. Ashikhmin, S. Premože, and P. Shirley, *A microfacet-based BRDF generator*, in Computer Graphics and Interactive Techniques: SIGGRAPH'2000 Conference Proceedings, 2000, pp. 65–74.

[6] R. H. Bartels, J. C. Beatty, and B. A. Barsky, *An Introduction to Splines for Use in Computer Graphics and Geometric Modeling*, Morgan Kaufmann, Los Altos, California, 1987. Forewords by P. Bézier and A.R. Forrest.

[7] P. Beckmann and A. Spizzichino, *The Scattering of Electromagnetic Waves from Rough Surfaces*, Macmillan, New York and Pergamon Press, Oxford, 1963.

[8] P. Bergeron, *A general version of Crow's shadow volumes*, IEEE Computer Graphics and Applications, 6 (1986), pp. 17–28.

[9] R. S. Berns, F. W. Billmeyer, and M. Saltzman, *Billmeyer and Saltzman's Principles of Color Technology*, John Wiley, New York, 3rd ed., 2000.

[10] P. Bézier, *Mathematical and practical possibilities of UNISURF*, in Computer Aided Geometric Design, Proceedings of Conference held at the University of Utah, Salt Lake City, March 1974, R. E. Barnhill and R. F. Riesenfeld, eds., Academic Press, New York, 1974, pp. 127–152.

[11] P. E. Bézier, *How Renault uses numerical control for car body design and tooling*, in Society of Automotive Engineers' Congress, 1968. SAE paper 680010.

[12] E. A. Bier and K. R. Sloan Jr., *Two-part texture mappings for ray tracing*, IEEE Computer Graphics and Applications, 6 (1986), pp. 40–53.

[13] J. Blinn, *Models of light reflection for computer synthesized pictures*, Computer Graphics, 11 (1973), pp. 192–193. SIGGRAPH'77.

[14] ——, *Simulation of wrinkled surfaces*, Computer Graphics, 12 (1978). SIGGRAPH'78. Reprinted in [124].

[15] ——, *What, teapots again?*, IEEE Computer Graphics and Applications, 7 (1987), pp. 61–63. Reprinted in [18], pp. 17-20.

[16] ——, *Hyperbolic interpolation*, IEEE Computer Graphics and Applications, 12 (1992), pp. 89–94. Reprinted in [17].

[17] ——, *Jim Blinn's Corner: A Trip Down the Graphics Pipeline*, Morgan Kaufmann, San Francisco, 1996.

[18] ——, *Jim Blinn's Corner: Dirty Pixels*, Morgan Kaufmann, San Francisco, 1998.

[19] W. Böhm, *Inserting new knots into B-spline curves*, Computer-Aided Design, 12 (1980), pp. 199–201.

[20] W. Böhm and H. Prautsch, *The insertion algorithm*, Computer-Aided Design, 17 (1985), pp. 58–59.

[21] P. J. Bouma, *Physical Aspects of Colour: An Introduction to the Scientific Study of Colour Stimuli and Colour Sensations*, Philips Technical Library, Macmillan, London, 2nd ed., 1971. Edited by W. de Groot and A.A. Kruithof and J.L. Guweltjes.

[22] L. S. Brotman and N. I. Badler, *Generating soft shadows with a depth buffer algorithm*, IEEE Computer Graphics and Applications, 4 (1984), pp. 5–12.

[23] S. R. Buss and J. Fillmore, *Spherical averages and applications to spherical splines and interpolation*, ACM Transactions on Graphics, 20 (2001), pp. 95–126.

[24] S. E. Chen and L. Williams, *View interpolation for image synthesis*, Computer Graphics, 27 (1993), pp. 279–288. SIGGRAPH'92.

[25] E. Cohen, T. Lynch, and R. F. Riesenfeld, *Discrete* B*-splines and subdivision techniques in computer-aided geometric design and computer graphics*, Computer Graphics and Image Processing, 14 (1980), pp. 87–111.

[26] M. F. Cohen and D. P. Greenberg, *The hemi-cube: A radiosity solution for complex environments*, Computer Graphics, 19 (1985), pp. 31–40.

[27] M. F. Cohen and J. R. Wallace, *Radiosity and Realistic Image Synthesis*, Academic Press, Boston, 1993. Includes a chapter by P. Hanrahan.

[28] R. L. Cook, T. Porter, and L. Carpenter, *Distributed ray tracing*, Computer Graphics, 18 (1984), pp. 137–145. SIGGRAPH'84.

[29] R. L. Cook and K. E. Torrance, *A reflectance model for computer graphics*, ACM Transactions on Graphics, 1 (1982), pp. 7–24.

[30] M. G. Cox, *The numerical evaluation of* B-*splines*, Journal of the Institute of Mathematics and its Applications, (1972), pp. 134–149.

[31] H. S. M. Coxeter, *Projective Geometry*, Springer-Verlag, New York, second ed., 1974.

[32] F. C. Crow, *Shadow algorithms for computer graphics*, Computer Graphics, 11 (1977), pp. 242–248. SIGGRAPH'77.

[33] H. B. Curry and I. J. Shoenberg, *On spline distributions and their limits: The Pólya distribution function, Abstract 308t*, Bulletin of the American Mathematical Society, 53 (1947), p. 1114.

[34] M. Daniel and J. C. Daubisse, *The numerical problem of using Bézier curves and surfaces in the power basis*, Computer Aided Geometric Design, 6 (1989), pp. 121–128.

[35] M. de Berg, M. H. Overmars, M. V. Krevald, and O. Schwartzkopf, *Computational Geometry: Algorithms and Applications*, Springer, Berlin, 2nd ed., 2000.

[36] C. de Boor, *On calculating with* B-*splines*, Journal of Approximation Theory, 6 (1972), pp. 50–62.

[37] P. de Casteljau, *Outillages méthodes calcul.* Technical report, 1959.

[38] ——, *Courbes et surfaces à poles.* Technical report, 1963.

[39] C. Everitt and M. J. Kilgard, *Practical and robust stenciled shadow volumes for hardware-accelerated rendering.* Manuscript at `http://developer.nvidia.com`, 2002.

[40] M. D. Fairchild, *Color Appearence Models*, Addison-Wesley, Reading, Massachusetts, 1998.

[41] H. S. Fairman, M. H. Brill, and H. Hemmendinger, *How the CIE 1931 color-matching functions were derived from Wright-Guild data*, Color Research and Application, 22 (1997), pp. 11–23.

[42] G. Farin, *Curves and Surfaces for Computer Aided-Geometric Design: A Practical Guide*, Academic Press, San Diego, 4th ed., 1997. Contains chapters by P. Bézier and W. Böhm.

[43] R. T. Farouki, *On the stability of transformations between power and Bernstein polynomial forms*, Computer Aided Geometric Design, 8 (1991), pp. 29–36.

[44] R. T. Farouki and V. T. Rajan, *On the numerical condition of polynomials in Bernstein form*, Computer Aided Geometric Design, 4 (1987), pp. 191–216.

[45] ——, *Algorithms for polynomials in Bernstein form*, Computer Aided Geometric Design, 5 (1988), pp. 1–26.

[46] R. T. Farouki and T. Sakkalis, *Real rational curves are not "unit speed"*, Computer Aided Geometric Design, 8 (1991), pp. 151–157.

[47] J. Ferguson, *Multivariable curve interpolation*, Journal of the Association for Computing Machinery, 11 (1964), pp. 221–228.

[48] R. P. Feynman, *Lectures on Physics, Volume I*, Addison-Wesley, Redwood City, CA, 1989. Chapters 35 and 36.

[49] J. Foley, A. van Dam, S. K. Feiner, and J. F. Hughes, *Computer Graphics: Principles and Practice*, Addison-Wesley, Reading, Mass., 2nd ed., 1990.

[50] H. Fuchs, G. D. Abram, and E. D. Grant, *Near real-time shaded display of rigid objects*, Computer Graphics, 17 (1983). SIGGRAPH'83.

[51] H. Fuchs, Z. Kedem, and B. F. Naylor, *On visible surface generation by a priori tree structures*, Computer Graphics, 14 (1980), pp. 124–133. SIGGRAPH'80.

[52] E. G. Gilbert, D. W. Johnson, and S. S. Keerthi, *A fast procedure for computing the distance between objects in three-dimensional space*, IEEE J. Robotics and Automation, RA-4 (1988), pp. 193–203.

[53] M. Girard and A. A. Maciejewski, *Computational modeling for the computer animation of legged figures*, Computer Graphics, 19 (1985), pp. 263–270. SIGGRAPH'85.

[54] A. Glassner, ed., *An Introduction to Ray Tracing*, Academic Press, London, 1989.

[55] A. S. Glassner, *Principles of Digital Image Synthesis*, Morgan Kaufmann, San Francisco, 1995. Two volumes.

[56] S. Gottschalk, M. C. Lin, and D. Manocha, *OBBTree: A hierarchical structure for rapid interference detection*, Computer Graphics, 30 (1996), pp. 171–180. SIGGRAPH '96.

[57] H. Gouraud, *Continuous shading of curved surfaces*, IEEE Transactions on Computers, 20 (1971), pp. 623–629.

[58] B. Grünbaum, *Convex Polytopes*, Interscience, London, 1967.

[59] R. Hall, *Illumination and Color in Computer Generated Imagery*, Springer Verlag, New York, 1989.

[60] P. Hanrahan, D. Salzman, and L. Aupperle, *A rapid hierachical radiosity algorithm*, Computer Graphics, 25 (1991), pp. 197–206. SIGGRAPH'91.

[61] J. C. Hart, G. K. Francis, and L. H. Kauffman, *Visualizing quaternion rotation*, ACM Transactions on Graphics, 13 (1994), pp. 256–276.

[62] X. D. He, K. E. Torrance, F. X. Sillion, and D. P. Greenberg, *A comprehensive physical model for light reflection*, Computer Graphics, 25 (1991), pp. 175–186. SIGGRAPH'91.

[63] P. S. Heckbert and H. P. Moreton, *Interpolation for polygon texture mapping and shading*, in State of the Art in Computer Graphics: Visualization and Modeling, D. F. Rogers and R. A. Earnshaw, eds., Springer-Verlag, New York, 1991, pp. 101–111.

[64] T. Heidmann, *Real shadows real time*, Iris Universe, 18 (1991), pp. 28–31. Silicon Graphics, Inc.

[65] N. J. Higman, *Accuracy and Stability of Numerical Algorithms*, Society for Industrial and Applied Mathematics, Philadelphia, 1996.

[66] F. S. Hill, *Computer Graphics using OpenGL*, Prentice Hall, Upper Saddle River, NJ, 2001.

[67] J. Hoschek and D. Lasser, *Fundamentals of Computer Aided Geometric Design*, AK Peters, Wellesley, Mass., 1993. Translated from German by L. Schumaker.

[68] R. Jackson, L. MacDonald, and K. Freeman, *Computer Generated Colour: A Practical Guide to Presentation and Display*, John Wiley, Chichester, 1994.

[69] H. W. Jensen, *Realistic Image Synthesis using Photon Mapping*, A.K. Peters, Natick, Massachusetts, 2001.

[70] H. W. Jensen and N. J. Christensen, *Photon maps in bidirectional Monte Carlo ray tracing of complex objects*, Computers and Graphics, 19 (1995), pp. 215–224.

[71] K. I. Joy and M. N. Bhetanabhotla, *Ray tracing parametric surface patches utilizing numerical techniques and ray coherence*, Computer Graphics, 20 (1986), pp. 279–285. SIGGRAPH'86.

[72] J. T. Kajiya, *Anisotropic reflection models*, Computer Graphics, 19 (1985), pp. 15–21. SIGGRAPH'85.

[73] A. R. Klumpp, *Singularity-free extraction of a quaternion from a direction-cosine matrix*, Journal of Spacecraft and Rockets, 13 (1976), pp. 754–755.

[74] D. H. U. Kochanek and R. H. Bartels, *Interpolating splines with local tension, continuity and bias control*, Computer Graphics, 18 (1984), pp. 33–41. SIGGRAPH'84.

[75] E. P. Lafortune and Y. D. Willems, *Bi-directional path tracing*, in Proc. 3rd International Confernence on Computational Graphics and Visualization Techniques (Compugraphics '93), ACM, 1993, pp. 145–153.

[76] E. Lee, *Rational Bézier representation for conics*, in Geometric Modeling: Algorithms and New Trends, G. E. Farin, ed., Philadelphia, 1987, SIAM, pp. 3–19.

[77] M. Lin, *Collision Detection for Animation and Robotics*, PhD thesis, U.C. Berkeley, 1993.

[78] M. C. Lin and J. F. Canny, *Efficient algorithms for incremental distance computation*, in IEEE Conference on Robotics and Automation, 1991, pp. 1008–1014.

[79] M. D. McCool, *Shadow volume reconstruction from depth maps*, ACM Transactions on Graphics, 19 (2000), pp. 1–26.

[80] T. Möller and E. Haines, *Real-Time Rendering*, AK Peters, Natick, Massachusetts, 1999.

[81] T. Möller and B. Trumbore, *Fast, minimum storage ray-triangle intersection*, journal of graphics tools, 2 (1997), pp. 21–28.

[82] W. M. Newman and R. F. Sproull, *Principles of Interactive Computer Graphics*, McGraw-Hill, New York, second ed., 1979.

[83] A. Ngan, F. Durand, and W. Matusik, *Experimental validation of analytical BRDF models.* Technical Sketch, SIGGRAPH, 2004.

[84] T. Nishita, T. W. Sederberg, and M. Kakimoto, *Ray tracing trimmed rational surface patches*, Computer Graphics, 24 (1990), pp. 337–345. SIGGRAPH'90.

[85] M. Oren and S. K. Nayar, *Generalization of Lambert's reflectance model*, Computer Graphics, 28 (1994), pp. 239–246. SIGGRAPH'94.

[86] ——, *Generalization of the Lambertian model and implications for machine vision*, International Journal of Computer Vision, 14 (1995), pp. 227–251.

[87] A. Overhauser, *Analytic definition of curves and surfaces by parabolic blending*, tech. rep., Ford Motor Company, 1968.

[88] B. T. Phong, *Illumination for computer generated pictures*, Communications of the ACM, 18 (1975), pp. 311–317.

[89] L. Piegl and W. Tiller, *A menagerie of rational B-spline circles*, IEEE Computer Graphics and Applications, 9 (1989), pp. 48–56.

[90] L. Piegl and W. Tiller, *The NURBS Book*, Springer Verlag, Berlin, 2nd ed., 1997.

[91] H. Prautsch, *A short proof of the Oslo algorithm*, Computer Aided Geometric Design, 1 (1984), pp. 95–96.

[92] W. H. Press, B. P. Flannery, S. A. Teukolsky, and W. T. Vetterling, *Numerical Recipes: The Art of Scientific Computing*, Cambridge University Press, Cambridge, 1986.

[93] W. T. Reeves, D. H. Salesin, and R. L. Cook, *Rendering antialiased shadows with depth maps*, Computer Graphics, 21 (1987), pp. 283–291. SIGGRAPH'87.

[94] D. F. Rogers, *An Introduction to NURBS: with Historical Perspective*, Morgan Kaufmann, San Francisco, 2001.

[95] H. Samet, *Applications of Spatial Data Structures: Computer Graphics, Image Processing and GIS*, Addison-Wesley, Reading, Mass., 1990.

[96] ——, *The Design and Analysis of Spatial Data Structures*, Addison-Wesley, Reading, Mass., 1990.

[97] C. Schlick, *An inexpensive BRDF model for physically-based rendering*, Computer Graphics Forum, 13 (1994), pp. 233–246. Proceedings, Eurographics'94.

[98] P. Schröder, D. Zorin, et al., *Subdivision for Modeling and Animation*, SIGGRAPH'98 Course Notes #36, ACM, 1998.

[99] L. L. Schumaker, *Spline Functions: Basic Theory*, Wiley, New York, 1981.

[100] H.-P. Seidel, *Knot insertion from a blossoming point of view*, Computer Aided Geometric Design, 5 (1988), pp. 81–86.

[101] ——, *A new multiaffine approach to B-splines*, Computer Aided Geometric Design, 6 (1989), pp. 23–32.

[102] S. W. Shepperd, *Quaternion from rotation matrix*, Journal of Guidance and Control, 1 (1978), pp. 223–224.

[103] P. Shirley, *Realistic Ray Tracing*, AK Peters, Natick, Massachusetts, 2000.

[104] K. Shoemake, *Animating rotation with quaternion curves*, Computer Graphics, 19 (1985), pp. 245–254. SIGGRAPH'85.

[105] ——, *Quaternion calculus and fast animation*, in SIGGRAPH'87 Course Notes on State of the Art Image Synthesis, ACM, 1987, pp. 101–121.

[106] I. J. Shoenberg, *Contributions to the problem of approximation of equidistant data by analytic functions, Part A — on the problem of smoothing or gradation, a first class of analytic approximation formulae*, Quarterly of Applied Mathematics, 4 (1946), pp. 45–99.

[107] ——, *On spline functions*, in Inequalities, Proceedings of a Symposium held at Wright-Paterson Air Force Base, August 19-27, 1965, O. Shisha, ed., New York, 1967, Academic Press.

[108] F. X. Sillion and C. Puech, *Radiosity and Global Illumination*, Morgan Kaufmann, San Francisco, 1994.

[109] R. A. Spurrier, *Comment on "Singularity-free extraction of a quaternion from a direction-cosine matrix"*, Journal of Spacecraft and Rockets, 15 (1978), pp. 255–256.

[110] F. Thomas and O. Johnston, *Disney Animation: The Illusion of Life*, Abbeville Press, New York, 1981.

[111] D. L. Toth, *On ray tracing parametric surfaces*, Computer Graphics, 19 (1985), pp. 171–179. SIGGRAPH'85.

[112] Y. S. Touloukian and D. P. Witt, *Thermal Radiative Properties: Metallic Elements and Alloys*, Thermophysical Properties of Matter, Vol 7, IFI/Plenum, New York, 1970.

[113] ——, *Thermal Radiative Properties: Nonmetallic Solids*, Thermophysical Properties of Matter, Vol 8, IFI/Plenum, New York, 1972.

[114] Y. S. Touloukian, D. P. Witt, and R. S. Hernicz, *Thermal Radiative Properties: Coatings*, Thermophysical Properties of Matter, Vol 9, IFI/Plenum, New York, 1972.

[115] T. S. Trowbridge and K. P. Reitz, *Average irregularity representation of a rough surface for ray reflection*, Journal of the Optical Society of America, 65 (1975), pp. 531–536.

[116] E. Veach and L. Guibas, *Bidirectional estimators for light transport*, in Proceedings, Fifth Eurographics Workshop on Rendering, New York, 1994, Springer Verlag, pp. 147–162.

[117] J. Warren and H. Weimer, *Subdivision Methods for Geometric Design: A Constructive Approach*, Morgan Kaufmann, San Francisco, 2002.

[118] A. Watt, *3D Computer Graphics*, Addison-Wesley, Reading, MA, 2nd ed., 1993.

[119] A. Watt and M. Watt, *Advanced Animation and Rendering Techniques: Theory and Practice*, Addison-Wesley, Reading, MA, 1992.

[120] T. White, *The Animator's Workbook*, Phaidon Press, Oxford, 1986.

[121] T. Whitted, *An improved illumination model for shaded display*, Communications of the ACM, 23 (1980).

[122] L. Williams, *Casting curved shadows on curved surfaces*, Computer Graphics, 12 (1978), pp. 270–274. SIGGRAPH'78.

[123] ———, *Pyramidal parametrics*, Computer Graphics, 17 (1983), pp. 1–11. SIGGRAPH'83.

[124] R. Wolfe, ed., *Significant Seminal Papers of Computer Graphics: Pioneering Efforts that Shaped the Field*, Association for Computing Machinery, New York, 1998.

[125] L. B. Wolff and D. J. Kurlander, *Ray tracing with polarization parameters*, IEEE Computer Graphics and Applications, 10 (1990), pp. 44–55.

[126] M. Woo, J. Nieder, T. Davis, and D. Schreiner, *OpenGL Programming Guide: The Official Guide to Learning OpenGL, Version 1.2*, OpenGL Architecture Review Board, Addison-Wesley Developers Press, Reading, Mass., third ed., 1999.

[127] G. Wyszecki and W. S. Stiles, *Color Science: Concepts and Methods, Quantitative Data and Formulae*, John Wiley & Sons, New York, 2nd ed., 1982.

[128] J. Zhao and N. I. Badler, *Inverse kinematics positioning using nonlinear programming for highly articulated figures*, ACM Transactions on Graphics, 13 (1994), pp. 313–336.

[129] G. M. Ziegler, *Lectures on Polytopes*, Springer Verlag, New York, 1995.

Index

EmitVertex, 117
EndPrimitive, 117

AABB, *see* bounding box, axis aligned
Abram, G., 420
abutting polygons, 127
accumulation buffer, 397
additive colors, 253
adjoint, 156, 494
affine, 351
affine combination, 186, 188
  preserved under, 186
affine function, 93
affine transformation, 35, 41, 64, 67, 84, 155
  matrix, 53, 65
  orientation preserving, 47, 65
  preserved under, 186, 281
affine transformations, 36
afterimages, 250
Agrawala, M., 401
aliasing, 3, 31, 126, 226, 233
alpha channel, 397, 401
ambient light, 135, 142, 144
ambient reflection, 142--143
ambient reflectivity coefficient, 135, 143
angle brackets, 43
angle of incidence, 134, 135, 137--139, 379
angle of reflection, 134, 135, 139
angle of refraction, 379
animation, 29, 35, 47, 126, 149, 183, 445
anisotropic surface, 165
anitaliasing, 31
anti-aliasing, 233--236, 372, 386, 396
antipodal, 62, 81, 215
arclength, 306, 311
arctangent, 48
articulated object, 448, 467
Arvo, D., 394
Ashdown, I., 444
Ashikhmin, M., 164
aspect ratio, 100
associative law, 459
atan2, 48
attachment point, 469
attenuation, *see* distance attenuation
automorphism, inner, 461
averaging, *see* interpolation
axis aligned bounding box, *see* bounding box, axis aligned
axis conventions, 5
azimuth, 232, *see also* yaw, pitch and roll

back buffer, 30
back face, 14, 21, 163
back intersection, 412
background color, 383
backwards ray tracing, 372, 394--396
Badler, N., 400, 472
ball, 209
Barsky, B., 266
Bartels, R., 266, 314
barycentric coordinates, 21, 187--195, 218, 227, 409, 410
  calculating, 192
base position, 469

basic ray tracing, *see* recursive ray tracing
basis function, 326, *see* blending function
basis spline, 326, *see also* B-spline curve
Beatty, J., 266
Beckmann distribution, 169
Bergeron, P., 400
Berns, R., 249, 263
Bernstein polynomial, 268, 278, 337, 362
Bessel spline, *see* Overhauser spline
Bessel tangent, 314
Bessel twist method, 320
Bézier curve, 186, 213, 265--324, 467
  as B-spline, 336, 365
  degree three, 266
  derivative, 269, 270, 280
  general degree, 278--287
  in OpenGL, 294--296
  piecewise, 274--277, 282
  quadratic, 299--306
  rational, 53, 187, 212, 295, 297--306, 364
  subdivision, *see* recursive subdivision
Bézier patch, 287--294, 404, 417
  in OpenGL, 296--297
  rational, 306--309
Bézier, P., 266
Bhetanabhotla, M., 417
bias, 316
bicubic patch, 320
bidirectional path tracing, 395
bidirectional reflectivity, 164--166
Bier, E., 229
bilinear interpolation, 195--207, 227, 234, 240
  inverting, 202--207
BilinearInvert, 205, 207
Billmeyer, F., 249
binary space partitioning (BSP) tree, 404, 420
binomial theorem, 268, 279, 285
bitmap, 4
black, 11, 253
blending, 127, 255, 396, 401
blending function, 267, 326, 328, 329, 467
Blinn, J., xvi, 164, 168, 170, 213, 237, 297
blossom, 350--355
Böhm method, 359--361
Böhm, W., 359
Bouma, P., 264
bounding box, 417, 418
  axis aligned (AABB), 418
  discrete oriented polygon (k-DOP), 418, 419
  oriented (OBB), 418, 420
bounding sphere, 406, 417, 418
bounding volume, 417, 418, 420
box, 411
BRDF, 165
Bresenham algorithm, 121, 122, 125--126
BRIDF, *see* bidirectional reflectivity
brightness, 256, 425
Brotman, L., 400
browser-safe colors, 255
browsers, 255
Brunelleschi, F., 63
BSP tree, *see* binary space partitioning tree
B-spline curve, 186, 213, 306, 325--369, 467
  as Bézier curve, 362--363
  derivative, 355
  interpolating, 365--369
  knot insertion, 351, 358
  nonuniform knots, 330--344
  rational, 53, 187, 212, 364--365
  repeated knots, 343
  smoothness, 342, 343, 355--358
  uniform knots, 326--330, 334
buffer, 30
bump mapping, 237--240
Buss, S., 467

C^∞-continuous, 276
C^1-continuity, 276, 282, 289, 291, 310, 315, 339, 340
C^2-continuity, 329, 340
CalcTransmissionDirection, 381
calculus, 495
camera, 386, 448, 452
camera coordinates, 36
camera position, *see* viewpoint
Canny, J., 421
canvas, 5
Carpenter, L., 385
Casteljau method, 270--271, 282--284, 345, 363, 417, 467
Casteljau, P. de, 266, 282, 355
Catmull-Rom spline, 309--311, 315, 317, 369, 447
caustics, 395
cell, 419
central cylindrical projections, 232
centripetal parameterization, 311
Chen, S.E., 401
choice function, 267
chord-length parameterization, 309, 311, 313, 369
Christiansen, N., 395
chroma, 256
chromaticity, 256
CIE, 264
CIELAB, 264
CIELUV, 264
circle, 212, 300--304, 306--309, 366
C^k-continuity, 276
clip distance, 111, 117
clipping, 111, 112
clipping plane, 87
clockwise, 14, 22
clone, 399
clothoid, 306
CLUT, *see* color lookup table
CMY, 253
  to/from RGB, 253
CMYK, 254
codomain, 484
cofactor, 156, 494
Cohen, M., 433, 443
collinear, 487
color, 2, 3, 20, 119, 121, 249--264, 393, 534
  additive and subtractive, 253
color lookup table, 255
color perception, 249--252
colorfulness, 256
column span (colspan), 476, 495
column vector, 43, 46, 64, 492
commutative law, 459
complex numbers, 458
composition, 41, 463
ComputeG, 174
computer-aided design, 265
cone
  general, 400
conic section, 187, 212, 298--309, 362, 364--365
conjugate, 459
ConnectDots, 314
constant attenuation factor, 146
continuity, *see* C^1-, C^2-, *and* C^k-continuity
continuity (TCB), 315
control point, 186, 266, 297, 326, 330, 364, 366
control polygon, 280, 281, 324, 358
convex, 411
convex hull, 209, 273, 274
convex hull property, 273, 275, 279, 281, 303, 358, 417
convex polytope, *see* polytope
convex quadrilateral, 198
convex set, 208--210
Cook Torrance lighting model, 144
Cook, R., 164, 168, 170, 176, 385, 401
Cook-Torrance lighting, 133, 164--177, 371, 373
coordinate system, 5
Cornu spiral, 306
counter-clockwise, 14, 22

Cox-de Boor formula, 326, 333--337, 344
Coxeter, H., 63
cracking, 128, 292, 293
cross product, 6, 79, 459, 490
Crow, F., 400
cube, 229, 411
cubic curve, 282
culling, 21, 111, 112
Curry, H., 326
cutoff angle, 146
cyan, 20, 253, 257, 535
cylinder, 229, 415

data glove, 447
de Berg, M., 421
de Boor algorithm, 345--350, 353, 363, 467
de Boor, C., 326
de Casteljau, *see* Casteljau
degree elevation, 285--287, 303, 364
degree of freedom, 468
degree one polynomial, 93
denominator equals zero, 333
depth, 28, 88, 90, 92, 94, 119
depth buffer, 28, 37, 89, 94, 96, 112, 121, 125, 371, 398, *see also* pseudo-distance
depth cueing, 401
depth of field, 372, 386, 389, 397, 398, 542
derivative, 498
determinant, 44, 65, 485, 487, 493
device independent screen coordinates, 37, 85
diagonal property, 351
diameter, 432
different curves, 282
diffuse light, 135, 137
diffuse reflection, 134, 137--139
diffuse reflectivity coefficient, 137, 382
diffuse transmission, 382
diffuse transmission coefficient, 382
diode, 447
directional light, 142, 160
discrete oriented polygon, *see* bounding box
display list, 4
distance, *see* depth *and* pseudo-distance
distance attenuation, 144, 146, 157, 160
distributed ray tracing, 372, 385--394
distributive law, 459
dithering, 262
dot product, 156, 467, 485, 490
  preserved, 47, 64
double buffering, 29--31
Durand, F., 164
dynamics, 449

ease in, 450
  fixed target, 450--451
  moving target, 451--452
ease out, fixed target, 451
EduPhong, 147, 157--164
element array, 17
ellipse, 212
emissive intensity, 143
emissiveness, 427
emissivity, 135, 142--143
empty set, 352
end effector, 468
end effector point, 468
end link, 468
environment map, 240--243, 398
  in OpenGL, 246--248
equivalent, 251
Euclidean space, 484
Euler angles, 454
Euler spiral, 306
Euler's theorem, 67, 81--83, 456
event, 30
Everitt, C., 400
extended light, 390
extinction coefficient, 176
extrapolation, 184, 185
eye, 250
eye position, *see* viewpoint

face culling, 21
Fairchild, M., 263
Fairman, H., 264
far clipping plane, 87, 91, 92, 97--99
Farin, G., 266, 355, 360, 364
Farouki, R., 306
Ferguson patches, 319
Ferguson, J., 319
Ferris wheel, 35
Feuerbach, K., 63
Feynman, R., 249
field of view, *see* viewport
Fillmore, J., 467
Fisher-Yates shuffle, 392
fixed point, 50, 439
fixed point problem, 439
fixed target, *see* ease-in, fixed target
flat, 111, 219
flat shading, 27, 132, 536
flats, 319
flexible objects, 448
flocking, 448
focal plane, 388
focusing, 395
fog, 396, 401
Foley, J., 249, 256
form factor, 424, 428, 430--435
forward dynamics, 449
forward kinematics, 449
forward ray tracing, 394
FourTextures, 243, 245
fragment shader, 22, 26, 38, 109
frame, 29
frame rate, 29
framebuffer, 24
Freeman, K., 249
Fresnel equation, 163, 164, 167, 175--177
Fresnel specularity, 144--145
front buffer, 30
front face, 14, 15, 21, 163
front intersection, 412
frustum, 98, 99
Fuchs, H., 420
full rank factorization, 478
function, 484

g, 25
G^1-continuity, 276, 282, 289, 291
gamma correction, 259--263
gathering method, 441
Gauss-Seidel, 441
Gauss-Seidel iteration, 441--442
Gaussian elimination, 479
generalized rotation, 47, 49, 81, 83
generic vertex attribute, *see* vertex attribute, 74
generic vertex attributes, 73
geodesic, 215
geometric continuity, *see* G^1-continuity
geometric occlusion, 169--175
geometry shader, 114--118
Geuzaine, C., xvii
GIF, 255
Gilbert, E., 421
gimbal lock, 456
Girard, M., 472, 480
GL_ACCUM, 397, 398
GL_ACCUM_BUFFER_BIT, 398
GL_ADD, 397
GL_ARRAY_BUFFER, 8--10, 16, 20
GL_AUTO_NORMAL, 297
GL_BACK, 22
GL_BLEND, 13, 397
GL_CCW, 22
GL_CLAMP, 244
GL_CLAMP_TO_EDGE, 244
gl_ClipDistance, 111
gl_ClipDistance[], 111
GL_COLOR_BUFFER_BIT, 29, 398
GL_CULL_FACE, 22
GL_CW, 22
GL_DEPTH_BUFFER_BIT, 29, 398
GL_DEPTH_TEST, 28
GL_DYNAMIC_DRAW, 9
GL_ELEMENT_ARRAY_BUFFER, 17
GL_FILL, 22, 297
gl_FragCoord, 112
GL_FRONT, 22

GL_FRONT_AND_BACK, 22
gl_FrontFacing, 112, 164
gl_in, 117
gl_InstanceID, 109
GL_LEQUAL, 28
GL_LESS, 29
GL_LINE, 22, 295, 297
GL_LINE_LOOP, 12
GL_LINE_SMOOTH, 13, 396
GL_LINE_SMOOTH_HINT, 13, 397
GL_LINE_STRIP, 12, 296
GL_LINEAR, 245
GL_LINEAR_MIPMAP_LINEAR, 245
GL_LINEAR_MIPMAP_NEAREST, 245
GL_LINES, 11, 12
GL_LOAD, 397
GL_MAP1_COLOR_4, 295
GL_MAP1_VERTEX_3, 294
GL_MAP1_VERTEX_4, 295
GL_MAP2_COLOR_4, 296
GL_MAP2_TEXTURE_COORD_2, 296
GL_MAP2_VERTEX_3, 296
GL_MAP2_VERTEX_4, 296
GL_MULT, 397
GL_MULTISAMPLE, 31
GL_NEAREST, 245
GL_NEAREST_MIPMAP_LINEAR, 245
GL_NEAREST_MIPMAP_NEAREST, 245
GL_NICEST, 13, 397
GL_NORMALIZE, 297
GL_ONE_MINUS_SRC_ALPHA, 13, 397
GL_POINT, 22, 296, 297
GL_POINT_SMOOTH, 13, 396
GL_POINT_SMOOTH_HINT, 13, 397
GL_POINTS, 11, 12, 296
gl_PointSize, 111, 117
GL_POLYGON_OFFSET_FILL, 97
GL_POLYGON_OFFSET_LINE, 97
GL_POLYGON_OFFSET_POINT, 97
GL_POLYGON_SMOOTH, 396
GL_POLYGON_SMOOTH_HINT, 397
gl_Position, 24, 69, 111, 112
GL_REPEAT, 244
GL_RETURN, 397, 398
GL_RGB, 243
GL_RGBA, 243, 244
GL_S, 247
GL_SPHERE_MAP, 247
GL_SRC_ALPHA, 13, 397
GL_SRGB8, 261, 262
GL_SRGB8_ALPHA8, 261, 262
GL_STATIC_DRAW, 8, 9, 16, 20
GL_T, 247
GL_TEXTURE_1D, 246
GL_TEXTURE_2D, 243--246
GL_TEXTURE_3D, 246
GL_TEXTURE_GEN_MODE, 247
GL_TEXTURE_GEN_S, 247
GL_TEXTURE_GEN_T, 247
GL_TEXTURE_MAG_FILTER, 245
GL_TEXTURE_MIN_FILTER, 245
GL_TEXTURE_WRAP_S, 244
GL_TEXTURE_WRAP_T, 244
GL_TRIANGLE_FAN, 13--15, 17, 18
GL_TRIANGLE_STRIP, 13--15, 17, 18
GL_TRIANGLES, 13--16, 18
GL_UNPACK_ALIGNMENT, 243
GL_UNSIGNED_BYTE, 20
gl_VertexID, 109
glAccum, 397, 398
glAccumClear, 397, 398
Glassner, A., 249, 263, 396
glBegin, 295, 296
glBindBuffer, 8--10, 16, 17, 20
glBindTexture, 246
glBindVertexArray, 8, 10, 11, 16--18, 20
glBlend, 399
glBlendFunc, 13, 110, 113, 397, 401
glBufferData, 8, 9, 16, 17, 20
glClear, 29, 398
glClearBuffer, 29
glClearColor(), 29
glClearDepth, 29
glCullFace, 22, 110, 112
glDeleteTextures, 246
glDepthFunc, 28, 110, 112
glDisable, *see the* GL_ *options that can be disabled*
glDraw*, 110, 115
glDraw*, 111

glDraw*Instanced, 109
glDrawArrays, 11--13, 16, 17, 21
glDrawElements, 17, 18
glEnable, *see the* GL_ *options that can be enabled*
glEnableVertexAttribArray, 8, 10, 16, 20, 21, 74
glEnd, 295, 296
glEvalCoord1f, 295
glEvalCoord2f, 297
glEvalMesh1, 295, 296
glEvalMesh2, 297
glEvalPoint1, 296
glEvalPoint2, 297
glFog, 401
glFrontFace, 22, 110, 112
glFrustum, 70, 97, 98, 158
GLFW_SAMPLES, 31
glfwPollEvents, 31
glfwWaitEvents, 30
glfwWindowHint, 31
glGenBuffers, 8, 9, 17
glGenTextures, 246
glGenVertexArrays, 8
glGetAttribLocation, 74
glGetUniformLocation, 75, 76
glHint, 13
glide rotation, 83
glLineWidth, 13, 110, 111
glLoadMatrixf, 70
glMap1f, 294, 295
glMap2f, 296
glMapGrid1f, 295
glMapGrid2f, 297
glNormal*, 295
global coordinates, *see* world coordinates
global lighting, 133
global reflectivity coefficient, 375
glOrtho, 70, 97, 158
glPixelStorei, 243
glPointSize, 13, 110, 111
glPolygonMode, 22, 110, 111
glPolygonOffset, 97
glProvokingIndex, 27, 219
glRotatef, 70
glScalef, 70
GLSL, 25
glTexCoord*, 246, 295
glTexGeni, 247
glTexImage*, 246
glTexImage2D, 243, 244, 262
glTexParameter*, 246
glTexParameteri, 244, 245
glTranslatef, 70
gluBuild2DMipmaps, 244, 246
GLuint, 246
gluLookAt, 70, 72, 452
glUniform, 73, 75
glUniform*, 109, 112
glUniformMatrix4f, 73
glUniformMatrix4fv, 74, 75
gluPerspective, 70, 97, 98, 158
glUseProgram, 75
GLUT_ACCUM, 397, 398
glutInitDisplayMode, 397, 398
gluUnProject, 400
glVertex*, 295
glVertexAttrib, 73, 75
glVertexAttrib*, 109
glVertexAttrib3f, 11, 16, 18, 19, 74
glVertexAttribPointer, 8--10, 16, 20
goniometer, 166
Gottschalk, S., 420
Gouraud shading, 121, 125, 131, 132, 142, 148, 157, 190, 258, 259, 429, 536
Gouraud, H., 121
GPU, 1
gradient, 153, 416, 496
Grant, E., 420
graphics processing unit, 1
great circle, 62, 215
Greenberg, D., 164, 433

Haines, E., 403, 421
half-space, 209
halfway vector, 141, 143, 161, 163, 169

Hall, R., 249, 252
Hamilton, W.R., 458
He, X., 164
heading, 232, *see also* yaw,pitch and roll
Heckbert, P., 213
Heidmann, T., 400
Heirich, A., 401
helix, 306
Helmholtz, H., 249
hemicube, 433
hemicube method, 433--435
Hering, E., 250
Hermite polynomial, 277--278, 450, 451
Hernicz, R., 177
hidden surface, 22, 28, 29, 85, 90, 92, 371, 373
high color, 255
homogeneous coordinates, 52, 64, 297, 298, 364
  affine combinations, 187, 210--213
homogeneous matrix, 54, 65, 156
Horner's method, 270
HSL, 256--258
  from RGB, 256
hue, 256
hyperbola, 212
hyperbolic interpolation, 213--215, 218, 227--229

identity matrix, 491
identity transformation, 41
IK, *see* inverse kinematics
illumination maps, 394
implicitly defined surface, 153, 497
importance sampling, 395
inbetweener, 446
index of refraction, 175, 376, 379
indexed color, *see* color lookup table
inherent velocity, 451
inker, 446
inner automorphism, 461
inner product, *see* dot product
intensity, 256
interpolating points, 185, 266, 309--321, 365--369, 447, 450, *see also* Catmull-Rom spline, Bessel twist method, Ferguson patches, Overhauser spline, *and* tension-continuity-bias spline
  with surface, 317--322
interpolation (averaging), 147, 183--218, 446, *see also* bilinear interpolation, Gouraud shading, hyperbolic interpolation, linear interpolation, Phong shading, quaternion, scan line interpolation, *and* spherical linear interpolation
intersection testing, 273, 385, 403--421
  line-plane, 408
  ray-Bézier curve, 274
  ray-Bézier patch, 417
  ray-cylinder, 415
  ray-ellipsoid, 407
  ray-plane, 407--408
  ray-polytope, 408, 411--415
  ray-quadric, 416
  ray-sphere, 404--407
  ray-triangle, 409--411
intrinsically curved, 231, 232
inverse, 41, *see also* matrix inverse
inverse dynamics, 449
inverse kinematics, 446, 449, 472--481

Jackson, R., 249, 263
Jacobi iteration, 436, 440--441
Jacobian, 473--475, 498
JacobiIteration., 440
jaggies, 3, 126, 386, 387, 396, 540
JavaScript, 5
Jensen, H., 395
jittering, 236, 391, 433

jittering eye position, *see* viewpoint jittering
Johnson, D., 421
Johnston, O., 446
joint, 468
Joy, K., 417

Kakimoto, M., 417
k-DOP, *see* bounding box
Keerthi, S., 421
kernel, 476, 495
keyframe, 446
keyframing, 446, 450
Kilgard, M., 400
kinematics, 449, 467--481
Klein, F., 63
knot, 265, 330, 332
knot elimination, 364
knot insertion, 364
knot multiplicity, 343
knot refinement, 359, 364
knot vector, 331, 332, 360
  standard, 340, 344
Kochanek, D., 314
Krevald, M., 421

Lambertian surface, 137, 138
least squares minimization, 477, 481
Lee, E., 302
Lempel, A., 255
lerp, *see* linear interpolation
lerp, 185
level of detail, 235
level set, 153, 497
level surface, *see* implicitly defined surface
Lin, M., 420, 421
line at infinity, 61, 62, 64, 84
line width, 111
line-plane intersection, 408
linear attenuation factor, 146
linear combination, 186
linear interpolation, 121, 125, 149, 227, 270, 466
  inversion, 184
  three points, 187--195
  two points, 184--185
linear subspace, 83, 494--495
linear transformation, 35, 39, 47, 64
  matrix, 43, 44, 64
linearly independent, 494
LinearMapR4, 70
link, 448, 468
LoadMatrix, 72
local control, 327, 329, 342, 369
local coordinates, 36
local lighting, 133, 164, 377
local viewer, 142, 247, 248
LOD, *see* level of detail
luminance, 256
LUT, *see* color lookup table
LZW compression, 255

MacDonald, D., 249
Mach banding, 429
Maciejewski, A., 472, 480
magenta, 20, 253, 257, 535
magnitude, 38, 459, 485, 489, 490
major radius, 152, 232
Manfield, L., 326
Manocha, D., 420
mapping, 484
masking, 170
material properties, 135, 143
matrix, 491
matrix inverse, 44, 436, 491, 493
matrix, orthonormal, 48
matrix product, 491
matrix representation
  cross product, 79
  orthographic projection, 87
  quaternion, 463--465
  reflection, 106
  rotation, 48, 66, 77
  scaling, 66
  shadow projection, 95
  translation, 66
matrix representation of a transformation, 43, 46, 53, 64, 65
matrix transpose, 43, 46, 491

Matusik, W., 164
McCool, D., 401
Mercator map, 231
metal, 164
metamerism, 251, 252
Meyer, G., 252
microfacet, 164, 166--169
millions of colors, 119, 254
minor radius, 152, 232
mipmapping, 226, 233--236, 259, 386
mirror, 139, 240, 372, 399
mirror image, 72
Möbius, A., 63
model matrix, 36, 55
modelview matrix, 37, 158
modern OpenGL, 70
Moll, L., 401
Möller, T., 403, 421
Monte-Carlo, 395
moon, 138
Moore-Penrose inverse, *see* pseudo-inverse
Moreton, H., 213
mosaic, 2
motion blur, 372, 389, 390, 397, 542
motion capture, 447
move-to, 4
movie, 371
moving target, *see* ease-in, moving target
Mozzi-Chasles theorem, 83
Mult_glRotate, 71, 72
Mult_glScale, 71
Mult_glTranslate, 71, 72
multiaffine, 351
multibody, *see* articulated object
multiplication, quaternion, 458
multiplicative identity, 460
multiplicative inverse, 460
multiplicity, 331, 343
multivariable, 495
multum in parvo, 235

Nayar, S., 174
near clipping plane, 87, 91, 92, 97--99
Newman, W., 63
Newton's method, 208, 417
Ngan, A., 164
Nishita, T., 417
noise, 237
nonlocal viewer, 142, 247, 248
nonuniform B-spline, *see* B-spline
nonuniform scaling, 40
noperspective, 111, 219, 229
norm, 38, 459, 485, 489, 490
normal vector, 150, 155, 157, 202, 416, 489, 497
  interpolation, 150, *see also* Phong shading
normalization, 489
NURBS, *see* Bézier curve, rational *and* B-spline curve, rational

OBB, *see* bounding box, oriented
octtree, 404, 419
one-to-one, 484
onto, 484
opponent color theory, 249, 250
order, 296, 332, 341
Oren, M., 174
orientation, 452--467
orientation preserving, 46, 47, 65, 67, 81, 453, 456
oriented bounding box, *see* bounding box, oriented
origin, 38, 64
orthogonal, 486, 495
orthogonal complement, 476, 495
orthographic projection, 37, 86--87, 97, 219
orthonormal, 48
oscilloscope, 4
Oslo method, 359
out, 219
Overhauser spline, 309, 311--314, 317, 369, 447, *see also* Bessel twist method
Overmars, M., 421

oversampling, *see* jittering *and* supersampling
overshoot, 314, 316

painter's algorithm, 28, 401
Palmer, G., 249
parabola, 212
parallel, 487
parallelepiped, 417
parametric curve, 266--268, 306, 498
parametric surface, 151, 229, 232, 237, 287
partial derivative, 496
participating media, 396
particle systems, 448
partition of unity, 329
patch, 424
path tracing, 393
pen down, 4
pen plotter, 4
pen up, 4
penumbra, 390, 391
percentage closer filtering, 401
permutation, 392
perpendicular, 486
perspective division, 37, 85, 158, 214
perspective transformation, 36, 37, 85, 86, 88--92, 94, 97--100, 142
    preserved under, 212, 298
Phong interpolation, 74, *see* Phong shading
Phong lighting, 133--147, 166, 226, 237, 247, 252, 371, 373, 378, 381
    shader code, 157--164
Phong shading, 131, 142, 149, 157
Phong, B., 133
photon maps, 395
piecewise Bézier curve, *see* Bézier curve
Piegl, L., 299, 360, 364
pinhole camera, 386
pitch, 232, *see also* yaw, pitch and roll
pixel, 2, 3, 234, 534
pixel shader, *see* fragment shader, 240
plane, 6, 105, 106, 407
plane at infinity, 64, 84
point, 38, 43, 63
point at infinity, 53, 61, 62, 64, 83, 84, 298--300
point size, 111
pointillism, 2
points, 46
polar form, *see* blossom
polygon offset, 96
polygonal modeling, 5
polyhedron, *see* polytope
polynomial curve, 282
polytope, 411
Porter, T., 385
positional light, 142, 160
postscript, 5, 285
pow, 34
Precompute_for_Slerp, 217, 218, 467
Premože, S., 164
primary color, 2, 250--253
primitive assembly, 111
prism, 411
progressive refinement, 442
projected convexity condition, 198, 199, 206, 207
projection, 486, 490
    matrix, 77
projective geometry, 61--63, 83--84, 94
projective line, 62, 63, 84
projective plane, 61, 84
projective point, 62, 63, 83, 84
projective space, 84
pseudo-distance, 37, 38, 90, 92, 119
pseudo-inverse, 476--480
Puech, C., 443
pyramid, 411

quad strip, 19
quadratic attenuation factor, 146
quadratic curve, 282, 299--306
quadratic formula, 203, 204
quadric, 416
quadrilateral, 19
quadtree, 419
quasi-Newton method, 417, 479
quaternion, 80, 215, 448, 453, 456--467
- conjugate, 459
- equality, 458
- from matrix, 464--465
- interpolation, 465--467
- matrix form, 463--464
- multiplication, 458
- norm, 459
- unit, 459

radiosity, 128, 423--444
radiosity (brightness), 427
radiosity equation, 428, 436--444
Ramamoorthi, R., 401
Ramshaw, L., 355
RandInt(i), 392
RandomPermutation, 392
range, 484, 495
rank, 495
rasterization, 111
rational curve, 297, 364, *see also* Bézier curve *and* B-spline curve
rational linear interpolation, *see* hyperbolic interpolation
ray, 404
ray tracing, 168, 236, 240, 371--401, 433
Ray Tracing News, 396
ray-Bézier patch intersection, 417
ray-cylinder intersection, 415
ray-ellipsoid intersection, 407
ray-line, 404
ray-plane intersection, 407--408
ray-polytope intersection, 408, 411--415
ray-quadric intersection, 416
ray-sphere intersection, 404--407
ray-triangle intersection, 409--411
RayTrace, 383, 384
RayTraceMain, 384
reciprocity, 428, 432, 435
recursive ray tracing, 372--377
recursive subdivision, 270--275, 284--285, 290, 292, 324, 358, 417
Reeves, W., 401
reflection, 72, 105--107, 372, 398
reflection direction, 139, 163, *see also* view reflection
reflection map, *see* environment map
reflection ray, 374--378
reflectivity, 427
reflectivity coefficient, *see* ambient, diffuse, global, *and* specular
refraction, 372
rendering pipeline, 36, 84, 85, 89, 92, 214
repeated knots, 343
rest position, 480
retina, 250
RGB, 20, 253--256
- to HSL, 256
- to/from CMY, 253

righthand rule, 6, 65, 66, 454, 490
righthanded coordinate system, 6, 64, 489
rigid body, 448
rigid transformation, 46, 47, 64, 67, 81, 453, 456
Rogers, D., 266
roll, *see* yaw, pitch and roll
room, 419
root link, 468
rotation, 45--52, 66, 81, 452--467, *see also* generalized rotation
rotation interpolation, *see* quaternions
rotation matrix, 48, 66, 77--80, 448, 453--454, 463
rotational joint, *see* joint

roundoff error, 80, 96, 124, 126--128, 203, 231, 404, 479
row vector, 43, 46, 492
rowspan, 476, 495
Russian roulette, 395

Sakkalis, T., 306
Salesin, D., 401
Saltzman, M., 249
Samet, H., 421
saturation, 256
scalar, 38, 484
scalar quaternion, 460
scan line interpolation, 122--124, 127, 148, 190
Schlick, C., 133, 144, 164, 177
Schröder, P, 322
Schumaker, L., 266
Schwartzkopf, O., 421
screen coordinates, 37
Sederberg, T., 417
Seidel, H.-P., 355
self reflection, 399
Set, 72
Set_glFrustum, 98--100, 158
Set_glOrtho, 158
Set_glRotate, 71
Set_glScale, 71
Set_glTranslate, 71
Set_gluLookAt, 73
Set_gluPerspective, 98--100, 158
SetByRows, 72
SetIdentity, 71
shader-specific input and output, 24, 25, 27
shader-specific output, 111
shading, 5, 21, 23, 131, 147, *see also* flat shading
shadow feeler, 373--375, 382, 391
shadow map, 399, 400
shadow volume, 127, 399
shadowing, 170
shadows, 95--97, 372, 390, 399
shearing, 72
Shepperd, S., 464
shininess, *see* specular exponent
Shirley, P., 164, 396
Shoemake, K., 215, 467
Shoenberg, I., 326
shooting method, 442--443
Shooting_Method, 442
silhouette edges, 400
Sillion, F., 164, 443
SimpleNurbs, 296, 297, 308
singular value decomposition, 479
skeleton, 445
skinning, 445
Slerp, 218
slerp, *see* spherical linear interpolation
slerp, 216
Sloan, K., 229
smoke, 396, 448
smooth, 111, 219
smooth shading, *see* shading
smoothstep, 323
Snell's law, 175, 379, 382
soft shadows, 390, 399
SolarModern, 75
Southwell iteration, 442
spacecraft, 453
span, 476, 494
spectral sampling, 252
specular exponent, 135, 137, 140, 143
specular highlight, 131, 132, 134, 140, 149, 150, 536
specular light, 134, 139, 140
specular reflection, 134, 135, 139--142
specular reflectivity coefficient, 135, 140, 144, 145, 382
specular transmission, 382
specular transmission coefficient, 382
sphere, 231, 403, 404
spherical coordinates, 232
spherical linear interpolation, 215--218, 465, 466
spline, 265, *see also* Bézier curve *and* B-spline curve

spotlight, 144, 146, 149, 150, 157, 160
spotlight direction, 157
spotlight exponent, 146
sprite, 111
Sproull, R., 63
sRGB, 259--263
standard knot vector, 340, 344
Star Trek, 453
stencil buffer, 399, 400
Stiles, W., 263
stochastic supersampling, 236, 386, *see also* jittering
stratified stochastic supersampling, *see* jittering
stride, 10, 20
subdivision surface, 322
subpixel, 3
subtractive colors, 253
superposition principle, 134, 143
supersampling, 236, 386
support, 484
surface normal, *see* normal vector
surface of revolution, 154, 297, 306--309
symmetric function, 351

TCB spline, *see* tension-continuity-bias spline
teapot, 132, 297, 536
television, 250
tension, 315
tension-continuity-bias spline, 309, 314--317, 447
terrain, 206
tessellation shader, 114
texture, 262
texture coordinates, 119, 226, 227, 229
  cylinder, 229--231
  sphere, 231--232
  torus, 232
texture map, 5, 119, 195, 225--248, *see also* mipmapping
  decal/replace, 225
  in OpenGL, 243--248
  repeating, 230, 244
texture object, 243, 245
TextureBMP, 243
TextureTorus, 243
Thomas, F., 446
thousands of colors, 255
Tiller, W., 299, 360, 364
tilt, planetary, 77
torchiere, 423
Torrance, K., 164, 168, 170, 176
torus, 152, 232
total derivative, 496
total internal reflection, 175, 380, 381, 385
Toth, D., 417
Touloukian, Y., 177
trace, 79, 464
traditional animation, 446
transform feedback, 114, 118
transformation, 39, 64, *see also* affine transformation, linear transformation, *and* rigid transformation
translation, 41, 47, 64
transmission
  diffuse light, 382
  specular light, 382
transmission coefficient, 377
transmission ray, 376--377
  direction, 379--381
transparency, 255, 372, 382
transpose, 46, *see* matrix transpose
triangle, 5, 187, 409
triangle fan, 14, 18, 27
triangle strip, 14, 18
trichromatic theory, 249
tridiagonal matrix, 368
trilinear interpolation, 207--208
  inversion, 208
tristimulus method, 251
true color, 254
tuple, 483
turtle geometry, 4
twist vector, 290, 318, 319, 321

undershoot, 314, 316

uniform, 109, 112
uniform scaling, 40
uniform speed, 306
uniform variable, 24, 70
uniform variables, 73
unit circle, 485
unit quaternion, 459, 460
unit sphere, 62, 215, 461, 489
unit vector, 485, 489
up direction, 73

value, 256
vanishing point, 63, 88
VAO, *see* Vertex Array Object
variation diminishing, 281, 324, 361
VBO, *see* Vertex Buffer Object
vector, 38, 43, 46, 63, 460, 483, 484
vector graphics, 4
vector, as quaternion, 460
vector-valued function, 151, 497
VectorR3, 70, 71
VectorR4, 70, 72
Vertex Array Object, 8, 9
vertex attribute, 9, 10
  generic, 11, 19, 24
Vertex Buffer Object, 8, 9
vertex post-processing, 111
vertex shader, 22, 25, 38, 109
vertical synchronization, 30
view coordinates, 36, 37
view matrix, 73
view orientation, 73
view reflection, 241, 247
view vector, 136, 163
viewing transformation, 85, 97
viewpoint animation, 448, 452
viewpoint jittering, 386
viewport, 36, 119, 373, 386

Wallace, J., 443
Warren, J., 322
Watt, A., xvii, 396
Watt, M., xvii, 396
web-safe colors, 255
weighted average, 151, 186, 187, 208, 209, 268, 274, 279, 281, 329, 342
  homogeneous coordinates, 187, 210--213
Welch, T., 255
white, 253
White, T., 446
Whitted, T., 396, 417
Wiemar, H., 322
Williams, L., 235, 401
winding number, 231
wireframe, 22
Witt, D., 177
world coordinates, 36
writePixel, 125
Wyszecki, G., 263

yaw, pitch and roll, 448, 453--456
yellow, 20, 253, 257, 258, 535
Young, T., 249

z buffer, *see* depth buffer
z fighting, 96
Zandt, T. van, xvii
zero vector, 38, 64
Zhao, J., 472
Ziv, J., 255
Zorin, D., 322

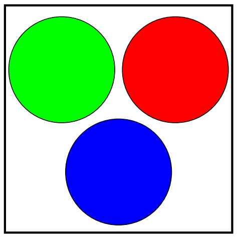

Color Plate C.1: (Figure I.1, page 3.) A pixel is formed from subregions or subpixels, each of which displays one of three colors.

Color	R	G	B	Color	R	G	B
Black: ⬛	0	0	0	White: ⬜	1	1	1
Red: 🟥	1	0	0	Cyan: 🟦	0	1	1
Green: 🟩	0	1	0	Magenta: 🟪	1	0	1
Blue: 🟦	0	0	1	Yellow: 🟨	1	1	0

Color Plate C.2: (Figure I.13, page 20.) Eight colors and their RGB values.

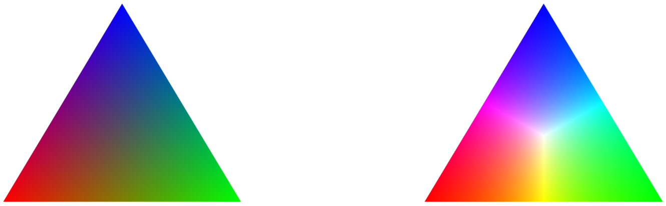

(a) The default smooth shading

(b) Full brightness shading

Color Plate C.3: (Figure I.14, page 21.) Two triangles: with the default smooth shading and the “full brightness” shading. The latter is created with the fragment shader on page 26.

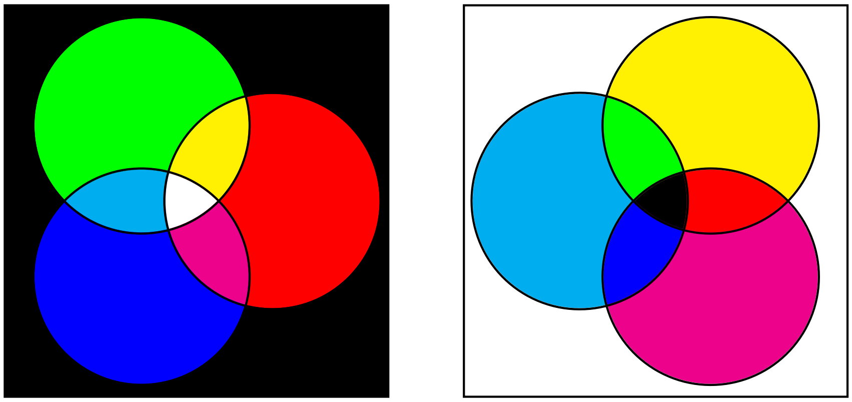

(a) (b)

Color Plate C.4: (Figure VII.1, page 254.) (a) The additive colors are red, green, and blue. (b) The subtractive colors are cyan, magenta, and yellow.

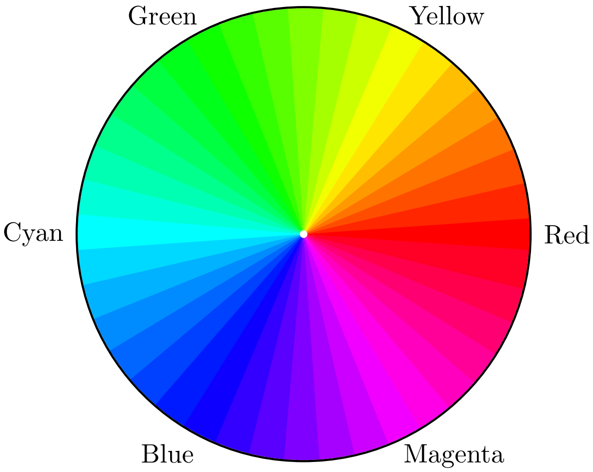

Color Plate C.5: (Figure VII.2, page 257.) Hue is measured in degrees, representing an angle around the color wheel. Pure red has hue equal to 0, pure green has hue equal to 120, and pure blue has hue equal to 240.

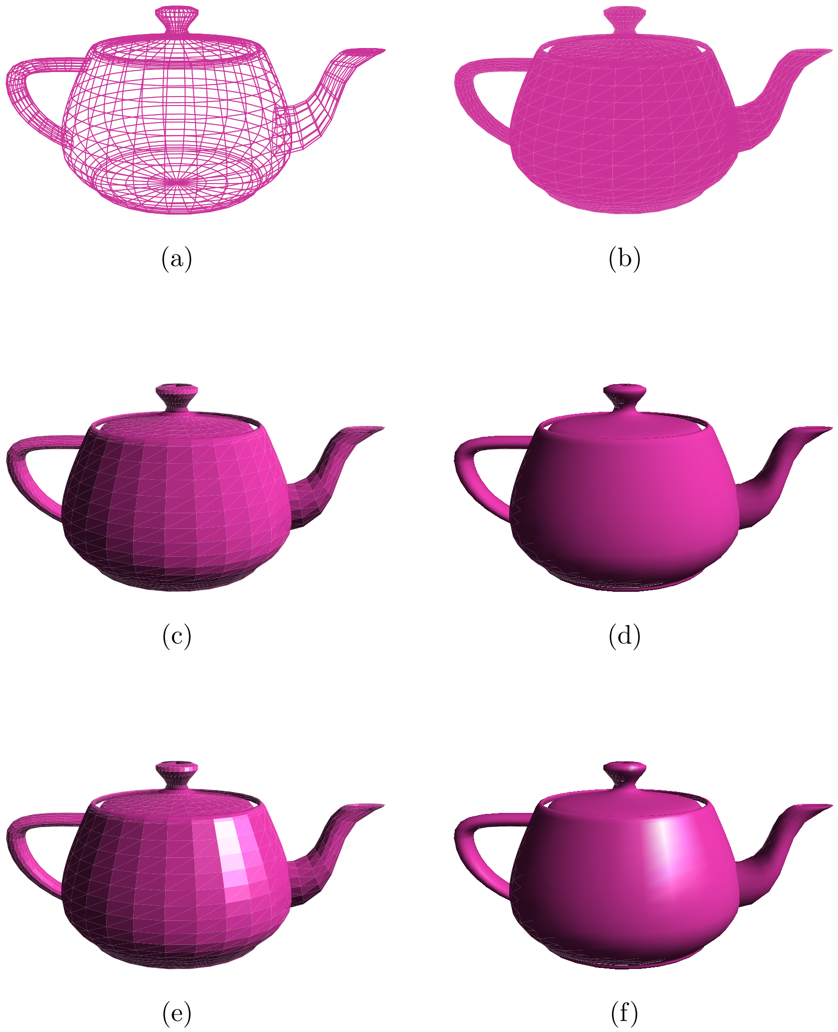

(a) (b)

(c) (d)

(e) (f)

Color Plate C.6: (Figure IV.1, page 132.) Six teapots with various shading and lighting options. (a) Wireframe teapot. (b) Teapot drawn with solid color, but no lighting or shading. (c) Teapot with flat shading, with only ambient and diffuse lighting. (d) Teapot drawn with Gouraud interpolation, with only ambient and diffuse reflection. (e) Teapot drawn with flat shading, with ambient, diffuse, and specular lighting. (f) Teapot with Gouraud shading, with ambient, diffuse, and specular lighting.

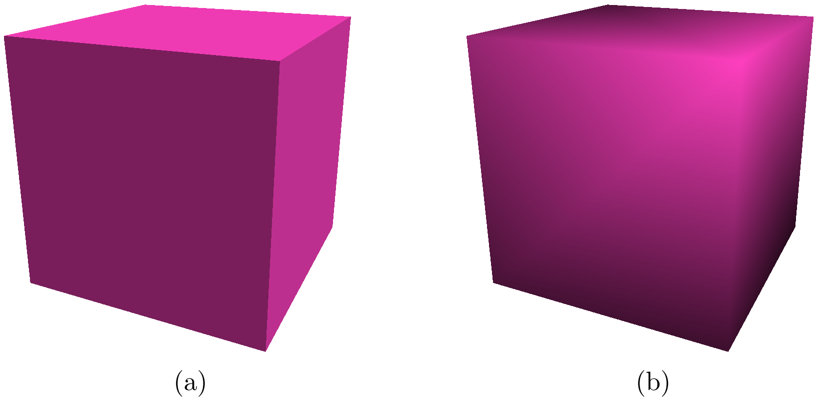

Color Plate C.7: (Figure IV.14, page 149.) Two cubes with (a) normals at vertices perpendicular to each face, and (b) normals outward from the center of the cube. Note that (a) is rendered with Gouraud shading, not flat shading.

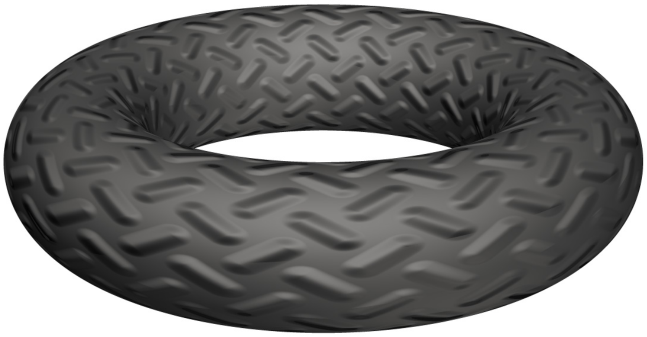

Color Plate C.8: (Figure VI.9, page 238.) A bump mapped torus. Note the lack of bumps on the silhouette. There are four white lights shining on the scene, plus a low level of ambient illumination. This picture was generated with the ray tracing software described in Appendix **??**.

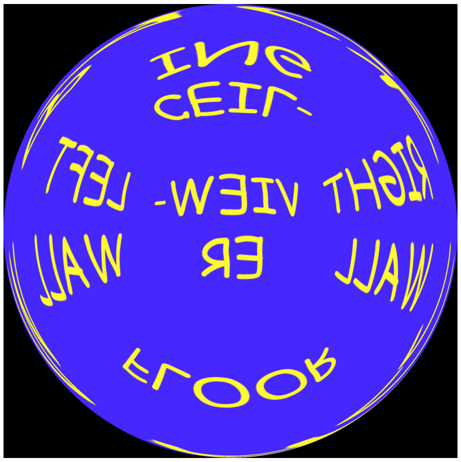

Color Plate C.9: (Figure VI.11, page 241.) An environment map mapped into a sphere projection. This is the kind of environment map supported by OpenGL. The scene is the same as is shown in Figure VI.12. Note that the front wall has the most fidelity, and the back wall the least. For this reason, spherical environment maps are best used when the view direction is close to the direction used to create the environment map.

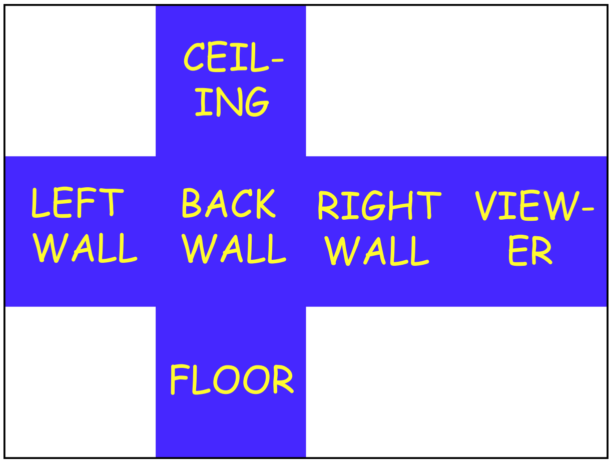

Color Plate C.10: (Figure VI.12, page 242.) An environment map mapped into a box projection consists of the six views from a point, mapped to the faces of a cube and then unfolded to make a flat image. This scene shows the reflection map from the point at the center of a room. The room is solid blue, except for yellow writing on the walls, ceiling and floor. The rectangular white regions of the environment map are not used.

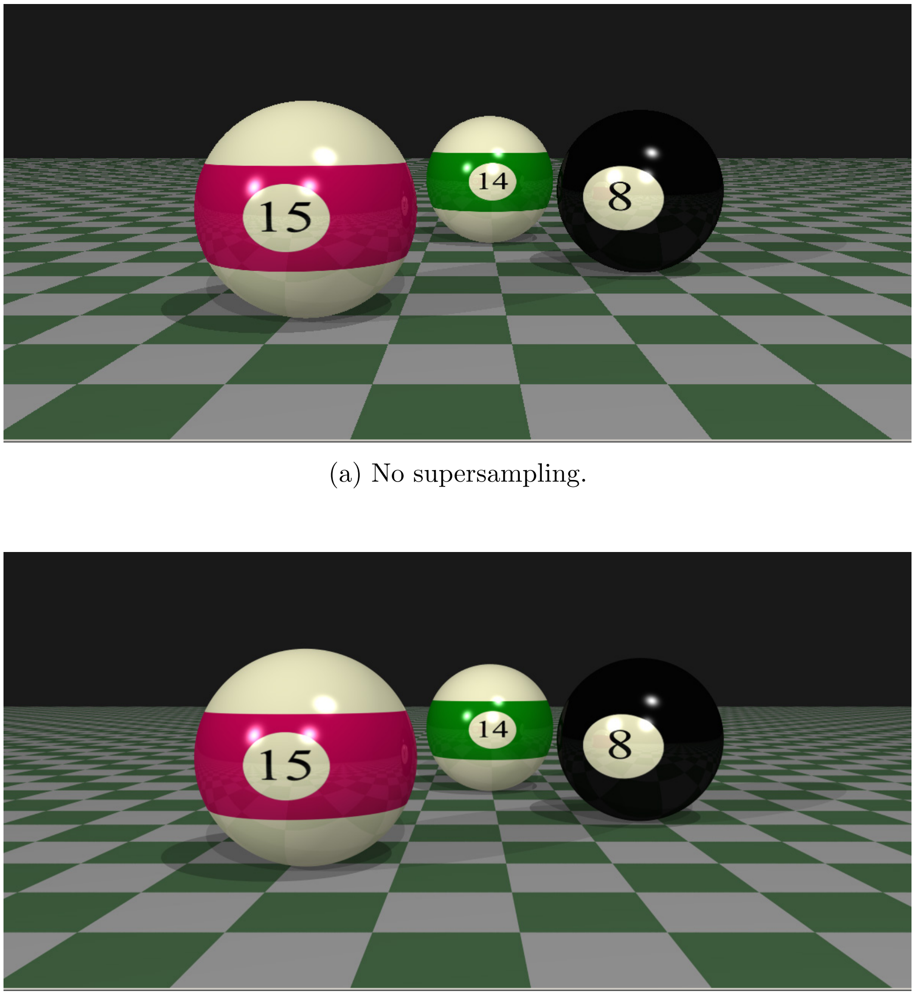

(a) No supersampling.

(b) Supersampling with jittered subpixel centers.

Color Plate C.11: (Figure X.9, page 387.) An example of anti-aliasing using jittered subpixel centers. (a) shows the scene rendered without supersampling; note the “jaggies” on the silhouettes of the balls, for instance. (b) is the scene with pixels selectively supersampled up to a maximum of 40 times.

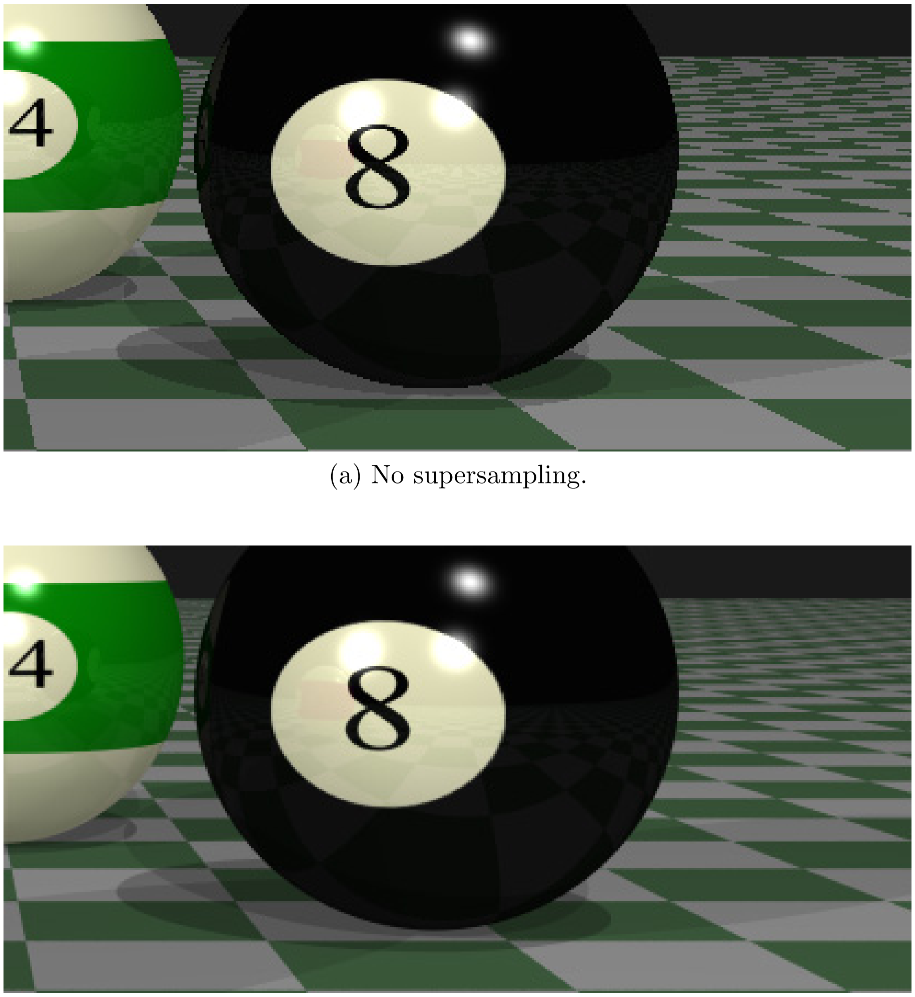

(a) No supersampling.

(b) Supersampling with jittered subpixel centers.

Color Plate C.12: (Figure X.10, page 388.) Close up views of the images in Figure X.9.

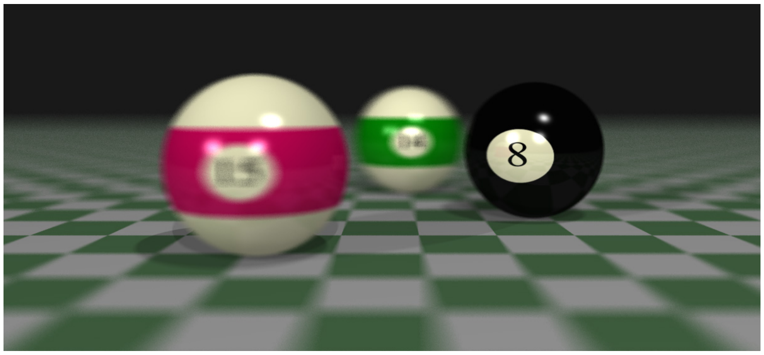

Color Plate C.13: (Figure X.12, page 389.) An example of depth of field. The front of the eight ball is the focal plane. Note also the blurring of the checkerboard plane. In this image, each pixel is selectively supersampled up to 40 times. The eye positions and the subpixel positions were independently jittered as described on page 391.

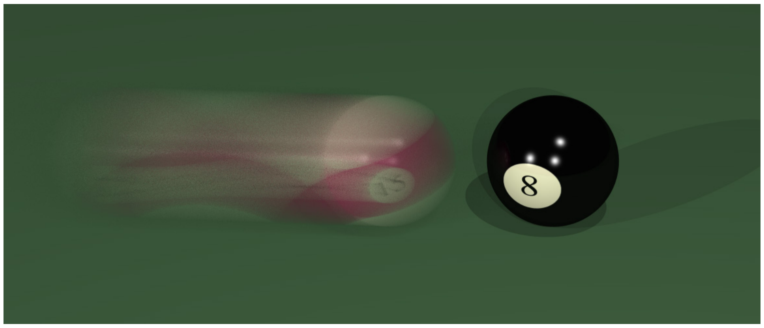

Color Plate C.14: (Figure X.13, page 390.) An example of motion blur. Pixels were selectively supersampled up to 40 times. Both motion supersampling and subpixel supersampling were used.

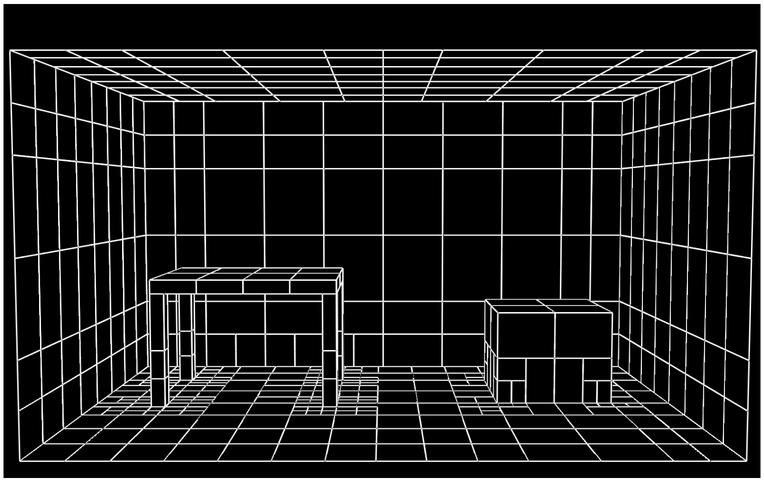

Color Plate C.15: (Figure XII.1, page 426.) The patches used to render the radiosity scene of Figures XII.2 and XII.3.

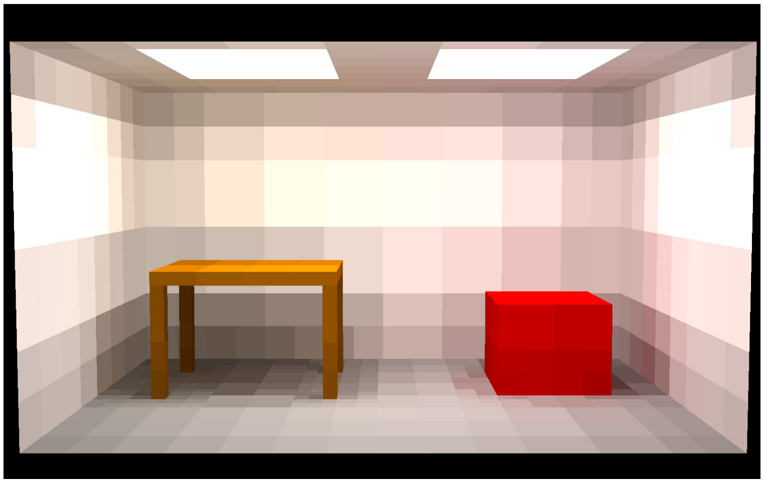

Color Plate C.16: (Figure XII.2, page 426.) A radiosity rendered figure, with flat shading. It is evident that this image is based on the patches shown in Figure XII.1.

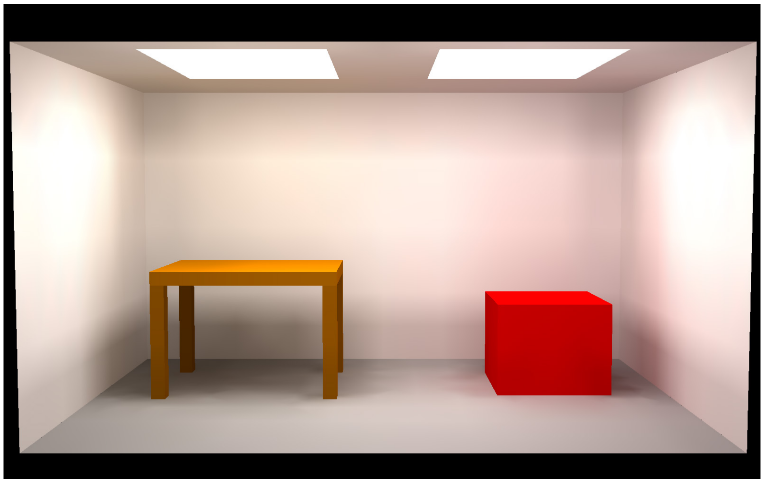

Color Plate C.17: (Figure XII.3, page 427.) A radiosity rendered figure, with smooth shading of illumination. The red color of the box is reflected onto the nearby walls, giving them a slight reddish hue. This is based on the patches shown in Figure XII.1.

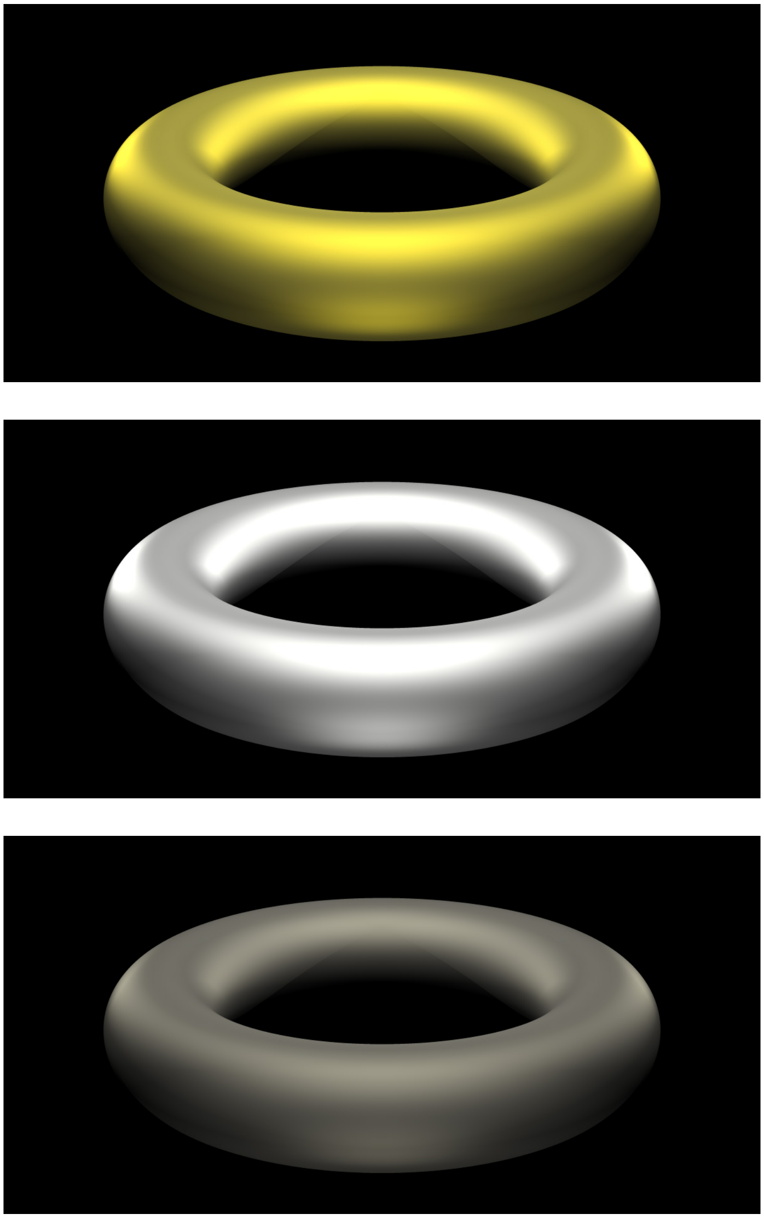

Color Plate C.18: (Figure IV.25, page 178.) Metallic tori, with specular component computed using the Cook-Torrance model. The materials are, from top to bottom, gold, silver and platinum. The roughness is $m = 0.4$ for all three materials. The tori are each illuminated by five positional white lights.